

TECHNISCHE UNIVERSITÄT MÜNCHEN

WACKER-Institut für Siliciumchemie

Professur für Siliciumchemie

NHC-stabilized Silyliumylidene Ions and Their Coordination Chemistry

Philipp Simon Frisch

Vollständiger Abdruck der von der Fakultät für Chemie der Technischen Universität München zur Erlangung des akademischen Grades eines

Doktors der Naturwissenschaften

genehmigten Dissertation.

Vorsitzender: Prof. Dr. Dr. h.c. Bernhard Rieger

Prüfer der Dissertation: 1. Prof. Dr. Shigeyoshi Inoue

2. Prof. Dr. Klaus Köhler

Die Dissertation wurde am 10.03.2020 bei der Technischen Universität München eingereicht und durch die Fakultät für Chemie am 26.05.2020 angenommen.

“Chemists do not usually stutter. It would be very awkward if they did, seeing that they have at times to get out such words as ‘methylethylamylphenylium’ ‘silyl-substituted silyliumylidene ion’.”

adapted from Sir William Crookes (1832–1919)

Diese Arbeit wurde in der Zeit von Juni 2016 bis Februar 2020 im Rahmen der Professur für Siliciumchemie der Technischen Universität München unter Betreuung von Herrn Prof. Dr. Shigeyoshi Inoue angefertigt.

Acknowledgments

Mein aufrichtiger Dank gilt meinem Doktorvater, Herrn Prof. Dr. Shigeyoshi Inoue, für die freundliche Aufnahme in seinen Arbeitskreis und das entgegengebrachte Vertrauen, mein Promotionsthema nach meinen eigenen Vorstellungen unter seiner Aufsicht bearbeiten zu können. Mit seiner Begeisterung für die Chemie im Allgemeinen und mit seinem beeindruckenden Wissen über die Hauptgruppenchemie brachte er meine Arbeit stetig mit Anregungen, Vorschlägen und Diskussionen voran.

Ferner möchte ich auch dem kompletten AK Inoue danken – ganz besonders meinen direkten Labornachbarn und guten Freunden Richard Holzner und Dominik Reiter sowie Franziska Hanusch. Der tägliche Wahnsinn der Laborarbeit wäre ohne die angenehme Atmosphäre und den „ein oder anderen“ Blödsinn im und außerhalb vom Labor bei Weitem nicht so spaßig gewesen. Das gleiche gilt auch für die „Jünglinge“ Ramona Baierl, Florian Tschernuth, Lisa Groll und Teresa Eisner. An dieser Stelle möchte ich auch Verena Goldberg für die regelmäßige Essensversorgung während langer Tage (und Nächte) im Labor danken.

Zusätzlich möchte ich auch Herrn Prof. Dr. Dr. h.c. Bernhard Rieger und Dr. Carsten Troll vom WACKER-Lehrstuhl für Makromolekulare Chemie danken: dass unsere Gruppe ohne zu zögern quasi in den Makro-Lehrstuhl aufgenommen wurden und dass wir die bestehende Infrastruktur und Ausrüstung mitbenutzen durften ist alles andere als selbstverständlich. Das hat gerade das erste Jahr der Promotion um ein Vielfaches einfacher und angenehmer gemacht. Auch den Makro-Mitgliedern des Silicium-Instituts, insbesondere Dr. Daniel Wendel, Fabian Herz, Daniel Henschel, Matthias Nobis und Andreas Saurwein will ich für die großartige Atmosphäre im Labor und die Hilfe danken.

Außerdem möchte ich mich bei meinem ehemaligen Masterarbeitsbetreuer Dr. Alexander Pöthig zusammen mit Dr. Christian Jandl für die Einführung in die Einkristall-Röntgendiffraktometrie bedanken – und auch dafür, dass beide immer bei sämtlichen Problemen mit Diffraktometern, Messungen oder Verfeinerungen mit Rat und Tat zur Verfügung standen. Ebenso möchte ich Dr. Tibor Szilvási danken für die Durchführung der theoretischen Berechnungen für meine Publikationen und die tolle unkomplizierte Zusammenarbeit. Ein großes Dankeschön gebührt auch Ulrike Ammari (Elementaranalyse), Maria Matthews (VT-NMR) und Dr. Oksana Storcheva (EPR Spektroskopie), genauso wie meinen Kollegen Dr. Lorenz Schiegerl (ESI-MS),

Maximilian Muhr (LIFDI-MS) und Patricia Heiß (IR Spektroskopie), für die Durchführung von zahlreichen Messungen während meiner Doktorarbeit.

Darüber hinaus gilt mein Dank noch meinen engagierten und interessierten Forschungspraktikanten Christopher Schiefer, Alexander Mutschke, Alina Denk, Sandra Paßreiter, Moritz Ludwig und Fiona Kiefer, die während meiner Promotion viel wichtige Arbeit für mich erledigt haben.

Abschließend möchte ich noch meiner ganzen Familie danken, insbesondere meinen Eltern Klaus und Brigitte und meiner Oma Erika für die andauernde Unterstützung – denn ohne euch wäre mir weder das Chemiestudium noch die Promotion möglich gewesen.

List of Abbreviations

CAAC	cyclic alkyl-amino carbene	NBO	natural bond orbital
<i>cf.</i>	Latin (<i>confer</i>): “compare”	NHC	<i>N</i> -heterocyclic carbene
COD	1,5-cyclooctadiene	NHCP	<i>N</i> -heterocyclic carbene phosphinidene
Cp*	1,2,3,4,5-pentamethyl-cyclopentadiene	NHI	<i>N</i> -heterocyclic imine
Dipp	2,6-di <i>is</i> opropylphenyl	NHSi	<i>N</i> -heterocyclic silylene
DMAP	4- <i>N,N</i> -dimethylamino-pyridine	NMR	nuclear magnetic resonance
<i>e.g.</i>	Latin (<i>exempli gratia</i>): “for example”	OTf	triflate
Eind	1,1,3,3,5,5,7,7-octaethyl- <i>s</i> -hydrindacen-4-yl	ppm	parts per million
EMind	1,1,7,7-tetraethyl-3,3,5,5-tetramethyl- <i>s</i> -hydrindacen-4-yl	<i>PR</i>	Piers-Rubinsztajn
<i>et al.</i>	Latin (<i>et alii</i>): “and others”	<i>p</i> -cymene	1- <i>is</i> opropyl-4-methylbenzene
HMPA	hexamethylphosphoramide	RCM	ring closing metathesis
HOMO	highest occupied molecular orbital	ROMP	ring opening metathesis polymerization
<i>i.e.</i>	Latin (<i>id est</i>): “that is”	SC-XRD	single crystal X-ray diffraction
IDipp	1,3-bis(2,6-di <i>is</i> opropylphenyl)-imidazol-2-ylidene	SIDipp	saturated IDipp; 1,3-bis(2,6-di <i>is</i> opropylphenyl)-imidazol-2-ylidene
IEt ₂ Me ₂	1,3-diethyl-4,5-dimethylimidazol-2-ylidene	Tbb	2,6-(CH(TMS) ₂) ₂ -4- ^t Bu-phenyl.
I ⁱ Pr ₂ Me ₂	1,3-di <i>is</i> opropyl-4,5-dimethylimidazol-2-ylidene	THF	tetrahydrofuran
IMe ₄	1,3,4,5-tetramethylimidazol-2-ylidene	Tipp	2,4,6-tri <i>is</i> opropylphenyl
LB	Lewis base	T ^{ipp} Ter	2,6-bis(2,4,6-tri <i>is</i> opropylphenyl)phenyl
LUMO	lowest unoccupied molecular orbital	TMS	trimethylsilyl
Mes	2,4,6-trimethylphenyl; mesityl	TON	turnover number
MesTer	2,6-bis(2,4,6-trimethylphenyl)phenyl	<i>vide infra</i>	Latin: “see below”
		<i>vide supra</i>	Latin: “see above”
		<i>vs.</i>	Latin (<i>versus</i>): “against”
		WCA	weakly coordinating anion

Publication List

Publications included in this thesis:

- P. Frisch and S. Inoue
Chemical Communications **2018**, *54*, 13658–13661
Title: “Coinage metal complexes of NHC-stabilized silyliumylidene ions”
DOI: [10.1039/c8cc07754a](https://doi.org/10.1039/c8cc07754a)
- P. Frisch and S. Inoue
Dalton Transactions **2019**, *48*, 10403–10406
Title: “NHC-stabilized silyl-substituted silyliumylidene ions”
DOI: [10.1039/c9dt02010a](https://doi.org/10.1039/c9dt02010a)
- P. Frisch, T. Szilvási, A. Porzelt and S. Inoue
Inorganic Chemistry **2019**, *58*, 14931–14937
Title: “Transition Metal Carbonyl Complexes of an N-Heterocyclic Carbene Stabilized Silyliumylidene Ion”
DOI: [10.1021/acs.inorgchem.9b02772](https://doi.org/10.1021/acs.inorgchem.9b02772)
- P. Frisch, T. Szilvási and S. Inoue
Chemistry – A European Journal, **2020**, *26*, 6271–6278
Title: “Facile Access to Dative, Single and Double Silicon–Metal Bonds Through M–Cl Insertion Reactions of Base-stabilized Si(II) Cations”
DOI: [10.1002/chem.202000866](https://doi.org/10.1002/chem.202000866)

Publications beyond the scope of this thesis:

- V. Nesterov, D. Reiter, P. Bag, P. Frisch, R. Holzner, A. Porzelt and S. Inoue
Chemical Reviews **2018**, *118*, 9678–9842
Title: “NHCs in Main Group Chemistry”
DOI: [10.1021/acs.chemrev.8b00079](https://doi.org/10.1021/acs.chemrev.8b00079)
- R. Holzner, A. Kaushansky, B. Tumanskii, P. Frisch, F. Linsenmann and S. Inoue
European Journal of Inorganic Chemistry **2019**, *25*, 2977–2981
Title: “Isolation of a Relatively Air-Stable, Bulky Silyl-Substituted, Neutral Silicon-Centered Radical”
DOI: [10.1002/ejic.201900522](https://doi.org/10.1002/ejic.201900522)
- D. Reiter, R. Holzner, A. Porzelt, P. J. Altmann, P. Frisch and S. Inoue
Journal of the American Chemical Society **2019**, *141*, 13536–13546
Title: “Disilene-Silylene Interconversion: A Synthetically Accessible Acyclic Bis(silyl)silylene”
DOI: [10.1021/jacs.9b05318](https://doi.org/10.1021/jacs.9b05318)

- D. Reiter, P. Frisch, T. Szilvási and S. Inoue
Journal of the American Chemical Society **2019**, *141*, 16991–16996
Title: “*Heavier Carbonyl Olefination: The Sila-Wittig Reaction*”
DOI: [10.1021/jacs.9b09379](https://doi.org/10.1021/jacs.9b09379)
- R. Holzner, D. Reiter, P. Frisch and S. Inoue
RSC Advances **2020**, *10*, 3402–3406
Title: “*DMAP-stabilized bis(silyl)silylenes as versatile synthons for organosilicon compounds*”
DOI: [10.1039/c9ra10628f](https://doi.org/10.1039/c9ra10628f)
- P. Frisch and S. Inoue
Dalton Transactions **2020**, *49*, 6176–6182
Title: “*Lewis base-stabilized silyliumylidene ions in transition metal coordination chemistry*”
DOI: [10.1039/d0dt00659a](https://doi.org/10.1039/d0dt00659a)
- D. Reiter, P. Frisch, D. Wendel, F. Hörmann and S. Inoue
Dalton Transactions **2020**, *49*, 7060–7068
Title: “*Oxidation reactions of a versatile, two-coordinate, acyclic iminosiloxy-silylene*”
DOI: [10.1039/d0dt01522a](https://doi.org/10.1039/d0dt01522a)

Conference Contributions

- P. Frisch and S. Inoue
Poster: “*NHC-stabilized Silyliumylidene Ions and Their Coordination Chemistry*”
The 15th International Symposium on Inorganic Ring Systems (IRIS), Kyoto, Japan, June 2018.
- P. Frisch and S. Inoue
Poster: “*Coordination Chemistry of NHC-stabilized Silyliumylidene Ions*”
9th European Silicon Days (ESD), Saarbrücken, Germany, September 2018.

Abstract

The still-young research field of silyliumylidene ions – Si(II) cations with a lone pair of electrons, two vacant orbitals and a positive charge – has started to garner an increased interest from both academia and industry, with a number of reports over the last 15 years focused on their potential for single-site small molecule activation and transition metal-free catalysis.

Importantly, due to the presence of a stereochemically active lone pair of electrons on the low-valent silicon center, they can also be employed as ligands in transition metal complexes like phosphines, carbenes or silylenes. Yet, compared to these commonly used ligand classes, their application in organometallic chemistry is still in its infancy. Understanding their reactivity with transition metals and their properties as ligands is of crucial importance, as the design of new and improved catalysts requires extensive knowledge about the coordination behavior of a variety of ligands. Notably, the extremely high inherent reactivity of silyliumylidene ions requires the coordination of up to two Lewis bases for their stabilization, which significantly reduces their π -acceptor ability.

Accordingly, this thesis describes the synthesis of novel NHC-stabilized silyliumylidene ions and their application as ligands in transition metal complexes. The first part of this dissertation focuses on the synthesis and isolation of the first silyl-substituted Si(II) cations. The introduction of new substituents with different steric and electronic properties is important, as the features of the single silyliumylidene substituent can have a significant influence on their stability and reactivity. As an interesting follow-up chemistry, it was also shown that NHC-stabilized silyliumylidene ions can undergo facile NHC exchange reactions from weaker to stronger σ -donating carbenes.

The second part of the thesis focuses solely on the coordination chemistry of NHC-stabilized silyliumylidene ions. As proof of principle – that coordination chemistry is indeed a possibility – group 11 (Cu, Ag, Au) complexes were synthesized directly from aryl-substituted Si(II) cations through reaction with simple coinage metal salts. It was shown that their solid-state structures and their stability in solution depends on the steric demand of the silyliumylidene substituent: bulky groups lead to stable monomers whereas smaller groups form dimeric complexes with a significantly reduced stability.

In a follow-up publication, the ligand properties of NHC-stabilized silyliumylidene ions were investigated experimentally and theoretically with the synthesis and analysis of group 6 (Cr, Mo, W) and group 8 (Fe) transition metal carbonyl complexes and then compared to other common ligand classes. It could be shown that NHC-stabilized Si(II) cations can be classified as weak σ -donor ligands with negligible π -acceptor character.

These investigations are followed by a final publication focused on the reactivity of various silyliumylidene ions with dimeric, chloro-bridged transition metal precursors: after the initial splitting of the dimeric complexes through coordination of the low-valent silicon moiety, an insertion reaction into the metal–chloride bond takes place with concomitant NHC-migration leading to chlorosilylene complexes with long Si–M bond distances. Reductive dechlorination of these complexes with either one or two equivalents of potassium graphite leads to an increase in the silicon–metal bond order, furnishing Si–M single and Si=M double bonds, respectively.

Zusammenfassung

Das noch junge Forschungsfeld der Silyliumyliden-Ionen – Si(II) Kationen mit einem freien Elektronenpaar, zwei unbesetzten Orbitalen und einer positiven Ladung – erfreut sich einem steigenden Interesse, sowohl aus der Wissenschaft, als auch aus der Industrie. Über die letzten 15 Jahre erschien eine Reihe von Berichten die auf das Potential dieser hochreaktiven, niedervalenten Silicium-Kationen in der Aktivierung kleiner Moleküle und in der metallfreien Katalyse fokussiert waren.

Aufgrund des vorhandenen stereochemisch aktiven freien Elektronenpaares am niedervalenten Siliciumzentrum, vergleichbar mit Phosphinen, Carbenen oder Silylenen, können Silyliumyliden-Ionen auch als Liganden in Übergangsmetallkomplexen eingesetzt werden. Im Vergleich zu diesen häufig verwendeten Ligandenklassen steht ihre Anwendung in der metallorganischen Chemie jedoch noch am Anfang. Das Verständnis ihrer Reaktivität mit Übergangsmetallen und ihrer Eigenschaften als Liganden ist von entscheidender Bedeutung, da das Design neuer und verbesserter Katalysatoren umfangreiche Kenntnisse über das Koordinationsverhalten einer Vielzahl an Liganden erfordert. Bedingt durch die hohe Reaktivität und Instabilität der Silyliumyliden-Ionen ist die Koordination von bis zu zwei Lewis-Basen an das Silicium-Zentrum für eine erfolgreiche Synthese nötig. Diese notwendige Stabilisierung verringert jedoch deren π -Akzeptoreigenschaften erheblich.

Dementsprechend beschreibt diese Arbeit die Synthese von neuartigen NHC-stabilisierten Silyliumyliden-Ionen und deren Anwendung als Liganden in Übergangsmetallkomplexen. Der erste Teil dieser Dissertation konzentriert sich auf die Synthese der ersten silyl-substituierten Si(II)-Kationen. Die Einführung von Substituenten mit unterschiedlichen sterischen und elektronischen Eigenschaften ist von Bedeutung, da die Charakteristiken des einzigen Silyliumyliden-Substituenten einen wesentlich Einfluss auf deren Reaktivität und Stabilität haben können. Als interessante Folgechemie konnte außerdem gezeigt werden, dass ein einfacher Austausch der koordinierten NHCs von schwächeren zu stärkeren Carbenen möglich ist.

Der zweite Teil dieser Arbeit konzentriert sich ausschließlich auf die Koordinationschemie von NHC-stabilisierten Silyliumyliden-Ionen. Als „Proof of Principle“ – dass Koordinationschemie tatsächlich möglich ist – wurden Gruppe 11

Komplexe (Cu, Ag, Au) direkt aus der Reaktion von aryl-substituierten Si(II)-Kationen mit Münzmetallsalzen synthetisiert. Es konnte gezeigt werden, dass ihre Struktur im Festkörper und ihre Stabilität in Lösung direkt vom sterischen Anspruch des Silyliumyliden-Substituenten abhängt: große Gruppen führen zu stabilen Monomeren, während kleinere Reste deutlich instabilere dimere Komplexe bilden.

In einer weiteren Publikation wurden die Ligandeneigenschaften von NHC-stabilisierten Silyliumyliden-Ionen sowohl experimentell als auch theoretisch durch die Synthese von Gruppe 6 (Cr, Mo, W) und Gruppe 8 (Fe) Metallcarbonylkomplexen untersucht und anschließend mit gängigen Ligandenklassen verglichen. Es konnte gezeigt werden, dass diese Art von Silyliumyliden-Ionen am besten als schwache σ -Donorliganden mit vernachlässigbarem π -Akzeptorcharakter beschrieben werden.

Auf diese Untersuchungen folgt eine abschließende Publikation bezüglich der Reaktivität verschiedener Silyliumyliden-Ionen mit dimeren, chloro-verbrückten Übergangsmetallkomplexen: Nach einer Spaltung des Dimers induziert durch die Koordination des niedervalenten Siliciumzentrums an das Metall findet eine Insertionsreaktion in die Metall–Chlor Bindung mit gleichzeitiger NHC-Wanderung statt, die zu Chlorosilylen-Metallkomplexen mit langen Si–M Bindungslängen führt. Eine reduktive Dechlorierung dieser Komplexe mit einem oder zwei Äquivalenten Kaliumgraphit führt zu Si–M Einfachbindungen bzw. Si=M Doppelbindungen mit jeweils signifikant verkürzten Bindungslängen.

Table of Contents

Acknowledgments	I
List of Abbreviations	III
Publication List	IV
Conference Contributions	V
Abstract	VI
Zusammenfassung	VIII
1. Introduction	1
2. Low-coordinate Silicon Compounds	3
2.1 Silylium Ions	3
2.2 Silylenes	6
2.2.1 <i>Milestones in Silylene Chemistry: Isolation and Reactivity</i>	7
2.2.2 <i>Silylenes as Ligands: A Superior Alternative to Carbenes?</i>	11
2.3 Silyliumylidene Ions	13
2.3.1 <i>Isolable Silyliumylidene Ions – an Overview</i>	16
2.3.2 <i>Donor-stabilized Silyliumylidene Ions (excluding NHCs)</i>	17
2.3.3 <i>NHC-stabilized Silyliumylidene Ions</i>	19
2.3.4 <i>Reactivity of Silyliumylidene Ions</i>	23
3. Scope of this Work	34
4. NHC-stabilized Silyl-substituted Silyliumylidene Ions	37
5. Coinage Metal Complexes of NHC-stabilized Silyliumylidene Ions	42
6. Transition Metal Carbonyl Complexes of an NHC-stabilized Silyliumylidene Ion	48
7. Facile Access to Dative, Single and Double Silicon–Metal Bonds Through M–Cl Insertion Reactions of Base-stabilized Si(II) Cations	56
8. Summary and Outlook	66
8.1 Novel NHC-stabilized Silyliumylidene Ions	66
8.2 Coordination Chemistry of NHC-stabilized Silyliumylidene Ions	68

8.2.1	<i>Coinage Metal Complexes – Monomeric vs. Dimeric Structures</i>	68
8.2.2	<i>Transition Metal Carbonyl Complexes and Ligand Properties</i>	69
8.2.3	<i>Insertion into M–Cl Bonds and Access to Si–M Multiple Bonds</i>	71
8.3	Outlook.....	73
9.	Zusammenfassung und Ausblick	75
9.1	Neuartige NHC-stabilisierte Silyliumyliden-Ionen	75
9.2	Koordinationschemie von NHC-stabilisierten Silyliumylidenen.....	77
9.2.1	<i>Münzmetallkomplexe – Monomere vs. Dimere Komplexe</i>	78
9.2.2	<i>Übergangsmetallcarbonylkomplexe und Ligandeneigenschaften</i>	79
9.2.3	<i>Insertion in M–Cl Bindungen und Zugang zu Si–M Mehrfachbindungen</i>	80
9.3	Ausblick.....	83
10.	Bibliography	85
11.	Appendix	97
11.1	Supporting Information Chapter 4	97
11.2	Supporting Information Chapter 5	123
11.3	Supporting Information Chapter 6	151
11.4	Supporting Information Chapter 7	201
11.5	Licenses for Copyrighted Content.....	313
11.5.1	<i>License for Chapter 4 and 5</i>	313
11.5.2	<i>License for Chapter 6</i>	314
11.5.3	<i>License for Chapter 7</i>	315

1. Introduction

The concept of catalysis lies at the heart of the modern chemical industry as it closely combines important economic and ecological principals. Without a doubt, it is the most important cornerstone regarding environmental protection, which will only become increasingly important in the coming decades: through catalysis, it becomes possible to reduce waste and emissions and also use finite resources and energy much more efficiently.¹

Since the original introduction of the concept by Berzelius almost 200 years ago², hetero- and homogeneous catalyst systems have been systematically investigated and developed and they are nowadays involved in the production of more than 85% of all manufactured goods.³⁻⁴ Hence, the importance of the large number of industrial scale catalytic processes for our society can hardly be overstated.⁵

The high activity and robustness of the many different heterogeneous catalyst systems – which make up the large majority (>80%) of the catalysts used in the chemical industry⁴ – is responsible for the millions of tons of fuels, fabrics, fertilizers and pharmaceuticals produced each year.⁵ On the other hand, the milder reaction conditions (e.g. lower temperature and pressure) possible for homogeneous systems and their impressive stereo- and chemoselectivity allows for an unprecedented control over the outcome of a reaction. This makes them especially attractive for laboratory scale preparations and fundamentally useful in the complex syntheses of pharmaceuticals and fine chemicals.⁶

Further development and improvement of these systems is of paramount importance for the future. However, almost all industrially relevant processes rely on the catalytic properties of transition metals, which bring the inherent downside of generally being rare, expensive, toxic and harmful to the environment. Therefore, over the past decades, the need for green and sustainable technologies and processes has been equally important.

A concept that has been gaining more and more attention in recent years is the utilization of (low-valent) main group compounds as an alternative to transition metals.⁷⁻⁹ Due to their high abundance – for example, silicon and aluminum being the 2nd and 3rd most abundant elements in the earth's crust¹⁰ – they are significantly less costly and often non-toxic. However, this rather young research field is still in its infancy

and until sustainable, transition metal-free alternatives are developed and adjusted to industrial scale chemical processes, the preparation of new and improved transition metal catalysts is also of significant interest. One of the easiest ways to change the behavior of a catalyst (*i.e.* activity, selectivity and stability) is to change the ligation of the transition metal. In this context, given the close relationship of silicon and carbon in the periodic table, silylene ligands are highly promising alternatives to the commonly used carbenes (*cf.* chapter 2.2.2), which is why they are starting to gather more and more attention in recent years.¹¹⁻¹⁴

The directly associated class of silyliumylidene ions, also known as Si(II) cations, is a new research field, that can also be of interest for the development of novel, intriguing catalyst systems. However, fundamental work in regard to their coordination chemistry with transition metals and their properties as ligands is necessary first, as a deep understanding of ligand properties and their influence on transition metals is vital to designing better catalytic systems.

2. Low-coordinate Silicon Compounds

The chemistry of low-coordinate and/or low-valent silicon compounds can be fundamentally different to that of related carbon compounds. These often incredibly reactive species have attracted much attention over the past several decades because of their interesting properties, reactivities and potential applications. Reported compounds include silylium ions $[\text{R}_3\text{Si}]^+$, silyl radicals $[\text{R}_3\text{Si}\cdot]$, disilenes $[\text{R}_2\text{Si}=\text{SiR}_2]$, disilynes $[\text{RSi}\equiv\text{SiR}]$, silylenes $[\text{R}_2\text{Si}:]$, silenes $[\text{R}_2\text{Si}=\text{CR}_2]$, silanones $[\text{R}_2\text{Si}=\text{O}]$, silyliumylidene ions $[\text{R}-\text{Si}:]^+$, silylones $[:\text{Si}:]$ and more, including a wealth of reported reactivities like the activation of small molecules and applications like transition metal-free catalysis.⁷⁻⁸ In this chapter, the chemistry of silylium ions $[\text{R}_3\text{Si}]^+$ and silylenes $[\text{R}_2\text{Si}:]$ will be briefly discussed and a particular emphasis will be placed on the development of the field of silyliumylidene ions $[\text{R}-\text{Si}:]^+$. Their syntheses, properties and reactivities will be discussed in detail.

2.1 Silylium Ions

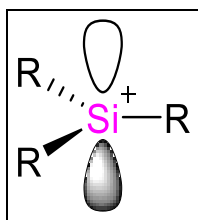


Figure 1 Schematic representation of the cationic part of a silylium ion $[\text{R}_3\text{Si}]^+$.

Silylium ions $[\text{R}_3\text{Si}]^+$ (Figure 1) are the direct heavier analogues of carbenium ions $[\text{R}_3\text{C}]^+$.¹⁵⁻¹⁶ As a three-coordinate silicon species with six valence electrons, a positive charge and a vacant p-orbital at the central Si(IV) atom, they are extraordinarily strong Lewis acids.

In principle, it should be easier to isolate silylium ions compared to carbenium ions, as silicon is larger, more electropositive and shows higher polarizability than carbon.¹⁷ While that is indeed the case in the gas phase, this does unfortunately not apply in the condensed phase due to the high electrophilicity of $[\text{R}_3\text{Si}]^+$. As a consequence, silicon cations strongly interact with most σ - and π -electron donors (e.g. nucleophiles, solvents and even arenes). In fact, it took a deliberate effort of over 100 years¹⁸ after the isolation of the first carbocation $[(\text{C}_6\text{H}_5)_3\text{C}]^+$ to isolate the first three-coordinate, solvent-free silylium ion $[(\text{Mes})_3\text{Si}]^+$ (**L-1**, Figure 2).¹⁹⁻²⁰

Consequently, it seems readily apparent that the approaches useful for the synthesis of carbenium ions are generally not suitable for the synthesis of the heavier analogues.¹⁶ Their successful isolation necessitates kinetic stabilization through bulky substituents and thermodynamic stabilization by electron-donating substituents, which reduce the electrophilicity of the silicon center. Furthermore, they also require non-nucleophilic non-coordinating reaction conditions (*i.e.* solvents and anions). Frequently employed weakly coordinating anions (WCAs) are (per)fluorinated borate anions²¹ or carboranate anions.²²

Silylium ions are most commonly prepared from four-coordinate neutral silanes through electrophilic abstraction of one substituent, for example, abstraction of a hydride substituent (*i.e.* cleavage of a Si–H bond) with a tritylium salt, the protonation of Si–H bonds with Brookhart's acid ($[\text{H}(\text{OEt}_2)_2][\text{B}(\text{Ar}^{\text{F}})_4]$, forming H_2) or the abstraction of alkyl groups with strong acids. Another approach to silylium ions is the abstraction of allylic substituents with an electrophile, which also allows for the synthesis of silylium ions with very bulky substituents.²²⁻²³ A number of free (although rare) as well as donor-stabilized silylium ions (both inter- and intramolecularly stabilized) have been reported over the last decades (see Figure 2 for examples).^{16,20,23} Very recently, Oestreich *et al.* even reported a series of isolable hydrogen-substituted carboranate-stabilized silylium ions, including a derivative of the parent silylium ion $[\text{H}_3\text{Si}]^+$ through a protonolysis strategy with a carborane acid.²²

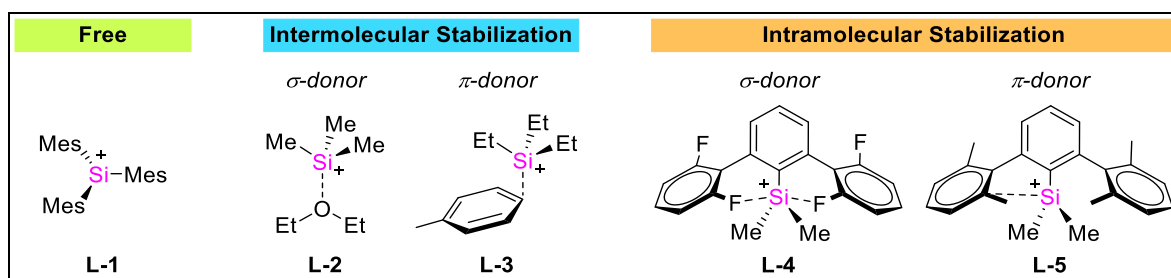
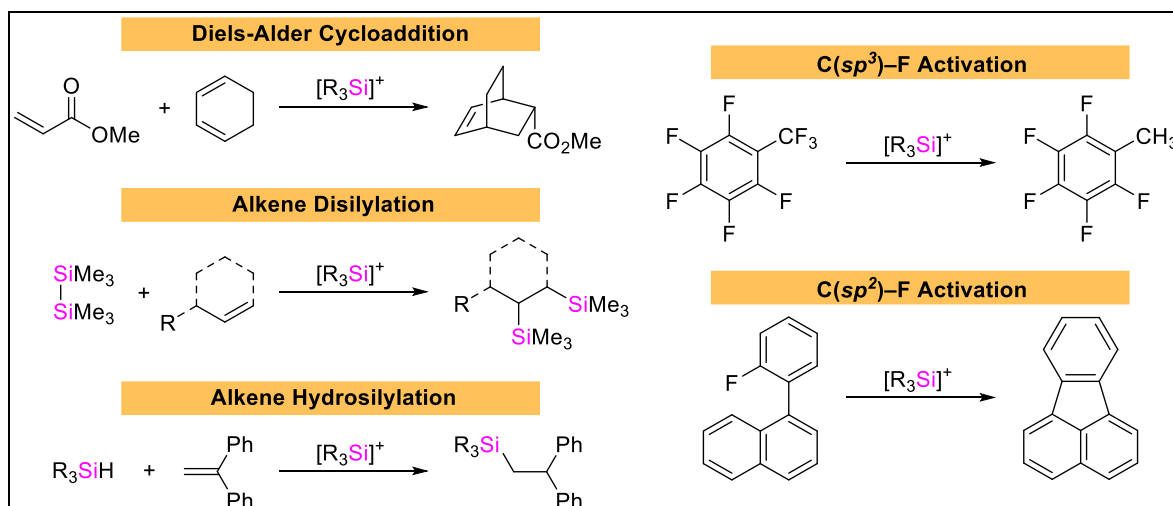


Figure 2 Examples for free silylium ions and through σ - and π -donors inter- and intramolecularly stabilized silylium ions (anions omitted).²³

Free silylium ions generally exhibit a characteristic ^{29}Si NMR resonance at very low field (>200 ppm).²³ For example, $[(\text{Mes})_3\text{Si}]^+$ (**L-1**) shows a resonance at 225.5 ppm.¹⁹ Upon interaction with donors such as anions or solvent molecules, a significant upfield shift can be observed. In the case of **L-1**, no coordination with benzene, toluene or *p*-xylene takes place, however, upon addition of MeCN or Et_3N , the expected shift to a higher field (37.0 and 47.1 ppm, respectively) occurs.

The increasing availability of isolable silylium ions has led to a growing interest regarding their reactivity as catalysts or reagents in synthetic organic chemistry (Scheme 1).^{20,23} Silicon-based Lewis acids can be efficient catalysts for cycloaddition reactions, for example, the toluene-stabilized silylium ion **L-3** catalyzes the Diels-Alder cycloaddition of methylacrylate and 1,3-cyclohexadiene even at low temperatures.²⁴ Further applications of silylium ions include the hydro-defluorination of C(sp³)-F bonds²⁵⁻²⁶, hydrosilylation of C=X bonds²⁷⁻²⁹ or carbonyl-deoxygenation.³⁰ Even the challenging cleavage of C(sp²)-F bonds has been reported.³¹⁻³² An application unique to this class of compounds is the silylium ion-catalyzed bis(silylation) of alkenes, where currently no alternative transition metal catalyst is known.³³ Furthermore, a modern field of research is the introduction of chiral substituents on silylium ions for the development of new and improved protocols in asymmetric catalysis.³⁴



Scheme 1 Selected examples for applications of silylium ions (adapted from ²³).

The use of stoichiometric amounts of silylium ions can also be useful, for example in the Friedel-Crafts C-H silylation of aromatic compounds, which is generally more difficult to achieve than the corresponding Friedel-Crafts alkylation. This is due to the competing reverse reaction (proto-desilylation), which is significantly more facile in the case of silylium ions and necessitates the removal of the protons from the reaction mixture with proton scavengers (*e.g.* bases).

With reliable methods for their synthesis and isolation becoming more and more available, silylium ions have continuously found an increasing number of applications in organic synthesis and catalysis. In the future, their incredibly high electrophilicity – which once prevented their isolation altogether – is sure to provide new and interesting reactivities and open up new catalytic pathways.

2.2 Silylenes

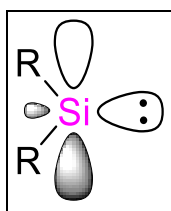


Figure 3 Schematic representation of a silylene [$R_2Si:$].

As the direct heavier congeners of carbenes, silylenes [$R_2Si:$] (Figure 3) are two-coordinate neutral Si(II) compounds with six valence electrons (two of them as the lone pair of electrons) and a vacant p-orbital on the low-valent silicon center.¹⁶

Despite their close relationship in the periodic table, the properties of carbenes and the heavier tetrylenes can differ significantly (Figure 4): for example, while the parent carbene [$H_2C:$] exhibits a triplet ground state (negative singlet-triplet gap ΔE_{S-T}), [$H_2E:$] ($E = Si, Ge, Sn, Pb$) prefer the singlet ground state due to an increasing singlet-triplet gap for the heavier tetrylenes.¹⁶ This singlet ground state of silylenes is responsible for the presence of the vacant orbital on the silicon center (high Lewis acidity) as well as a lone pair of electrons (Lewis basicity), leading directly to their Lewis ambiphilicity. Additionally, as hybridization becomes more and more difficult for the heavier elements (due to an increasing separation of the s and p-orbitals with an increasing nuclear charge), the lone pair of electrons of the heavier tetrylenes exhibits an increased s-character compared to the more pronounced p-character of the carbene lone pair. As a direct consequence of this “inert s-pair effect”³⁵, the stability of the +II oxidation state also increases significantly with an increase of the principal quantum number.³⁶⁻³⁷

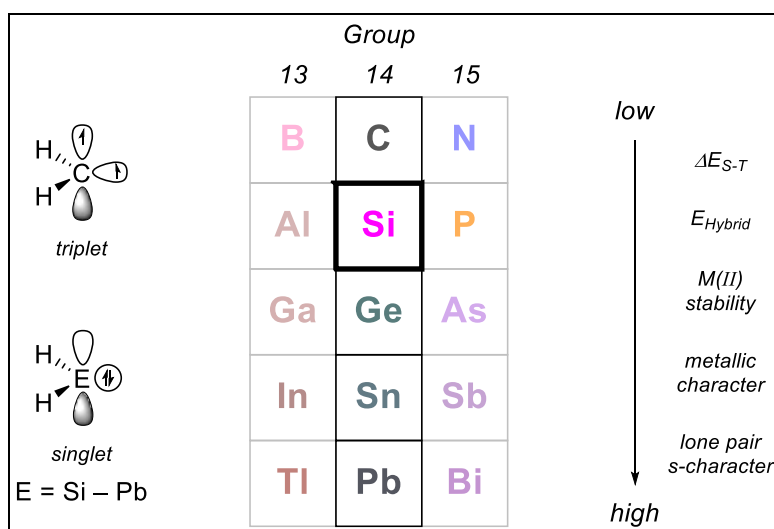


Figure 4 Schematic representation of triplet carbenes and heavier singlet tetrylenes and general trends of the most important electronic properties of group 14 elements (adapted from³⁸).

While silylenes were initially considered as elusive species and highly reactive intermediates, nowadays they represent arguably one of the most important research aspects of modern (low-valent) main group chemistry with their versatile reactivity (e.g. due to their Lewis ambiphilicity) and numerous promising applications. They are regularly shown to be indispensable building blocks for organosilicon chemistry and their incredible potential in the metal-free activation of small molecules (and, by extension, in metal-free catalysis) is currently under heavy investigation – as are transition metal silylene complexes for the development of improved and novel transition metal-catalyzed conversions.

To stabilize these species and allow them to be studied and utilized under ambient conditions, introduction of appropriate substituents is necessary. Similar to the concepts used for the isolation of silylium ions, either thermodynamic or kinetic stabilization (or a combination of both) is required.¹⁶ Over the past three decades, a large variety of bulky substituents with easily adjustable steric demand and strongly electron-donating systems have been developed, which has greatly increased the number of viable systems for the stabilization of highly reactive low-valent main group compounds. Furthermore, as silylenes can be highly electrophilic due to the presence of the empty p-orbital, additional stabilization can be achieved through inter- or intramolecular coordination of a Lewis base to the silicon center. This significantly reduces its electrophilicity, but also weakens the inherently high reactivity of the free silylenes at the same time.

2.2.1 Milestones in Silylene Chemistry: Isolation and Reactivity

Historically, silylenes have been postulated as transient intermediates and extensively studied *via* low-temperature matrix isolation studies, various trapping reactions and theoretical investigations.³⁹

The concepts of thermodynamic and kinetic stabilization as well as stabilization through Lewis bases have been successfully employed for the isolation of a plethora of silylenes. While most of the reported examples are three-coordinate compounds with external donor molecules^{36,40-41} such as NHCs⁴², even a handful of acyclic, two-coordinate examples have been reported and studied extensively. The most important milestones in this field are briefly summed up below.

(i) Isolation of Silylenes

The first major breakthrough in regards to isolable, room temperature stable Si(II) compounds was achieved by Jutzi and co-workers in 1986, with the isolation of decamethylsilicocene $[\text{Cp}^*_2\text{Si}]^{43}$ (**L-6**) (Figure 5). However, due to the hyper-coordinate nature (η^{10}) of the silicon center in **L-6**, it cannot be considered a true two-coordinate silylene. Nevertheless, because of the η^5 - η^3 - η^1 rearrangement processes⁴⁴ easily possible for the Cp* group, **L-6** still shows the reactivity expected for a nucleophilic silylene.⁴⁵ This discovery was soon followed by the isolation of **L-7**, an actual two-coordinate silylene and the first representative of the now well investigated class of *N*-heterocyclic silylenes (NHSis) – the heavier analogues of the well-known and widely utilized NHCs – by Denk and co-workers in 1994.⁴⁶

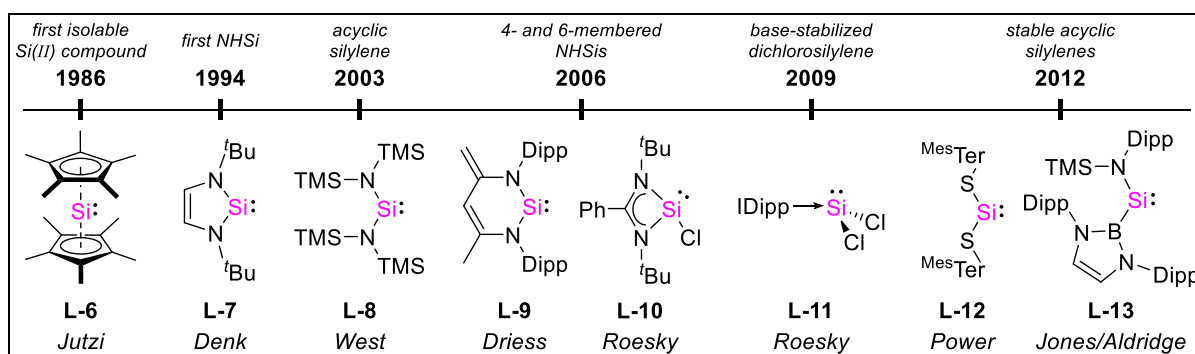


Figure 5 Selection of important milestones in the synthesis of silylene compounds.

Just like in NHCs, the cyclic framework and the π -donating *N*-substituents can effectively stabilize the low-valent silicon center. Since then, a wealth of new cyclic silylenes have been synthesized, including a bis(alkyl)-substituted example⁴⁷ and the 6- and 4-membered NHSis **L-9**⁴⁸ and **L-10**.⁴⁹ Importantly, the amidinate-stabilized three-coordinate silylene **L-10** is also the first example of a compound with a Si(II)–Cl bond that is stable at room temperature. Thanks to the easy functionalizability of the chloride substituent, numerous derivatives of this silylene with a variety of substituents have been reported since the initial synthesis of **L-10**.⁵⁰⁻⁵¹

With the isolation of the NHC-stabilized dichlorosilylene **L-11** in 2009 through the reductive elimination of HCl from HSiCl_3 *via* NHCs (or reduction of $\text{NHC} \rightarrow \text{SiCl}_4$ with KC_8), the chemistry of low-valent silicon finally caught up with that of the heavier group 14 elements germanium, tin and lead, where comparable precursors were already known and readily available.⁵² The availability of an easily accessible Si(II) precursor for salt metathesis reactions paved the way for an abundance of novel low-valent silicon compounds.⁵³ It is worth mentioning, that the NHC-stabilized dibromo- and

diiido-silylene analogues have since also been prepared through reduction of the corresponding SiBr_4 and SiI_4 NHC adducts.⁵⁴⁻⁵⁵

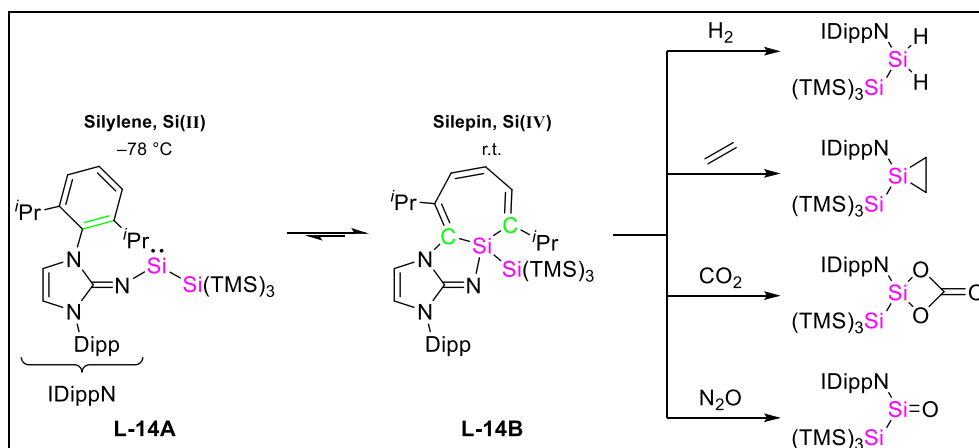
The acyclic silylene **L-8** was synthesized in 2003 through the reductive debromination of the corresponding dibromosilane precursor.⁵⁶ However, the compound is unstable under ambient conditions (as opposed to the germanium and tin analogues⁵⁷⁻⁵⁸) and decomposes quickly at temperatures higher than $-20\text{ }^\circ\text{C}$. The breakthrough in the chemistry of stable, acyclic, two-coordinate silylenes came only very recently: in 2012, the groups of Power and Jones/Aldridge independently, at the same time, reported the isolation of silylenes **L-12**⁵⁹ and **L-13**⁶⁰, respectively. Over the past few years, this compound class has been extended with a handful of other examples.³⁸ However, some representatives, e.g. the highly reactive bis(silyl)silylenes, still remain elusive with no room temperature stable examples reported so far.⁶¹

(ii) Activation of Small Molecules

Recent years have started to reveal the true possibilities of silylenes (especially that of acyclic, two-coordinate systems) in terms of reactivity, not just as synthons for organosilicon compounds^{50,62-63} and ligands in transition metal complexes^{12-14,39}, but also as transition metal mimics in the activation of small molecules, with the potential to become genuine environmentally friendly alternatives to transition metal complexes in catalysis. The single-site activation of enthalpically strong molecules such as H_2 used to be a domain that was essentially entirely dominated by transition metal complexes, but since 2012, several silylenes have been reported that easily cleave the H–H bond (even under very mild conditions), most notably silylene **L-13**⁶⁰, silepin **L-14B**⁶⁴ (as a masked variant of the acyclic silylene **L-14A**) (Scheme 2) and a masked bis(silyl)silylene.⁶¹ Furthermore, silylenes are also capable of facilely activating other challenging small molecules such as CO_2 ⁶⁵, CO ⁶⁶⁻⁶⁷, N_2O ⁶⁵, ethylene⁶⁸, white phosphorus (P_4)⁶⁹ and NH_3 .^{38,65,70-71} Even the reversible, temperature dependent insertion into a C=C double bond has been reported with the NHI-substituted silylene **L-14A**. Interestingly, at room temperature, **L-14B** also easily undergoes oxidative additions with CO_2 , N_2O and ethylene (Scheme 2).⁶⁴⁻⁶⁵

While a full catalytic cycle (*i.e.* involving oxidative addition and product formation followed by reductive elimination) with a silylene has not been found yet, the reported

reactivities are a promising starting point for further investigations regarding true catalytic applications of silylenes.



Scheme 2 Temperature dependent, reversible insertion into a C=C double bond of a silylene and examples for silylene-based small molecule activation reactions with a masked silylene.

(iii) Coordination Chemistry with Transition Metals

In terms of transition metal complex chemistry, the close relationship of silicon with carbon and the isolation of the first carbene complexes by Fischer and Schrock inspired the early attempts in the coordination chemistry of silylenes.⁷² While silylene complexes have also been postulated as intermediates in transition metal-catalyzed organosilicon reactions⁷³⁻⁷⁴, the chemistry of isolable representatives started out with the synthesis of complexes with silylene moieties that would often not be stable under ambient conditions and therefore require the metal fragment for stabilization (e.g. **L-15**⁷⁵ and **L-16**⁷⁶, Figure 6). Early synthetic methodology involved abstraction of anionic groups (e.g. triflate, hydride) from silyl-substituted complexes, α -hydrogen migration or the generation of a transient silylene and subsequent trapping as a metal complex.⁷² Soon after, complexes were also synthesized directly from stable silylenes (e.g. **L-17-L-19**)⁷⁷⁻⁷⁹ and a variety of complexes have been reported since.³⁹

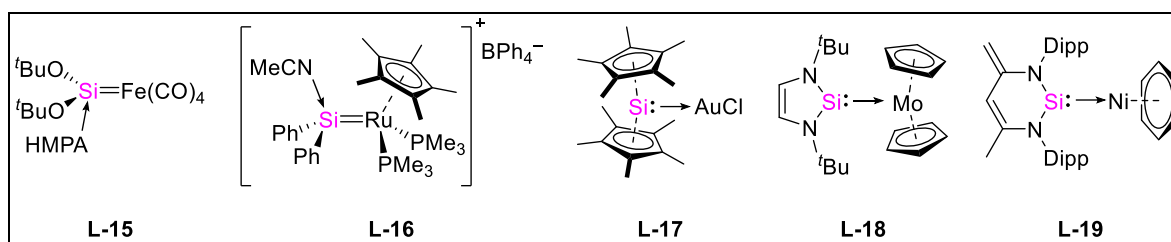


Figure 6 Examples for early silylene transition metal complexes (**L-15** and **L-16**) and complexes of stable silylenes (**L-17-L-19**).

Unfortunately, this area of silylene chemistry has been largely overshadowed by the success of carbene transition metal complexes. However, with the incredible developments in the field of isolable silylenes, their coordination chemistry has also seen advances.³⁹ In recent years, it has been shown that silylenes can be potent ligands for a variety of transformations and that they might have the potential to supersede carbene ligands in the near future.¹¹⁻¹⁴

2.2.2 Silylenes as Ligands: A Superior Alternative to Carbenes?

One of the most important cornerstones of modern carbene chemistry are the class of *N*-heterocyclic carbenes (NHCs) and their ability to function as incredibly diverse ligands in transition metal chemistry. This versatility and the ability to stabilize highly reactive and otherwise elusive species has also found widespread success in main group chemistry as of late.⁴² Over the past decades, an absolutely staggering amount of NHC transition metal complexes has been isolated and a plethora of catalytic applications of these complexes have been reported.⁸⁰⁻⁸³ Similarly, Fischer and Schrock carbene complexes have shown to be impressive catalysts for a range of organic reactions.⁸⁴⁻⁸⁵ Most notably, they are efficient and versatile catalysts for a variety of olefin metathesis reactions (e.g. ring opening metathesis polymerization (ROMP) and ring closing metathesis (RCM)) and their incredible impact was recognized with the Nobel prize in chemistry in 2005.⁸⁶

Considering that modification of the ligation of the transition metal is one of the easiest ways to change catalytic behavior, combined with the ever-growing number of isolable free silylenes – which facilitates the synthesis of novel silylene transition metal complexes – and a wealth of isolated silylene complexes^{39,72,87}, an interesting question arises: *can silylenes as ligands compete with or even surpass carbenes in terms of complex stability, catalytic ability and versatility?*

A recent theoretical investigation sought to provide an answer to this question by comparing the most important ligand properties (*i.e.* σ -donor and π -acceptor ability, steric factors (e.g. buried volume⁸⁸) and ligand-to-metal charge transfer) of model phosphines (PPh₃ and PCy₃) and NHCs (IDipp) with a large selection of synthetically available low-valent silicon compounds (for proton affinity as an indicator for σ -donor ability as a comparative example, see Figure 7).⁸⁹

The authors concluded that some reported silylenes can indeed compete and sometimes even outperform carbenes regarding all important favorable ligand features. For example, donor-stabilized silylenes can offer incredibly strong σ -donating effects – combined with a small buried volume, these ligands can promote the oxidative addition step of the catalytic cycle. Conversely, strongly π -accepting low-valent silicon ligands with a large buried volume can speed up the reductive elimination step.⁸⁹

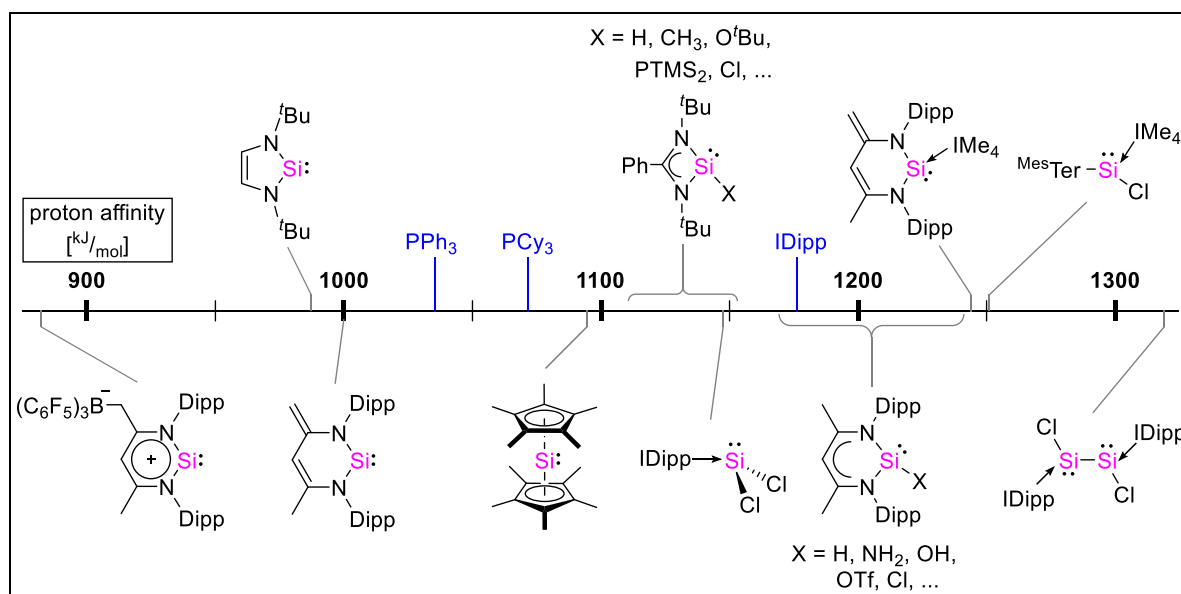


Figure 7 Calculated proton affinity (in kJ/mol) as a quantification of σ -donor ability for selected silylene examples; PPh_3 , PCy_3 and IDipp are added for comparison (adapted from ⁸⁹).

Unfortunately, even though the number of isolable silylene complexes continues to grow, investigations into their catalytic potential are still lacking, especially compared to those of carbene complexes. Hence, direct real-world comparisons of carbenes and silylenes are difficult, as analogue complexes of carbenes and silylenes are scarce and comparable catalytic investigations even more so. But from the handful of reported catalytic applications, it is evident that silylene ligands in transition metal-catalyzed transformations have a large untapped potential. At the same time, this so far limited number of applications makes it also obvious that silylene complexes do not appear to generate the same interest and uptake that NHC complexes have enjoyed over the last several decades.

Nevertheless, several recent reports undoubtedly suggest that the use of silylenes as ligands in transition metal-catalyzed organic transformations can offer advantages compared to carbenes or phosphines.^{11-14,90} While the direct relationship of NHSis with NHCs makes them prime candidates for improving existing conversions, these publications also show that not only improved catalytic performance is a possibility.

Specifically designed silylene ligands can play an essential role in the catalytic cycle by enabling new reactions through cooperative effects.⁹⁰⁻⁹¹ For example, Driess *et al.* reported the hydrosilylation of ketones catalyzed by a hydridosilylene iron complex where the NHSi ligand plays a key role, as the first step of the proposed catalytic cycle includes a silicon-iron hydride transfer.⁹¹ In the upcoming years, comprehensive studies on the feasibility of silylenes as ligands and reports on novel or improved catalytic applications are expected.

2.3 Silyliumylidene Ions

This chapter is intended as a comprehensive summary of the chemistry of silyliumylidene ions, including reported compounds and their reactivity.

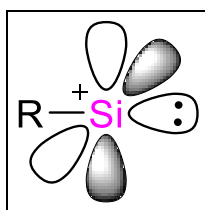


Figure 8 Schematic representation of a silyliumylidene ion $[R-Si:]^+$.

Silyliumylidene ions $[R-Si:]^+$ (Figure 8) are one-coordinate Si(II) cations, with four valence electrons (two of them as the stereochemically active lone pair of electrons), two vacant degenerate p-orbitals and a positive charge located at the central silicon atom.¹⁸ Due to this unique electronic structure, they can be considered related to silylium ions (empty p-orbital and cationic charge) as well as silylenes (empty p-orbital and lone pair of electrons) (Figure 9).

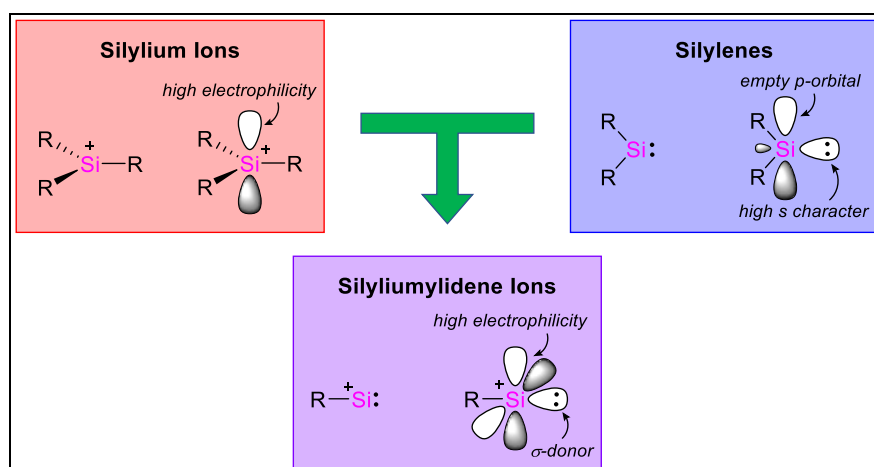
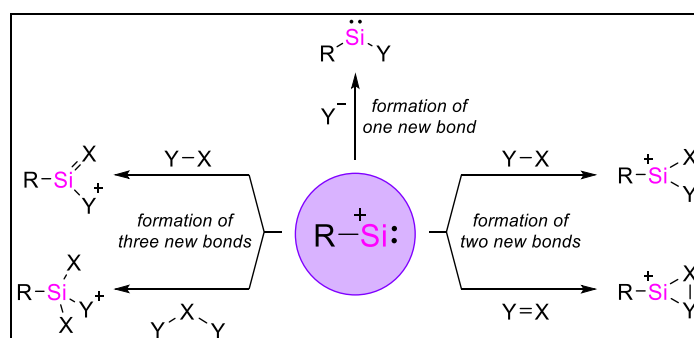


Figure 9 Formal combination of properties of silylenes (empty p-orbital, lone pair of electrons, Lewis ambiphilicity) and silylium ions (empty p-orbital, cationic charge, high electrophilicity) to silyliumylidene ions.

With that, they of course also combine the Lewis ambiphilic nature of silylenes and the high electrophilicity of silylium ions, which further means Si(II) cations can be highly useful in a wide range of synthetic and catalytic applications. Gaspar even theorized, that this exceptional combination of properties could result in an incredible synthetic potential of silyliumylidene ions (which he initially dubbed “supersilylenes”) in organosilicon chemistry, theoretically allowing the simultaneous formation of up to three new bonds in a single reaction (Scheme 3).⁹² Unfortunately, because of that, the challenges that make the isolation of silylium ions and silylenes so difficult are also combined in the case of Si(II) cations.



Scheme 3 Schematic representation of the synthetic potential of silyliumylidene ions.⁹²⁻⁹³

The smallest possible representative of the silyliumylidene class, which is also the smallest possible polyatomic silicon moiety, $[\text{H-Si}]^+$, can only be observed experimentally under mass spectrometric conditions in the gas phase as a short-lived intermediate⁹⁴ as well as spectroscopically in astrochemical processes.⁹⁵⁻⁹⁶

In the condensed phase, no one-coordinate silyliumylidene ions have been isolated. This is quite easily understandable, as the single substituent of a Si(II) cation simply cannot provide the steric and electronic protection necessary to stabilize such reactive species. Therefore, the isolation of silyliumylidene ions in the condensed phase requires the same concepts presented for silylenes and silylium ions (*vide supra*): kinetic stabilization of the extremely electron deficient silicon center with a sterically demanding and protecting substituent is necessary, as is the thermodynamic stabilization provided by coordination of one or two Lewis bases (LB, Figure 10). While the isolation of silyliumylidene ions initially required the use of WCAs and non-nucleophilic solvents, the use of relatively bulky substituents and NHCs as stabilizing Lewis bases also opened the door for simple halides as counter anions and the use of lower-priced solvents such as acetonitrile. Unfortunately, the bulky substituents and coordinated Lewis bases that are needed to tame the extreme inherent reactivity and

electrophilic nature of the $[R-Si]^+$ moiety also influence and somewhat weaken its reactivity. For example, coordination of two Lewis bases to the silicon center – which is the most common method utilized for the stabilization of silyliumylidene ions (*vide infra*) – occupy both empty p-orbitals and thereby significantly reduce the π -acceptor ability of the silyliumylidene ion.

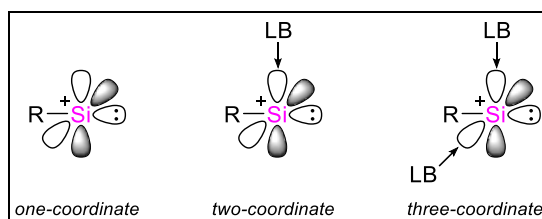


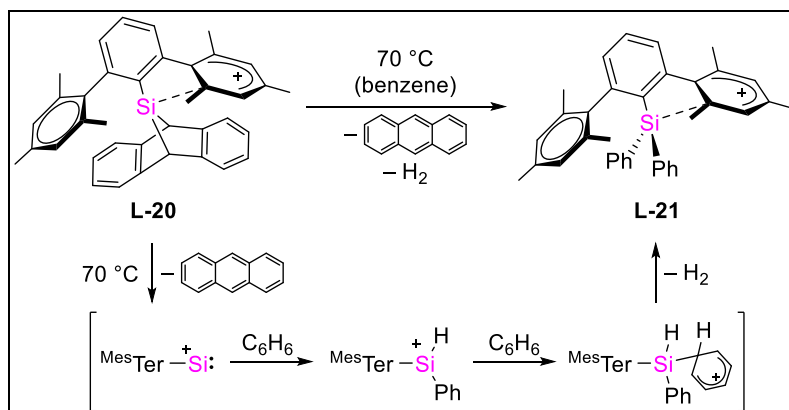
Figure 10 Schematic representation of one-, two- and three-coordinate silyliumylidene ions.⁹⁷

These three-coordinate silyliumylidene ions generally exhibit a pyramidal structure. Comparable to silyl radicals⁹⁸⁻¹⁰⁰, electropositive substituents lead to an increase of the sum of the bond angles around the central silicon atom (*i.e.* a reduced pyramidalization, which corresponds to a reduced s-character of the silicon-centered lone pair), whereas electronegative substituents lead to an increased pyramidalization and with that an increased s-character.¹⁰¹⁻¹⁰²

The group of Müller computationally investigated the electronic properties of a series of one-coordinate silyliumylidene ions as well as the principal reactivity of silyliumylidene ions (*e.g.* σ -bond insertion and π -bond addition reactions).¹⁰³ The calculations revealed a singlet ground state and the presence of a sp-type HOMO (*i.e.* the lone pair) and two low-lying degenerate p-type LUMOs (*i.e.* the empty p-orbitals). The singlet-triplet gaps (up to 450 kJ/mol) are predicted to be substantially higher than those of the related silylenes. Electronegative and/or π -donating substituents (*e.g.* NH_2 , OH , F) increase both the stability of the Si(II) cation as well as the singlet-triplet gap significantly due to the destabilization of the LUMO through the conjugation between the lone pair and the heteroatom. Conversely, electropositive substituents (*e.g.* SiH_3 , GeH_3) lead to decreased singlet-triplet gaps.¹⁰³

The group further predicted that the *m*-terphenyl substituent should be very effective at stabilizing a silyliumylidene ion due to potential “through-space” interactions with the π -system of the flanking aryl groups (*cf.* silylium ion **L-5**, Figure 2).¹⁰³ This concept was later put into practice with the thermally induced generation of the Mes^sTer -substituted silyliumylidene ion from the corresponding 7-silanorbornadienyl cation **L-20** (Scheme 4).¹⁰⁴ Immediate C–H activation of the solvent benzene leading to silylium

ion **L-21** showcases the extremely high reactivity of this almost completely unstabilized species (meaning, without donor stabilization by Lewis bases).



Scheme 4 Generation of the mono-substituted silyliumylidene ion [^{MesTer}Si:]⁺ from **L-20** and its C–H activation of benzene (anions omitted).¹⁰⁴

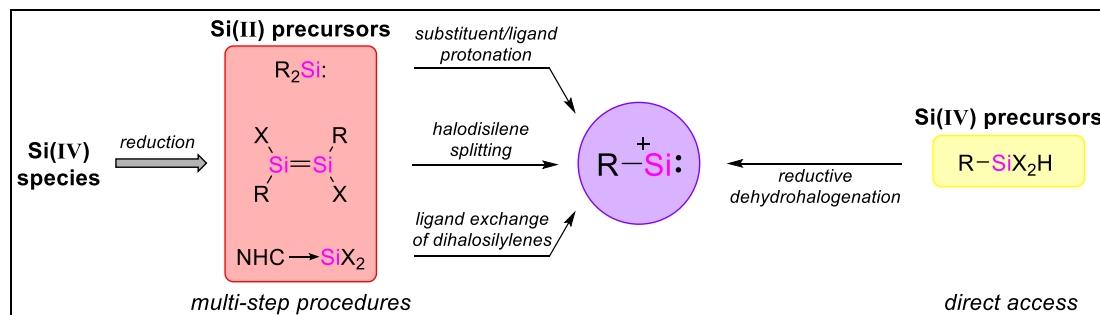
Going down the periodic table, the heavier tetryliumylidene ions [R–E]⁺ (E = Ge, Sn, Pb) are generally easier to synthesize and isolate due to the increased stability of the +II oxidation state for the heavier elements (just like in the case of tetrylenes).³⁷ It is therefore unsurprising, that examples of the heavier congeners appeared much earlier and more frequently in the literature^{37,44,105-110} (e.g. [Cp*Sn:]⁺ in 1979¹¹¹ and [Cp*Ge:]⁺ in 1980¹¹² vs. [Cp*Si:]⁺ in 2004¹¹³). Similarly, while the synthesis of [Cp*E:]⁺ (E = Ge, Sn) could be carried out with a simple protonation of [Cp*₂E:] with HBF₄¹¹¹⁻¹¹², the synthesis of [Cp*Si:]⁺ required a more nuanced approach (*vide infra*).¹¹³ In the context of the C–H activation of benzene with the essentially unstabilized [^{MesTer}Si:]⁺ (Scheme 4)¹⁰³, the isolation of the “quasi one-coordinate” plumblyliumylidene ion clearly demonstrates the much higher stability of the heavier analogues.¹¹⁴

2.3.1 Isolable Silyliumylidene Ions – an Overview

Generally, the synthesis and isolation of silyliumylidene ions involve multi-step approaches including the reduction of suitable Si(IV) species followed by isolation and purification of the Si(II) precursors and their subsequent conversion to the cationic species (Scheme 5).

These work-intensive and difficult syntheses have generally limited their potential applications, however, in recent years a significant amount of progress has been made in a more facile approach to their targeted synthesis and isolation. Furthermore,

reactivity studies of these highly reactive species are starting to appear more frequently in the literature (see chapter 2.3.4).



Scheme 5 Commonly used routes to isolable silyliumylidene ions.

The vast majority of reported silyliumylidene ions are three-coordinate species with either an aryl or halide substituent on the central silicon moiety and utilize NHCs for their stabilization. Nevertheless, a handful of other two- and three-coordinate Si(II) cations have been reported throughout the last 15 years. Figure 11 gives an overview over the most important milestones in the isolation of silyliumylidenes: from the major breakthrough in 2004 with the isolation of a η^5 -Cp*-coordinated Si(II) cation and the synthesis of a two-coordinate silyliumylidene ion in 2006, to the first synthesis of an NHC-stabilized silyliumylidene ion in 2013 up to the isolation of the NHC-stabilized parent silyliumylidene ion in 2017 – the history of and progress in the field of silyliumylidene ion chemistry will be discussed in detail below.

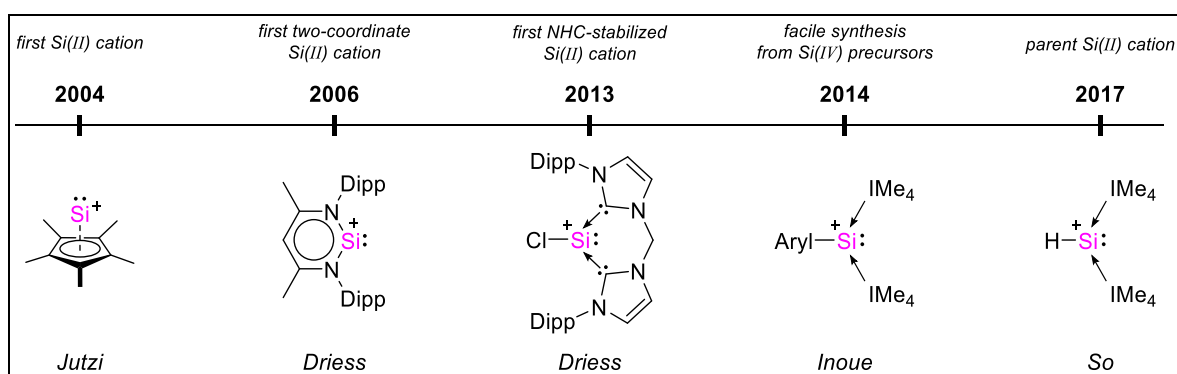


Figure 11 Most important milestones in the isolation of silyliumylidene cations (anions omitted).

2.3.2 Donor-stabilized Silyliumylidene Ions (excluding NHCs)

The first derivative of $[\text{H-Si}]^+$ was reported by Jutzi and co-workers in 2004.¹¹³ They were able to successfully isolate the cationic π -complex $[(\text{C}_5\text{Me}_5)\text{Si}][\text{B}(\text{C}_6\text{F}_5)_4]$ (**L-22**) (Figure 12) by taking advantage of silicon's ability to form hyper-coordinate compounds as well as the stabilizing effects of the Cp* ligand *via* protonation of

decamethylsilicocene $[\text{Cp}^*_2\text{Si}]$ with the proton-transfer agent $[\text{Me}_5\text{C}_5\text{H}_2][\text{B}(\text{C}_6\text{F}_5)_4]$. Initial experiments with HBF_4 as the proton source – an approach comparable to Jutzi's earlier efforts for the isolation of the heavier analogues $[\text{Cp}^*\text{Ge}]^+$ and $[\text{Cp}^*\text{Sn}]^+$ ¹¹¹⁻¹¹² – were unsuccessful and only led to decomposition products. In the ^{29}Si NMR of **L-22**, an extreme high-field shift of -400.2 ppm could be observed, which is characteristic for π -complexes of divalent silicon (*cf.* -398.0 ppm for $[(\text{C}_5\text{Me}_5)_2\text{Si}]$ (**L-6**)).¹¹⁵

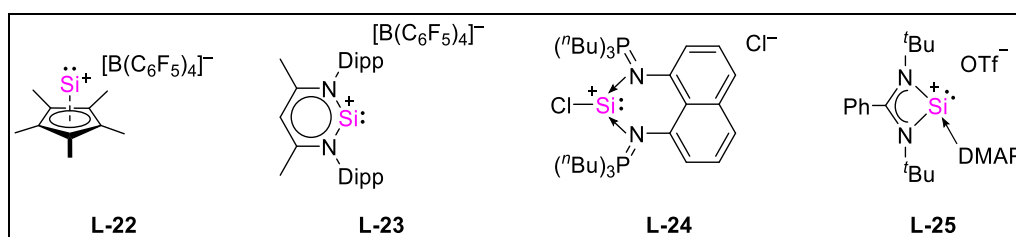


Figure 12 Literature reported silyliumylidene ions (excluding NHC-stabilized variants).

While, technically, **L-22** cannot be considered a true one-coordinate silyliumylidene ion due to the hyper-coordination of the Cp^* ligand (*cf.* silylene **L-6**, Figure 5), it can be regarded as the “resting state” of the actual one-coordinate Si(II) cation $[\eta^1\text{-Cp}^*\text{Si}]^+$, and its reported reactivities support this assumption (*vide infra*). An updated, more convenient method for its preparation with higher yield was later reported by Filippou *et al.*: reaction of $\text{NHC} \rightarrow \text{SiX}_2$ ($\text{NHC} = \text{IDipp}, \text{SIDipp}$; $\text{X} = \text{Cl}, \text{Br}$) with two equivalents of KCp^* yields $[\text{Cp}^*_2\text{Si}]$, which can then be protonated with Brookhart's acid.¹¹⁶ Very recently, the WACKER Chemie AG disclosed a technical scale preparation method through hydride abstraction of $[\text{Cp}^*_2\text{Si}]$ with a tritylium salt, resulting in tetramethylfulvene and **L-22** in high yield.¹¹⁷ This approach is also suitable for the convenient introduction of a variety of different anions. A derivative of **L-22** with C_5^iPr_5 instead of Cp^* was also synthesized through protonation of the mixed silicocene $[(\text{C}_5\text{Me}_5)(\text{C}_5^i\text{Pr}_5)\text{Si}]$.¹¹⁸

In 2006, Driess *et al.* utilized a sterically demanding β -diketiminato ligand to isolate the two-coordinate Si(II) cation **L-23**, which is stabilized by 6π -electron delocalization into the β -diketiminato ligand.¹¹⁹ **L-23** is formed *via* protonation of the ligand backbone of the corresponding zwitterionic *N*-heterocyclic silylene with Brookhart's acid. It is important to note that **L-23** was the first reported two-coordinate Si(II) cation and still remains one of only two reported silyliumylidene ions of this class (*cf.* complex **L-33**, Figure 14). The group further reported a silicon(II) cation stabilized by a bis(iminophosphorane) ligand *via* reaction of $\text{NHC} \rightarrow \text{SiCl}_2$ with the free ligand.¹²⁰ Due to the three-coordinate silicon center in **L-24**, the ^{29}Si NMR resonance is shifted

significantly upfield to -3.3 ppm compared to the $+69.3$ ppm observed for the two-coordinate **L-23**.

In 2013, So and co-workers split and oxidized an amidinate-stabilized Si(I) dimer through addition of *N*-TMS-dimethylamino-pyridinium triflate in the presence of additional DMAP and were able to isolate the amidinate-based DMAP-stabilized silyliumylidene triflate **L-25**.¹²¹ The ^{29}Si NMR resonance (-82.3 ppm) is shifted upfield even further because of the three strong *N*-donor substituents/ligands. The high pyramidalization around the central silicon atom (sum of bond angles: 266.1°) is indicative of a high *s*-character of the silicon-centered lone pair.

Since then, only silyliumylidene ions utilizing either one or two NHC moieties for the stabilization of the low-valent silicon center have been reported.

2.3.3 NHC-stabilized Silyliumylidene Ions

As NHCs are excellent donors, capable of stabilizing a wide variety of low-valent main group species⁴², it is unsurprising that the majority of reported silyliumylidene ions employ up to two NHC moieties for the kinetic and thermodynamic stabilization of the highly electrophilic silicon center. However, an important point regarding NHC-stabilized silyliumylidene ions is the location of the positive charge and, consequently, their representation either as a donor-acceptor complex (Figure 13A) with the positive charge localized on the silicon center or as the zwitterionic form (Figure 13B) as a silyl-anion with the positive charge distributed over the NHCs. Directly related to that, the use of arrows in regards to NHCs in main group compounds is a frequent point of contention in the literature as well.¹²²⁻¹²⁴

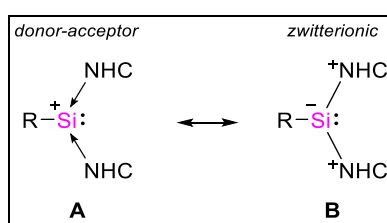


Figure 13 Donor-acceptor (**A**) and zwitterionic (**B**) canonical structures of NHC-stabilized Si(II) cations (anions omitted).

On the one hand, the zwitterionic form (which diminishes the cationic charge at the silicon center) can be justified from the relatively short $\text{Si}-\text{C}^{\text{NHC}}$ bond lengths and the relatively high-field ^{13}C NMR resonance of the carbene carbon atom (~ 150 –

160 ppm).^{37,42,97} This resonance is closer to imidazolium salts (~130–140 ppm) than free carbenes (~200 ppm) and generally upfield shifted from metal NHC complexes. On the other hand, the pyramidal structure observed for NHC-stabilized silyliumylidene ions and the silicon-centered positive charge suggested by NBO analysis clearly support the depiction as the donor-acceptor complex.¹²⁵ It is reasonable to assume that both resonance structures contribute to the overall electronic structure, however, for simplicity and consistency, NHC-stabilized silyliumylidene ions throughout this thesis are always depicted using arrows with the positive charge located at the central silicon atom.

The first NHC-stabilized Si(II) cations **L-26**¹²⁶ and **L-27**⁵⁵ were reported by the groups of Driess and Filippou, respectively, at essentially the same time in 2013 (Figure 14). For **L-26**, Driess *et al.* opted for the same approach they already utilized for the bis(iminophosphorane) silyliumylidene ion **L-24**. Compared to the ²⁹Si NMR shift observed for **L-24** (–3.3 ppm¹²⁰), the bis(NHC)-stabilized compound exhibits a significantly high-field shifted silicon resonance of –58.4 ppm, which can be attributed to the strong electron donation of the bis(NHC) ligand.¹²⁶ The chelating ligand forces a relatively pyramidalized geometry around the central silicon atom with a sum of bond angles of 282.1°.

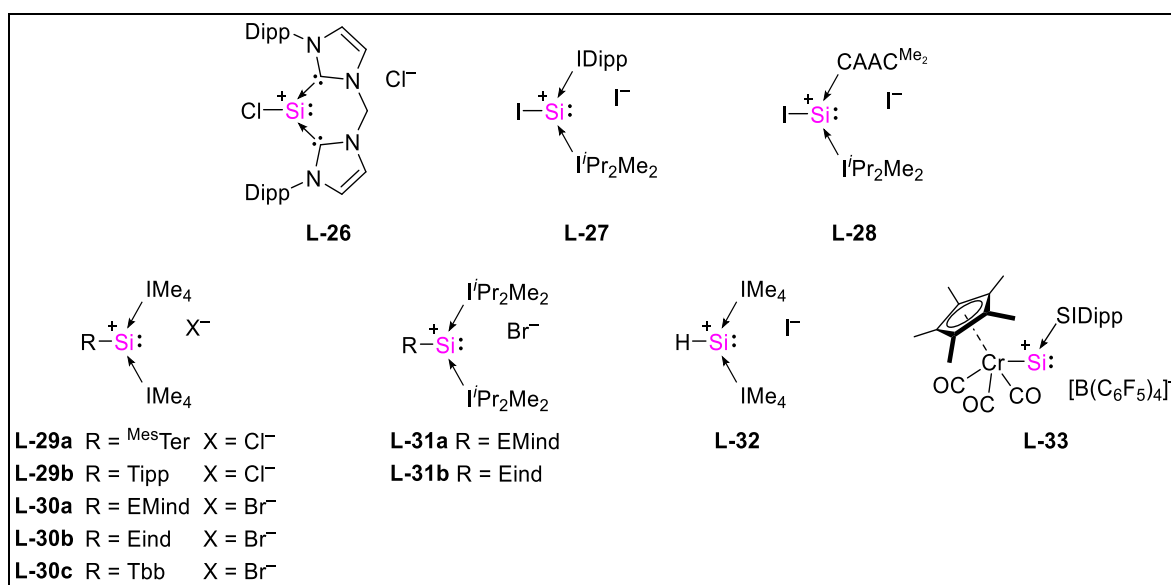
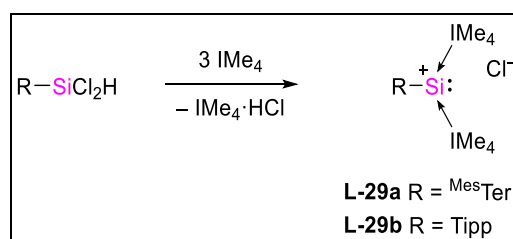


Figure 14 NHC-stabilized silyliumylidene ions **L-26-L-33**; Eind = 1,1,3,3,5,5,7,7-octaethyl-*s*-hydrindacen-4-yl; EMind = 1,1,7,7-tetraethyl-3,3,5,5-tetramethyl-*s*-hydrindacen-4-yl; Tbb = 2,6-(CH(TMS)₂)₂-4-^tBu-C₆H₂.

L-27 could be isolated from the reaction of the NHC-stabilized diiodosilylene IDipp→SiI₂ with ⁱPr₂Me₂, which led to the displacement of one iodide substituent. A fascinating feature of this silyliumylidene ion is the presence of a doublet at –55.3 ppm

($J_{\text{Si-H}} = 10.4 \text{ Hz}$) in the ^{29}Si NMR, which stems from the “through-space” coupling of the silicon center with one methine proton of the *iso*-propyl wingtip due to their close spatial proximity, which can also be observed in the solid-state structure ($d_{\text{Si}\cdots\text{H}} = 2.57 \text{ \AA}$).⁵⁵ Interestingly, addition of the smaller NHC IMe_4 to $\text{IDipp}\rightarrow\text{SiI}_2$ leads to the formation of the unprecedented silicon(II) dication $[\text{Si}(\text{IMe}_4)_3]^{2+}$ through a carbene substitution reaction instead of a silyliumylidene ion.⁵⁵ The mixed CAAC/NHC iodo-silyliumylidene iodide **L-28** was synthesized *via* the same route from the $\text{CAAC}\rightarrow\text{SiI}_2$ precursor.¹²⁷

In 2014, Inoue *et al.* reported the facile access to NHC-stabilized aryl-substituted silyliumylidene ions through abstraction of HCl from easily accessible Si(IV) dichlorosilane precursors.¹²⁵ Addition of three equivalents of NHC to suitable precursors leads to the formation of the desired silyliumylidene chlorides **L-29** with concomitant formation of one equivalent of imidazolium chloride (Scheme 6). The advantages of this route are that it completely avoids the need for the highly reactive Si(II) precursors and the silyliumylidene ion can be synthesized in a simple one-pot reaction. Furthermore, it is anticipated that this synthetic route can be employed to access silyliumylidene ions with different substituents and other NHCs.



Scheme 6 Synthesis of aryl-silyliumylidene ions **L-29**.

Initially, the isolable yield was limited to ~50% as the work-up procedure involved the separation of large crystals of **L-29** from fine imidazolium chloride powder *via* hexane suspension. However, the yield was later improved to 66% through an amended procedure.¹²⁸

The same method was later used by Sasamori, Tokitoh and co-workers for the isolation of silyliumylidene bromide **L-30b** from the corresponding dibromosilane.¹²⁹ Interestingly, these aryl-substituted silyliumylidene ions **L-30** are also accessible through splitting of various arylbromodisilenes by addition of 4 equivalents of NHC. (e.g. the disilene $(\text{Eind})\text{BrSi}=\text{SiBr}(\text{Eind})$ with IMe_4 leads to **L-30b**).¹²⁹⁻¹³⁰ Distinctive for bis(NHC)-stabilized silyliumylidene ions, the ^{29}Si NMR shifts can be observed in the high-field region between -50 and -80 ppm (*cf.* Table 1).

An important milestone was achieved by So *et al.* in 2017 with the isolation of the NHC-stabilized parent silyliumylidene ion **L-32**. Upon homoleptic Si–Si bond cleavage of the NHC-stabilized iodosilicon(I) dimer [IDippI₂Si]₂ with four equivalents of IMe₄, they were able to isolate [H–Si(IMe₄)₂] *via* intermediate formation of a silicon(I) radical, which abstracts H· from the solvent toluene.¹³¹ The ²⁹Si NMR exhibits a doublet at –77.9 ppm (¹J_{Si–H} = 283 Hz) and the Si–H moiety can be observed at 9.73 ppm in the ¹H NMR. The sum of bond angles around the central silicon atom (292.2°) is significantly smaller (which equals an increased pyramidalization and therefore a higher s-character of the lone pair) than in the case of the aryl-substituted silyliumylidene ions **L-29-L-31** (*cf.* Table 1), but nevertheless indicates the presence of a stereochemically active lone pair.

Table 1 Comparison of ²⁹Si NMR shifts and sum of bond angles around the central silicon atom of reported silyliumylidene ions (left: excluding NHCs, right: including NHCs).

#	²⁹ Si NMR [ppm]	Σ∠Si [°]	#	²⁹ Si NMR [ppm]	Σ∠Si [°]
L-22	–400.2	×	L-26	–58.4	282.1
L-23	+69.3	×	L-27	–55.3	301.4
L-24	–3.3	286.6	L-28	–51.5	322.9
L-25	–82.3	266.1	L-29a	–68.8	310.2
			L-29b	–69.5	313.0
			L-30a	–60.8	×
			L-30b	–63.3	×
			L-30c	–70.9	314.7
			L-31a	–75.9	327.0
			L-31b	–59.6	327.3
			L-32	–77.9	292.2
			L-33	+828.6	×

The cationic compound **L-33** with a transition metal-bound silicon moiety can be considered a silyliumylidene ion with a transition metal substituent, as NBO and NRT calculations indicated the presence of a lone pair and a positive charge at the silicon center.¹³² The complex, which was synthesized through addition of CO gas to a chromium silylidyne complex, represents one of only two known two-coordinate silyliumylidene ions (*cf.* **L-23**, Figure 12). The compound is also notable for exhibiting the most downfield shifted ²⁹Si NMR resonance (+828.6 ppm) reported to date, which clearly indicates the difference in the electronic structures and also illustrates the significant difference the silyliumylidene substituent can make.

Nevertheless, even with all of the advances made over the past 15 years in the field of silyliumylidene chemistry, the notoriously difficult synthetic target of a genuinely one-coordinate Si(II) cation as an actual derivative of $[\text{H-Si:}]^+$ remains elusive.

2.3.4 Reactivity of Silyliumylidene Ions

In general, reactivity studies of silyliumylidene ions are quite limited (especially compared to silylenes), as their restricted availability and their generally demanding synthesis makes related follow-up chemistry more difficult. Nonetheless, as this chapter will highlight, Si(II) cations can offer a variety of intriguing reactivities, from acting as synthons for highly reactive, novel low-valent silicon species such as silylones or donor-free silylenes to small molecule activation reactions, transition metal coordination chemistry and even catalytic applications (Figure 15).

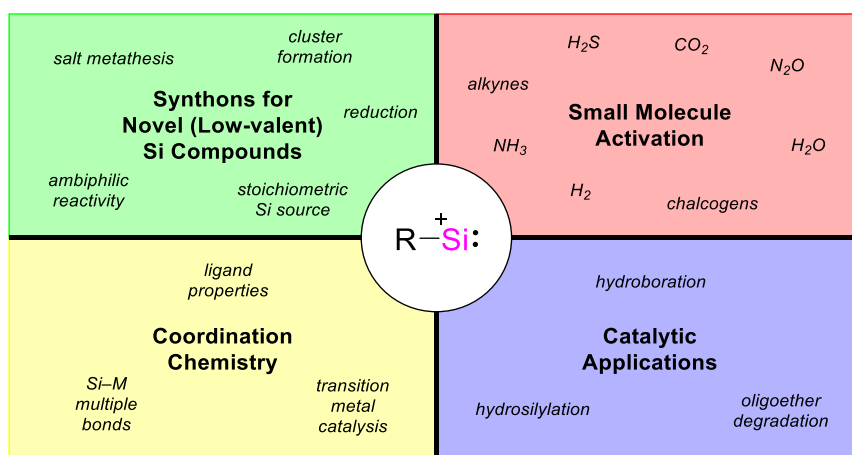
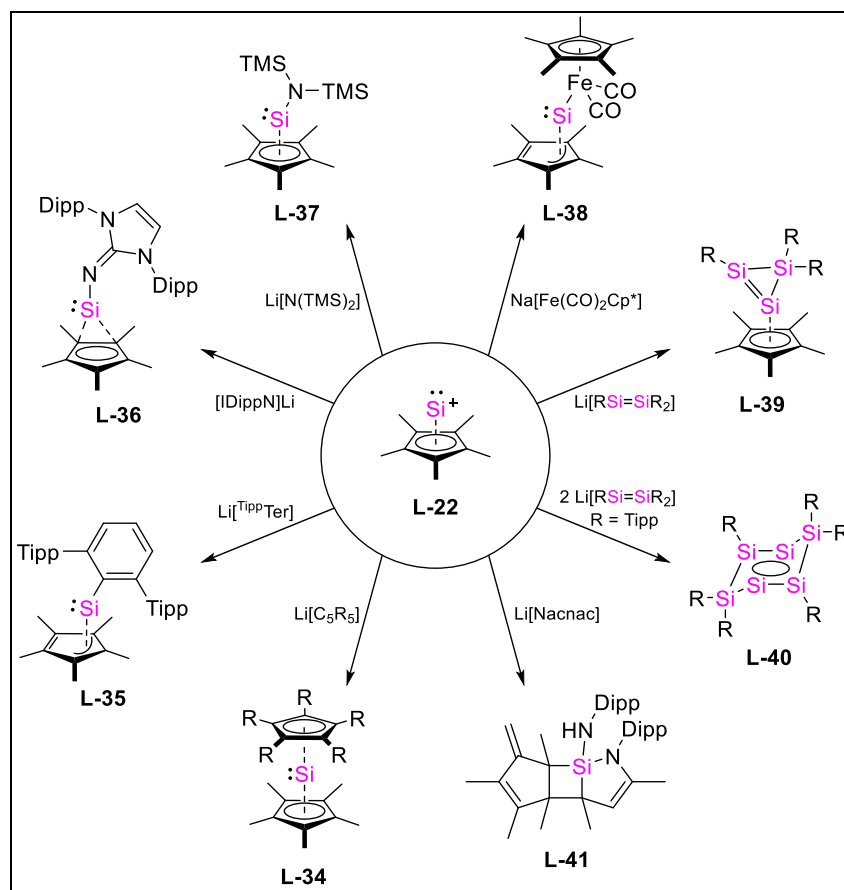


Figure 15 General overview over the fields of applications of silyliumylidene ions $[\text{R-Si:}]^+$.

(i) Synthons for Novel (Low-valent) Silicon Compounds

It is of course unsurprising that the most expansive reactivity investigations reported so far center around the first isolated silyliumylidene ion **L-22**. In addition to its impressive stabilizing effects allowing the isolation of **L-22**, the Cp^* substituent also has the added benefit of coordinative flexibility (*i.e.* the possibility of a hapticity shift from η^5 to η^1), giving **L-22** a range of possible applications. Jutzi himself has previously comprehensively reviewed the reported reactivities of $[\text{Cp}^*\text{Si:}]^+$ in 2014.¹³³ Nevertheless, an outline is given in Scheme 7 which will be briefly discussed below.

A large part of the reported reactivities focus on the synthesis of novel acyclic silylenes *via* reaction of **L-22** with suitable precursors that generally incorporate a small cation (e.g. Li^+ , Na^+) to remove the counter anion of **L-22** *via* salt metathesis. Jutzi and co-workers reported multiple new sandwich complexes **L-34** related to decamethylsilicocene, which were synthesized by reaction of **L-22** with different lithiated Cp-derivatives like $\text{Li}(\text{C}_5^i\text{Pr}_5)$.¹¹⁸ Similarly, utilization of a lithiated bulky aryl¹³⁴, imino¹³⁵ or amino group¹³⁶ furnished the corresponding Cp*-substituted aryl-, imino- and amino- silylenes **L-35**, **L-36** and **L-37**, respectively. Interestingly, while the amino-substituted complex **L-37** exhibits a monomeric structure with a π -bonded Cp* substituent in solution, dimerization to a *trans*-disilene with a σ -bonded Cp* substituent can be observed in the solid state.¹³⁶ Furthermore, the metallo-substituted silylene **L-38** could be obtained after addition of $\text{Na}[\text{Fe}(\text{CO})_2\text{Cp}^*]$.¹³⁷

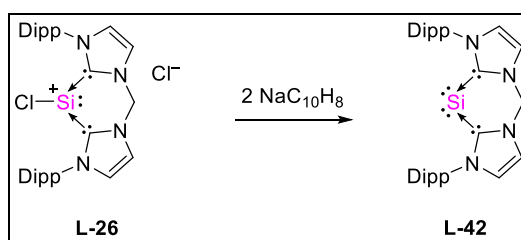


Scheme 7 Selected reported reactivities of $[\text{Cp}^*\text{Si}]^+$ (anion omitted).

Jutzi and Scheschkewitz *et al.* also described a novel route to cyclotrisilene **L-39** *via* addition of the lithium-disilene $\text{Li}(\text{TippSi}=\text{SiTipp}_2)$.¹³⁸ Addition of 2 equivalents of this reagent leads to the formation of the hexasilabenzene isomer **L-40**.¹³⁹⁻¹⁴⁰ The concept of utilizing $[\text{Cp}^*\text{Si}]^+$ and $[\text{Cp}^*_2\text{Si}]$ as a stoichiometric source of silicon was further used by Scheschkewitz and co-workers to isolate several silicon-based clusters.¹⁴¹

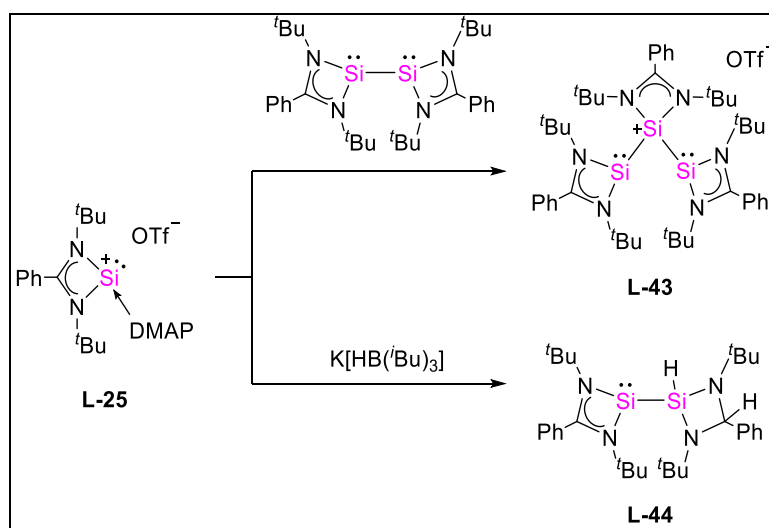
Remarkably, reaction of **L-22** with the lithium salt of the β -diketiminate ligand (LiNacnac) leads to the tricyclic Si(IV) compound **L-41** through cleavage of the ligand framework and multiple rearrangement reactions.¹⁴²

Driess *et al.* showed in 2013 that Si(II) cations can offer a remarkably simple access route to silylones. Reductive dehalogenation of their bis(NHC)-stabilized silyliumylidene ion **L-26** with sodium naphthalenide led to the silylone (“sila-dicarbene”) **L-42** (Scheme 8).¹²⁶



Scheme 8 Conversion of silyliumylidene **L-26** to silylone **L-42**.

So and co-workers were also able to demonstrate the nucleophilic and electrophilic character of the DMAP-stabilized silyliumylidene **L-25** through unique reactivities: addition of the amidinate Si(I)-dimer¹⁴³ (the precursor of Si(II) cation **L-25**) resulted in the formation of **L-43**, which is the first example of a silylium cation with low-valent silicon substituents. Reduction of **L-25** using *K*-selectride yielded the silylsilylene **L-44** (Scheme 9).¹²¹



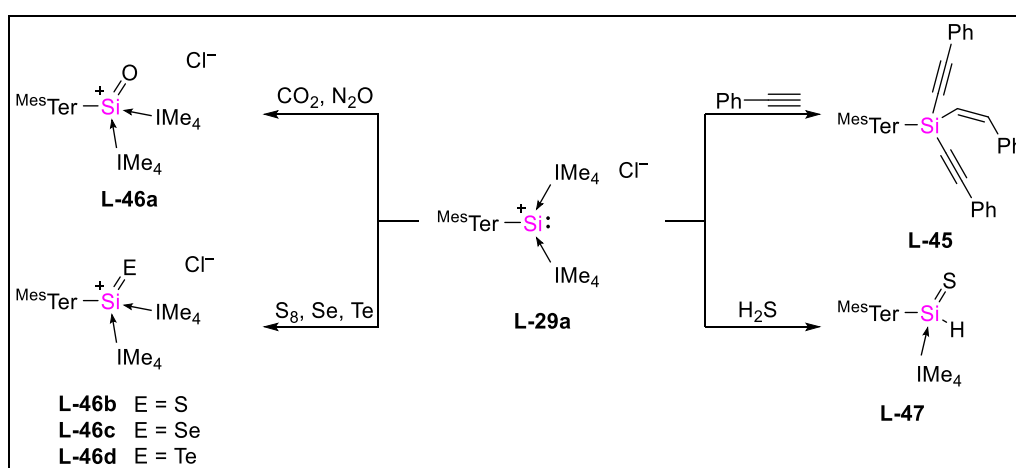
Scheme 9 Unique reactivity of DMAP-stabilized silyliumylidene **L-25**.

(ii) Small Molecule Activation

The activation of (relatively) inert small molecules is one of the most important fields of modern main group chemistry, especially in the context of transition metal-free catalysis. Silyliumylidene ions have been employed in a variety of activation reactions, ranging from chalcogens, to C–H bonds in terminal alkynes and small gaseous molecules such as N₂O, CO₂ and H₂S, which is a testament to the high reactivity of even three-coordinate Si(II) cations.

Inoue and co-workers reported multiple diverse and interesting reactivities of their NHC-stabilized silyliumylidene ions **L-29**, which were recently reviewed in a personal account.⁹⁷ Initially, the reactivity towards phenylacetylene was investigated: addition of three equivalents of phenylacetylene to **L-29a** results in the formation of alkenyl-dialkynyl-silane **L-45** (Scheme 10) *via* multiple C–H bond activations.¹²⁵ The observed formation of the (*Z*)-isomer as the sole product was explained using DFT calculations, where formation of the (*E*)-isomer could be excluded due to high activation barriers.

Furthermore, it was shown that activation of CO₂ using **L-29** is also possible.¹⁴⁴ Utilization of the bulky *m*-terphenyl group (**L-29a**) allowed the isolation of sila-acylium ion **L-46a**, the silicon analogue of an acylium ion. Using the smaller Tipp substituent (**L-29b**) lead to the same activation product, although the compound decomposes above –30 °C because of the reduced steric protection, presumably undergoing polymerization.



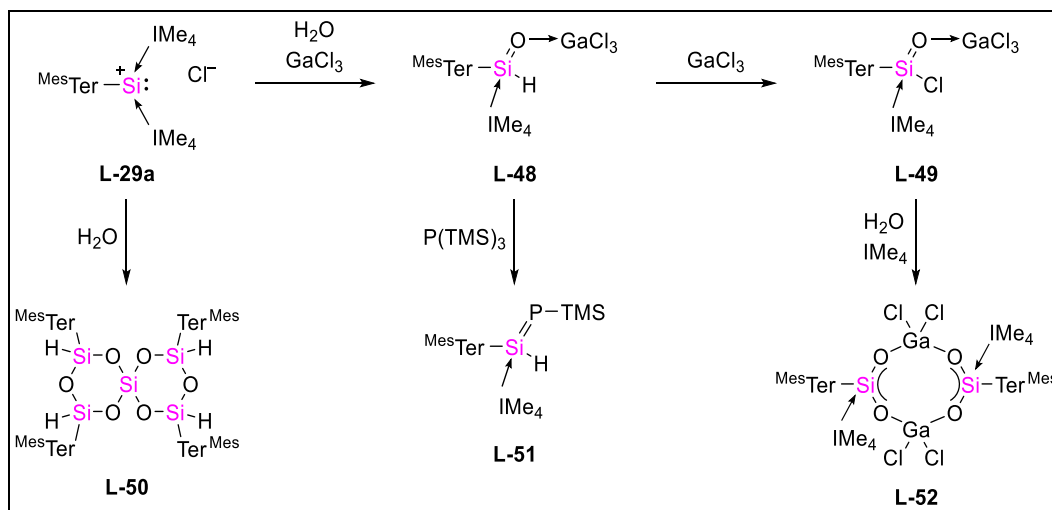
Scheme 10 Reported small molecule activation reactions of silyliumylidene ion **L-29a**.

Using N₂O as the oxidation agent leads to the same product. The related heavier homologues **L-46b-d** of sila-acylium ion **L-46a** could also be isolated *via* reaction of **L-29a** with S₈, Se and Te.¹⁴⁵ For these compounds, unique chalcogen exchange

reactions could be observed, going from $\text{Te} \rightarrow \text{Se} \rightarrow \text{S}$, which corresponds well with the calculated $\text{Si}=\text{E}$ bond dissociation energies. Further examples of sulfur activation were reported by Driess and co-workers as well as So *et al.*, furnishing the expected sila-thionium compounds.¹²⁰⁻¹²¹

Recently, Inoue *et al.* also reported the activation of S–H bonds in H_2S .¹²⁸ Reaction of the silyliumylidene ion with hydrogen sulfide furnished thio-sila-aldehyde **L-47** with concomitant formation of imidazolium chloride. Detailed computational studies elucidated the mechanism of formation, which commences with a proton transfer from H_2S to **L-29a**, followed by an attack of the SH^- moiety on the silicon center.

Furthermore, sila-aldehyde **L-48** as the lighter congener of **L-47** could also be isolated by reaction of **L-29a** with water (Scheme 11). However, as opposed to the sulfur-containing compound, **L-48** requires the presence of a Lewis acid (e.g. GaCl_3) for donor-acceptor stabilization.¹⁴⁶ In the absence of a Lewis acid, only formation of spiro-siloxane **L-50** could be observed. The sila-aldehyde was then further functionalized to sila-acyl-chloride **L-49** through chlorination with additional GaCl_3 and hydrolysis of this heavier acid chloride in the presence of free NHC (leading to **L-52**) was also presented. Moreover, convenient conversion to phosphasilene **L-51** using $\text{P}(\text{TMS})_3$ was achieved as well.



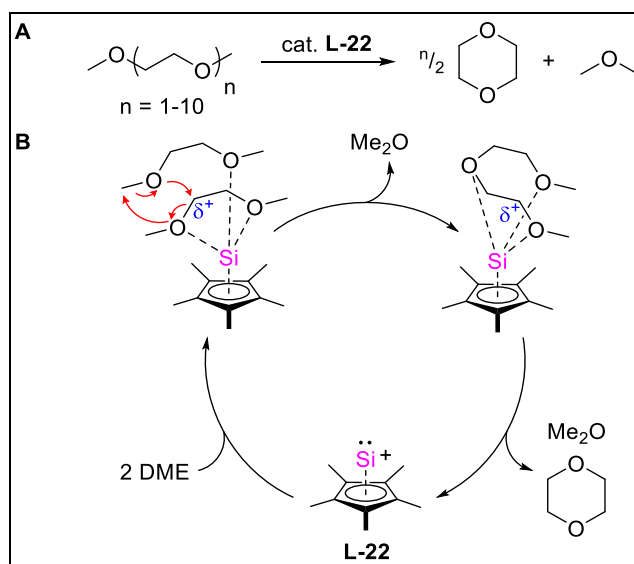
Scheme 11 Conversion of **L-29a** to sila-aldehyde **L-48** and follow-up chemistry.

Filippou and co-workers also demonstrated the use of N_2O as oxidation agent with the isolation of a metalla-sila-acylium ion from the metalla-silyliumylidene ion **L-33**.¹³² They further reported that, due to the small HOMO-LUMO gap of the metalla-silyliumylidene ion, activation of H_2 , NH_3 , H_2O and HCl is also possible, but no further details were disclosed.

(iii) Catalytic Applications

Due to their unique electronic structure, silyliumylidene ions are promising transition metal-free alternatives for catalytic applications. Especially Si(II) cations with a formal coordination number of two or less have the potential to supersede transition metal complexes in various organic transformations. Accordingly, silyliumylidene ions are one of the few low-valent main group compounds with multiple reported catalytic reactivities that even include applications that can be relevant on an industrial scale.

The first report of a catalytic activity of a silyliumylidene ion was published in 2011, when Jutzi and co-workers discovered the facile degradation of oligoethers (e.g. dimethoxyethane) to dioxane and dimethylether (Scheme 12A) in the presence of catalytic amounts of **L-22** without any decomposition of the Si(II) cation.¹⁴⁷

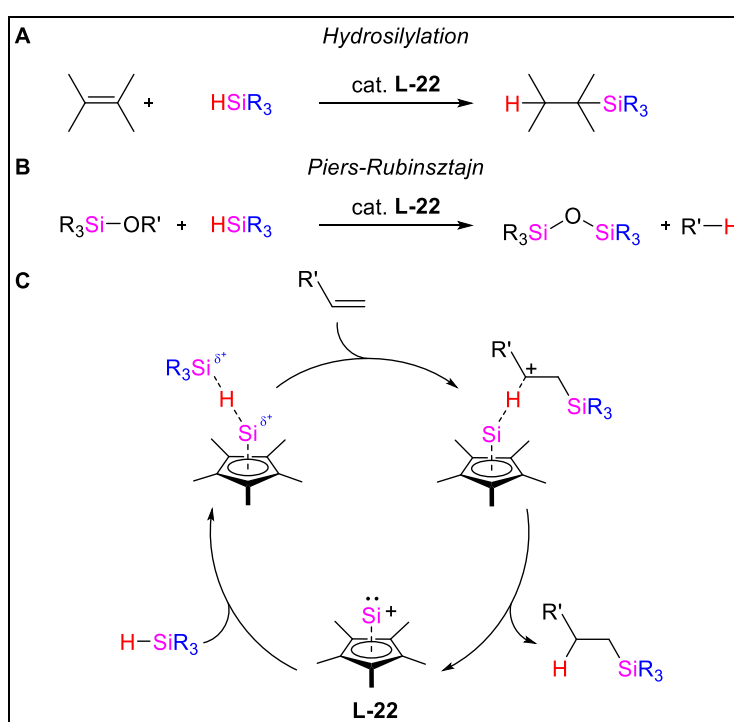


Scheme 12 Catalytic conversion of oligoethers to 1,4-dioxane and dimethylether by **L-22** (A) and suggested mechanism for the conversion (B) (anions omitted).

The free coordination sites at silicon – available due to the open coordination sphere of **L-22** – were deemed essential for the catalytic activity, with calculations showing multiple weak and non-rigid Si–O interactions between the silicon cation and two DME molecules being responsible for the rearrangement reactions (Scheme 12B). Similarly, degradation of cyclic ethers (e.g. 12-crown-4) lead to the formation of 1,4-dioxane without byproducts. While catalytic activity is rather low at room temperature (15 days for full conversion with 7 mol% catalyst), the observed reactivity clearly serves as a proof of concept for catalytic applications of a Si(II) cation.

The WACKER Chemie AG has also taken notice of the catalytic potential of silyliumylidene ions: very recently, the company reported the utilization of Jutzi's

silyliumylidene ion **L-22** as a catalyst in technically relevant organosilicon reactions: in the transition metal-free hydrosilylation of olefins (Scheme 13A) and the Piers-Rubinsztajn (*PR*) reaction (Scheme 13B).¹¹⁷ **L-22** efficiently catalyzes the hydrosilylation of C=C double bonds, with terminal olefins showing higher reaction rates. It was even possible to achieve full conversion with a catalyst loading as low as 0.0013 mol% with a turnover number (TON) of ~80000, which is in the range of the commonly employed platinum-based catalysts. As **L-22** is still active even after full consumption of the starting materials, recovery of the catalyst and reuse in further hydrosilylation reactions is a possibility. The potential recycling of the catalyst makes this especially attractive for industrial applications.

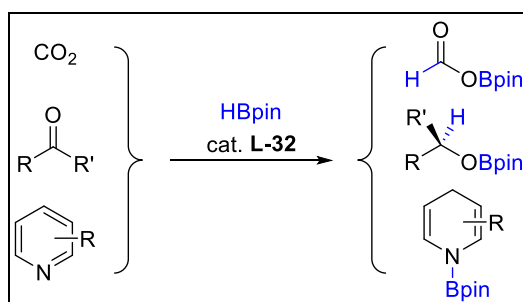


Scheme 13 Catalytic hydrosilylation of olefins (**A**) and Piers-Rubinsztajn reaction (**B**) using **L-22** as the catalyst and suggested mechanism of the hydrosilylation (**C**) (anions omitted).

Hydrosilylation of double bonds attached to silicon is more difficult due to a competing redistribution reaction between the Si-bound H and the Si-bound vinyl group taking place. Similarly, hydrosilylation of C≡C bonds is more limited in its application, giving a mixture of hydrosilylation and dehydrogenative silylation products. Once again, the open coordination sphere of **L-22** was found to be crucial for the catalytic activity, with the presumed mechanism involving “activation” of the silane Si-H bond (Scheme 13C). **L-22** is also able to efficiently catalyze the *PR* reaction between Si-OR and Si-H groups (0.1 mol% catalyst at 60 °C), giving siloxanes without significant catalyst deactivation. Importantly, addition of alkoxy silanes to a hydrosilylation mixture inhibits

the catalytic activity through coordination of the oxygen to the silicon center. However, this inhibition is fully reversible, as heating to 60 °C leads to consumption of the coordinated alkoxy silane through the *PR* reaction, allowing the hydrosilylation to continue uninhibited.

Also very recently, So and co-workers reported hydroboration reactions of a variety of substrates (e.g. carbonyl compounds and pyridine derivatives) with the NHC-stabilized parent silyliumylidene ion **L-32**, including the catalytic reduction of CO₂ (Scheme 14).¹⁴⁸ Hydroboration of aliphatic aldehydes as well as aromatic aldehyde substrates, including derivatives with electron-donating and electron-withdrawing substituents is possible at a high rate at room temperature. On the other hand, ketones and pyridine-based substrates require temperatures of up to 90 °C. While higher catalyst loadings are necessary (10 mol%) in comparison to the aforementioned hydrosilylation catalysis, it is nevertheless equal parts surprising and impressive that catalytic reactions – especially the reduction of CO₂ – can also be carried out with an NHC-stabilized low-valent silicon compound.



Scheme 14 Catalytic hydroboration of CO₂, carbonyl compounds and pyridine derivatives by **L-32**.

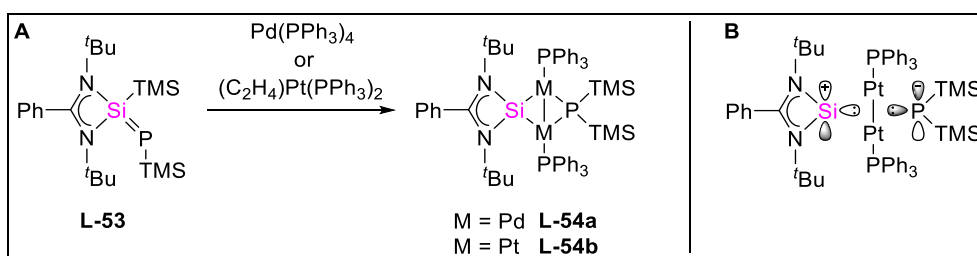
The mechanism of the aldehyde/ketone hydroboration is presumed to proceed *via* activation of the substrate with the silyliumylidene ion lone pair, followed by addition of the B–H bond to the C=O functional group with elimination of the catalyst.

These reported examples strikingly demonstrate the potential of silyliumylidene ions to serve as efficient and versatile catalysts in organic transformations. The industrially relevant hydrosilylation with Jutzi's silyliumylidene ion stands out as one of the most promising catalytic applications of a low-valent main group compound to date and even the three-coordinate silyliumylidene ion **L-32** with two NHC moieties attached to the silicon center shows promising activity in a catalytic transformation. As the investigation of catalytic activity of silyliumylidene ions is still in its infancy, further interesting developments over the next years are expected.

(iv) Transition Metal Coordination Chemistry

As discussed in chapter 2.2.2 of this thesis, silylenes have an extraordinary potential in transition metal coordination chemistry. With their relationship to silylenes – *i.e.* the presence of a lone pair on the central silicon atom – the same can also apply to silyliumylidene ions. For example, a (formally) one-coordinate silyliumylidene ion could be used to form a $\text{Si}\equiv\text{M}$ triple bond – a notoriously difficult synthetic target – in a single reaction step. The low-coordinate nature of Si(II) cations would also potentially allow further functionalization of silyliumylidene transition metal complexes to isolate hitherto unobtainable silylene and silyl-substituted complexes. Furthermore, due to their ionic nature, facile salt metathesis reactions with anionic transition metal complexes (*i.e.* using the precipitation of a salt as the driving force of the reaction) can be employed. Additionally, silicon-coordinated NHC moieties can be of interest for transition metal coordination chemistry, as the migration of NHCs to the metal center could allow for the synthesis of novel, interesting complexes. However, just like the area of silyliumylidene ions compared to silylenes, the coordination chemistry of Si(II) cations is far less developed than the field of silylene ligands. In fact, only a handful of (formal) silyliumylidene complexes have been reported in the literature and no studies regarding the properties of silyliumylidene ions as ligands have been carried out.

The first example was reported in 2013 by Inoue *et al.*: rearrangement reactions of zwitterionic phosphasilene **L-53** in the presence of group 10 d^{10} transition metal phosphine complexes ($\text{Pd}(\text{PPh}_3)_4$ or $(\eta^2\text{-C}_2\text{H}_4)\text{Pt}(\text{PPh}_3)_2$) give the formal silyliumylidene phosphide complexes **L-54** (Scheme 15A).¹⁴⁹ Interestingly, such a rearrangement does not take place with $\text{Ni}(\text{COD})_2$, forming a bis(silylene)nickel complex instead.

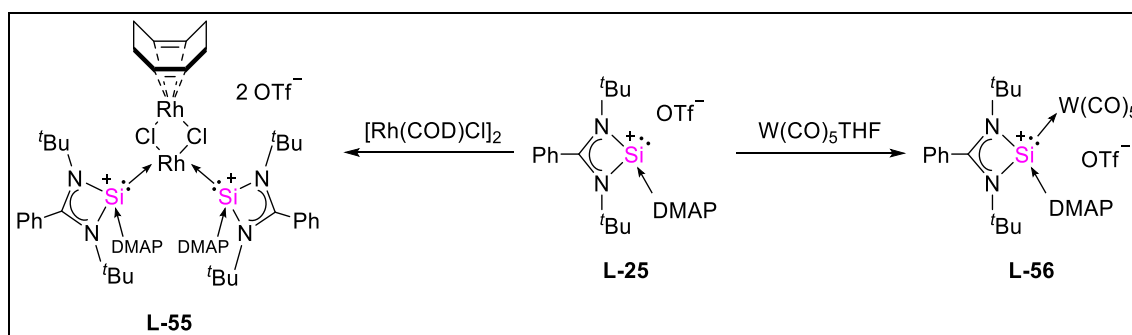


Scheme 15 Synthesis of formal silyliumylidene ion complexes **L-54** from phosphasilene **L-53** (**A**) and schematic representation of the bonding situation in **L-54b** (**B**).

According to molecular orbital calculations, the bonding situation is best described as an interaction between the lone pair orbital of the silyliumylidene moiety and the lone pair orbital of the phosphide with the empty d-orbitals of the metal (Scheme 15B). NBO

charge analysis revealed a positive charge on the silicon atom (+0.974) and a negative charge on the phosphorus atom (−0.715), also indicating the silyliumylidene-type character of the silicon moiety. In the ^{29}Si NMR the central silicon atom resonates at 187.8 ppm and 234.5 ppm for Pd and Pt, respectively, which is a considerable downfield shift to comparable silylene or silyl bis(palladium) and bis(platinum) complexes.

One year later, So and co-workers described the synthesis of tungsten and rhodium complexes directly from a stable silyliumylidene ion (Scheme 16).¹⁵⁰ Addition of $[\text{Rh}(\text{COD})\text{Cl}]_2$ or $\text{W}(\text{CO})_5(\text{THF})$ to the amidinate-substituted DMAP-stabilized Si(II) cation **L-25**¹²¹ results in the formation of complexes **L-55** and **L-56**, respectively.¹⁵⁰ In the case of $\text{W}(\text{CO})_5\text{THF}$, the monomeric complex is formed *via* displacement of the coordinated THF moiety by the silyliumylidene ion. Unexpectedly, for $[\text{Rh}(\text{COD})\text{Cl}]_2$, one cyclooctadiene ligand in the transition metal dimer is replaced by two silyliumylidene ligands instead of the expected cleavage of the dimer.

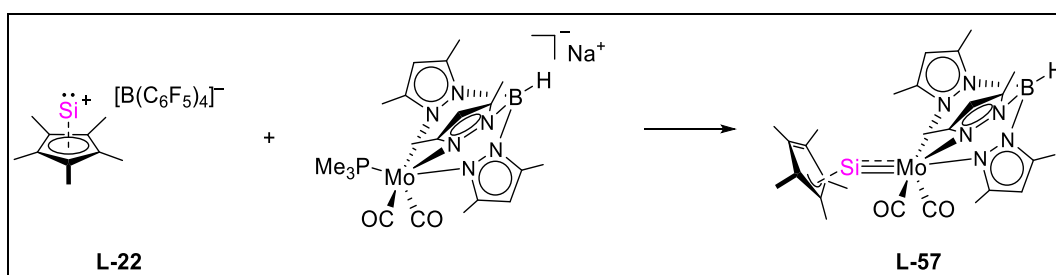


Scheme 16 Synthesis of Rh and W complexes **L-55** and **L-56** from **L-25**.

SC-XRD analysis of complex **L-56** revealed a Si(II)–W bond length of 2.497(1) Å, which is in the range of typical Si–W bonds (2.388–2.708 Å).¹⁵⁰ Unfortunately, crystal quality of the rhodium complex was not sufficient enough for a detailed structural analysis. ^{29}Si NMR (40.5 ppm (**L-55**) and 51.6 ppm (**L-56**)) shifts exhibit an expected downfield shift compared to **L-25** (−82.3 ppm). Regrettably, IR spectra and σ -donor/ π -acceptor strength of **L-56** were not discussed.

Very recently, Filippou *et al.* reported the silyliidyne molybdenum complex **L-57** synthesized from Jutzi's $[\text{Cp}^*\text{Si}][\text{B}(\text{C}_6\text{F}_5)_4]$ (**L-22**) *via* a salt metathesis reaction with a sodium metallate precursor (Scheme 17).¹¹⁶ The PMe_3 ligand on the metal was introduced to offer a more easily displaceable ligand than CO to promote the formation of a multiple-bonded complex. ^{29}Si NMR data revealed a strong downfield shift from −400.2 ppm in **L-22** to −272.4 ppm in **L-57**. SC-XRD analysis of **L-57** showed a short

Mo–Si bond length of 2.309(1) Å, which is considerably shorter than Mo–Si single bonds (~2.56 Å) and is at the short end of Mo=Si double bonds (2.287–2.387 Å), which confirms a significant multiple bond character between Si and Mo. Interestingly, the Cp*⁺-ring in **L-57** is coordinated to silicon in a η^3 -fashion. Charge analysis *via* natural resonance theory (NRT) revealed a high positive charge located at the silicon center (+1.13), which is even higher than that found in the starting material **L-22** (+0.89). Hence, the complex can also be described as a silyliumylidene complex with a very short metal–silicon bond.



Scheme 17 Synthesis of silylydyne complex **L-57** from **L-22**.

These reported examples already demonstrate the potential of silyliumylidene ions as ligands in transition metal complexes. It is understandable, however, that much like any reactivity investigations of Si(II) cations, the field of silyliumylidene ion coordination chemistry is still in its infancy, especially given how young the field of silyliumylidene ions itself still is. Add that to the fact that syntheses and isolation of these cations are often laborious and difficult procedures, the small number of reported coordination compounds as well as the limited knowledge about their properties is not surprising.

3. Scope of this Work

The past 15 years have shown silyliumylidene ions to be highly interesting low-valent silicon species worth investigating, with a breadth of possible applications, from stoichiometric activation of small molecules to acting as metal-free catalysts in organic transformations. However, as pointed out in the introduction, silyliumylidenes are still in their infancy regarding the investigation of their properties and applications, especially concerning their possible coordination chemistry with transition metals. In fact, prior to this thesis, only a single report detailed a transition metal complex synthesized directly from a silyliumylidene ion.¹⁵⁰ However, no further studies on the properties of the ligand were disclosed. Hence, the primary goal of this thesis was the investigation of the possible coordination chemistry of NHC-stabilized silyliumylidene ions and to achieve a fundamental understanding of their properties as ligands.

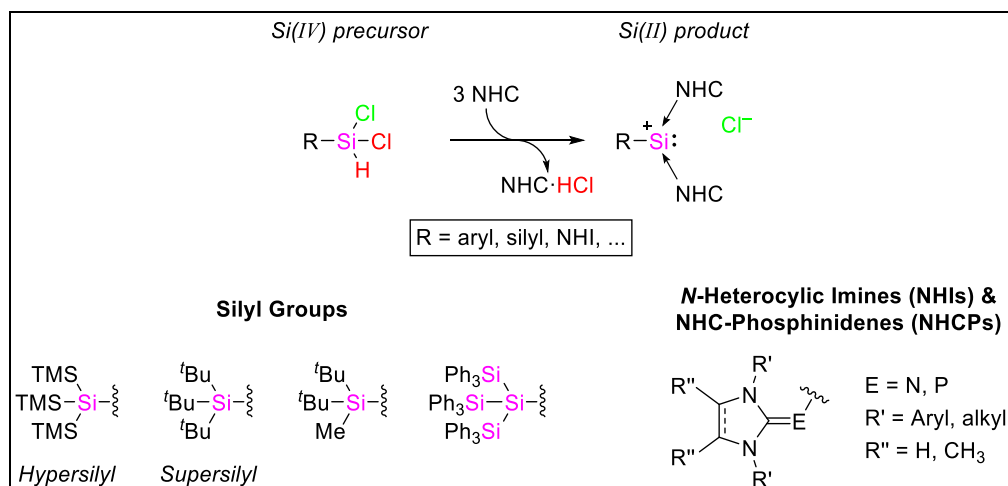
Furthermore, the overwhelming majority of reported Si(II) cations feature either an aryl or halide substituent. Keeping in mind that the electronic and steric properties of the sole substituent in silyliumylidene ions has a profound influence on the properties and reactivity of the low-valent silicon center, another focus of this work was to introduce other substituents on the central silicon moiety.

Therefore, the work in this thesis can be divided into two parts: first, the isolation of novel NHC-stabilized silyliumylidene ions with different substituents (i), followed by investigation of the possible coordination chemistry of these Si(II) cations with a variety of transition metals (ii), including investigation of the properties and reactivities of the obtained complexes.

(i) Increasing the Variety of Available Substituents on Si(II) Cations

The initial goal was to expand the previously reported, convenient silyliumylidene ion synthesis method (*i.e.* utilization of NHCs for the abstraction of HCl from an easily accessible Si(IV) dichlorosilane precursor¹²⁵) (Scheme 18, for details *cf.* chapter 2.3.1) to other substituents with different steric and electronic properties in order to increase the available range of substituents on NHC-stabilized silyliumylidene ions. Obviously, dichlorosilane (R–SiCl₂H) derivatives of the selected substituents needed to be easily accessible to be able to increase the scope of this synthesis route. With that in mind, we selected three promising substituent classes, based on their excellent electron-

donating properties and their easily tunable steric demand: **silyl groups**, **N-heterocyclic imines** (NHIs) and the related **N-heterocyclic carbene-phosphinidenes** (NHCPs). Additionally, **aryl groups** with low steric demand to allow facile reaction with bulky substrates as well as sterically demanding transition metal complexes were also considered.



Scheme 18 Schematic representation of the synthesis of silyliumylidene ions through abstraction of HCl from dichlorosilane precursors with NHCs and promising substituents for the isolation of novel NHC-stabilized Si(II) cations.

Furthermore, as the desired silyliumylidene ion and the imidazolium salt [NHC·HCl] byproduct are formed in a 1:1 ratio during the synthesis and their separation is difficult, the work-up of the reaction was deemed to be an essential target for further improvements.

(ii) Utilization of Literature Known and Novel NHC-stabilized Si(II) Cations as Ligands in Transition Metal Complexes and Investigation of Their Properties

With the presence of a stereochemically active lone pair on the silicon center, silyliumylidene ions can act as ligands in transition metal complexes. Even though a number of Si(II) cations have been reported in recent years, the corresponding transition metal coordination chemistry is still very much in its infancy. However, this is understandable, considering that silyliumylidene ion chemistry itself is still a very young field and that transition metal complexes incorporating a positively charged silicon-based ligand are an incredibly challenging synthetic target. The general low stability and simultaneous often extremely high reactivity of Si(II) cations with multiple reactive sites makes predictions about their general behavior with transition metals difficult.

Furthermore, reactivity investigations are also made difficult with the limitations of usable solvents, as generally polar, coordinating solvents are needed for homogeneous reactions, which bring their own challenges in transition metal chemistry. Additionally, chlorinated solvents often lead to decomposition.

NHC-stabilized silyliumylidene ions $[R-Si(NHC)_2]X$ offer three distinct reactive sites that can possibly be taken advantage of regarding coordination chemistry with transition metals (Figure 16).¹⁵¹

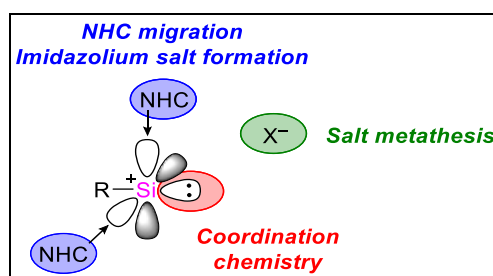


Figure 16 Potential reactive sites of an NHC-stabilized silyliumylidene ion (adapted from ¹⁵¹).

Each reactive site can be specifically targeted through the choice of a complementing transition metal precursor:

- **Silicon-centered Lone Pair**

Due to the presence of the stereochemically active lone pair on the silicon center, the silyliumylidene ion can act as a σ -donor. Using either labile ligands (e.g. solvent molecules, ethylene, ...) on the transition metal, dimeric metal precursors that can be easily cleaved or simple metal salts can facilitate the coordination.

- **Counter Anion**

Reaction with an anionic transition metal complex with a counter cation and using a salt metathesis reaction with precipitation of a simple salt as the driving force of the reaction can be a simple access route to transition metal complexes. Additionally, anion exchange reactions can increase the spectrum of available silyliumylidene ions with potentially different reactivities and solubilities.

- **Coordinated NHCs**

It is conceivable, that the coordinated NHC moieties can potentially migrate to a transition metal. Furthermore, the anion of the silyliumylidene and a hydride substituent of a transition metal complex can be used in conjunction with the NHC moiety to form and precipitate an imidazolium salt and with that free up an additional coordination site on the silicon center. Access to Si–M multiple bonds is also a possibility with this route.

4. NHC-stabilized Silyl-substituted Silyliumylidene Ions

Title: “NHC-stabilized silyl-substituted silyliumylidene ions”¹⁵²

Status: Communication; published online: June 18, 2019.

Journal: *Dalton Transactions* **2019**, *48*, 10403–10406.

Publisher: Royal Society of Chemistry

DOI: [10.1039/C9DT02010A](https://doi.org/10.1039/C9DT02010A)

Authors: Philipp Frisch and Shigeyoshi Inoue^a

Reproduced by permission of The Royal Society of Chemistry. © 2019 The Royal Society of Chemistry.

Content: So far, the available substituent range on silyliumylidene ions remains very limited, with the overwhelming majority of Si(II) cations featuring either aryl or halide substituents. However, as the choice of substituent can have a profound impact on the electronic situation of the central silicon atom, it is desirable to increase the variety of possible substituents in these highly reactive species. Different substituents can markedly influence the reactivity and stability of the low-valent silicon species itself and also that of any possible reaction products. Importantly, isolation of silyliumylidene ions with a broader range of substituents has been generally hampered by the lack of availability of a suitable synthetic approach.

This publication outlines the synthesis and isolation of the first silyl-substituted silyliumylidene ions through a convenient one-pot synthesis directly from a Si(IV) precursor. Before that, this previously reported synthesis route was limited to aryl-based substituents on the central silicon atom. Addition of three equivalents of free NHC (NHC = IMe₄, IEt₂Me₂) to a solution of a dichlorosilane precursor R–SiCl₂H (R = ^tBu₃Si, ^tBu₂MeSi) results in rapid formation of the desired silyliumylidene ions [R–Si(NHC)₂]Cl and concomitant formation of imidazolium chloride [NHC·HCl]. Separation of the product and byproduct can be achieved through simple extraction with a mixture of toluene and acetonitrile.

Introduction of the highly electropositive silyl-based substituents results in a reduced pyramidalization around the central silicon atom and with that a reduced s-character of the silicon-centered lone pair. Additionally, the stronger σ -donating properties of the silyl substituent compared to aryl-based substituents are reflected in a significant upfield shift in the ²⁹Si NMR. Furthermore, the facile exchange reaction of the coordinated IEt₂Me₂ moieties to the more σ -electron donating NHCs IMe₄ could be demonstrated. The kinetics of the reaction were analyzed *via* reaction progress monitoring through ¹H NMR, which revealed an associative S_N2-type mechanism.

^aP. Frisch planned and executed all experiments, conducted the SC-XRD measurements including processing of the data and wrote the manuscript. All work was performed under the supervision of S. Inoue.



NHC-stabilized silyl-substituted silyliumylidene ions†

Philipp Frisch and Shigeyoshi Inoue *

Cite this: *Dalton Trans.*, 2019, **48**, 10403Received 14th May 2019,
Accepted 18th June 2019

DOI: 10.1039/c9dt02010a

rsc.li/dalton

The first silyl-substituted silyliumylidene ions are reported. The scope of a previously described convenient one-step procedure for the preparation of N-heterocyclic carbene (NHC) stabilized silyliumylidene ions via dehydrochlorination from a Si(IV) precursor with NHCs is expanded to silyl-based substituents as well as aryl substituents with reduced steric bulk.

As a novel class of low-valent silicon compounds, silyliumylidene ions $[\text{RSi}]^+$ have gained increasing scientific interest over the last decade, as they exhibit a unique electronic structure: they combine the properties of silylenes $[\text{R}_2\text{Si}]$ and silylium ions $[\text{R}_3\text{Si}]^+$ into one silicon center and therefore feature a lone pair of electrons (with four total valence electrons), a positive charge and two vacant orbitals on the central silicon atom.¹ Si(II) cations are extremely reactive species² and their isolation generally necessitates kinetic and thermodynamic stabilization by bulky substituents and electron-donating ligands. Since Jutzi's initial report on the Me_5C_5 -stabilized Si(II) cation **I** in 2004³ (Fig. 1), the overwhelming majority of isolated silyliumylidene ions are three-coordinate and utilize two Lewis bases such as NHCs⁴ for stabilization and bear either an aryl- or halo-substituent at the silicon center (e.g. **IV–VII**).^{4a,5} Notable exceptions are the β -diketiminato-based (**II**)⁶ and the amidinate-stabilized (**III**)⁷ Si(II) cations and the impressive isolation of the NHC-stabilized parent silyliumylidene ion **V**.⁸

The synthetic approach for most reported silyliumylidene ions involves multi-step procedures with Si(II) precursors. These often laborious and difficult syntheses have unfortunately limited potential applications.^{5g,7,9} However, in 2014, our group reported a simple one-pot procedure for the isolation of NHC-stabilized silyliumylidene ions from easily accessible Si(IV) precursors.^{5b} Addition of three equivalents of IME_4

(1,3,4,5-tetramethylimidazol-2-ylidene) to aryldichlorosilanes $\text{R-SiCl}_2\text{H}$ ($\text{R} = m\text{-Ter, Tipp}$) leads to the selective formation of silyliumylidene ions **IV** and concomitant formation of imidazolium chloride. Since then, we have shown a variety of reactivities, including small molecule activation¹⁰ and transition metal coordination chemistry.¹¹ Unfortunately, this protocol has so far been limited to aryl substituents. Very recently, this approach was also utilized to isolate the Eind-substituted silyliumylidene **VI** from the corresponding aryldibromosilane.^{5d}

In order to generalize this synthetic protocol as well as expand the available substituent possibilities for silyliumylidenes, we envisioned the introduction of other groups on the central silicon atom using the same reductive dehydrochlorination approach. Because of the lack of a suitable synthetic procedure, no silyl-substituted silyliumylidene ions have been isolated so far. Owing to their tunable steric demand and strong σ -electron-donating properties,¹² silyl groups are excellent substituents for main group chemistry. In fact, our group has already demonstrated that they are useful and valuable for the isolation of various highly reactive and otherwise elusive low-valent main group compounds.¹³ We now report the first

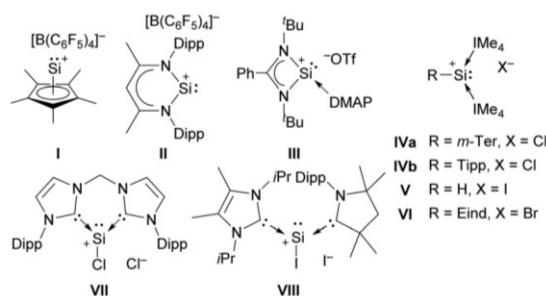


Fig. 1 Selected examples of silyliumylidene ions (I–III) and NHC-stabilized silyliumylidenes (IV–VIII); $m\text{-Ter} = 2,6\text{-Me}_2\text{C}_6\text{H}_3$, $\text{Mes} = 2,4,6\text{-Me}_3\text{C}_6\text{H}_2$, $\text{Tipp} = 2,4,6\text{-}i\text{Pr}_3\text{C}_6\text{H}_2$, $\text{Dipp} = 2,6\text{-}i\text{Pr}_2\text{C}_6\text{H}_3$, $\text{Eind} = 1,1,3,3,5,5,7,7\text{-octaethyl-s-hydrindacen-4-yl}$.

Department of Chemistry, WACKER-Institute of Silicon Chemistry and Catalysis Research Center, Technische Universität München, Lichtenbergstraße 4, 85748 Garching bei München, Germany. E-mail: s.inoue@tum.de

† Electronic supplementary information (ESI) available: Experimental details and crystallographic data. CCDC 1914471 for **1** and 1914472 for **2a**. For ESI and crystallographic data in CIF or other electronic format see DOI: 10.1039/c9dt02010a

silyl-substituted silyliumylidene ions synthesized *via* the same approach.

Similarly to the previously reported synthesis of **IV**,^{5b} addition of three equivalents of NHC (IME₄ or IET₂Me₂) to a silyl-substituted dichlorosilane precursor solution in toluene (or benzene) (Scheme 1) led to the formation of a yellow precipitate, consisting of a mixture of imidazolium chloride and silyliumylidene chloride. Product separation can be achieved by extraction of the precipitate with an acetonitrile/toluene mixture. The products can be isolated in moderate yields (56–65%) as yellow to orange air- and moisture sensitive solids. Furthermore, we set out to expand this one-pot procedure to aryl substituents with reduced steric bulk, because the size of the substituent has a profound influence on possible reactivities like activation of small organic substrates and coordination to transition metal complexes. Based on this, in addition to the previously reported bulky aryl substituents, we have been able to apply this approach to the less bulky mesityl system, affording **3**.

All silyliumylidene ions **1–3** show good solubility in pyridine, acetonitrile and (di-)fluorobenzene. Additionally, **2b** (NHC = IET₂Me₂) also shows good solubility in THF. While **IV** (R = *m*-Ter/Tipp) as well as **1–2** (R = ^tBu₃Si and ^tBu₂MeSi) are indefinitely stable in MeCN solution, **3** (R = Mes) fully decomposes to an unidentified mixture of products in less than four hours. However, compound **3** is stable in pyridine solution for at least three days.

It is worth mentioning that isolation of a silyliumylidene ion incorporating both the bulky supersilyl (^tBu₃Si) group as well as two IET₂Me₂ NHCs could not be achieved, presumably due to steric reasons. Similarly, employing sterically more demanding NHCs (*e.g.* I^tPr₂Me₂) with the ^tBu₂MeSi substituent did also not yield the desired products. We have also attempted to utilize the (TMS)₃Si group (TMS = Me₃Si) as a possible substituent with (TMS)₃Si–SiCl₂H as the starting material. Unfortunately, we were not able to isolate the corresponding NHC-stabilized silyliumylidene ion. In our experience, decomposition occurred at temperatures above –40 °C (presumably TMS group migration), which led to a mixture of products with TMS₄Si and imidazolium chloride as the main products.

²⁹Si NMR spectra for compounds **1–3** show sharp singlets in the expected range. The resonance of the central silicon atom in **3** (–71.2 ppm) is shifted slightly upfield compared to the bulky aryl substituted derivatives **IVa/b** (–68.8/–69.5 ppm). Introduction of the silyl substituent expectedly causes a more pronounced upfield shift to –82.0 ppm (**1**) and

–90.7/–86.2 ppm (**2a/2b**), presumably due to the stronger σ-donating properties of the silyl group. A similar trend can be observed between Müllers terphenyl-substituted IME₄-stabilized hydrosilylenes (–80.3/–87.6 ppm)¹⁴ and the ^tBu₃Si-substituted IME₄-stabilized hydrosilylene (–137.8 ppm) reported by our group.^{13a} ¹H NMR and ¹³C NMR spectra each show one signal set corresponding to the silyliumylidene substituent and the NHCs.

Single crystals suitable for X-ray diffraction (XRD) analysis of compound **1** and **2a** were obtained by slow diffusion of Et₂O into a concentrated MeCN solution at –35 °C and by storing a concentrated C₆H₄F₂ solution at –35 °C, respectively. Both silyliumylidene ions show the expected structure with a three-coordinate silicon centre with two NHC moieties and a distorted trigonal-pyramidal geometry around the central silicon atom (Fig. 2). A summary of the most important NMR and XRD data of the different silyliumylidene ions is given in Table 1. The shortest Si...Cl distances are 5.720/5.759 Å for **1** and **2a**, respectively (*cf.* 6.234 Å in **IVa**).^{5b} Si–Si bond lengths in **1** and **2a** (**1**: 2.424(1) Å; **2**: 2.388(1)/2.396(1) Å) are very similar to the Si–Si distance (2.415(1) Å) in the ^tBu₃Si-substituted hydrosilylene and of course significantly longer than the Si1–C1 bond length in **IVa** (1.935(2) Å (*ref.* 5b)). Si–C_{NHC} bond distances are very similar (1.937(2)/1.943(3) Å for **1**, *avg.* 1.944 Å for **2a** and 1.948(2)/1.967(2) Å for **IVa**^{5b}). The sum of the bond angles around the central silicon atom (*i.e.* the

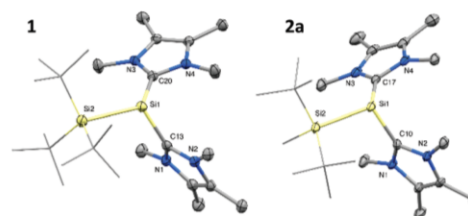
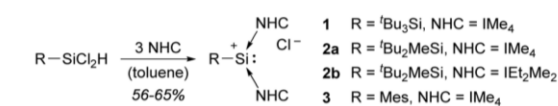


Fig. 2 Ellipsoid plot (50% probability level) of the molecular structures of silyl-silyliumylidene ions **1** (left) and **2a** (right, one out of two independent molecules in the asymmetric unit shown). Hydrogen atoms and anions are omitted for clarity. Selected bond lengths [Å] and angles [°]: **1**: Si1–Si2 2.424(1), Si1–C13 1.937(2), Si1–C20 1.943(3), Si2–Si1–C13 122.1(1), Si2–Si1–C20 113.5(1), C13–Si1–C20 93.1(1); **2a**: Si1–Si2 2.388(1)/2.396(1), Si1–C10 1.943(2)/1.940(3), Si1–C17 1.945(3)/1.947(3), Si2–Si1–C10 107.4(1)/105.8(1), Si2–Si1–C17 117.9(1)/117.5(1).

Table 1 Comparison of the ²⁹Si NMR data in CD₃CN (central Si atom) and XRD data of aryl-substituted (**IV**, **3**) and silyl-substituted (**1**, **2**) silyliumylidene ions

#	R	NHC	²⁹ Si NMR [ppm]	Si1–R [Å]	∑∠Si1 [°]
IVa	<i>m</i> -Ter	IME ₄	–68.8 (<i>ref.</i> 5b)	1.935(2)	310.2
IVb	Tipp	IME ₄	–69.5 (<i>ref.</i> 5b)	—	—
3	Mes	IME ₄	–71.2	—	—
1	^t Bu ₃ Si	IME ₄	–82.0	2.424(1)	328.7
2a	^t Bu ₂ MeSi	IME ₄	–90.7	Avg. 2.392	319.0
2b	^t Bu ₂ MeSi	IET ₂ Me ₂	–86.2	—	—



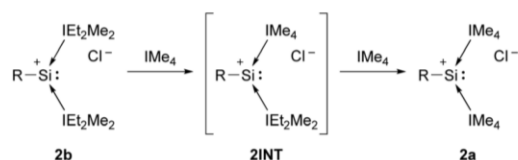
Scheme 1 Synthesis of silyl-substituted silyliumylidene ions **1–2** and aryl-substituted silyliumylidene ion **3**; IME₄ = 1,3,4,5-tetramethylimidazol-2-ylidene; IET₂Me₂ = 1,3-diethyl-4,5-dimethylimidazol-2-ylidene; Mes = 2,4,6-Me₃C₆H₂.

degree of pyramidalization) is 319.0° for **2a** and 328.7° in the case of **1**, which corresponds to a reduced pyramidalization compared to the 310.2° observed for **IVa**, and with that a reduced s character of the silicon-centered lone pair of the silyl-substituted silyliumylidene ions. This reduced pyramidalization can presumably be attributed to the introduction of the silyl-group and its strong σ -donor properties, as electropositive substituents lead to a lower degree of pyramidalization.¹⁵ This effect can also be observed in silyl-substituted silyl-radicals, which show a very low degree of pyramidalization.¹⁶

As multiple NHC exchange reactions of NHC-stabilized low-valent group 14 compounds have been reported in recent years,¹⁷ we examined whether an exchange of the coordinated IEt_2Me_2 moieties in **2b** to the more σ -electron-donating and less bulky NHC IME_4 could be achieved. Indeed, treatment of an orange THF solution of **2b** with two molar equivalents of IME_4 at room temperature resulted in rapid precipitation of a yellow solid (Scheme 2). After washing the precipitate with THF to remove free IEt_2Me_2 , compound **2a** could be isolated in 82% yield.

Importantly, precipitation as the driving force is not necessary, as the exchange reaction can also be carried out in fluorobenzene- d_5 where both starting material **2b** and product **2a** are well soluble and then easily monitored *via* ^1H NMR (*cf.* ESI Fig. S22–S23[†]). Intermediate formation of a mixed $\text{IEt}_2\text{Me}_2/\text{IME}_4$ silyliumylidene **2INT** can be clearly observed *via* ^1H and ^{29}Si NMR (*cf.* ESI Fig. S24[†]). As expected, the ^{29}Si NMR resonance of the central silicon atom of **2INT** (-89.2 ppm) falls between the resonances of **2b** (-86.2 ppm) and **2a** (-90.7 ppm). Unfortunately, isolation of **2INT** was, so far, not possible.

Fig. 3 shows the time-dependent relative concentrations of starting material **2b**, intermediate **2INT** and product **2a**, which can be derived from the NMR data. Because of the presence of two molar equivalents of free IME_4 , the first NHC exchange occurs rapidly, with about 90% of **2b** being consumed after just 27 minutes. This exchange slows down as more IME_4 is consumed to form **2a** from **2INT**, therefore full consumption of **2b** occurs after roughly 150 minutes. The maximum concentration of **2INT** (62%) is reached after 20 minutes of reaction time. After 300 minutes, 91% **2a** and 9% **2INT** is present in the mixture while full conversion to **2a** is achieved after 24 hours. Presumably, these exchange reactions follow the 2nd order rate law (*i.e.* linear relation between $1/c_{\text{2INT}}$ and the reaction time, *cf.* ESI Fig. S28[†]), indicating an associative $\text{S}_{\text{N}}2$ -type mechanism, similarly to the NHC exchange reactions observed for NHC-stabilized silylenes by Jana and Scheschkewitz *et al.*^{17b}



Scheme 2 NHC exchange of silyliumylidene ion **2b** to **2a** via the mixed-NHC silyliumylidene **2INT**; $\text{R} = ^t\text{Bu}_2\text{MeSi}$.

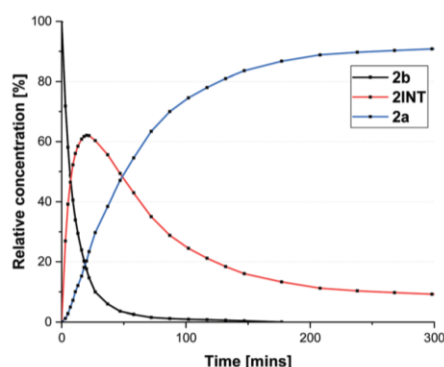


Fig. 3 Plot of the change in the relative concentrations of **2b**, **2INT** and **2a** with time in the NHC exchange reaction of **2b** to **2a** with IME_4 .

The reverse reaction, *i.e.* exchange of IME_4 with IEt_2Me_2 could not be achieved, even with a large excess of IEt_2Me_2 . This can be attributed to the increased σ -donor strength of IME_4 .

Conclusions

In conclusion, we present the expansion of a convenient preparation method for NHC-stabilized silyliumylidene ions to silyl groups as well as sterically less demanding aryl substituents. The first silyl-substituted silyliumylidene ions **1**, **2a** and **2b** have been prepared and fully characterized. Furthermore, we were able to show that the coordinated IEt_2Me_2 moieties in **2b** can easily be exchanged to the more σ -electron-donating NHC IME_4 . Novel reactivity investigations of these silyliumylidene ions, including coordination chemistry with transition metals, are currently under investigation in our laboratory and will be reported in due course.

Conflicts of interest

The authors declare no conflicts of interest.

Acknowledgements

We are exceptionally grateful to the WACKER Chemie AG and the H2020 European Research Council (SILION 637394) for continued financial support. We are also thankful to Dr A. Pöthig and Dr C. Jandl for advice pertaining to crystallography and to L. Schiegerl for recording the ESI-MS spectra.

References

- G. Bertrand, *Science*, 2004, **305**, 783–785.
- C. Gerdes, W. Saak, D. Haase and T. Müller, *J. Am. Chem. Soc.*, 2013, **135**, 10353–10361.

- 3 P. Jutzi, A. Mix, B. Rummel, W. W. Schoeller, B. Neumann and H.-G. Stammer, *Science*, 2004, **305**, 849–851.
- 4 (a) V. Nesterov, D. Reiter, P. Bag, P. Frisch, R. Holzner, A. Porzelt and S. Inoue, *Chem. Rev.*, 2018, **118**, 9678–9842; (b) S. L. Powley and S. Inoue, *Chem. Rec.*, 2019, DOI: 10.1002/tcr.201800188.
- 5 (a) Y. Xiong, S. Yao, S. Inoue, E. Irran and M. Driess, *Angew. Chem., Int. Ed.*, 2012, **51**, 10074–10077; (b) S. U. Ahmad, T. Szilvási and S. Inoue, *Chem. Commun.*, 2014, **50**, 12619–12622; (c) A. C. Filippou, Y. N. Lebedev, O. Chernov, M. Straßmann and G. Schnakenburg, *Angew. Chem., Int. Ed.*, 2013, **52**, 6974–6978; (d) N. Hayakawa, K. Sadamori, S. Mizutani, T. Agou, T. Sugahara, T. Sasamori, N. Tokitoh, D. Hashizume and T. Matsuo, *Inorganics*, 2018, **6**, 30; (e) T. Agou, N. Hayakawa, T. Sasamori, T. Matsuo, D. Hashizume and N. Tokitoh, *Chem. – Eur. J.*, 2014, **20**, 9246–9249; (f) Y. Li, Y.-C. Chan, Y. Li, I. Purushothaman, S. De, P. Parameswaran and C.-W. So, *Inorg. Chem.*, 2016, **55**, 9091–9098; (g) Y. Xiong, S. Yao, S. Inoue, J. D. Epping and M. Driess, *Angew. Chem., Int. Ed.*, 2013, **52**, 7147–7150.
- 6 M. Driess, S. Yao, M. Brym and C. van Wüllen, *Angew. Chem., Int. Ed.*, 2006, **45**, 6730–6733.
- 7 H.-X. Yeong, H.-W. Xi, Y. Li, K. H. Lim and C.-W. So, *Chem. – Eur. J.*, 2013, **19**, 11786–11790.
- 8 Y. Li, Y.-C. Chan, B.-X. Leong, Y. Li, E. Richards, I. Purushothaman, S. De, P. Parameswaran and C.-W. So, *Angew. Chem., Int. Ed.*, 2017, **56**, 7573–7578.
- 9 P. Jutzi, *Chem. – Eur. J.*, 2014, **20**, 9192–9207.
- 10 (a) S. U. Ahmad, T. Szilvási, E. Irran and S. Inoue, *J. Am. Chem. Soc.*, 2015, **137**, 5828–5836; (b) D. Sarkar, D. Wendel, S. U. Ahmad, T. Szilvási, A. Pöthig and S. Inoue, *Dalton Trans.*, 2017, **46**, 16014–16018; (c) D. Sarkar, V. Nesterov, T. Szilvasi, P. J. Altmann and S. Inoue, *Chem. – Eur. J.*, 2019, **25**, 1198–1202; (d) A. Porzelt, J. Schweizer, R. Baierl, P. J. Altmann, M. Holthausen and S. Inoue, *Inorganics*, 2018, **6**, 54.
- 11 P. Frisch and S. Inoue, *Chem. Commun.*, 2018, **54**, 13658–13661.
- 12 N. Wiberg, K. Amelunxen, H. W. Lerner, H. Schuster, H. Nöth, I. Krossing, M. Schmidt-Amelunxen and T. Seifert, *J. Organomet. Chem.*, 1997, **542**, 1–18.
- 13 (a) S. Inoue and C. Eisenhut, *J. Am. Chem. Soc.*, 2013, **135**, 18315–18318; (b) P. Bag, A. Porzelt, P. J. Altmann and S. Inoue, *J. Am. Chem. Soc.*, 2017, **139**, 14384–14387; (c) D. Wendel, T. Szilvási, C. Jandl, S. Inoue and B. Rieger, *J. Am. Chem. Soc.*, 2017, **139**, 9156–9159; (d) D. Wendel, D. Reiter, A. Porzelt, P. J. Altmann, S. Inoue and B. Rieger, *J. Am. Chem. Soc.*, 2017, **139**, 17193–17198.
- 14 D. Lutters, C. Severin, M. Schmidtman and T. Müller, *J. Am. Chem. Soc.*, 2016, **138**, 6061–6067.
- 15 B. Tumanskii, M. Karni and Y. Apeloig, in *Encyclopedia of Radicals in Chemistry, Biology and Materials*, ed. C. Chatgililoglu and A. Studer, 2012, DOI: 10.1002/9781119953678.rad066.
- 16 (a) A. Sekiguchi, T. Fukawa, M. Nakamoto, V. Y. Lee and M. Ichinohe, *J. Am. Chem. Soc.*, 2002, **124**, 9865–9869; (b) A. Sekiguchi, S. Inoue, M. Ichinohe and Y. Arai, *J. Am. Chem. Soc.*, 2004, **126**, 9626–9629.
- 17 (a) A. Jana, I. Omlor, V. Huch, H. S. Rzepa and D. Scheschkewitz, *Angew. Chem., Int. Ed.*, 2014, **53**, 9953–9956; (b) A. Maiti, D. Mandal, I. Omlor, D. Dhara, L. Klemmer, V. Huch, M. Zimmer, D. Scheschkewitz and A. Jana, *Inorg. Chem.*, 2019, **58**, 4071–4075; (c) H. Cui, M. Wu and P. Teng, *Eur. J. Inorg. Chem.*, 2016, **2016**, 4123–4127; (d) B. J. Guddorf, A. Hepp and F. Lips, *Chem. – Eur. J.*, 2018, **24**, 10334–10338.

5. Coinage Metal Complexes of NHC-stabilized Silyliumylidene Ions

Title: “Coinage metal complexes of NHC-stabilized silyliumylidene ions”¹⁵³

Status: Communication; published online: October 18, 2018.

Journal: *Chemical Communications* **2018**, *54*, 13658–13661.

Publisher: Royal Society of Chemistry

DOI: [10.1039/C8CC07754A](https://doi.org/10.1039/C8CC07754A)

Authors: Philipp Frisch and Shigeyoshi Inoue^a

Reproduced by permission of The Royal Society of Chemistry. © 2018 The Royal Society of Chemistry.

Content: In recent years, silyliumylidene ions [R–Si:]⁺ have shown to be intriguing low-valent silicon species with a unique electronic structure: they combine the properties of silylenes [R₂Si:] – a lone pair of electrons and an empty p-orbital – with those of silylium ions [R₃Si]⁺ – a positive charge and an empty p-orbital – into a single silicon center. Because of the presence of this stereochemically active lone pair on the silicon center, Si(II) cations can act as ligands in transition metal complexes just like silylenes or carbenes.

This publication describes the synthesis of the first coinage metal complexes of a silyliumylidene ion through addition of simple metal salt precursors (CuCl, AgOTf, (Me₂S)AuCl) directly to NHC-stabilized silyliumylidene ions [R–Si(IMe₄)₂]Cl (R = *m*-terphenyl, Tipp) and constitutes the entry of our group into the coordination chemistry of Si(II) cations. Isolation of these complexes can be seen as a proof of concept that NHC-stabilized silyliumylidene ions can in fact act as ligands in transition metal complexes.

Coordination of the silyliumylidene ion to the group 11 metal is readily apparent by the rapid decolorization of the initially bright orange solution and a significant downfield shift of the ²⁹Si NMR resonance that gets progressively stronger with increasing atomic number of the transition metal. The complexes show a monomeric structure in the solid state with a four-coordinate silicon center that still carries both NHC ligands and Si–M bond lengths in the expected range. A reduction in steric bulk of the aryl substituent (from *m*-terphenyl to Tipp) on the silyliumylidene ion leads to a dimerization of the complexes *via* the M–Cl bonds. Additionally, the complexes with the smaller substituents show significantly lower stability in solution, rapidly decomposing at room temperature to unidentified silicon species and transition metal bis(NHC) complexes.

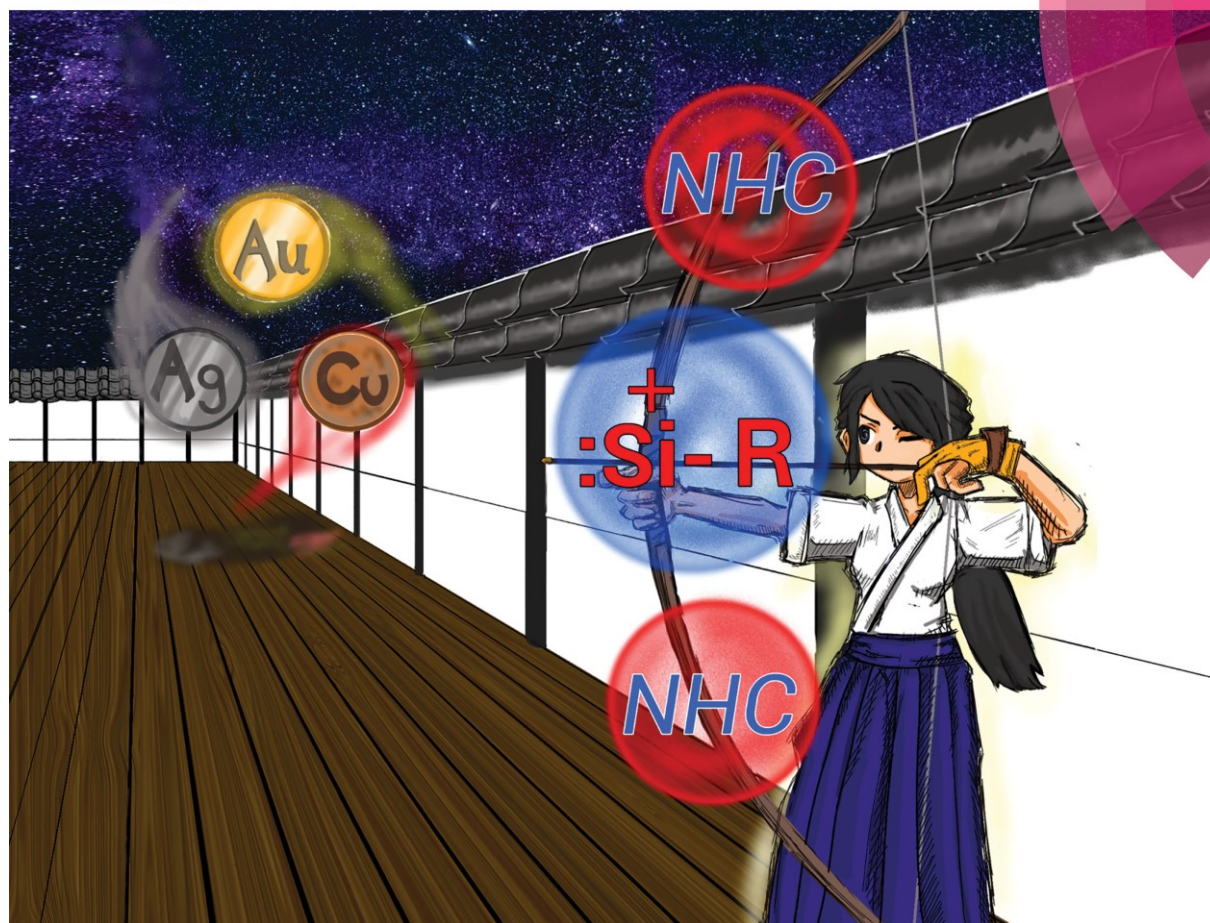
^aP. Frisch planned and executed all experiments, conducted the SC-XRD measurements including processing of the data and wrote the manuscript. All work was performed under the supervision of S. Inoue.

Inside Front Cover of Chemical Communications Volume 54, Number 97.

Volume 54 | Number 97 | 18 December 2018 | Pages 13609–13752

ChemComm

Chemical Communications
rsc.li/chemcomm



ISSN 1359-7345



COMMUNICATION
Philipp Frisch and Shigeyoshi Inoue
Coinage metal complexes of NHC-stabilized silyliumylidene ions



ChemComm

COMMUNICATION

View Article Online

View Journal | View Issue



Coinage metal complexes of NHC-stabilized silyliumylidene ions†

Philipp Frisch and Shigeyoshi Inoue *

 Cite this: *Chem. Commun.*, 2018, **54**, 13658

 Received 27th September 2018,
Accepted 18th October 2018

DOI: 10.1039/c8cc07754a

rsc.li/chemcomm

The first silyliumylidene ion coinage metal complexes are reported. Treatment of N-heterocyclic carbene (NHC) stabilized silyliumylidene ions (R = *m*-Ter, Tipp) with transition metal precursors (CuCl, AgOTf, (Me₂S)AuCl) yields the first silyliumylidene coinage metal (M = Cu, Ag, Au) complexes, which have been fully characterized including X-ray diffraction analyses.

Silyliumylidene ions [RSi:]⁺ are a relatively new class of low-valent silicon compounds that feature a positive charge, a lone pair of electrons and two vacant orbitals on the silicon center.¹ Their successful isolation generally requires steric and electronic stabilization of the Si(II) cation by utilization of bulky substituents as well as external donors (e.g. NHCs).² A number of silyliumylidenes³ have been reported since Jutzi's seminal work on the pentamethylcyclopentadienyl silyliumylidene ion [Cp*Si:][B(C₆F₅)₄] in 2004.⁴ So far, reactivity investigations remain limited to the activation of few small molecules and some specific subsequent reactions.^{3c,i,j,5}

Due to the presence of a lone pair on the silicon atom – similarly to silylenes⁶ – silyliumylidene ions should also be able to act as ligands in transition metal complexes. However, it is important to note that the external donors required to stabilize the Si(II) cations generally reduce their π-acceptor ability by (partially) filling the vacant orbitals on the silicon center.

In contrast to silylenes, the coordination behavior of silyliumylidene ions has been barely explored. In 2013, we described bis(platinum) and bis(palladium) complexes **I** and **II** (Fig. 1), which can formally be regarded as base-stabilized silyliumylidene-phosphide complexes.⁷ In 2014, So *et al.* reported rhodium (**III**) and tungsten (**IV**) complexes of a base-stabilized Si(II) cation.⁸ Very recently, Filippou *et al.* also

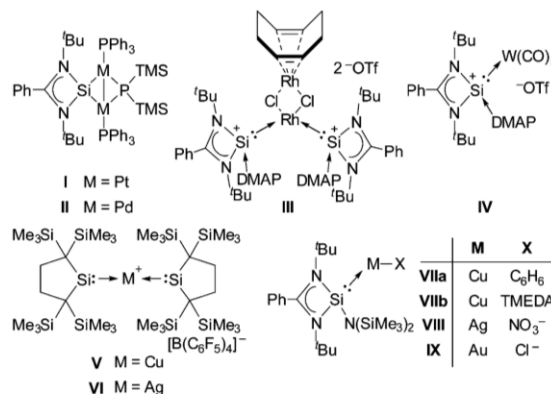


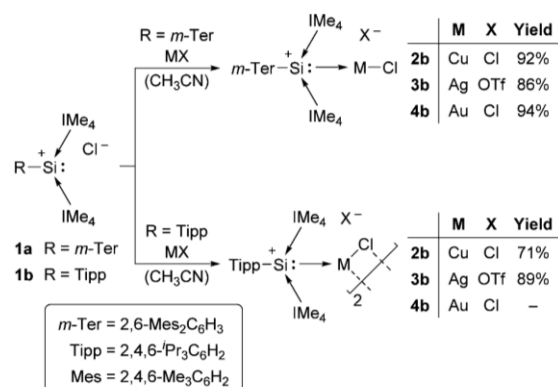
Fig. 1 Examples of (formal) silyliumylidene transition metal complexes (I–IV) as well as silylene coinage metal complexes (V–IX); DMAP = 4-dimethylaminopyridine; TMEDA = tetramethylethylenediamine.

reported a molybdenum silyliumylidene complex synthesized from [Cp*Si:][B(C₆F₅)₄].^{5e}

While a variety of coinage metal compounds with silyl-based substituents have been reported over the last decades,⁹ group 11 complexes incorporating ligands with a low-valent silicon atom are quite rare. For example, Jutzi *et al.* described the AuCl complex of [(Cp*)₂Si:], however, no crystal structure was reported.¹⁰ Dialkylsilylene complexes of copper (V) and silver (VI)¹¹ and silacyclopropylidene complexes of copper and gold were structurally characterized.¹² In recent years, Roesky's silylene [PhC(N^tBu)₂]SiX (X = Cl, N(SiMe₃)₂)¹³ has shown great potential in the isolation of various monomeric and dimeric silylene coinage metal complexes VII–IX.¹⁴ However, no coinage metal complexes with silyliumylidene ions as a ligand have been reported so far. Motivated by our recent reports on the interesting chemistry of NHC-stabilized silyliumylidene ions **1**^{3e,5a,b,15} we set out to utilize **1** as ligands in transition metal complexes. Herein we disclose the first silyliumylidene coinage metal complexes synthesized from stable NHC-stabilized Si(II) cations.

Department of Chemistry, WACKER-Institute of Silicon Chemistry and Catalysis Research Center, Technische Universität München, Lichtenbergstraße 4, 85748 Garching bei München, Germany. E-mail: s.inoue@tum.de

† Electronic supplementary information (ESI) available: Experimental details and crystallographic data. CCDC 1870254 (2a), 1870256 (3a), 1870258 (3b), 1870255 (4a) and 1870257 (5). For ESI and crystallographic data in CIF or other electronic format see DOI: 10.1039/c8cc07754a



Scheme 1 Synthesis of NHC-stabilized silyliumylidene ion coinage metal complexes **2–4** (MX = CuCl (**2**), AgOTf (**3**), (Me₂S)AuCl (**4**)); IMe₄ = 1,3,4,5-tetramethylimidazol-2-ylidene.

As shown in Scheme 1, the coinage metal complexes **2–4** can be conveniently synthesized by addition of simple metal precursors (CuCl, AgOTf, (Me₂S)AuCl) to the silyliumylidene ions **1**. Treatment of an acetonitrile solution of **1a** or **1b** with one equivalent of copper(i)chloride (Scheme 1) results in dissolution of the salt accompanied by rapid decolorization of the orange solution. A similar reactivity can be observed upon addition of (Me₂S)AuCl. In the case of AgOTf, addition of the coinage metal salt leads to immediate precipitation of a colorless solid (AgCl) without any color change of the solution. This is due to an anion exchange of the chloride counter anion in **1** to a triflate anion. After stirring for 5 minutes, the colorless precipitate gradually dissolves and the solution changes color from orange to colorless. Complexes **2–4** can be isolated as air- and moisture-sensitive (in the case of **3a** and **3b** also light-sensitive) colorless solids in good to excellent yield (71–94%) by crystallization from a MeCN–Et₂O mixture at –40 °C. The complexes are insoluble in benzene, hexane and Et₂O and show good solubility in pyridine, difluorobenzene and acetonitrile.

The coordination of the coinage metal to the silyliumylidene ion is accompanied by a downfield shift of the ²⁹Si NMR resonance (Table 1) from –68.8/–69.5 ppm (**1a/1b**)^{3e} to –46.6/–48.8 (**2a/2b**, M = Cu), –44.1/–46.6 (**3a/3b**, M = Ag) and –34.6/–38.0 ppm (**4a/4b**, M = Au), however the downfield shift is significantly less pronounced than the one observed by So *et al.* upon coordination of their DMAP-stabilized silyliumylidene to rhodium and tungsten (–82.3 to +40.5 and +51.6 ppm, respectively).⁸ For comparison, the reported silylene coinage metal complexes show resonances in a relatively narrow range, e.g. 4.4 ppm (**VIIa**),^{14d} 7.9 ppm (**VIII**)^{14a} and 8.8 ppm (**IX**).^{14a} It is noteworthy that the ²⁹Si NMR of silver complex **3a** shows two doublets at –44.1 ppm corresponding to the ¹⁰⁹Ag and ¹⁰⁷Ag isotopes with coupling constants of ¹J_{Si¹⁰⁹Ag} = 408.1 Hz and ¹J_{Si¹⁰⁷Ag} = 352.6 Hz. Similarly, complex **3b** also shows two doublets at –46.6 ppm, with coupling constants of ¹J_{Si¹⁰⁹Ag} = 410.1 Hz and ¹J_{Si¹⁰⁷Ag} = 355.8 Hz. The ¹H NMR spectra of the *m*-Ter substituted complexes **2a–4a** are quite similar, each

Table 1 Comparison of the ²⁹Si NMR and XRD data of silyliumylidene ions **1**^{3e} and the coinage metal complexes **2–4**

#	R	M	²⁹ Si NMR [ppm]	Si1–M1 [Å]	Si1–M1–Cl1 [°]
1a	<i>m</i> -Ter	—	–68.8	—	—
1b	Tipp	—	–69.5	—	—
2a	<i>m</i> -Ter	Cu	–46.6	2.238(2)	169.3(1)
2b	Tipp	Cu	–48.8	—	—
3a	<i>m</i> -Ter	Ag	–44.1	2.379(1)	171.8(1)
3b	Tipp	Ag	–46.6	2.398(1)	141.2(1)
4a	<i>m</i> -Ter	Au	–34.6	2.281(1)	176.8(1)
4b	Tipp	Au	–38.0	—	—

showing a single signal set for the *m*-terphenyl ligand with a broadened singlet for the mesityl CH-groups, which split into two separate singlets at –40 °C (*cf.* ESI,† Fig. S5 for VT-NMR). The NHC wingtip CH₃ groups split into two broad signals from one broad signal observed for the silyliumylidene ion **1a**,^{3e} which also coalesce into one signal at +60 °C. The NHC backbone methyl groups as well as the mesityl methyl groups give only one broad signal in total. At low temperature (–40 °C) as well as high temperature (+60 °C), this broad signal splits into multiple singlets corresponding to each unique methyl group. The ¹³C NMR spectra show resonances for the carbene carbon atoms and one signal set for the *m*-terphenyl ligand. Line broadening can also be observed. The ¹³C NMR spectra of **3** also exhibit a quartet at 122.1 ppm corresponding to the CF₃SO₃[–] anion (¹J_{CF} = 321.0 Hz).

Interestingly, no signal broadening or splitting in the ¹H NMR spectra of the Tipp substituted complexes **2b–4b** can be observed. This corresponds to a less restricted rotation of the Tipp group and the coordinated NHCs due to the reduced steric bulk of the Tipp substituent compared to the *m*-Ter group. Compared to starting material **1b**, the signals in the complexes appear slightly shifted downfield, except for the septet corresponding to the *ortho* iso-propyl groups, which appears shifted upfield. While we could observe gold complex **4b** by ¹H and ²⁹Si NMR, we were unable to obtain satisfactory analytical data due to rapid decomposition (*cf.* ESI,† Fig. S20–S25).

Single crystals suitable for XRD measurements of all three *m*-Ter substituted complexes **2a–4a** were obtained by slow diffusion of Et₂O into a concentrated acetonitrile solution at –40 °C. As expected, the solid-state structures of the complexes are very similar (Fig. 2). All three compounds are monomers in the solid state and feature a four-coordinate silicon(II) center with a distorted tetrahedral geometry. Going from copper to silver, an increase in the Si–M bond length (2.238(2) and 2.379(1) Å, respectively) is observed while going from Ag to Au the bond length decreases (2.379(1) to 2.281(1) Å, respectively). This is unsurprising since it has been previously shown that gold is indeed smaller than silver.¹⁶ Frenking *et al.* also reported that, among the coinage metals, silylenes form their strongest coordination complexes with gold,¹⁷ which could also explain a decrease in bond length. Furthermore, a similar trend can be observed in the coinage metal silylene complexes

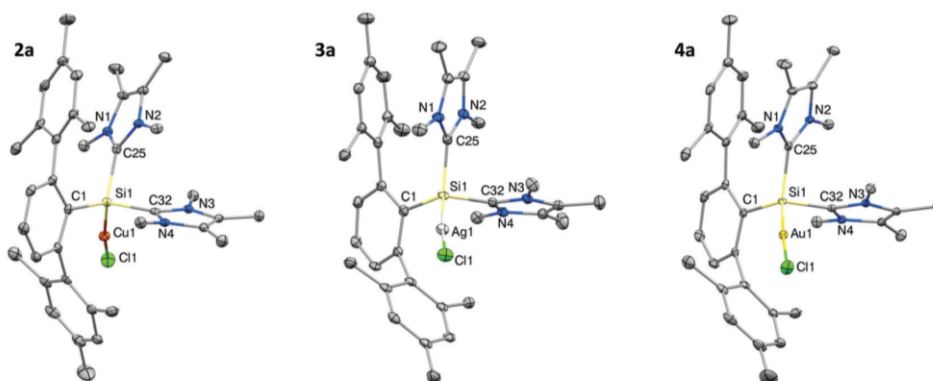


Fig. 2 Ellipsoid plot (50% probability level) of the molecular structures of complexes **2a** (left), **3a** (middle) and **4a** (right). Hydrogen atoms and anions are omitted for clarity. Selected bond lengths [Å] and angles [°]: **2a**: Si1–C1 1.916(3), Si1–C25 1.939(2), Si1–C32 1.938(2), Si1–Cu1 2.238(2), Cu1–Cl1 2.1477(6), Si1–Cu1–Cl1 169.3(1), C25–Si1–C32 95.5(2), C1–Si1–Cu1 119.4(2); **3a**: Si1–C1 1.911(4), Si1–C25 1.936(3), Si1–C32 1.938(4), Si1–Ag1 2.379(1), Ag1–Cl1 2.366(1), Si1–Ag1–Cl1 171.8(1), C25–Si1–C32 95.8(1), C1–Si1–Ag1 114.8(1); **4a**: Si1–C1 1.916(2), Si1–C25 1.942(2), Si1–C32 1.941(2), Si1–Au1 2.281(1), Au1–Cl1 2.354(1), Si1–Au1–Cl1 176.8(1), C25–Si1–C32 96.5(1), C1–Si1–Au1 119.0(1).

reported by Khan *et al.*^{14a} The M–Si bond length in all three complexes lies in the same range as previously reported Si(II) coinage metal complexes (Cu: 2.171^{14e}–2.289¹⁸ Å; Ag: 2.337^{14a}–2.425^{14c} Å; Au: 2.246^{14b}–2.318^{14b} Å). With increasing atomic number of the transition metal, the linearity of the M–Si1–Cl1 bond increases from 169.3(1)° to 171.8(1)° from Cu to Ag and finally to 176.8(1)° for the gold complex. The angle between the two coordinated NHCs (C25–Si1–C32) increases slightly from the silyliumylidene ion **1a** (93.8(1)°)^{3e} to 95.5(2)°, 95.8(2)° and 96.5(1)° for **2a**, **3a** and **4a**, respectively.

Single crystals suitable for XRD analysis for complex **3b** were obtained by diffusion of Et₂O into a concentrated solution of **3b** in CH₃CN:C₇H₈ (2:1) at –40 °C. Interestingly, the complex shows a dimeric structure in the solid state (Fig. 3). The two silyliumylidene ligands are bridged *via* a 4-membered Ag₂Cl₂ ring. The Si1–Ag1–Cl1 angle (141.2(1)°) is significantly smaller than in the monomeric complexes. The dimerization is most

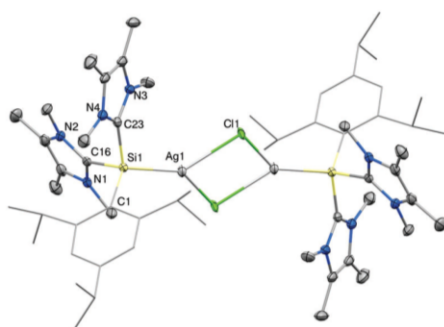
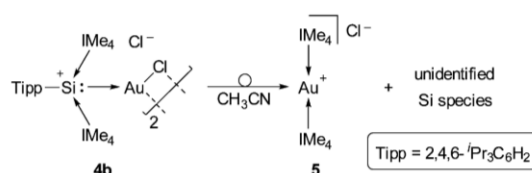


Fig. 3 Ellipsoid plot (50% probability level) of the molecular structure of complex **3b**. Hydrogen atoms and anions are omitted for clarity and the Tipp substituents are depicted as wireframes. Selected bond lengths [Å] and angles [°]: Si1–C1 1.919(2), Si1–C16 1.935(2), Si1–C23 1.931(2), Si1–Ag1 2.398(1), Ag1–Cl1 2.562(1), Si1–Ag1–Cl1 141.2(1), C16–Si1–C23 100.8(1), C1–Si1–Ag1 118.0(1).

likely a result of the reduced steric bulk of the Tipp ligand. The Si–Ag bond length (2.398(1) Å) is slightly longer than in **3a**, a possible consequence of the dimeric structure, but still well within the reported Si–Ag bond range. Due to their marked instability, we were not able to obtain single crystals of complex **2b** and **4b**, but judging from their comparable reactivity and similar ¹H and ²⁹Si NMR data, it is expected that their structures are analogous.

While the *m*-terphenyl substituted compounds are stable indefinitely in the solid state and for weeks in acetonitrile solution at room temperature (under exclusion of light for **3a**), slow decomposition occurs in C₆H₄F₂ and pyridine. Decomposition also occurs slowly in acetonitrile upon heating at 90 °C, resulting in an unidentified product mixture. In contrast, the Tipp substituted complexes undergo full decomposition over a period of 2 to 4 hours (Scheme 2), which is accompanied by an NHC migration to the metal center. For example, the decomposition of an acetonitrile solution of gold complex **4b** results in a linearly coordinated [(IME₄)₂Au]Cl complex (**5**, *cf.* ESI[†] for SC-XRD and NMR data) and two silicon-containing species with a significantly upfield shifted ²⁹Si NMR resonance (40.5 and 64.0 ppm, respectively; *cf.* –38 ppm for **4b**). Unfortunately, we were not able to unambiguously determine the composition of these silicon-containing species.

In summary, we have reported the first coinage metal complexes 2–4 of an NHC-stabilized silyliumylidene ion. They were



Scheme 2 Decomposition of the Tipp-substituted Au complex **4b** in solution to [Au(IME₄)₂]Cl (**5**) and unidentified Si species.

synthesized from the NHC-stabilized silyliumylidene ions **1** via addition of simple metal salts. The complexes bearing the sterically demanding *m*-terphenyl substituent show a monomeric structure in the solid state and are stable for weeks in acetonitrile solution. On the other hand, the complexes having the smaller Tipp substituent reveal a dimeric structure and a significant decrease in stability. Possible catalytic applications of the complexes as well as their reactivity are currently under investigation in our laboratory.

We are grateful to the WACKER Chemie AG and the European Research Council (SILION 637394) for continued financial support. We are also thankful to Dr A. Pöthig and Dr C. Jandl for advice pertaining to crystallography and L. Schiegl, MSc for recording the ESI-MS spectra.

Conflicts of interest

There are no conflicts of interest.

References

- G. Bertrand, *Science*, 2004, **305**, 783–785.
- V. Nesterov, D. Reiter, P. Bag, P. Frisch, R. Holzner, A. Porzelt and S. Inoue, *Chem. Rev.*, 2018, **118**, 9678–9842.
- For silyliumylidene ions, see: (a) M. Driess, S. Yao, M. Brym and C. van Wüllen, *Angew. Chem., Int. Ed.*, 2006, **45**, 6730–6733; (b) A. C. Filippou, Y. N. Lebedev, O. Chernov, M. Straßmann and G. Schnakenburg, *Angew. Chem., Int. Ed.*, 2013, **52**, 6974–6978; (c) Y. Xiong, S. Yao, S. Inoue, J. D. Epping and M. Driess, *Angew. Chem., Int. Ed.*, 2013, **52**, 7147–7150; (d) T. Agou, N. Hayakawa, T. Sasamori, T. Matsuo, D. Hashizume and N. Tokitoh, *Chem. – Eur. J.*, 2014, **20**, 9246–9249; (e) S. U. Ahmad, T. Szilvási and S. Inoue, *Chem. Commun.*, 2014, **50**, 12619–12622; (f) N. Hayakawa, K. Sadamori, S. Mizutani, T. Agou, T. Sugahara, T. Sasamori, N. Tokitoh, D. Hashizume and T. Matsuo, *Inorganics*, 2018, **6**, 30; (g) Y. Li, Y.-C. Chan, Y. Li, I. Purushothaman, S. De, P. Parameswaran and C.-W. So, *Inorg. Chem.*, 2016, **55**, 9091–9098; (h) Y. Li, Y. C. Chan, B. X. Leong, Y. Li, E. Richards, I. Purushothaman, S. De, P. Parameswaran and C.-W. So, *Angew. Chem., Int. Ed.*, 2017, **56**, 7573–7578; (i) H.-X. Yeong, H.-W. Xi, Y. Li, K. H. Lim and C.-W. So, *Chem. – Eur. J.*, 2013, **19**, 11786–11790; (j) Y. Xiong, S. Yao, S. Inoue, E. Irran and M. Driess, *Angew. Chem., Int. Ed.*, 2012, **51**, 10074–10077, and references therein.
- P. Jutzi, A. Mix, B. Rummel, W. W. Schoeller, B. Neumann and H.-G. Stammer, *Science*, 2004, **305**, 849–851.
- For reactivity of silyliumylidenes, see: (a) D. Sarkar, D. Wendel, S. U. Ahmad, T. Szilvási, A. Pöthig and S. Inoue, *Dalton Trans.*, 2017, **46**, 16014–16018; (b) A. Porzelt, J. Schweizer, R. Baierl, P. Altmann, M. Holthausen and S. Inoue, *Inorganics*, 2018, **6**, 54; (c) P. Jutzi, K. Leszczyńska, A. Mix, B. Neumann, W. W. Schoeller and H.-G. Stammer, *Organometallics*, 2009, **28**, 1985–1987; (d) K. Leszczyńska, A. Mix, R. J. F. Berger, B. Rummel, B. Neumann, H.-G. Stammer and P. Jutzi, *Angew. Chem., Int. Ed.*, 2011, **50**, 6843–6846; (e) P. Ghana, M. I. Arz, G. Schnakenburg, M. Straßmann and A. C. Filippou, *Organometallics*, 2018, **37**, 772–780; (f) P. Jutzi, *Chem. – Eur. J.*, 2014, **20**, 9192–9207.
- B. Blom, M. Stoelzel and M. Driess, *Chem. – Eur. J.*, 2013, **19**, 40–62.
- N. C. Breit, T. Szilvási, T. Suzuki, D. Gallego and S. Inoue, *J. Am. Chem. Soc.*, 2013, **135**, 17958–17968.
- H.-X. Yeong, Y. Li and C.-W. So, *Organometallics*, 2014, **33**, 3646–3648.
- For coinage metal silyl complexes, see: (a) J. D. Farwell, P. B. Hitchcock, M. F. Lappert and A. V. Protchenko, *J. Organomet. Chem.*, 2007, **692**, 4953–4961; (b) G. Tan, B. Blom, D. Gallego, E. Irran and M. Driess, *Chem. – Eur. J.*, 2014, **20**, 9400–9408; (c) M. Walewska, J. Hlina, W. Gaderbauer, H. Wagner, J. Baumgartner and C. Marschner, *Z. Anorg. Allg. Chem.*, 2016, **642**, 1304–1313; (d) M. J. Sgro, W. E. Piers and P. E. Romero, *Dalton Trans.*, 2015, **44**, 3817–3828; (e) M. Joost, P. Gualco, S. Mallet-Ladeira, A. Amgoune and D. Bourissou, *Angew. Chem., Int. Ed.*, 2013, **52**, 7160–7163; (f) M. Wilfling and K. W. Klinkhammer, *Angew. Chem., Int. Ed.*, 2010, **49**, 3219–3223; (g) M. Theil, P. Jutzi, B. Neumann, A. Stammer and H.-G. Stammer, *J. Organomet. Chem.*, 2002, **662**, 34–42, and references therein.
- P. Jutzi and A. Möhrke, *Angew. Chem., Int. Ed. Engl.*, 1990, **29**, 893–894.
- Y. Inagawa, S. Ishida and T. Iwamoto, *Chem. Lett.*, 2014, **43**, 1665–1667.
- T. Troadec, A. Prades, R. Rodriguez, R. Mirgalet, A. Baceiredo, N. Saffon-Merceron, V. Branchadell and T. Kato, *Inorg. Chem.*, 2016, **55**, 8234–8240.
- (a) C.-W. So, H. W. Roesky, J. Magull and R. B. Oswald, *Angew. Chem., Int. Ed.*, 2006, **45**, 3948–3950; (b) R. Azhakar, R. S. Ghadwal, H. W. Roesky, H. Wolf and D. Stalke, *Organometallics*, 2012, **31**, 4588–4592.
- (a) S. Khan, S. K. Ahirwar, S. Pal, N. Parvin and N. Kathewad, *Organometallics*, 2015, **34**, 5401–5406; (b) S. Khan, S. Pal, N. Kathewad, I. Purushothaman, S. De and P. Parameswaran, *Chem. Commun.*, 2016, **52**, 3880–3882; (c) N. Parvin, R. Dasgupta, S. Pal, S. S. Sen and S. Khan, *Dalton Trans.*, 2017, **46**, 6528–6532; (d) N. Parvin, S. Pal, J. Echeverria, S. Alvarez and S. Khan, *Chem. Sci.*, 2018, **9**, 4333–4337; (e) G. Tan, B. Blom, D. Gallego and M. Driess, *Organometallics*, 2014, **33**, 363–369.
- S. U. Ahmad, T. Szilvási, E. Irran and S. Inoue, *J. Am. Chem. Soc.*, 2015, **137**, 5828–5836.
- (a) A. Bayler, A. Schier, G. A. Bowmaker and H. Schmidbauer, *J. Am. Chem. Soc.*, 1996, **118**, 7006–7007; (b) P. Pykkö, *Angew. Chem., Int. Ed.*, 2004, **43**, 4412–4456; (c) P. Schwerdtfeger, *Heteroat. Chem.*, 2002, **13**, 578–584.
- C. Boehme and G. Frenking, *Organometallics*, 1998, **17**, 5801–5809.
- A. G. Avent, B. Gehrhus, P. B. Hitchcock, M. F. Lappert and H. Maciejewski, *J. Organomet. Chem.*, 2003, **686**, 321–331.

6. Transition Metal Carbonyl Complexes of an NHC-stabilized Silyliumylidene Ion

Title: “Transition Metal Carbonyl Complexes of an *N*-Heterocyclic Carbene Stabilized Silyliumylidene Ion”¹⁵⁴

Status: Article; published online: October 22, 2019.

Journal: *Inorganic Chemistry* **2019**, 58, 14931–14937.

Publisher: American Chemical Society

DOI: [10.1021/acs.inorgchem.9b02772](https://doi.org/10.1021/acs.inorgchem.9b02772)

Authors: Philipp Frisch, Tibor Szilvási, Amelie Porzelt and Shigeyoshi Inoue^a

Reprinted with permission from the American Chemical Society. © 2019 American Chemical Society.

Content: The properties of ligands in transition metal complexes like σ -donor and π -acceptor strength can significantly influence the stability and reactivity of complexes, including their catalytic activity. It is therefore of crucial importance to understand the properties of novel ligand systems and their influence on the transition metal itself and its coordination sphere. Not much is known about the properties of Si(II) cations as ligands, as no studies into their σ -donor/ π -acceptor ability have been carried out so far. A common method for the study of ligand properties is the investigation of the IR carbonyl stretching frequencies of the respective carbonyl transition metal complexes.

This publication outlines the synthesis of several novel transition metal carbonyl complexes incorporating a silyliumylidene ligand, including the first Fe, Cr and Mo complexes of a Si(II) cation. It constitutes a logical continuation of our previous work on silyliumylidene transition metal complexes. However, contrary to our previous publication on coinage metal complexes, the bulky *m*-terphenyl substituent did not react with the transition metal precursors, whereas utilization of the Tipp substituent allowed us to isolate a series of stable group 6 and group 8 carbonyl complexes.

Coordination of the silyliumylidene ion to the transition metal is once again apparent by a significant downfield shift of the ²⁹Si NMR resonance and the solid-state structures revealed long Si–M bond lengths. A combination of experimentally determined IR stretching frequencies of the carbonyl ligands on the transition metal together with DFT calculations give insight into the relative donor/acceptor strength of the Si(II) cation, which revealed weak σ -donor as well as negligible π -acceptor properties. Furthermore, comparisons to common ligand classes like NHCs and other low-valent silicon ligands are drawn.

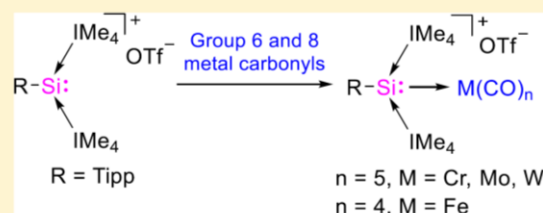
^aP. Frisch planned and executed all experiments involving transition metal carbonyl complexes, conducted the SC-XRD measurements including processing of the data and wrote the manuscript. T. Szilvási carried out the computational studies. A. Porzelt provided the synthetic protocol for the anion exchange reactions. All work was performed under the supervision of S. Inoue.

Transition Metal Carbonyl Complexes of an N-Heterocyclic Carbene Stabilized Silyliumylidene Ion

Philipp Frisch,[†] Tibor Szilvási,[‡] Amelie Porzelt,[†] and Shigeyoshi Inoue^{*,†}[†]Department of Chemistry, WACKER-Institute of Silicon Chemistry and Catalysis Research Center, Technische Universität München, Lichtenbergstraße 4, 85748 Garching bei München, Germany[‡]Department of Chemical and Biological Engineering, University of Wisconsin–Madison, 1415 Engineering Drive, Madison, Wisconsin 53706-1607, United States

Supporting Information

ABSTRACT: Silyliumylidene ions—Si(II) cations with a stereochemically active lone pair of electrons—can act as ligands in transition metal complexes comparable to silylenes. However, no investigations concerning their donor abilities have been carried out. Carbonyl complexes lend themselves exceptionally well to determine the donor/acceptor strength of various ligand systems. We now report the synthesis of novel group 6 and group 8 transition metal carbonyl complexes 2–5 of N-heterocyclic carbene (NHC) stabilized silyliumylidene ion **1b**, including the first Cr, Mo, and Fe complexes of a Si(II) cation. The complexes were fully characterized by multinuclear NMR and IR spectroscopy and SC-XRD studies. A combination of experimentally determined IR bands together with theoretical calculations revealed weak σ -donor properties and a negligible π -acceptor ability of NHC-stabilized Si(II) cation **1b**.



INTRODUCTION

Since Jutzi's initial report on the pentamethylcyclopentadiene-silicon(II) cation $[\text{Cp}^*\text{Si}]^+$ in 2004,¹ silyliumylidene ions have gained increasing scientific interest. Because of their unique electronic structure—a silicon center with a lone pair of electrons, a positive charge, and two vacant orbitals²—they are promising candidates for the facile activation of various bond types, as well as small molecules and, importantly, main-group catalysis. These highly reactive species can also give new access routes to novel low-valent silicon compounds, such as silylenes.³ Their potential in the activation of small molecules has already been shown with the isolation of sila-acylium ions through the activation of CO_2 ⁴ and their heavier homologues directly from S,⁵ Se, and Te.⁵ Other reported reactivities include the activation of O–H,⁶ S–H,⁷ and C–H⁸ bonds and even the catalytic degradation of oligoethers to dioxane.⁹

Another possible application of Si(II) cations is their use as ligands in transition metal complexes. Because of the presence of a lone pair of electrons on the silicon center, silyliumylidene ions can function as ligands just like silylenes and carbenes. However, one-coordinate silyliumylidene ions $[\text{R-Si}]^+$ (i.e., without donor-stabilization) have not been isolated so far due to their instability and high reactivity.^{8b} Hence, isolation of these Si(II) cations necessitates their kinetic and thermodynamic stabilization through generally sterically demanding substituents as well as electron donating ligands, such as NHCs.^{2b,10} On the other hand, introduction of these moieties generally hampers their reactivity and in the case of the stabilization through Lewis bases also (partially) fills the vacant

orbitals on the silicon center, therefore reducing their π -acceptor ability.

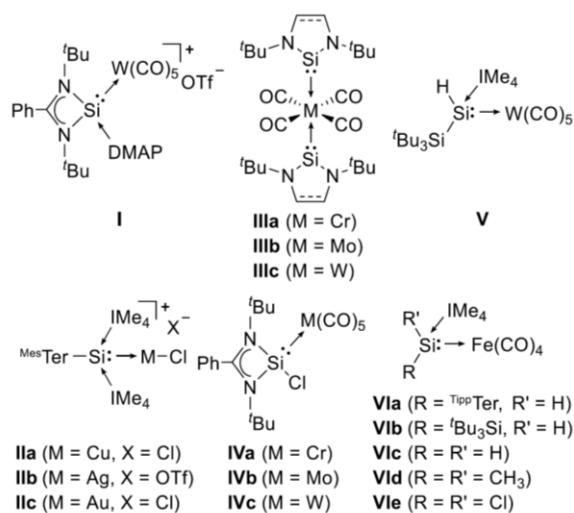
Understandably, the reported transition metal coordination chemistry of silyliumylidene ions is significantly more limited than the related silylene coordination chemistry: our group described formal Pd_2 and Pt_2 silyliumylidene-phosphide complexes, obtained from a rearrangement reaction of a phosphasilene.¹¹ So et al. reported a Rh- and W-complex (**I**) (Chart 1) of a DMAP-stabilized silyliumylidene ion.¹² Recently, we described the first coinage metal complexes **II** of Si(II) cations, synthesized directly from an NHC-stabilized silyliumylidene ion.¹³ The synthesis of a silyliumylidene molybdenum complex from $[\text{Cp}^*\text{Si}]^+$ was also recently accomplished.¹⁴ It is important to note that the donor strength of silyliumylidene ions as ligands in transition metal complexes has not been studied so far.

In contrast, a variety of group 6 and group 8 metal carbonyl complexes with silylenes as ligands have been isolated.¹⁵ For example, West et al. reported a series of saturated and unsaturated bis(*N*-heterocyclic silylene) (NHSi) complexes **III** of group 6 carbonyls.¹⁶ Related group 8 complexes with Fe and Ru,¹⁶ as well as monosilylene complexes,¹⁷ were also described. Complexes **IV** of an amidinate-stabilized chlorosilylene were prepared and utilized for the isolation of the corresponding fluorosilylene derivatives.¹⁸ Furthermore, related amidinate-stabilized hydrosilylene complexes of $\text{Fe}(\text{CO})_4$ ¹⁹ and various $\text{Fe}(\text{CO})_4$ complexes **VI**²⁰ from NHC-stabilized silylenes have

Received: September 17, 2019

Published: October 22, 2019

Chart 1. Examples of Reported Silyliumylidene Transition Metal Complexes (I, II) and Silylene Transition Metal Carbonyl Complexes (III–VI)^a



^aDMAP = 4-dimethylaminopyridine, IMe₄ = 1,3,4,5-tetramethylimidazol-2-ylidene, ^{Mes/Tipp}Ter = 2,6-(Mes/Tipp)₂-C₆H₃, Mes = 2,4,6-Me₃-C₆H₂, Tipp = 2,4,6-ⁱPr₃-C₆H₂.

been reported in recent years. The electronic properties of silylenes as ligands have also been investigated computationally.^{16,21}

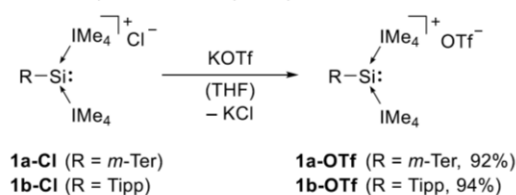
Therefore, to start of any investigation into the donor strength of NHC-stabilized silyliumylidene ions and to determine their donor ability, we set out to synthesize transition metal carbonyl complexes utilizing our previously described NHC-stabilized silyliumylidene ions^{8a} as ligands. Herein, we report the synthesis and full characterization of several novel group 6 (Cr, Mo, W) and group 8 (Fe) transition metal carbonyl complexes of NHC-stabilized Si(II) cations and an investigation of the donor ability of the silyliumylidene ligand by experimental as well as theoretical means.

RESULTS AND DISCUSSION

Synthesis and NMR Analysis. In an initial attempt, we reacted the group 6 transition metal carbonyl W(CO)₆ with the bulky *m*-terphenyl (*m*-Ter = 2,6-(2,4,6-Me₃-C₆H₂)₂-C₆H₃) substituted silyliumylidene chloride^{8a} **1a-Cl** as a suspension in THF. However, no reaction occurred, even at elevated temperatures and prolonged reaction times. Irradiation of the mixture with UV light led to the full consumption of W(CO)₆ accompanied by complete dissolution of the Si(II) cation, however, no change in the ¹H and ²⁹Si NMR could be observed. Interestingly, the ¹³C NMR indicated formation of the chloropentacarbonyl tungstate anion²² [W(CO)₅Cl]⁻. This prompted us to exchange the chloride counteranion from the silyliumylidene ion **1a-Cl** to a triflate anion via reaction with KOTf to prevent any undesired anion formation (Scheme 1).

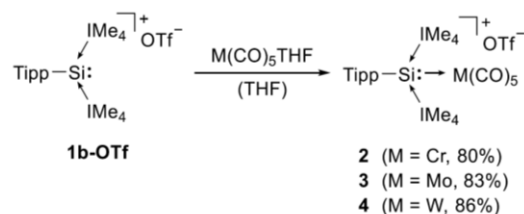
Introduction of the OTf⁻ anion also brings the additional benefit of increased solubility in THF, allowing for a homogeneous reaction. Unfortunately, even with the triflate anion, the steric bulk of the *m*-terphenyl substituent in **1a-OTf** seemed to prevent any reaction with W(CO)₆ or W(CO)₅(THF). Hence, we moved our efforts to the sterically

Scheme 1. Synthesis of Silyliumylidene Triflates **1-OTf**



less demanding Tipp substituent (**1b-Cl**, Tipp = 2,4,6-ⁱPr₃-C₆H₂) and, consequently, introduced the OTf⁻ anion. Finally, reaction of a THF solution of silyliumylidene triflate **1b-OTf** with a freshly prepared solution of M(CO)₅(THF) (M = Cr, Mo, W) in THF allowed us to isolate the desired [Tipp-Si(IME₄)₂ → M(CO)₅]⁺ complexes **2–4** in high yield (80–86%) as pale to bright yellow solids (Scheme 2). The successful complex formation can be observed by a visible color change from bright orange (**1b-OTf** in THF) to pale to bright yellow (**2–4**).

Scheme 2. Synthesis of Group 6 Carbonyl Complexes **2–4**



While no direct reaction could be observed with M(CO)₆, initial preparation of M(CO)₅(THF) is not necessary, as irradiation of a simple mixture of the starting materials with UV light led to formation of the same complexes, albeit slightly less clean. The complexes are well soluble in THF, C₆H₅F, acetonitrile, and pyridine and are slightly soluble in Et₂O. They are stable for about 2 days in THF, Et₂O, and C₆H₅F solution at room temperature, but after 48 h, small amounts of unidentified decomposition products can be observed in the ¹H NMR. They decompose rapidly in acetonitrile to an unidentified mixture of products.

Coordination of the silicon center to the transition metal is accompanied by marked downfield shift in the ²⁹Si NMR (−69.5 ppm for **1b-OTf**), which gets progressively weaker with an increasing atomic number of the group 6 metal. The Cr(CO)₅ complex **2** resonates at +6.3 ppm, whereas the Mo(CO)₅ and W(CO)₅ complexes (**3** and **4**) are shifted upfield to −17.3 and −30.5 ppm, respectively. The same trend was also observed for the related group 6 silylene complexes **III** (unsat./sat.; Cr, 136.9/170.3 ppm; Mo, 119.3/155.3 ppm; W, 97.8/137.1 ppm)¹⁶ and **IV** (Cr, 92.3 ppm; Mo, 72.8 ppm; W, 53.0 ppm).¹⁸ However, this is in stark contrast to the coinage metal silyliumylidene complexes **II**, where an increasing atomic number resulted in a stronger downfield shift (Cu, −48.8 ppm; Ag, −46.6 ppm; Au, −38.0 ppm).¹³ For comparison, the only other silyliumylidene ion W(CO)₅ complex **I** shows a significantly stronger downfield shift of the ²⁹Si NMR resonance from −82.3 ppm in the uncoordinated silyliumylidene ion^{5b} to +51.6 ppm in the complex.¹² We were also able to observe the coupling of the central Si atom with ¹⁸³W (~14% natural abundance, S = 1/2; cf., Figure S28),

resulting in a doublet with $^1J_{\text{SiW}} = 123.0$ Hz, which is in line with other reported Si(II) \rightarrow W(CO)₅ complexes.¹⁷ No coupling with $^{95/97}\text{Mo}$ (^{95}Mo , ~16%; ^{97}Mo , ~10% natural abundance; $S = 5/2$) could be observed, even with a high concentration and significantly increased number of scans. ^{29}Si NMR shifts as well as other important analytical parameters are summed up in Table 1.

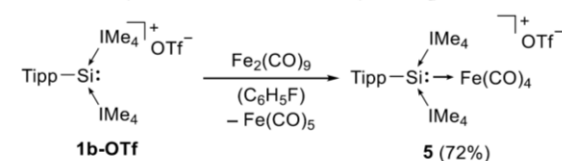
Table 1. Comparison of ^{29}Si NMR & ^{13}C NMR (THF-*d*₈) and Si–M Bond Lengths of Silyliumylidene Ion **1b**-OTf and Its Transition Metal Complexes **2–5**

M	^{29}Si NMR [ppm]	^{13}C NMR (CO) [ppm]	Si1–M1 [Å]
1b	–69.5		
2 Cr	6.3	225.2, 222.0	
3 Mo	–17.3	210.0, 202.2	2.673(1)/2.740(1)
4 W	–30.5	201.9, 192.4	
5 Fe	5.4	217.4	2.349(1)

The ^1H NMR spectra of complexes **2–4** are very similar, showing a single set of resonances for the Tipp-substituent and the NHCs. The biggest difference, also compared to silyliumylidene **1b**-OTf, is the broadening of the septet corresponding to the *iso*-propyl groups in ortho-position to the central silicon atom. The ^{13}C NMR spectra show one set of resonances for the Tipp-substituent and the coordinated NHCs and two separate resonances for the metal-bound CO ligands, presumably due to the trans effect,²² which is consistent with other low-valent silicon complexes.^{17,18} The CO resonances can be observed in the expected range, with a gradual upfield shift going from Cr (225.5/222.0 ppm) to Mo (210.0/202.2 ppm) to W (201.9/192.4 ppm).

To further expand the coordination chemistry of silyliumylidene ions, we also attempted the synthesis of group 8 carbonyl complexes. No reaction could be observed between Fe(CO)₅ and **1b**-OTf. However, addition of one equivalent of the more reactive iron carbonyl compound Fe₂(CO)₉ to **1b**-OTf in THF resulted in the formation of Fe(CO)₄ complex **5**, which unfortunately was accompanied by slow polymerization of the solvent. We, therefore, switched to fluorobenzene, which allowed us to isolate complex **5** in good yield (72%) and purity as a colorless solid (Scheme 3). Fe(CO)₅ as the byproduct can

Scheme 3. Synthesis of Iron Carbonyl Complex **5**



be easily removed under reduced pressure and no further polymerization occurred when the NMR measurements of the purified product were carried out in THF-*d*₈. As expected, coordination of iron to the silicon center once again causes a significant downfield shift of the ^{29}Si NMR resonance from –69.5 ppm (**1b**-OTf) to +5.4 ppm (**5**) (cf., Table 1). For comparison, the hydrosilylene complexes **VIa** and **VIb** show resonances at –11.1 ppm and –48.3 ppm, respectively (downfield from –80.5 ppm and –137.8 ppm in the free silylenes). The ^1H NMR spectrum is comparable to **2–4**, with a key difference being the significant upfield shift of the septet

corresponding to the ortho 'Pr groups to 3.14 ppm (for **5**) compared to 4.10–4.24 ppm observed for **2–4** (and 3.74 ppm for **1b**-OTf). Interestingly, no signal broadening of this septet occurs in this case. It is important to note that the ^{13}C NMR of complex **5** only shows a single resonance for the CO ligands at 217.5 ppm compared to the two resonances observed for the group 6 complexes.

Single-Crystal X-ray Diffraction (SC-XRD) Structure Determination. Single crystals suitable for XRD measurements of Mo(CO)₅ complex **3** were obtained by cooling a concentrated solution of **3** in Et₂O to –35 °C and single crystals of Fe(CO)₄ complex **5** were obtained by cooling a concentrated solution of **5** in C₆H₅F to –35 °C. The complexes are monomers in the solid state and feature a four-coordinate Si(II) center with a distorted tetrahedral geometry (Figure 1). As expected, the Mo atom in **3** features an octahedral coordination sphere with five terminal carbonyl ligands. The Si1–Mo1 bond lengths in **3** (2.673(1)/2.740(1) Å) are at the upper end of the reported Si–Mo bond lengths (2.41–2.71 Å).²³ In fact, 2.740(1) Å is the longest reported Mo–Si bond to date. They are much longer than the Si–Mo bonds in the silylene complexes **IIIb** (unsat./sat. = 2.471/2.480 Å)¹⁶ and **IVb** (2.455(1) Å).¹⁸ The bond is also significantly longer than the Si–W bond in silyliumylidene W(CO)₅ complex **1** (2.497(1) Å).¹² The Si1–C_{NHC} (avg. 1.956 Å) bond lengths, as well as the Mo1–C (avg. 2.035 Å) and C–O (avg. 1.142 Å) bond lengths, are in the expected range. So far, we were unable to obtain single crystals of the analogous Cr and W complexes, but because of their very similar NMR data and reactivity, they should exhibit comparable structures. The solid-state structure of iron complex **5** is very similar to that of tungsten complex **3**, except that the Fe atom adopts a trigonal bipyramidal structure with four terminal CO ligands (Figure 1, right) instead of five. Similarly, the Si1–Fe1 bond (2.349(1) Å) is also quite long. It is only slightly shorter than the longest reported Si–Fe bond to date (**VIb**, 2.372(1) Å).^{20b} Similar to those in complex **3**, the Si1–C_{NHC}, Fe1–C, and C–O bonds are in the expected range.

IR Spectroscopic Analysis. All complexes **2–5** were characterized by IR spectroscopy. Experimentally determined values (solid state, neat) of CO stretching frequencies and the calculated bands of complexes **2–5** are listed in Table 2. Conclusions about the σ -donor or π -acceptor ability of silyliumylidene ion **1b** as a ligand can be drawn from the characteristic CO stretching frequencies in these complexes. To put the relative donor/acceptor strength of **1b** into perspective, we selected multiple literature known complexes and compared the CO stretching frequencies: strong(er) σ -donors/weak(er) π -acceptors increase the π -backbonding from the metal to the CO ligand and therefore strengthen the M–C bond while simultaneously weakening the C–O bond (which results in lower wave numbers of the CO stretching frequency, i.e., a bathochromic shift). Conversely, ligands with weak(er) σ -donor/strong(er) π -acceptor properties lead to higher wave numbers observed in the IR spectrum (i.e., a hypsochromic shift). In general, strong σ -donors are weaker π -acceptors and vice versa. However, in the case of **1**, the two coordinated NHC moieties occupy the p-orbitals, significantly reducing the π -acceptor ability of the central silicon atom. This drastically reduces the π -backbonding contribution from the metal fragment to the silicon center. Hence, any changes of the carbonyl stretching frequency observed in the IR spectrum

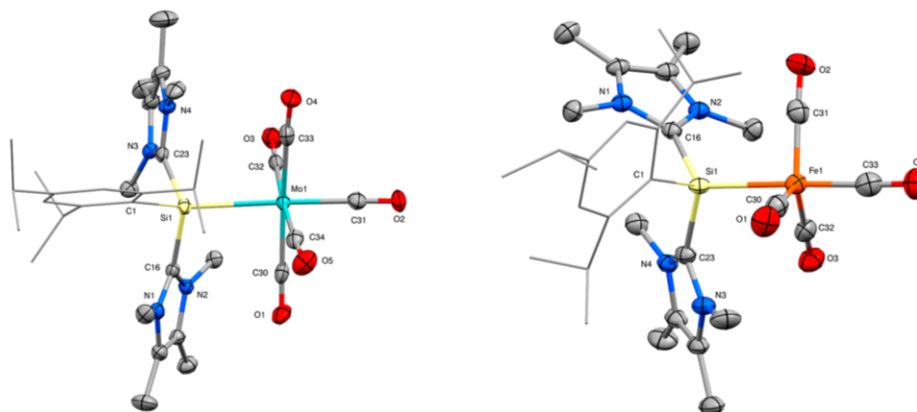


Figure 1. Ellipsoid plot (50% probability level) of the molecular structure of Mo(CO)₅ complex **3** (one out of two independent molecules in the asymmetric unit shown) and Fe(CO)₄ complex **5**. Tipp-substituents are simplified as wireframes. Hydrogen atoms, solvent molecules, and anions are omitted for clarity. Selected bond lengths [Å] and angles [°]: **3** Si1–Mo1 2.673(1)/2.740(1), Si1–C1 1.942(3)/1.966(3), Si1–C16 1.951(2)/1.950(3), Si1–C23 1.962(4)/1.960(3), Mo1–C30 2.037(3)/2.040(3), Mo1–C31 2.004(3)/1.998(3), Mo1–C32 2.043(4)/2.018(3), Mo1–C33 2.052(3)/2.057(3), Mo1–C34 2.041(4)/2.056(4), C30–O1 1.143(4)/1.140(4), C31–O2 1.140(4)/1.146(4), C32–O3 1.144(5)/1.154(5), C33–O4 1.140(3)/1.139(4), C34–O5 1.142(5)/1.142(4), Mo1–Si1–C1 132.7(1)/131.2(1), Mo1–Si1–C16 103.1(1)/102.2(1), Mo1–Si1–C23 108.1(1)/109.3(1), C1–Si1–C16 104.3(1)/108.6(1), C1–Si1–C23 98.9(1)/98.5(1), C16–Si1–C23 108.1(1)/104.8(1), Si1–Mo1–C31 169.4(1)/171.5(1); **5** Si1–Fe1 2.349(1), Si1–C1 1.91(2), Si1–C16 1.949(2), Si1–C23 1.956(2), Fe1–C30 1.768(2), Fe1–C31 1.775(2), Fe1–C32 1.781(3), Fe1–C33 1.790(3), C30–O1 1.160(3), C31–O2 1.157(3), C32–O3 1.154(3), C33–O4 1.146(3), Fe1–Si1–C1 115.5(6), Fe1–Si1–C16 116.5(1), Fe1–Si1–C23 106.4(1), C1–Si1–C16 104.9(6), C1–Si1–C23 112.1(6), C16–Si1–C23 100.6(1), Si1–Fe1–C33 176.5(1).

Table 2. Experimentally Determined (Solid State, Neat) and Calculated CO Stretching Frequencies of Complexes **2–5** and Relevant IR Data for Reported Complexes **1**, **12**, **V**,^{20b} and **VI**²⁰

M	CO stretching frequencies $\delta_{\text{C}\equiv\text{O}}$ [cm ⁻¹] ^a		
	experimental	calculated	
2	Cr	2037, 1965, 1889	2026, 1964, 1946, 1915, 1907
3	Mo	2054, 1969, 1897	2039, 1967, 1961, 1921, 1916
4	W	2052, 1963, 1891	2034, 1961, 1954, 1913, 1907
1	W	2070, 1991, 1921	
V	W	2042, 1952, 1879	
5	Fe	2021, 1943, 1887	2030, 1962, 1919, 1903
VIa	Fe	2009, 1922, 1884	
VIb	Fe	2002, 1919, 1878	
VIc	Fe	2011, 1904, 1855	
VI d	Fe	1999, 1911, 1855	
VI e	Fe	2029, 1950, 1893	

^aThe difference in the number of observed and calculated IR bands can most likely be attributed to the overlap of close bands in the IR spectra.

should be mainly attributable to the σ -donor ability of Si(II) cation **1b**.

In general, common ligand classes like phosphines (e.g., Ph₃P \rightarrow W(CO)₅, $\delta_{\text{C}\equiv\text{O}}$ = 2060, 1914, 1887 cm⁻¹)²⁴ or NHCs (e.g., IMes \rightarrow W(CO)₅, $\delta_{\text{C}\equiv\text{O}}$ = 2057, 1911, 1876 cm⁻¹)²⁵ are (significantly) stronger σ -donors than Si(II) cation **1b**, presumably because of the cationic nature of the silyliumylidene, as well as stronger π -acceptors, because of the presence of two NHC ligands on the central silicon atom reducing its π -acceptor ability. However, as this was expected, a comparison to other (donor-stabilized) low-valent silicon species is more fitting and interesting: the IR bands of silyliumylidene W(CO)₅ complexes **1**¹² and **4** (Table 2) show that silyliumylidene **1** is a stronger σ -donor/weaker π -acceptor

than the corresponding DMAP-stabilized silyliumylidene ion.^{5b} An increased σ -donor ability might be attributable to the two coordinated NHC moieties in **1** (vs the weaker N-donors in **I**), as it has been predicted that coordination of strong donors to silylenes actually increases their σ -donor strength considerably.²¹ The substantial difference in bond lengths (cf., SC-XRD discussion) of these complexes could stem from the bulkier ligand framework present in our system. Comparison to complex **V**^{20b} shows **1** to be a slightly weaker σ -donor than the respective hydrosilylene, presumably attributable to the cationic nature of **1**.²⁶

Since no Fe(CO)₄ complexes of a Si(II) cation have been reported so far, we chose various related silylene complexes **VI**²⁰ for comparison. From this data, we can see that the σ -donor ability of silyliumylidene **1b** is very similar to the NHC-stabilized aryl-hydrosilylene ligand in **VIa** and, again, slightly lower than the NHC-stabilized silyl-hydrosilylene ligand in **VIb** (cf., W(CO)₅ complex). Considering that silyl groups have an increased σ -electron donating ability compared to aryl substituents, this is not surprising. Complex **VIe** (IMe₄ \rightarrow SiCl₂ \rightarrow Fe(CO)₄) shows comparable IR bands and with that should be very similar in relative σ -donor/ π -acceptor strength. Furthermore, we have calculated the Tolman Electronic Parameters (TEPs) of the [Tipp–Si(IMe₄)₂ \rightarrow Ni(CO)₃]⁺ complex (TEPs: 2063, 2017, 2001 cm⁻¹), which support the weak σ -donor/ π -acceptor strength of **1b**.^{20b,27}

Computational Studies. Density functional theory (DFT) calculations were performed to gain further insight into the ligand properties of silyliumylidene **1b** and the electronic structure and bonding situation in complexes **2–5**. We calculated the proton affinity (PA) of silyliumylidene **1**, which can be used to quantify its σ -donor ability.²⁸ For easy comparability, we employed the same method and basis set (B97-D/Def2-TZVP//B97-D/6-31G*) utilized in our previous publication discussing σ -donor/ π -acceptor strength and ligand properties of various silylenes.²¹ Expectedly, the

predicted PA of 917 kJ/mol for **1b** was found to be rather low, which can most likely be attributed to the cationic nature of the silyliumylidene ion. This value does take the zwitterionic mesomeric structures of **1b** into consideration.^{8a} Driess et al. reported a zwitterionic β -diketiminato silyliumylidene²⁹ that exhibits a similarly low PA (888 kJ/mol), which also stems from the cationic charge in the π -system of the ligand framework.²¹ For comparison, these PAs are significantly lower than model phosphine compounds (Ph_3P , 1031 kJ/mol; Cy_3P , 1072 kJ/mol), NHCs (IDipp, 1176 kJ/mol), and donor-stabilized NHSis (~ 1200 kJ/mol) and slightly lower than nonstabilized NHSis (~ 980 kJ/mol).²¹ These results agree well with those derived from the IR analysis.

Additionally, we calculated the frontier orbitals of all complexes: as expected, the HOMO and LUMO of **2–5** are very similar (as an example, see Figure 2 for HOMO and

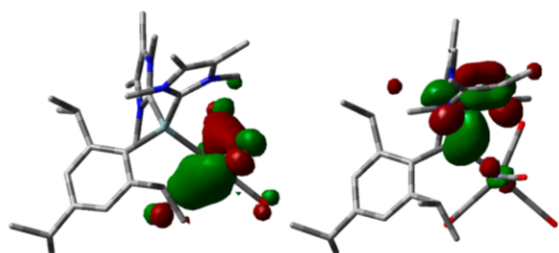


Figure 2. DFT-calculated frontier orbitals of silyliumylidene $\text{Fe}(\text{CO})_4$ complex **5**: HOMO (left, -7.08 eV) and LUMO (right, -4.76 eV).

LUMO of **5**, cf., Figures S39–S41 for complexes **2–4**). While the HOMO of **5** is localized on the transition metal fragment, the LUMO is mainly located on the silicon center and the adjacent NHC framework. Furthermore, we also calculated the Wiberg Bond Indices (WBI) (Table 3). The low values for the WBIs (i.e., 0.63 – 0.78) correlate well with the long Si–M bond distances observed for the complexes. Investigation of the atomic charge distribution in complexes **2–5** via natural population analysis (NPA) shows a substantial positive charge located on the silyliumylidene silicon with a significant negative charge on the transition metal center. The negative charge located on the metal center decreases considerably with increasing atomic number of the metal (i.e., Cr (-2.61) \rightarrow Mo (-2.25) \rightarrow W (-1.66)), which is most likely the consequence of the orbital size differences that makes donation of the silicon-centered lone pair to the metal more difficult with its increasing size. Additionally, this conclusion is in line with the obtained bond polarization values and the increasing s character of silicon, which also indicate a decreasing donation of the silicon centered lone pair.

Interestingly, the calculated bond dissociation energies (BDEs) of **2–4** follow an opposite trend, showing the

strongest binding for **4** (51.9 kcal/mol) and the weakest binding for **2** (41.5 kcal/mol). We presume that this trend can be traced back to an increased ionic nature of the Si \rightarrow M bond with an increasing atomic number. This results in an increased bond strength with a decreasing covalent character, which is also reflected in the calculated WBI values. Finally, we note that **5** has both a much larger BDE than **2–4**, as well as an increased covalent character (WBI = 0.78). These results are comparable to the results of our previous study where we have systematically investigated Fe-carbonyl silylene complexes.^{20b} Additionally, NBO analysis (cf., Table S2–S5) of iron complex **5** revealed a small contribution of π -backdonation from a metal d-orbital to the central silicon atom, while no π -backdonation for the group 6 complexes **2–4** was found. These substantial differences are also reflected in the thermal stability of the complexes: whereas the group 6 complexes **2–4** melt under decomposition between 74 and 83 °C, solid **5** only decomposes at temperatures higher than 195 °C.

CONCLUSIONS

In summary, we have synthesized and fully characterized a series of novel group 6 (Cr, Mo, W) and group 8 (Fe) carbonyl complexes **2–5** of an NHC-stabilized silyliumylidene ion, which includes the first reported Fe, Cr and Mo complexes of a silyliumylidene ion, by directly reacting silyliumylidene triflate **1b-OTf** with transition metal carbonyl precursors. Coordination of the Si(II) cation to the metal is accompanied by a significant downfield shift of the ^{29}Si NMR resonance. SC-XRD analysis revealed surprisingly long Si–M bond lengths. Analysis of the complexes via carbonyl IR stretching frequencies together with DFT calculations give insight into the σ -donor ability of the Si(II) cation, which is significantly lower than in model NHC or phosphine complexes, most likely because of the positive charge located on the silicon center. Further coordination chemistry of NHC-stabilized Si(II) cations toward other metals and their application in organometallic transformations is currently under investigation in our laboratory.

ASSOCIATED CONTENT

Supporting Information

The Supporting Information is available free of charge on the ACS Publications website at DOI: 10.1021/acs.inorgchem.9b02772.

Experimental details, crystallographic data, NMR spectra, IR spectra, and computational details (PDF)

Accession Codes

CCDC 1949742–1949745 contain the supplementary crystallographic data for this paper. These data can be obtained free of charge via www.ccdc.cam.ac.uk/data_request/cif, or by emailing data_request@ccdc.cam.ac.uk, or by contacting The

Table 3. Summary of the Calculated Si–M Bond Lengths, Bond Dissociation Energies (BDEs), Percentage of s Character on the Silicon Center, NPA Atomic Charges, Wiberg Bond Index (WBI) for Complexes **2–5**

	M	theor. Si–M [Å]	BDE Si–M [kcal/mol]	s character of silicon [%]	bond polarization		NPA atomic charge		WBI
					Si [%]	M [%]	Si	M	Si–M
2	Cr	2.541	41.5	33.4	60.4	39.6	+1.24	–2.61	0.69
3	Mo	2.686	45.2	35.3	64.7	35.3	+1.18	–2.25	0.66
4	W	2.679	51.9	36.9	69.0	31.0	+1.12	–1.66	0.63
5	Fe	2.340	62.1	31.8	53.0	47.0	+1.32	–1.59	0.78

Cambridge Crystallographic Data Centre, 12 Union Road, Cambridge CB2 1EZ, UK; fax: +44 1223 336033.

AUTHOR INFORMATION

Corresponding Author

*E-mail: s.inoue@tum.de.

ORCID

Tibor Szilvási: 0000-0002-4218-1570

Shigeyoshi Inoue: 0000-0001-6685-6352

Notes

The authors declare no competing financial interest.

ACKNOWLEDGMENTS

The authors are exceptionally grateful to the WACKER Chemie AG and the European Research Council (SILION 637394) for continued financial support. We are also thankful to Dr A. Pöthig and Dr C. Jandl for advice regarding crystallography and K. Huber for his experimental work concerning the anion exchange reactions.

REFERENCES

- Jutzi, P.; Mix, A.; Rummel, B.; Schoeller, W. W.; Neumann, B.; Stammer, H.-G. The $\text{Me}_2\text{C}_5\text{Si}$ Cation: A Stable Derivative of HSi^+ . *Science* **2004**, *305*, 849–851.
- (a) Bertrand, G. The Modest Undressing of a Silicon Center. *Science* **2004**, *305*, 783–785. (b) Powley, S. L.; Inoue, S. NHC-Stabilised Silyliumylidene Ions. *Chem. Rec.* **2019**, DOI: 10.1002/tcr.201800188.
- Xiong, Y.; Yao, S.; Inoue, S.; Epping, J. D.; Driess, M. A Cyclic Silylone (“Siladicarbene”) with an Electron-Rich Silicon(0) Atom. *Angew. Chem., Int. Ed.* **2013**, *52*, 7147–7150.
- Ahmad, S. U.; Szilvási, T.; Irran, E.; Inoue, S. An NHC-Stabilized Silicon Analogue of Acylium Ion: Synthesis, Structure, Reactivity, and Theoretical Studies. *J. Am. Chem. Soc.* **2015**, *137*, 5828–5836.
- (a) Xiong, Y.; Yao, S.; Inoue, S.; Irran, E.; Driess, M. The Elusive Silyliumylidene $[\text{ClSi}]^+$ and Silathionium $[\text{ClSi}=\text{S}]^+$ Cations Stabilized by Bis(Iminophosphorane) Chelate Ligand. *Angew. Chem., Int. Ed.* **2012**, *51*, 10074–10077. (b) Yeong, H.-X.; Xi, H.-W.; Li, Y.; Lim, K. H.; So, C.-W. A Silyliumylidene Cation Stabilized by an Amidinate Ligand and 4-Dimethylaminopyridine. *Chem. - Eur. J.* **2013**, *19*, 11786–11790. (c) Sarkar, D.; Wendel, D.; Ahmad, S. U.; Szilvási, T.; Pöthig, A.; Inoue, S. Chalcogen-atom transfer and exchange reactions of NHC-stabilized heavier silaacylium ions. *Dalton Trans* **2017**, *46*, 16014–16018.
- Sarkar, D.; Nesterov, V.; Szilvási, T.; Altmann, P. J.; Inoue, S. The Quest for Stable Sila-aldehydes: Synthesis and Reactivity of a Masked Silacarbonyl. *Chem. - Eur. J.* **2019**, *25*, 1198–1202.
- Porzelt, A.; Schweizer, J.; Baierl, R.; Altmann, P.; Holthausen, M.; Inoue, S. S-H Bond Activation in Hydrogen Sulfide by NHC-Stabilized Silyliumylidene Ions. *Inorganics* **2018**, *6*, 54.
- (a) Ahmad, S. U.; Szilvási, T.; Inoue, S. A facile access to a novel NHC-stabilized silyliumylidene ion and C-H activation of phenylacetylene. *Chem. Commun.* **2014**, *50*, 12619–12622. (b) Gerdes, C.; Saak, W.; Haase, D.; Müller, T. Dibenzosilanorbornadienyl Cations and Their Fragmentation into Silyliumylidenes. *J. Am. Chem. Soc.* **2013**, *135*, 10353–10361.
- Leszczyńska, K.; Mix, A.; Berger, R. J. F.; Rummel, B.; Neumann, B.; Stammer, H.-G.; Jutzi, P. The Pentamethylcyclopentadienylsilicon(II) Cation as a Catalyst for the Specific Degradation of Oligo(ethyleneglycol) Diethers. *Angew. Chem., Int. Ed.* **2011**, *50*, 6843–6846.
- Nesterov, V.; Reiter, D.; Bag, P.; Frisch, P.; Holzner, R.; Porzelt, A.; Inoue, S. NHCs in Main Group Chemistry. *Chem. Rev.* **2018**, *118*, 9678–9842.
- Breit, N. C.; Szilvási, T.; Suzuki, T.; Gallego, D.; Inoue, S. From a Zwitterionic Phosphasilene to Base Stabilized Silyliumylidene-

Phosphide and Bis(silylene) Complexes. *J. Am. Chem. Soc.* **2013**, *135*, 17958–17968.

(12) Yeong, H.-X.; Li, Y.; So, C.-W. A Base-Stabilized Silyliumylidene Cation as a Ligand for Rhodium and Tungsten Complexes. *Organometallics* **2014**, *33*, 3646–3648.

(13) Frisch, P.; Inoue, S. Coinage metal complexes of NHC-stabilized silyliumylidene ions. *Chem. Commun.* **2018**, *54*, 13658–13661.

(14) Ghana, P.; Arz, M. I.; Schnakenburg, G.; Straßmann, M.; Filippou, A. C. Metal-Silicon Triple Bonds: Access to $[\text{Si}(\eta^5\text{-C}_5\text{Me}_5)]^+$ from $\text{SiX}_2(\text{NHC})$ and its Conversion to the Silyliumylidene Complex $[\text{TpMe}(\text{CO})_2\text{MoSi}(\eta^3\text{-C}_5\text{Me}_5)]$ (TpMe = $\kappa^3\text{-N,N',N''}$ -hydridotris(3,5-dimethyl-1-pyrazolyl)borate). *Organometallics* **2018**, *37*, 772–780.

(15) Iwamoto, T.; Ishida, S. Stable Silylenes and Their Transition Metal Complexes. In *Organosilicon Compounds*; Lee, V. Y., Ed.; Academic Press, 2017; Chapter 8, pp 361–532.

(16) Schmedake, T. A.; Haaf, M.; Paradise, B. J.; Millevolte, A. J.; Powell, D. R.; West, R. Electronic and steric properties of stable silylene ligands in metal(0) carbonyl complexes. *J. Organomet. Chem.* **2001**, *636*, 17–25.

(17) Zark, P.; Schäfer, A.; Mitra, A.; Haase, D.; Saak, W.; West, R.; Müller, T. Synthesis and reactivity of N-aryl substituted N-heterocyclic silylenes. *J. Organomet. Chem.* **2010**, *695*, 398–408.

(18) Azhakar, R.; Ghadwal, R. S.; Roesky, H. W.; Wolf, H.; Stalke, D. Stabilization of Low Valent Silicon Fluorides in the Coordination Sphere of Transition Metals. *J. Am. Chem. Soc.* **2012**, *134*, 2423–2428.

(19) Blom, B.; Pohl, M.; Tan, G.; Gallego, D.; Driess, M. From Unsymmetrically Substituted Benzamidinato and Guanidinato Dichlorohydrosilanes to Novel Hydrido N-Heterocyclic Silylene Iron Complexes. *Organometallics* **2014**, *33*, 5272–5282.

(20) (a) Lutters, D.; Severin, C.; Schmidtmann, M.; Müller, T. Activation of 7-Silanorbornadienes by N-Heterocyclic Carbenes: A Selective Way to N-Heterocyclic-Carbene-Stabilized Silylenes. *J. Am. Chem. Soc.* **2016**, *138*, 6061–6067. (b) Eisenhut, C.; Szilvási, T.; Dübek, G.; Breit, N. C.; Inoue, S. Systematic Study of N-Heterocyclic Carbene Coordinate Hydrosilylene Transition-Metal Complexes. *Inorg. Chem.* **2017**, *56*, 10061–10069.

(21) Benedek, Z.; Szilvási, T. Can low-valent silicon compounds be better transition metal ligands than phosphines and NHCs? *RSC Adv.* **2015**, *5*, 5077–5086.

(22) Buchner, W.; Schenk, W. A. ^{13}C NMR spectra of monosubstituted tungsten carbonyl complexes. NMR trans influence in octahedral tungsten (0) compounds. *Inorg. Chem.* **1984**, *23*, 132–137.

(23) Ghana, P.; Arz, M. I.; Chakraborty, U.; Schnakenburg, G.; Filippou, A. C. Linearly Two-Coordinated Silicon: Transition Metal Complexes with the Functional Groups $\text{M}\equiv\text{Si}-\text{M}$ and $\text{M}=\text{Si}=\text{M}$. *J. Am. Chem. Soc.* **2018**, *140*, 7187–7198.

(24) Yih, K.-H.; Lee, G.-H.; Wang, Y. Synthesis and Structural Characterization of Configurational Isomers of Tungsten-Palladium Complexes with Bridging Diphenyl(dithioalkoxycarbonyl)phosphine as a Ligand and Phosphine Transfer from Tungsten to Palladium. *Inorg. Chem.* **2000**, *39*, 2445–2451.

(25) Wang, Z.; Li, S.; Teo, W. J.; Poh, Y. T.; Zhao, J.; Hor, T. S. A Molybdenum (0) and tungsten (0) carbonyl N-heterocyclic carbene complexes as catalyst for olefin epoxidation. *J. Organomet. Chem.* **2015**, *775*, 188–194.

(26) Inoue, S.; Eisenhut, C. A Dihydrodisilene Transition Metal Complex from an N-Heterocyclic Carbene-Stabilized Silylene Monohydride. *J. Am. Chem. Soc.* **2013**, *135*, 18315–18318.

(27) Ardizzoia, G. A.; Brenna, S. Interpretation of Tolman electronic parameters in the light of natural orbitals for chemical valence. *Phys. Chem. Chem. Phys.* **2017**, *19*, 5971–5978.

(28) (a) Fey, N.; Tsipis, A. C.; Harris, S. E.; Harvey, J. N.; Orpen, A. G.; Mansson, R. A. Development of a Ligand Knowledge Base, Part 1: Computational Descriptors for Phosphorus Donor Ligands. *Chem. - Eur. J.* **2006**, *12*, 291–302. (b) Jover, J.; Fey, N.; Harvey, J. N.; Lloyd-

Jones, G. C.; Orpen, A. G.; Owen-Smith, G. J. J.; Murray, P.; Hose, D. R. J.; Osborne, R.; Purdie, M. Expansion of the Ligand Knowledge Base for Monodentate P-Donor Ligands (LKB-P). *Organometallics* **2010**, *29*, 6245–6258.

(29) Driess, M.; Yao, S.; Brym, M.; van Wüllen, C. Low-Valent Silicon Cations with Two-Coordinate Silicon and Aromatic Character. *Angew. Chem., Int. Ed.* **2006**, *45*, 6730–6733.

7. Facile Access to Dative, Single and Double Silicon–Metal Bonds Through M–Cl Insertion Reactions of Base-stabilized Si(II) Cations

Title: “Facile Access to Dative, Single and Double Silicon–Metal Bonds Through M–Cl Insertion Reactions of Base-stabilized Si(II) Cations”¹⁵⁵

Status: Article; published online: February 19, 2020.

Journal: *Chemistry – A European Journal* **2020**, *26*, 6271–6278.

Publisher: Wiley-VCH Verlag GmbH & Co. KGaA, Weinheim.

DOI: [10.1002/chem.202000866](https://doi.org/10.1002/chem.202000866)

Authors: Philipp Frisch, Tibor Szilvási and Shigeyoshi Inoue^a

Reproduced with permission from the Wiley-VCH Verlag. © 2020 Wiley-VCH Verlag GmbH & Co. KGaA.

Content: Dimeric, halide-bridged metal precursors are often used in metalorganic chemistry as convenient starting materials for a variety of complexes. They can easily dissociate into monomers and therefore can offer an essentially free coordination site for the reaction with additional ligands. With the presence of multiple halides, they also have the potential for further functionalization and follow-up chemistry.

This publication outlines the synthesis of a variety of NHC-stabilized chlorosilylene metal complexes through reaction of NHC-stabilized Si(II) cations with chloro-bridged dimeric transition metal precursors. The mechanism of formation was investigated in-depth by theoretical means: the initial coordination of the silyliumylidene ion with concomitant cleavage of the metal dimer is followed by a rapid insertion into the M–Cl bond with simultaneous migration of a silicon-bound NHC to the metal. The mechanism could also be verified experimentally with NMR and SC-XRD characterization of the initially formed silyliumylidene complex.

Due to the presence of three chlorides in the complexes, they were presumed to be ideal starting materials for further functionalization. Initial reduction with one equivalent of potassium graphite leads to an unexpected outcome: the NHC coordinated to silicon dissociates with simultaneous migration of the metal-bound chloride substituent to the silicon center. SC-XRD analysis revealed a substantial decrease in the Si–M bond length. Further reductive dechlorination of the di(chloro)silyl ruthenium complex with additional KC₈ furnishes an unstabilized chlorosilylene transition metal complex. The solid-state structure once again showed a significant decrease in the Si–Ru bond distance, suggesting a double bond character. However, it remains to be seen whether an isolation of a Si≡M triple bond can also be realized with this system, either through further reductive dechlorination or through salt metathesis chloride abstraction.

^aP. Frisch planned and executed all experiments, conducted the SC-XRD measurements including processing of the data and wrote the manuscript. T. Szilvási carried out the computational studies. All work was performed under the supervision of S. Inoue.

Transition Metals | *Hot Paper*

Facile Access to Dative, Single, and Double Silicon–Metal Bonds Through M–Cl Insertion Reactions of Base-Stabilized Si^{II} Cations

Philipp Frisch,^[a] Tibor Szilvási,^[b] and Shigeyoshi Inoue*^[a]

Abstract: Silicon(II) cations can offer fascinating reactivity patterns due to their unique electronic structure: a lone pair of electrons, two empty p orbitals and a positive charge combined on a single silicon center. We now report the facile insertion of N-heterocyclic carbene (NHC)-stabilized silyliumylidene ions into M–Cl bonds (M = Ru, Rh), forming a series of novel chlorosilylene transition-metal complexes. Theoretical investigations revealed a reaction mechanism in which the insertion into the M–Cl bond with concomitant

1,2-migration of a silicon-bound NHC to the transition metal takes place after formation of an initial silyliumylidene transition-metal complex. The mechanism could be verified experimentally through characterization of the intermediate complexes. Furthermore, the obtained chlorosilylene complexes can be conveniently utilized as synthons to access Si–M and Si=M bonding motifs through reductive dehalogenation.

Introduction

The presence of a lone pair of electrons, two vacant orbitals and a positive charge on the silicon center makes silyliumylidene ions an incredibly versatile and promising class of low-valent silicon compounds.^[1] They offer a large, yet untapped synthetic potential in organosilicon chemistry with the possibility to form up to three new bonds in a single reaction.^[2] They are promising candidates for the activation of small molecules, transition metal free catalysis^[3] and can act as synthons for novel (low-valent) silicon compounds. Further, with the presence of a stereochemically active lone pair, they can also function as ligands in transition metal complexes. So far, no one-coordinate Si^{II} cation has been isolated^[4] and most reported examples are three-coordinate and utilize two Lewis bases for their stabilization (e.g. NHCs).^[5] This brings the drawback of a generally reduced reactivity by blocking the empty p-orbitals.

Hence, both amount and diversity of reported reactivities lag behind those of silylenes, where common reactivity patterns include insertion reactions into various types of (strong) bonds. A staggering number of examples for the insertion into E–H (E = H, N, O, S, C, B, ...) and E–Halogen bonds have been reported in recent years.^[6] Similarly, the coordination chemistry of silylenes with transition metals is a continuously expanding research field with various catalytic applications.^[6d,7]

In contrast, even as the number of isolable base-stabilized silyliumylidenes continues to grow,^[4a,8] reported reactivities remain scarce.^[5,9] Only few reactivity studies with small molecules^[10] have been found and E–H bond activation reactions are limited to S–H, O–H and acidic C–H bonds.^[8g,11]

The chemistry of Si^{II} cations as transition metal ligands has seen some progress in recent years.^[12] Reported examples include complexes with coinage metals^[12d] and group 6 and 8 metal carbonyls,^[12b,e] but no further reactivity of these complexes has been reported to date. Importantly, the synthesis of new types of complexes with silicon-based ligands and substituents is of high interest for the development of improved catalysts.^[7a–c,13] With their intriguing synthetic potential, silyliumylidenes are uniquely suited for the facile synthesis of various types of Si–M (multiple) bonds (e.g. through salt metathesis or formation of coordination complexes followed by abstraction/migration of stabilizing Lewis bases). This was elegantly demonstrated by Filippou et al. with the direct synthesis of a molybdenum silylidyne complex.^[12c]

For silylene complexes, a variety of follow-up chemistry is known.^[6d,7] For instance, multiple insertion reactions into metal-chloride bonds of a coordinated transition metal fragment have been reported. For example, Jutzi and co-workers disclosed the insertion of Decamethylsilicocene into a Hg–X bond, furnishing silyl-substituted Hg compounds (I, Scheme 1 A).^[14] The group further reported analogous insertion

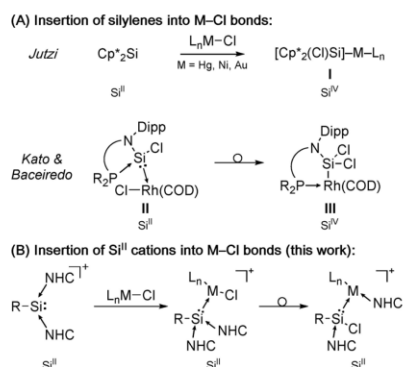
[a] P. Frisch, Prof. Dr. S. Inoue
Department of Chemistry
WACKER-Institute of Silicon Chemistry and Catalysis Research Center
Technische Universität München, Lichtenbergstraße 4, 85748 Garching bei München (Germany)
E-mail: s.inoue@tum.de

[b] Dr. T. Szilvási
Department of Chemical and Biological Engineering
University of Wisconsin-Madison, 1415 Engineering Drive
Madison, Wisconsin 53706-1607 (USA)

Supporting information and the ORCID identification number(s) for the author(s) of this article can be found under:
<https://doi.org/10.1002/chem.202000866>.

© 2020 The Authors. Published by Wiley-VCH Verlag GmbH & Co. KGaA. This is an open access article under the terms of the Creative Commons Attribution License, which permits use, distribution and reproduction in any medium, provided the original work is properly cited.

7. Facile Access to Dative, Single and Double Silicon–Metal Bonds Through M–Cl Insertion Reactions of Base-stabilized Si(II) Cations



Scheme 1. (A) Examples for silylene insertion reactions into M–Cl bonds. (B) Formation of chlorosilylenes via insertion of Si^{III} cations into M–Cl bonds.

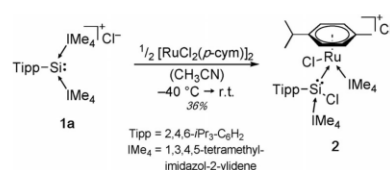
reactions into Ni–Cl and Au–Cl bonds^[15] and related reactivities with Pt–Cl bonds were also reported by Lappert et al.^[16] Recently, Kato, Baceiredo, and co-workers reported the insertion of a chlorosilylene ligand into the Rh–Cl bond of a coordinated [RhCl(COD)] fragment (II), forming the corresponding RSiCl₂–Rh(COD) compound III.^[17] For silyliumylidene ions and their transition-metal complexes, no analogous reactivity has been observed so far. In fact, insertion reactions into E–Halogen bonds have not been reported at all.

Herein, we now report the first reactivity studies regarding insertion reactions of a Si^{III} cation into transition metal-chloride bonds. Reactions of NHC-stabilized silyliumylidene ions with dimeric, chloro-bridged transition-metal precursors lead to coordination of the Si^{III} cation to the metal fragment, followed by insertion of the silyliumylidene ligand into the M–Cl (M = Ru, Rh) bond, furnishing NHC-stabilized transition metal silylene complexes (Scheme 1B). The complexes have been fully characterized by multinuclear NMR spectroscopy and SC-XRD (single crystal X-ray diffraction) and the insertion mechanism has been investigated theoretically and verified experimentally. Furthermore, we present a facile access route to Si–M and Si=M bonds through stepwise reduction of the isolated complexes with KC₈, initially furnishing silyl-substituted complexes, followed by the formation of the corresponding Si=M double bond through additional reductive dehalogenation. Importantly, while these types of insertion reactions are generally accompanied by an increase of the silicon oxidation state from II to IV, no such change occurs for silyliumylidene ions (cf. Scheme 1).

Results and Discussion

Insertion of a Si^{III} cation into a Ru–Cl Bond

While exploring the coordination chemistry of NHC-stabilized Si^{III} cations, we investigated the reaction of the Tipp-substituted silyliumylidene ion **1a**^[8a] with the transition metal precursor [RuCl₂(*p*-cym)]₂ (Scheme 2, *p*-cym = 1-Me-4-*i*Pr-benzene). Addi-



Scheme 2. Synthesis of chlorosilylene ruthenium complex **2**.

tion of cold acetonitrile to a mixture of **1a** and the precursor at –40 °C led to an immediate color change of the solution to deep red. At about –20 to –15 °C, the color of the solution rapidly changed to orange. Even at –40 °C, a color change to orange can be observed within 2 hours. The ²⁹Si NMR of the orange solution displays one resonance with an expected downfield shift at 17.6 ppm (from –69.5 ppm (**1a**)^[8a]), indicating the formation of a single coordination product. Interestingly, the corresponding ¹H NMR (cf. Supporting Information, Figure S8) showed a highly asymmetric species with four separate septets and eight doublets (corresponding to four chemically unique *iso*-propyl groups) and two distinct signal sets for the NHCs. The ¹³C NMR showed two resonances for the carbene carbon atoms at 169.9 and 154.8 ppm, indicating the possible migration of one NHC to the transition metal.

The complex rapidly decomposes at room temperature in solution to a mixture of products, making further investigation and functionalization difficult. Nevertheless, crystals suitable for SC-XRD analysis could be obtained by storing a concentrated solution of **2** in MeCN at –35 °C. Figure 1 shows the solid-state structure of **2**, unambiguously confirming the asymmetric nature of the complex and the shift of one NHC to the metal. The half-sandwich complex with a piano-stool configuration

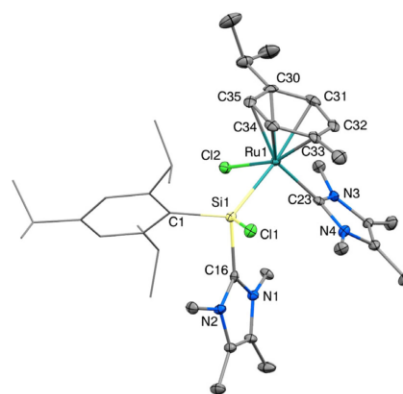


Figure 1. Ellipsoid plot (50%) of the molecular structure of **2**. Hydrogen atoms and the anion are omitted. The Tipp substituent is simplified as a wireframe for clarity. Selected bond lengths (Å) and angles [°]: Si1–Ru1 2.409(1), Si1–Cl1 2.167(1), Si1–C1 1.941(4), Si1–C16 1.970(4), Ru1–Cl2 2.404(1), Ru1–C23 2.077(4), Ru1–*p*-cym_⊥ 1.770(1), C1–Si1–Ru1 123.3(1), Si1–Ru1–*p*-cym_⊥ 131.1(1), Cl1–Si1–Ru1–Cl2 –173.1(1), C16–Si1–Ru1–C23 –11.1(2).

7. Facile Access to Dative, Single and Double Silicon–Metal Bonds Through M–Cl Insertion Reactions of Base-stabilized Si(II) Cations

features an NHC-stabilized aryl-chlorosilylene ligand with a tetrahedral coordination sphere around the silicon center and a Si1–Ru1 bond length (2.409(1) Å) typical for Si–Ru bonds.^[18] The Si–C_{NHC} (1.970(4) Å) and Ru–C_{NHC} (2.077(4) Å) bond lengths are in the typical range for Si–C_{NHC} and Ru–C_{NHC} bonds.

It is worth noting that attempts to stabilize the complex by employing the significantly bulkier *m*-terphenyl (2,6-(2,4,6-Me₃-C₆H₂)₂-C₆H₃) substituent were unsuccessful and no reaction could be observed, presumably due to its large steric hindrance. Similarly, we envisioned the introduction of a Cp* ligand (Cp* = 1,2,3,4,5-pentamethyl-cyclopentadienyl) on the metal. The *p*-cymene ligand is often a weak spot in such complexes, as it can be relatively easily cleaved from the metal. Unfortunately, no reaction of the related precursor [RhCl₂(Cp*)]₂ with **1a** could be observed, most likely due to the increased steric demand of the Cp* substituent.

Formation of complex **2**—mechanistic insights

To elucidate the mechanism of formation of chlorosilylene complex **2**, we performed DFT calculations at the B97-D/def2-SVP level of theory (Figure 2). In a first step, the coordination of a silyliumylidene moiety to each transition metal center leads to the splitting of the dimer, forming the silyliumylidene complex **2'**. This also indicates why no reaction could be observed at all for the significantly bulkier *m*-terphenyl and Cp*: the initial coordination step is blocked due to their large steric hindrance, which completely stops any product formation. After the coordination, the insertion reaction of the low-valent silicon into the Ru–Cl bond occurs with concomitant 1,2-migration of one NHC moiety to the transition metal. We have previously observed a related NHC migration reaction involving NHC-stabilized silyliumylidene ions with the formation of a [(IMe₄)₂Au]Cl complex from a silyliumylidene gold complex.^[12d] This migration/insertion reaction is similar to the mentioned in-

sertion reaction of a chlorosilylene ligand into a Rh–Cl bond (II→III, Scheme 1).^[17] However, a key distinction to the insertion reactions of silylenes is that in the case of the Si^{II} cation, the formal oxidation state of the silicon center does not change: here, the insertion reaction leads from [R–Si^{II}]⁺ to [R–Si^{II}–Cl], whereas silylenes [R₂Si^{IV}] yield silyl-substituted complexes [R₂ClSi^{IV}–M] (cf. Scheme 1).

Based on the calculated reaction profile we presumed that the deep red species observed at low temperatures during the synthesis should be the silyliumylidene complex **2'**. Indeed, low-temperature ²⁹Si NMR analysis (–30 °C) showed a weak resonance at considerably higher field (–21.1 ppm vs. +17.6 ppm for **2**) that immediately vanished upon warming and even disappeared at low temperatures within 2 hours. This upfield shifted resonance is expected for a Si^{II} center with two coordinated NHC moieties and is in line with our previously reported group 6 silyliumylidene complexes (Cr: +6.3 ppm; Mo: –17.3 ppm; W: –30.5 ppm and the related iron complex (+5.4 ppm)).^[12e] To further reinforce the suggestion that **2'** is in fact the intermediate observed at low temperatures, we calculated the ²⁹Si NMR shifts for **2** and **2'**: we find that the calculated chemical shifts (19.8 ppm for **2** and –23.4 ppm for **2'** (HCTH407/def2-SVP//B97-D/def2-SVP)) are in good agreement with the experimentally observed values.

Due to the relatively rapid insertion reaction occurring even at low temperatures, we were unable to structurally characterize **2'**. However, based on these results we hypothesized, that the insertion/migration reaction from **2'** to **2** occurs so rapidly to reduce the considerable steric congestion at the silicon center and that reducing the size of the aryl substituent could enable us to isolate the intermediate silyliumylidene complex. Consequently, we utilized **1b**^[8k] and performed the same reaction (Scheme 3). Indeed, ²⁹Si NMR analysis of the resulting red-orange solution showed a resonance at –20.5 ppm, considerably upfield shifted compared to **2** (17.6 ppm) and very close to

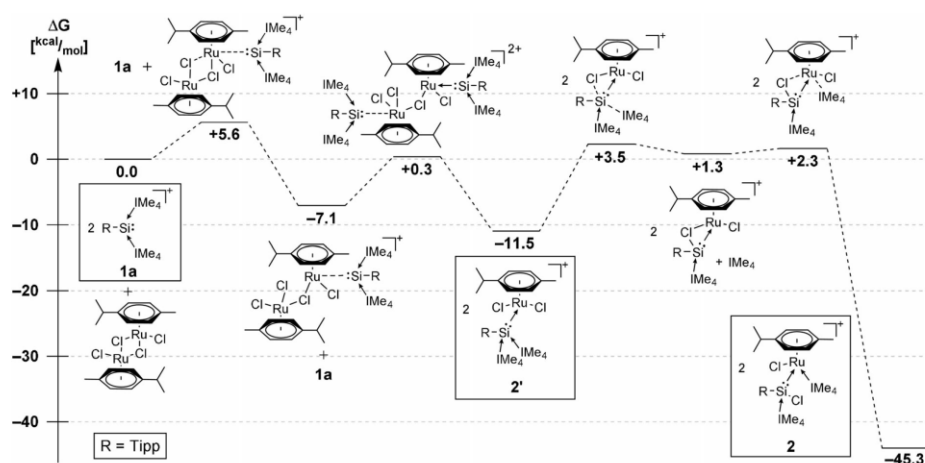
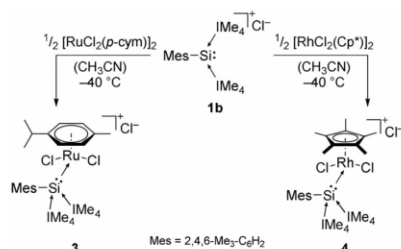


Figure 2. DFT-derived reaction mechanism and energy profile for the formation of **2** from **1a** via **2'**.

7. Facile Access to Dative, Single and Double Silicon–Metal Bonds Through M–Cl Insertion Reactions of Base-stabilized Si(II) Cations



Scheme 3. Synthesis of silyliumylidene complexes **3** and **4**.

the -21.1 ppm for **2'**. However, **3** decomposes incredibly quickly at room temperature (even faster than **2**) and slowly at -35 °C, preventing further characterization and analysis (especially through SC-XRD). Hence, to stabilize the desired complex, we also attempted the reaction with $[\text{RhCl}_2(\text{Cp}^*)]_2$, which proceeds instantly even at -40 °C. ^{29}Si NMR analysis of the deep red solution showed a resonance at -24.2 ppm (d , $^1J_{\text{Si-Rh}} = 66.9$ Hz), indicating the formation of the desired complex **4**. While **4** is somewhat more stable in solution than **3**, it still decomposes rapidly (for details concerning the decomposition, see Supporting Information). Still, we were able to obtain single crystals of **4** through quick diffusion of Et_2O into a MeCN solution at -35 °C. The solid-state structure (Figure 3) revealed a silyliumylidene complex with a geometry comparable to the chlorosilylene complex **3**, except that in **4** both NHCs are still located on the silicon center and both chlorides are still bound to the metal. The compound features a long Rh1–Si1 bond length of 2.426(2) Å with typical Si–C_{NHC} bond lengths (1.958(7) and 1.944(7) Å). The angle between the coordinated NHCs ($93.9(3)^\circ$) is comparable to uncoordinated silyliumylidene ions (e.g. **1a**: $94.3(1)^\circ$).^[12e]

Attempts to convert **4** into the chlorosilylene complex analogous to **2** through prolonged stirring failed due to the low stability of **4** in solution. No conversion could be detected after 12 hours at -35 °C and at higher temperatures only decomposition products were observed.

Reactivity of silyl-substituted silyliumylidene ions

Silyl groups have proven to be excellent substituents for the stabilization of elusive main group species because of their

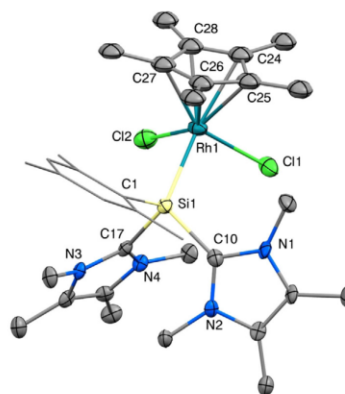
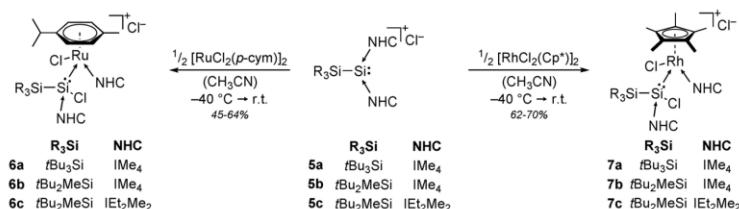


Figure 3. Ellipsoid plot (50%) of the molecular structure of **4**. Hydrogen atoms and the anion are omitted. The mesityl substituent is simplified as a wireframe for clarity. Selected bond lengths [Å] and angles [°]: Si1–Rh1 2.426(2), Si1–C1 1.899(7), Si1–C10 1.958(7), Si1–C17 1.944(7), Rh1–C1 2.420(2), Rh1–Cl2 2.404(2), Rh1–Cp*₁ 1.857(1), C1–Si1–Rh1 112.7(2), C10–Si1–C17 93.9(3), Si1–Rh1–Cp*₁ 132.3(1).

tuneable steric demand as well as their strong σ -electron-donating properties.^[19] Consequently, we attempted the same conversions with our recently reported silyl-substituted silyliumylidenes^[8k] **5** in the hope of furnishing analogous silyliumylidene or chlorosilylene complexes with increased stability in solution to allow further functionalization. Reaction of **5** with $[\text{RuCl}_2(p\text{-cym})]_2$ and $[\text{RhCp}^*\text{Cl}_2]_2$ (Scheme 4) furnished the orange to red chlorosilylene complexes **6** and **7**, respectively. Only **5c** did not react in a clean fashion with $[\text{RhCp}^*\text{Cl}_2]_2$, giving a mixture of products containing the desired complex with less than 40% (cf. Supporting Information Figure S56). Purification attempts were not successful. This can presumably be attributed to the increased steric demand of the bulkier NHCs together with the Cp* ligand, thus favouring side reactions. ^{29}Si NMR analysis of **6–7** (see Table 1) revealed resonances close to **2**, clearly indicating the formation of the analogous chlorosilylene complexes. Furthermore, ^1H and ^{13}C NMR spectra show formation of asymmetric species with clear signal sets for NHCs bound to both silicon and the metal. Generally, reactions with the rhodium precursor give higher yields than the analogous ruthenium reactions due to higher stability of the Rh complexes in solution. While complexes **6** still slowly



Scheme 4. Synthesis of **6** and **7** from **5** ($\text{IEt}_2\text{Me}_2 = 1,3\text{-diethyl-4,5-dimethylimidazol-2-ylidene}$).

7. Facile Access to Dative, Single and Double Silicon–Metal Bonds Through M–Cl Insertion Reactions of Base-stabilized Si(II) Cations

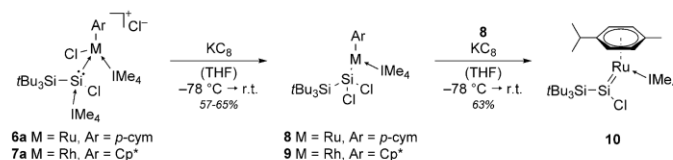
R	M	^{29}Si NMR [ppm]	Si–M [Å]	M–aryl _⊥ [Å]
1a	Tipp	–69.5 ^[9a]		
1b	Mes	–71.2 ^[9a]		
5a	<i>t</i> Bu ₃ Si	–82.0 ^[9a]		
5b	<i>t</i> Bu ₂ MeSi	–90.7 ^[9a]		
5c	<i>t</i> Bu ₂ MeSi ^[b]	–86.2 ^[9a]		
3	Mes	Ru	–20.5	
4	Mes	Rh	–24.2	2.426(2)
2	Tipp	Ru	+17.6	2.409(1)
6a	<i>t</i> Bu ₃ Si	Ru	+29.4	2.499(1)
6b	<i>t</i> Bu ₂ MeSi	Ru	+29.4	
6c	<i>t</i> Bu ₂ MeSi ^[b]	Ru	+23.5	
7a	<i>t</i> Bu ₃ Si	Rh	+23.5	2.423(2)
7b	<i>t</i> Bu ₂ MeSi	Rh	+23.9	2.384(1)
7c	<i>t</i> Bu ₂ MeSi ^[b]	Rh	+18.6	
8	<i>t</i> Bu ₃ Si	Ru		2.374(1)
9	<i>t</i> Bu ₃ Si	Rh		2.328(1)/2.331(1)
10	<i>t</i> Bu ₃ Si	Ru	+240.6 ^[c]	2.236(1)

[a] Ordered according to structural relationship. [b] NHC = IEt₂Me₂. [c] C₆D₆.

decompose at room temperature in solution (**6a** being the most stable of all ruthenium complexes with full decomposition after roughly 12 hours), **7a** and **7b** are stable for at least two weeks.

To further elucidate and strengthen our proposed reaction mechanism, we used the *t*Bu₃Si-substituted silyliumylidene triflate **5a-OTf** (instead of chloride) and carried out the same reaction: the corresponding complex **7a-OTf** could be obtained (cf. Supporting Information, Figures S46–S48), excluding any relevant involvement of the anion in the reaction mechanism. This reactivity also further underscores the hypothesis that the Si^{II} cation indeed inserts into the M–Cl bond.

SC-XRD analysis of complexes **6a**, **7a** and **7b** (for details, see Supporting Information Figure S82–S84) revealed the same general structural motif present in **2**. The Si–M bonds (**2**: 2.409(1) Å, **6a**: 2.499(1) Å, **7a**: 2.423(2) Å, **7b**: 2.384(1) Å) in all complexes are quite long. Interestingly, **2** exhibits a shorter bond length ($\Delta = 0.09$ Å, 3.6%) than **6a**. This trend in bond lengths can also be observed in the related silyl- and aryl-substituted hydrosilylene iron complexes (e.g. Si–Fe distance in *Ar*yl(H)Si(NHC)→Fe(CO)₄ (2.3268(6) Å^[20]) is shorter than in *Silyl*yl(H)Si(NHC)→Fe(CO)₄ (2.3717(16) Å^[21])). The distance between the metal and the centroid of the aryl ligand M–aryl_⊥ are statistically identical in **2** and **6a** (1.770(1) Å vs. 1.767(1) Å).



Scheme 5. Reduction of **6a** and **7a** with KC_8 to silyl complexes **8** and **9** and to silylene complex **10**.

Si1–Cl1 bonds are essentially identical in all complexes, with Si1–C_{NHC} bonds being slightly longer for the *t*Bu₃Si substituted complexes. The two chloride substituents are oriented almost completely opposite to each other in **2** (dihedral angle Cl–Si–M–Cl: –173.1(1)°), while they exhibit a slightly more staggered position in **6a** and **7a** (–156.1(1)° and –154.8(1)°, respectively). A similar trend can be observed for the dihedral angle between the two NHC ligands: **2** shows a C_{NHC}–Si–M–C_{NHC} dihedral angle of –11.1(2)°, whereas narrowing of this angle can be observed for **6a** and **7a** (–0.2(2)° and –4.2(3), respectively). The angle between the calculated planes of the two NHC scaffolds in the *t*Bu₃Si-substituted complexes (**6a**: 25.0°, **7a**: 32.5°) are significantly smaller compared to the Tipp-substituted complex (**2**: 45.8°), meaning they are oriented in a more parallel fashion.

Access to Si–M single and Si–M double bonds

As complexes **2**, **6** and **7** exhibit a halide counterion and one halide bound to the silicon and transition metal each, we thought them to be ideal precursors for the synthesis of Si–Ru and Si–Rh multiple bonds through reductive dehalogenation. We utilized the *t*Bu₃Si-substituted complexes **6a** and **7a** for further investigations due to their significantly increased stability in solution. After treatment of **6a** and **7a** with one equivalent of potassium graphite (Scheme 5), we were able to isolate the unexpected paramagnetic silyl-substituted complexes **8** (bright green) and **9** (grey-black) in moderate and good yield, respectively. EPR analysis of **8** and **9** revealed only a single band in both cases (cf. Supporting Information, Figures S64 and S67). No hyperfine coupling to α - or β -silicon could be observed. The *g*-values (**8**: *g* = 2.1062, **9**: *g* = 2.1003) are in line with other paramagnetic ruthenium and rhodium complexes.^[22] We successfully confirmed the composition of **8** and **9** through SC-XRD analysis (Figure 4, left and center). Formation of these complexes most likely takes place through 1,2-migration of the metal-bound chloride to silicon under dissociation of the silicon-bound NHC. As expected, the chloride counterion was the first halide to be removed through reductive dehalogenation.

The Si1–Ru1 bond length in **8** (2.374(1) Å) is shortened significantly ($\Delta = 0.125$ Å, 5.0%) in comparison to **6a**, which is consistent with a reduction of the complex and an increase in the bond order of the Si–Ru bond. Similarly, the Si1–Rh1 bond length in **9** (2.328(1)/2.331(1) Å) is also reduced ($\Delta = 0.094$ Å (average), 3.9%) in comparison to **7a**. Interestingly, the Ru–*p*-cym_⊥ distance in **8** (1.756(1) Å) is slightly shorter than in **6a**

7. Facile Access to Dative, Single and Double Silicon–Metal Bonds Through M–Cl Insertion Reactions of Base-stabilized Si(II) Cations

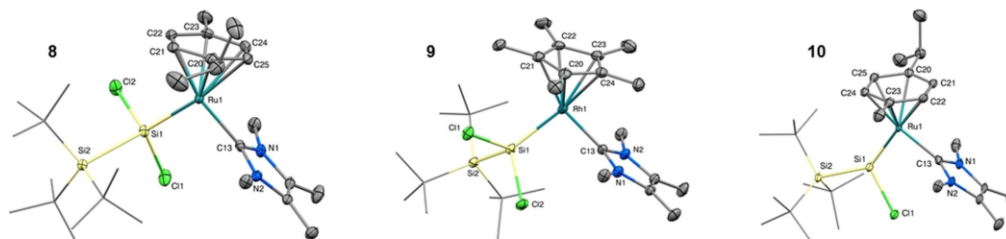


Figure 4. Ellipsoid plot (50%) of the molecular structures of **8** (left), **9** (middle, one out of two independent molecules in the asymmetric unit shown) and **10** (right). Hydrogen atoms are omitted and the *t*Bu substituents are simplified as wireframes for clarity. Selected bond lengths [Å] and angles [°]: **8**: Si1–Ru1 2.374(1), Si1–Cl1 2.161(1), Si1–Cl2 2.160(1), Si1–Si2 2.424(1), Ru1–C13 2.064(2), Ru1–*p*-cym_⊥ 1.756(1), Si2–Si1–Ru1 128.0(1), Si1–Ru1–*p*-cym_⊥ 134.0(1); **9**: Si1–Rh1 2.328(1)/2.331(1), Si1–Cl1 2.145(1)/2.146(1), Si1–Cl2 2.170(1)/2.171(1), Si1–Si2 2.430(1)/2.429(1), Rh1–C13 2.033(3)/2.018(3), Rh1–Cp*_⊥ 1.911(1)/1.909(1), Si2–Si1–Rh1 126.6(1)/126.0(4), Si1–Rh1–Cp*_⊥ 135.7(1)/136.1(1); **10**: Si1–Ru1 2.236(1), Si1–Cl1 2.169(1), Si1–Si2 2.416(1), Ru1–C13 2.055(4), Ru1–*p*-cym_⊥ 1.751(1), Si2–Si1–Ru1 143.8(1), Si1–Ru1–*p*-cym_⊥ 147.7(1).

(1.767(1) Å), whereas the Rh–Cp*_⊥ distance is slightly increased from 1.895(1) Å in **7a** to 1.911(1)/1.909(1) Å in **9**.

We further attempted the reaction of **6a** with two equivalents of KC₈ in the hopes of furnishing a Si–Ru bond. Indeed, two-electron reduction of **6a** or additional reduction of **8** with 1 KC₈ yielded the ruthenium silylene complex **10** (Scheme 5, 63% from **8**, 41% from **6a**). During the reaction, an intense color change from bright green (**8**) to deep red (**10**) can be easily observed. We also attempted the reduction of complex **7a** (or **9**; color change from black to purple) to a similar Si=Rh species. While ²⁹Si NMR and mass spectrometry analysis (for details, see Supporting Information) suggest that formation of the analogous complex takes place (albeit in a significantly less clean fashion), we have been unable to obtain satisfactory analytical data so far.

With the additional reductive step, **10** is no longer paramagnetic. The ²⁹Si NMR exhibits a significantly downfield shifted resonance at 240.6 ppm, which falls in the expected range of Si=M bonds with a three coordinate Si center^[23] and indicates the multiple-bond character of the Si–Ru bond. The observed resonance is even more downfield shifted than the previously reported structurally related aryl-chlorosilylene complexes Cp*(R₃P)(H)Ru=SiCl(aryl) (aryl=Tipp (221.7 ppm), *m*-terphenyl (205.0 ppm)).^[23a] No signal splitting analogous to complexes **6** and **7** could be observed in the ¹H/¹³C NMR spectra. The carbene carbon atom of the metal-bound NHC also exhibits a significantly more downfield shifted resonance at 188.5 ppm compared to the 172.1 ppm observed for **6a**.

SC-XRD analysis of **10** (Figure 4, right) revealed the expected structure with only one chloride atom bound to the silicon center. The silylene silicon adopts a trigonal planar coordination sphere (sum of angles around Si1: 359.4°). Again, a significant shortening (Δ = 0.138 Å, 5.8%) of the Si–Ru bond takes place from 2.374(1) Å (**8**) to 2.236(1) Å (**10**) (cf. Δ = 0.263 Å, 10.5% from **6a**), further indicating double-bond character. In fact, the Si–Ru bond length is easily in the range of other Si–Ru double bonds (2.18^[23a]–2.34 Å^[18,24]).

Computational studies

To better understand the bonding situation and the electronic structure of the isolated complexes, we also carried out DFT calculations (for details, see Supporting Information). The calculated metric parameters (Table 2, Supporting Information Table S10) show good agreement with the experimentally ob-

Table 2. Summary of the calculated Si–M bond lengths, NPA atomic charges and Wiberg bond index (WBI)/Mayer bond order (MBO) of the investigated complexes.

	M	Theor.		NPA atomic charge		WBI	MBO
		Si–M [Å]	Si	M	Si–M		
2	Ru	2.392	+1.31	–0.56	0.73	0.83	
4	Rh	2.365	+1.23	–0.25	0.64	0.81	
6a	Ru	2.481	+0.81	–0.53	0.73	0.72	
7a	Rh	2.428	+0.74	–0.21	0.64	0.70	
8	Ru	2.371	+0.74	–0.46	0.60	0.86	
9	Rh	2.324	+0.68	–0.21	0.68	0.91	
10	Ru	2.225	+0.62	–0.73	1.35	1.52	

served values, indicating the validity of the computational method. Analysis of the Natural Bond Orbitals (NBO, Supporting Information Table S3–S9) revealed that the Si–M bond polarity can change in different complexes: for example, the Si–Ru bond is polarized towards the metal center in complexes **2**, **8**, and **10**. In contrast, the bond is polarized towards the Si atom in **6a**. Combined with the very long Si–Ru bond distance in **6a** (2.499(1) Å), we conclude that the Si–Ru bond in **6a** is more dative in nature while it exhibits an increased covalent character in the other complexes. Natural Population Analysis (NPA, Table 2 and Supporting Information Table S10) shows that for the aryl-substituted complexes **2** and **4** the central Si atom bears a more positive charge than in the silyl-substituted complexes **6a**, **7a** and **8–10**. This can presumably be attributed to the stronger σ -donating properties of the silyl moieties compared to aryl groups. In general, the ruthenium center in complexes **2**, **6a** and **8** exhibits a more negative charge than

7. Facile Access to Dative, Single and Double Silicon–Metal Bonds Through M–Cl Insertion Reactions of Base-stabilized Si(II) Cations

the Rh atom in **4**, **7a** and **9**. The Ru center in complex **10** exhibits the highest negative charge (−0.73) out of all complexes. This increased negative charge is most likely the consequence of the double bond character of the Si–Ru bond in **10** suggested by the NBOs (cf. Supporting Information, Table S9). The Wiberg Bond Index (WBI) and Mayer Bond Order (MBO) also support the double bond character, as both WBI and MBO for complex **10** are significantly higher than in the other complexes. These results agree well with the experimentally determined Si–M bond lengths. The calculated frontier orbitals also confirm the validity of the Si–Ru bond in **10** (Figure 5), where the HOMO (highest occupied molecular orbital) and LUMO (lowest unoccupied molecular orbital) correspond to the bonding and anti-bonding orbital of the Si–Ru π -bond. Additionally, we were unable to find similar orbitals for the other investigated complexes (cf. Supporting Information, Figure S88–S93), in which the HOMO and LUMO are associated with the metal d orbitals and the π -system of the Cp* or *p*-cymene ligands.

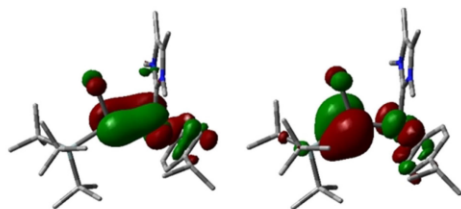


Figure 5. Calculated frontier orbitals of Si=Ru complex **10**: HOMO (left, −3.52 eV) and LUMO (right, −1.43 eV).

Conclusions

In summary, we have used NHC-stabilized Si^{II} cations as a convenient entry point for the isolation of Si→M, Si–M and Si=M moieties via the insertion of silyliumylidenes into M–Cl (M = Ru, Rh) bonds with simultaneous silicon-to-metal NHC-migration, followed by reductive dehalogenation. This work significantly expands the still-young field of silyliumylidene transition metal coordination chemistry and showcases the ease with which relatively bulky aryl- and silyl-substituted silyliumylidenes insert into M–Cl bonds, forming chlorosilylene transition metal complexes. This is an important distinction to previously reported M–Cl insertion reactions of low-valent silicon compounds, where the insertion leads to Si^{IV} compounds. The mechanism of formation was investigated theoretically and predicted to include an initially formed silyliumylidene transition metal complex followed by insertion of the Si^{II} cation into the M–Cl bond with concomitant 1,2-migration of a silicon-bound NHC moiety to the metal. This could be verified experimentally through NMR and XRD characterization of the silyliumylidene complexes.

The presence of multiple halides on the isolated chlorosilylene complexes gives a simple access route to Si–M single and Si=M double bonds through successive reductive dechlorination. The possible utilization of this synthetic approach to

access various transition metal silylidene and silyldiynes complexes is currently under investigation in our laboratory.

Acknowledgements

The authors are exceptionally grateful to the WACKER Chemie AG and the European Research Council (SILION 637394) for continued financial support. We are also thankful to Dr. A. Pöthig and Dr. C. Jandl for advice regarding crystallography, to M. Muhr for recording the LIFDI-MS spectra and to Dr. O. Storcheva for recording the EPR spectra.

Conflict of interest

The authors declare no conflict of interest.

Keywords: carbene ligands · insertion · reduction · silylene · transition metals

- [1] G. Bertrand, *Science* **2004**, *305*, 783–785.
- [2] P. P. Gaspar, *Organosilicon Chemistry VI: From Molecules to Materials* (Eds.: N. Auner, J. Weis), Wiley-VCH, Weinheim **2005**, pp. 10–92.
- [3] a) K. Leszczyńska, A. Mix, R. J. F. Berger, B. Rummel, B. Neumann, H.-G. Stammer, P. Jutzi, *Angew. Chem. Int. Ed.* **2011**, *50*, 6843–6846; *Angew. Chem.* **2011**, *123*, 6975–6978; b) E. Fritz-Langhals, *Org. Process Res. Dev.* **2019**, *23*, 2369–2377; c) B. X. Leong, J. Lee, Y. Li, M.-C. Yang, C.-K. A. Siu, M.-D. Su, C.-W. So, *J. Am. Chem. Soc.* **2019**, *141*, 17629–17636.
- [4] a) P. Jutzi, A. Mix, B. Rummel, W. W. Schoeller, B. Neumann, H.-G. Stammer, *Science* **2004**, *305*, 849–851; b) T. Müller, *Organometallics* **2010**, *29*, 1277–1283; c) C. Gerdes, W. Saak, D. Haase, T. Müller, *J. Am. Chem. Soc.* **2013**, *135*, 10353–10361.
- [5] a) V. Nesterov, D. Reiter, P. Bag, P. Frisch, R. Holzner, A. Porzelt, S. Inoue, *Chem. Rev.* **2018**, *118*, 9678–9842; b) S. L. Powlley, S. Inoue, *Chem. Rec.* **2019**, *19*, 2179–2188.
- [6] a) Y. Mizuhata, T. Sasamori, N. Tokitoh, *Chem. Rev.* **2009**, *109*, 3479–3511; b) N. J. Hill, R. West, *J. Organomet. Chem.* **2004**, *689*, 4165–4183; c) T. Chu, G. I. Nikonov, *Chem. Rev.* **2018**, *118*, 3608–3680; d) T. Iwamoto, S. Ishida, *Organosilicon Compounds: Theory and Experiment (Synthesis)* (Ed.: V. Y. Lee), Academic Press, Massachusetts **2017**, pp. 361–532.
- [7] a) Y.-P. Zhou, M. Driess, *Angew. Chem. Int. Ed.* **2019**, *58*, 3715–3728; *Angew. Chem.* **2019**, *131*, 3753–3766; b) S. Raoufmoqhammad, Y.-P. Zhou, Y. Wang, M. Driess, *J. Organomet. Chem.* **2017**, *829*, 2–10; c) B. Blom, M. Stoelzel, M. Driess, *Chem. Eur. J.* **2013**, *19*, 40–62; d) M. Okazaki, H. Tobita, H. Ogino, *Dalton Trans.* **2003**, 493–506; e) L. Álvarez-Rodríguez, J. A. Cabeza, P. García-Álvarez, D. Polo, *Coord. Chem. Rev.* **2015**, *300*, 1–28.
- [8] a) M. Driess, S. Yao, M. Brym, C. van Wüllen, *Angew. Chem. Int. Ed.* **2006**, *45*, 6730–6733; *Angew. Chem.* **2006**, *118*, 6882–6885; b) Y. Xiong, S. Yao, S. Inoue, E. Irran, M. Driess, *Angew. Chem. Int. Ed.* **2012**, *51*, 10074–10077; *Angew. Chem.* **2012**, *124*, 10221–10224; c) H.-X. Yeong, H.-W. Xi, Y. Li, K. H. Lim, C.-W. So, *Chem. Eur. J.* **2013**, *19*, 11786–11790; d) Y. Xiong, S. Yao, S. Inoue, J. D. Epping, M. Driess, *Angew. Chem. Int. Ed.* **2013**, *52*, 7147–7150; *Angew. Chem.* **2013**, *125*, 7287–7291; e) A. C. Filippou, Y. N. Lebedev, O. Chernov, M. Straßmann, G. Schnakenburg, *Angew. Chem. Int. Ed.* **2013**, *52*, 6974–6978; *Angew. Chem.* **2013**, *125*, 7112–7116; f) Y. Li, Y.-C. Chan, Y. Li, I. Purushothaman, S. De, P. Parameswaran, C.-W. So, *Inorg. Chem.* **2016**, *55*, 9091–9098; g) S. U. Ahmad, T. Szilvási, S. Inoue, *Chem. Commun.* **2014**, 50, 12619–12622; h) T. Agou, N. Hayakawa, T. Sasamori, T. Matsuo, D. Hashizume, N. Tokitoh, *Chem. Eur. J.* **2014**, *20*, 9246–9249; i) N. Hayakawa, K. Sadamori, S. Mizutani, T. Agou, T. Sugahara, T. Sasamori, N. Tokitoh, D. Hashizume, T. Matsuo, *Inorganics* **2018**, *6*, 30; j) Y. Li, Y.-C. Chan, B.-X. Leong, Y. Li, E. Richards, I. Purushothaman, S. De, P. Parameswaran, C.-W. So, *Angew. Chem. Int. Ed.*

7. Facile Access to Dative, Single and Double Silicon–Metal Bonds Through M–Cl Insertion Reactions of Base-stabilized Si(II) Cations

- 2017, 56, 7573–7578; *Angew. Chem.* **2017**, 129, 7681–7686; k) P. Frisch, S. Inoue, *Dalton Trans.* **2019**, 48, 10403–10406.
- [9] P. Jutzi, *Chem. Eur. J.* **2014**, 20, 9192–9207.
- [10] a) S. U. Ahmad, T. Szilvási, E. Irran, S. Inoue, *J. Am. Chem. Soc.* **2015**, 137, 5828–5836; b) A. C. Filippou, B. Baars, O. Chernov, Y. N. Lebedev, G. Schnakenburg, *Angew. Chem. Int. Ed.* **2014**, 53, 565–570; *Angew. Chem.* **2014**, 126, 576–581; c) D. Sarkar, D. Wendel, S. U. Ahmad, T. Szilvási, A. Pöthig, S. Inoue, *Dalton Trans.* **2017**, 46, 16014–16018.
- [11] a) A. Porzelt, J. Schweizer, R. Baierl, P. Altmann, M. Holthausen, S. Inoue, *Inorganics* **2018**, 6, 54; b) D. Sarkar, V. Nesterov, T. Szilvási, P. J. Altmann, S. Inoue, *Chem. Eur. J.* **2019**, 25, 1198–1202.
- [12] a) N. C. Breit, T. Szilvási, T. Suzuki, D. Gallego, S. Inoue, *J. Am. Chem. Soc.* **2013**, 135, 17958–17968; b) H.-X. Yeong, Y. Li, C.-W. So, *Organometallics* **2014**, 33, 3646–3648; c) P. Ghana, M. I. Arz, G. Schnakenburg, M. Straßmann, A. C. Filippou, *Organometallics* **2018**, 37, 772–780; d) P. Frisch, S. Inoue, *Chem. Commun.* **2018**, 54, 13658–13661; e) P. Frisch, T. Szilvási, A. Porzelt, S. Inoue, *Inorg. Chem.* **2019**, 58, 14931–14937.
- [13] Z. Benedek, T. Szilvási, *RSC Adv.* **2015**, 5, 5077–5086.
- [14] M. Theil, P. Jutzi, B. Neumann, A. Stämmler, H.-G. Stämmler, *Organometallics* **2000**, 19, 2937–2940.
- [15] M. Theil, P. Jutzi, B. Neumann, A. Stämmler, H.-G. Stämmler, *J. Organomet. Chem.* **2002**, 662, 34–42.
- [16] B. Gehrhuis, P. B. Hitchcock, M. F. Lappert, H. Maciejewski, *Organometallics* **1998**, 17, 5599–5601.
- [17] S. Takahashi, E. Bellan, A. Baceiredo, N. Saffon-Merceron, S. Massou, N. Nakata, D. Hashizume, V. Branchadell, T. Kato, *Angew. Chem. Int. Ed.* **2019**, 58, 10310–10314; *Angew. Chem.* **2019**, 131, 10416–10420.
- [18] H. Hashimoto, J. Sato, H. Tobita, *Organometallics* **2009**, 28, 3963–3965.
- [19] N. Wiberg, K. Amelunxen, H. W. Lerner, H. Schuster, H. Nöth, I. Krossing, M. Schmidt-Amelunxen, T. Seifert, *J. Organomet. Chem.* **1997**, 542, 1–18.
- [20] D. Lutters, C. Severin, M. Schmidtman, T. Müller, *J. Am. Chem. Soc.* **2016**, 138, 6061–6067.
- [21] C. Eisenhut, T. Szilvási, G. Dübek, N. C. Breit, S. Inoue, *Inorg. Chem.* **2017**, 56, 10061–10069.
- [22] a) M. A. Casado, J. J. Pérez-Torrente, J. A. López, M. A. Ciriano, P. J. Alonso, F. J. Lahoz, L. A. Oro, *Inorg. Chem.* **2001**, 40, 4785–4792; b) B. B. Wayland, A. E. Sherry, A. G. Bunn, *J. Am. Chem. Soc.* **1993**, 115, 7675–7684; c) A. H. Maki, N. Edelstein, A. Davison, R. H. Holm, *J. Am. Chem. Soc.* **1964**, 86, 4580–4587; d) M. M. T. Khan, D. Srinivas, R. I. Kureshy, N. H. Khan, *Inorg. Chem.* **1990**, 29, 2320–2326; e) R. E. DeSimone, *J. Am. Chem. Soc.* **1973**, 95, 6238–6244.
- [23] a) P. G. Hayes, R. Waterman, P. B. Glaser, T. D. Tilley, *Organometallics* **2009**, 28, 5082–5089; b) A. C. Filippou, O. Chernov, G. Schnakenburg, *Angew. Chem. Int. Ed.* **2011**, 50, 1122–1126; *Angew. Chem.* **2011**, 123, 1154–1158.
- [24] M. Ochiai, H. Hashimoto, H. Tobita, *Angew. Chem. Int. Ed.* **2007**, 46, 8192–8194; *Angew. Chem.* **2007**, 119, 8340–8342.

Manuscript received: February 17, 2020

Accepted manuscript online: February 19, 2020

Version of record online: ■■■, 0000

7. Facile Access to Dative, Single and Double Silicon–Metal Bonds Through M–Cl Insertion Reactions of Base-stabilized Si(II) Cations

FULL PAPER



A facile access route to Si–M, Si–M, and Si=M (M = Ru, Rh) moieties through the insertion of NHC-stabilized silylium-ylidene ions into metal–chloride bonds and subsequent reductive dehalogenation is reported. The coordination–insertion–

tion–migration mechanism was investigated theoretically and verified experimentally through NMR and XRD characterization of the intermediate silylium-ylidene transition-metal coordination complexes.

Transition Metals

P. Frisch, T. Szilvási, S. Inoue*

■ ■ – ■ ■

Facile Access to Dative, Single, and Double Silicon–Metal Bonds Through M–Cl Insertion Reactions of Base-Stabilized Si^{II} Cations

8. Summary and Outlook

Since Jutzi's seminal work on the pentamethylcyclopentadiene silicon(II) cation **L-22** in 2004¹¹³, the field of silyliumylidene ions has been expanding ever since and these highly reactive species have been garnering increasing interest in both academia and industry. As detailed in chapter 2.3.4 of this thesis, not just the stoichiometric activation of a variety of small molecules has been reported, but also transition metal-free catalytic applications, the use of silyliumylidene ions as synthons for novel low-valent silicon compounds and coordination chemistry with transition metals.

In 2014, our group reported the novel aryl-substituted NHC-stabilized silyliumylidene ions **L-29**, isolated through a convenient one-pot procedure from readily available aryl-dichlorosilane precursors through abstraction of HCl with free NHCs.¹²⁵ Motivated by the interesting chemistry reported on the activation of phenylacetylene¹²⁵ and CO₂¹⁴⁴ with **L-29** as well as the first report of a transition metal coordination complex synthesized directly from a silyliumylidene ion from So *et al.*¹⁵⁰ with their DMAP-stabilized silyliumylidene ion **L-25**¹²¹, this thesis sought to expand the scope of transition metal coordination chemistry with Si(II) cations as ligands.

Furthermore, as the sole substituent of a silyliumylidene ion can have a pronounced impact on their reactivity and stability including the coordination behavior, the isolation of novel silyliumylidene ions with different substituents was also targeted and the previously reported dichlorosilane-based one-pot procedure chosen as the synthetic approach.

8.1 Novel NHC-stabilized Silyliumylidene Ions

To isolate the first silyl-substituted silyliumylidene ions, a variety of literature known silyl-dichlorosilanes were synthesized and then reacted with three equivalents of NHCs (Figure 17A).¹⁵² Addition of free NHCs to the dichlorosilane precursors leads to a rapid precipitation of a 1:1 mixture of imidazolium chloride and silyliumylidene chlorides **1-3**. While the reaction is essentially quantitative, removal of the imidazolium chloride byproduct reduces the isolable yield to ~55-65%. Separation of the low-valent silicon species and the imidazolium salt was conveniently achieved through extraction with a mixture of acetonitrile and toluene. This procedure can also be applied to other silyliumylidene ions synthesized *via* the same route. Adapting to the different

solubilities of various combinations of imidazolium salt and Si(II) cation as well as the stability in different solvents is easily possible by varying the polar solvent and the solvent mixture ratio.

Whereas the bulky ${}^t\text{Bu}_3\text{Si}$ substituent does not allow isolation of silyliumylidene ions with NHCs larger than IMe_4 , replacement of the ${}^t\text{Bu}_3\text{Si}$ moiety with ${}^t\text{Bu}_2\text{MeSi}$ makes the isolation of the IEt_2Me_2 coordinated Si(II) cation **2b** possible. In comparison to the previously utilized aryl substituents, introduction of these silyl groups leads to a strong upfield shift in the observed ${}^{29}\text{Si}$ NMR resonance due the stronger σ -electron donating properties of the silyl moieties and a decreased pyramidalization around the central silicon atom.

Moreover, implementation of the mesityl group as a substituent with a relatively small steric demand was also achieved. As **3** is not stable in acetonitrile solution, separation of the $\text{IMe}_4\cdot\text{HCl}$ byproduct was achieved by using pyridine as the solvent.

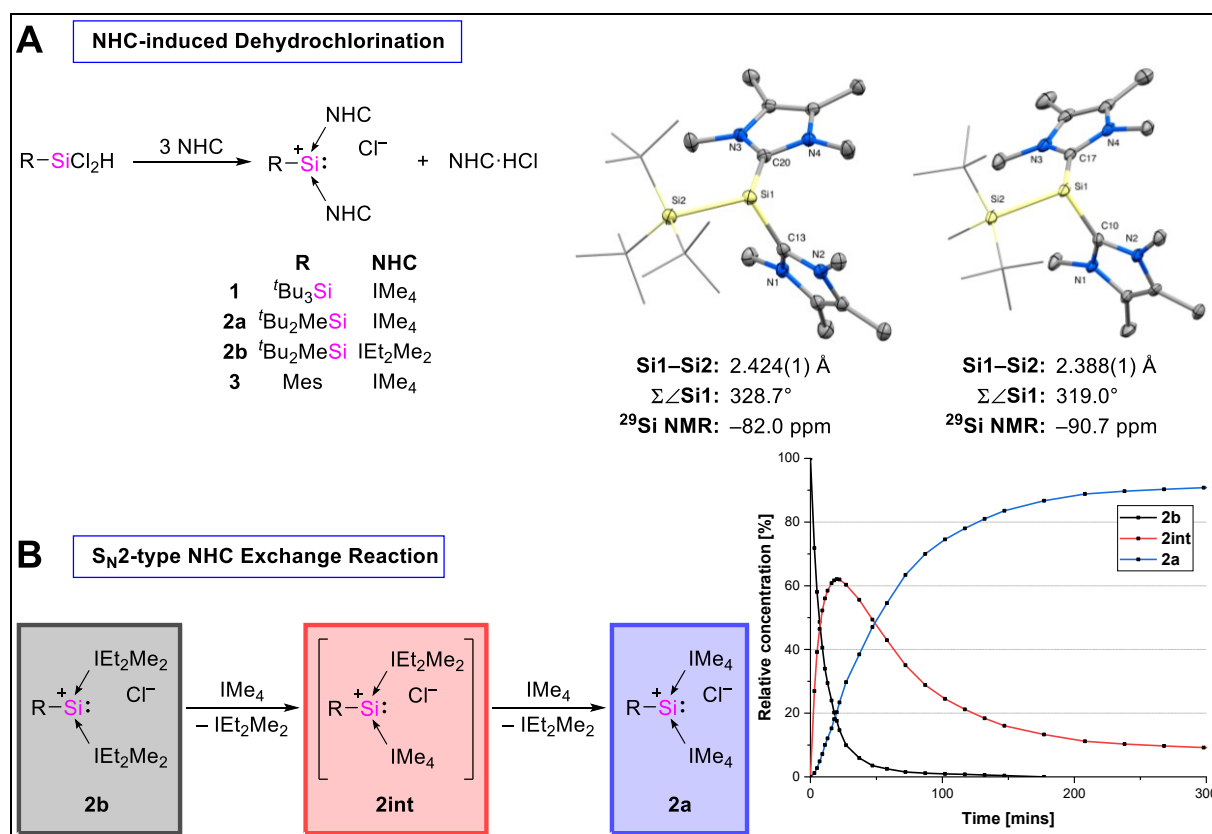


Figure 17 Synthesis of novel NHC-stabilized silyliumylidene ions **1-3** and SC-XRD structures of **1** and **2a** (A); NHC exchange reaction of silyliumylidene **2b** with plot of the relative concentrations of **2b**, **2int** and **2a** over time (B).

Interestingly, it is easily possible to exchange the coordinated IEt_2Me_2 moieties in **2b** with the smaller, stronger Lewis base IMe_4 . The reaction progress can be conveniently monitored *via* ${}^1\text{H}$ NMR analysis, which also allows investigation of the reaction kinetics:

the exchange reactions follow the 2nd order rate law, which indicates an associative S_N2-type mechanism. Exchange of IMe₄ with IEt₂Me₂ cannot be achieved due to the increased σ -donor strength of IMe₄.

8.2 Coordination Chemistry of NHC-stabilized Silyliumylidene Ions

With a variety of different silyliumylidene ions in hand, the field of coordination chemistry with Si(II) cations as ligands was tackled. The transition metals, that could be successfully utilized for the synthesis of a variety of different NHC-stabilized silyliumylidene complexes are indicated in Figure 18.

Group								
4	5	6	7	8	9	10	11	12
Ti	V	Cr	Mn	Fe	Co	Ni	Cu	Zn
Zr	Nb	Mo	Tc	Ru	Rh	Pd	Ag	Cd
Hf	Ta	W	Re	Os	Ir	Pt	Au	Hg

Figure 18 Successfully employed transition metals in the coordination chemistry with NHC-stabilized silyliumylidene ions during this thesis.

It was possible to isolate and fully characterize a range of complexes with transition metals from groups 6, 8, 9 and 11. A more detailed summary of the obtained results is given below.

8.2.1 Coinage Metal Complexes – Monomeric vs. Dimeric Structures

In an initial experiment, the *m*-terphenyl-substituted silyliumylidene ion **L-29a** was reacted with the simple coinage metal salts CuCl, AgOTf and (Me₂S)AuCl (Figure 19A).¹⁵³ Addition of these salts to an acetonitrile solution of **L-29a** led to the rapid decolorization of the initially bright orange solution. After recrystallization, the full series of the first coinage metal complexes **4a**, **5a** and **6a** of a silyliumylidene ion could be isolated in high yield. ²⁹Si NMR analysis of the complexes revealed the expected downfield shifts in comparison to the free Si(II) cation. In this context, the most interesting feature is the observation of two doublets in the ²⁹Si NMR of the silver complex **5a** due to the coupling with the ¹⁰⁷Ag and ¹⁰⁹Ag nuclei.

In the case of the sterically demanding ^{Mes}Ter substituent on **L-29a**, the formed complexes **4a**, **5a** and **6a** are indefinitely stable in solution and display a monomeric structure in the solid state. Reducing the steric bulk of the silyliumylidene substituent to the Tipp group results in a dimerization along the M–Cl bond (complexes **4b**, **5b** and **6b**) and a significantly decreased stability in solution. Upon decomposition, NHC migration to the transition metal takes place, furnishing bis(NHC) metal complexes (Figure 19B). The resulting silicon species could not be identified.

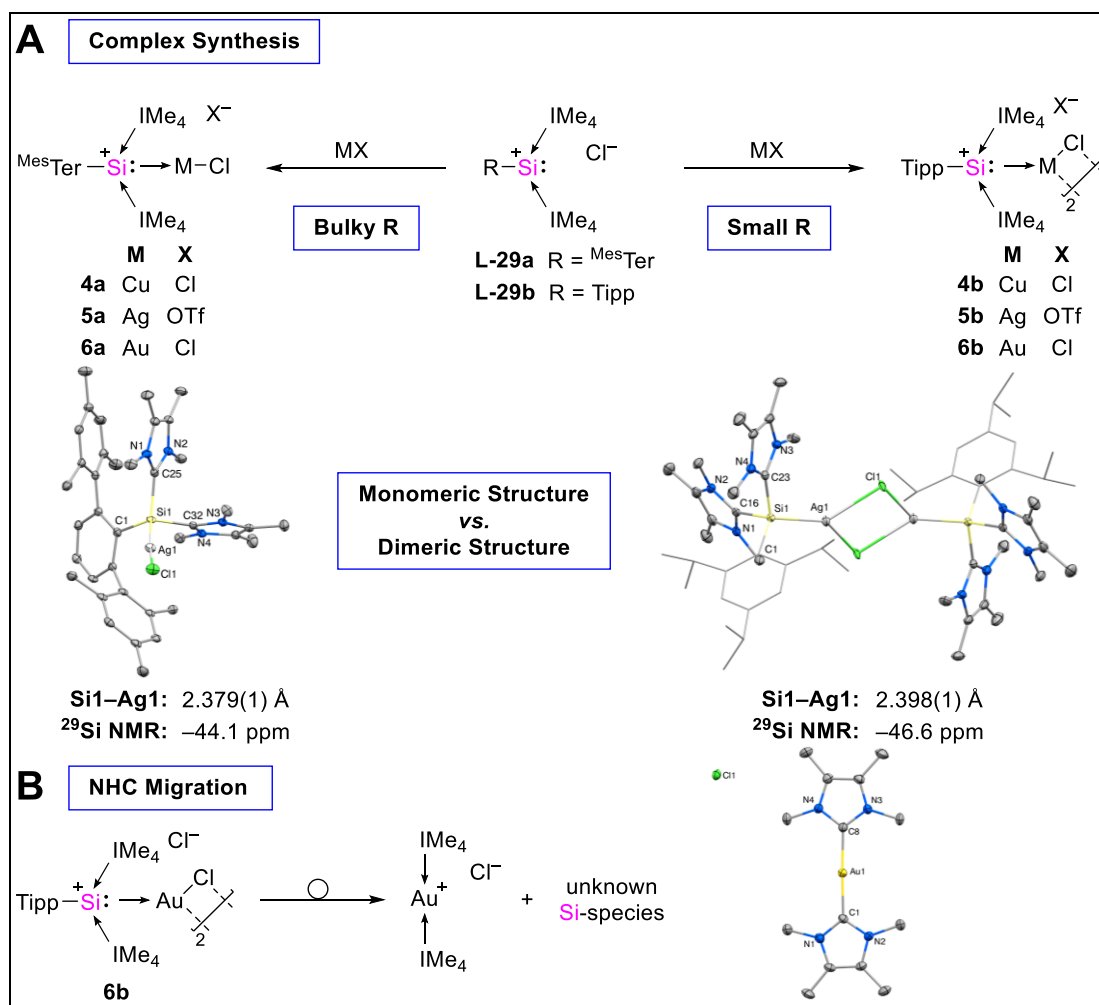


Figure 19 Synthesis of the first coinage metal complexes **4-6** of a silyliumylidene ion with the SC-XRD structures of the monomeric and dimeric Ag complexes (**A**); NHC migration reaction observed for the dimeric Au complex **6b** (**B**).

8.2.2 Transition Metal Carbonyl Complexes and Ligand Properties

Since no investigations of the properties of silyliumylidene ions as ligands had been reported and transition metal carbonyl complexes are exceptionally useful in the determination of σ -donor and/or π -acceptor properties of ligands, we decided to

approach this research field as a continuation of our previous efforts on silyliumylidene coordination chemistry.

Reaction of the Tipp-substituted silyliumylidene ion **L-29b-OTf** with group 6 carbonyl THF complexes ($M(\text{CO})_5(\text{THF})$, $M = \text{Cr}, \text{Mo}, \text{W}$) resulted in the clean formation of the metal carbonyl complexes **7-9** (Figure 20), which includes the first Cr and Mo complexes of a Si(II) cation.¹⁵⁴

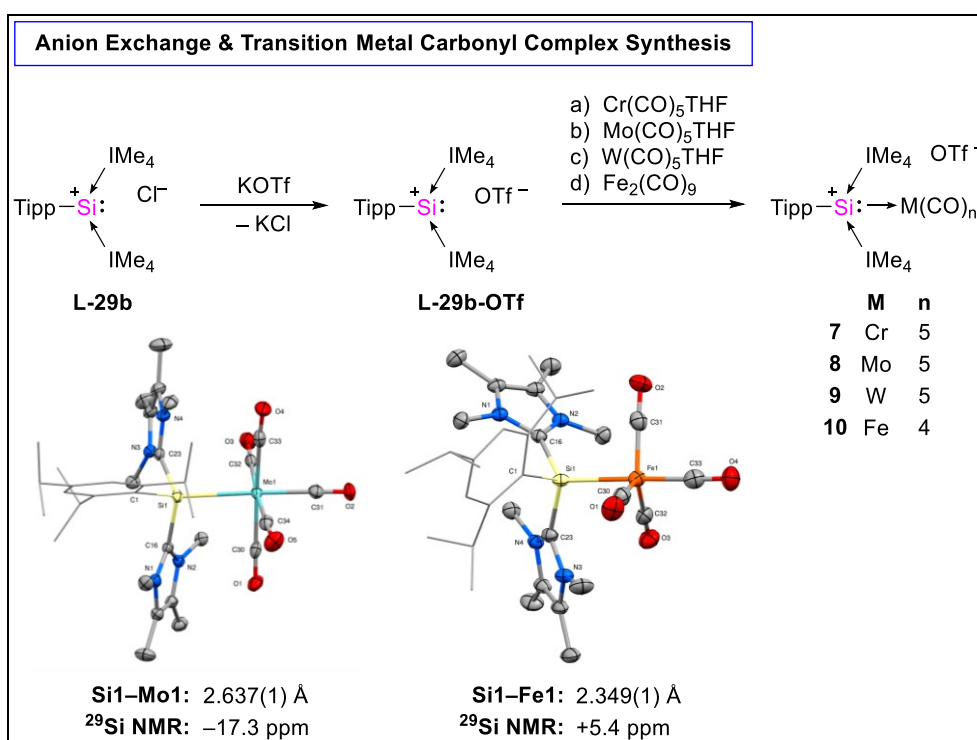


Figure 20 Silyliumylidene anion exchange, synthesis of transition metal carbonyl complexes **7-10** and SC-XRD structures of complexes **8** and **10**.

Importantly, introduction of a triflate anion *via* an anion exchange reaction is necessary, as the chloride anion in **L-29b** readily reacts with $M(\text{CO})_5(\text{THF})$ to form $[\text{M}(\text{CO})_5\text{Cl}]^-$. The analogous Mes^tTer -substituted complexes could not be obtained due to the increased steric hindrance of the larger aryl substituent. Furthermore, it was possible to isolate the first iron complex of a silyliumylidene ion by reaction of **L-29b-OTf** with $\text{Fe}_2(\text{CO})_9$. Utilization of the more reactive iron carbonyl dimer is necessary, as no reaction takes place upon addition of $\text{Fe}(\text{CO})_5$. SC-XRD analysis of the complexes revealed surprisingly long Si-M bonds and IR analysis together with theoretical investigations gave insight into the donor/acceptor properties of the silyliumylidene ligand, which showed **L-29b** to be a weak σ -donor ligand (presumably due to the positive charge located on the silicon atom) with negligible π -acceptor ability (because of the presence of 2 NHCs on the silicon center).

8.2.3 Insertion into M–Cl Bonds and Access to Si–M Multiple Bonds

Dimeric, chloro-bridged transition metal complexes are well known and often employed precursors in transition metal carbene complex chemistry. As these conveniently accessible dimers can easily dissociate, they can essentially offer a “free” coordination site that facilitates coordination of a new ligand. Moreover, the presence of multiple halides allows the use of transmetalation reactions with, for example, Ag and Li compounds in addition to having the potential for further functionalization *via* the halide substituents.

Hence, we were interested in exploring the coordination chemistry of silyliumylidene ions with these versatile dimers. Reaction of either silyl-based ($R = {}^t\text{Bu}_3\text{Si}$ and ${}^t\text{Bu}_2\text{MeSi}$) or aryl-based ($R = \text{Tipp}$) silyliumylidene ions with $[\text{RuCl}_2(p\text{-cymene})]_2$ or $[\text{RhCl}_2(\text{Cp}^*)]_2$ leads to highly asymmetric chlorosilylene complexes **11-15** through coordination of the silyliumylidene ion to the transition metal accompanied by splitting of the dimer, followed by insertion of the coordinated silyliumylidene ion into the metal–chloride bond and migration of a silicon bound NHC to the transition metal (Figure 21A).¹⁵⁵

The mechanism of the coordination/insertion/migration reaction was investigated theoretically (Figure 21B) and also verified experimentally with the isolation of the silyliumylidene ion complexes **16** and **17** ($R = \text{Mes}$), which represent the first step of the reaction mechanism before the insertion. Reaction of a silyliumylidene triflate (instead of chloride) with the same transition metal precursors led to the identical complexes with OTf^- as the counter anion, providing further evidence for the insertion and rearrangement reaction mechanism and excluding the potential involvement of a chlorosilylene in the coordination reaction.

Presumably, increasing the steric bulk of the silyliumylidene substituent favors the insertion reaction to decrease the steric congestion around the silicon center. The mesityl substituent in **3** is small enough to allow isolation of the silyliumylidene complexes **16-17**, whereas the slightly larger Tipp substituent in **L-29b** forces the rapid insertion/migration reaction. Further increase of the steric bulk with the *m*-terphenyl substituent prevents the initial coordination altogether, which explains why no insertion reaction can take place in this case. Unfortunately, the low thermal stability of the mesityl substituted complexes prevented the isolation of the corresponding chlorosilylene complexes through prolonged reaction time or heating.

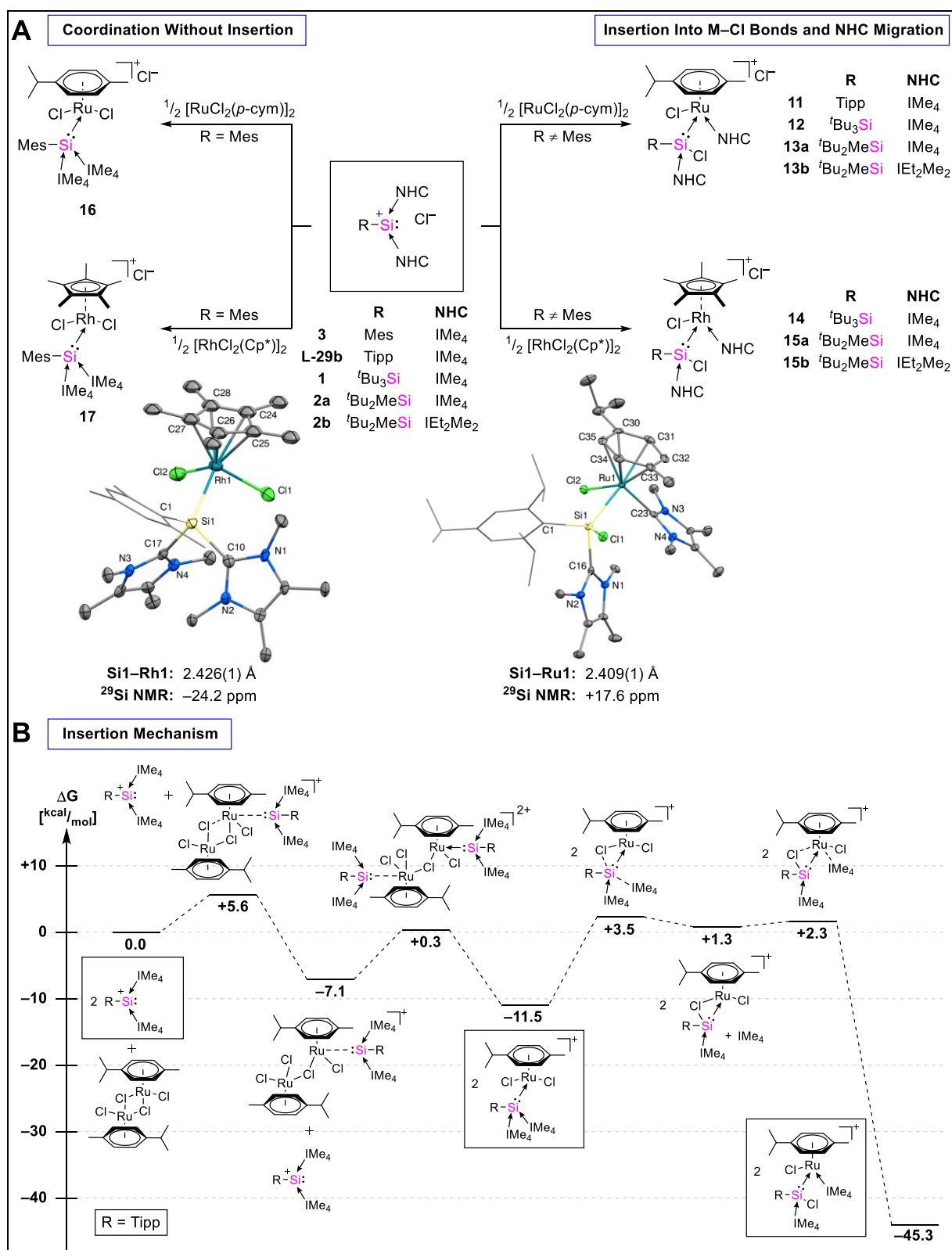


Figure 21 Coordination/insertion behavior of various silyliumylidene ions with dimeric $[\text{MCl}_2(\text{Aryl})]_2$ complexes and crystal structures of silyliumylidene complex **17** and chlorosilylene complex **11** (A); Calculated mechanism of the coordination and insertion reaction (B).

The presence of three chlorides in the obtained complexes makes them ideal starting points for further functionalization. Reduction of the ${}^t\text{Bu}_3\text{Si}$ -substituted ruthenium and rhodium complexes **12** and **14** with one equivalent of KC_8 led to the expected removal

of the chloride counter anion with a surprising rearrangement reaction: the chloride bound to the transition metal migrates to the silicon center with concomitant dissociation of the silicon-bound NHC, resulting in di(chloro)silyl-substituted complexes **18** and **19** (Figure 22). In both cases, a color change (**12**→**18**: orange→green; **14**→**19**: orange-red→black) can be observed. SC-XRD analysis of these complexes revealed substantially shortened Si–M bond lengths in comparison to the chlorosilylene complexes **12** and **14**. Further reduction of complex **18** with an additional equivalent of KC_8 gave the unstabilized chlorosilylene complex **20**. Once again, SC-XRD analysis revealed a significantly shorter Si–M bond distance, indicating a double bond character. An intense color change (**18**→**20**: green→red) can be observed as well.

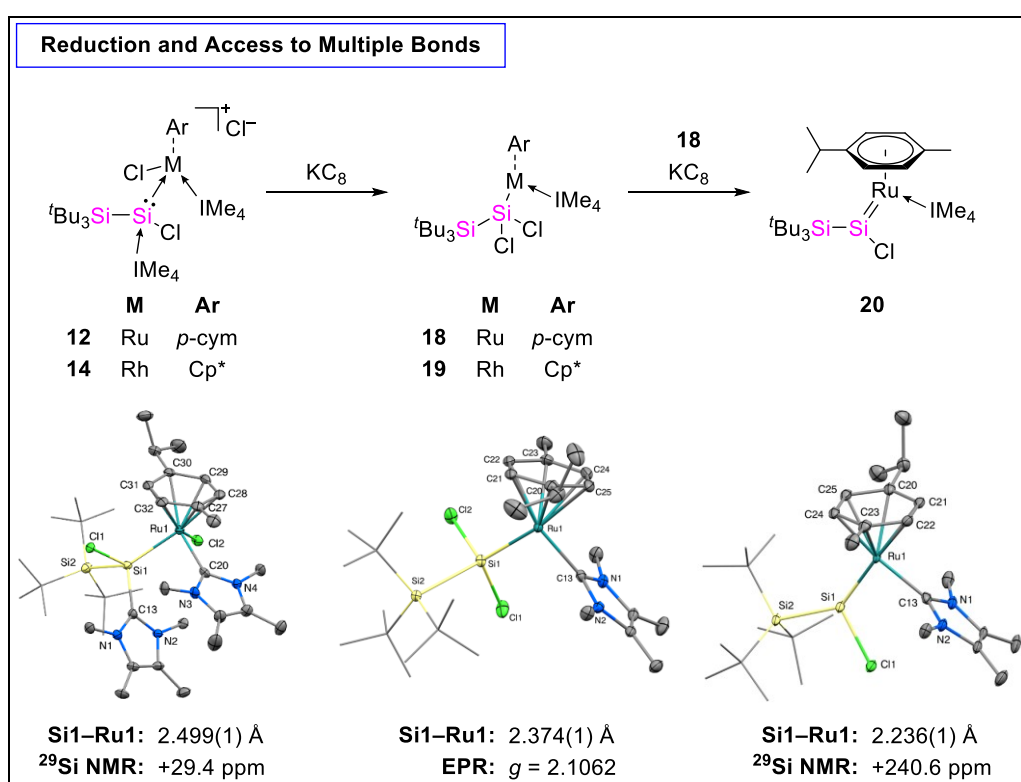


Figure 22 Reduction of chlorosilylene complexes **12** and **14** to silyl-substituted complexes **18** and **19** and further reduction of **18** to the Si=Si double bond **20**.

8.3 Outlook

This thesis has succeeded in significantly expanding the scope of the field of coordination chemistry with silyliumylidene ions as ligands. It was possible to synthesize, isolate and fully characterize the first transition metal complexes of NHC-stabilized silyliumylidene ions. The coinage metal complexes **4-6** can be regarded as a proof of principle, that NHC-stabilized Si(II) cations can indeed act as ligands in

complex chemistry. Building on this, experimental and theoretical analysis of transition metal carbonyl complexes **7-10** gave insight into the σ -donor and π -acceptor properties of NHC-stabilized silyliumylidene ions. Moreover, interesting reactivity patterns could be observed, for example the migration of the silicon-bound NHCs to a transition metal (Figure 19B, complex **6b**), or the insertion of the low-valent silicon moiety into the M–Cl bonds of a coordinated transition metal fragment, resulting in chlorosilylene complexes **11-15** (Figure 21). Nevertheless, further investigations into the influence of the silyliumylidene substituent on their coordination behavior would allow for a better understanding of the possible coordination chemistry.

While it was already shown that the obtained chlorosilylene complexes can offer a relatively simple access route to Si=M double bonds through reductive dehalogenation, further investigations are required as to whether they are also useful precursors for Si≡M triple bonds. Conceivable approaches include either the further reductive dehalogenation of the Si=M chlorosilylene complexes, or formation of a cationic complex through abstraction of a chloride and exchange with a suitable weakly coordinating anion. Additional functionalization of the chloride substituents is also a possibility, which could give access to a series of otherwise unobtainable, asymmetric silylene complexes.

However, the most important follow-up chemistry of the isolated complexes is their application as catalysts in organic transformations. For example, iron-catalyzed hydroboration reactions, ruthenium-catalyzed transfer hydrogenations or gold-catalyzed hydroamination reactions could be attractive targets for silyliumylidene complexes. In this context, isolation of nickel and palladium complexes could also open up even more potential catalytic applications.

9. Zusammenfassung und Ausblick

Seit Jutzis bahnbrechender Arbeit über das Pentamethylcyclopentadien-Silicium(II)-Kation **L-22** in 2004¹¹³ hat sich das Forschungsfeld der Silyliumyliden-Ionen stetig erweitert und das Interesse von Wissenschaft und Industrie an diesen hochreaktiven Verbindungen nimmt kontinuierlich zu. Wie in Kapitel 2.3.4 dieser Dissertation detailliert dargelegt, wurde nicht nur über die stöchiometrische Aktivierung einer Vielzahl an kleinen Molekülen berichtet, sondern auch metallfreie katalytische Anwendungen. Ebenso wurde die Verwendung von Silyliumyliden-Ionen als Synthone für neuartige niedervalente Siliciumverbindungen beschrieben und die Koordinationschemie mit Übergangsmetallen untersucht.

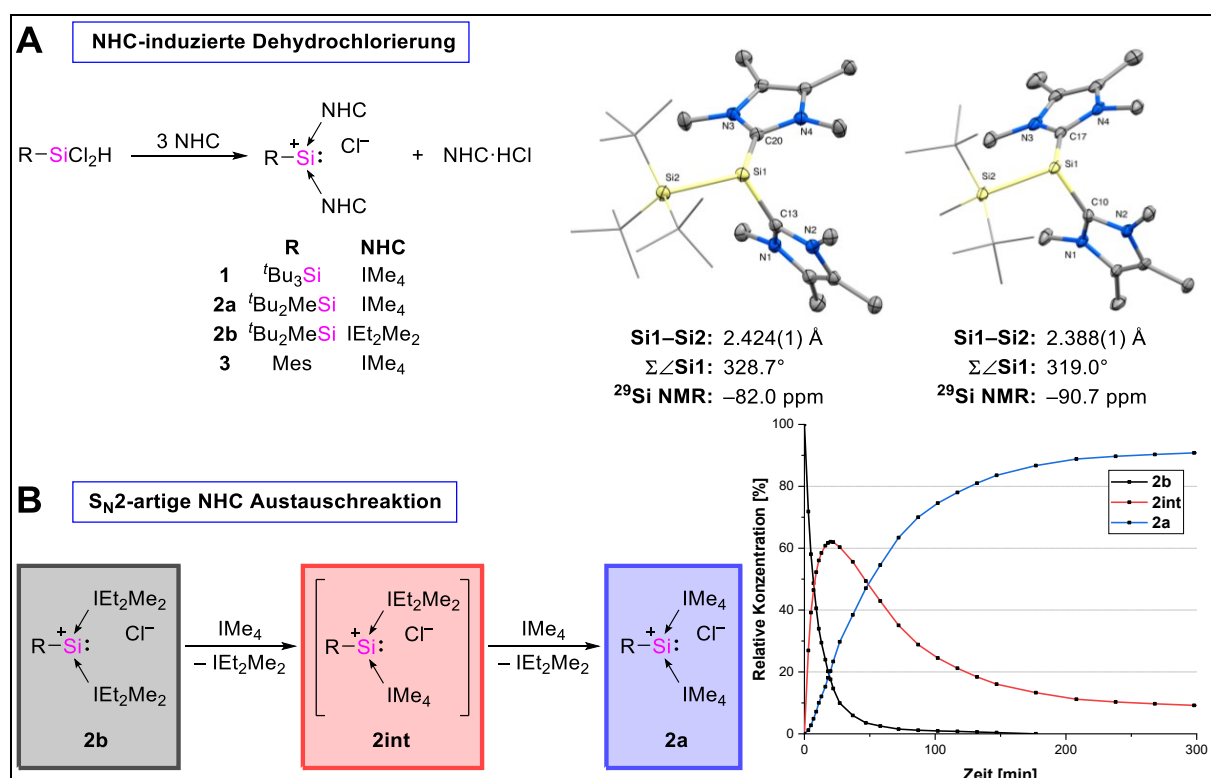
Im Jahr 2014 berichtete unsere Gruppe über die Synthese von neuartigen, NHC-stabilisierten Silyliumyliden-Ionen **L-29** mit sterisch anspruchsvollen Aryl-Resten, die in einer einfachen „one-pot“-Reaktion aus leicht verfügbaren Aryl-Dichlorsilanen durch Abstraktion von HCl mit Hilfe von freien NHCs dargestellt wurden.¹²⁵ Motiviert durch die spannende und vielversprechende Chemie von **L-29**, die die Aktivierung von Phenylacetylen¹²⁵ und CO₂¹⁴⁴ aufzeigte, sowie die erste Publikation von So *et al.* über Übergangsmetall-Koordinationskomplexe¹⁵⁰, die direkt aus einem Silyliumyliden-Ion synthetisiert wurden, zielte diese Arbeit darauf ab, das Forschungsgebiet der Übergangsmetall-Koordinationschemie mit Si(II)-Kationen als Liganden signifikant zu erweitern.

Da der alleinige Substituent eines Silyliumyliden-Ions einen ausgeprägten Einfluss auf dessen Stabilität und Reaktivität (einschließlich des Koordinationsverhaltens) haben kann, wurde auch die Isolation neuartiger Silyliumyliden-Ionen mit unterschiedlichen Substituenten angestrebt, wobei das zuvor erwähnte Dichlorsilan-basierte „one-pot“-Verfahren als synthetischer Zugang gewählt wurde.

9.1 Neuartige NHC-stabilisierte Silyliumyliden-Ionen

Um die ersten silyl-substituierten Silyliumyliden-Ionen zu isolieren, wurden mehrere literaturbekannte Silyl-dichlorsilane synthetisiert und anschließend mit je drei Äquivalenten NHC umgesetzt (Abbildung 23A).¹⁵² Die Zugabe von freien NHCs zu den Dichlorsilanen führt zu einer schnellen Bildung einer 1:1-Mischung aus Imidazoliumchlorid und den gewünschten Silyliumyliden-Chloriden **1-3**. Obwohl die

Reaktionen im Wesentlichen quantitativ verlaufen, reduziert sich die isolierbare Ausbeute auf ~55-65% durch die Abtrennung des Nebenproduktes. Die Trennung der niedervalenten Siliciumspezies und des Imiazoliumsalses kann bequem durch Extraktion mit einer Mischung aus Toluol und Acetonitril erfolgen. Dieses Vorgehen kann auch auf andere Silyliumyliden-Ionen angewendet werden, die mit der gleichen Vorschrift synthetisiert wurden. Eine Anpassung an die unterschiedlichen Löslichkeiten verschiedener Kombinationen von Imidazoliumsalzen und Si(II)-Kationen, sowie die Stabilität in verschiedenen Lösungsmitteln kann problemlos durch eine Variation des polaren Lösungsmittels und des Lösungsmittelverhältnisses erreicht werden.



Synthese der NHC-stabilisierten Silyliumyliden-Ionen **1-3** mit Kristallstrukturen von **1** und **2a** (**A**); NHC Austauschreaktion von Silyliumyliden **2b** mit zugehörigem Plot der relativen Konzentrationen von **2b**, **2int** und **2a** aufgetragen gegen die Zeit (**B**).

Um Silyliumyliden-Ionen mit größeren NHCs als IME₄ zu isolieren, muss die sterisch anspruchsvolle ^tBu₃Si-Gruppe durch kleinere Silylreste wie beispielsweise ^tBu₂MeSi ersetzt werden. Die kleinere Silylgruppe ermöglicht problemlos die Synthese des IEt₂Me₂-koordinierten Si(II)-Kations **2b**.

Im Vergleich zu den bisher verwendeten Aryl-Substituenten wird aufgrund der stärkeren elektronenschiebenden Eigenschaften der Silylgruppen eine starke Hochfeldverschiebung der ²⁹Si-NMR-Resonanz und eine verminderte Pyramidalisierung um das zentrale Siliciumatom beobachtet.

Darüber hinaus war es möglich ein Silyliumyliden-Ion mit dem sterisch wenig anspruchsvollen Substituenten Mesityl zu isolieren. Da **3** allerdings in Acetonitril nur eine geringe Stabilität aufweist, wurde die Abtrennung des Imiazoliumsalz-Nebenproduktes mit Pyridin als Lösungsmittel durchgeführt.

Interessanterweise ist es leicht möglich die koordinierten NHCs in **2b** mit der kleineren, stärkeren Lewis Base IMe_4 auszutauschen (Abbildung 23B). Der Reaktionsfortschritt kann bequem über $^1\text{H-NMR}$ Analyse verfolgt werden, was ebenfalls eine Untersuchung der Reaktionskinetik ermöglicht: die Austauschreaktionen folgen dem Geschwindigkeitsgesetz 2. Ordnung, was auf einen assoziativen $\text{S}_{\text{N}}2$ -artigen Mechanismus hindeutet. Der umgekehrte Austausch von IMe_4 durch $\text{I}(\text{Et})_2\text{Me}_2$ ist aufgrund der höheren σ -Donorstärke von IMe_4 nicht möglich.

9.2 Koordinationschemie von NHC-stabilisierten Silyliumylidenen

Anschließend wurde die Möglichkeit der Übergangsmetall-Koordinationschemie mit Silyliumyliden-Ionen als Liganden genauer untersucht. Die Übergangsmetalle, von denen erfolgreich Komplexe mit NHC-stabilisierten $\text{Si}(\text{II})$ -Kationen als Liganden erhalten werden konnten, sind in Abbildung 24 dargestellt.

Gruppe								
4	5	6	7	8	9	10	11	12
Ti	V	Cr	Mn	Fe	Co	Ni	Cu	Zn
Zr	Nb	Mo	Tc	Ru	Rh	Pd	Ag	Cd
Hf	Ta	W	Re	Os	Ir	Pt	Au	Hg

Abbildung 24 Im Laufe dieser Arbeit erfolgreich eingesetzte Übergangsmetalle in der Koordinationschemie mit NHC-stabilisierten Silyliumyliden-Ionen.

Es war möglich eine Reihe von Komplexen mit Übergangsmetallen der Gruppen 6, 8, 9 und 11 zu isolieren und vollständig zu charakterisieren. Eine detailliertere Zusammenfassung der erzielten Ergebnisse ist im Anschluss aufgeführt.

9.2.1 Münzmetallkomplexe – Monomere vs. Dimere Komplexe

Als Ausgangsexperiment wurde das *m*-terphenyl-substituierte Si(II)-Kation **L-29a** mit den einfachen Münzmetallverbindungen CuCl, AgOTf und (Me₂S)AuCl umgesetzt (Abbildung 25A).¹⁵³ Die Zugabe der Metallverbindungen zu einer orangefarbenen Acetonitrillösung von **L-29a** führte zu einer raschen Entfärbung. Nach Umkristallisation konnte die gesamte Reihe **4a**, **5a** und **6a** der ersten Münzmetallkomplexe eines Silyliumyliden-Ions in hoher Ausbeute isoliert werden. Eine ²⁹Si-NMR-Analyse der Komplexe ergab die erwartete Tieffeldverschiebung im Vergleich zum freien Silyliumyliden-Ion. Das interessanteste Merkmal sind die zwei Dubletts, die im ²⁹Si-NMR-Spektrum des Silberkomplexes **5a** aufgrund der Kopplung des Siliciumzentrums mit den ¹⁰⁷Ag- und ¹⁰⁹Ag-Kernen beobachtet wurden.

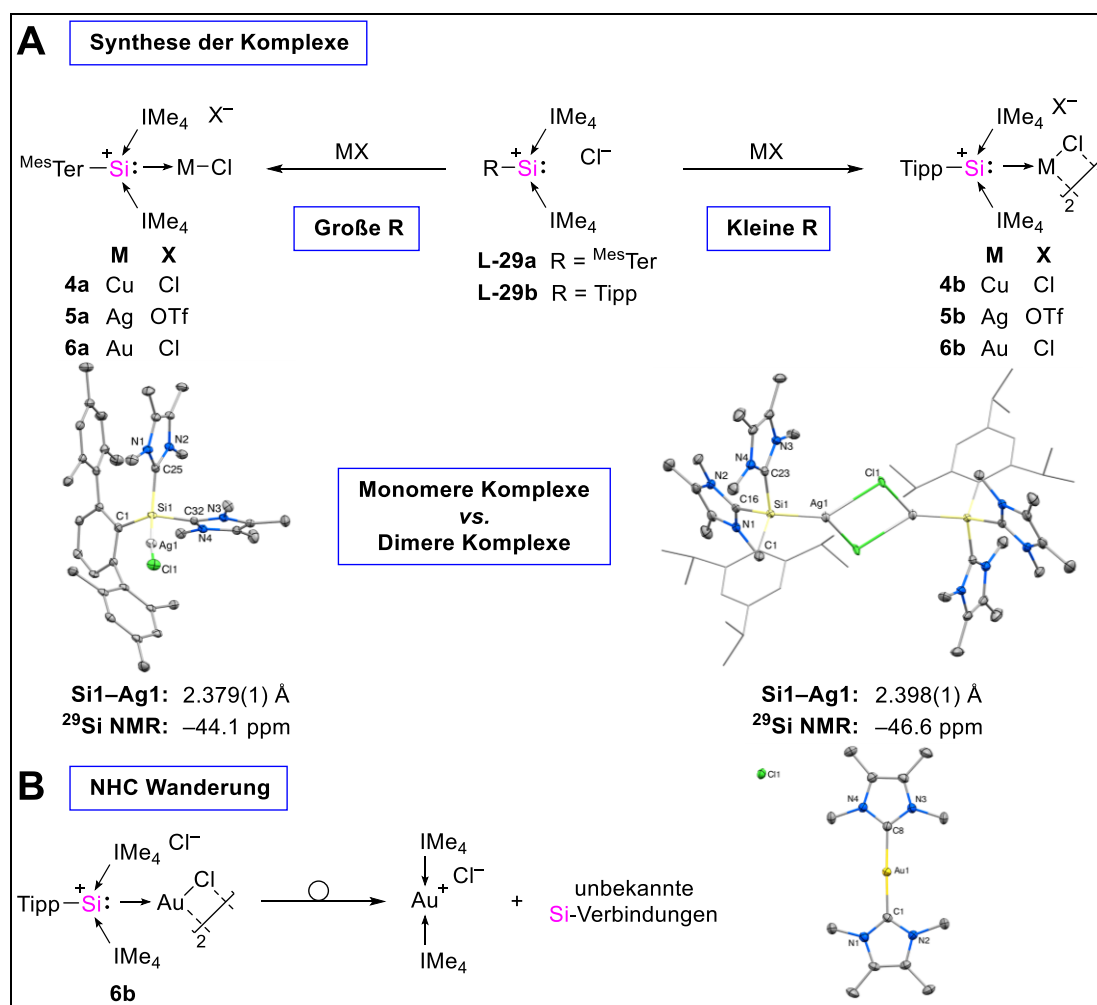


Abbildung 25 Synthese der ersten Münzmetallkomplexe **4-6** eines Silyliumyliden-Ions und Einkristallstrukturen der monomeren und dimeren Silberkomplexe (**A**); NHC Wanderung, die bei dem dimeren Goldkomplex **6b** beobachtet werden konnte (**B**).

Während sich im Falle des sterisch anspruchsvollen MesTer-Substituenten in Lösung die stabilen Komplexe **4a**, **5a** und **6a** bilden, die in der Kristallstruktur eine monomere

Struktur zeigen, führt eine Reduzierung des sterischen Anspruchs des Substituenten zur Bildung der dimeren Komplexe **4b**, **5b** und **6b**. Diese weisen in Lösung eine deutlich reduzierte Stabilität auf. Bei der Zersetzung der dimeren Komplexe findet eine NHC-Wanderung zum Übergangsmetall statt, was zu einer Bildung von Bis(NHC)-Metallkomplexen führt (Abbildung 25B). Die in dieser Reaktion gebildeten Siliciumverbindungen konnten nicht isoliert und eindeutig charakterisiert werden.

9.2.2 Übergangsmetallcarbonylkomplexe und Ligandeneigenschaften

Da bisher keine Untersuchungen der Eigenschaften von Silyliumyliden-Ionen als Liganden veröffentlicht wurden und Übergangsmetallcarbonylkomplexe sich zur Bestimmung der σ -Donor- bzw. π -Akzeptor-Eigenschaften eines Liganden außerordentlich gut eignen, haben wir beschlossen, dieses Forschungsfeld als direkte Fortsetzung unserer bisherigen Bemühungen anzugehen.

Die Reaktion des Tipp-substituierten Silyliumyliden-Ions **L-29b-OTf** mit den Carbonyl-THF-Komplexen der Gruppe 6 Metalle ($M(\text{CO})_5(\text{THF})$, $M = \text{Cr}, \text{Mo}, \text{W}$) führte zu einer direkten Bildung der Metallcarbonylkomplexe **7-9**, wobei es sich hierbei um die ersten synthetisierten Chrom- und Molybdän-Komplexe eines Si(II)-Kations handelt (Abbildung 26).¹⁵⁴

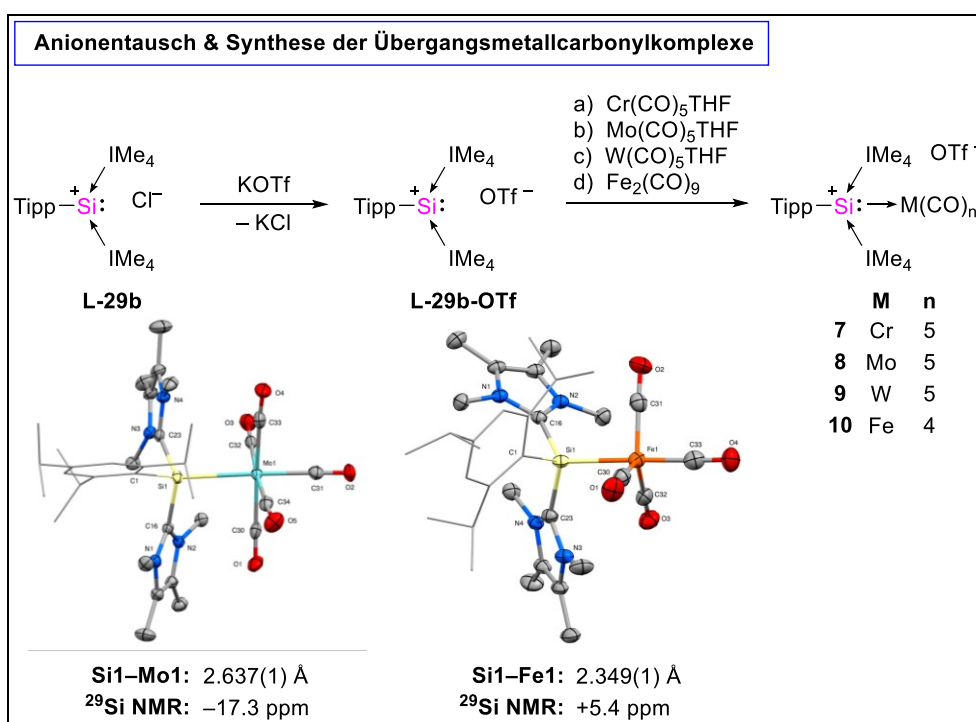


Abbildung 26 Anionenaustausch des Silyliumyliden-Ions **L-29b**, Synthese der Übergangsmetallcarbonylkomplexe **7-10** und Einkristallstrukturen der Komplexe **8** und **10**.

Der Austausch des Chlorid-Anions durch ein Triflat-Anion muss erfolgen, da das Chlorid-Anion in **L-29b** direkt mit $M(\text{CO})_5(\text{THF})$ zu $[M(\text{CO})_5\text{Cl}]^-$ reagiert. Die analogen ^{Mes}Ter-substituierten Komplexe konnten aufgrund des großen sterischen Anspruchs des größeren Aryl-Substituenten nicht erhalten werden.

Darüber hinaus war es möglich, den ersten Eisenkomplex eines Silyliumyliden-Ions durch Reaktion von **L-29b-OTf** mit $\text{Fe}_2(\text{CO})_9$ zu isolieren. Der Einsatz des im Vergleich zum Monomer $\text{Fe}(\text{CO})_5$ reaktiveren Eisencarbonyl-Dimers ist notwendig, da mit dem Monomer keine Reaktion stattfindet. Die Einkristallstrukturanalyse der Komplexe zeigte überraschend lange Silicium–Metall-Bindungen. IR-Analyse kombiniert mit theoretischen Untersuchungen gaben Einblicke in die Donor-/Akzeptor-Eigenschaften des Silyliumyliden-Liganden **L-29b**, der sich am besten als schwacher σ -Donor-Ligand (vermutlich aufgrund der positiven Ladung am Siliciumatom) mit vernachlässigbarer π -Akzeptorfähigkeit (aufgrund der zwei koordinierten NHCs) beschreiben lässt.

9.2.3 Insertion in M–Cl Bindungen und Zugang zu Si–M Mehrfachbindungen

Dimere, chloro-verbrückte Übergangsmetallkomplexe werden häufig als Ausgangsverbindungen in der Übergangsmetallcarbenkomplex-Chemie verwendet. Da diese Verbindungen in Gegenwart von zusätzlichen Liganden leicht in Monomere dissoziieren können, stellen sie Vorläuferverbindungen mit einer leicht zugänglichen, effektiv freien Koordinationsstelle dar, die die Koordination neuer Liganden signifikant vereinfacht. Darüber hinaus ermöglichen die Chlorid-Substituenten den Einsatz von Transmetallierungsreaktionen mit beispielsweise Silber- oder Lithium-Verbindungen. Ebenso ist das Potential für weitere Funktionalisierungsreaktionen groß. Aufgrund dieser Eigenschaften waren wir daran interessiert, die Koordinationschemie von Silyliumylidenen mit diesen flexiblen Komplexen zu untersuchen.

Die Reaktion von Silyl-basierten ($R = \text{}^t\text{Bu}_3\text{Si}$ and $\text{}^t\text{Bu}_2\text{MeSi}$) oder Aryl-basierten ($R = \text{Tipp}$) Silyliumylidenen mit $[\text{RuCl}_2(p\text{-cymene})]_2$ oder $[\text{RhCl}_2(\text{Cp}^*)]_2$ führt zu den hoch-
asymmetrischen NHC-stabilisierten Chlorosilylenkomplexen **11-15**. Deren Bildung erfolgt durch Koordination des Silyliumyliden-Ions an das Übergangsmetallzentrum (unter Spaltung des Dimers), mit anschließender Insertion des niedervalenten Siliciums in die Metall–Chlor-Bindung und gleichzeitiger Wanderung eines NHCs vom Silicium-Liganden auf das Metallzentrum (Abbildung 27A).¹⁵⁵

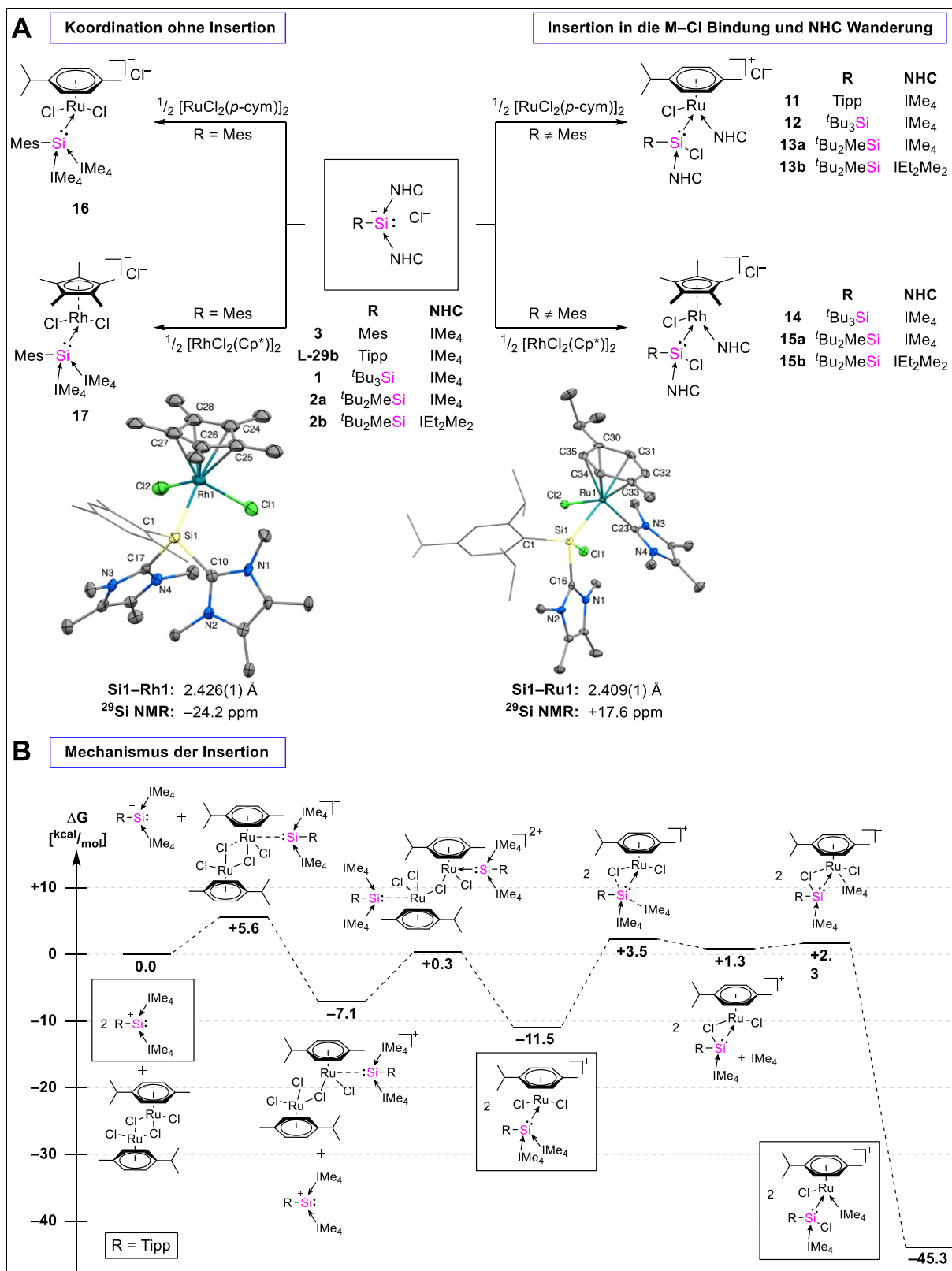


Abbildung 27 Koordinations-/Insertionsverhalten von verschiedenen Silyliumyliden-Ionen mit den dimeren Komplexen $[\text{MCl}_2(\text{Aryl})]_2$, Kristallstrukturen des Silyliumyliden-Komplexes **17** und des Chlorosilylen-Komplexes **11** (A); Berechneter Mechanismus der Koordinations- und Insertionsreaktion (B).

Der Mechanismus der Koordinations-/Insertions-/Migrationsreaktion wurde sowohl theoretisch untersucht (Abbildung 27B), als auch experimentell mit der Isolierung der

Komplexe **16** und **17** (R = Mesityl) belegt, die den ersten Schritt des Reaktionsmechanismus vor der Insertionsreaktion repräsentieren. Einen weiteren Beweis für den Insertions-/Umlagerungsmechanismus liefert die Reaktion eines Silyliumyliden-Triflats (anstelle von Chlorid) mit den gleichen Übergangsmetall-Ausgangsverbindungen, wobei die entsprechenden Komplexe mit Triflat als Gegenion erhalten wurden. Dies schließt ebenso eine mögliche Beteiligung eines Chlorosilylens an der Koordinationsreaktion aus.

Vermutlich begünstigt ein größerer sterischer Anspruch des Silyliumyliden-Substituenten die Insertionsreaktion, um die sterische Überlastung um das Siliciumzentrum herum zu reduzieren. Der Mesityl-Substituent in **3** ist scheinbar klein genug, um die Isolierung der Silyliumyliden-Komplexe zu ermöglichen, wohingegen der Tipp-Substituent in **L-29b** eine schnelle Insertions-/Migrationsreaktion erzwingt. Ein noch größerer sterischer Anspruch des Restes, sprich ^{Mes}Ter als Substituent in **L-29a**, verhindert die gesamte Koordination komplett, weshalb in diesem Falle überhaupt keine Reaktion beobachtet werden kann. Leider verhindert die geringe thermische Stabilität der Mesityl-substituierten Komplexe die Isolierung der entsprechenden Chlorosilylen-Komplexe durch eine verlängerte Reaktionszeit oder höhere Reaktionstemperaturen.

Die drei Chloride in den erhaltenen Komplexen machen sie zu idealen Ausgangspunkten für weitere Funktionalisierungsreaktionen. Die Reduktion der ^tBu₃Si-substituierten Ruthenium- oder Rhodiumkomplexe **12** und **14** mit einem Äquivalent KC₈ führte zu der erwarteten Abstraktion des Chlorid-Gegenions mit einer überraschenden Umlagerungsreaktion: das an das Übergangsmetall gebundene Chlorid wandert an den Siliciumliganden unter gleichzeitiger Dissoziation des Silicium-gebundenen NHCs, was zu den di(chloro)silyl-substituierten Komplexen **18** und **19** führt (Abbildung 28). Eine Einkristallstrukturanalyse der Komplexe ergab im Vergleich zu den Chlorosilylenkomplexen **12** und **14** deutlich verkürzte Si–M-Bindungen. Während der Reaktion tritt außerdem eine eindeutig erkennbare Farbänderung (**12**→**18**: orange→grün; **14**→**19**: orange-rot→schwarz) auf. Eine Folgereduktion von Komplex **18** mit einem weiteren Äquivalent KC₈ ergab den unstabilierten Chlorosilylenkomplex **20**. Wie bereits bei der ersten Reduktion tritt hier eine deutliche Verkürzung der Si–M-Bindungslänge auf, was auf den Doppelbindungscharakter des Komplexes hindeutet. Ebenso kann auch hier eine Farbänderung beobachtet werden (**18**→**20**: grün→rot).

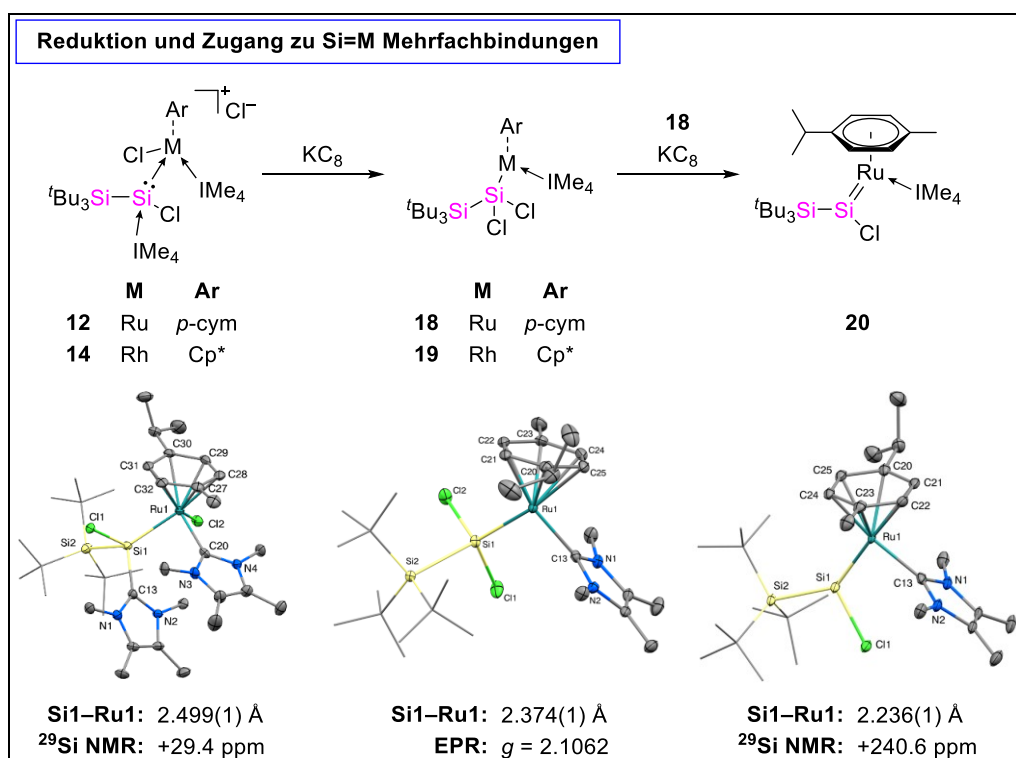


Abbildung 28 Reduktion der Chlorosilylenkomplexe **12** und **14** zu silyl-substituierten Komplexen **18** und **19** und weitere Reduktion von **18** zu der Si=Si Doppelbindung **20**.

9.3 Ausblick

Im Rahmen dieser Dissertation ist es gelungen, den Umfang des Forschungsfeldes der Koordinationschemie von Silyliumyliden-Ionen signifikant zu erweitern. Es war möglich die ersten Übergangsmetallkomplexe von NHC-stabilisierten Silyliumyliden-Ionen zu isolieren und vollständig zu charakterisieren. Die berichteten Münzmetallkomplexe **4-6** können als „Proof of Concept“ angesehen werden, dass NHC-stabilisierte Si(II)-Kationen tatsächlich als Liganden in der Komplexchemie agieren können. Darauf aufbauend gab die experimentelle und theoretische Analyse von Übergangsmetallcarbonylkomplexen **7-10** Einblick in die σ -Donor- und π -Akzeptoreigenschaften von NHC-stabilisierten Silyliumyliden-Ionen. Darüber hinaus konnten interessante Reaktivitätsmuster beobachtet werden, z.B. die Migration der Silicium-gebundenen NHCs zu einem Übergangsmetall (Abbildung 25B, Komplex **6b**), oder die Insertion des niedervalenten Silicium-Zentrums in eine Metall–Chlor-Bindung eines koordinierten Übergangsmetallfragments (Abbildung 27, Komplexe **11-15**). Dennoch würden weitere Untersuchungen bezüglich des Einflusses der Silyliumyliden-Substituenten bessere Rückschlüsse auf ihr Koordinationsverhalten ermöglichen.

Während bereits gezeigt werden konnte, dass die erhaltenen Chlorosilylen-Komplexe einen relativ einfachen Zugang zu Si=M-Doppelbindungen durch reduktive Dehalogenierung bieten können, sind weitere Untersuchungen erforderlich, ob sie auch für die Synthese von Si≡M-Dreifachbindungen geeignet sind. Denkbar wäre hier beispielweise eine weitere reduktive Dehalogenierung der Si=M-Komplexe, oder die Bildung eines kationischen Komplexes durch Abstraktion des verbleibenden Chlorids und der Austausch mit einem geeigneten schwach-koordinierenden Anion. Eine zusätzliche Funktionalisierung der Chloridsubstituenten wäre ebenfalls möglich, die so den Zugang zu einer Reihe von sonst unzugänglichen, asymmetrischen Silylenkomplexen ermöglichen könnte.

Die wichtigste Folgechemie der isolierten Komplexe ist jedoch ihre Anwendung als Katalysatoren in organischen Reaktionen. Beispielsweise könnten eisenkatalysierte Hydroborierungsreaktionen, rutheniumkatalysierte Transferhydrierungen oder goldkatalysierte Hydroaminierungsreaktionen attraktive Ziele für Silyliumyliden-Komplexe sein. In diesem Zusammenhang könnte auch die Isolierung von Nickel- und Palladiumkomplexen noch mehr potentielle katalytische Anwendungen eröffnen.

10. Bibliography

- [1] B. Lindström and L. J. Pettersson, A Brief History of Catalysis, *CATTECH* **2003**, 7, 130-138.
- [2] J. Wisniak, The History of Catalysis: From the Beginning to Nobel Prizes, *Educación Química* **2010**, 21, 60-69.
- [3] C. R. Catlow, M. Davidson, C. Hardacre and G. J. Hutchings, Catalysis making the world a better place, *Phil. Trans. R. Soc. A* **2016**, 374, 20150089.
- [4] J. Hagen, Economic Importance of Catalysts in *Industrial Catalysis: A Practical Approach*, J. Hagen (Editor), Wiley-VCH, Weinheim, **2015**.
- [5] J. M. Thomas, The societal significance of catalysis and the growing practical importance of single-site heterogeneous catalysts, *Proc. R. Soc. A* **2012**, 468, 1884-1903.
- [6] M. Beller, Applying Homogeneous Catalysis for the Synthesis of Pharmaceuticals in *New Avenues to Efficient Chemical Synthesis*, P. H. Seeberger, T. Blume (Editors), Springer-Verlag, Berlin, **2007**.
- [7] P. P. Power, Main-group elements as transition metals, *Nature* **2010**, 463, 171-177.
- [8] C. Weetman and S. Inoue, The Road Travelled: After Main-Group Elements as Transition Metals, *ChemCatChem* **2018**, 10, 4213-4228.
- [9] L. C. Wilkins and R. L. Melen, Enantioselective Main Group Catalysis: Modern Catalysts for Organic Transformations, *Coord. Chem. Rev.* **2016**, 324, 123-139.
- [10] W. M. Haynes, CRC Handbook of Chemistry and Physics, 97th ed., CRC Press, Florida, **2016**.
- [11] S. Inoue, The Next Generation of Silylene Ligands for Better Catalysts in *Discovering the Future of Molecular Sciences*, B. Pignataro (Editor), Wiley-VCH, Weinheim, **2014**.
- [12] S. Raoufmoghaddam, Y.-P. Zhou, Y. Wang and M. Driess, *N*-heterocyclic silylenes as powerful steering ligands in catalysis, *J. Organomet. Chem.* **2017**, 829, 2-10.
- [13] Y.-P. Zhou, *N*-Heterocyclic Silylenes as Tools in Coordination Chemistry and Catalysis, PhD Thesis, Technische Universität Berlin, Berlin, **2018**.
- [14] Y.-P. Zhou and M. Driess, Isolable Silylene Ligands Can Boost Efficiencies and Selectivities in Metal-Mediated Catalysis, *Angew. Chem. Int. Ed.* **2019**, 58, 3715-3728.
- [15] C. A. Reed, The Silylium Ion Problem, R_3Si^+ : Bridging Organic and Inorganic Chemistry, *Acc. Chem. Res.* **1998**, 31, 325-332.

- [16] V. Y. Lee and A. Sekiguchi, Organometallic Compounds of Low-Coordinate Si, Ge, Sn and Pb, John Wiley & Sons, New Jersey, **2010**.
- [17] V. Y. Lee and A. Sekiguchi, Silicon-Centered Cations - Chapter 5 in *Organosilicon Compounds: Theory and Experiment (Synthesis)*, V. Y. Lee (Editor), Academic Press, Massachusetts, **2017**.
- [18] G. Bertrand, The Modest Undressing of a Silicon Center, *Science* **2004**, *305*, 783-785.
- [19] J. B. Lambert and Y. Zhao, Das Trimesitylsilylium-Ion, *Angew. Chem.* **1997**, *109*, 389-391.
- [20] H. F. T. Klare and M. Oestreich, Silylium ions in catalysis, *Dalton Trans.* **2010**, *39*, 9176-9184.
- [21] J. B. Lambert and S. Zhang, Tetrakis(pentafluorophenyl)borate: a new anion for silylium cations in the condensed phase, *J. Chem. Soc., Chem. Commun.* **1993**, 383-384.
- [22] Q. Wu, E. Irran, R. Müller, M. Kaupp, H. F. T. Klare and M. Oestreich, Characterization of hydrogen-substituted silylium ions in the condensed phase, *Science* **2019**, *365*, 168-172.
- [23] J. C. L. Walker, H. F. T. Klare and M. Oestreich, Cationic silicon Lewis acids in catalysis, *Nat Rev Chem* **2019**.
- [24] K. Hara, R. Akiyama and M. Sawamura, Strong Counteranion Effects on the Catalytic Activity of Cationic Silicon Lewis Acids in Mukaiyama Aldol and Diels–Alder Reactions, *Organic Letters* **2005**, *7*, 5621-5623.
- [25] T. Stahl, H. F. T. Klare and M. Oestreich, Main-Group Lewis Acids for C–F Bond Activation, *ACS Catal.* **2013**, *3*, 1578-1587.
- [26] G. Meier and T. Braun, Catalytic C–F Activation and Hydrodefluorination of Fluoroalkyl Groups, *Angew. Chem. Int. Ed.* **2009**, *48*, 1546-1548.
- [27] J. B. Lambert, Y. Zhao and H. Wu, β -Silyl and β -Germyl Carbocations Stable at Room Temperature, *The Journal of Organic Chemistry* **1999**, *64*, 2729-2736.
- [28] K. Müther, J. Mohr and M. Oestreich, Silylium Ion Promoted Reduction of Imines with Hydrosilanes, *Organometallics* **2013**, *32*, 6643-6646.
- [29] K. Müther and M. Oestreich, Self-regeneration of a silylium ion catalyst in carbonyl reduction, *Chem. Commun.* **2011**, *47*, 334-336.
- [30] K. Mitsuo, H. Takakazu and S. Hideki, Siloxycarbenium Tetrakis[3,5-bis(trifluoromethyl)phenyl]borates and Their Role in Reactions of Ketones with Nucleophiles, *Chem. Lett.* **1992**, *21*, 555-558.
- [31] H. F. T. Klare, Catalytic C–H Arylation of Unactivated C–H Bonds by Silylium Ion-Promoted C(sp²)–F Bond Activation, *ACS Catal.* **2017**, *7*, 6999-7002.

- [32] S. Duttwyler, C. Douvris, N. L. P. Fackler, F. S. Tham, C. A. Reed, K. K. Baldridge and J. S. Siegel, C–F Activation of Fluorobenzene by Silylium Carboranes: Evidence for Incipient Phenyl Cation Reactivity, *Angew. Chem. Int. Ed.* **2010**, *49*, 7519-7522.
- [33] Q. Wu, A. Roy, E. Irran, Z.-W. Qu, S. Grimme, H. F. T. Klare and M. Oestreich, Catalytic Difunctionalization of Unactivated Alkenes with Unreactive Hexamethyldisilane through Regeneration of Silylium Ions, *Angew. Chem. Int. Ed.* **2019**, *58*, 17307-17311.
- [34] P. Shaykhutdinova and M. Oestreich, Achieving Enantioselectivity in Difficult Cyclohexa-1,3-diene Diels–Alder Reactions with Sulfur-Stabilized Silicon Cations as Lewis Acid Catalysts, *Organic Letters* **2018**, *20*, 7029-7033.
- [35] P. Pyykko, Relativistic effects in structural chemistry, *Chem. Rev.* **1988**, *88*, 563-594.
- [36] Y. Mizuhata, T. Sasamori and N. Tokitoh, Stable Heavier Carbene Analogues, *Chem. Rev.* **2009**, *109*, 3479-3511.
- [37] V. S. V. S. N. Swamy, S. Pal, S. Khan and S. S. Sen, Cations and dications of heavier group 14 elements in low oxidation states, *Dalton Trans.* **2015**, *44*, 12903-12923.
- [38] D. Wendel, Synthesis and Reactivity of Acyclic Silylenes: On the Way to Metal-free Catalysis, PhD Thesis, Technische Universität München, Garching bei München, **2018**.
- [39] T. Iwamoto and S. Ishida, Stable Silylenes and Their Transition Metal Complexes - Chapter 8 in *Organosilicon Compounds: Theory and Experiment (Synthesis)*, V. Y. Lee (Editor), Academic Press, Massachusetts, **2017**.
- [40] M. Asay, C. Jones and M. Driess, *N*-Heterocyclic Carbene Analogues with Low-Valent Group 13 and Group 14 Elements: Syntheses, Structures, and Reactivities of a New Generation of Multitalented Ligands, *Chem. Rev.* **2011**, *111*, 354-396.
- [41] S. Yao, Y. Xiong and M. Driess, Zwitterionic and Donor-Stabilized *N*-Heterocyclic Silylenes (NHSis) for Metal-Free Activation of Small Molecules, *Organometallics* **2011**, *30*, 1748-1767.
- [42] V. Nesterov, D. Reiter, P. Bag, P. Frisch, R. Holzner, A. Porzelt and S. Inoue, NHCs in Main Group Chemistry, *Chem. Rev.* **2018**, *118*, 9678-9842.
- [43] P. Jutzi, D. Kanne and C. Krüger, Decamethylsilicocene – Synthesis and Structure, *Angew. Chem. Int. Ed.* **1986**, *25*, 164-164.
- [44] P. Jutzi and N. Burford, Structurally Diverse π -Cyclopentadienyl Complexes of the Main Group Elements, *Chem. Rev.* **1999**, *99*, 969-990.
- [45] T. Kühler and P. Jutzi, Decamethylsilicocene: Synthesis, Structure, Bonding and Chemistry in *Adv. Organomet. Chem.*, Academic Press, **2003**. Vol. 49.

- [46] M. Denk, R. Lennon, R. Hayashi, R. West, A. V. Belyakov, H. P. Verne, A. Haaland, M. Wagner and N. Metzler, Synthesis and Structure of a Stable Silylene, *J. Am. Chem. Soc.* **1994**, *116*, 2691-2692.
- [47] M. Kira, S. Ishida, T. Iwamoto and C. Kabuto, The First Isolable Dialkylsilylene, *J. Am. Chem. Soc.* **1999**, *121*, 9722-9723.
- [48] M. Driess, S. Yao, M. Brym, C. van Wüllen and D. Lentz, A New Type of *N*-Heterocyclic Silylene with Ambivalent Reactivity, *J. Am. Chem. Soc.* **2006**, *128*, 9628-9629.
- [49] C.-W. So, H. W. Roesky, J. Magull and R. B. Oswald, Synthesis and Characterization of $[\text{PhC}(\text{N}^t\text{Bu})_2]\text{SiCl}$: A Stable Monomeric Chlorosilylene, *Angew. Chem. Int. Ed.* **2006**, *45*, 3948-3950.
- [50] S. S. Sen, S. Khan, P. P. Samuel and H. W. Roesky, Chemistry of functionalized silylenes, *Chem. Sci.* **2012**, *3*, 659-682.
- [51] R. Azhakar, R. S. Ghadwal, H. W. Roesky, H. Wolf and D. Stalke, Facile Access to the Functionalized *N*-Donor Stabilized Silylenes $\text{PhC}(\text{N}^t\text{Bu})_2\text{SiX}$ ($\text{X} = \text{PPh}_2$, NPh_2 , NCy_2 , N^iPr_2 , NMe_2 , $\text{N}(\text{SiMe}_3)_2$, O^tBu), *Organometallics* **2012**, *31*, 4588-4592.
- [52] R. S. Ghadwal, H. W. Roesky, S. Merkel, J. Henn and D. Stalke, Lewis Base Stabilized Dichlorosilylene, *Angew. Chem. Int. Ed.* **2009**, *48*, 5683-5686.
- [53] R. S. Ghadwal, R. Azhakar and H. W. Roesky, Dichlorosilylene: A High Temperature Transient Species to an Indispensable Building Block, *Acc. Chem. Res.* **2013**, *46*, 444-456.
- [54] A. C. Filippou, O. Chernov and G. Schnakenburg, $\text{SiBr}_2(\text{Idipp})$: A Stable *N*-Heterocyclic Carbene Adduct of Dibromosilylene, *Angew. Chem. Int. Ed.* **2009**, *48*, 5687-5690.
- [55] A. C. Filippou, Y. N. Lebedev, O. Chernov, M. Straßmann and G. Schnakenburg, Silicon(II) Coordination Chemistry: *N*-Heterocyclic Carbene Complexes of Si^{2+} and Si^+ , *Angew. Chem. Int. Ed.* **2013**, *52*, 6974-6978.
- [56] G.-H. Lee, R. West and T. Müller, Bis[bis(trimethylsilyl)amino]silylene, an Unstable Divalent Silicon Compound, *J. Am. Chem. Soc.* **2003**, *125*, 8114-8115.
- [57] D. H. Harris and M. F. Lappert, Monomeric, volatile bivalent amides of group IV elements, $\text{M}(\text{NR}^{12})_2$ and $\text{M}(\text{NR}^1\text{R}^2)_2$ ($\text{M} = \text{Ge}, \text{Sn}, \text{or Pb}$; $\text{R}^1 = \text{Me}_3\text{Si}$, $\text{R}^2 = \text{Me}_3\text{C}$), *J. Chem. Soc., Chem. Commun.* **1974**, 895-896.
- [58] M. J. S. Gynane, D. H. Harris, M. F. Lappert, P. P. Power, P. Rivière and M. Rivière-Baudet, Subvalent Group 4B metal alkyls and amides. Part 5. The synthesis and physical properties of thermally stable amides of germanium(II), tin(II), and lead(II), *J. Chem. Soc., Dalton Trans.* **1977**, 2004-2009.
- [59] B. D. Reken, T. M. Brown, J. C. Fettinger, H. M. Tuononen and P. P. Power, Isolation of a Stable, Acyclic, Two-Coordinate Silylene, *J. Am. Chem. Soc.* **2012**, *134*, 6504-6507.

- [60] A. V. Protchenko, K. H. Birjkumar, D. Dange, A. D. Schwarz, D. Vidovic, C. Jones, N. Kaltsoyannis, P. Mountford and S. Aldridge, A Stable Two-Coordinate Acyclic Silylene, *J. Am. Chem. Soc.* **2012**, *134*, 6500-6503.
- [61] D. Reiter, R. Holzner, A. Porzelt, P. J. Altmann, P. Frisch and S. Inoue, Disilene–Silylene Interconversion: A Synthetically Accessible Acyclic Bis(silyl)silylene, *J. Am. Chem. Soc.* **2019**, *141*, 13536-13546.
- [62] N. Muthukumar, K. Velappan, K. Gour and G. Prabusankar, *N*-heterocyclic carbene supported halosilylenes: New frontiers in an emerging field, *Coord. Chem. Rev.* **2018**, *377*, 1-43.
- [63] P. Bag, S. U. Ahmad and S. Inoue, Synthesis and Reactivity of Functionalized Silicon(II) Compounds: Iminosilylene, Phosphinosilylene, Hydrosilylene, and Related Compounds, *Bull. Chem. Soc. Jpn.* **2016**, *90*, 255-271.
- [64] D. Wendel, A. Porzelt, F. A. D. Herz, D. Sarkar, C. Jandl, S. Inoue and B. Rieger, From Si(II) to Si(IV) and Back: Reversible Intramolecular Carbon–Carbon Bond Activation by an Acyclic Iminosilylene, *J. Am. Chem. Soc.* **2017**, *139*, 8134-8137.
- [65] D. Wendel, D. Reiter, A. Porzelt, P. J. Altmann, S. Inoue and B. Rieger, Silicon and Oxygen’s Bond of Affection: An Acyclic Three-Coordinate Silanone and Its Transformation to an Iminosiloxysilylene, *J. Am. Chem. Soc.* **2017**, *139*, 17193-17198.
- [66] A. V. Protchenko, P. Vasko, D. C. H. Do, J. Hicks, M. Á. Fuentes, C. Jones and S. Aldridge, Reduction of Carbon Oxides by an Acyclic Silylene: Reductive Coupling of CO, *Angew. Chem. Int. Ed.* **2019**, *58*, 1808-1812.
- [67] Y. Wang, A. Kostenko, T. J. Hadlington, M. P. Luecke, S. Yao and M. Driess, Silicon-Mediated Selective Homo- and Heterocoupling of Carbon Monoxide, *J. Am. Chem. Soc.* **2019**, *141*, 626-634.
- [68] D. Wendel, W. Eisenreich, C. Jandl, A. Pöthig and B. Rieger, Reactivity of an Acyclic Silylsilylene toward Ethylene: Migratory Insertion into the Si–Si Bond, *Organometallics* **2016**, *35*, 1-4.
- [69] M. M. D. Roy, M. J. Ferguson, R. McDonald, Y. Zhou and E. Rivard, A vinyl silylsilylene and its activation of strong homo- and heteroatomic bonds, *Chem Sci* **2019**, *10*, 6476-6481.
- [70] T. J. Hadlington, J. A. B. Abdalla, R. Tirfoin, S. Aldridge and C. Jones, Stabilization of a two-coordinate, acyclic diaminosilylene (ADASi): completion of the series of isolable diaminotetrylenes, :E(NR₂)₂ (E = group 14 element), *Chem. Commun.* **2016**, *52*, 1717-1720.
- [71] B. Blom and M. Driess, Recent Advances in Silylene Chemistry: Small Molecule Activation En-Route Towards Metal-Free Catalysis in *Functional Molecular Silicon Compounds II: Low Oxidation States*, D. Scheschkewitz (Editor), Springer International Publishing, Cham, **2014**.

- [72] R. Waterman, P. G. Hayes and T. D. Tilley, Synthetic Development and Chemical Reactivity of Transition-Metal Silylene Complexes, *Acc. Chem. Res.* **2007**, *40*, 712-719.
- [73] M. D. Curtis and P. S. Epstein, Redistribution Reactions on Silicon Catalyzed by Transition Metal Complexes in *Adv. Organomet. Chem.*, F. G. A. Stone, R. West (Editors), Academic Press, **1981**. Vol. 19.
- [74] T. D. Tilley, Mechanistic Aspects of Transition-Metal Catalyzed Dehydrogenative Silane Coupling Reactions, *Comments Inorg. Chem.* **1990**, *10*, 37-51.
- [75] C. Zybill and G. Müller, Synthesis and Structure of $[(OC)_4Fe=Si(O^tBu)_2 \cdot HMPT]$, a Donor-Stabilized Silanediyl ("Silylene") Complex, *Angew. Chem. Int. Ed.* **1987**, *26*, 669-670.
- [76] D. A. Straus, T. D. Tilley, A. L. Rheingold and S. J. Geib, Preparation, characterization, and x-ray crystal structure of an acetonitrile-complexed ruthenium silylene, *J. Am. Chem. Soc.* **1987**, *109*, 5872-5873.
- [77] P. Jutzi and A. Möhrke, Bis(pentamethylcyclopentadienyl)silylene as Ligand in Gold(I) Chloride Complexes, *Angew. Chem. Int. Ed.* **1990**, *29*, 893-894.
- [78] S. H. A. Petri, D. Eikenberg, B. Neumann, H.-G. Stammer and P. Jutzi, Reaction of Molybdenocene and Tungstenocene Derivatives with the Divalent Silicon Species $SiN^tBuCHCHN^tBu$ and $(C_5Me_5)_2Si$, *Organometallics* **1999**, *18*, 2615-2618.
- [79] A. Meltzer, C. Präsang, C. Milsman and M. Driess, The Striking Stabilization of $Ni^0(\eta^6\text{-Arene})$ Complexes by an Ylide-Like Silylene Ligand, *Angew. Chem. Int. Ed.* **2009**, *48*, 3170-3173.
- [80] F. Glorius, *N-Heterocyclic Carbenes in Transition Metal Catalysis*, Springer-Verlag, Berlin, **2007**. Vol. 21.
- [81] S. Díez-González, N. Marion and S. P. Nolan, *N-Heterocyclic Carbenes in Late Transition Metal Catalysis*, *Chem. Rev.* **2009**, *109*, 3612-3676.
- [82] M. G. Gardiner and C. C. Ho, Recent advances in bidentate bis(*N*-heterocyclic carbene) transition metal complexes and their applications in metal-mediated reactions, *Coord. Chem. Rev.* **2018**, *375*, 373-388.
- [83] E. Peris, Smart *N*-Heterocyclic Carbene Ligands in Catalysis, *Chem. Rev.* **2018**, *118*, 9988-10031.
- [84] K. H. Dötz and J. Stendel, Fischer Carbene Complexes in Organic Synthesis: Metal-Assisted and Metal-Templated Reactions, *Chem. Rev.* **2009**, *109*, 3227-3274.
- [85] A. de Meijere, H. Schirmer and M. Duetsch, Fischer Carbene Complexes as Chemical Multitalents: The Incredible Range of Products from Carbenepentacarbonylmetal α,β -Unsaturated Complexes, *Angew. Chem. Int. Ed.* **2000**, *39*, 3964-4002.

- [86] C. P. Casey, 2005 Nobel Prize in Chemistry. Development of the Olefin Metathesis Method in Organic Synthesis, *J. Chem. Educ.* **2006**, *83*, 192.
- [87] M. Okazaki, H. Tobita and H. Ogino, Reactivity of silylene complexes, *Dalton Trans.* **2003**, 493-506.
- [88] H. Clavier and S. P. Nolan, Percent buried volume for phosphine and *N*-heterocyclic carbene ligands: steric properties in organometallic chemistry, *Chem. Commun.* **2010**, *46*, 841-861.
- [89] Z. Benedek and T. Szilvási, Can low-valent silicon compounds be better transition metal ligands than phosphines and NHCs?, *RSC Adv.* **2015**, *5*, 5077-5086.
- [90] B. Blom, D. Gallego and M. Driess, *N*-heterocyclic silylene complexes in catalysis: new frontiers in an emerging field, *Inorg. Chem. Front.* **2014**, *1*, 134-148.
- [91] B. Blom, S. Enthaler, S. Inoue, E. Irran and M. Driess, Electron-Rich *N*-Heterocyclic Silylene (NHSi)–Iron Complexes: Synthesis, Structures, and Catalytic Ability of an Isolable Hydridosilylene–Iron Complex, *J. Am. Chem. Soc.* **2013**, *135*, 6703-6713.
- [92] P. P. Gaspar, Organosilicon-Based Reactive Intermediates in *Organosilicon Chemistry VI: From Molecules to Materials*, N. Auner, J. Weis (Editors), Wiley-VCH, Weinheim, **2005**.
- [93] C. Gerdes, Terphenylsubstituierte 7-Silanorbornadiene und das erste 7-Silanorbornadienylkation als Precursorverbindung für ein intermediäres Silyliumyliden, PhD Thesis, Carl von Ossietzky Universität Oldenburg, Oldenburg, **2012**.
- [94] A. E. Douglas and B. L. Lutz, Spectroscopic identification of the SiH⁺ molecule: The A₁Π–X₁Σ⁺ system, *Can. J. Phys.* **1970**, *48*, 247-253.
- [95] N. Grevesse and A. J. Sauval, Identification of SiH⁺ in the Solar Photospheric Spectrum, *Astron. Astrophys.* **1970**, *9*, 232-238.
- [96] P. D. Singh and F. G. Vanlandingham, Line Positions and Oscillator Strengths of Rotation-vibration Bands of Possible Interstellar SiH and SiH⁺, *Astron. Astrophys.* **1978**, *66*, 87-92.
- [97] S. L. Powley and S. Inoue, NHC-Stabilised Silyliumylidene Ions, *Chem. Rec.* **2019**, *19*, 2179–2188.
- [98] A. Sekiguchi, T. Fukawa, M. Nakamoto, V. Y. Lee and M. Ichinohe, Isolable Silyl and Gerym Radical Lacking Conjugation with π-Bonds: Synthesis, Characterization, and Reactivity, *J. Am. Chem. Soc.* **2002**, *124*, 9865-9869.
- [99] A. Sekiguchi, S. Inoue, M. Ichinohe and Y. Arai, Isolable Anion Radical of Blue Disilene (^tBu₂MeSi)₂Si=Si(SiMe^tBu₂)₂ Formed upon One-Electron Reduction: Synthesis and Characterization, *J. Am. Chem. Soc.* **2004**, *126*, 9626-9629.

- [100] R. Holzner, A. Kaushansky, B. Tumanskii, P. Frisch, F. Linsenmann and S. Inoue, Isolation of a Relatively Air-Stable, Bulky Silyl-Substituted, Neutral Silicon-Centered Radical, *Eur. J. Inorg. Chem.* **2019**, 2019, 2977-2981.
- [101] B. Tumanskii, M. Karni and Y. Apeloig, Persistent and Stable Silyl Radicals in *Encyclopedia of Radicals in Chemistry, Biology and Materials*, C. Chatgililoglu, A. Studer (Editors), John Wiley & Sons, New Jersey, **2012**.
- [102] B. Tumanskii, M. Karni and Y. Apeloig, Silicon-Centered Radicals - Chapter 6 in *Organosilicon Compounds: Theory and Experiment (Synthesis)*, V. Y. Lee (Editor), Academic Press, Massachusetts, **2017**.
- [103] T. Müller, Stability, Reactivity, and Strategies for the Synthesis of Silyliumylidenes, RSi^+ . A Computational Study, *Organometallics* **2010**, 29, 1277-1283.
- [104] C. Gerdes, W. Saak, D. Haase and T. Müller, Dibenzosilanorbornadienyl Cations and Their Fragmentation into Silyliumylidenes, *J. Am. Chem. Soc.* **2013**, 135, 10353-10361.
- [105] C. P. Sindlinger, F. S. W. Aicher and L. Wesemann, Cationic Stannylenes: *In Situ* Generation and NMR Spectroscopic Characterization, *Inorg. Chem.* **2017**, 56, 548-560.
- [106] M. A. C. Holger Braunschweig, Rian D. Dewhurst, Magdalena Heid, Florian Huppa and Sakya S. Sen, Stepwise isolation of low-valent, low-coordinate Sn and Pb mono- and dications in the coordination sphere of platinum, *Chem. Sci.* **2015**, 6, 425-435.
- [107] M. Bouška, L. Dostál, A. Růžicka and R. Jambor, Stabilization of Three-Coordinated Germanium(II) and Tin(II) Cations by a Neutral Chelating Ligand, *Organometallics* **2013**, 32, 1995-1999.
- [108] C. S. Jiaye Li, Florian Winter, Harald Scherer, Nils Trapp, Alexander Higelin, Sarah Keller, Rainer Pçttgen, Ingo Krossing, and Cameron Jones, Weak Arene Stabilization of Bulky Amido-Germanium(II) and Tin(II) Monocations, *Angew. Chem. Int. Ed.* **2012**, 51.
- [109] M. J. Taylor, A. J. Saunders, M. P. Coles and J. R. Fulton, Low-Coordinate Tin and Lead Cations, *Organometallics* **2011**, 30, 1334-1339.
- [110] M. M. D. Roy, P. A. Lummis, M. J. Ferguson, R. McDonald and E. Rivard, Accessing Low-Valent Inorganic Cations by Using an Extremely Bulky *N*-Heterocyclic Carbene, *Chem. Eur. J.* **2017**, 23, 11249-11252.
- [111] P. Jutzi, F. Kohl and C. Krüger, Synthesis and Structure of the nido-Cluster $(\text{CH}_3)_5\text{C}_5\text{Sn}^+$, *Angew. Chem. Int. Ed.* **1979**, 18, 59-60.
- [112] P. Jutzi, F. Kohl, P. Hofmann, C. Krüger and Y.-H. Tsay, Bis(pentamethylcyclopentadienyl)germanium und -zinn sowie (Pentamethylcyclopentadienyl)germanium- und -zinn-Kationen: Synthese, Struktur und Bindungsverhältnisse, *Chemische Berichte* **1980**, 113, 757-769.

- [113] P. Jutzi, A. Mix, B. Rummel, W. W. Schoeller, B. Neumann and H.-G. Stammer, The $\text{Me}_5\text{C}_5\text{Si}$ Cation: A Stable Derivative of HSi^+ , *Science* **2004**, *305*, 849-851.
- [114] S. Hino, M. Brynda, A. D. Phillips and P. P. Power, Synthesis and Characterization of a Quasi-One-Coordinate Lead Cation, *Angew. Chem. Int. Ed.* **2004**, *43*, 2655-2658.
- [115] P. Jutzi, U. Holtmann, D. Kanne, C. Krüger, R. Blom, R. Gleiter and I. Hyla-Kryspin, Decamethylsilicocene – The first stable silicon(II) compound: Synthesis, structure, and bonding, *Chemische Berichte* **1989**, *122*, 1629-1639.
- [116] P. Ghana, M. I. Arz, G. Schnakenburg, M. Straßmann and A. C. Filippou, Metal–Silicon Triple Bonds: Access to $[\text{Si}(\eta^5\text{-C}_5\text{Me}_5)]^+$ from $\text{SiX}_2(\text{NHC})$ and its Conversion to the Silylidyne Complex $[\text{TpMe}(\text{CO})_2\text{MoSi}(\eta^3\text{-C}_5\text{Me}_5)]$ ($\text{TpMe} = \kappa^3\text{-N,N',N''-hydridotris(3,5-dimethyl-1-pyrazolyl)borate}$), *Organometallics* **2018**, *37*, 772-780.
- [117] E. Fritz-Langhals, Silicon(II) Cation $\text{Cp}^*\text{Si}^+ \text{X}^-$: A New Class of Efficient Catalysts in Organosilicon Chemistry, *Org. Process Res. Dev.* **2019**, *23*, 2369-2377.
- [118] P. Jutzi, A. Mix, B. Neumann, B. Rummel and H.-G. Stammer, Novel π -complexes of divalent silicon: mixed substituted neutral sandwich compounds and the half-sandwich cation $(i\text{Pr}_5\text{C}_5)\text{Si}^+$, *Chem. Commun.* **2006**, *33*, 3519-3521.
- [119] M. Driess, S. Yao, M. Brym and C. van Wüllen, Low-Valent Silicon Cations with Two-Coordinate Silicon and Aromatic Character, *Angew. Chem. Int. Ed.* **2006**, *45*, 6730-6733.
- [120] Y. Xiong, S. Yao, S. Inoue, E. Irran and M. Driess, The Elusive Silyliumylidene $[\text{ClSi}]^+$ and Silathionium $[\text{ClSi}=\text{S}]^+$ Cations Stabilized by Bis(Iminophosphorane) Chelate Ligand, *Angew. Chem. Int. Ed.* **2012**, *51*, 10074-10077.
- [121] H.-X. Yeong, H.-W. Xi, Y. Li, K. H. Lim and C.-W. So, A Silyliumylidene Cation Stabilized by an Amidinate Ligand and 4-Dimethylaminopyridine, *Chem. Eur. J.* **2013**, *19*, 11786-11790.
- [122] G. Frenking, Dative Bonds in Main-Group Compounds: A Case for More Arrows!, *Angew. Chem. Int. Ed.* **2014**, *53*, 6040-6046.
- [123] D. Himmel, I. Krossing and A. Schnepf, Dative Bonds in Main-Group Compounds: A Case for Fewer Arrows!, *Angew. Chem. Int. Ed.* **2014**, *53*, 370-374.
- [124] A. Nandi and S. Kozuch, History and Future of Dative Bonds, *Chem. Eur. J.* **2019**, *25*, 1-15.
- [125] S. U. Ahmad, T. Szilvási and S. Inoue, A facile access to a novel NHC-stabilized silyliumylidene ion and C–H activation of phenylacetylene, *Chem. Commun.* **2014**, *50*, 12619-12622.

- [126] Y. Xiong, S. Yao, S. Inoue, J. D. Epping and M. Driess, A Cyclic Silylone ("Siladibene") with an Electron-Rich Silicon(0) Atom, *Angew. Chem. Int. Ed.* **2013**, *52*, 7147-7150.
- [127] Y. Li, Y.-C. Chan, Y. Li, I. Purushothaman, S. De, P. Parameswaran and C.-W. So, Synthesis of a Bent 2-Silaallene with a Perturbed Electronic Structure from a Cyclic Alkyl(amino) Carbene-Diidosilylene, *Inorg. Chem.* **2016**, *55*, 9091-9098.
- [128] A. Porzelt, J. Schweizer, R. Baierl, P. Altmann, M. Holthausen and S. Inoue, S-H Bond Activation in Hydrogen Sulfide by NHC-Stabilized Silyliumylidene Ions, *Inorganics* **2018**, *6*, 54.
- [129] N. Hayakawa, K. Sadamori, S. Mizutani, T. Agou, T. Sugahara, T. Sasamori, N. Tokitoh, D. Hashizume and T. Matsuo, Synthesis and Characterization of *N*-Heterocyclic Carbene-Coordinated Silicon Compounds Bearing a Fused-Ring Bulky Eind Group, *Inorganics* **2018**, *6*, 30.
- [130] T. Agou, N. Hayakawa, T. Sasamori, T. Matsuo, D. Hashizume and N. Tokitoh, Reactions of Diaryldibromodisilenes with *N*-Heterocyclic Carbenes: Formation of Formal Bis-NHC Adducts of Silyliumylidene Cations, *Chem. Eur. J.* **2014**, *20*, 9246-9249.
- [131] Y. Li, Y.-C. Chan, B.-X. Leong, Y. Li, E. Richards, I. Purushothaman, S. De, P. Parameswaran and C.-W. So, Trapping a Silicon(I) Radical with Carbenes: A Cationic cAAC-Silicon(I) Radical and an NHC-Parent-Silyliumylidene Cation, *Angew. Chem. Int. Ed.* **2017**, *56*, 7573-7578.
- [132] A. C. Filippou, B. Baars, O. Chernov, Y. N. Lebedev and G. Schnakenburg, Silicon-Oxygen Double Bonds: A Stable Silanone with a Trigonal-Planar Coordinated Silicon Center, *Angew. Chem. Int. Ed.* **2014**, *53*, 565-570.
- [133] P. Jutzi, The Pentamethylcyclopentadienylsilicon(II) Cation: Synthesis, Characterization, and Reactivity, *Chem. Eur. J.* **2014**, *20*, 9192-9207.
- [134] P. Jutzi, K. Leszczyńska, B. Neumann, W. W. Schoeller and H.-G. Stämmler, [2,6-(Trip)₂H₃C₆](Cp*)Si: A Stable Monomeric Arylsilicon(II) Compound, *Angew. Chem. Int. Ed.* **2009**, *48*, 2596-2599.
- [135] S. Inoue and K. Leszczyńska, An Acyclic Imino-Substituted Silylene: Synthesis, Isolation, and its Facile Conversion into a Zwitterionic Silamine, *Angew. Chem. Int. Ed.* **2012**, *51*, 8589-8593.
- [136] P. Jutzi, A. Mix, B. Neumann, B. Rummel, W. W. Schoeller, H.-G. Stämmler and A. B. Rozhenko, Reversible Transformation of a Stable Monomeric Silicon(II) Compound into a Stable Disilene by Phase Transfer: Experimental and Theoretical Studies of the System $\{[(\text{Me}_3\text{Si})_2\text{N}](\text{Me}_5\text{C}_5)\text{Si}\}_n$ with $n = 1, 2$, *J. Am. Chem. Soc.* **2009**, *131*, 12137-12143.
- [137] P. Jutzi, K. Leszczyńska, A. Mix, B. Neumann, B. Rummel, W. Schoeller and H.-G. Stämmler, Synthesis and Characterization of the Ferrio-Substituted Silicon(II) Compound $\text{Me}_5\text{C}_5(\text{CO})_2\text{FeSiC}_5\text{Me}_5$, *Organometallics* **2010**, *29*, 4759-4761.

- [138] K. Leszczyńska, K. Abersfelder, A. Mix, B. Neumann, H.-G. Stammler, M. J. Cowley, P. Jutzi and D. Scheschkewitz, Reversible Base Coordination to a Disilene, *Angew. Chem. Int. Ed.* **2012**, *51*, 6785-6788.
- [139] K. Abersfelder, A. J. P. White, H. S. Rzepa and D. Scheschkewitz, A Tricyclic Aromatic Isomer of Hexasilabenzene, *Science* **2010**, *327*, 564-566.
- [140] K. Leszczyńska, K. Abersfelder, M. Majumdar, B. Neumann, H.-G. Stammler, H. S. Rzepa, P. Jutzi and D. Scheschkewitz, The Cp*Si⁺ cation as a stoichiometric source of silicon, *Chem. Commun.* **2012**, *48*, 7820-7822.
- [141] K. I. Leszczyńska, V. Huch, C. Präsang, J. Schwabedissen, R. J. F. Berger and D. Scheschkewitz, Atomically Precise Expansion of Unsaturated Silicon Clusters, *Angew. Chem. Int. Ed.* **2019**, *58*, 5124-5128.
- [142] P. Jutzi, K. Leszczyńska, A. Mix, B. Neumann, W. W. Schoeller and H.-G. Stammler, Reaction of the (Pentamethylcyclopentadienyl)silicon(II) Cation with a Sterically Encumbered β -Diketiminato Anion: Unexpected Formation of a Tricyclic Silicon(IV) Compound, *Organometallics* **2009**, *28*, 1985-1987.
- [143] S. S. Sen, A. Jana, H. W. Roesky and C. Schulzke, A Remarkable Base-Stabilized Bis(silylene) with a Silicon(I)–Silicon(I) Bond, *Angew. Chem. Int. Ed.* **2009**, *48*, 8536-8538.
- [144] S. U. Ahmad, T. Szilvási, E. Irran and S. Inoue, An NHC-Stabilized Silicon Analogue of Acylium Ion: Synthesis, Structure, Reactivity, and Theoretical Studies, *J. Am. Chem. Soc.* **2015**, *137*, 5828-5836.
- [145] D. Sarkar, D. Wendel, S. U. Ahmad, T. Szilvási, A. Pöthig and S. Inoue, Chalcogen-atom transfer and exchange reactions of NHC-stabilized heavier silaacylium ions, *Dalton Trans.* **2017**, *46*, 16014-16018.
- [146] D. Sarkar, V. Nesterov, T. Szilvasi, P. J. Altmann and S. Inoue, The Quest for Stable Silaaldehydes: Synthesis and Reactivity of a Masked Silacarbonyl, *Chem. Eur. J.* **2019**, *25*, 1198-1202.
- [147] K. Leszczyńska, A. Mix, R. J. F. Berger, B. Rummel, B. Neumann, H.-G. Stammler and P. Jutzi, The Pentamethylcyclopentadienylsilicon(II) Cation as a Catalyst for the Specific Degradation of Oligo(ethyleneglycol) Diethers, *Angew. Chem. Int. Ed.* **2011**, *50*, 6843-6846.
- [148] B. X. Leong, J. Lee, Y. Li, M.-C. Yang, C.-K. A. Siu, M.-D. Su and C.-W. So, A Versatile NHC-Parent Silyliumylidene Cation for Catalytic Chemo- and Regioselective Hydroboration, *J. Am. Chem. Soc.* **2019**, *141*, 17629-17636.
- [149] N. C. Breit, T. Szilvási, T. Suzuki, D. Gallego and S. Inoue, From a Zwitterionic Phosphasilene to Base Stabilized Silyliumylidene-Phosphide and Bis(silylene) Complexes, *J. Am. Chem. Soc.* **2013**, *135*, 17958-17968.
- [150] H.-X. Yeong, Y. Li and C.-W. So, A Base-Stabilized Silyliumylidene Cation as a Ligand for Rhodium and Tungsten Complexes, *Organometallics* **2014**, *33*, 3646-3648.

- [151] P. Frisch and S. Inoue, Lewis base-stabilized silyliumylidene ions in transition metal coordination chemistry, *Dalton Trans.* **2020**, 49, 6176-6182.
- [152] P. Frisch and S. Inoue, NHC-stabilized silyl-substituted silyliumylidene ions, *Dalton Trans.* **2019**, 48, 10403-10406.
- [153] P. Frisch and S. Inoue, Coinage metal complexes of NHC-stabilized silyliumylidene ions, *Chem. Commun.* **2018**, 54, 13658-13661.
- [154] P. Frisch, T. Szilvási, A. Porzelt and S. Inoue, Transition Metal Carbonyl Complexes of an *N*-Heterocyclic Carbene Stabilized Silyliumylidene Ion, *Inorg. Chem.* **2019**, 58, 14931-14937.
- [155] P. Frisch, T. Szilvási and S. Inoue, Facile Access to Dative, Single, and Double Silicon–Metal Bonds Through M–Cl Insertion Reactions of Base-Stabilized Si(II) Cations, *Chem. Eur. J.* **2020**, 26, 6271-6278.

11. Appendix

11.1 Supporting Information Chapter 4

Electronic Supplementary Material (ESI) for Dalton Transactions.
This journal is © The Royal Society of Chemistry 2019

Supporting Information

NHC-stabilized Silyl-substituted Silyliumylidene Ions

*Philipp Frisch and Shigeyoshi Inoue**

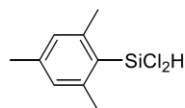
Table of Contents

1. Experimental Section	2
1.1. General Methods and Instrumentation	2
1.2 Synthesis of Mes–SiCl ₂ H	3
1.3 Synthesis of [^t Bu ₃ Si–Si(IME ₄) ₂]Cl (1)	5
1.4 Synthesis of [^t Bu ₂ MeSi–Si(NHC) ₂]Cl (2a,b)	7
1.5 Synthesis of [Mes–Si(IME ₄) ₂]Cl (3)	13
1.6 NHC exchange reaction of 2b to 2a	16
2. X-ray Crystallographic Data	23
2.1 SC-XRD structure of [^t Bu ₃ Si–Si(IME ₄) ₂]Cl (1)	24
2.2 SC-XRD structure of [^t Bu ₂ MeSi–Si(IME ₄) ₂]Cl (2a)	24
3. References	26

1. Experimental Section

1.1. General Methods and Instrumentation

All reactions were carried out under exclusion of water and oxygen in an atmosphere of argon 4.6 ($\geq 99.996\%$) using standard Schlenk techniques or in a Labstar glovebox from *MBraun* with H_2O and O_2 levels below 0.5 ppm. Glassware was heat dried under vacuum prior to use. Acetonitrile, pyridine, Acetonitrile- d_3 , pyridine- d_5 , fluorobenzene and fluorobenzene- d_5 were refluxed over CaH_2 , distilled under argon, deoxygenated by three freeze-pump-thaw cycles and stored over 3 Å molecular sieve in a glovebox. Diethylether, THF and *n*-hexane were refluxed over sodium/benzophenone, distilled under argon, deoxygenated by three freeze-pump-thaw cycles and stored over 3 Å molecular sieve in a glovebox. C_6D_6 was stirred over Na-K-alloy, distilled under argon, deoxygenated by three freeze-pump-thaw cycles and stored over 3 Å molecular sieve in a glovebox. All NMR samples were prepared under argon in *J. Young* PTFE valve NMR tubes. NMR spectra at ambient temperature (300 K) were recorded on a *Bruker* AV400US or DRX400 (^1H : 400.13 MHz, ^{13}C : 100.62 MHz, ^{29}Si : 79.49 MHz), AVHD300 (^1H : 300.13 MHz) or AV500C (^1H : 500.36 MHz, ^{13}C : 125.83 MHz, ^{29}Si : 99.41 MHz). The ^1H , ^{13}C and ^{29}Si NMR spectroscopic chemical shifts δ are reported in ppm relative to tetramethylsilane. ^1H and ^{13}C NMR spectra are calibrated against the residual proton and natural abundance carbon resonances of the respective deuterated solvent as internal standard (C_6D_6 : $\delta(^1\text{H}) = 7.16$ ppm and $\delta(^{13}\text{C}) = 128.0$ ppm; CD_3CN : $\delta(^1\text{H}) = 1.94$ ppm and $\delta(^{13}\text{C}) = 118.3$ ppm; $\text{C}_6\text{D}_5\text{N}$: $\delta(^1\text{H}) = 8.74$ ppm and $\delta(^{13}\text{C}) = 150.4$ ppm; $\text{C}_6\text{D}_5\text{F}$: $\delta(^1\text{H}) = 6.90$ ppm). ^{29}Si NMR spectra are referenced to the resonance of tetramethylsilane ($\delta = 0$ ppm) as external standard. The following abbreviations are used to describe signal multiplicities: s = singlet, d = doublet, t = triplet, sept = septet, bs = broad signal, m = multiplet. Quantitative elemental analyses (EA) were carried out using a *HEKAtech* EURO EA instrument equipped with a CHNS combustion analyzer at the Laboratory for Microanalysis at the TUM Catalysis Research Center. Melting Points (M.P.) were determined in sealed glass capillaries under inert gas with a *Büchi* M-565 melting point apparatus. ESI-MS spectra were recorded on a *Bruker* HCT Instrument with a dry gas temperature of 300 °C and an injection speed of 240 μLs^{-1} . Unless otherwise stated, all commercially available chemicals were purchased from *abcr* or *Sigma-Aldrich* and used without further purification. The compounds 1,3,4,5-tetramethylimidazol-2-ylidene (IMe_4)^{S1}, 1,3-diethyl-4,5-dimethylimidazol-2-ylidene (IEt_2Me_2)^{S1}, MeSi ^{S2}, $^t\text{Bu}_3\text{Si-SiCl}_2\text{H}$ ^{S3} and $^t\text{Bu}_2\text{MeSi-SiCl}_2\text{H}$ ^{S4} were prepared as described in the literature.

1.2 Synthesis of Mes-SiCl₂H

HSiCl₃ (10 mL, 13.5 g, 99.7 mmol, 5.0 eq) was dissolved in 30 mL Et₂O and slowly added to a suspension of MesLi (2.50 g, 19.8 mmol, 1.0 eq) in 50 mL Et₂O cooled to -78 °C. The suspension was allowed to warm to room temperature and then stirred for 48 hours. The solvent was removed under reduced pressure and the residue was extracted with hexane (3×20 mL). Hexane was removed under reduced pressure and after bulb-to-bulb distillation (6×10⁻³ mbar, 70 °C) the product (3.61 g, 19.8 mmol, 83%) was obtained as a colorless oil.

¹H NMR (400 MHz, C₆D₆, 300 K): δ [ppm] = 6.52 (s, 2H, C_{mes}H), 6.27 (s, 1H, SiCl₂H), 2.34 (s, 6H, C_{ortho}H), 1.96 (s, 3H, C_{para}H).

¹³C{¹H} NMR (100 MHz, C₆D₆, 300 K): δ [ppm] = 144.7, 142.6, 129.8, 125.4, 22.8, 21.1.

²⁹Si{¹H} NMR (79 MHz, C₆D₆, 300 K): δ [ppm] = -6.9 (SiCl₂H).

EA: C₉H₁₂Cl₂Si

calculated [%]: C (49.32), H (5.52).

measured [%]: C (49.53), H (5.49).

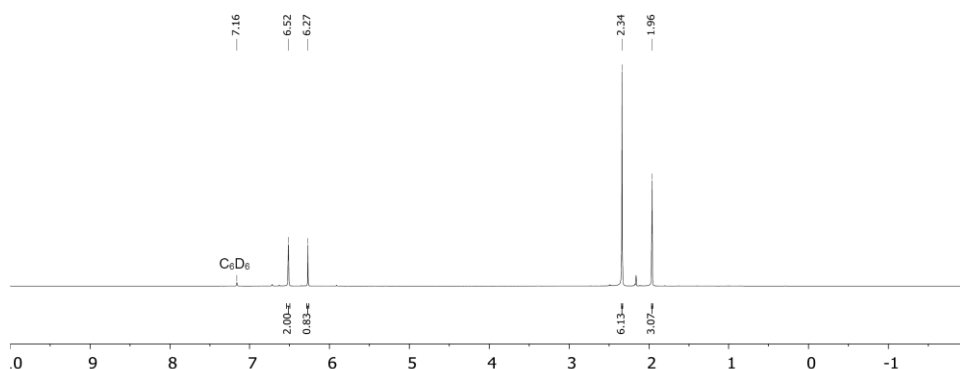


Fig. S1 ¹H NMR spectrum of Mes-SiCl₂H in C₆D₆ at 300 K.

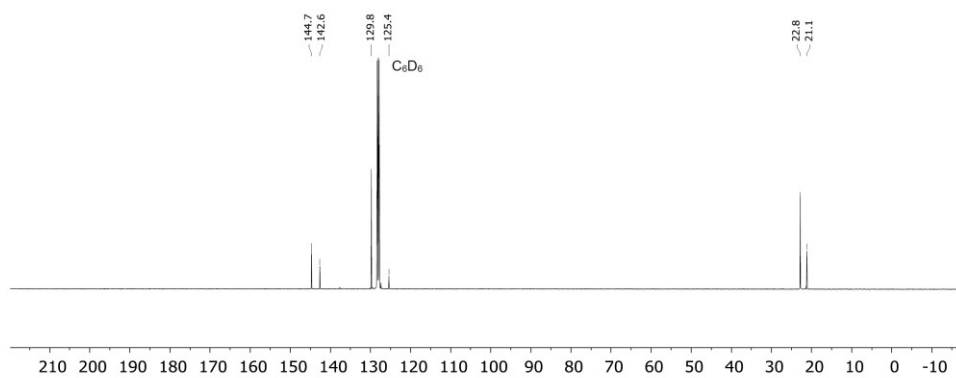


Fig. S2 $^{13}\text{C}\{^1\text{H}\}$ NMR spectrum of Mes-SiCl₂H in C₆D₆ at 300 K.

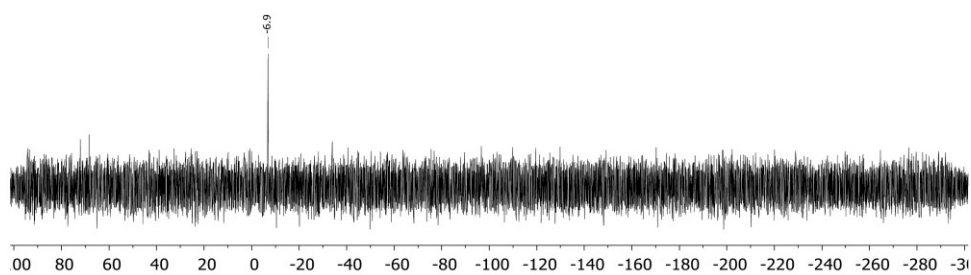
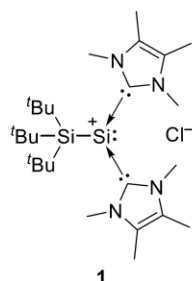


Fig. S3 $^{29}\text{Si}\{^1\text{H}\}$ NMR spectrum of Mes-SiCl₂H in C₆D₆ at 300 K.

1.3 Synthesis of [^tBu₃Si–Si(IME₄)₂]Cl (**1**)

^tBu₃Si–SiCl₂H (1.00 g, 3.34 mmol, 1.0 eq) was dissolved in 50 mL toluene and cooled to –50 °C. IMe₄ (1.24 g, 10.0 mmol, 3.0 eq) was dissolved in 20 mL toluene and then added dropwise to the silane solution. The mixture was slowly warmed to room temperature overnight. The orange precipitate was collected by filtration, the residue washed with toluene (2×10 mL) and hexane (2×10 mL) and finally extracted with a mixture of toluene and acetonitrile (5:1, 2×30 mL). The solvent was removed under reduced pressure and after drying under vacuum the product **1** (1.11 g, 2.17 mmol, 65%) was isolated as an orange air- and moisture-sensitive powder.

Single crystals suitable for XRD analysis of **1** were obtained by slow diffusion of Et₂O into a concentrated MeCN solution of **1** at –35 °C.

¹H NMR (400 MHz, CD₃CN, 300 K): δ [ppm] = 3.69 (s, 12H, N_{NHC}CH₃), 2.15 (s, 12H, C_{NHC}CH₃), 1.22 (s, 27H, C(CH₃)₃).

¹³C{¹H} NMR (100 MHz, CD₃CN, 300 K): δ [ppm] = 164.1, 128.6, 36.6, 33.0, 26.1, 9.4.

²⁹Si{¹H} NMR (79 MHz, CD₃CN, 300 K): δ [ppm] = 21.8 (SiSi[#]Bu₃), –82.0 (SiSi[#]Bu₃).

ESI-MS: calculated: 475.36 (C₂₆H₅₁N₄Si₂⁺ = **1** – Cl[–])
measured: 475.2

EA: C₂₆H₅₁ClN₄Si₂ calculated [%]: C (61.07), H (10.05), N (10.96).
measured [%]: C (60.86), H (9.78), N (10.73).

M.P.: 161–162 °C (decomposition, change to red oil).

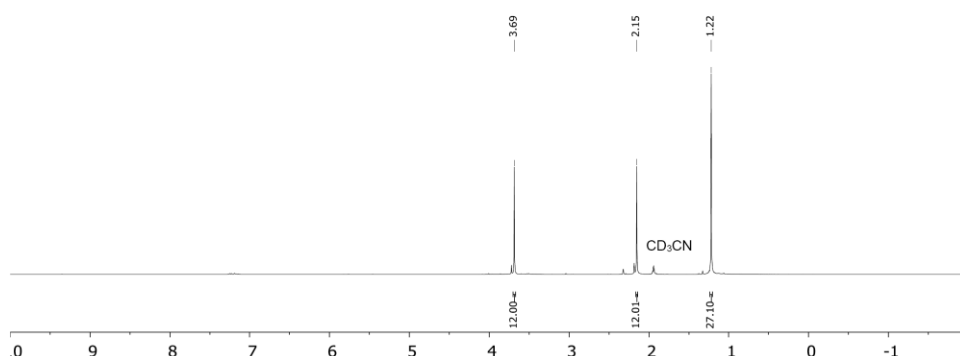


Fig. S4 ¹H NMR spectrum of [^tBu₃Si–Si(IME₄)₂]Cl (**1**) in CD₃CN at 300 K.

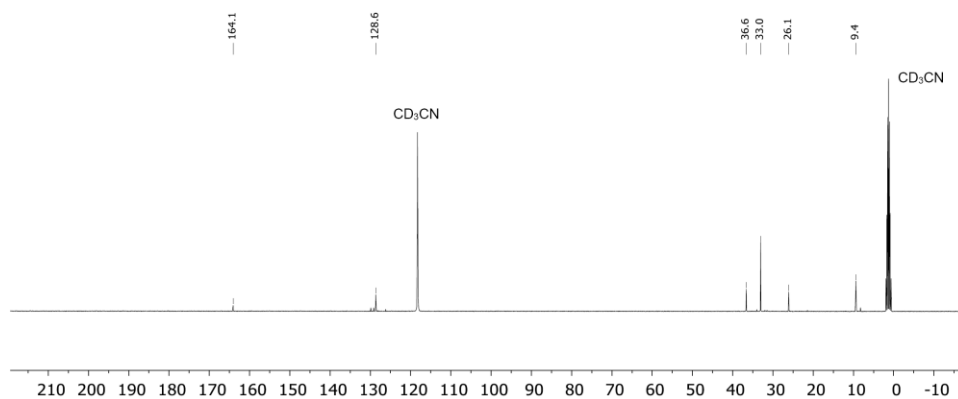


Fig. S5 $^{13}\text{C}\{^1\text{H}\}$ NMR spectrum of $[\text{tBu}_3\text{Si-Si}(\text{Ime}_4)_2]\text{Cl}$ (**1**) in CD_3CN at 300 K.

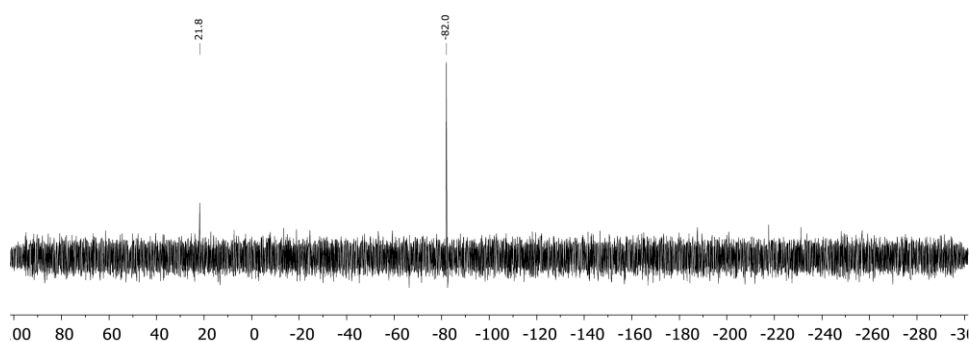


Fig. S6 $^{29}\text{Si}\{^1\text{H}\}$ NMR spectrum of $[\text{tBu}_3\text{Si-Si}(\text{Ime}_4)_2]\text{Cl}$ (**1**) in CD_3CN at 300 K.

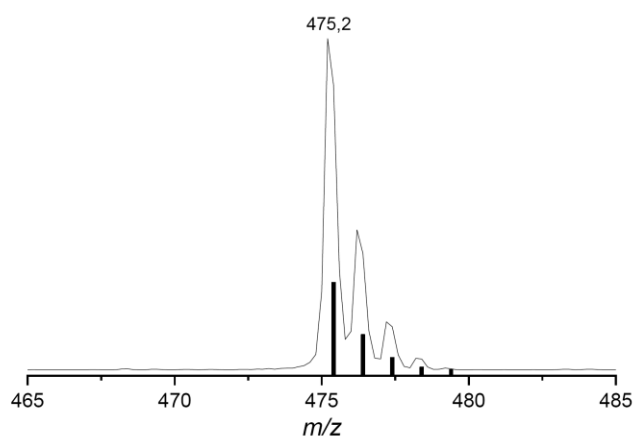
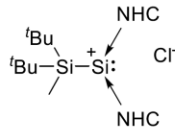


Fig. S7 ESI-MS spectrum (detailed view) of $[\text{tBu}_3\text{Si-Si}(\text{Ime}_4)_2]^+$ (**1** - Cl^-) (positive mode, 300 °C, -4000 V; line: measured spectrum; bars: simulated spectrum).

S6

1.4 Synthesis of [^tBu₂MeSi–Si(NHC)₂]Cl (**2a,b**)


^tBu₂MeSi–SiCl₂H (1.00 g, 3.89 mmol, 1.0 eq) was dissolved in 50 mL toluene and cooled to –50 °C. NHC (11.7 mmol, 3.0 eq) was dissolved in 20 mL toluene and then added dropwise to the silane solution. The mixture was allowed to warm to room temperature overnight. The yellow precipitate was collected by filtration, the residue washed with toluene (2×10 mL) and hexane (2×10 mL), dried under reduced pressure and finally extracted with a mixture of toluene and acetonitrile (8:1, 2×30 mL). The solvent was removed under reduced pressure and after drying under vacuum the products **2a,b** were isolated as yellow to orange air- and moisture-sensitive powders.

2a NHC = IMe₄
2b NHC = IEt₂Me₂

[^tBu₂MeSi–Si(IMe₄)₂]Cl (**2a**)

Yield: 1.19 g, 2.54 mmol, 65%.

Single crystals suitable for XRD analysis of **2a** were obtained by storing a concentrated solution of **2a** in 1,2-difluorobenzene at –35 °C.

¹H NMR (400 MHz, CD₃CN, 300 K): δ [ppm] = 3.64 (s, 12H, N_{NHC}CH₃), 2.15 (s, 12H, C_{NHC}CH₃), 0.94 (s, 18H, C(CH₃)₃), 0.40 (SiCH₃).

¹³C{¹H} NMR (100 MHz, CD₃CN, 300 K): δ [ppm] = 163.2, 128.6, 35.8, 29.9, 22.4, 9.3, –1.7.

²⁹Si{¹H} NMR (79 MHz, CD₃CN, 300 K): δ [ppm] = 9.0 (SiSi[#]Bu₂Me), –90.7 (Si/Si[#]Bu₂Me).

ESI-MS: calculated: 433.32 (C₂₃H₄₅N₄Si₂⁺ = **2a** – Cl[–])

measured: 433.2

EA: C₂₃H₄₅CIN₄Si₂ calculated [%]: C (58.87), H (9.67), N (11.94).

measured [%]: C (58.62), H (9.63), N (11.77).

M.P.: 158-159 °C (decomposition, change to red oil).

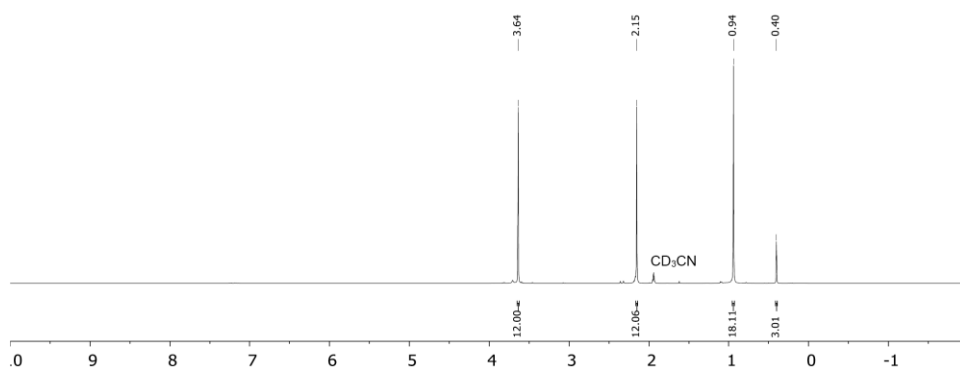


Fig. S8 ¹H NMR spectrum of [^tBu₂MeSi–Si(IMe₄)₂]Cl (**2a**) in CD₃CN at 300 K.

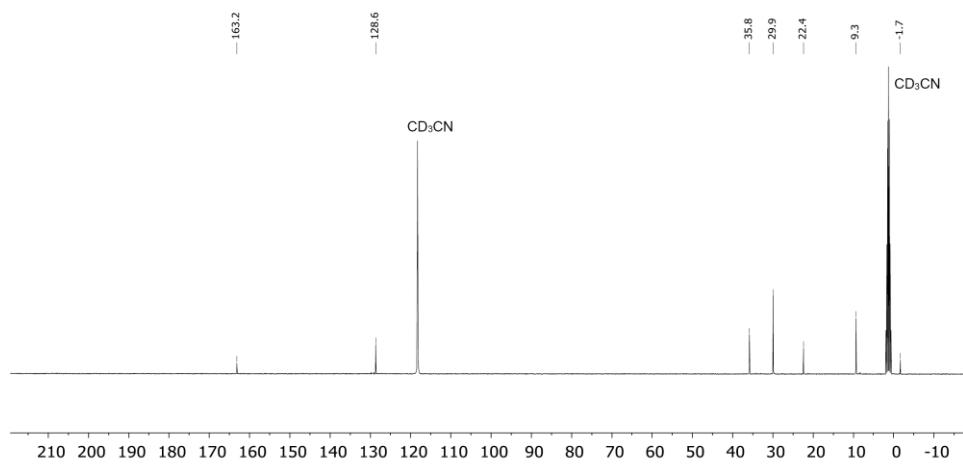


Fig. S9 $^{13}\text{C}\{^1\text{H}\}$ NMR spectrum of $[\text{Bu}_2\text{MeSi-Si}(\text{Ime}_4)_2]\text{Cl}$ (**2a**) in CD_3CN at 300 K.

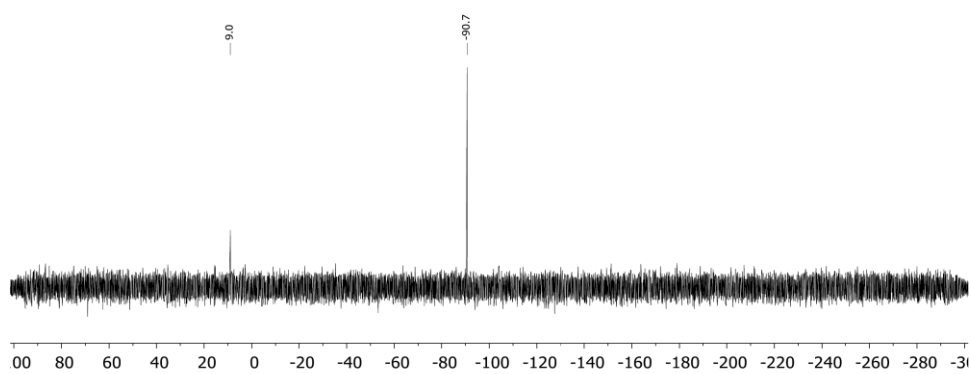


Fig. S10 $^{29}\text{Si}\{^1\text{H}\}$ NMR spectrum of $[\text{Bu}_2\text{MeSi-Si}(\text{Ime}_4)_2]\text{Cl}$ (**2a**) in CD_3CN at 300 K.

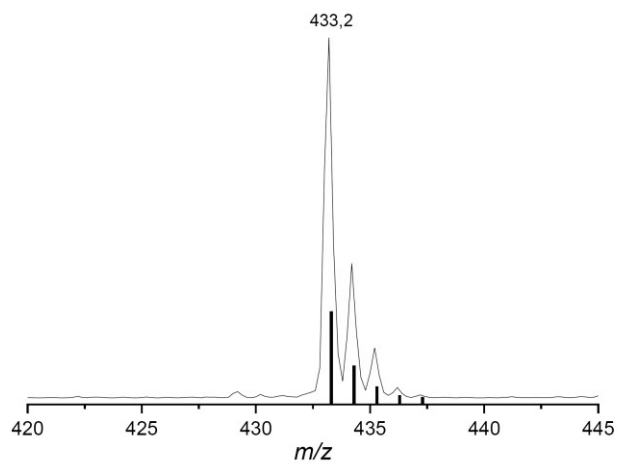


Fig. S11 ESI-MS spectrum (detailed view) of $[\text{tBu}_2\text{MeSi-Si}(\text{Me}_4)_2]^+$ (**2a** - Cl^-) (positive mode, 300 °C, -4000 V; line: measured spectrum; bars: simulated spectrum).

[^tBu₂MeSi–Si(IEt₂Me₂)₂]Cl (2b)

Yield: 1.15 g, 2.19 mmol, 56%.

¹H NMR (400 MHz, CD₃CN, 300 K): δ [ppm] = 4.41 (q, *J* = 7.2 Hz, 8H, CH₂CH₃), 2.22 (s, 12H, C_{NHC}CH₃), 1.04 (t, *J* = 7.2 Hz, 12H, CH₂CH₃), 0.92 (s, 18H, C(CH₃)₃), 0.36 (s, 3H, SiCH₃).

¹H NMR (400 MHz, C₆D₅F, 300 K): δ [ppm] = 4.46 (q, *J* = 7.2 Hz, 8H, CH₂CH₃), 2.07 (s, 12H, C_{NHC}CH₃), 1.05–0.99 (m, 30H, CH₂CH₃, C(CH₃)₃), 0.28 (s, 3H, SiCH₃).

Note: The signal for the ethyl wingtip substituent (t, 12H, CH₂CH₃) overlaps with the signal for the ^tBu-substituent (s, 18H, C(CH₃)₃).

¹³C{¹H} NMR (100 MHz, CD₃CN, 300 K): δ [ppm] = 162.3, 129.3, 44.7, 30.0, 22.5, 14.7, 9.4, –2.4.

²⁹Si{¹H} NMR (79 MHz, CD₃CN, 300 K): δ [ppm] = 9.7 (SiSi[#]Bu₂Me), –86.2 (SiSi[#]Bu₂Me).

ESI-MS: calculated: 489.38 (C₂₇H₅₃N₄Si₂⁺ = **2b** – Cl[–])

measured: 489.2

EA: C₂₇H₅₃ClN₄Si₂ calculated [%]: C (61.73), H (10.17), N (10.66).

measured [%]: C (61.31), H (10.43), N (10.94).

M.P.: 147–148 °C (decomposition, change to red oil).

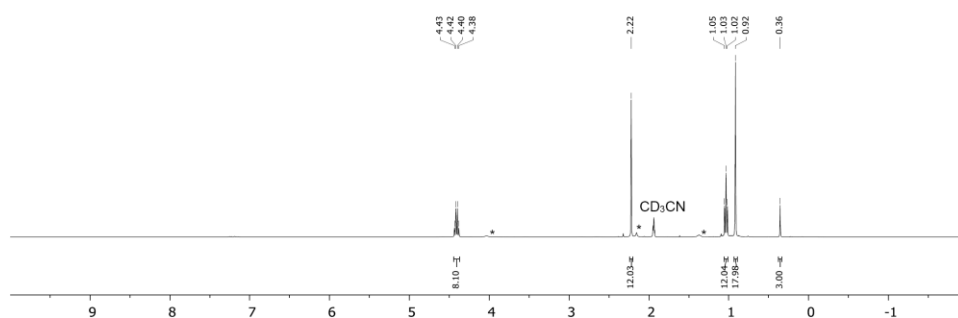


Fig. S12 ¹H NMR spectrum of [^tBu₂MeSi–Si(IEt₂Me₂)₂]Cl (**2b**) in CD₃CN at 300 K. Signals from small amounts of residual IEt₂Me₂·HCl are marked with *.

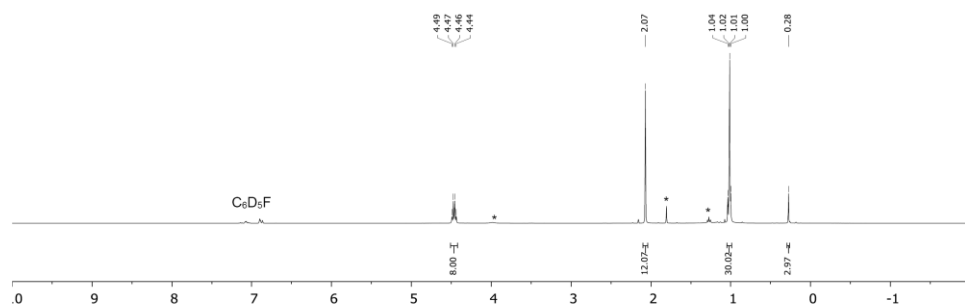


Fig. S13 ^1H NMR spectrum of $[\text{Bu}_2\text{MeSi-Si}(\text{IEt}_2\text{Me}_2)_2]\text{Cl}$ (**2b**) in $\text{C}_6\text{D}_5\text{F}$ at 300 K. Signals from small amounts of residual $\text{IEt}_2\text{Me}_2\cdot\text{HCl}$ are marked with *.

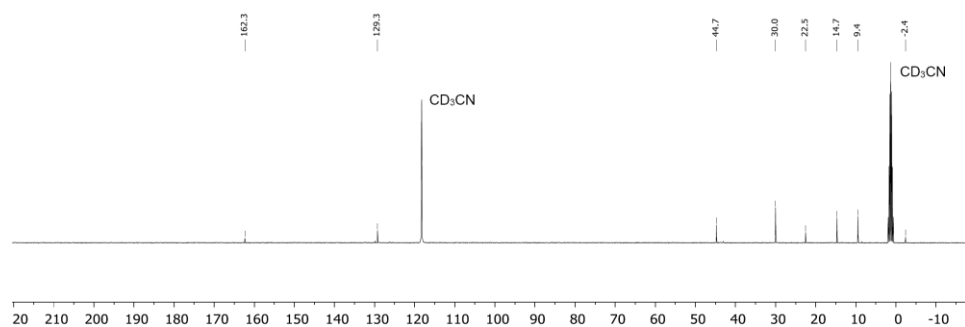


Fig. S14 $^{13}\text{C}\{^1\text{H}\}$ NMR spectrum of $[\text{Bu}_2\text{MeSi-Si}(\text{IEt}_2\text{Me}_2)_2]\text{Cl}$ (**2b**) in CD_3CN at 300 K.

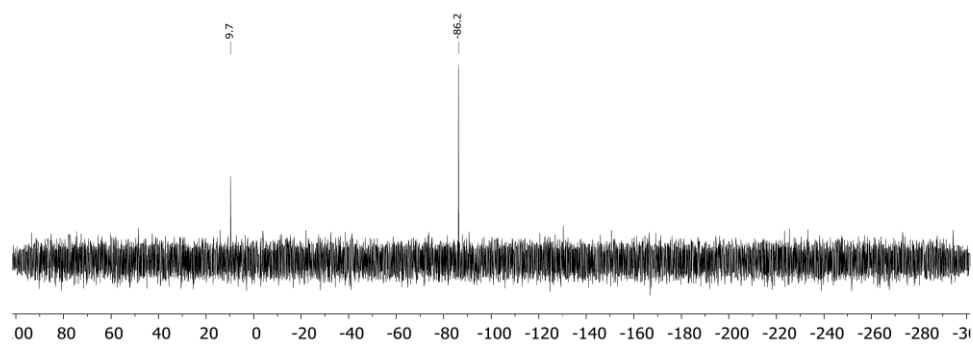


Fig. S15 $^{29}\text{Si}\{^1\text{H}\}$ NMR spectrum of $[\text{Bu}_2\text{MeSi-Si}(\text{IEt}_2\text{Me}_2)_2]\text{Cl}$ (**2b**) in CD_3CN at 300 K.

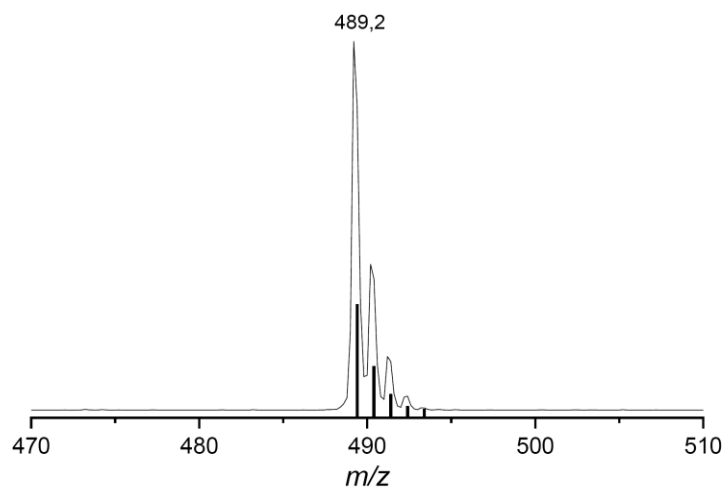
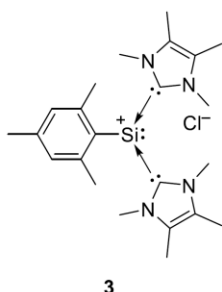


Fig. S16 ESI-MS spectrum (detailed view) of $[\text{tBu}_2\text{MeSi-Si}(\text{IEt}_2\text{Me}_2)_2]^+$ (**2b** - Cl^-) (positive mode, 300 °C, -4000 V; line: measured spectrum; bars: simulated spectrum).

1.5 Synthesis of [Mes–Si(IME₄)₂]Cl (**3**)**3**

Mes–SiCl₂H (1.00 g, 4.56 mmol, 1.0 eq) was dissolved in 60 mL toluene and cooled to –50 °C. IME₄ (1.70 g, 13.69 mmol, 3.0 eq) was dissolved in 20 mL toluene and then added dropwise to the silane solution. The mixture was allowed to warm to room temperature overnight. The yellow precipitate was collected by filtration, the residue washed with toluene (2×10 mL) and hexane (2×10 mL), dried under reduced pressure and then extracted with pyridine (3×15 mL). The solvent was removed under reduced

pressure and after drying under vacuum the product **3** (1.20 g, 2.78 mmol, 61%) was isolated as a pale yellow air- and moisture-sensitive powder.

The compound is very poorly soluble in benzene and well soluble in acetonitrile, pyridine and fluorobenzene. Decomposition occurs in acetonitrile (<4 hours).

¹H NMR (400 MHz, C₅D₅N, 300 K): δ [ppm] = 6.92 (s, 2H, C_{mes}H), 3.68 (s, 12H, N_{NHC}CH₃), 2.29 (s, 6H, C_{mes}CH_{3,ortho}), 2.28 (s, 3H, C_{mes}CH_{3,para}), 2.12 (s, 12H, C_{NHC}CH₃).

¹³C{¹H} NMR (100 MHz, C₅D₅N, 300 K): δ [ppm] = 160.6, 144.8, 137.9, 137.3, 130.0, 128.7, 34.3, 25.2, 21.5, 9.4.

²⁹Si{¹H} NMR (79 MHz, C₅D₅N, 300 K): δ [ppm] = –68.7 (MesSi).

²⁹Si{¹H} NMR (79 MHz, CD₃CN, 300 K): δ [ppm] = –71.2 (MesSi).

ESI-MS: calculated: 311.15 (C₁₄H₂₄N₄SiCl (**3** – Mesityl))
measured: 311.0

Note: The molecular ion peak of **3** – Cl[–] (395.2) could only be observed for a short time upon fast injection. Regular injection speed led to quantitative cleavage of the Si–C bond to the mesityl substituent.

EA: C₂₃H₃₅ClN₄Si calculated [%]: C (64.08), H (8.18), N (13.00).
measured [%]: C (63.62), H (8.02), N (13.32).

M.P.: 180–181 °C (decomposition, color change to black).

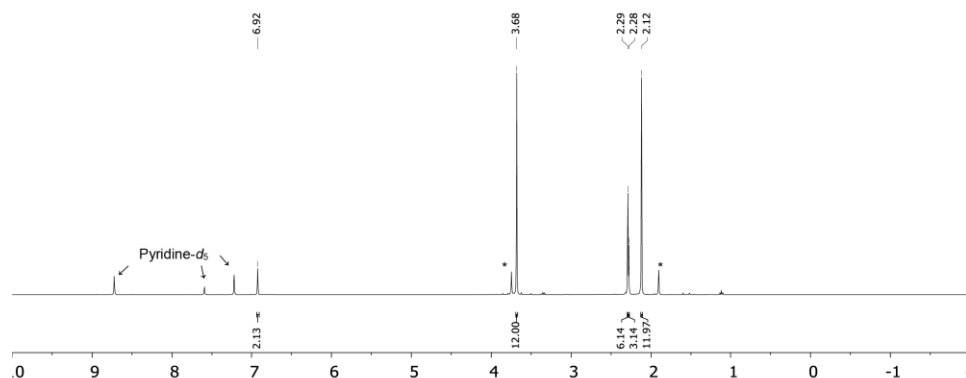


Fig. S17 ^1H NMR spectrum of $[\text{Mes-Si}(\text{IME}_4)_2]\text{Cl}$ (**3**) in pyridine- d_5 at 300 K. Signals from small amounts of residual $\text{IME}_4\cdot\text{HCl}$ are marked with *.

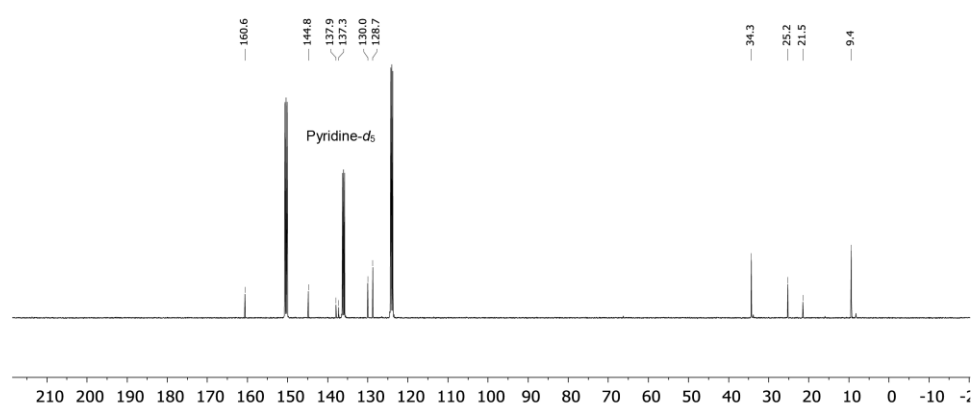


Fig. S18 $^{13}\text{C}\{^1\text{H}\}$ NMR spectrum of $[\text{Mes-Si}(\text{IME}_4)_2]\text{Cl}$ (**3**) in pyridine- d_5 at 300 K.

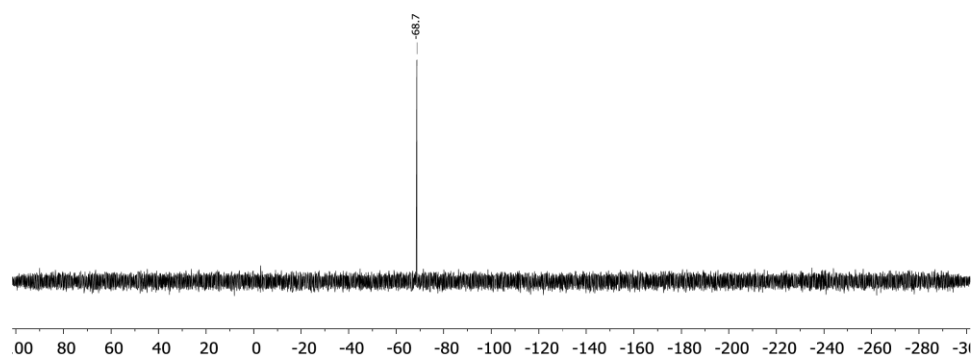


Fig. S19 $^{29}\text{Si}\{^1\text{H}\}$ NMR spectrum of $[\text{Mes-Si}(\text{IME}_4)_2]\text{Cl}$ (**3**) in pyridine- d_5 at 300 K.

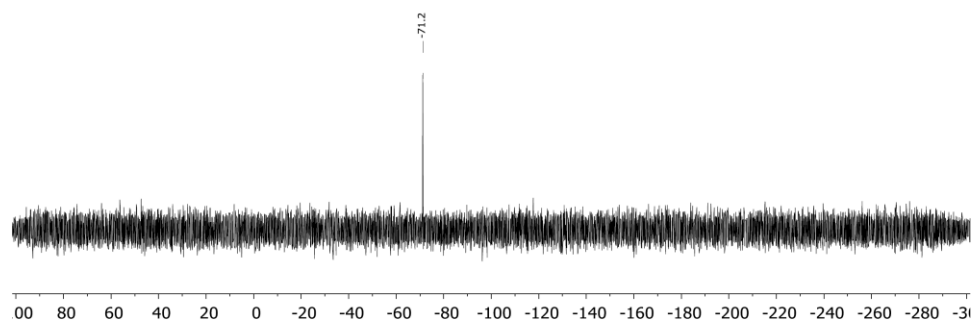


Fig. S20 $^{29}\text{Si}\{^1\text{H}\}$ NMR spectrum of $[\text{Mes-Si}(\text{IME}_4)_2]\text{Cl}$ (**3**) in CD_3CN at 300 K.

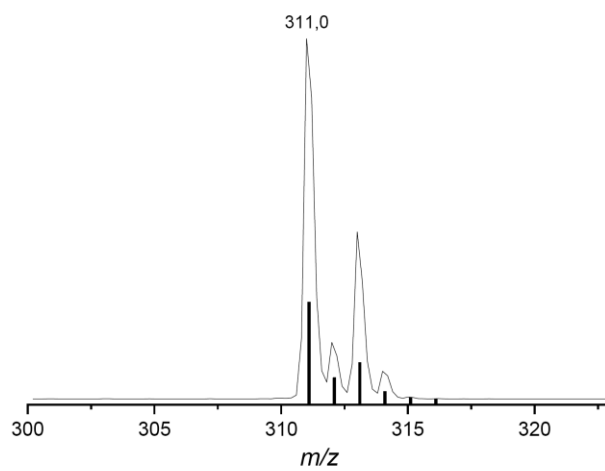
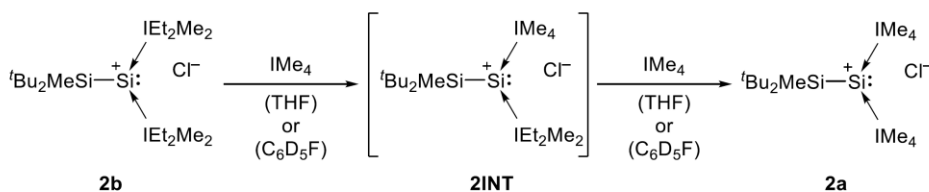


Fig. S21 ESI-MS spectrum (detailed view) of $[\text{Si}(\text{IME}_4)_2]\text{Cl}$ (**3** - Mes) (positive mode, 300 °C, -4000 V; line: measured spectrum; bars: simulated spectrum).

1.6 NHC exchange reaction of **2b** to **2a**

Procedure for the NHC exchange reaction:

[^tBu₂MeSi–Si(IEt₂Me₂)₂]Cl (**2b**) (50.0 mg, 95.2 μmol, 1.0 eq) was dissolved in 2 mL THF and a solution of IMe₄ (23.6 mg, 190.3 μmol, 2.0 eq) in 0.5 mL THF was added dropwise. Rapid formation of a yellow precipitate was observed, which was collected by filtration and washed with THF (2×2 mL) and hexane (1×1 mL) and after drying under vacuum product **2a** (36.6 mg, 78.0 μmol, 82%) was isolated as a yellow powder. Analytical data in CD₃CN are the same as previously mentioned (*cf.* section 1.4)

Procedure for the NHC exchange reaction (NMR scale):

[^tBu₂MeSi–Si(IEt₂Me₂)₂]Cl (**2b**) (20.0 mg, 38.1 μmol, 1.0 eq) and Si(TMS)₄ (12.2 mg, 38.1 μmol, 1.0 eq) were dissolved in 0.3 mL C₆D₅F, transferred to a J. Young NMR tube and then frozen at –78 °C. IMe₄ (9.5 mg, 76.1 μmol, 2.0 eq) was dissolved in 0.2 mL C₆D₅F and then slowly added to the frozen solution. The frozen mixture was then allowed to warm up slightly, then shaken strongly and several ¹H NMR measurements were taken immediately followed by ¹H NMR measurements in selected intervals (*cf.* Table S1). Si(TMS)₄ was used as internal standard.

Fig. S22 and Fig. S23 show the time resolved NMR data in C₆D₅F with 2.5 eq of IMe₄. The third set of signals belongs to the intermediate **2INT** [(^tBu₂MeSi–Si(IME₄)(IEt₂Me₂)]Cl. While we have been unable to isolate **2INT** in a clean fashion, in addition to the observations made in the ¹H NMR measurements, we were able to investigate the reaction mixture with ²⁹Si NMR (Fig. S24). As expected, the ²⁹Si NMR resonances of **2INT** (9.2 ppm (^tBu₂MeSiSi), –89.2 ppm (^tBu₂MeSiSi)) fall between that of **2b** (9.8 ppm (^tBu₂MeSiSi), –86.2 ppm (^tBu₂MeSiSi)) and **2a** (9.0 ppm (^tBu₂MeSiSi), –90.7 ppm (^tBu₂MeSiSi)).

To record a ²⁹Si NMR of the mixture in CD₃CN for better comparability, C₆H₅F was removed quickly from the reaction mixture after roughly 20 minutes of reaction time. The residue was dissolved in CD₃CN, the suspension was filtered and a ²⁹Si NMR was measured immediately.

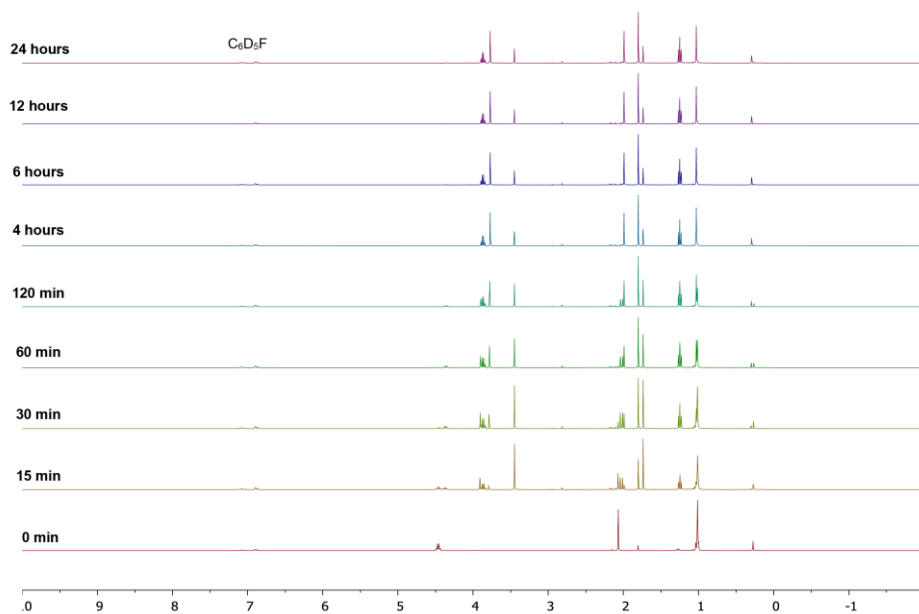


Fig. S22 Time resolved ^1H NMR spectra (overview) of the NHC exchange of **2b** with excess IMe_4 to **2a**.

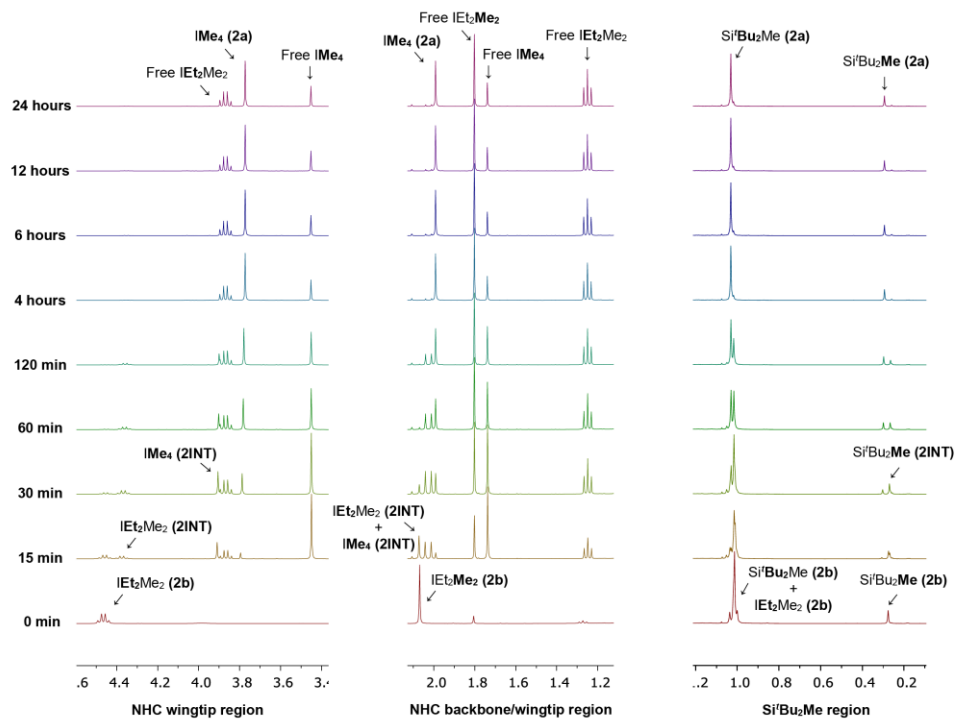


Fig. S23 Time resolved ^1H NMR spectra (detail view) of the NHC exchange of **2b** with excess IMe_4 to **2a**.

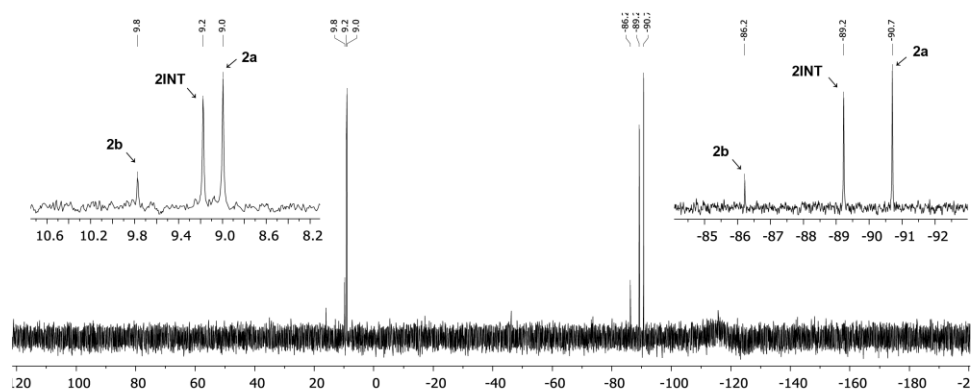


Fig. S24 $^{29}\text{Si}\{^1\text{H}\}$ NMR spectrum in CD_3CN of the reaction mixture of the NHC exchange of **2b** to **2a** via the intermediate **2INT**.

11. Appendix

Table S1 Relative [%] and absolute [mmol/L] molar concentrations of **2b**, **2INT** and **2a** by time as determined by ¹H NMR.

t [min]	Δt [min]	2b		2INT		2a	
		[%]	[mmol/L]	[%]	[mmol/L]	[%]	[mmol/L]
0	–	100.0	76.1	0.0	0.0	0.0	0.0
3	3	71.9	54.7	26.9	20.5	1.2	0.9
5	2	58.1	44.2	39.2	29.8	2.8	2.1
7	2	48.7	37.0	46.5	35.4	4.9	3.7
9	2	40.6	30.9	52.2	39.8	7.2	5.5
11	2	34.0	25.9	56.0	42.7	10.0	7.6
13	2	29.5	22.4	58.5	44.5	12.1	9.2
16	3	24.0	18.2	60.8	46.3	15.2	11.6
18	2	20.2	15.4	61.7	47.0	18.1	13.8
20	2	17.6	13.4	62.1	47.3	20.3	15.5
22	2	14.7	11.1	62.0	47.2	23.4	17.8
27	5	10.0	7.6	60.3	45.9	29.7	22.6
37	10	5.9	4.5	55.6	42.3	38.5	29.3
47	10	3.5	2.7	49.4	37.6	47.1	35.8
58	11	2.5	1.9	42.9	32.7	54.6	41.5
72	14	1.5	1.2	35.0	26.7	63.4	48.3
87	15	1.2	0.9	28.8	22.0	70.0	53.3
102	15	0.9	0.7	24.5	18.7	74.6	56.8
117	15	0.8	0.6	21.2	16.1	78.0	59.4
132	15	0.6	0.5	18.4	14.0	81.0	61.7
147	15	0.3	0.3	16.0	12.2	83.6	63.6
177	30	0.0	0.0	13.3	10.1	86.7	66.0
208	31	–	–	11.2	8.5	88.8	67.6
238	30	–	–	10.3	7.8	89.7	68.3
268	30	–	–	9.7	7.4	90.3	68.7
298	30	–	–	9.2	7.0	90.8	69.1
328	30	–	–	8.9	6.8	91.1	69.4
358	30	–	–	8.5	6.4	91.5	69.7
388	30	–	–	8.0	6.1	91.9	70.0
448	60	–	–	7.7	5.9	92.3	70.3
508	60	–	–	7.6	5.8	92.4	70.4
568	60	–	–	7.5	5.7	92.5	70.5
628	60	–	–	7.3	5.6	92.7	70.6

Plotting the relative molar concentrations vs. the reaction time (Fig. S25 (overview), Fig. S26 (**2b**), Fig. S27 (**2INT**), Fig. S29 (**2a**)) allows easy observation of the reaction progress.

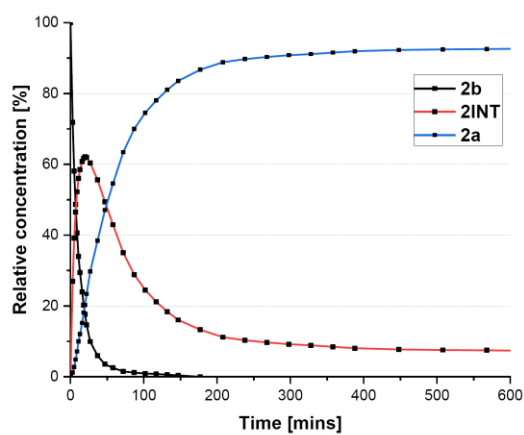


Fig. S25 Plot of the relative concentration of **2b**, **2INT** and **2a** vs. the time in the NHC exchange reaction of **2b** to **2a** via **2INT**.

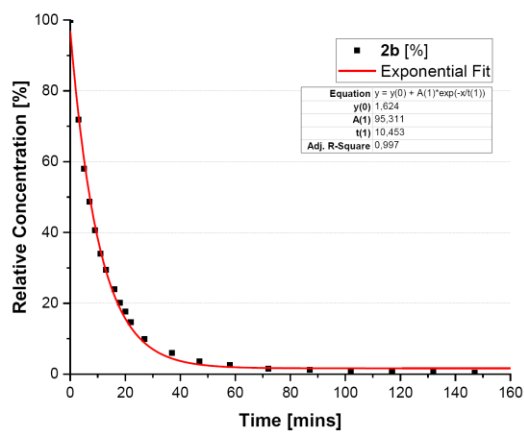


Fig. S26 Plot of the relative concentration of **2b** vs. time in the NHC exchange reaction of **2b** to **2a** via **2INT**.

The kinetics of a reaction can be deduced from a linear correlation between either $1/c_{2b}$ vs. the time (2^{nd} order kinetics) or $\ln(c_{2b})$ vs. the time (1^{st} order kinetics). However, the first NHC exchange from **2b** to **2INT** is heavily influenced by the concentration of IME_4 , which changes during the reaction because of the additional consumption of IME_4 from the second step of the reaction. Choosing a smaller time window to determine the reaction order does not allow reliable conclusions to be drawn from the data. We therefore looked at the second step of the reaction from **2INT** to **2a** in a time period where the overwhelming majority of **2b** had already been consumed (Fig. S27 and Fig. S28).

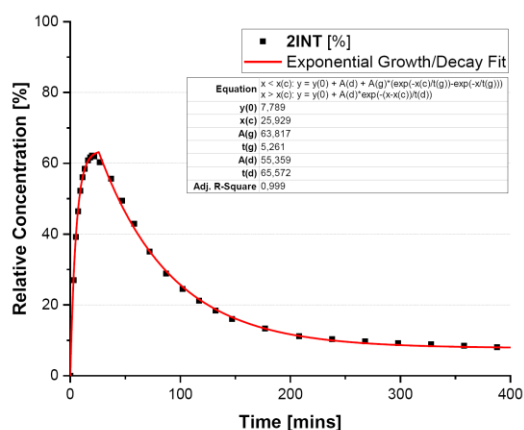


Fig. S27 Plot of the relative concentration of **2INT** vs. time in the NHC exchange reaction of **2b** to **2a** via **2INT**.

Plotting $1/c_{2\text{INT}}$ vs. the reaction time shows a linear correlation (Fig. S28, excluding the startup period where **2INT** is formed from **2b**), which indicates the reaction follows 2^{nd} order kinetics. The rate constant of the second exchange reaction is $0.558 \text{ L} \cdot \text{mol}^{-1} \cdot \text{min}^{-1}$. The first exchange reaction should exhibit the same reaction kinetics.

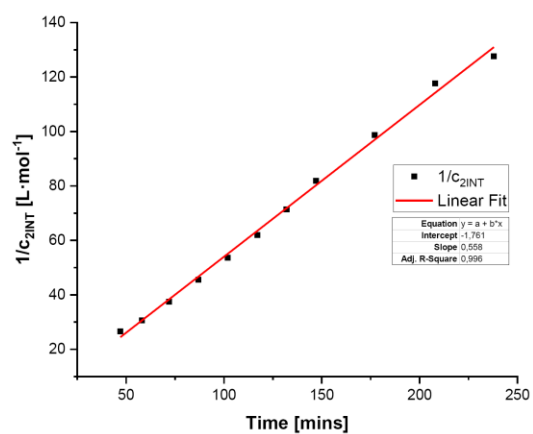


Fig. S28 Plot of $1/c_{2INT}$ vs. time in the NHC exchange reaction of **2b** to **2a** via **2INT**.

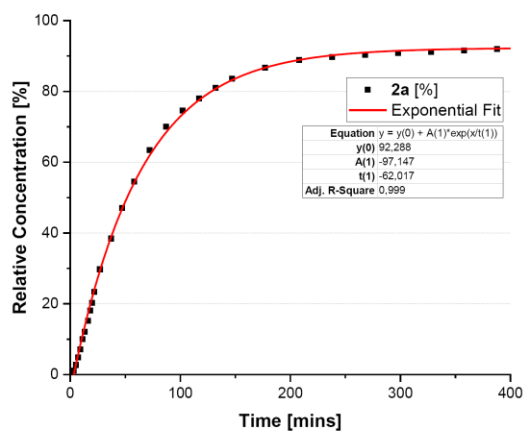


Fig. S29 Plot of the relative concentration of **2a** vs. the time in the NHC exchange reaction of **2b** to **2a** via **2INT**.

2. X-ray Crystallographic Data

General Information

The X-ray intensity data of **1** and **2a** were collected on an X-ray single crystal diffractometer equipped with a CMOS detector (Bruker Photon-100), a rotating anode (Bruker TXS) with MoK α radiation ($\lambda = 0.71073 \text{ \AA}$) and a Helios mirror optic by using the APEX III software package.^{S5} The measurements were performed on single crystals coated with the perfluorinated ether Fomblin® Y. The crystals were fixed on the top of a micro sampler, transferred to the diffractometer and frozen under a stream of cold nitrogen. A matrix scan was used to determine the initial lattice parameters. Reflections were merged and corrected for Lorenz and polarization effects, scan speed, and background using SAINT.^{S6} Absorption corrections, including odd and even ordered spherical harmonics were performed using SADABS.^{S6} Space group assignments were based upon systematic absences, E statistics, and successful refinement of the structures. Structures were solved by direct methods with the aid of successive difference Fourier maps, and were refined against all data using the APEX III software in conjunction with SHELXL-2014^{S7} and SHELXLE.^{S8} All H atoms were placed in calculated positions and refined using a riding model, with methylene and aromatic C–H distances of 0.99 and 0.95 \AA , respectively, and $U_{\text{iso}}(\text{H}) = 1.2 \cdot U_{\text{eq}}(\text{C})$. Full-matrix least-squares refinements were carried out by minimizing $\Delta w(F_o^2 - F_c^2)^2$ with SHELXL-97 weighting scheme.^{S9} Neutral atom scattering factors for all atoms and anomalous dispersion corrections for the non-hydrogen atoms were taken from International Tables for Crystallography.^{S10} The images of the crystal structures were generated by Mercury.^{S11} The CCDC numbers CCDC-1914471 (**1**) and CCDC-1914472 (**2a**) contain the supplementary crystallographic data for the structures. These data can be obtained free of charge from the Cambridge Crystallographic Data Centre *via* <https://www.ccdc.cam.ac.uk/structures/>.

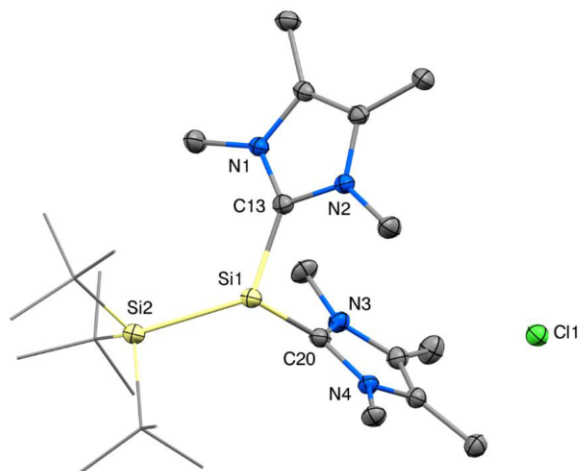
2.1 SC-XRD structure of [^tBu₃Si–Si(IME₄)₂]Cl (1)

Fig. S30 Ellipsoid plot (50% probability level) of the molecular structure of compound **1**. Hydrogen atoms and solvent molecules are omitted for clarity. Selected bond lengths [Å] and angles [°]: Si1–Si2 2.424(1), Si1–C13 1.937(2), Si1–C20 1.943(3), Si2–Si1–C13 122.1(1), Si2–Si1–C20 113.5(1), C13–Si1–C20 93.1(1).

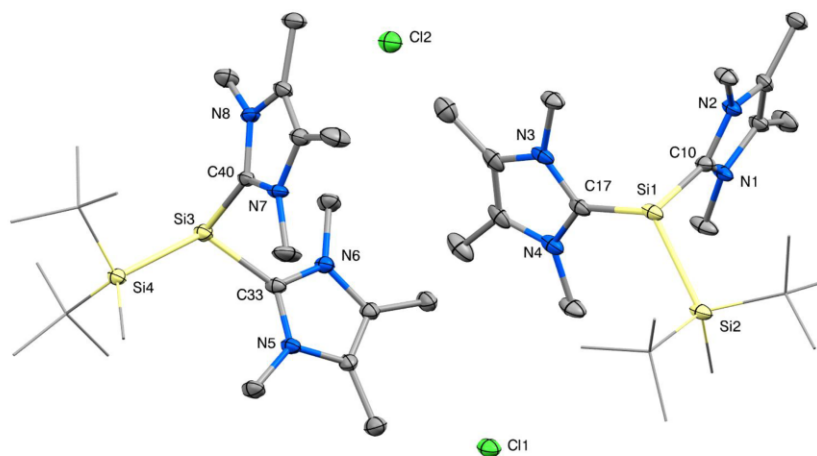
2.2 SC-XRD structure of [^tBu₂MeSi–Si(IME₄)₂]Cl (2a)

Fig. S31 Ellipsoid plot (50% probability level) of the molecular structure of compound **2a**. Hydrogen atoms and solvent molecules are omitted for clarity. Selected bond lengths [Å] and angles [°]: Si1–Si2 2.388(1), Si1–C10 1.943(2), Si1–C17 1.945(3), Si2–Si1–C10 107.4(1), Si2–Si1–C17 117.9(1), C10–Si1–C17 93.6(1), Si3–Si4 2.396(1), Si3–C33 1.940(3), Si3–C40 1.947(3), Si4–Si3–C33 117.5(1), Si4–Si3–C40 105.8(1), C33–Si3–C40 94.1(1).

11. Appendix

Table S2 Crystal data and structural refinement parameters for compounds **1** and **2a**.

Compound #	1	2a
Chemical formula	C ₃₀ H ₅₇ Cl ₁ N ₆ Si ₂	C ₅₂ H ₈₄ Cl ₂ F ₂ N ₆ Si ₄
Formula weight	593.45	1052.62
Temperature	100(2) K	100(2) K
Wavelength	0.71073 Å	0.71073 Å
Crystal size	0.178 x 0.243 x 0.472 mm	0.199 x 0.226 x 0.272 mm
Crystal habit	clear orange fragment	clear yellow fragment
Crystal system	trigonal	triclinic
Space group	R-3	P-1
Unit cell dimensions	a = 45.605(5) Å, α = 90° b = 45.605(5) Å, β = 90° c = 9.2968(11) Å, γ = 120°	a = 11.0482(19) Å, α = 66.805(5)° b = 17.171(3) Å, β = 74.978(5)° c = 21.066(4) Å, γ = 88.261(6)°
Volume	16745(4) Å ³	3536.2(11) Å ³
Z	6	4
Density (calculated)	1.059 g/cm ³	0.989 g/cm ³
Absorption coefficient	0.193 mm ⁻¹	0.199 mm ⁻¹
F(000)	5832	1140
Diffractometer	Bruker D8 Venture	Bruker D8 Venture
Radiation source	TXS rotating anode, Mo	TXS rotating anode, Mo
Theta range for data collection	2.25 to 25.35° -54<=h<=54	2.22 to 25.68° -13<=h<=13
Index ranges	-54<=k<=54 -11<=l<=11	-20<=k<=20 -25<=l<=25
Reflections collected	226492	63614
Independent reflections	6800 [R(int) = 0.0716]	13410 [R(int) = 0.0838]
Coverage of independent reflections	99.9%	99.9%
Absorption correction	Multi-Scan	Multi-Scan
Max. and min. transmission	0.9660 and 0.9140	0.9610 and 0.9470
Refinement method	Full-matrix least-squares on F ²	Full-matrix least-squares on F ²
Refinement program	SHELXL-2016/6 (Sheldrick, 2016)	SHELXL-2016/6 (Sheldrick, 2016)
Function minimized	Σ w(F _o ² - F _c ²) ²	Σ w(F _o ² - F _c ²) ²
Data / restraints / parameters	6800 / 0 / 371	13410 / 132 / 716
Goodness-of-fit on F ²	1.104	1.024
Δ/σ _{max}	0.002	0.001
Final R indices	5960 data; I>2σ(I) R1 = 0.0432, wR2 = 0.1240 all data R1 = 0.0512, wR2 = 0.1296	9895 data; I>2σ(I) R1 = 0.0521, wR2 = 0.1114 all data R1 = 0.0802, wR2 = 0.1207
Weighting scheme	w=1/[σ ² (F _o ²)+(0.0634P) ² +45.3570P] where P=(F _o ² +2F _c ²)/3	w=1/[σ ² (F _o ²)+(0.0378P) ² +3.4602P] where P=(F _o ² +2F _c ²)/3
Largest diff. peak and hole	0.857 and -0.262 eÅ ⁻³	0.728 and -0.336 eÅ ⁻³
R.M.S. deviation from mean	0.061 eÅ ⁻³	0.056 eÅ ⁻³

3. References

- S1 N. Kuhn and T. Kratz, *Synthesis*, 1993, **1993**, 561-562.
- S2 A. Hübner, T. Bernert, I. Sängler, E. Alig, M. Bolte, L. Fink, M. Wagner and H.-W. Lerner, *Dalton Trans.*, 2010, **39**, 7528-7533.
- S3 N. Wiberg, W. Niedermayer, H. Nöth, J. Knizek, W. Ponikwar and K. Polborn, *Z. Naturforsch. B.*, 2000, **55**, 389.
- S4 V. Y. Lee, K. Takanashi, R. Kato, T. Matsuno, M. Ichinohe and A. Sekiguchi, *J. Organomet. Chem.*, 2007, **692**, 2800-2810.
- S5 *APEX suite of crystallographic software*, APEX 3 version 2015.5-2; Bruker AXS Inc.: Madison, Wisconsin, USA, 2015.
- S6 *SAINT*, Version 7.56a and *SADABS* Version 2008/1; Bruker AXS Inc.: Madison, Wisconsin, USA, 2008.
- S7 G. M. Sheldrick, *SHELXL-2014*, University of Göttingen, Göttingen, Germany, 2014.
- S8 C. B. Hübschle, G. M. Sheldrick and B. Dittrich, *J. Appl. Cryst.*, 2011, **44**, 1281-1284.
- S9 G. M. Sheldrick, *SHELXL-97*, University of Göttingen, Göttingen, Germany, 1998.
- S10 A. J. C. Wilson, *International Tables for Crystallography*, Vol. C, Tables 6.1.1.4 (pp. 500-502), 4.2.6.8 (pp. 219-222), and 4.2.4.2 (pp. 193-199); Kluwer Academic Publishers: Dordrecht, The Netherlands, 1992.
- S11 C. F. Macrae, I. J. Bruno, J. A. Chisholm, P. R. Edgington, P. McCabe, E. Pidcock, L. Rodriguez-Monge, R. Taylor, J. van de Streek and P. A. Wood, *J. Appl. Cryst.*, 2008, **41**, 466-470.

11.2 Supporting Information Chapter 5

Electronic Supplementary Material (ESI) for Chemical Communications.
This journal is © The Royal Society of Chemistry 2018

Supporting Information

Coinage-metal Complexes of NHC-stabilized Silyliumylidene Ions

*Philipp Frisch and Shigeyoshi Inoue**

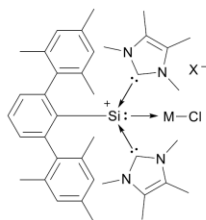
Table of Contents

1. Experimental Section.....	S2
1.1. General Methods and Instrumentation.....	S2
1.2 Synthesis of [<i>m</i> -Terphenyl-Si(IME ₄) ₂ -MCl]X (2a , 3a , 4a).....	S3
1.3 Synthesis of [Tipp-Si(IME ₄) ₂ -MCl]X (2b , 3b , 4b).....	S13
1.4 Decomposition of 4b	S19
2. X-ray Crystallographic Data.....	S23
2.1 SC-XRD structure of [<i>m</i> -Ter-Si(IME ₄) ₂ -CuCl]Cl (2a).....	S24
2.2 SC-XRD structure of [<i>m</i> -Ter-Si(IME ₄) ₂ -AgCl]OTf (3a).....	S24
2.3 SC-XRD structure of [<i>m</i> -Ter-Si(IME ₄) ₂ -AuCl]Cl (4a).....	S25
2.4 SC-XRD structure of [[Tipp-Si(IME ₄) ₂ -AgCl]OTf] ₂ (3b).....	S25
2.5 SC-XRD structure of [(IME ₄) ₂ Au]Cl (5).....	S26
3. References.....	S28

1. Experimental Section

1.1. General Methods and Instrumentation

All reactions were carried out under exclusion of water and oxygen in an atmosphere of argon 4.6 ($\geq 99.996\%$) using standard Schlenk techniques or in a Labstar glovebox from *MBraun* with H_2O and O_2 levels below 0.5 ppm. Glassware was heat dried under vacuum prior to use. Acetonitrile and Acetonitrile- d_3 were refluxed over CaH_2 , distilled under argon, deoxygenated by three freeze-pump-thaw cycles and stored over 3 Å molecular sieve in a glovebox. Diethylether was refluxed over sodium/benzophenone, distilled under argon, deoxygenated by three freeze-pump-thaw cycles and stored over 3 Å molecular sieve in a glovebox. All NMR samples were prepared under argon in *J. Young* PTFE valve NMR tubes. NMR spectra at ambient temperature (300 K) were recorded on a *Bruker* AV400US or DRX400 (^1H : 400.13 MHz, ^{13}C : 100.62 MHz, ^{29}Si : 79.49 MHz), AVHD300 (^1H : 300.13 MHz) or AV500C (^1H : 500.36 MHz, ^{13}C : 125.83 MHz, ^{29}Si : 99.41 MHz). Variable temperature NMR spectra were recorded on a *Bruker* DRX400 (^1H : 400.13 MHz, ^{13}C : 100.62 MHz, ^{29}Si : 79.49 MHz) spectrometer. The ^1H , ^{13}C and ^{29}Si NMR spectroscopic chemical shifts δ are reported in ppm relative to tetramethylsilane. ^1H and ^{13}C NMR spectra are calibrated against the residual proton and natural abundance carbon resonances of the respective deuterated solvent as internal standard (CD_3CN : $\delta(^1\text{H}) = 1.94$ ppm and $\delta(^{13}\text{C}) = 118.3$ ppm). ^{29}Si NMR spectra are referenced to the resonance of tetramethylsilane ($\delta = 0$ ppm) as external standard. The following abbreviations are used to describe signal multiplicities: s = singlet, d = doublet, t = triplet, sept = septet, bs = broad signal, m = multiplet. Quantitative elemental analyses (EA) were carried out using a *HEKAtech* EURO EA instrument equipped with a CHNS combustion analyzer at the Laboratory for Microanalysis at the TUM Catalysis Research Center. Melting Points (M.P.) were determined in sealed glass capillaries under inert gas by a *Büchi* M-565 melting point apparatus. ESI-MS spectra were recorded on a *Bruker* HCT Instrument with a dry gas temperature of 300 °C and an injection speed of 240 μLs^{-1} . Samples were prepared in a glovebox and spectra were visualized using OriginPro 2018. Unless otherwise stated, all commercially available chemicals were purchased from abcr or Sigma-Aldrich and used without further purification. The compounds [*m*-Terphenyl-Si(IME $_4$) $_2$]Cl (**1a**)^{S1} and [Tipp-Si(IME $_4$) $_2$]Cl (**1b**)^{S1} were prepared as described in the literature.

1.2 Synthesis of [*m*-Terphenyl-Si(IME₄)₂-MCl]X (**2a**, **3a**, **4a**)

	M	X
2a	Cu	Cl
3a	Ag	OTf
4a	Au	Cl

General procedure:

[*m*-Terphenyl-Si(IME₄)₂]Cl (**1a**) (100.0 mg, 159.9 μmol, 1.0 eq) was dissolved in 3 mL acetonitrile and the coinage metal precursor (CuCl (**2a**)/AgOTf (**3a**)/(SMe₂)AuCl (**4a**), 159.9 μmmol, 1.0 eq) was added in one portion at room temperature while stirring (under exclusion of light for **3a**). After stirring for 5 minutes the solution was filtered, concentrated under vacuum until incipient precipitation and Et₂O (4-5 mL) was added. After storing the solution at -40 °C for 48 hours the microcrystalline

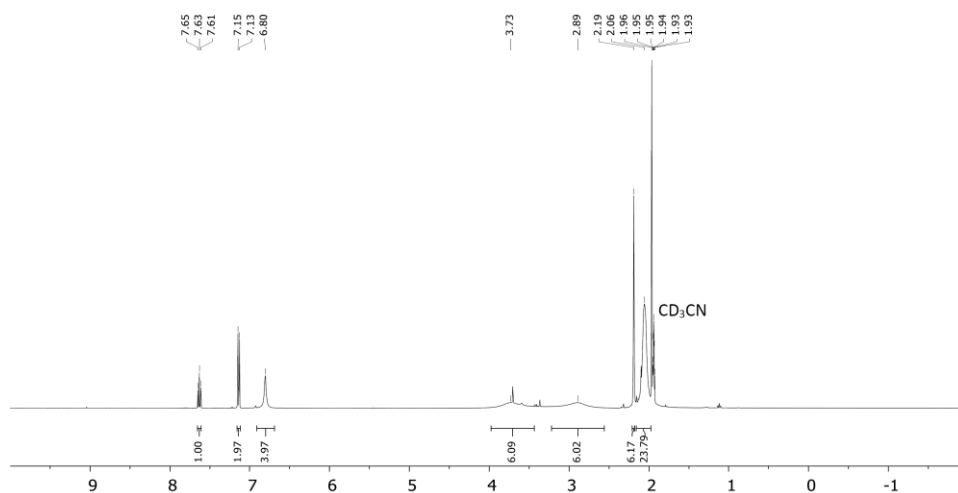
precipitate was collected by filtration, washed with Et₂O (2 × 2 mL) and after drying under vacuum the products **2a**, **3a** and **4a** were obtained as colorless air-, (light-) and moisture-sensitive solids. The compounds are stable in the solid state and in acetonitrile solution at room temperature but decompose slowly upon heating to 90 °C in acetonitrile.

[*m*-Terphenyl-Si(IME₄)₂-CuCl]Cl (2a**)**

Yield = 92%.

Single crystals suitable for XRD analysis were obtained by slow diffusion of Et₂O into a concentrated acetonitrile solution of **2a** at -40 °C.**¹H NMR (400 MHz, CD₃CN, 300 K):** δ [ppm] = 7.63 (t, *J* = 7.6 Hz, 1H, C_{ar}H_{para}), 7.14 (d, *J* = 7.6 Hz, 2H, C_{ar}H_{meta}), 6.80 (bs, 4H, C_{mes}H), 3.73 (bs, 6H, N_{NHC}CH₃), 2.89 (bs, 6H, N_{NHC}CH₃), 2.19 (s, 6H, C_{mes}CH_{3,para}), 2.06 (bs, 24H, C_{mes}CH_{3,ortho} + C_{NHC}CH₃).**¹³C NMR (126 MHz, CD₃CN, 300 K):** δ [ppm] = 150.7, 150.4, 140.5, 138.1, 135.7, 134.7, 131.7, 131.7, 130.4, 129.8, 129.2, 36.3, 22.8, 21.4, 21.1, 9.2.**²⁹Si NMR (99 MHz, CD₃CN, 300 K):** δ [ppm] = -46.6.**EA:** C₃₈H₄₉CuCl₂N₄Si calculated: C (63.01), H (6.82), N (7.73).

measured: C (62.85), H (7.13), N (7.49).

ESI-MS: calculated: 687.27 (C₃₈H₄₉ClCuN₄Si⁺).measured: 687.2 (**2a** - Cl⁻).**M.P.:** 125-126 °C (decomposition, color change to orange).**Fig. S1** ¹H NMR spectrum of [*m*-Terphenyl-Si(IME₄)₂-CuCl]Cl (**2a**) in CD₃CN at 300 K.

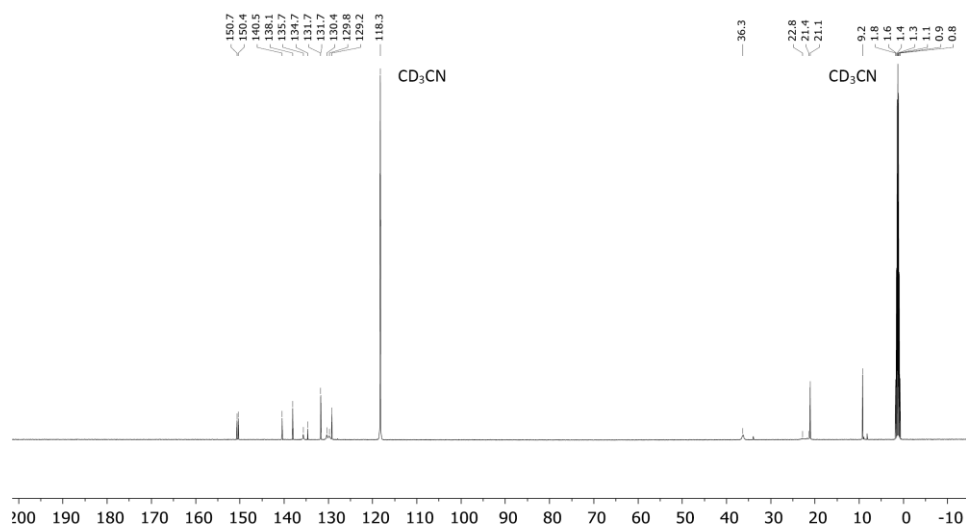


Fig. S2 ^{13}C NMR spectrum of $[m\text{-Terphenyl-Si}(\text{IMe}_4)_2\text{-CuCl}]\text{Cl}$ (**2a**) in CD_3CN at 300 K.

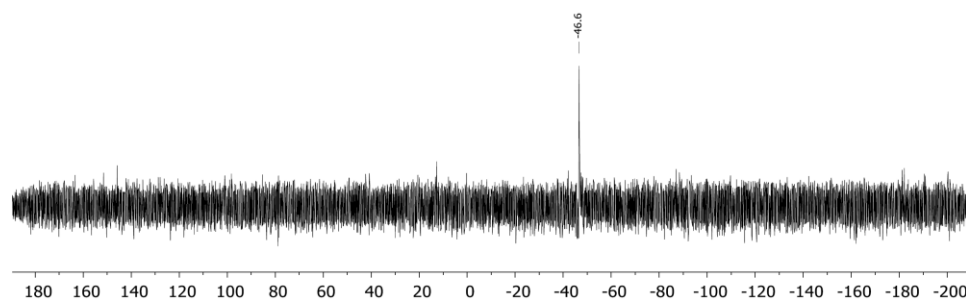


Fig. S3 ^{29}Si NMR spectrum of $[m\text{-Terphenyl-Si}(\text{IMe}_4)_2\text{-CuCl}]\text{Cl}$ (**2a**) in CD_3CN at 300 K.

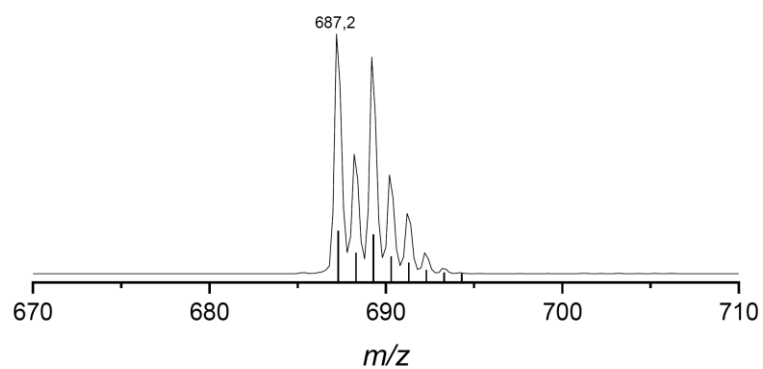


Fig. S4 ESI-MS spectrum (detail view) of **2a** (positive mode, 300 °C, -4000 V; line: measured spectrum; bars: simulated spectrum).

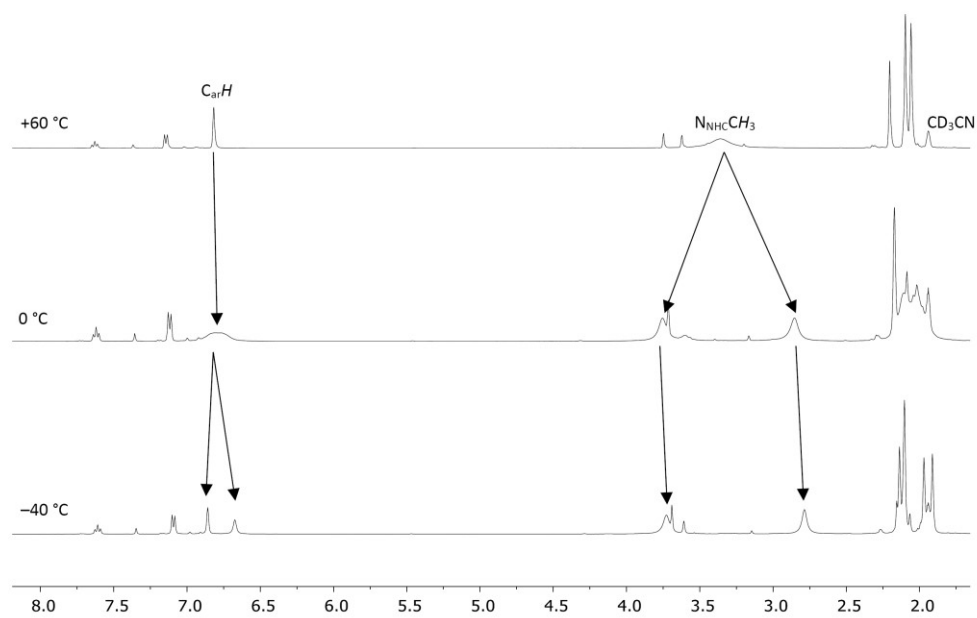


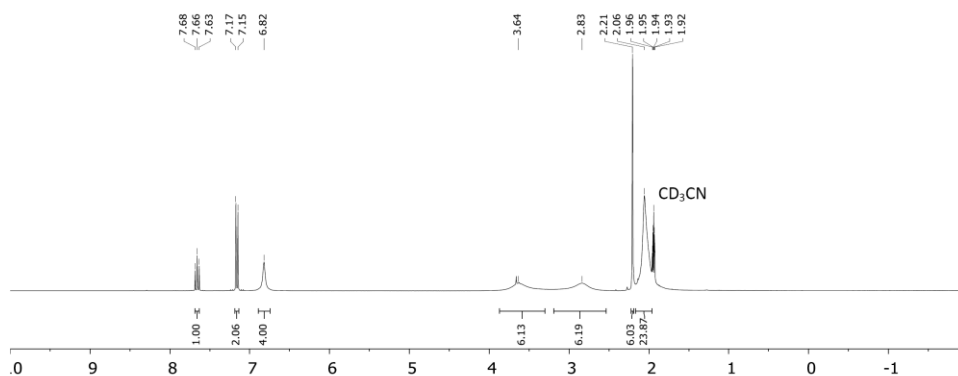
Fig. S5 Variable temperature NMR spectra of **2a** in CD₃CN (bottom: -40 °C, middle: 0 °C, top: +60 °C).

[*m*-Terphenyl-Si(IME₄)₂-AgCl]OTf (3a**)**

Yield = 86%.

Single crystals suitable for XRD analysis were obtained by slow diffusion of Et₂O into a concentrated acetonitrile solution of **3a** at -40 °C.**¹H NMR** (300 MHz, CD₃CN, 300 K): δ [ppm] = 7.66 (t, *J* = 7.6 Hz, 1H, C_{ar}H_{para}), 7.16 (d, *J* = 7.6 Hz, 2H, C_{ar}H_{meta}), 6.82 (bs, 4H, C_{mes}H), 3.64 (bs, 6H, N_{NHC}CH₃), 2.83 (bs, 6H, N_{NHC}CH₃), 2.21 (s, 6H, C_{mes}CH_{3,para}), 2.06 (bs, 24H, C_{mes}CH_{3,ortho} + C_{NHC}CH₃).**¹³C NMR** (126 MHz, CD₃CN, 300 K): δ [ppm] = 151.3, 150.4, 150.3, 140.4, 138.6, 136.1, 133.6, 133.5, 132.2, 132.1, 130.6, 129.6, 36.5, 35.9, 22.8, 21.5, 21.2, 9.2.**²⁹Si NMR** (99 MHz, CD₃CN, 300 K): δ [ppm] = -44.1 (d, ¹*J*_{SiAg} = 352.6 Hz), -44.1 (d, ¹*J*_{SiAg} = 408.1 Hz).**EA:** C₃₉H₄₉AgClF₃N₄O₃SSi calculated: C (53.09), H (5.60), N (6.35), S (3.63).

measured: C (53.41), H (5.70), N (6.40), S (3.41).

ESI-MS: calculated: 731.25 (C₃₈H₄₉ClAgN₄Si⁺).measured: 731.2 (**3a** - Cl⁻).**M.P.:** 170–171 °C (decomposition, color change to black).**Fig. S6** ¹H NMR spectrum of [*m*-Terphenyl-Si(IME₄)₂-AgCl]OTf (**3a**) in CD₃CN at 300 K.

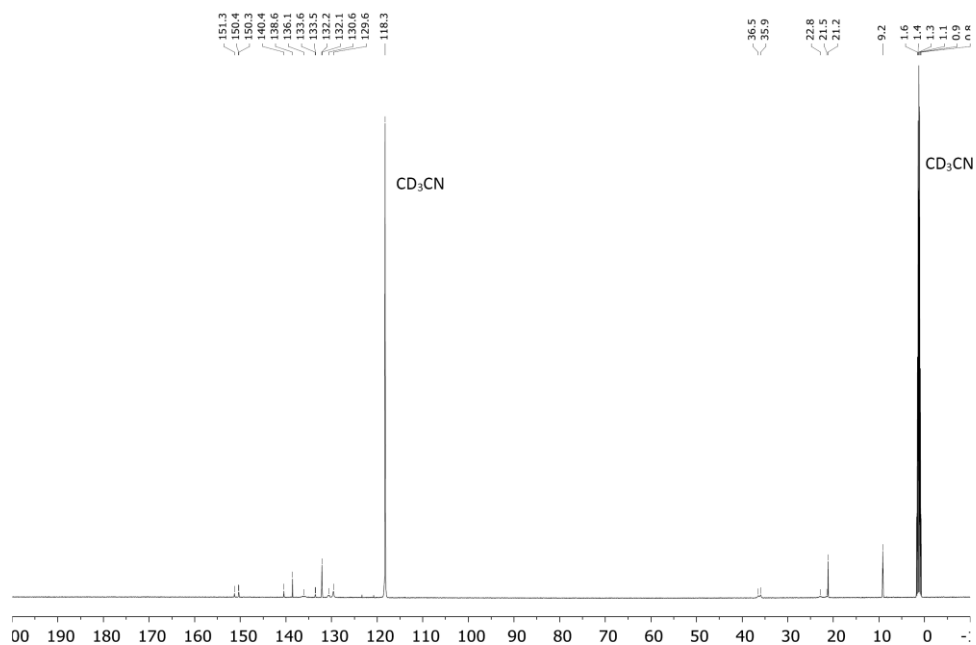


Fig. S7 ^{13}C NMR spectrum of [m-Terphenyl-Si(Ime₄)₂-AgCl]OTf (**3a**) in CD_3CN at 300 K.

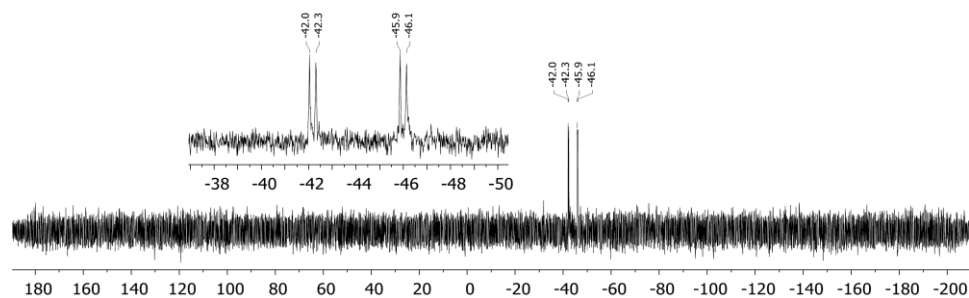


Fig. S8 ^{29}Si NMR spectrum of [m-Terphenyl-Si(Ime₄)₂-AgCl]OTf (**3a**) in CD_3CN at 300 K.

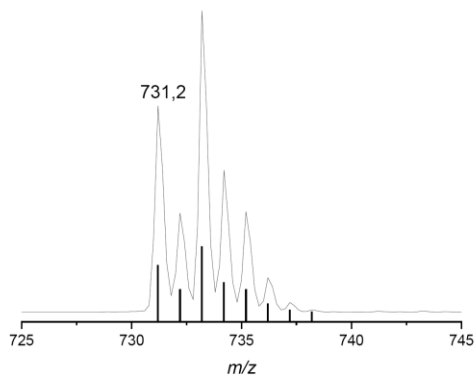


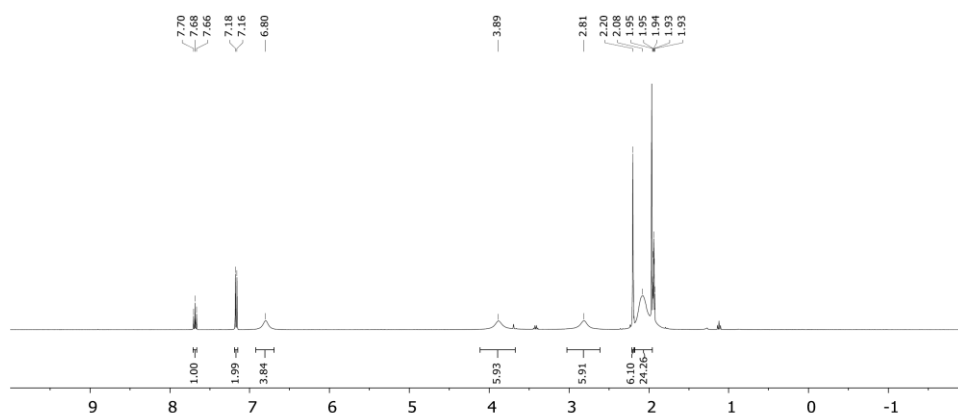
Fig. S9 ESI-MS spectrum (detail view) of **3a** (positive mode, 300 °C, -4000 V; line: measured spectrum; bars: simulated spectrum).

[*m*-Terphenyl-Si(IME₄)₂-AuCl]Cl (4a**)**

Yield = 94%.

Single crystals suitable for XRD analysis were obtained by slow diffusion of Et₂O into a concentrated acetonitrile solution of **4a** at -40 °C.**¹H NMR (400 MHz, CD₃CN, 300 K):** δ [ppm] = 7.68 (t, *J* = 7.6 Hz, 1H, C_{ar}H_{para}), 7.17 (d, *J* = 7.6 Hz, 2H, C_{ar}H_{meta}), 6.80 (s, 4H, C_{mes}H), 3.89 (bs, 6H, N_{NHC}CH₃), 2.81 (bs, 6H, N_{NHC}CH₃), 2.20 (s, 6H, C_{mes}CH_{3,para}), 2.08 (bs, 24H, C_{mes}CH_{3,ortho} + C_{NHC}CH₃).**¹³C NMR (126 MHz, CD₃CN, 300 K):** δ [ppm] = 151.5, 148.6, 140.7, 138.4, 132.7, 132.6, 131.1, 129.5, 129.2, 37.4, 36.1, 23.0, 21.8, 21.2, 17.9, 9.3.**²⁹Si NMR (79 MHz, CD₃CN, 300 K):** δ [ppm] = -34.6.**EA:** C₃₈H₄₉Cl₂AuN₄Si calculated: C (53.21), H (5.76), N (6.53).

measured: C (52.99), H (5.86), N (6.42).

ESI-MS: calculated: 821.31 (C₃₈H₄₉ClAuN₄Si⁺).measured: 821.3 (**4a** - Cl⁻).**M.P.:** 234–235 °C (decomposition, color change to dark red).**Fig. S10** ¹H NMR spectrum of [*m*-Terphenyl-Si(IME₄)₂-AuCl]Cl (**4a**) in CD₃CN at 300 K.

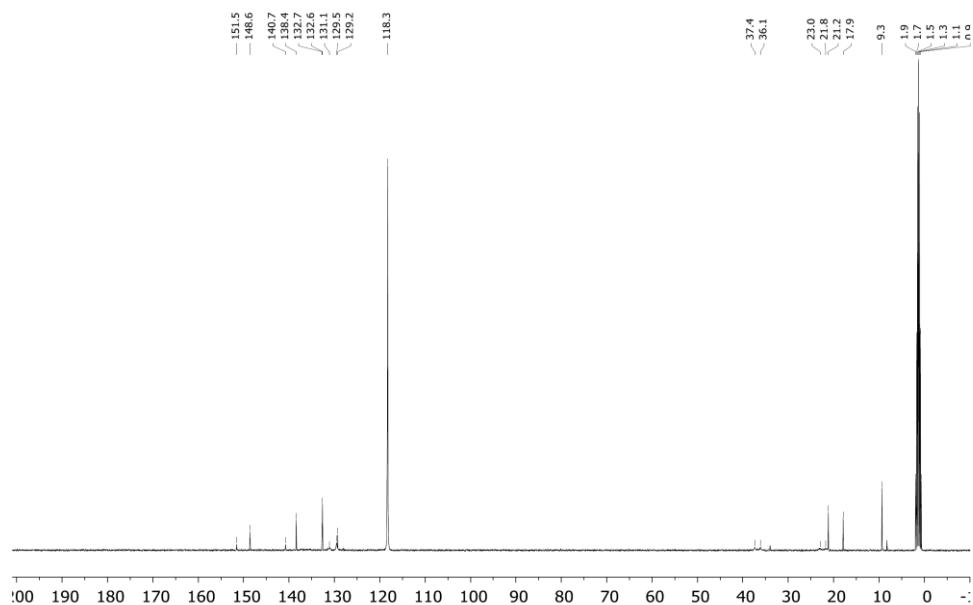


Fig. S11 ^{13}C NMR spectrum of [m-Terphenyl-Si(Ime₄)₂-AuCl]Cl (**4a**) in CD_3CN at 300 K.

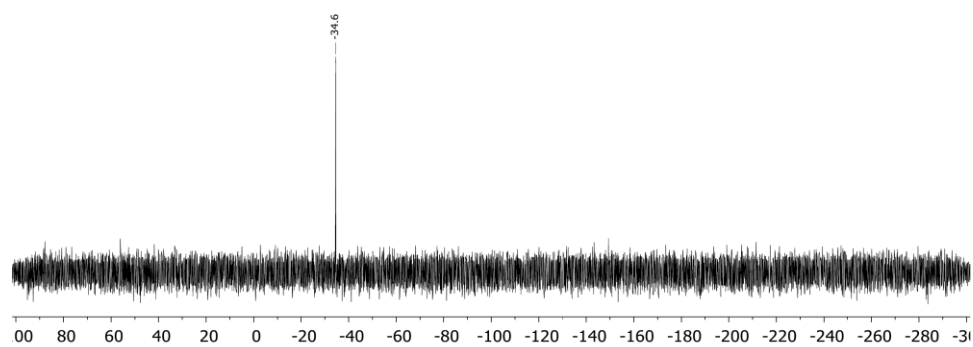


Fig. S12 ^{29}Si NMR spectrum of [m-Terphenyl-Si(Ime₄)₂-AuCl]Cl (**4a**) in CD_3CN at 300 K.

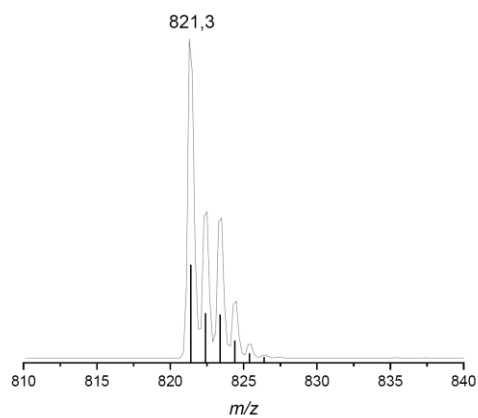
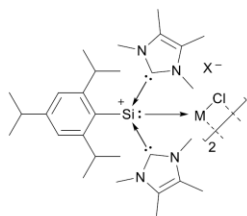


Fig. S13 ESI-MS spectrum (detail view) of **4a** (positive mode, 300 °C, -4500 V; line: measured spectrum; bars: simulated spectrum).

1.3 Synthesis of [Tipp-Si(IME₄)₂-MCl]X (**2b**, **3b**, **4b**)

	M	X
2b	Cu	Cl
3b	Ag	OTf
4b	Au	Cl

General procedure:

[Tipp-Si(IME₄)₂]Cl (**1b**) (50.0 mg, 97.1 μmol, 1.0 eq) was dissolved in 1.5 mL acetonitrile and cooled to -40 °C. The coinage metal precursor (MX = CuCl (**2b**)/AgOTf (**3b**)/(SMe₂)AuCl (**4b**), 97.1 μmol, 1.0 eq) was added in one portion while stirring (under exclusion of light for **3b**).

The solution was quickly filtered and Et₂O (10 mL) was added to precipitate a colorless solid. The solid was collected by filtration, washed with Et₂O (2 × 2 mL) and after drying under vacuum the

products **2b** and **3b** were obtained as colorless air-, (light-), moisture-sensitive solids. The complexes are stable in the solid state but decompose rapidly in solution. Due to the rapid decomposition, no satisfactory analytical data could be obtained for complex **4b**.

[Tipp-Si(IME₄)₂-CuCl]Cl (2b)

Yield = 71%.

¹H NMR (500 MHz, CD₃CN, 300 K): δ [ppm] = 7.12 (s, 2H, C_{ar}H), 3.60 (hept, *J* = 6.8 Hz, 2H, C_{ortho}H(CH₃)₂), 3.55 (s, 12H, N_{NHC}CH₃), 2.88 (hept, *J* = 6.9 Hz, 1H, C_{para}H(CH₃)₂), 2.20 (s, 12H, C_{NHC}CH₃), 1.22 (d, *J* = 6.9 Hz, 6H, C_{para}H(CH₃)₂), 1.02 (d, *J* = 6.8 Hz, 12H, C_{ortho}H(CH₃)₂).

¹³C NMR (126 MHz, CD₃CN, 300 K): δ [ppm] = 157.4, 153.6, 152.2, 129.9, 129.2, 123.3, 36.4, 35.0, 34.8, 25.0, 24.0, 9.2.

²⁹Si NMR (99 MHz, CD₃CN, 300 K): δ [ppm] = -48.8.

EA: C₂₉H₄₇Cl₂CuN₄Si calculated: C (56.71), H (7.71), N (9.12).

measured: C (56.89), H (7.92), N (9.01).

M.P.: 132-134 °C (decomposition, color change to yellow-orange).

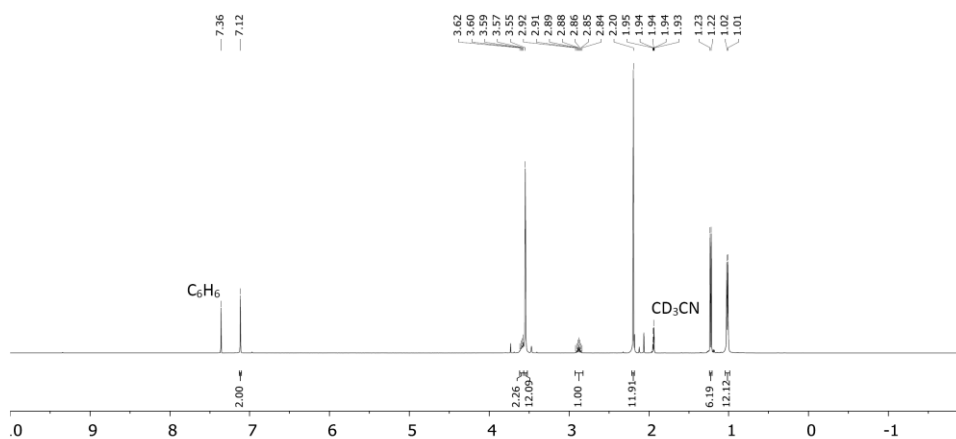


Fig. S14 ¹H NMR spectrum of [Tipp-Si(IME₄)₂-CuCl]Cl (**2b**) in CD₃CN at 300 K. Residual C₆H₆ (7.36 ppm) stems from the crystallization of starting material **1b**. NMR spectra were recorded immediately after mixing the starting materials due to rapid decomposition.

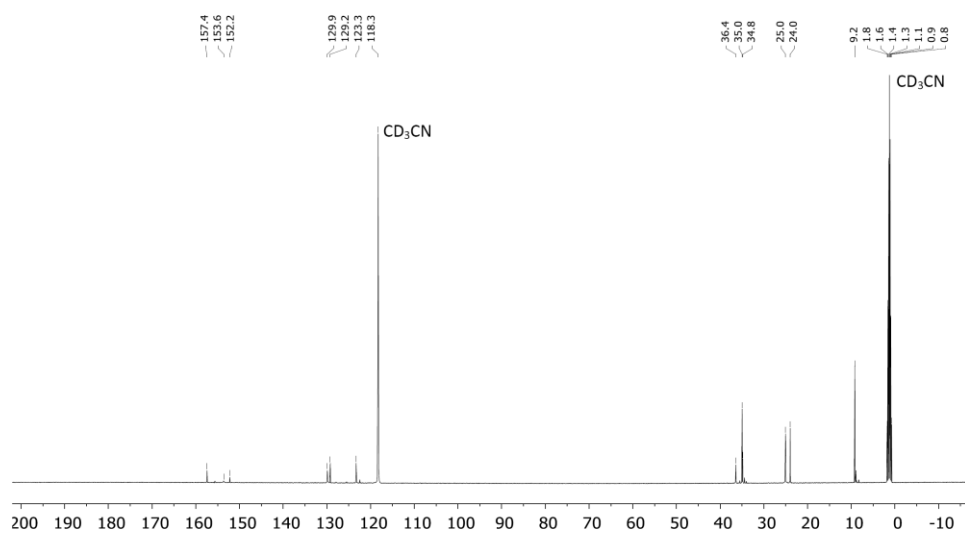


Fig. S15 ^{13}C NMR spectrum of $[\text{Tipp-Si}(\text{IME}_4)_2\text{-CuCl}]\text{Cl}$ (**2b**) in CD_3CN at 300 K.

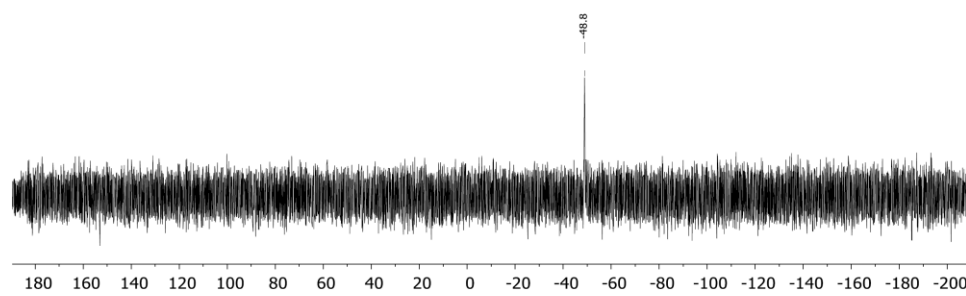


Fig. S16 ^{29}Si NMR spectrum of $[\text{Tipp-Si}(\text{IME}_4)_2\text{-CuCl}]\text{Cl}$ (**2b**) in CD_3CN at 300 K.

[Tipp-Si(Ime₄)₂-AgCl]OTf (3b)

Single crystals suitable for XRD analysis were obtained by slow diffusion of Et₂O into a concentrated solution of **3b** in acetonitrile:toluene (2:1) at -40 °C.

Yield = 89%.

¹H NMR (500 MHz, CD₃CN, 300 K): δ [ppm] = 7.16 (s, 2H, C_{ar}H), 3.49 (s, 12H, N_{NHC}CH₃), 3.29 (hept, *J* = 6.8 Hz, 2H, C_{ortho}H(CH₃)₂), 2.90 (hept, *J* = 6.9 Hz, 1H, C_{para}H(CH₃)₂), 2.21 (s, 12H, C_{NHC}CH₃), 1.23 (d, *J* = 6.9 Hz, 6H, C_{para}H(CH₃)₂), 1.05 (d, *J* = 6.7 Hz, 12H, C_{ortho}H(CH₃)₂).

¹³C NMR (126 MHz, CD₃CN, 300 K): δ [ppm] = 157.1, 153.4, 150.4, 131.0, 127.1, 123.9, 122.0 (q, ¹*J*_{CF} = 321.0 Hz) 36.7, 34.8, 35.1, 24.8, 23.9, 9.1.

²⁹Si NMR (99 MHz, CD₃CN, 300 K): δ [ppm] = -46.6 (d, ¹*J*_{SiAg} = 355.8 Hz), -46.6 (d, ¹*J*_{SiAg} = 410.1 Hz).

EA: C₃₀H₄₇AgClF₃N₄O₃SSi calculated: C (46.66), H (6.14), N (7.26), S (4.15).

measured: C (46.29), H (5.99), N (7.38), S (4.04).

M.P.: 190-191 °C (decomposition, color change to black).

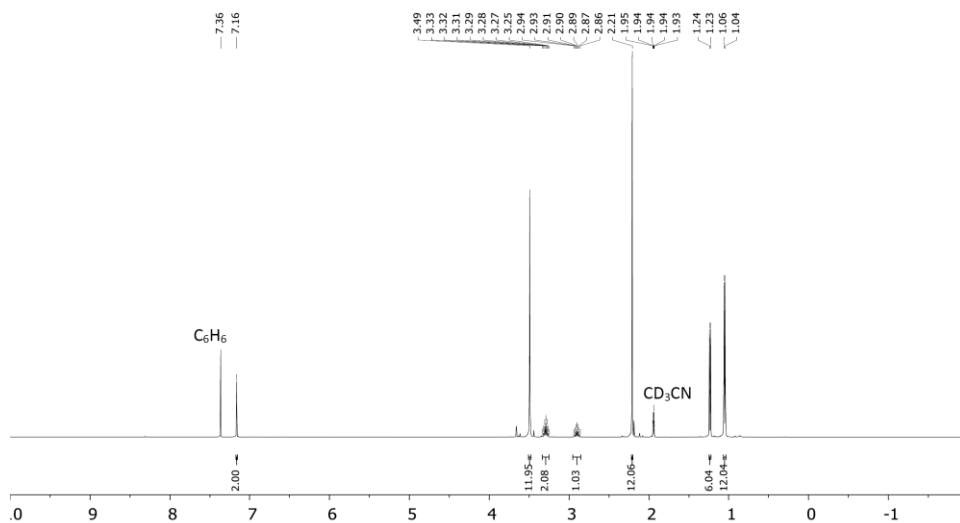


Fig. S17 ¹H NMR spectrum of [Tipp-Si(Ime₄)₂-AgCl]OTf (**3b**) in CD₃CN at 300 K. Residual C₆H₆ (7.36 ppm) stems from the crystallization of starting material **1b**. NMR spectra were recorded immediately after mixing the starting materials due to rapid decomposition.

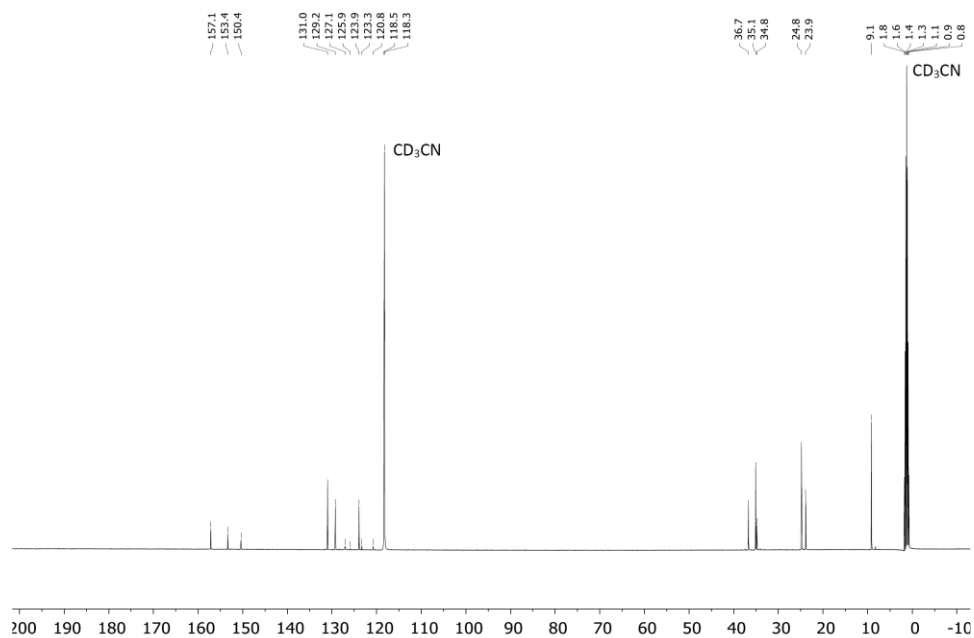


Fig. S18 ^{13}C NMR spectrum of $[\text{Tipp-Si}(\text{Ime}_4)_2\text{-AgCl}]\text{OTf}$ (**3b**) in CD_3CN at 300 K.

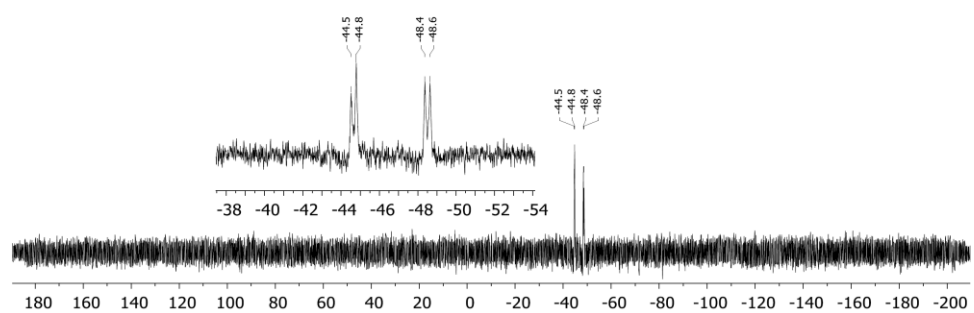


Fig. S19 ^{29}Si NMR spectrum of $[\text{Tipp-Si}(\text{Ime}_4)_2\text{-AgCl}]\text{OTf}$ (**3b**) in CD_3CN at 300 K.

[Tipp-Si(Ime₄)₂-AuCl]Cl (4b)

¹H NMR (500 MHz, CD₃CN, 300 K): δ [ppm] = 7.19 (s, 2H, C_{ar}H), 3.63 (s, 12H, N_{NHC}CH₃), 3.38 (hept, *J* = 6.7 Hz, 2H, C_{ortho}H(CH₃)₂), 2.90 (hept, *J* = 6.8 Hz, 1H, C_{para}H(CH₃)₂), 2.24 (s, 12H, C_{NHC}CH₃), 1.23 (d, *J* = 6.7 Hz, 6H, C_{para}H(CH₃)₂), 1.06 (d, *J* = 6.8 Hz, 12H, C_{ortho}H(CH₃)₂).

CH groups of the ⁱPr-substituents of **4b** overlap with CH groups of the ⁱPr substituents of the decomposition products.

²⁹Si NMR (99 MHz, CD₃CN, 300 K): δ [ppm] = -38.0.

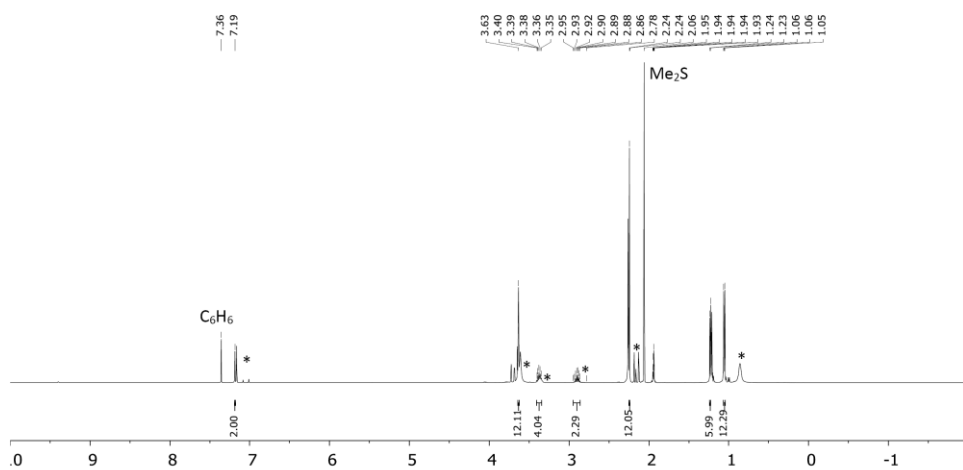


Fig. S20 ¹H NMR spectrum of [Tipp-Si(Ime₄)₂-AuCl]Cl (**4b**) in CD₃CN at 300 K. Residual C₆H₆ (7.36 ppm) stems from the crystallization of starting material **1b**. NMR spectra were recorded immediately after dissolution of the complex. Because of the rapid decomposition even at low temperature, no satisfactory NMR data was obtained. Decomposition products are marked with *.

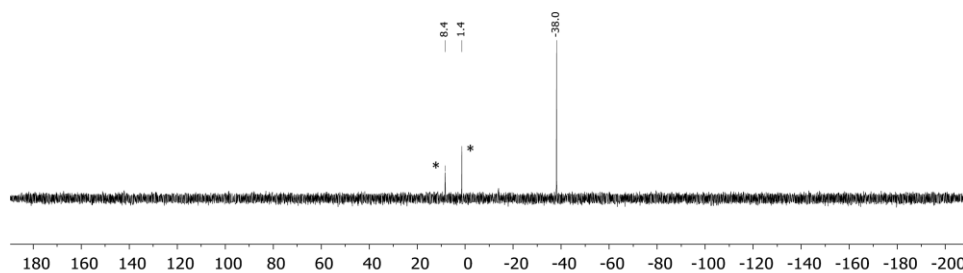


Fig. S21 ²⁹Si NMR spectrum of [Tipp-Si(Ime₄)₂-AuCl]Cl (**4b**) in CD₃CN at 300 K. Beginning decomposition is marked with *.

1.4 Decomposition of 4b

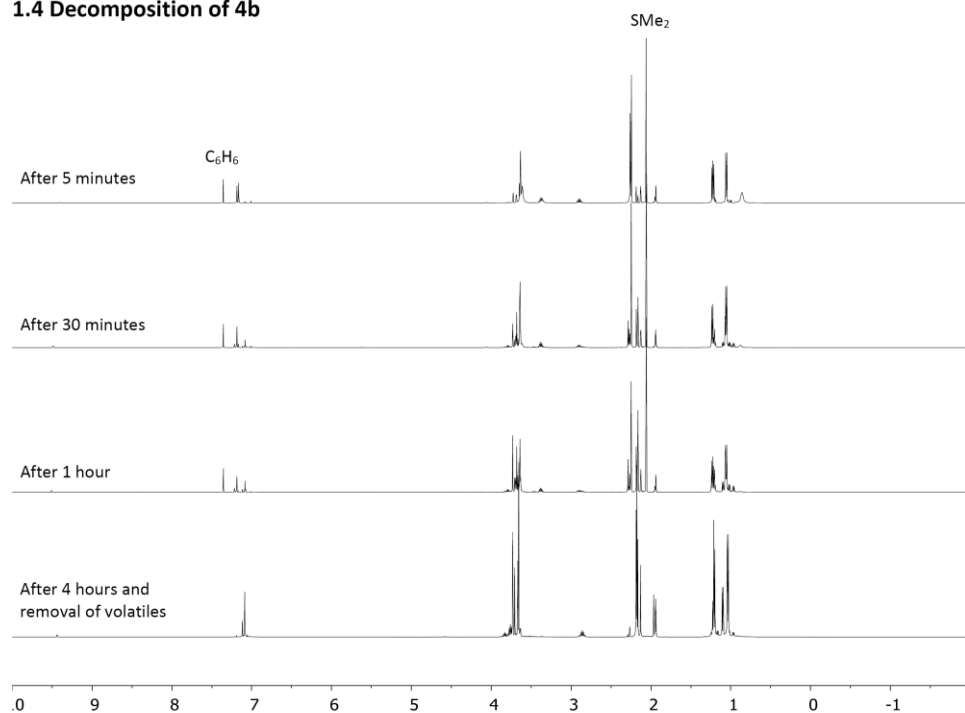


Fig. S22 ^1H NMR spectra of $[\text{Tipp-Si}(\text{Ime}_4)_2\text{-AuCl}]\text{Cl}$ (**4b**) after 5 minutes, 30 minutes, 1 hour and 4 hours. Initially fast formation of intermediate decomposition products can be observed that slowly change to the final product mixture. After around 3 hours no further changes could be observed. (cf. Fig. S23 for detailed view)

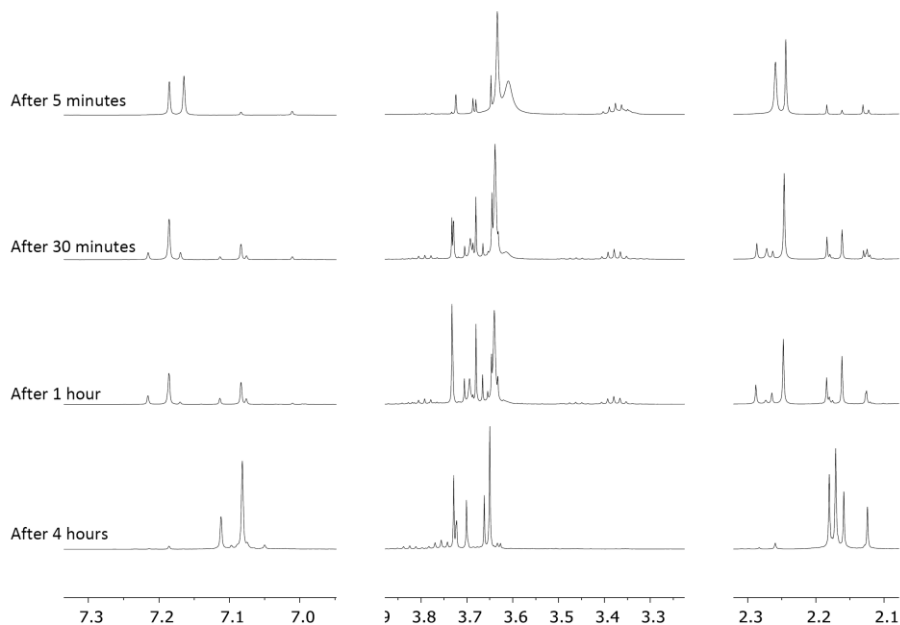


Fig. S23 Detailed look at the changing signals observed in the ^1H NMR spectra of $[\text{Tipp-Si}(\text{IME}_4)_2\text{-AuCl}]\text{Cl}$ (**4b**) after 5 minutes, 30 minutes, 1 hour and 4 hours (left: $\text{C}_{\text{ar}}\text{H}$ region, middle: NHCCH_3 and $\text{CH}(\text{CH}_3)_2$ region, right: $\text{C}_{\text{NHCCH}_3}$ region).

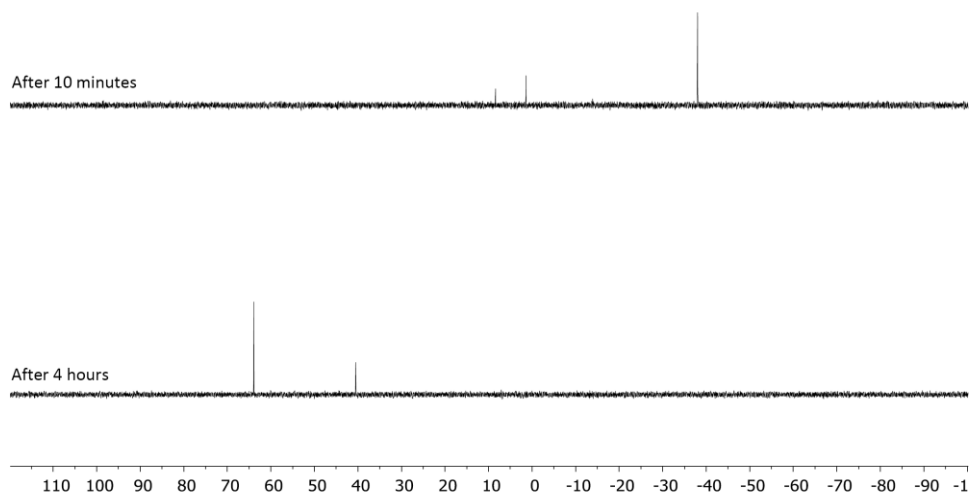


Fig. S24 ^{29}Si NMR spectrum of $[\text{Tipp-Si}(\text{IME}_4)_2\text{-AuCl}]\text{Cl}$ (**4b**) and thermal decomposition in CD_3CN at 300 K immediately after mixing of the starting materials (top) and after complete decomposition (bottom). Signals at -38.0 (**4b**) and intermediates (8.4 & 1.4 ppm) vanish completely over a period of 4 hours and signals at $+40.5$ and $+64.0$ emerge.

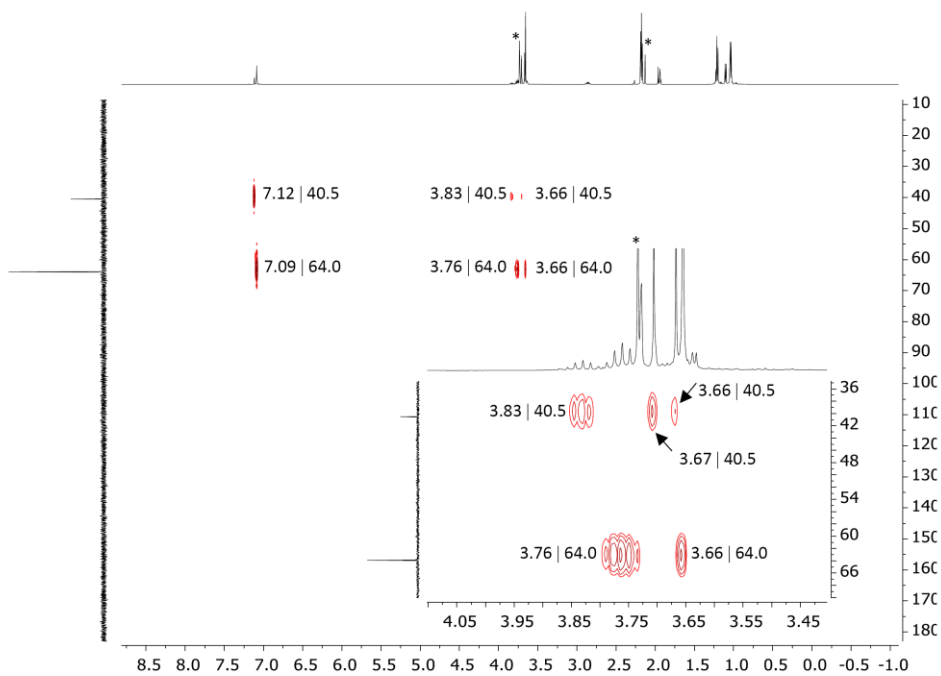


Fig. S25 $^1\text{H}/^{29}\text{Si}$ HMBC NMR spectrum of the decomposition products of complex **4b**. Clear correlation between the minor species in the ^1H NMR and the Si resonance at +40.5 ppm as well as the major species in the ^1H NMR and the Si resonance at +64.0 ppm can be observed. Signals corresponding to $[(\text{IMe}_4)_2\text{Au}]\text{Cl}$ are marked with * (*cf.* Fig. S26).

[(IMe₄)₂Au]Cl

¹H NMR (500 MHz, CD₃CN, 300 K): δ [ppm] = 3.73 (s, 6H, NCH₃), 2.16 (s, 6H, CCH₃).

¹³C NMR (126 MHz, CD₃CN, 300 K): δ [ppm] = 183.0, 127.1, 35.8, 9.0.

EA: (C₁₄H₂₄AuClN₄) calculated: C (34.97), H (5.03), N (11.65).

measured: C (34.84), H (5.24), N (11.73).

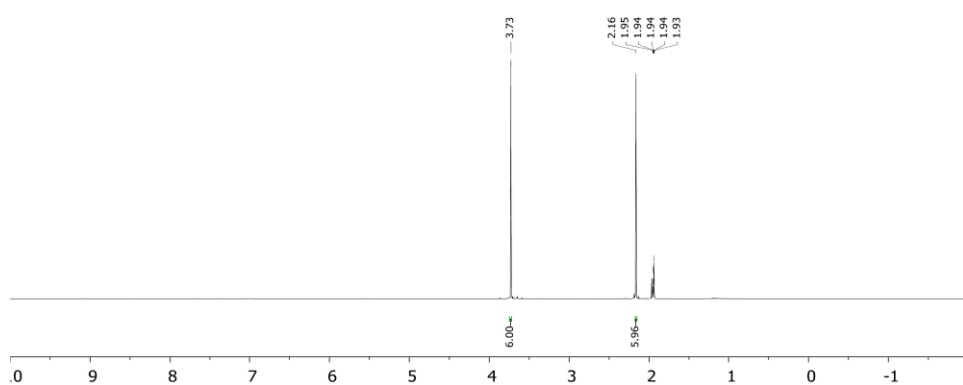


Fig. S26 ¹H NMR spectrum of [(IMe₄)₂Au]Cl (5) in CD₃CN at 300 K.

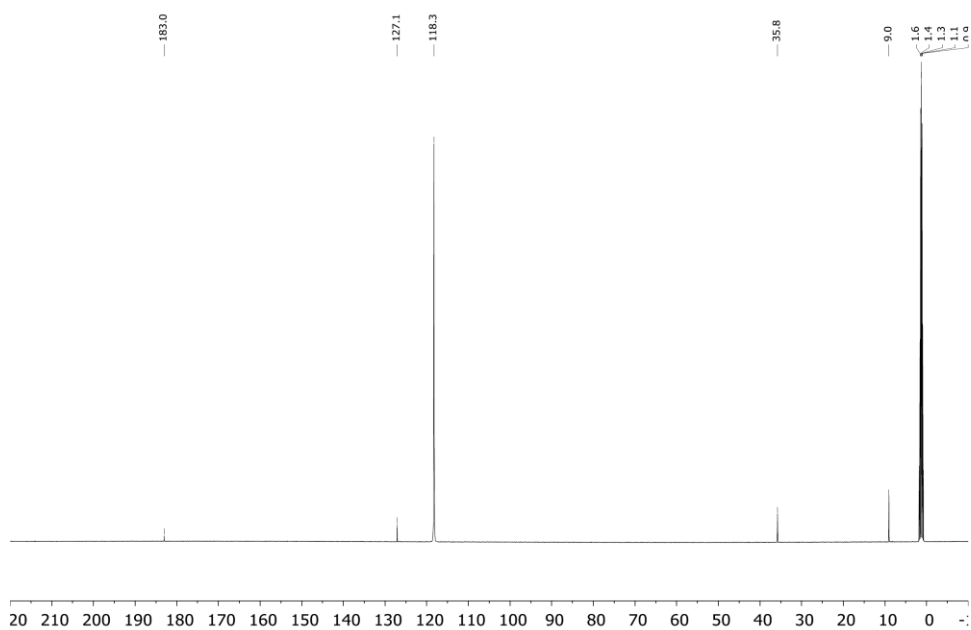


Fig. S27 ¹³C NMR spectrum of [(IMe₄)₂Au]Cl (5) in CD₃CN at 300 K.

2. X-ray Crystallographic Data

General Information

The X-ray intensity data of **4a** was collected on an X-ray single crystal diffractometer equipped with a CMOS detector (Bruker Photon-100), an IMS microsource with MoK α radiation ($\lambda = 0.71073 \text{ \AA}$) and a Helios mirror optic by using the APEX III software package.⁵² The X-ray intensity data of **2a**, **3a**, **3b** and **5** were collected on an X-ray single crystal diffractometer equipped with a CMOS detector (Bruker Photon-100), a rotating anode (Bruker TXS) with MoK α radiation ($\lambda = 0.71073 \text{ \AA}$) and a Helios mirror optic by using the APEX III software package.⁵² The measurements were performed on single crystals coated with the perfluorinated ether Fomblin[®] Y. The crystals were fixed on the top of a micro sampler, transferred to the diffractometer and frozen under a stream of cold nitrogen. A matrix scan was used to determine the initial lattice parameters. Reflections were merged and corrected for Lorenz and polarization effects, scan speed, and background using SAINT.⁵³ Absorption corrections, including odd and even ordered spherical harmonics were performed using SADABS.⁵³ Space group assignments were based upon systematic absences, E statistics, and successful refinement of the structures. Structures were solved by direct methods with the aid of successive difference Fourier maps, and were refined against all data using the APEX III software in conjunction with SHELXL-2014⁵⁴ and SHELXL.⁵⁵ All H atoms were placed in calculated positions and refined using a riding model, with methylene and aromatic C–H distances of 0.99 and 0.95 \AA , respectively, and $U_{\text{iso}}(\text{H}) = 1.2 \cdot U_{\text{eq}}(\text{C})$. Full-matrix least-squares refinements were carried out by minimizing $\Delta w(F_o^2 - F_c^2)^2$ with SHELXL-97 weighting scheme.⁵⁶ Neutral atom scattering factors for all atoms and anomalous dispersion corrections for the non-hydrogen atoms were taken from International Tables for Crystallography.⁵⁷ The images of the crystal structures were generated by Mercury.⁵⁸ The CCDC numbers CCDC-1870254 (**2a**), CCDC-1870256 (**3a**), CCDC-1870258 (**3b**), CCDC-1870255 (**4a**) and CCDC-1870257 (**5**) contain the supplementary crystallographic data for the structures. These data can be obtained free of charge from the Cambridge Crystallographic Data Centre *via* <https://www.ccdc.cam.ac.uk/structures/>.

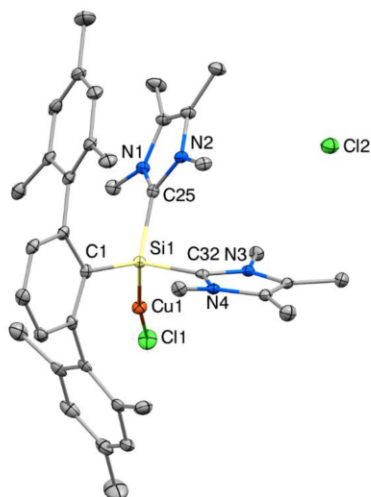
2.1 SC-XRD structure of [*m*-Ter-Si(IMe₄)₂-CuCl]Cl (**2a**)

Fig. S28 Ellipsoid plot (50% probability level) of the molecular structures of complex **2a**. Hydrogen atoms are omitted for clarity. Selected bond lengths [Å] and angles [°]: Si1–C1 1.916(3), Si1–C25 1.939(2), Si1–C32 1.938(2), Si1–Cu1 2.238(2), Cu1–Cl1 2.1477(6), Si1–Cu1–Cl1 169.3(1), C25–Si1–C32 95.5(2), C1–Si1–Cu1 119.4(2).

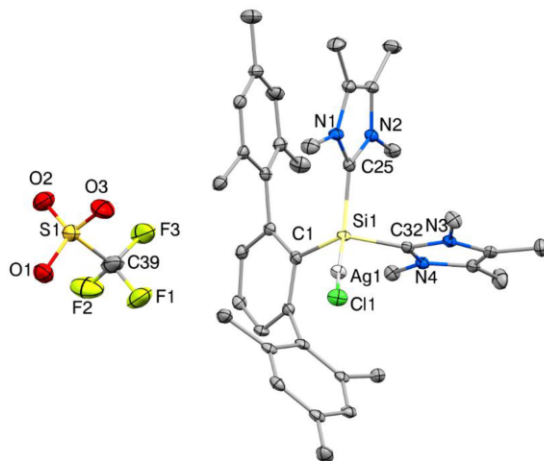
2.2 SC-XRD structure of [*m*-Ter-Si(IMe₄)₂-AgCl]OTf (**3a**)

Fig. S29 Ellipsoid plot (50% probability level) of the molecular structures of complex **3a**. Hydrogen atoms are omitted for clarity. Selected bond lengths [Å] and angles [°]: Si1–C1 1.911(4), Si1–C25 1.936(3), Si1–C32 1.938(4), Si1–Ag1 2.379(1), Ag1–Cl1 2.366(1), Si1–Ag1–Cl1 171.8(1), C25–Si1–C32 95.8(1), C1–Si1–Ag1 114.8(1).

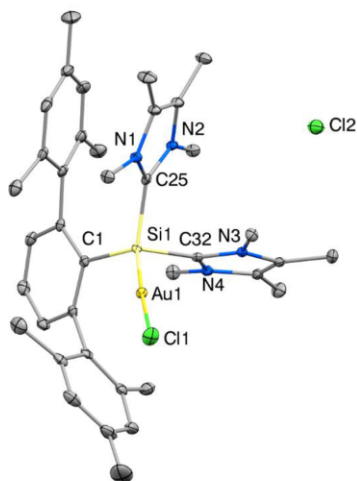
2.3 SC-XRD structure of [*m*-Ter-Si(IME₄)₂-AuCl]Cl (**4a**)

Fig. S30 Ellipsoid plot (50% probability level) of the molecular structures of complex **4a**. Hydrogen atoms are omitted for clarity. Selected bond lengths [Å] and angles [°]: Si1–C1 1.916(2), Si1–C25 1.942(2), Si1–C32 1.941(2), Si1–Au1 2.281(1), Au1–Cl1 2.354(1), Si1–Au1–Cl1 176.8(1), C25–Si1–C32 96.5(1), C1–Si1–Au1 119.0(1).

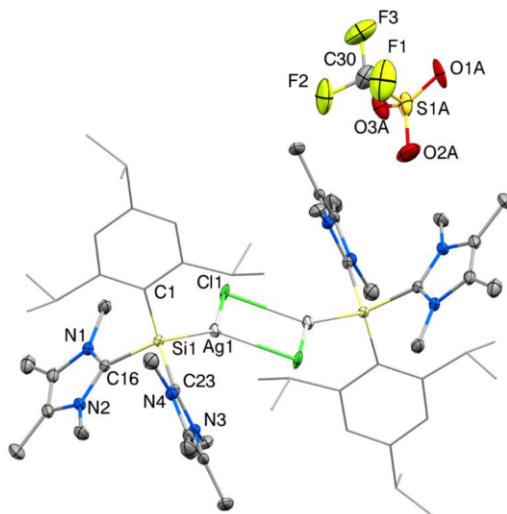
2.4 SC-XRD structure of [[Tipp-Si(IME₄)₂-AgCl]OTf]₂ (**3b**)

Fig. S31 Ellipsoid plot (50% probability level) of the molecular structure of complex **3b**. Hydrogen atoms are omitted for clarity. Only one triflate anion is shown and the Tipp substituents are depicted as wireframes. Selected bond lengths [Å] and angles [°]: Si1–C1 1.919(2), Si1–C16 1.935(2), Si1–C23 1.931(2), Si1–Ag1 2.398(1), Ag1–Cl1 2.562(1), Si1–Ag1–Cl1 141.2(1), C16–Si1–C23 100.8(1), C1–Si1–Ag1 118.0(1).

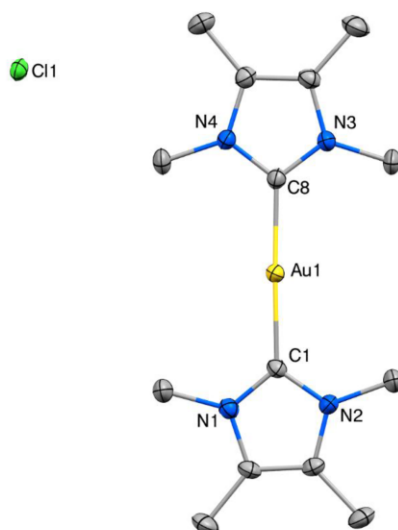
2.5 SC-XRD structure of $[(\text{IMe}_4)_2\text{Au}]\text{Cl}$ (5)

Fig. S32 Ellipsoid plot (50% probability level) of the molecular structure of complex 5. Hydrogen atoms are omitted for clarity. Selected bond lengths [Å] and angles [°]: Au1–C1 2.030(4), Au1–C8 2.022(4), C1–Au–C8 176.9(2).

Table S1 Crystal data and structural refinement parameters for compounds 2a, 3a, 3b, 4a and 5.

Compound #	2a	3a	3b	4a	5
Chemical formula	C ₃₁ H ₂₆ Cl ₂ CuN ₂ Si	C ₃₁ H ₂₆ AgClF ₂ N ₂ O ₂ Si	C ₃₁ H ₂₆ AgClF ₂ N ₂ O ₂ Si	C ₃₁ H ₂₆ AuCl ₂ N ₂ Si	C ₃₁ H ₂₆ Au ₂ Cl ₂ N ₂ Si
Formula weight	765.39 g/mol	964.39 g/mol	864.32	939.88 g/mol	1043.68
Temperature	100(2) K	100(2) K	100(2) K	100(2) K	100(2) K
Wavelength	0.71073 Å	0.71073 Å	0.71073 Å	0.71073 Å	0.71073 Å
Crystal size	0.106 × 0.146 × 0.218 mm	0.161 × 0.164 × 0.182 mm	0.084 × 0.194 × 0.245 mm	0.135 × 0.318 × 0.433 mm	0.120 × 0.294 × 0.402 mm
Crystal habit	clear colorless fragment	clear colorless fragment	clear colorless fragment	clear colorless fragment	clear colorless fragment
Crystal system	triclinic	monoclinic	triclinic	triclinic	triclinic
Space group	P-1	C1 2/c 1	P-1	P-1	P-1
Unit cell dimensions	a = 11.7503(10) Å, α = 89.784(4)° b = 12.5328(11) Å, β = 88.660(4)° c = 15.2070(14) Å, γ = 68.230(4)° 2079(3) Å ³	a = 28.241(2) Å, α = 90° b = 24.601(2) Å, β = 125.378(2)° c = 17.0773(13) Å, γ = 90° 9673.8(13) Å ³	a = 9.2078(5) Å, α = 86.901(2)° b = 15.2567(7) Å, β = 74.733(2)° c = 17.3518(8) Å, γ = 68.401(5)° 2266.13(19) Å ³	a = 11.8414(17) Å, α = 89.739(6)° b = 12.5669(19) Å, β = 88.886(5)° c = 15.180(2) Å, γ = 68.401(5)° 2100.3(8) Å ³	a = 9.656(2) Å, α = 76.210(7)° b = 10.844(3) Å, β = 79.390(8)° c = 19.427(5) Å, γ = 88.399(7)° 1941.5(8) Å ³
Volume	Z	Z	Z	Z	Z
Density (calculated)	1.223 g/cm ³	1.324 g/cm ³	g/cm ³	1.494 g/cm ³	1.785 g/cm ³
Absorption coefficient	0.715 mm ⁻¹	0.594 mm ⁻¹	mm ⁻¹	3.713 mm ⁻¹	7.722 mm ⁻¹
F(000)	808	4000	900	952	1016
Diffractometer	Bruker D8 Venture	Bruker D8 Venture	Bruker D8 Venture	Bruker D8 Venture Duo IMS	Bruker D8 Venture
Radiation source	TXS rotating anode (Mo)	TXS rotating anode (Mo)	TXS rotating anode (Mo)	IMS microsource (Mo)	TXS rotating anode (Mo)
Theta range for data collection	2.21 to 25.68°	2.21 to 25.68°	2.37 to 25.68°	2.20 to 25.35°	2.15 to 25.68°
Index ranges	-14 ≤ h ≤ 14, -15 ≤ k ≤ 15, -18 ≤ l ≤ 18	-34 ≤ h ≤ 34, -30 ≤ k ≤ 30, -20 ≤ l ≤ 20	-11 ≤ h ≤ 11, -18 ≤ k ≤ 18, -21 ≤ l ≤ 21	-14 ≤ h ≤ 14, -15 ≤ k ≤ 15, -18 ≤ l ≤ 18	-11 ≤ h ≤ 11, -12 ≤ k ≤ 12, -23 ≤ l ≤ 23
Reflections collected	45489	141925	97351	78718	59756
Independent reflections	7896 [R(int) = 0.0424]	9197 [R(int) = 0.0734]	8606 [R(int) = 0.0385]	7652 [R(int) = 0.0224]	7387 [R(int) = 0.0633]
Coverage of independent reflections	99.9%	100.0%	100.0%	99.9%	100.0%
Absorption correction	Multi-Scan	Multi-Scan	Multi-Scan	Multi-Scan	Multi-Scan
Max. and min. transmission	0.6820 and 0.7461	0.6782 and 0.7454	0.5713 and 0.7464	0.7063 and 0.7466	0.4181 and 0.7454
Refinement method	Full-matrix least-squares on F ²	Full-matrix least-squares on F ²	Full-matrix least-squares on F ²	Full-matrix least-squares on F ²	Full-matrix least-squares on F ²
Refinement program	SHELXL-2014/7 (Sheldrick, 2014)	SHELXL-2014/7 (Sheldrick, 2014)	SHELXL-2014/7 (Sheldrick, 2014)	SHELXL-2014/7 (Sheldrick, 2014)	SHELXL-2014/7 (Sheldrick, 2014)
Function minimized	Σ w(F _o ² - F _c ²) ²	Σ w(F _o ² - F _c ²) ²	Σ w(F _o ² - F _c ²) ²	Σ w(F _o ² - F _c ²) ²	Σ w(F _o ² - F _c ²) ²
Data / restraints / parameters	7896 / 0 / 458	9197 / 0 / 548	8606 / 0 / 512	7652 / 75 / 514	7387 / 0 / 434
Goodness-of-fit on F ²	1.025	1.065	1.061	1.100	1.066
Δ/σ _{max}	0.001	0.001	0.002	0.006	0.001
Final R indices	6967 data; >2σ(I); R1 = 0.0326, wR2 = 0.0801	7530 data; >2σ(I); R1 = 0.0403, wR2 = 0.0951	7908 data; >2σ(I); R1 = 0.0261, wR2 = 0.0625	7541 data; >2σ(I); R1 = 0.0135, wR2 = 0.0344	6833 data; >2σ(I); R1 = 0.0255, wR2 = 0.0698
Weighting scheme	all data: R1 = 0.0389, wR2 = 0.0832 w = 1/(σ ² (F _o ²) + (0.0330P) ² + 2.4865P) where P = (F _o ² + 2F _c ²)/3	all data: R1 = 0.0559, wR2 = 0.1024 w = 1/(σ ² (F _o ²) + (0.0483P) ² + 33.9538P) where P = (F _o ² + 4F _c ²)/3	all data: R1 = 0.0297, wR2 = 0.0640 w = 1/(σ ² (F _o ²) + (0.0280P) ² + 2.1058P) where P = (F _o ² + 2F _c ²)/3	all data: R1 = 0.0138, wR2 = 0.0346 w = 1/(σ ² (F _o ²) + (0.0171P) ² + 1.6279P) where P = (F _o ² + 2F _c ²)/3	all data: R1 = 0.0273, wR2 = 0.0711 w = 1/(σ ² (F _o ²) + (0.0411P) ² + 2.0259P) where P = (F _o ² + 2F _c ²)/3
Largest diff. peak and hole	0.763 and -0.374 eÅ ⁻³	1.012 and -0.678 eÅ ⁻³	0.807 and -0.630 eÅ ⁻³	0.305 and -0.745 eÅ ⁻³	2.385 and -0.961 eÅ ⁻³
R.M.S. deviation from mean	0.060 eÅ ⁻³	0.088 eÅ ⁻³	0.056 eÅ ⁻³	0.064 eÅ ⁻³	0.154 eÅ ⁻³

3. References

- S1 S. U. Ahmad, T. Szilvási and S. Inoue, *Chem. Commun.*, **2014**, 50, 12619-12622.
- S2 *APEX suite of crystallographic software*, APEX 3 version 2015.5-2; Bruker AXS Inc.: Madison, Wisconsin, USA, **2015**.
- S3 *SAINT*, Version 7.56a and *SADABS* Version 2008/1; Bruker AXS Inc.: Madison, Wisconsin, USA, **2008**.
- S4 G. M. Sheldrick, *SHELXL-2014*, University of Göttingen, Göttingen, Germany, **2014**.
- S5 C. B. Hübschle, G. M. Sheldrick and B. Dittrich, *J. Appl. Cryst.* **2011**, 44, 1281-1284.
- S6 G. M. Sheldrick, *SHELXL-97*, University of Göttingen, Göttingen, Germany, **1998**.
- S7 A. J. C. Wilson, *International Tables for Crystallography*, Vol. C, Tables 6.1.1.4 (pp. 500-502), 4.2.6.8 (pp. 219-222), and 4.2.4.2 (pp. 193-199); Kluwer Academic Publishers: Dordrecht, The Netherlands, **1992**.
- S8 C. F. Macrae, I. J. Bruno, J. A. Chisholm, P. R. Edgington, P. McCabe, E. Pidcock, L. Rodriguez-Monge, R. Taylor, J. van de Streek and P. A. Wood, *J. Appl. Cryst.* **2008**, 41, 466-470.

11.3 Supporting Information Chapter 6

Supporting Information

Transition Metal Carbonyl Complexes of an *N*-Heterocyclic Carbene Stabilized Silyliumylidene Ion

*Philipp Frisch, Tibor Szilvási, Amelie Porzelt, and Shigeyoshi Inoue**

Table of Contents

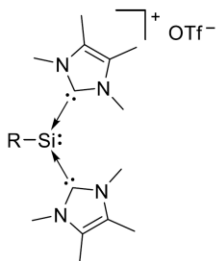
1. Experimental Section.....	S2
1.1. General Methods and Instrumentation	S2
1.2 Synthesis of [R–Si(Ime ₄) ₂]OTf (R = <i>m</i> -Ter (1a-OTf), Tipp (1b-OTf))	S4
1.3 Synthesis of [Tipp–Si(Ime ₄) ₂ →M(CO) ₅]OTf (M = Cr (2), Mo (3), W (4)).....	S15
1.4 Synthesis of [Tipp–Si(Ime ₄) ₂ –Fe(CO) ₄]OTf (5)	S23
2. X-ray Crystallographic Data.....	S26
2.1 SC-XRD structure of [<i>m</i> -Ter–Si(Ime ₄) ₂]OTf (1a-OTf , CCDC-1949742)	S27
2.2 SC-XRD structure of [Tipp–Si(Ime ₄) ₂]OTf (1b-OTf , CCDC-1949743).....	S28
2.3 SC-XRD structure of [Tipp–Si(Ime ₄) ₂ →Mo(CO) ₅]OTf (3 , CCDC-1949744)	S29
2.4 SC-XRD structure of [Tipp–Si(Ime ₄) ₂ →Fe(CO) ₄]OTf (5 , CCDC-1949745)	S30
3. DFT Calculations	S32
4. References	S50

1. Experimental Section

1.1. General Methods and Instrumentation

All manipulations were carried out under exclusion of water and oxygen in an atmosphere of argon 4.6 ($\geq 99.996\%$) using standard Schlenk techniques or in a Labstar glovebox from *MBraun* with H_2O and O_2 levels below 0.5 ppm. Glassware was heat dried under vacuum prior to use. Acetonitrile, $\text{C}_6\text{H}_5\text{F}$, $\text{C}_6\text{H}_4\text{F}_2$ and Acetonitrile- d_3 were refluxed over CaH_2 , distilled under argon, deoxygenated by three freeze-pump-thaw cycles and stored over 3 Å molecular sieve in a glovebox. Diethylether, THF and *n*-hexane were refluxed over sodium/benzophenone, distilled under argon, deoxygenated by three freeze-pump-thaw cycles and stored over 3 Å molecular sieve in a glovebox. THF- d_8 was stirred over Na-K alloy, distilled under argon, deoxygenated by three freeze-pump-thaw cycles and stored over 3 Å molecular sieve in a glovebox. All NMR samples were prepared under argon in *J. Young* PTFE valve NMR tubes. NMR spectra at ambient temperature (300 K) were recorded on a *Bruker* AV400US or DRX400 (^1H : 400.13 MHz) or AV500C (^1H : 500.36 MHz, ^{13}C : 125.83 MHz, ^{29}Si : 99.41 MHz, ^{19}F : 470.77 MHz). The ^1H , ^{13}C , and ^{29}Si NMR spectroscopic chemical shifts δ are reported in ppm relative to tetramethylsilane. ^1H and ^{13}C NMR spectra are calibrated against the residual proton and natural abundance carbon resonances of the respective deuterated solvent as internal standard (CD_3CN : $\delta(^1\text{H}) = 1.94$ ppm and $\delta(^{13}\text{C}) = 118.3$ ppm; THF- d_8 : $\delta(^1\text{H}) = 1.73$ ppm and $\delta(^{13}\text{C}) = 25.4$ ppm). ^{19}F NMR spectra are referenced to the resonance of CFCl_3 ($\delta = 0$ ppm) as external standard. NMR spectra in THF- d_8 include a resonance for silicon grease ($\delta(^1\text{H}) = 0.11$ ppm, $\delta(^{13}\text{C}) = 1.4$ ppm), derived from *B. Braun AG Sterican®* cannulas, which is marked with # in the corresponding spectra. The following abbreviations are used to describe signal multiplicities: s = singlet, d = doublet, t = triplet, q = quartet, sext = sextet, sept = septet, bs = broad signal, m = multiplet. NMR spectra were visualized using MestReNova 12. Reactions requiring UV irradiation were carried out using an *Asahi Spectra* MAX-302 Xenon Light Source. Quantitative elemental analyses (EA) were carried out using a *HEKAtech* EURO EA instrument equipped with a CHNS combustion analyzer. Carbon values for the group 6 complexes were consistently and reproducibly low ($\sim 1\%$ deviation), presumably due to the formation of incombustible silicon-carbides. Nevertheless, the EA data is provided to show the best values obtained so far. IR spectra were recorded in the solid state (neat) on a Perkin Elmer FT-IR spectrometer (diamond ATR, Spectrum Two) in a range of 400–4000 cm^{-1} at room temperature inside an argon filled glovebox. Spectra were visualized using

OriginPro 2018. IR bands are reported in cm^{-1} and the intensities are abbreviated as following: s = strong, m = medium, w = weak. Melting Points (M.P.) were determined in sealed glass capillaries under inert gas by a *Büchi* M-565 melting point apparatus. Unless otherwise stated, all commercially available chemicals were purchased from abcr or Sigma-Aldrich and used without further purification. The compounds [*m*-Ter-Si(IME₄)₂]Cl (**1a-Cl**)^{S1} (*m*-Ter = 2,6-(2,4,6-Me₃-C₆H₂)₂-C₆H₃) and [Tipp-Si(IME₄)₂]Cl (**1b-Cl**)^{S2} (Tipp = 2,4,6-Pr₃-C₆H₂) were prepared as described in the literature.

1.2 Synthesis of [R-Si(IME₄)₂]OTf (R = *m*-Ter (1a-OTf), Tipp (1b-OTf))1a-OTf (R = *m*-Ter)

1b-OTf (R = Tipp)

General Procedure: [R-Si(IME₄)₂]Cl (**1-CI**) (300.0 mg, 1.0 eq) and KOTf (1.0 eq) were suspended in 8 mL THF and stirred at r.t. until the starting material dissolved. The cloudy, bright orange suspension was concentrated under reduced pressure to about 5 mL, filtered and the clear solution was further concentrated under reduced pressure until precipitation began. *n*-Hexane (12-15 mL) was added to precipitate an orange solid which was collected by filtration, washed with *n*-hexane (3 mL) and after drying under vacuum the products **1-OTf** were obtained as orange air- and moisture-sensitive solids.

[*m*-Ter-Si(IME₄)₂]OTf (1a-OTf)

Yield: 327.4 mg, 443.0 μmol, 92%.

1a-OTf is well soluble in acetonitrile and THF. Single crystals suitable for XRD analysis of compound **1a-OTf** were obtained by slow diffusion of pentane into a saturated solution of **1a-OTf** in 1,2-difluorobenzene.

¹H NMR (500 MHz, THF-*d*₈, 300 K): δ [ppm] = 7.29 (t, ³J_{H-H} = 7.5 Hz, 1H, C_{ar}H_{para}), 6.91 (d, ³J_{H-H} = 7.5 Hz, 2H, C_{ar}H_{meta}), 6.64 (s, 4H, C_{mes}H), 3.44 (s, 12H, N_{NHC}CH₃), 2.14 (s, 6H, C_{mes}CH_{3,para}), 2.11 (s, 12H, C_{mes}CH_{3,ortho}), 2.06 (s, 12H, C_{NHC}CH₃).

¹H NMR (500 MHz, CD₃CN, 300 K): δ [ppm] = 7.35 (t, ³J_{H-H} = 7.5 Hz, 1H C_{ar}H_{para}), 6.94 (d, ³J_{H-H} = 7.5 Hz, 2H, C_{ar}H_{meta}), 6.69 (s, 4H, C_{mes}H), 3.29 (bs, 12H, N_{NHC}CH₃), 2.15 (s, 6H, C_{mes}CH_{3,para}), 2.07 (s, 12H, C_{mes}CH_{3,ortho}), 2.01 (s, 12H, C_{NHC}CH₃).

¹³C{¹H} NMR (126 MHz, THF-*d*₈, 300 K): δ [ppm] = 159.7, 148.4, 146.0, 141.1, 136.5, 130.0, 128.3, 128.3, 127.5, 122.3 (q, ¹J_{C-F} = 322.6 Hz, CF₃), 34.2, 22.0, 21.1, 9.0.

¹³C{¹H} NMR (126 MHz, CD₃CN, 300 K): δ [ppm] = 160.3, 148.7, 144.7, 141.0, 137.0, 130.2, 128.4, 128.2, 128.1, 122.1 (q, ¹J_{C-F} = 320.9 Hz, CF₃), 35.4, 21.9, 21.0, 9.1.

²⁹Si{¹H} NMR (99 MHz, THF-*d*₈, 300 K): δ [ppm] = -70.0.

²⁹Si{¹H} NMR (99 MHz, CD₃CN, 300 K): δ [ppm] = -69.2.

¹⁹F{¹H} NMR (471 MHz, THF-*d*₈, 300 K): δ [ppm] = -79.2.

¹⁹F{¹H} NMR (471 MHz, CD₃CN, 300 K): δ [ppm] = -79.3.

EA: C₃₉H₄₉N₄SiO₃F₃ calculated [%]: C (63.39), H (6.68), N (7.58), S (4.34).
 measured [%]: C (62.64), H (6.74), N (7.50), S (4.08).

M.P.: 143-144 °C (decomposition, change to orange oil).

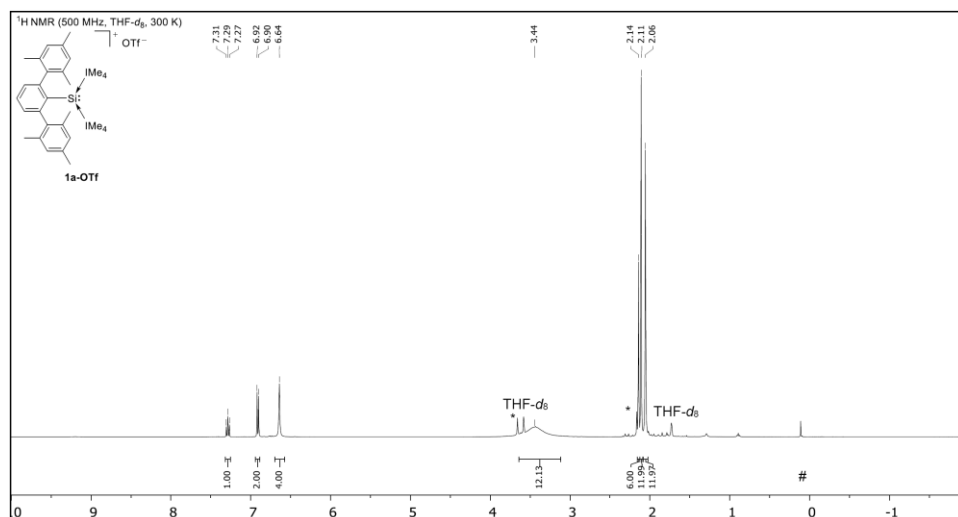


Fig. S1 ¹H NMR spectrum of [Tipp-Si(IME₄)₂]OTf (1a-OTf) in THF-*d*₈ at 300 K. Residual imidazolium triflate (IME₄·HOTf) is marked with *.

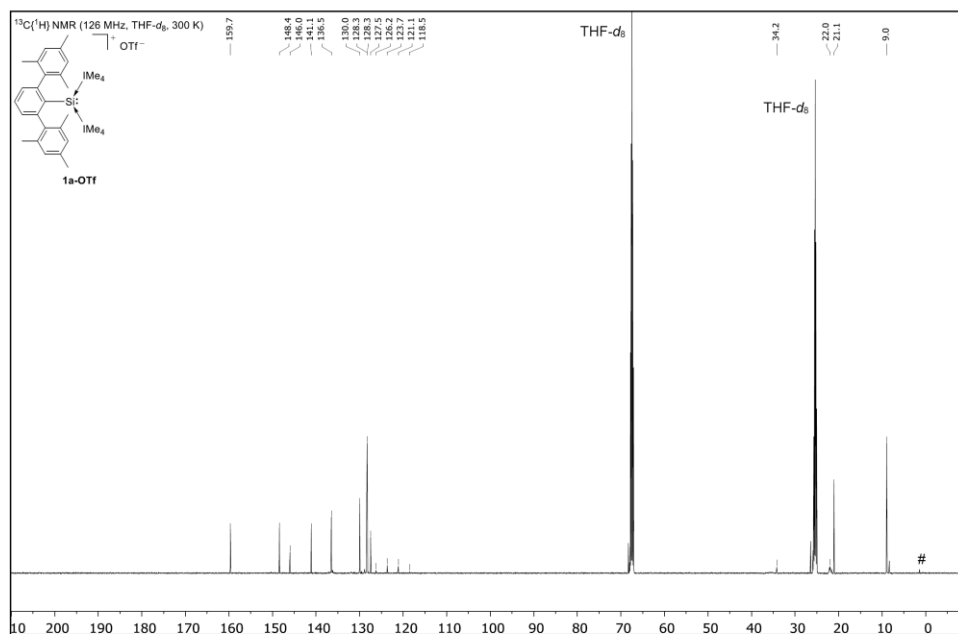


Fig. S2 ¹³C{¹H} NMR spectrum of [Tipp-Si(IME₄)₂]OTf (1a-OTf) in THF-*d*₈ at 300 K.

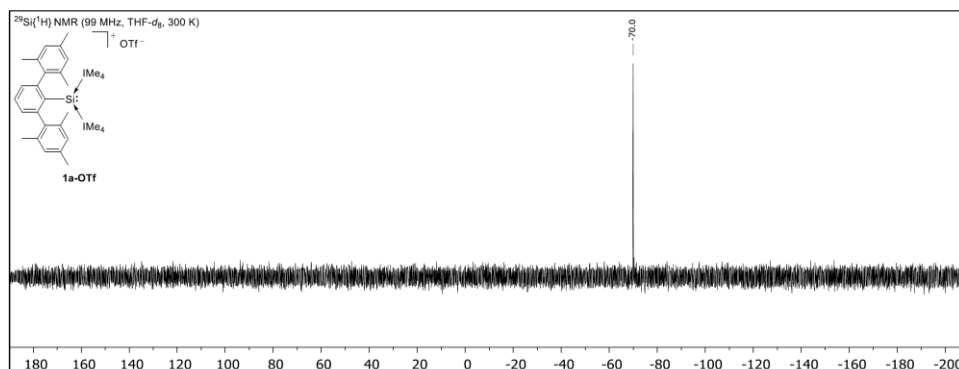


Fig. S3 ²⁹Si{¹H} NMR spectrum of [Tipp-Si(Ime₄)₂]OTf (**1a-OTf**) in THF-*d*₆ at 300 K.

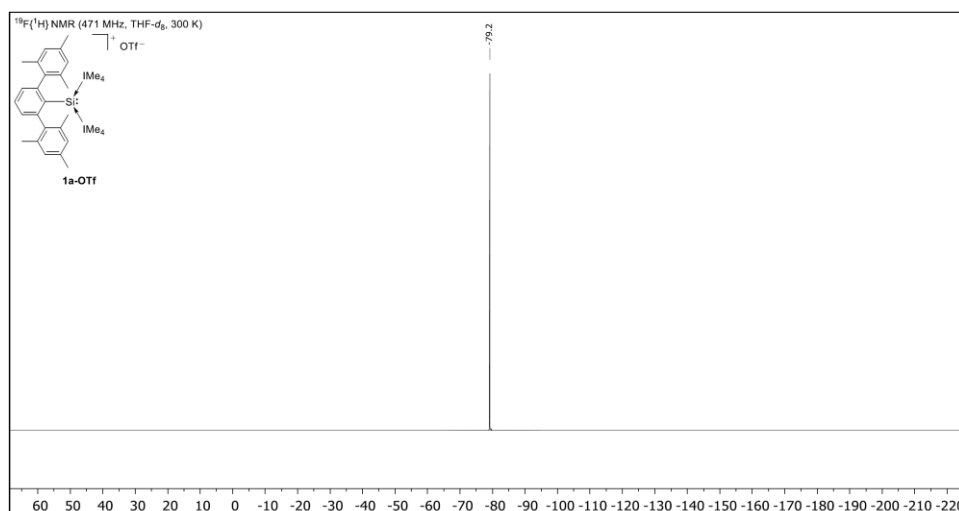


Fig. S4 ¹⁹F{¹H} NMR spectrum of [Tipp-Si(Ime₄)₂]OTf (**1a-OTf**) in THF-*d*₆ at 300 K.

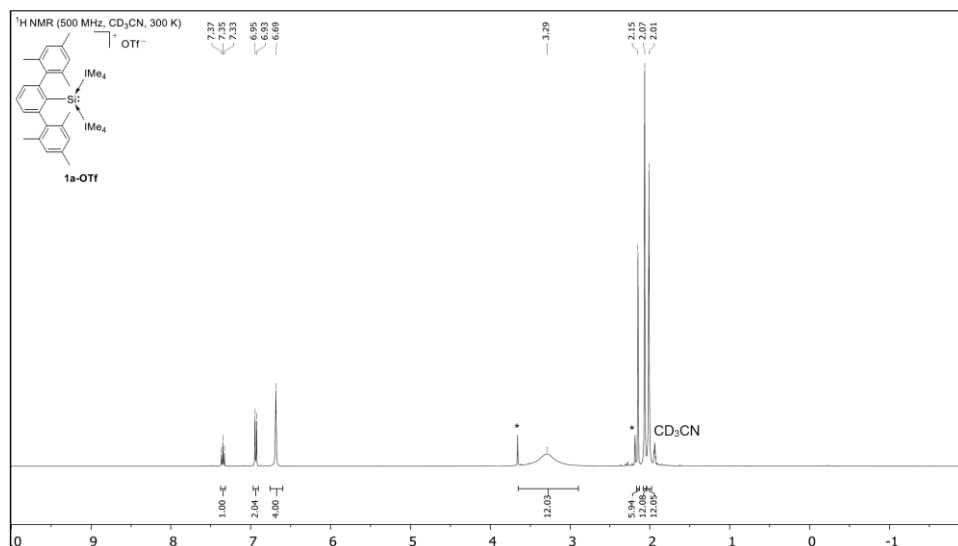


Fig. S5 ¹H NMR spectrum of [Tipp-Si(Ime₄)₂]OTf (**1a-OTf**) in CD₃CN at 300 K. Residual imidazolium triflate (Ime₄⁺·HOTf) is marked with *.

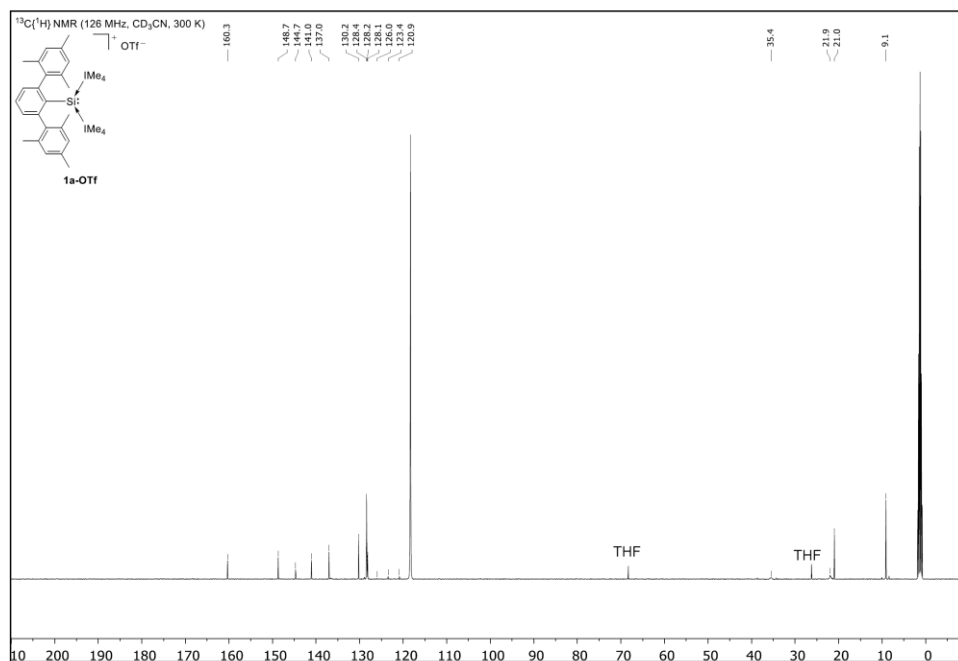


Fig. S6 ¹³C{¹H} NMR spectrum of [Tipp-Si(Ime₄)₂]OTf (**1a-OTf**) in CD₃CN at 300 K.

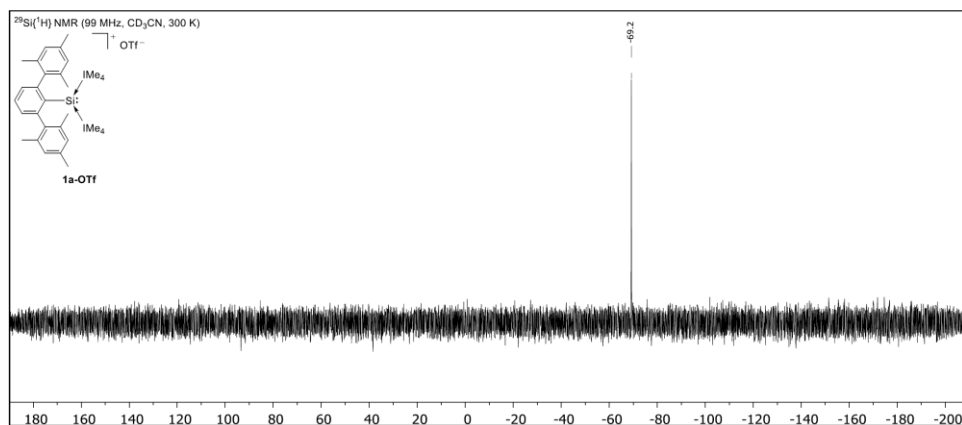


Fig. S7 ²⁹Si{¹H} NMR spectrum of [Tipp-Si(IMe₄)₂]OTf (**1a-OTf**) in CD₃CN at 300 K.

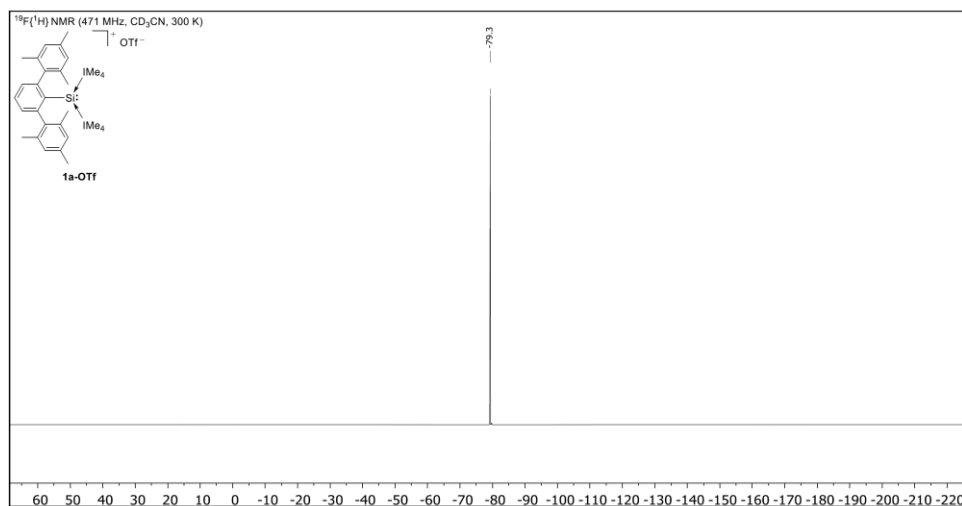


Fig. S8 ¹⁹F{¹H} NMR spectrum of [Tipp-Si(IMe₄)₂]OTf (**1a-OTf**) in CD₃CN at 300 K.

11. Appendix

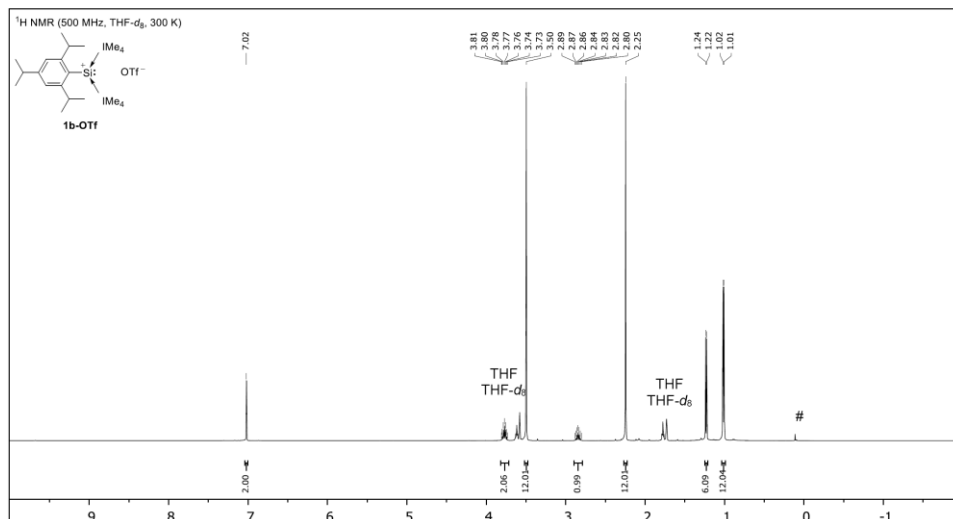


Fig. S9 ¹H NMR spectrum of [Tipp-Si(Ime₄)₂]OTf (**1b-OTf**) in THF-*d*₆ at 300 K.

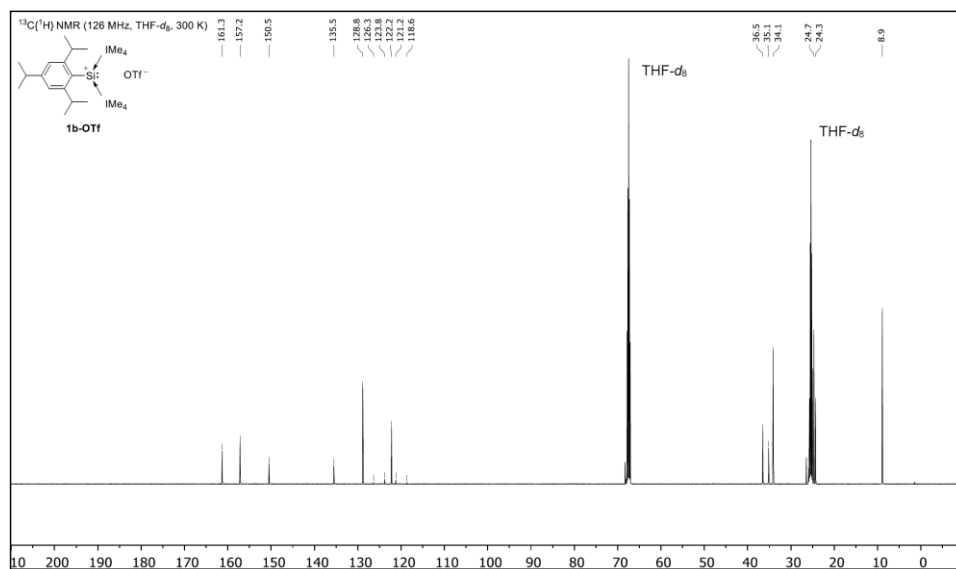


Fig. S10 ¹³C NMR spectrum of [Tipp-Si(Ime₄)₂]OTf (**1b-OTf**) in THF-*d*₆ at 300 K.

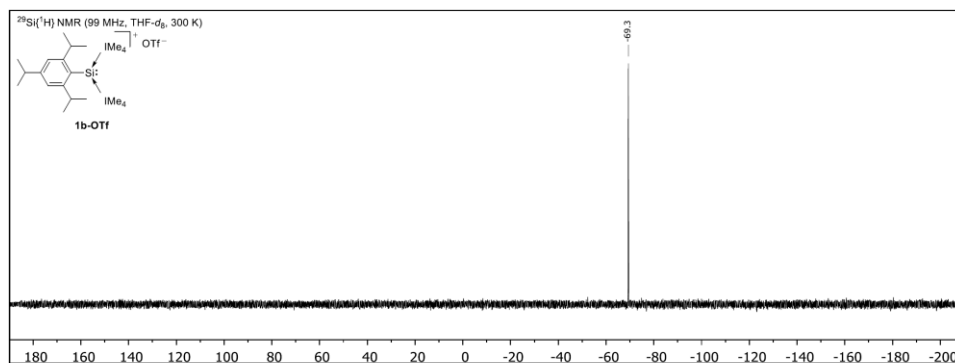


Fig. S11 ²⁹Si{¹H} NMR spectrum of [Tipp-Si(Ime₄)₂]OTf (**1b-OTf**) in THF-*d*₆ at 300 K.

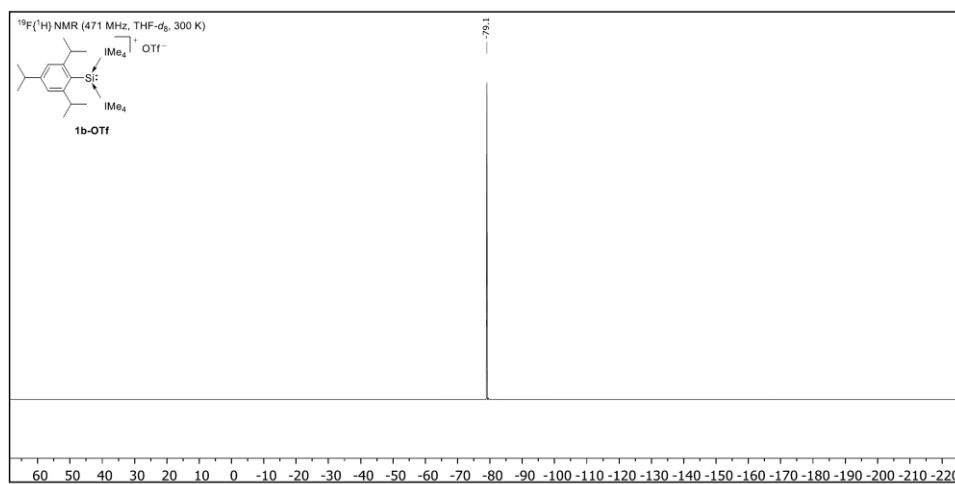


Fig. S12 ¹⁹F{¹H} NMR spectrum of [Tipp-Si(Ime₄)₂]OTf (**1b-OTf**) in THF-*d*₆ at 300 K.

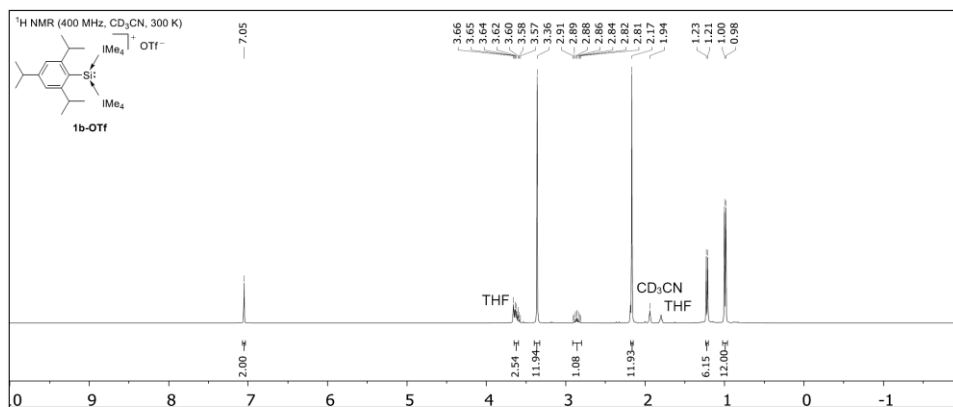


Fig. S13 ¹H NMR spectrum of [Tipp-Si(IME₄)₂]OTf (**1b-OTf**) in CD₃CN at 300 K.

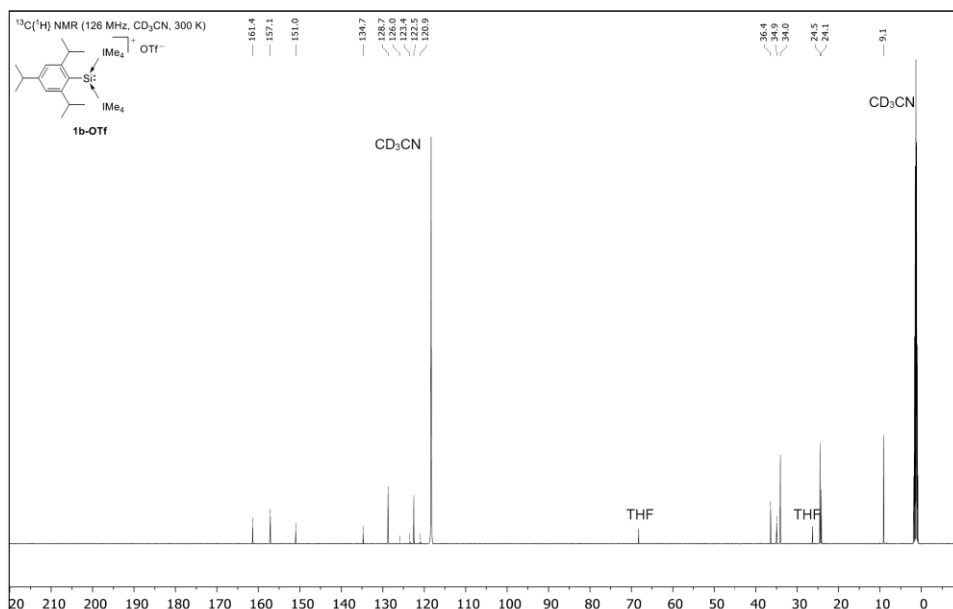


Fig. S14 ¹³C{¹H} NMR spectrum of [Tipp-Si(IME₄)₂]OTf (**1b-OTf**) in CD₃CN at 300 K.

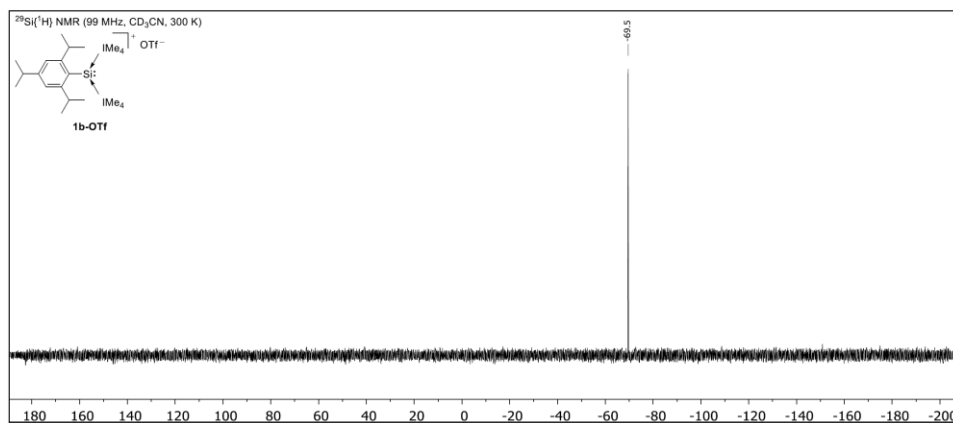


Fig. S15 ²⁹Si{¹H} NMR spectrum of [Tipp-Si(IME₄)₂]⁺OTf⁻ (**1b-OTf**) in CD₃CN at 300 K.

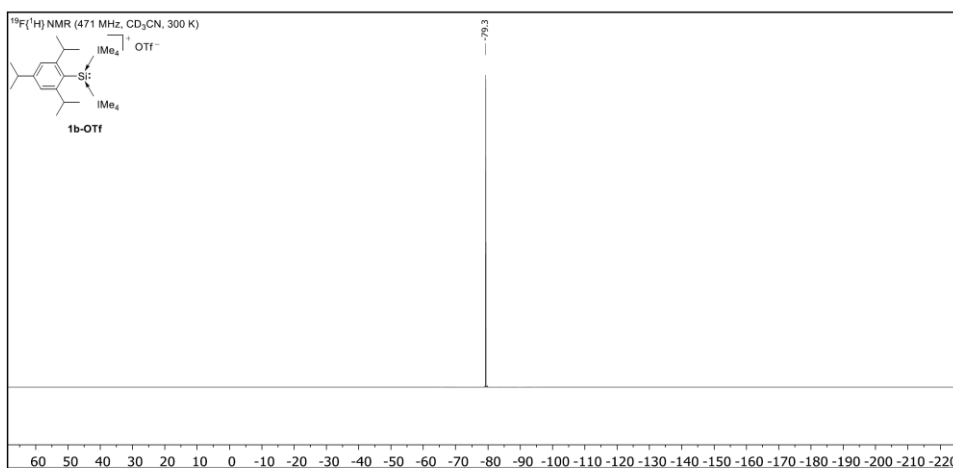


Fig. S16 ¹⁹F{¹H} NMR spectrum of [Tipp-Si(IME₄)₂]⁺OTf⁻ (**1b-OTf**) in CD₃CN at 300 K.

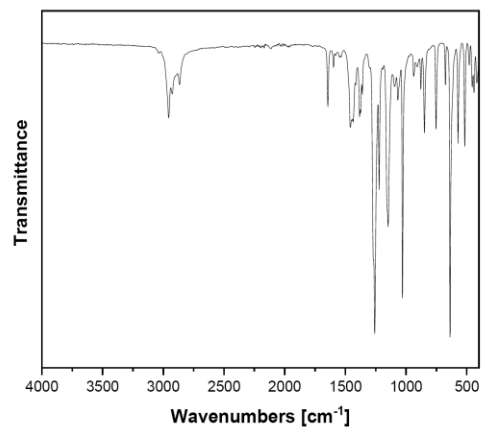
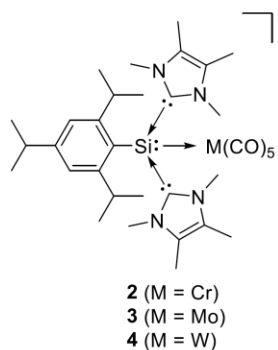


Fig. S17 Solid state FT-IR spectrum of [Tipp-Si(IME₄)₂]OTf (**1b-OTf**).

1.3 Synthesis of [Tipp-Si(Ime₄)₂→M(CO)₅]OTf (M = Cr (2), Mo (3), W (4))



General procedure: M(CO)₆ (M = Cr, Mo, W; 174.9 μmol, 1.1 eq) was dissolved in 5 mL THF and irradiated with UV light for 6 hours. Solid [Tipp-Si(Ime₄)₂]OTf (**1b-OTf**) (100.0 mg, 159.0 μmol, 1.0 eq) was added to the yellow-orange M(CO)₅THF solution in one portion and then stirred for one hour at room temperature. The bright yellow solution was concentrated under reduced pressure to about 1-2 mL and hexane (15 mL) was added slowly to precipitate a

(pale) yellow solid. The solid was collected by filtration, washed with hexane (2×3 mL) and after drying under vacuum the complexes **2-4** were obtained as pale to bright yellow air- and moisture-sensitive solids.

Alternate procedure: M(CO)₆ and [Tipp-Si(Ime₄)₂]OTf (**1b-OTf**) can be mixed in THF and simply irradiated with UV light for 4-6 hours. However, the reaction is less clean than preparing M(CO)₅THF before adding **1b-OTf**.

[Tipp-Si(Ime₄)₂→Cr(CO)₅]OTf (**2**)

Yield = 104.3 mg, 127.0 μmol, 80%.

¹H NMR (400 MHz, THF-*d*₈, 300 K): δ [ppm] = 7.18 (s, 2H, C_{ar}H), 4.10 (bs, 2H, C_{ortho}H(CH₃)₂), 3.80 (s, 12H, N_{NHC}CH₃), 2.88 (sept, *J* = 7.0 Hz, 1H, C_{para}H(CH₃)₂), 2.26 (s, 12H, C_{NHC}CH₃), 1.24 (d, *J* = 7.0 Hz, 6H, C_{para}H(CH₃)₂), 1.08 (d, *J* = 6.5 Hz, 12H, C_{ortho}H(CH₃)₂).

¹³C{¹H} NMR (126 MHz, THF-*d*₈, 300 K): δ [ppm] = 225.2 (CO), 222.0 (CO), 156.8, 155.2, 152.4, 131.3, 130.6, 124.5, 37.2, 34.8, 34.5, 24.0, 8.9.

Note: The CF₃ group in the triflate anion (normally a weak quartet around 120-125 ppm) was not observed.

²⁹Si{¹H} NMR (99 MHz, THF-*d*₈, 300 K): δ [ppm] = 6.3.

FT-IR (solid): $\tilde{\nu}$ [cm⁻¹] = 2037 (m, $\tilde{\nu}_{C=O}$), 1889 (s, $\tilde{\nu}_{C=O}$).

EA: C₃₅H₄₇N₄SiSO₈F₃Cr calculated [%]: C (51.21), H (5.77), N (6.83), S (3.91).
measured [%]: C (50.09), H (5.57), N (6.61), S (3.81).

M.P.: 74–75 °C (decomposition, change to brown oil).

11. Appendix

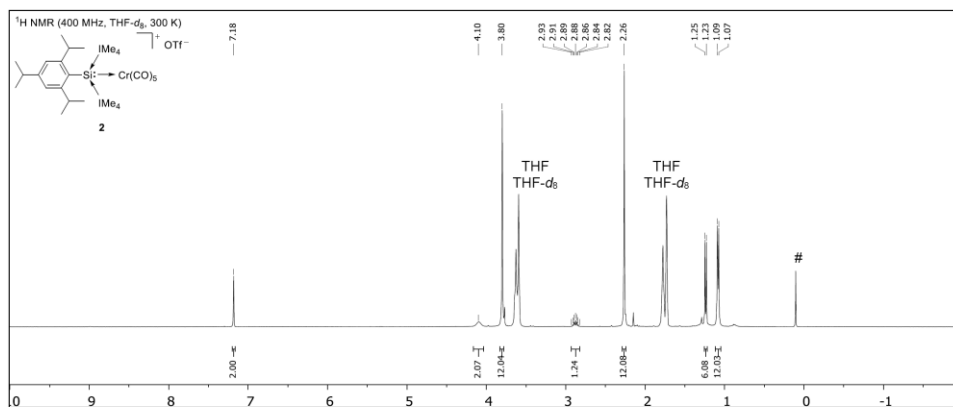


Fig. S18 ¹H NMR spectrum of [Tipp-Si(IME₄)₂→Cr(CO)₅]OTf (**2**) in THF-*d*₈ at 300 K.

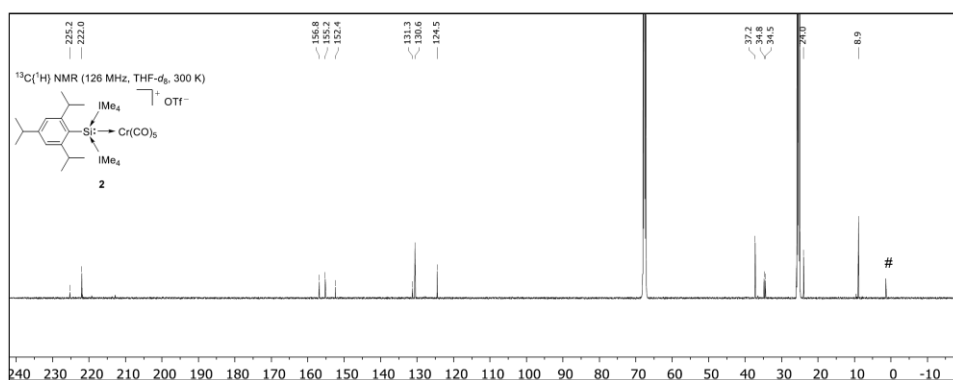


Fig. S19 ¹³C{¹H} NMR spectrum of [Tipp-Si(IME₄)₂→Cr(CO)₅]OTf (**2**) in THF-*d*₈ at 300 K.

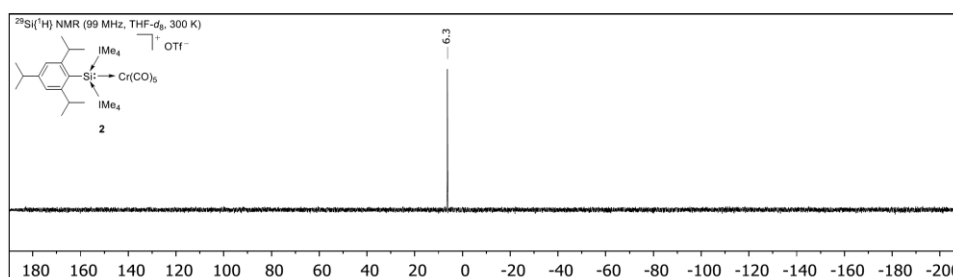


Fig. S20 ²⁹Si{¹H} NMR spectrum of [Tipp-Si(IME₄)₂→Cr(CO)₅]OTf (**2**) in THF-*d*₈ at 300 K.

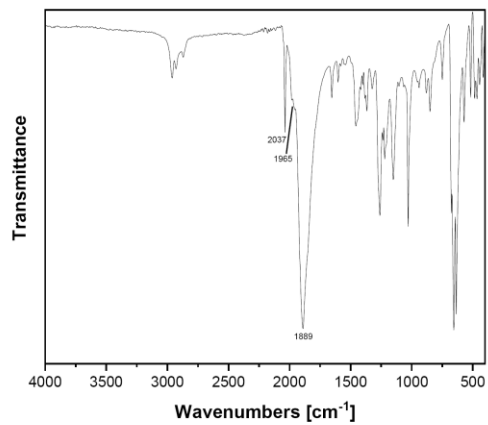


Fig. S21 Solid state FT-IR spectrum of [Tipp-Si(IME₄)₂→Cr(CO)₅]OTf (**2**).

[Tipp–Si(IME₄)₂→Mo(CO)₅]OTf (3)

Yield = 114.3 mg, 132.2 μmol, 83%.

Single crystals suitable for XRD analysis of compound **3** were obtained by cooling a concentrated solution of **3** in Et₂O to –35 °C.

¹H NMR (400 MHz, CD₃CN, 300 K): δ [ppm] = 7.16 (s, 2H, C_{ar}H), 4.20 (bs, 2H, C_{ortho}H(CH₃)₂), 3.63 (s, 12H, N_{NHC}CH₃), 2.88 (sept, *J* = 6.9 Hz, 1H, C_{para}H(CH₃)₂), 2.17 (s, 12H, C_{NHC}CH₃), 1.22 (d, *J* = 6.9 Hz, 6H, C_{para}H(CH₃)₂), 1.02 (d, *J* = 6.6 Hz, 12H, C_{ortho}H(CH₃)₂).

¹H NMR (400 MHz, THF-*d*₆, 300 K): δ [ppm] = 7.16 (s, 2H, C_{ar}H), 4.24 (bs, 2H, C_{ortho}H(CH₃)₂), 3.80 (s, 12H, N_{NHC}CH₃), 2.87 (sept, *J* = 6.9 Hz, 1H, C_{para}H(CH₃)₂), 2.25 (s, 12H, C_{NHC}CH₃), 1.24 (d, *J* = 6.9 Hz, 6H, C_{para}H(CH₃)₂), 1.07 (d, *J* = 6.6 Hz, 12H, C_{ortho}H(CH₃)₂).

¹³C{¹H} NMR (126 MHz, THF-*d*₆, 300 K): δ [ppm] = 210.0 (CO), 202.2 (sext, ¹J_{Si^{95/97}Mo} = 68.3 Hz, CO), 156.9, 156.0, 152.2, 131.2, 130.5, 124.3, 37.1, 34.9, 34.9, 24.0, 8.9.

Note: (a) Coupling to Mo (~16% ⁹⁵Mo (*S* = 5/2), ~10% ⁹⁷Mo (*S* = 5/2)) can be observed for the CO signal at 202.2 ppm; (b) The CF₃ group in the triflate anion (normally a very weak quartet around 120–125 ppm) was not observed.

²⁹Si{¹H} NMR (99 MHz, THF-*d*₆, 300 K): δ [ppm] = –17.3.

Note: No coupling of Si to Mo could be observed, even with a concentrated solution and a significantly increased number of scans.

FT-IR (solid): $\tilde{\nu}$ [cm⁻¹] = 2054 (m, $\tilde{\nu}_{C=O}$), 1969 (w, $\tilde{\nu}_{C=O}$), 1897 (s, $\tilde{\nu}_{C=O}$), 1860 (s, $\tilde{\nu}_{C=O}$).

EA: C₃₅H₄₇N₄SiSO₈F₃Mo calculated [%]: C (48.61), H (5.48), N (6.48), S (3.71).

measured [%]: C (47.72), H (5.45), N (6.29), S (3.47).

M.P.: 79–80 °C (decomposition, change to red-brown oil).

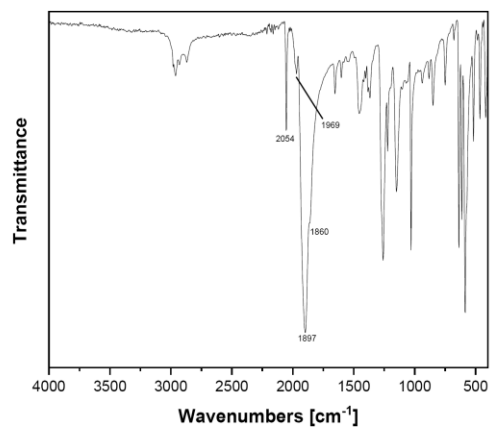


Fig. S25 Solid state FT-IR spectrum of [Tipp-Si(IME₄)₂→Mo(CO)₅]OTf (**3**).

[Tipp-Si(IME₄)₂→W(CO)₅]OTf (4)

Yield = 130.6 mg, 137.1 μmol, 86%.

¹H NMR (500 MHz, THF-*d*₆, 300 K): δ [ppm] = 7.17 (s, 2H, C_{ar}H), 4.15 (bs, 2H, C_{ortho}H(CH₃)₂), 3.80 (s, 12H, N_{NHC}CH₃), 2.88 (sept, *J* = 6.9 Hz, 1H, C_{para}H(CH₃)₂), 2.26 (s, 12H, C_{NHC}CH₃), 1.24 (d, *J* = 6.9 Hz, 6H, C_{para}H(CH₃)₂), 1.08 (d, *J* = 6.6 Hz, 12H, C_{ortho}H(CH₃)₂).

¹³C{¹H} NMR (126 MHz, THF-*d*₆, 300 K): δ [ppm] = 201.9 (d, ¹*J*_{C¹⁸³W} = 123.8 Hz, CO), 192.4 (d, ¹*J*_{C¹⁸³W} = 126.6 Hz, CO), 156.9, 155.5, 152.3, 130.5, 130.2, 124.4, 37.4, 35.1, 34.9, 25.7, 24.0, 8.9.

Note: (a) Coupling to W (~14% ¹⁸³W (*S* = 1/2)) can be observed for the CO signals at 201.9 ppm and 192.4 ppm. (b) The CF₃ group in the triflate anion (normally a very weak quartet around 120-125 ppm) was not observed.

²⁹Si{¹H} NMR (99 MHz, THF-*d*₆, 300 K): δ [ppm] = -30.5 (d, ¹*J*_{Si¹⁸³W} = 122.6 Hz)

Note: Coupling to W (~14% ¹⁸³W (*S* = 1/2)) can be observed for the Si signal.

FT-IR (solid): $\tilde{\nu}$ [cm⁻¹] = 2052 (m, $\tilde{\nu}_{C=O}$), 1963 (w, $\tilde{\nu}_{C=O}$), 1891 (s, $\tilde{\nu}_{C=O}$), 1850 (s, $\tilde{\nu}_{C=O}$).

EA: C₃₅H₄₇N₄SiSO₈F₃W calculated [%]: C (44.12), H (4.97), N (5.88), S (3.36).
measured [%]: C (43.09), H (4.82), N (5.67), S (3.19).

M.P.: 82-83 °C (decomposition, change to brown oil).

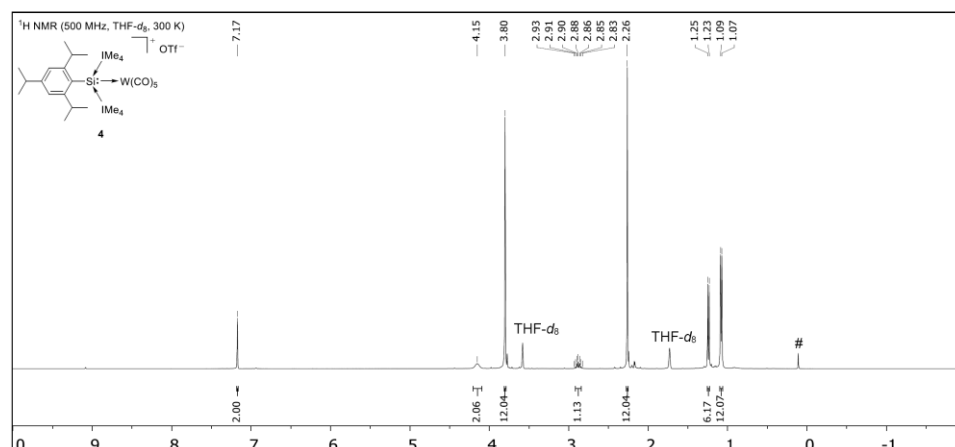


Fig. S26 ¹H NMR spectrum of [Tipp-Si(IME₄)₂→W(CO)₅]OTf (4) in THF-*d*₆ at 300 K.

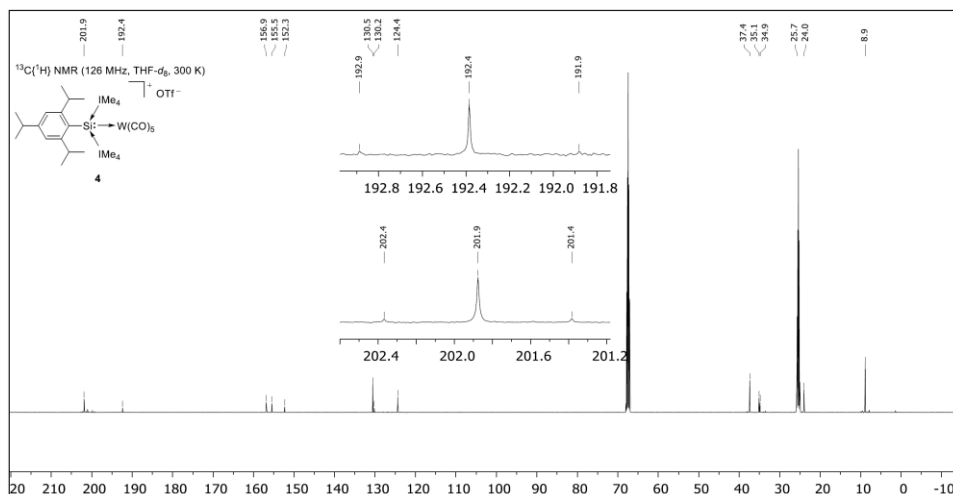


Fig. S27 $^{13}\text{C}\{^1\text{H}\}$ NMR spectrum of $[\text{Tipp-Si}(\text{IMe}_4)_2\text{-W}(\text{CO})_5]\text{OTf}$ (**4**) in THF- d_6 at 300 K.

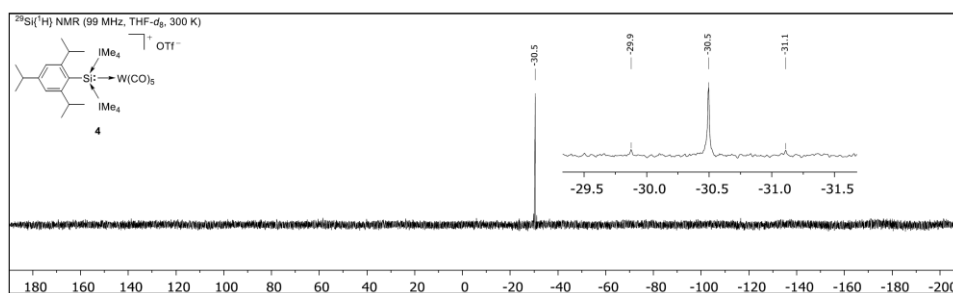


Fig. S28 $^{29}\text{Si}\{^1\text{H}\}$ NMR spectrum of $[\text{Tipp-Si}(\text{IMe}_4)_2\text{-W}(\text{CO})_5]\text{OTf}$ (**4**) in THF- d_6 at 300 K.

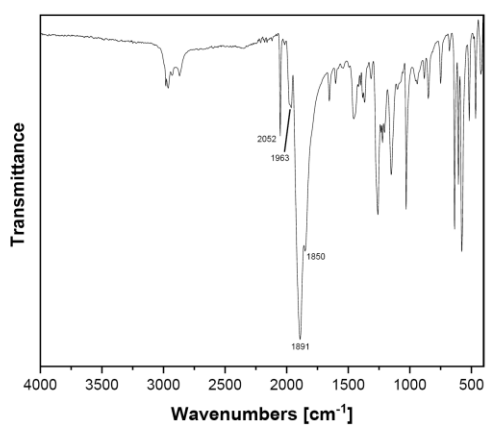
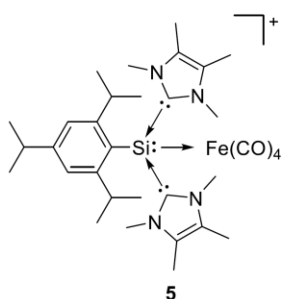


Fig. S29 Solid state FT-IR spectrum of $[\text{Tipp-Si}(\text{IMe}_4)_2\text{-W}(\text{CO})_5]\text{OTf}$ (**4**).

1.4 Synthesis of [Tipp-Si(IME₄)₂-Fe(CO)₄]OTf (5)

$\text{Fe}_2(\text{CO})_9$ (57.9 mg, 159.0 μmol , 1.0 eq) was mixed with [Tipp-Si(IME₄)₂]OTf (1) (100.0 mg, 159.0 μmol , 1.0 eq) and suspended in 5 mL C₆H₅F. After stirring for 4 hours at r.t. the pale brown cloudy solution was filtered and the solvent and Fe(CO)₅ was removed under reduced pressure. The residue was extracted with 2 mL C₆H₅F, filtered and then stored over night at -35 °C. The microcrystalline precipitate was collected by filtration,

washed with hexane (2x, 3 mL) and after drying under vacuum the complex **5** (91.2 mg, 114.5 μmol , 72%) was obtained as a pale beige air- and moisture sensitive solid.

Single crystals suitable for XRD analysis of compound **5** were obtained by cooling a concentrated solution of **5** in C₆H₅F to -35 °C.

¹H NMR (400 MHz, THF-*d*₈, 300 K): δ [ppm] = 7.16 (s, 2H, C_{ar}H), 3.70 (s, 12H, N_{NHC}CH₃), 3.15 (sept, *J* = 6.5 Hz, 2H, C_{ortho}H(CH₃)₂), 2.91 (sept, *J* = 6.9 Hz, 1H, C_{para}H(CH₃)₂), 2.31 (s, 12H, C_{NHC}CH₃), 1.24 (d, *J* = 6.9 Hz, 6H, C_{para}H(CH₃)₂), 1.09 (d, *J* = 6.5 Hz, 12H, C_{ortho}H(CH₃)₂).

¹³C{¹H} NMR (126 MHz, THF-*d*₈, 300 K): δ [ppm] = 217.4 (CO), 157.0, 153.0, 152.0, 132.6, 131.9, 123.9, 122.3 (q, *J*_{CF} = 322.4 Hz, CF₃). 36.8, 35.8, 35.0, 24.0, 9.1.

²⁹Si{¹H} NMR (99 MHz, THF-*d*₈, 300 K): δ [ppm] = 5.4.

FT-IR (solid): $\tilde{\nu}$ [cm⁻¹] = 2021 (s), 1943 (m), 1903 (s), 1887 (s).

EA: C₃₄H₄₇N₄SiSO₇F₃Fe·C₆H₅F calculated [%]: C (54.42), H (5.79), N (6.19), S (3.54).
measured [%]: C (54.50), H (5.72), N (6.02), S (3.85).

M.P.: 195-196 °C (decomposition, change to black oil).

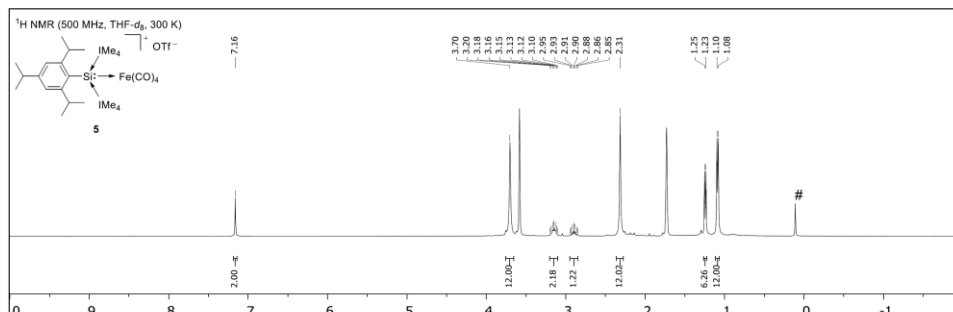


Fig. S30 ¹H NMR spectrum of [Tipp-Si(Ime₄)₂->Fe(CO)₄]OTf (**5**) in THF-*d*₈ at 300 K.

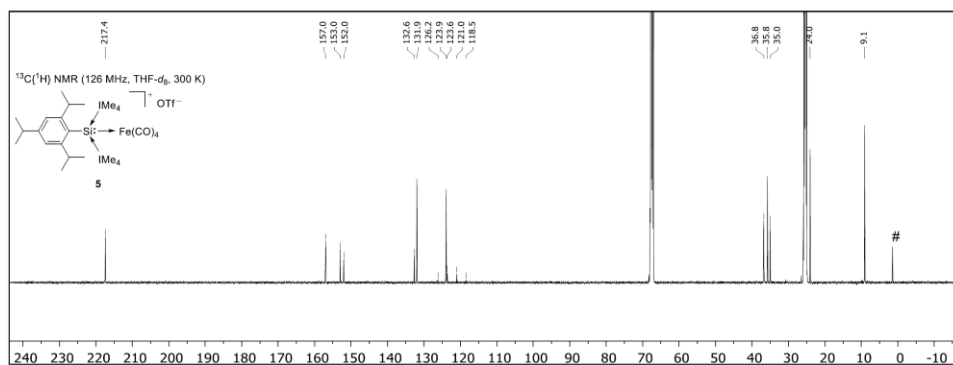


Fig. S31 ¹³C{¹H} NMR spectrum of [Tipp-Si(Ime₄)₂->Fe(CO)₄]OTf (**5**) in THF-*d*₈ at 300 K.

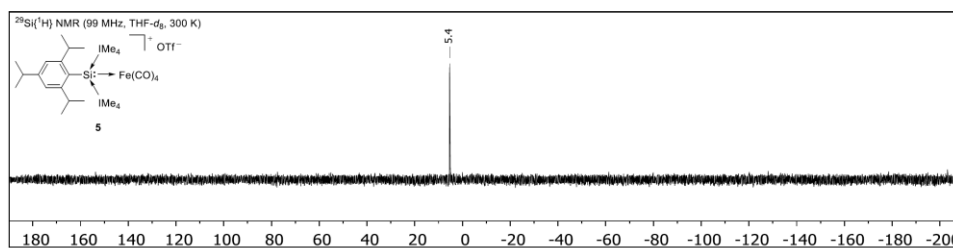


Fig. S32 ²⁹Si{¹H} NMR spectrum of [Tipp-Si(Ime₄)₂->Fe(CO)₄]OTf (**5**) in THF-*d*₈ at 300 K.

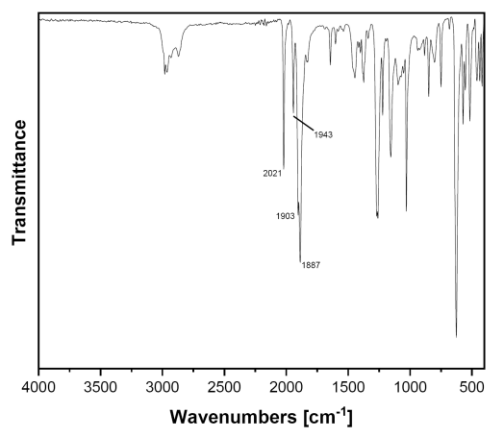


Fig. S33 Solid state FT-IR spectrum of [Tipp-Si(IME₄)₂→Fe(CO)₄]OTf (**5**).

2. X-ray Crystallographic Data

General Information

The X-ray intensity data of **1a-OTf**, **1b-OTf**, **3** and **5** were collected on an X-ray single crystal diffractometer equipped with a CMOS detector (Bruker Photon-100), an IMS microsource with MoK α radiation ($\lambda = 0.71073 \text{ \AA}$) and a Helios mirror optic by using the APEX III software package.^{S3} The measurements were performed on single crystals coated with the perfluorinated ether Fomblin® Y. The crystals were fixed on the top of a micro sampler, transferred to the diffractometer and frozen under a stream of cold nitrogen. A matrix scan was used to determine the initial lattice parameters. Reflections were merged and corrected for Lorenz and polarization effects, scan speed, and background using SAINT.^{S4} Absorption corrections, including odd and even ordered spherical harmonics were performed using SADABS.^{S4} Space group assignments were based upon systematic absences, E statistics, and successful refinement of the structures. Structures were solved by direct methods with the aid of successive difference Fourier maps, and were refined against all data using the APEX III software in conjunction with SHELXL-2014^{S5} and SHELXLE.^{S6} All H atoms were placed in calculated positions and refined using a riding model, with methylene and aromatic C–H distances of 0.99 and 0.95 Å, respectively, and $U_{\text{iso}}(\text{H}) = 1.2 \cdot U_{\text{eq}}(\text{C})$. Full-matrix least-squares refinements were carried out by minimizing $\Delta w(F_o^2 - F_c^2)^2$ with SHELXL-97 weighting scheme.^{S7} Neutral atom scattering factors for all atoms and anomalous dispersion corrections for the non-hydrogen atoms were taken from International Tables for Crystallography.^{S8} The images of the crystal structures were generated by Mercury.^{S9} The CCDC numbers CCDC-1949742 (**1a-OTf**), CCDC-1949743 (**1b-OTf**), CCDC-1949744 (**3**) and CCDC-1949745 (**5**) contain the supplementary crystallographic data for the structures. These data can be obtained free of charge from the Cambridge Crystallographic Data Centre via <https://www.ccdc.cam.ac.uk/structures/>.

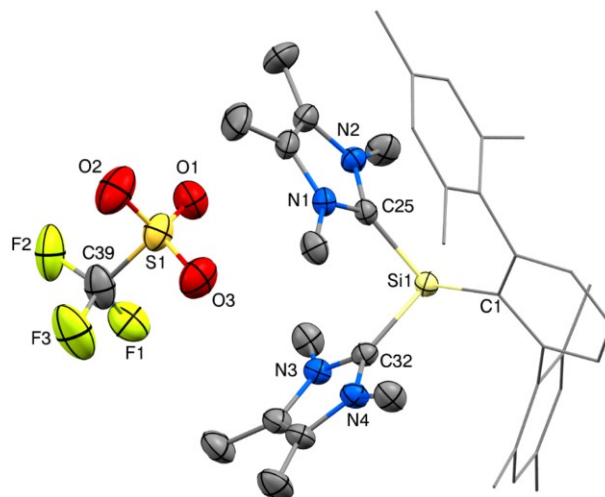
2.1 SC-XRD structure of [*m*-Ter-Si(Ime₄)₂OTf] (1a-OTf, CCDC-1949742)

Fig. S34 Ellipsoid plot (50% probability level) of the molecular structure of silyliumylidene triflate **1a-OTf**. The *m*-Ter-substituent is simplified as a wireframe and hydrogen atoms are omitted for clarity. Selected bond lengths [Å] and angles [°]: Si1–C1 1.932(2), Si1–C25 1.964(2), Si1–C32 1.940(2), C1–Si1–C25 111.7(1), C1–Si1–C32 104.0(1), C25–Si1–C32 94.3(1), sum of angles around Si1: $\sum \angle \text{Si1}$ 310.0.

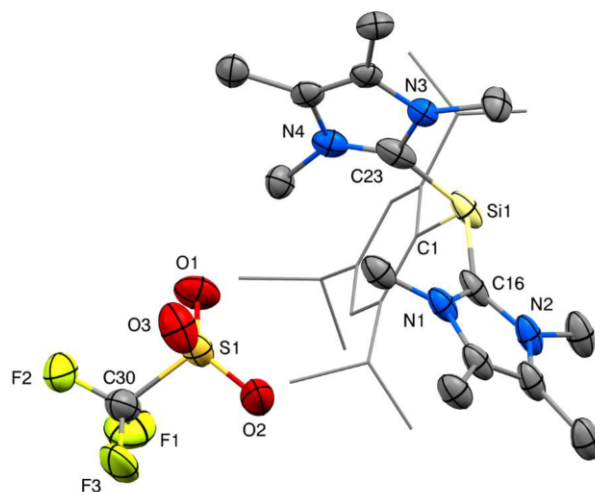
2.2 SC-XRD structure of [Tipp-Si(Ime₄)₂]OTf (1b-OTf, CCDC-1949743)

Fig. S35 Ellipsoid plot (50% probability level) of the molecular structure of silyliumylidene triflate **1b-OTf**. The Tipp-substituent is simplified as a wireframe and hydrogen atoms are omitted for clarity. Selected bond lengths [Å] and angles [°]: Si1–C1 1.892(3), Si1–C16 1.925(2), Si1–C23 1.926(3), C1–Si1–C16 111.6(1), C1–Si1–C23 102.0(1), C16–Si1–C23 99.4(1), sum of angles around Si1: $\sum \angle \text{Si1}$ 313.0.

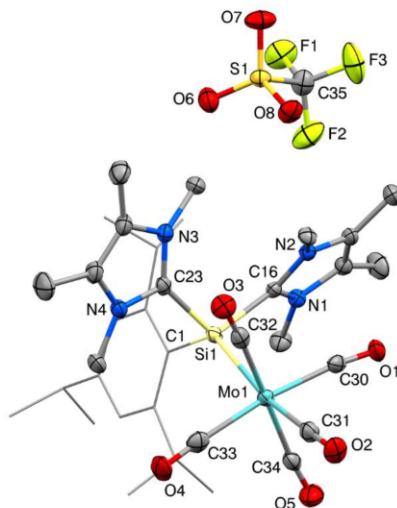
2.3 SC-XRD structure of [Tipp-Si(Ime₄)₂→Mo(CO)₅]OTf (3, CCDC-1949744)

Fig. S36 Ellipsoid plot (50% probability level) of the molecular structure of Mo(CO)₅ complex **3**·Et₂O. One out of two independent molecules in the asymmetric unit is depicted. The Tipp-substituent is simplified as a wireframe, hydrogen atoms and solvent molecules are omitted for clarity. Selected bond lengths [Å] and angles [°]: Si1–Mo1 2.673(1), Si2–Mo2 2.740(1), Si1–C1 1.942(3), Si2–C36 1.966(3), Si1–C16 1.951(2), Si2–C51 1.960(3), Si1–C23 1.962(4), Si2–C58 1.950(3), Mo1–C30 2.037(3), Mo2–C65 2.040(3), Mo1–C31 2.004(3), Mo2–C66 1.998(3), Mo1–C32 2.043(4), Mo2–C67 2.018(4), Mo1–C33 2.052(3), Mo2–C68 2.057(3), Mo1–C34 2.041(4), Mo2–C69 2.056(4), C30–O1 1.143(4), C65–O9 1.140(4), C31–O2 1.140(4), C66–O10 1.146(4), C32–O3 1.144(5), C67–O11 1.154(5), C33–O4 1.140(3), C68–O12 1.139(4), C34–O5 1.142(5), C69–O13 1.142(4), Mo1–Si1–C1 132.7(1), Mo2–Si2–C36 131.2(1), Mo1–Si1–C16 103.1(1), Mo2–Si2–C51 109.3(1), Mo1–Si1–C23 108.1(1), Mo2–Si2–C58 102.2(1), C1–Si1–C16 104.3(1), C36–Si2–C51 98.5(1), C1–Si1–C23 98.9(1), C36–Si2–C58 108.6(1), C16–Si1–C23 108.1(1), C51–Si2–C58 104.8(1), Si1–Mo1–C31 169.4(1), Si2–Mo2–C66 171.5(1); sum of angles around Mo1 of in-plane CO ligands (C30, C32, C33, C34) = 359.97°, sum of angles around Mo2 of in-plane CO ligands (C65, C67, C68, C69) = 359.52°.

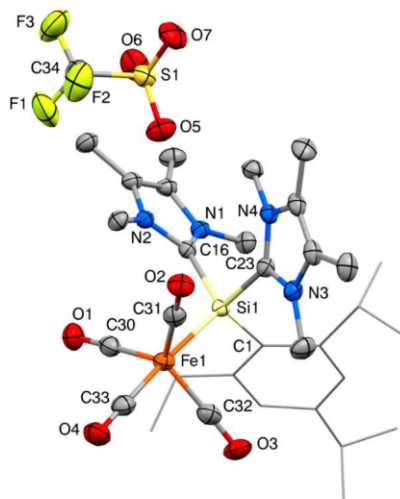
2.4 SC-XRD structure of [Tipp-Si(IME₄)₂→Fe(CO)₄]OTf (5, CCDC-1949745)

Fig. S37 Ellipsoid plot (50% probability level) of the molecular structure of Fe(CO)₄ complex **5**·C₆H₅F. The Tipp-substituent is simplified as a wireframe, hydrogen atoms and solvent molecules are omitted for clarity. Selected bond lengths [Å] and angles [°]: Si1–Fe1 2.349(1), Si1–C1 1.91(2), Si1–C16 1.949(2), Si1–C23 1.956(2), Fe1–C30 1.768(2), Fe1–C31 1.775(2), Fe1–C32 1.781(3), Fe1–C33 1.790(3), C30–O1 1.160(3), C31–O2 1.157(3), C32–O3 1.154(3), C33–O4 1.146(3), Fe1–Si1–C1 115.5(6), Fe1–Si1–C16 116.5(1), Fe1–Si1–C23 106.4(1), C1–Si1–C16 104.9(6), C1–Si1–C23 112.1(6), C16–Si1–C23 100.6(1), Si1–Fe1–C33 176.5(1); Sum of angles around Fe1 of in-plane CO ligands (C30, C31, C32) = 359.52°.

Table S1 Crystal data and structural refinement parameters for compounds 1a-OTf, 1b-OTf, 3 and 5.

Compound #	1a-OTf	1b-OTf	3-EtO	5-C ₆ H ₅ F
CCDC #	CCDC-1949742	CCDC-1949743	CCDC-1949744	CCDC-1949745
Chemical formula	C ₂₃ H ₁₈ F ₁₀ N ₂ O ₇ SSi	C ₂₃ H ₁₈ F ₁₀ N ₂ O ₇ SSi	C ₂₇ H ₂₄ F ₁₀ N ₂ O ₇ Si ₂	C ₂₇ H ₁₈ F ₁₀ N ₂ O ₇ Si ₂
Formula weight	738.97	628.87	1803.83	1688.60
Temperature	100(2) K	100(2) K	100(2) K	100(2) K
Wavelength	0.71073 Å	0.71073 Å	0.71073 Å	0.71073 Å
Crystal size	0.320 × 0.411 × 0.483 mm	0.219 × 0.372 × 0.450 mm	0.106 × 0.172 × 0.178 mm	0.150 × 0.193 × 0.274 mm
Crystal habit	clear yellow fragment	clear orange fragment	clear pale yellow plate	clear colourless fragment
Crystal system	monoclinic	triclinic	triclinic	monoclinic
Space group	P 2 ₁ /c	P -1	P -1	P 2 ₁ /n
Unit cell dimensions	a = 15.564(7) Å, α = 90° b = 14.250(6) Å, β = 96.16(3)° c = 17.466(9) Å, γ = 90°	a = 9.525(10) Å, α = 96.743(3)° b = 11.254(3)(12) Å, β = 96.448(3)° c = 18.3058(18) Å, γ = 104.553(4)°	a = 13.752(5) Å, α = 110.156(13)° b = 16.774(7) Å, β = 104.315(13)° c = 21.449(9) Å, γ = 95.770(13)°	a = 9.672(6) Å, α = 90° b = 28.6808(14) Å, β = 92.439(2)° c = 14.6856(7) Å, γ = 90°
Volume	3863(3) Å ³	1867(13) Å ³	4406(3) Å ³	4069(7) Å ³
Z	4	2	2	2
Density (calculated)	1.271 g/cm ³	1.119 g/cm ³	1.360 g/cm ³	1.378 g/cm ³
Absorption coefficient	0.171 mm ⁻¹	0.166 mm ⁻¹	0.437 mm ⁻¹	0.518 mm ⁻¹
F(000)	1568	672	1876	1770
Diffractometer	Bruker D8 Venture Duo IMS	Bruker D8 Venture Duo IMS	Bruker D8 Venture Duo IMS	Bruker D8 Venture Duo IMS
Radiation source	IMS microsource, Mo	IMS microsource, Mo	IMS microsource, Mo	IMS microsource, Mo
Theta range for data collection	2.20 to 25.48°	1.89 to 25.68°	1.99 to 25.68°	2.22 to 25.68°
Index ranges	-18<h<=18, -17<k<=17, -21<l<=21	-11<h<=11, -13<k<=13, -22<l<=22	-16<h<=16, -20<k<=20, -26<l<=26	-11<h<=11, -34<k<=34, -17<l<=17
Reflections collected	127048	71526	186471	188211
Independent reflections	7090 [R(int) = 0.0694]	7099 [R(int) = 0.0476]	16724 [R(int) = 0.0933]	7711 [R(int) = 0.0506]
Coverage of independent reflections	98.8%	99.9%	99.9%	99.9%
Absorption correction	Multi-Scan	Multi-Scan	Multi-Scan	Multi-Scan
Refinement method	Full-matrix least-squares on F ²	Full-matrix least-squares on F ²	Full-matrix least-squares on F ²	Full-matrix least-squares on F ²
Refinement program	SHELXL-2016/6 (Sheldrick, 2016)	SHELXL-2016/6 (Sheldrick, 2016)	SHELXL-2016/6 (Sheldrick, 2016)	SHELXL-2016/6 (Sheldrick, 2016)
Function minimized	Σ w(F _o ² - F _c ²) ²	Σ w(F _o ² - F _c ²) ²	Σ w(F _o ² - F _c ²) ²	Σ w(F _o ² - F _c ²) ²
Data / restraints / parameters	7090 / 0 / 474	7099 / 201 / 582	16724 / 0 / 1030	7711 / 94 / 594
Goodness-of-fit on F ²	1.035	1.026	1.055	1.112
Final R indices	6074 data; I>2σ(I); R1 = 0.0420, wR2 = 0.1060	5800 data; I>2σ(I); R1 = 0.0502, wR2 = 0.1156	13856 data; I>2σ(I); R1 = 0.0411, wR2 = 0.0916	6595 data; I>2σ(I); R1 = 0.0373, wR2 = 0.0867
Weighting scheme	all data: R1 = 0.0560, wR2 = 0.1135 w = 1/(σ ² (F _o ²) + (0.0560P) ² + 2.0762P)	all data: R1 = 0.0635, wR2 = 0.1258 w = 1/(σ ² (F _o ²) + (0.0448P) ² + 1.8306P)	all data: R1 = 0.0643, wR2 = 0.0976 w = 1/(σ ² (F _o ²) + (0.0374P) ² + 6.1588P)	all data: R1 = 0.0493, wR2 = 0.0980 w = 1/(σ ² (F _o ²) + (0.0319P) ² + 4.5088P)
Largest diff. peak and hole	where P = (F _o ² + 2F _c ²)/3	where P = (F _o ² + 2F _c ²)/3	where P = (F _o ² + 2F _c ²)/3	where P = (F _o ² + 2F _c ²)/3
R.M.S. deviation from mean	0.329 and -0.403 eÅ ⁻³	0.814 and -0.706 eÅ ⁻³	0.802 and -0.597 eÅ ⁻³	0.498 and -0.359 eÅ ⁻³
	0.053 eÅ ⁻³	0.046 eÅ ⁻³	0.073 eÅ ⁻³	0.053 eÅ ⁻³

S31

3. DFT Calculations

DFT calculations were carried out at the B97-D/Def2-TZVP//B97-D/def2-SVP level of theory using Gaussian 09.^{S10-13} For consistency reasons with our previous study^{S14}, σ -donor strength and π -acceptor ability was calculated at the B97-D/Def2-TZVP//B97-D/6-31G* level of theory.^{S15} Stationary points on the potential energy surface were characterized by harmonic vibrational frequency calculations. Table S2-S5 contain the respective relevant data for the NBO analysis of complexes **2-5**. Table S6 contains the calculated Si–M and Si–C_{NHC} bond lengths, WBIs/MBOs and NPA charges. Table S7 contains the calculated CO stretching frequencies for complexes **2-5**. Fig. S38-S41 contain the respective HOMOs and LUMOs for complexes **2-5**.

Table S2 NBO-Analysis of the central [Tipp–Si(Ime₄)₂→Cr] moiety in silyliumylidene Cr(CO)₅ complex **2**.

2	Occupation	Atom	Polarization	s-character	p-character	d-character
Bond	1.69	Si	60.37%	33.37%	66.61%	0.03%
		Cr	39.63%	14.01%	49.56%	36.43%
Bond	1.95	Si	24.97%	20.75%	78.51%	0.74%
		C _{NHC}	75.03%	44.31%	55.68%	0.01%
Bond	1.95	Si	24.81%	19.72%	79.53%	0.75%
		C _{NHC}	75.19%	43.81%	56.18%	0.01%
Bond	1.93	Si	29.37%	26.44%	72.98%	0.58%
		C _{aryl}	70.63%	29.06%	70.93%	0.02%

Table S3 NBO-Analysis of the central [Tipp–Si(Ime₄)₂→Mo] moiety in silyliumylidene Mo(CO)₅ complex **3**.

3	Occupation	Atom	Polarization	s-character	p-character	d-character
Bond	1.71	Si	64.73%	35.29%	64.69%	0.03%
		Mo	35.27%	16.48%	53.49%	30.01%
Bond	1.95	Si	24.87%	19.68%	79.57%	0.75%
		C _{NHC}	75.13%	44.45%	55.54%	0.01%
Bond	1.95	Si	24.66%	18.82%	80.42%	0.76%
		C _{NHC}	75.34%	44.03%	55.97%	0.00%
Bond	1.94	Si	29.35%	26.36%	73.06%	0.58%
		C _{aryl}	70.65%	29.20%	70.79%	0.01%

Table S4 NBO-Analysis of the central [Tipp–Si(IME₄)₂→W] moiety in silyliumylidene W(CO)₅ complex **4**.

4	Occupation	Atom	Polarization	s-character	p-character	d-character
Bond	1.70	Si	68.95%	36.86%	63.11%	0.04%
		W	31.05%	17.01%	53.39%	29.58%
Bond	1.95	Si	24.84%	18.92%	80.32%	0.76%
		C _{NHC}	75.16%	44.65%	55.34%	0.01%
Bond	1.95	Si	75.34%	44.22%	55.78%	0.00%
		C _{NHC}	24.66%	18.16%	81.07%	0.77%
Bond	1.94	Si	29.43%	26.18%	73.24%	0.57%
		C _{aryl}	70.57%	29.44%	70.55%	0.02%

Table S5 NBO-Analysis of the central [Tipp–Si(IME₄)₂→Fe] moiety in silyliumylidene Fe(CO)₄ complex **5**.

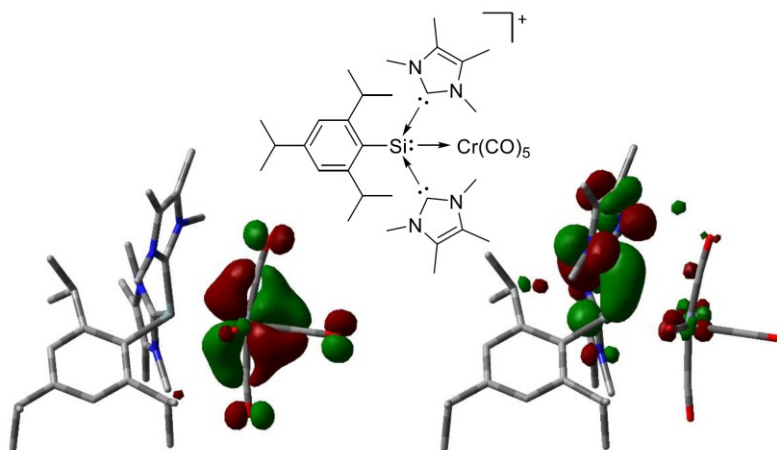
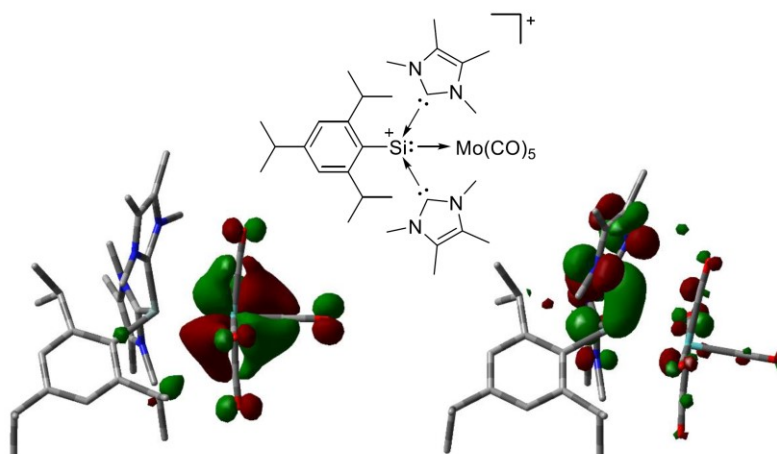
5	Occupation	Atom	Polarization	s-character	p-character	d-character
Bond	1.70	Si	53.01%	31.81%	68.11%	0.07%
		Fe	46.99%	15.60%	50.47%	33.92%
Bond	1.61	Si	1.90%	0.03%	59.74%	40.22%
		Fe	98.10%	0.00%	1.61%	98.39%
Bond	1.83	Si	19.63%	20.59%	53.28%	26.13%
		C _{NHC}	80.37%	44.44%	55.55%	0.01%
Bond	1.87	Si	21.18%	20.09%	61.96%	17.96%
		C _{NHC}	78.82%	44.29%	55.70%	0.01%
Bond	1.93	Si	28.40%	27.92%	70.78%	1.30%
		C _{aryl}	71.60%	30.36%	69.62%	0.02%

Table S6 Calculated Si–M and Si–C_{NHC} bond lengths [Å], NPA charges of Si and Metal atoms, Wiberg Bond Index (WBI) and Mayer Bond Order (MBO) in silyliumylidene transition metal complexes **2-5**.

#	M	Bond length [Å]			NPA charge		WBI/MBO		
		Si–M	Si–C _{NHC}	Si–C _{NHC}	Si	Metal	Si–M	Si–C _{NHC}	Si–C _{NHC}
2	Cr	2.541	1.994	1.959	+1.24	–2.61	0.69/0.77	0.71/0.83	0.73/0.85
3	Mo	2.686	1.990	1.958	+1.18	–2.25	0.66/0.56	0.71/0.84	0.74/0.87
4	W	2.679	1.986	1.953	+1.12	–1.66	0.63/0.65	0.72/0.84	0.74/0.86
5	Fe	2.340	1.974	1.961	+1.32	–1.59	0.78/1.02	0.69/0.81	0.70/0.82

Table S7 Calculated CO stretching frequencies [cm^{-1}] of silyliumylidene $\text{M}(\text{CO})_n$ complexes 2-5.

M	CO stretching frequency [cm^{-1}]
Cr	2026, 1964, 1946, 1915, 1907
Mo	2039, 1967, 1961, 1921, 1916
W	2034, 1961, 1954, 1913, 1907
Fe	2030, 1962, 1919, 1903

**Fig. S38** HOMO (left, -7.31 eV) and LUMO (right, -4.55 eV) of silyliumylidene $\text{Cr}(\text{CO})_5$ complex 2.**Fig. S39** HOMO (left, -7.39 eV) and LUMO (right, -4.56 eV) of silyliumylidene $\text{Mo}(\text{CO})_5$ complex 3.

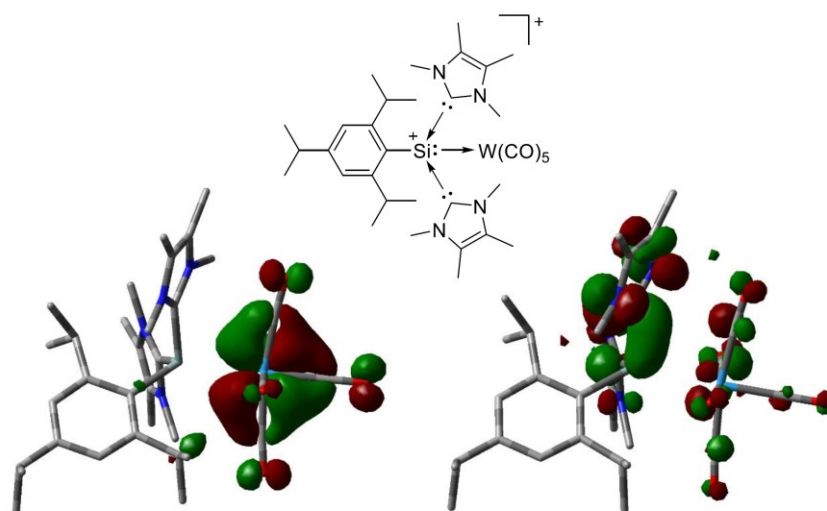


Fig. S40 HOMO (left, -7.39 eV) and LUMO (right, -4.60 eV) of silyliumylidene W(CO)₅ complex 4.

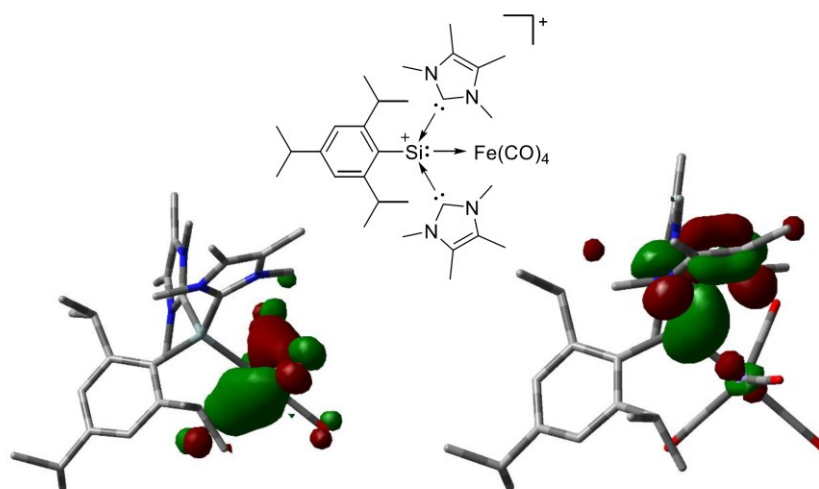


Fig. S41 HOMO (left, -7.08 eV) and LUMO (right, -4.76 eV) of silyliumylidene Fe(CO)₄ complex 5.

11. Appendix

Table S8 Cartesian coordinates of 2.

Atomtype	X Coordinate [Å]	Y Coordinate [Å]	Z Coordinate [Å]
C	1.341943	-2.287068	3.20611
N	0.511842	-1.830169	2.179619
C	1.030136	-0.706214	1.601091
N	2.204892	-0.472156	2.261178
C	2.415081	-1.427053	3.25416
C	3.234384	0.507478	1.91386
C	-0.691972	-2.549304	1.738558
Si	0.381078	0.0304	-0.094143
C	0.438376	2.020299	0.027858
N	0.037053	2.737173	-1.063168
C	0.229774	4.102106	-0.877659
C	0.754107	4.250106	0.383324
N	0.867602	2.965298	0.920049
C	-0.51624	2.203605	-2.308323
C	1.256237	2.807271	2.318043
C	-0.099737	5.120515	-1.918433
C	1.141147	5.480308	1.135727
C	3.641827	-1.442902	4.103806
C	1.050655	-3.498193	4.030665
Cr	2.121162	-0.862609	-1.716583
C	1.171415	-0.382477	-3.283978
O	0.688423	-0.112534	-4.304405
C	2.838804	0.868267	-1.569528
O	3.257514	1.948627	-1.432535
C	3.425875	-1.444493	-2.925292
O	4.233152	-1.795402	-3.677713
C	3.269628	-1.550475	-0.404109
O	4.013157	-2.063716	0.332043
C	1.295359	-2.556104	-1.542566
O	0.864837	-3.618479	-1.353672
C	-1.579213	-0.164083	0.024839
C	-2.365637	-0.828377	-0.976683
C	-3.762223	-0.934727	-0.826639
C	-4.452286	-0.424339	0.279065
C	-3.686783	0.222757	1.256987
C	-2.289797	0.366492	1.157263
C	-1.80795	-1.484126	-2.239745
C	-2.373605	-0.844284	-3.527031
C	-5.961178	-0.568665	0.40578
C	-6.68821	0.177476	-0.733788
C	-1.640337	1.118761	2.320168
C	-2.071082	2.601142	2.319715
C	-2.083339	-3.004298	-2.251851
C	-6.377615	-2.054663	0.446569

S36

11. Appendix

C	-1.912596	0.470275	3.694371
H	-4.331922	-1.448419	-1.609334
H	-4.203106	0.635615	2.13335
H	-0.720051	-1.344602	-2.245061
H	-1.721455	-3.493738	-1.330317
H	-1.57371	-3.478641	-3.110975
H	-3.167546	-3.205468	-2.344319
H	-2.214479	0.248981	-3.555642
H	-3.461757	-1.026374	-3.610156
H	-1.884556	-1.281825	-4.416307
H	-6.259627	-0.101907	1.365625
H	-7.472913	-2.145669	0.574708
H	-5.882302	-2.587968	1.280093
H	-6.102487	-2.563524	-0.497646
H	-6.415714	1.249746	-0.74949
H	-7.784796	0.096281	-0.609618
H	-6.42441	-0.25842	-1.716987
H	-0.555559	1.076428	2.18365
H	-1.372486	1.019847	4.489781
H	-1.576514	-0.58281	3.715411
H	-2.988545	0.488843	3.947605
H	-1.598448	3.151875	3.156181
H	-3.166368	2.683248	2.447347
H	-1.806201	3.099078	1.368591
H	-1.360403	2.839931	-2.621297
H	-0.894157	1.186367	-2.150375
H	0.25371	2.198949	-3.097277
H	0.164095	6.127668	-1.555514
H	-1.179666	5.116387	-2.16469
H	0.458828	4.932926	-2.855691
H	2.208094	5.458718	1.431605
H	0.539535	5.600577	2.058203
H	0.979606	6.370553	0.505689
H	0.578446	3.411318	2.943191
H	2.290179	3.162034	2.461807
H	1.173103	1.761022	2.624124
H	3.430182	1.166025	2.775663
H	2.909714	1.101433	1.051121
H	4.163148	-0.022632	1.652131
H	3.574631	-2.249846	4.851873
H	3.78231	-0.485105	4.641427
H	4.544853	-1.620169	3.487111
H	0.071471	-3.419987	4.541334
H	1.830211	-3.619178	4.801029
H	1.038858	-4.418179	3.413501
H	-1.604832	-2.029004	2.070875
H	-0.662386	-3.56729	2.154829

S37

11. Appendix

H	-0.703632	-2.615144	0.641361
---	-----------	-----------	----------

Table S9 Cartesian coordinates of **3**.

Atomtype	X Coordinate [Å]	Y Coordinate [Å]	Z Coordinate [Å]
C	1.000747	1.394292	3.8415
N	0.250769	0.766874	2.842939
C	0.758254	1.04706	1.605829
N	1.846377	1.843161	1.837566
C	2.011308	2.074276	3.202414
C	2.854338	2.264782	0.865351
C	-0.849834	-0.164704	3.12413
Si	0.226891	0.091903	-0.0188
C	0.15718	1.398077	-1.519001
N	-0.18813	0.930751	-2.755379
C	-0.096196	1.926731	-3.722298
C	0.309214	3.064733	-3.068732
N	0.449708	2.71961	-1.721711
C	-0.647607	-0.415436	-3.098949
C	0.712815	3.763631	-0.73594
C	-0.400758	1.685035	-5.163556
C	0.563675	4.442237	-3.585035
C	3.149161	2.870081	3.74931
C	0.700599	1.280315	5.300587
Mo	2.291148	-1.591932	-0.361834
C	1.416654	-2.625102	-1.908746
O	0.990291	-3.258915	-2.780874
C	2.951841	-0.152141	-1.645117
O	3.284208	0.710356	-2.353879
C	3.937944	-2.721553	-0.700163
O	4.886059	-3.352816	-0.906883
C	3.286848	-0.813398	1.237168
O	3.87523	-0.457399	2.176071
C	1.586783	-2.935893	1.032978
O	1.26159	-3.667088	1.8698
C	-1.716512	-0.148445	0.169587
C	-2.344529	-1.432527	0.048449
C	-3.742739	-1.551228	0.169379
C	-4.58123	-0.457181	0.417191
C	-3.967839	0.79656	0.536611
C	-2.576485	0.975479	0.416478
C	-1.598778	-2.74823	-0.174456
C	-2.058237	-3.478723	-1.455388
C	-6.085606	-0.628937	0.561685
C	-6.709218	-1.230154	-0.715611
C	-2.096887	2.420638	0.561048

S38

11. Appendix

C	-2.593849	3.283336	-0.618711
C	-1.758998	-3.681268	1.046017
C	-6.426381	-1.486799	1.799662
C	-2.491476	3.057163	1.911017
H	-4.191684	-2.546357	0.073026
H	-4.602628	1.671361	0.729071
H	-0.527881	-2.521981	-0.28501
H	-1.411702	-3.197987	1.977632
H	-1.172164	-4.607216	0.905742
H	-2.819993	-3.963854	1.183903
H	-1.975743	-2.837351	-2.351645
H	-3.112544	-3.803319	-1.370916
H	-1.439216	-4.379155	-1.622823
H	-6.520744	0.378913	0.714375
H	-7.523002	-1.572743	1.920584
H	-6.006204	-1.043767	2.722546
H	-6.014501	-2.509078	1.69172
H	-6.485079	-0.608252	-1.602909
H	-7.808003	-1.305729	-0.609325
H	-6.316109	-2.248531	-0.90139
H	-1.002246	2.417636	0.541591
H	-2.074756	4.080222	1.988967
H	-2.107848	2.464786	2.762466
H	-3.589353	3.133903	2.017642
H	-2.237644	4.327617	-0.523663
H	-3.699037	3.311293	-0.638825
H	-2.250742	2.875585	-1.587603
H	-1.640913	-0.343352	-3.574525
H	-0.736058	-1.034295	-2.199453
H	0.063255	-0.887836	-3.796814
H	-0.25412	2.612441	-5.741478
H	-1.446862	1.350859	-5.306864
H	0.2595	0.90436	-5.588571
H	1.600193	4.770945	-3.375221
H	-0.122303	5.183363	-3.129489
H	0.412899	4.465539	-4.677004
H	-0.052602	4.549907	-0.841755
H	1.708505	4.203833	-0.910499
H	0.654662	3.356416	0.277469
H	2.955496	3.362324	0.883455
H	2.570105	1.930969	-0.139023
H	3.824016	1.813678	1.129611
H	3.046369	2.976494	4.841803
H	3.193043	3.884045	3.306667
H	4.114852	2.368159	3.542672
H	-0.324437	1.625993	5.536702
H	1.411017	1.898545	5.874077

S39

11. Appendix

H	0.797652	0.23596	5.657094
H	-1.820671	0.276098	2.846994
H	-0.837551	-0.406731	4.197225
H	-0.707225	-1.091337	2.546061

Table S10 Cartesian coordinates of **4**.

Atomtype	X Coordinate [Å]	Y Coordinate [Å]	Z Coordinate [Å]
C	0.719414	1.525275	3.87702
N	-0.00512	0.874573	2.874881
C	0.463831	1.214122	1.638311
N	1.498511	2.077732	1.871536
C	1.670884	2.287148	3.238749
C	2.446241	2.605104	0.890732
C	-1.02935	-0.143129	3.142998
Si	0.003843	0.231446	0.014832
C	-0.135799	1.52839	-1.482893
N	-0.381396	1.034868	-2.731879
C	-0.336845	2.036793	-3.695356
C	-0.070038	3.205979	-3.025214
N	0.041608	2.871421	-1.673229
C	-0.662777	-0.355408	-3.089659
C	0.176926	3.930242	-0.678278
C	-0.540788	1.771069	-5.149974
C	0.082864	4.602532	-3.530208
C	2.762712	3.144187	3.786252
C	0.454923	1.353316	5.337298
W	2.199147	-1.270814	-0.302878
C	1.406516	-2.447483	-1.813385
O	1.045773	-3.151131	-2.662759
C	2.711665	0.19011	-1.653184
O	2.938656	1.066703	-2.388634
C	3.937347	-2.297333	-0.633602
O	4.925258	-2.86739	-0.837757
C	3.210979	-0.376387	1.247544
O	3.824482	0.037849	2.147418
C	1.589463	-2.595938	1.177026
O	1.290992	-3.28688	2.059038
C	-1.907177	-0.1784	0.183262
C	-2.420362	-1.513178	0.066899
C	-3.805546	-1.750232	0.160756
C	-4.740323	-0.729432	0.373262
C	-4.238532	0.572665	0.495771
C	-2.86493	0.868782	0.406409
C	-1.561637	-2.762805	-0.125136
C	-1.925002	-3.534393	-1.411944

S40

11. Appendix

C	-6.229297	-1.024859	0.469344
C	-6.763855	-1.626491	-0.847797
C	-2.511681	2.348095	0.567923
C	-3.070182	3.178662	-0.607033
C	-1.670237	-3.700384	1.096837
C	-6.53928	-1.94896	1.66632
C	-2.972627	2.930207	1.921187
H	-4.164615	-2.781893	0.070376
H	-4.949694	1.391372	0.667586
H	-0.513074	-2.446146	-0.209942
H	-1.402174	-3.181837	2.035259
H	-0.991128	-4.564724	0.98089
H	-2.701864	-4.086178	1.203381
H	-1.853533	-2.897126	-2.312031
H	-2.95721	-3.929013	-1.359467
H	-1.240481	-4.391346	-1.54772
H	-6.747026	-0.05985	0.639805
H	-7.629076	-2.122447	1.747829
H	-6.183152	-1.507487	2.616442
H	-6.047487	-2.932848	1.539415
H	-6.568479	-0.953893	-1.704376
H	-7.854825	-1.798246	-0.778982
H	-6.279304	-2.599669	-1.058119
H	-1.42035	2.438303	0.561434
H	-2.649563	3.985325	2.015732
H	-2.544641	2.362829	2.768459
H	-4.073804	2.906723	2.01833
H	-2.816276	4.250288	-0.491211
H	-4.172533	3.10274	-0.644107
H	-2.676731	2.819862	-1.576316
H	-1.554354	-0.381986	-3.738605
H	-0.869944	-0.948133	-2.190861
H	0.197718	-0.787612	-3.626131
H	-0.429366	2.705769	-5.723953
H	-1.54988	1.361522	-5.351872
H	0.198949	1.040564	-5.530538
H	1.079242	5.01747	-3.281915
H	-0.680319	5.279631	-3.098706
H	-0.029441	4.618199	-4.62688
H	-0.668697	4.629476	-0.784614
H	1.119791	4.477642	-0.841632
H	0.158571	3.51019	0.331212
H	2.425565	3.707185	0.904386
H	2.193515	2.23473	-0.109392
H	3.461716	2.266939	1.148463
H	2.66143	3.234783	4.8803
H	2.74356	4.162485	3.352235

S41

11. Appendix

H	3.753984	2.700379	3.567904
H	-0.588096	1.616347	5.599659
H	1.128561	2.007617	5.9151
H	0.635017	0.310344	5.664573
H	-2.026837	0.214771	2.843087
H	-1.019529	-0.376447	4.217906
H	-0.796297	-1.05717	2.573892

Table S11 Cartesian coordinates of **5**.

Atomtype	X Coordinate [Å]	Y Coordinate [Å]	Z Coordinate [Å]
N	-1.511046	-1.728665	-2.138968
C	-1.755197	-0.988016	-1.014645
N	-3.074526	-1.208318	-0.732837
C	-3.644548	-2.083754	-1.648088
C	-2.651085	-2.415245	-2.544273
Si	-0.446096	-0.04936	0.125848
Fe	-0.841041	-0.290939	2.419474
C	-1.584746	-1.858073	2.03837
O	-2.112362	-2.870716	1.786124
C	-3.872095	-0.577931	0.319428
C	-5.065873	-2.532647	-1.562338
C	-2.676184	-3.325415	-3.728217
C	-0.289967	-1.734247	-2.944618
C	-0.772188	1.832204	-0.31897
N	-1.717771	2.41449	-1.114728
C	-1.748559	3.796433	-0.91404
C	-0.77751	4.073232	0.022331
N	-0.188704	2.859435	0.355576
C	-2.506815	1.73783	-2.142281
C	0.90386	2.737159	1.324071
C	-0.366063	5.371787	0.632173
C	-2.690788	4.715045	-1.621645
C	1.326822	-0.456576	-0.498971
C	1.941748	-1.641261	0.024687
C	3.341747	-1.738001	0.069207
C	4.178955	-0.721512	-0.417112
C	3.568596	0.35143	-1.088831
C	2.170885	0.48379	-1.181802
C	1.134196	-2.880804	0.417195
C	1.386225	-4.00367	-0.619466
C	5.684553	-0.786446	-0.216847
C	1.648699	1.51679	-2.188881
C	2.018976	1.061578	-3.622626
C	1.411351	-3.413799	1.834576
C	2.162257	2.953445	-1.966209

S42

11. Appendix

C	-1.79048	1.211415	2.422256
O	-2.398935	2.211853	2.42586
C	0.925478	-0.128259	2.632756
O	2.067651	0.009982	2.815048
C	-1.090428	-0.539139	4.179731
O	-1.251245	-0.703356	5.312993
H	4.203386	1.092993	-1.58801
H	3.80044	-2.637171	0.499526
H	0.546421	1.530261	-2.139402
H	3.116009	1.077937	-3.76097
H	1.568835	1.740692	-4.373079
H	1.674376	0.032068	-3.826546
H	3.255571	3.004435	-2.125888
H	1.957569	3.319669	-0.947787
H	1.690062	3.646774	-2.688027
H	0.059838	-2.634864	0.354841
H	1.215565	-3.656729	-1.654619
H	0.717661	-4.862575	-0.417687
H	2.430822	-4.362592	-0.557398
H	2.480124	-3.670579	1.958328
H	0.818453	-4.330685	2.010929
H	1.133132	-2.674219	2.601641
H	-0.448194	-1.131247	-3.857919
H	-0.050955	-2.76967	-3.235045
H	0.537934	-1.316261	-2.355014
H	-2.383803	-2.798043	-4.656784
H	-3.691222	-3.732596	-3.867869
H	-1.980905	-4.177371	-3.59488
H	-5.767009	-1.676173	-1.584644
H	-5.2498	-3.090312	-0.623229
H	-5.304988	-3.197429	-2.408716
H	-4.569629	0.152359	-0.131522
H	-3.202252	-0.088072	1.038264
H	-4.448304	-1.353607	0.848768
H	1.488888	3.66981	1.310688
H	1.560864	1.903822	1.037506
H	0.497164	2.554865	2.332258
H	0.692424	5.60842	0.406871
H	-0.481768	5.347828	1.732636
H	-0.989793	6.189966	0.23617
H	-2.546115	5.745797	-1.25811
H	-3.746908	4.435449	-1.440815
H	-2.522805	4.718861	-2.71725
H	-2.841706	2.483054	-2.880342
H	-3.392205	1.242663	-1.709539
H	-1.88205	0.990151	-2.654388
H	5.926686	-1.814599	0.117811

S43

11. Appendix

C	6.481217	-0.505722	-1.506026
C	6.093626	0.185931	0.913803
H	7.176922	0.101443	1.124861
H	5.880625	1.231736	0.616276
H	5.533395	-0.02567	1.843909
H	7.563946	-0.635694	-1.320554
H	6.181826	-1.190143	-2.322433
H	6.327352	0.534697	-1.852708

Table S12 Cartesian coordinates of [Tipp-Si(Ime₄)₂]⁺.

Atomtype	X Coordinate [Å]	Y Coordinate [Å]	Z Coordinate [Å]
N	-3.388481	-1.088629	0.479765
C	-2.047484	-1.184234	0.178621
N	-1.938547	-2.334001	-0.560177
C	-3.183613	-2.945519	-0.720922
C	-4.103736	-2.151904	-0.073604
Si	-0.71046	-0.160751	1.115389
C	-1.003218	1.669939	0.54735
N	-1.866266	2.321602	-0.294984
C	-1.687098	3.706008	-0.218585
C	-0.68034	3.924426	0.693194
N	-0.286308	2.669128	1.153803
C	-2.7192	1.71658	-1.310492
C	-2.477084	4.667064	-1.044768
C	-0.059928	5.202744	1.15485
C	0.794942	2.431224	2.108688
C	-0.702422	-2.924527	-1.067311
C	-3.361847	-4.220732	-1.478556
C	-5.582323	-2.31087	0.072354
C	-3.95094	-0.067626	1.354701
C	1.057522	-0.4853	0.386884
C	1.504221	-0.032349	-0.900372
C	2.86535	-0.114733	-1.239274
C	3.824185	-0.663127	-0.36853
C	3.37451	-1.15581	0.864128
C	2.022954	-1.081197	1.259365
C	0.555492	0.509712	-1.971401
C	0.670341	-0.264242	-3.303307
C	1.662788	-1.695719	2.614559
C	1.855854	-3.226632	2.590573
C	5.291362	-0.737994	-0.765826
C	5.490915	-1.635664	-2.005784
C	2.444876	-1.051338	3.776549
C	5.879544	0.669339	-1.001531
C	0.771288	2.018043	-2.214786

S44

11. Appendix

H	3.19133	0.246626	-2.222511
H	4.104352	-1.61647	1.542787
H	-0.472724	0.358946	-1.605824
H	1.660156	-0.113362	-3.773186
H	-0.096432	0.089865	-4.019791
H	0.532816	-1.350581	-3.153062
H	1.780122	2.197524	-2.632601
H	0.686768	2.601445	-1.281625
H	0.03356	2.410105	-2.942673
H	0.58736	-1.501853	2.800999
H	1.255962	-3.690518	1.783524
H	1.545381	-3.671688	3.555574
H	2.916847	-3.491354	2.417451
H	3.533171	-1.226431	3.67526
H	2.122265	-1.481622	4.743858
H	2.279519	0.04267	3.811213
H	-0.831281	-3.193423	-2.129959
H	-0.457331	-3.837499	-0.492982
H	0.117615	-2.20238	-0.959777
H	-3.034567	-4.119449	-2.532253
H	-4.424138	-4.516818	-1.477249
H	-2.775141	-5.044936	-1.027622
H	-6.128413	-1.425177	-0.307931
H	-5.877622	-2.45756	1.130427
H	-5.922583	-3.19208	-0.496794
H	-4.12467	0.880442	0.815315
H	-3.232527	0.119262	2.179649
H	-4.906337	-0.426523	1.768933
H	1.0206	3.365612	2.645299
H	1.696017	2.065342	1.583977
H	0.471593	1.655424	2.829493
H	1.027069	5.224106	0.94397
H	-0.194814	5.355675	2.243795
H	-0.525378	6.055234	0.632648
H	-2.196764	5.703066	-0.791636
H	-3.565726	4.555021	-0.873535
H	-2.294001	4.519656	-2.127774
H	-2.423787	2.09239	-2.306331
H	-3.77895	1.976538	-1.134999
H	-2.595531	0.626015	-1.287954
H	5.838592	-1.199209	0.080029
H	6.958009	0.602718	-1.240841
H	5.37401	1.16801	-1.851599
H	5.758013	1.308822	-0.106663
H	6.566217	-1.718829	-2.254125
H	5.09214	-2.652962	-1.831668
H	4.971407	-1.209348	-2.886138

S45

11. Appendix

Table S13 Cartesian coordinates of Cr(CO)₅.

Atomtype	X Coordinate [Å]	Y Coordinate [Å]	Z Coordinate [Å]
C	1.351529	1.351424	-0.389643
O	2.168677	2.168555	-0.381964
Cr	-0.00011	0.000018	-0.350361
C	1.351175	-1.351595	-0.38962
O	2.16858	-2.168478	-0.381662
C	-1.351585	1.351433	-0.388828
O	-2.168772	2.168551	-0.380788
C	-1.351724	-1.351122	-0.389454
O	-2.168988	-2.168157	-0.381636
C	0.000318	-0.000119	1.476039
O	0.001048	-0.00054	2.638263

Table S14 Cartesian coordinates of Mo(CO)₅.

Atomtype	X Coordinate [Å]	Y Coordinate [Å]	Z Coordinate [Å]
C	1.426312	-1.495037	-0.339144
O	2.224523	-2.33025	-0.316976
Mo	-0.000103	-0.000297	-0.325834
C	-1.495662	-1.425962	-0.339082
O	-2.331514	-2.223574	-0.317257
C	1.494776	1.425713	-0.339895
O	2.329997	2.22402	-0.31831
C	-1.425897	1.494958	-0.338939
O	-2.223487	2.330768	-0.316783
C	0.00031	0.000111	1.61944
O	0.001145	0.000758	2.783169

Table S15 Cartesian coordinates of W(CO)₅.

Atomtype	X Coordinate [Å]	Y Coordinate [Å]	Z Coordinate [Å]
C	-1.522042	1.449408	-0.180621
O	-2.356494	2.251138	-0.18974
W	-0.018723	0.00157	-0.225523
C	1.459148	1.471306	-0.340602
O	2.297887	2.265066	-0.406253
C	-1.446306	-1.505123	-0.347151
O	-2.238491	-2.346082	-0.414523
C	0.011402	-0.029932	1.715785
O	0.037912	-0.046118	2.876527
C	1.52461	-1.39377	-0.282324

11. Appendix

O	2.412264	-2.132441	-0.203738
---	----------	-----------	-----------

Table S16 Cartesian coordinates of Fe(CO)₄.

Atomtype	X Coordinate [Å]	Y Coordinate [Å]	Z Coordinate [Å]
C	0.000997	-0.000413	1.361597
O	0.001629	-0.000319	2.521815
Fe	-0.000441	-0.000061	-0.362033
C	1.022229	-1.502049	-0.435893
O	1.674509	-2.45859	-0.462994
C	-1.812998	-0.134083	-0.435415
O	-2.967598	-0.219986	-0.460839
C	0.789484	1.636582	-0.435695
O	1.293108	2.679065	-0.46232

Table S17 Cartesian coordinates of [Tipp-Si(IME₄)₂]⁺→Ni(CO)₃.

Atomtype	X Coordinate [Å]	Y Coordinate [Å]	Z Coordinate [Å]
C	2.121641	0.25	-1.150336
C	1.392248	-0.459399	-0.134166
C	2.139058	-1.30584	0.757626
C	3.546001	-1.298956	0.70484
C	4.263959	-0.50064	-0.199382
C	3.527587	0.243235	-1.134728
Si	-0.463216	-0.116028	0.267773
C	-0.801913	1.682967	-0.414083
N	-1.68725	2.169733	-1.332984
C	-1.783854	3.562984	-1.241419
C	-0.91023	3.946493	-0.250371
N	-0.314072	2.783025	0.226227
C	-2.365494	1.390782	-2.364308
C	-2.689753	4.382727	-2.100498
C	-0.590687	5.298637	0.294039
C	0.72314	2.781286	1.259432
C	1.452272	-2.303043	1.695221
C	2.257773	-2.677657	2.952273
C	5.785033	-0.47007	-0.191717
C	6.30525	0.937983	0.170861
C	1.466542	0.924393	-2.362326
C	1.714004	2.44586	-2.425309
C	-1.591781	-1.260061	-0.863512
N	-1.233952	-2.231397	-1.760192
C	-2.33639	-2.988293	-2.15071
C	-3.423731	-2.46737	-1.484871
N	-2.944671	-1.417971	-0.708788

11. Appendix

C	0.089207	-2.464141	-2.33885
C	-3.83264	-0.605107	0.119363
C	-4.859845	-2.876299	-1.494834
C	-2.23747	-4.132458	-3.105361
Ni	-1.204006	0.05319	2.453653
C	-2.06925	-1.512324	2.731108
O	-2.633412	-2.523399	2.784431
C	-2.20403	1.551481	2.497002
O	-2.757452	2.570936	2.438744
C	0.303771	0.297757	3.425247
O	1.29264	0.507534	3.98774
C	1.047283	-3.577957	0.920515
C	6.37178	-0.946614	-1.537257
C	1.953121	0.281291	-3.684051
H	4.068018	0.811017	-1.901953
H	4.113993	-1.935057	1.392579
H	0.378816	0.746845	-2.304229
H	3.018849	0.514067	-3.863736
H	1.373991	0.679591	-4.539946
H	1.853278	-0.818068	-3.670143
H	2.793022	2.649298	-2.560767
H	1.38802	2.959815	-1.50715
H	1.178613	2.893097	-3.285186
H	0.513266	-1.842055	2.042085
H	0.326214	-3.346067	0.117381
H	0.566309	-4.302746	1.605003
H	1.933318	-4.063388	0.466238
H	3.125766	-3.319719	2.707202
H	1.612929	-3.248578	3.645962
H	2.626429	-1.779693	3.47902
H	0.074116	-2.192489	-3.409558
H	0.348105	-3.531263	-2.238934
H	0.832953	-1.859433	-1.805014
H	-1.805128	-3.818937	-4.075301
H	-3.238818	-4.553857	-3.293886
H	-1.595915	-4.940023	-2.701224
H	-5.519985	-2.038942	-1.793595
H	-5.187118	-3.216391	-0.492704
H	-5.012289	-3.705916	-2.204921
H	-4.525426	-0.030159	-0.522246
H	-3.227659	0.069526	0.740647
H	-4.419076	-1.264334	0.780519
H	1.394786	3.637715	1.081946
H	1.310086	1.853322	1.196371
H	0.265809	2.865757	2.25971
H	0.476711	5.555468	0.145927
H	-0.803225	5.349877	1.379362

S48

11. Appendix

H	-1.199193	6.065039	-0.213874
H	-2.630591	5.441468	-1.798065
H	-3.744895	4.059255	-2.007412
H	-2.411026	4.322446	-3.171747
H	-2.519308	2.028385	-3.249812
H	-3.34665	1.025944	-2.014741
H	-1.737025	0.533192	-2.648501
H	6.124377	-1.171613	0.595743
H	7.410592	0.938855	0.22571
H	6.002603	1.676719	-0.597279
H	5.906456	1.273122	1.147024
H	7.477248	-0.961666	-1.491474
H	6.018261	-1.96386	-1.791163
H	6.07737	-0.264683	-2.358763

4. References

- S1 A. Porzelt, J. Schweizer, R. Baierl, P. Altmann, M. Holthausen and S. Inoue, *Inorganics*, **2018**, *6*, 54-67.
- S2 S. U. Ahmad, T. Szilvási and S. Inoue, *Chem. Commun.*, **2014**, *50*, 12619-12622.
- S3 *APEX suite of crystallographic software*, APEX 3 version 2015.5-2; Bruker AXS Inc.: Madison, Wisconsin, USA, 2015.
- S4 *SAINT*, Version 7.56a and *SADABS* Version 2008/1; Bruker AXS Inc.: Madison, Wisconsin, USA, 2008.
- S5 G. M. Sheldrick, *SHELXL-2014*, University of Göttingen, Göttingen, Germany, 2014.
- S6 C. B. Hübschle, G. M. Sheldrick and B. Dittrich, *J. Appl. Cryst.*, **2011**, *44*, 1281-1284.
- S7 G. M. Sheldrick, *SHELXL-97*, University of Göttingen, Göttingen, Germany, 1998.
- S8 A. J. C. Wilson, *International Tables for Crystallography*, Vol. C, Tables 6.1.1.4 (pp. 500-502), 4.2.6.8 (pp. 219-222), and 4.2.4.2 (pp. 193-199); Kluwer Academic Publishers: Dordrecht, The Netherlands, 1992.
- S9 C. F. Macrae, I. J. Bruno, J. A. Chisholm, P. R. Edgington, P. McCabe, E. Pidcock, L. Rodriguez-Monge, R. Taylor, J. van de Streek and P. A. Wood, *J. Appl. Cryst.*, **2008**, *41*, 466-470.
- S10 A. D. Becke, *The Journal of Chemical Physics*, **1997**, *107*, 8554-8560.
- S11 S. Grimme, *J. Comput. Chem.*, **2006**, *27*, 1787-1799.
- S12 F. Weigend and R. Ahlrichs, *PCCP*, **2005**, *7*, 3297-3305.
- S13 M. J. Frisch, G. W. Trucks, H. B. Schlegel, G. E. Scuseria, M. A. Robb, J. R. Cheeseman, G. Scalmani, V. Barone, B. Mennucci, G. A. Petersson, H. Nakatsuji, M. Caricato, X. Li, H. P. Hratchian, A. F. Izmaylov, J. Bloino, G. Zheng, J. L. Sonnenberg, M. Hada, M. Ehara, K. Toyota, R. Fukuda, J. Hasegawa, M. Ishida, T. Nakajima, Y. Honda, O. Kitao, H. Nakai, T. Vreven, J. A. Montgomery, Jr., J. E. Peralta, F. Ogliaro, M. Bearpark, J. J. Heyd, E. Brothers, K. N. Kudin, V. N. Staroverov, R. Kobayashi, J. Normand, K. Raghavachari, A. Rendell, J. C. Burant, S. S. Iyengar, J. Tomasi, M. Cossi, N. Rega, J. M. Millam, M. Klene, J. E. Knox, J. B. Cross, V. Bakken, C. Adamo, J. Jaramillo, R. Gomperts, R. E. Stratmann, O. Yazyev, A. J. Austin, R. Cammi, C. Pomelli, J. W. Ochterski, R. L. Martin, K. Morokuma, V. G. Zakrzewski, G. A. Voth, P. Salvador, J. J. Dannenberg, S. Dapprich, A. D. Daniels, Ö. Farkas, J. B. Foresman, J. V. Ortiz, J. Cioslowski and D. J. Fox, *Gaussian 09, Revision E.01*, Gaussian, Inc., Wallingford CT, 2009.
- S14 Z. Benedek and T. Szilvási, *RSC Adv.*, **2015**, *5*, 5077-5086.
- S15 M. J. Frisch, J. A. Pople and J. S. Binkley, *The Journal of Chemical Physics*, **1984**, *80*, 3265-3269.

11.4 Supporting Information Chapter 7

Chemistry—A European Journal

Supporting Information

Facile Access to Dative, Single, and Double Silicon–Metal Bonds Through M–Cl Insertion Reactions of Base-Stabilized Si^{II} Cations

Philipp Frisch,^[a] Tibor Szilvási,^[b] and Shigeyoshi Inoue^{*[a]}

Supporting Information

Facile Access to Dative, Single and Double Silicon–Metal Bonds Through M–Cl Insertion Reactions of Base-stabilized Si(II) cations

Philipp Frisch, Tibor Szilvási and Shigeyoshi Inoue*

Table of Contents

1. Experimental Section	S3
1.1 General Methods and Instrumentation	S3
1.2 Synthesis of [^t Bu ₃ Si–Si(IME ₄) ₂]OTf (5a-OTf).....	S5
1.3 General Synthetic Procedure for [R–Si(NHC)Cl→RuCl(NHC)(<i>p</i> -cym)]Cl	S9
1.3.1 [^t Tipp–Si(IME ₄)Cl→RuCl(IME ₄)(<i>p</i> -cymene)]Cl (2)	S10
1.3.2 [^t Bu ₃ Si–Si(IME ₄)Cl→RuCl(IME ₄)(<i>p</i> -cymene)]Cl (6a).....	S17
1.3.3 [^t Bu ₂ MeSi–Si(IME ₄)Cl→RuCl(IME ₄)(<i>p</i> -cymene)]Cl (6b).....	S22
1.3.4 [^t Bu ₂ MeSi–Si(IEt ₂ Me ₂)Cl→RuCl(IEt ₂ Me ₂)(<i>p</i> -cymene)]Cl (6c)	S27
1.4 General Synthetic Procedure for [R–Si(NHC)Cl→RhCl(NHC)(Cp [*])]Cl	S33
1.4.1 [^t Bu ₃ Si–Si(IME ₄)Cl→RhCl(IME ₄)(Cp [*])]X (7a , X = Cl, OTf).....	S34
1.4.2 [^t Bu ₂ MeSi–Si(IME ₄)Cl→RhCl(IME ₄)(Cp [*])]Cl (7b)	S42
1.4.3 [^t Bu ₂ MeSi–Si(IEt ₂ Me ₂)Cl→RhCl(IEt ₂ Me ₂)(Cp [*])]Cl (7c)	S47
1.5 General Synthetic Procedure for [R–Si(NHC) ₂ →MCl ₂ (Ar)]Cl.....	S49
1.5.1 [Mes–Si(IME ₄) ₂ →RuCl ₂ (<i>p</i> -cymene)]Cl (3).....	S50
1.5.2 [Mes–Si(IME ₄) ₂ →RhCl ₂ (Cp [*])]X (4 , X = Cl, [RhCl ₃ Cp [*]]).....	S51

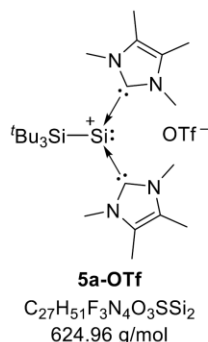
1.6	General Synthetic Procedure for [^t Bu ₃ Si–SiCl ₂ –M(IMe ₄)(Ar)]	S56
1.6.1	[^t Bu ₃ Si–SiCl ₂ –Ru(IMe ₄)(<i>p</i> -cymene)] (8)	S57
1.6.2	[^t Bu ₃ Si–SiCl ₂ –Rh(IMe ₄)(Cp*)] (9)	S60
1.7	Synthesis of [^t Bu ₃ Si–Si(Cl)=Ru(IMe ₄)(<i>p</i> -cymene)] (10)	S62
2.	X-ray Crystallographic Data	S69
2.1	General Information	S69
2.2	SC-XRD structure of 2 (CCDC-1976774)	S70
2.3	SC-XRD structure of 4-RhCl₃Cp* (CCDC-1976772)	S71
2.4	SC-XRD structure of 6a (CCDC-1976773)	S72
2.5	SC-XRD structure of 7a (CCDC-1976776)	S73
2.6	SC-XRD structure of 7b (CCDC-1976775)	S74
2.7	SC-XRD structure of 8 (CCDC-1976777)	S75
2.8	SC-XRD structure of 9 (CCDC-1976778)	S76
2.9	SC-XRD structure of 10 (CCDC-1976779)	S77
2.10	Crystal data and structural refinement parameters	S78
3.	DFT Calculations	S80
3.1	NBO Analysis of Complexes 2 , 4 , 6a , 7a , 8 , 9 and 10	S80
3.2	HOMOs and LUMOs of Complexes 2 , 4 , 6a , 7a , 8 , 9 and 10	S83
3.3	Calculated Mechanism for the Formation of 2 via 2'	S87
3.4	Cartesian Coordinates of the Calculated Structures	S88
4.	References	S110

1. Experimental Section

1.1 General Methods and Instrumentation

All reactions were carried out under exclusion of water and oxygen in an atmosphere of argon 4.6 ($\geq 99.996\%$) using standard Schlenk techniques or in a Labstar glovebox from *MBraun* with H_2O and O_2 levels below 0.5 ppm. Glassware was heat dried under vacuum prior to use. Acetonitrile and Acetonitrile- d_3 were refluxed over CaH_2 , distilled under argon, deoxygenated by three freeze-pump-thaw cycles and stored over 3 Å molecular sieve in a glovebox. Diethylether, benzene, toluene, THF and *n*-hexane were refluxed over sodium/benzophenone, distilled under argon, deoxygenated by three freeze-pump-thaw cycles and stored over 3 Å molecular sieve in a glovebox. C_6D_6 and THF- d_8 were stirred over Na/K alloy, distilled under argon, deoxygenated by three freeze-pump-thaw cycles and stored over 3 Å molecular sieve in a glovebox. All NMR samples were prepared under argon in *J. Young* PTFE valve NMR tubes. NMR spectra at ambient temperature (300 K) were recorded on a *Bruker AV500C* (^1H : 500.36 MHz, ^{13}C : 125.83 MHz, ^{29}Si : 99.41 MHz) spectrometer. Low temperature NMR spectra were recorded on a *Bruker DRX400* (^1H : 400.13 MHz, ^{13}C : 100.62 MHz, ^{29}Si : 79.49 MHz) spectrometer. The ^1H , ^{13}C and ^{29}Si NMR spectroscopic chemical shifts δ are reported in ppm relative to tetramethylsilane. ^1H and $^{13}\text{C}\{^1\text{H}\}$ NMR spectra are calibrated against the residual proton and natural abundance carbon resonances of the respective deuterated solvent as internal standard (CD_3CN : $\delta(^1\text{H}) = 1.94$ ppm and $\delta(^{13}\text{C}) = 118.3$ ppm; THF- d_8 : $\delta(^1\text{H}) = 1.73$ ppm and $\delta(^{13}\text{C}) = 25.4$ ppm; C_6D_6 : $\delta(^1\text{H}) = 7.16$ ppm and $\delta(^{13}\text{C}) = 128.1$ ppm). ^{29}Si NMR spectra are referenced to the resonance of tetramethylsilane ($\delta = 0$ ppm) as external standard. ^{19}F NMR spectra are referenced to the resonance of CFCl_3 ($\delta = 0$ ppm) as external standard. Individual peaks were assigned on the basis of 2D ($^1\text{H}/^1\text{H}$ COSY, $^1\text{H}/^{13}\text{C}$ HSQC, $^1\text{H}/^{13}\text{C}$ HMBC, $^1\text{H}/^{29}\text{Si}$ HMBC) NMR experiments. The following abbreviations are used to describe signal multiplicities: s = singlet, d = doublet, t = triplet, q = quartet, sept = septet, m = multiplet. NMR spectra were visualized using MestReNova 12. Spectra recorded in C_6D_6 include a resonance for silicone grease (C_6D_6 : $\delta(^1\text{H}) = 0.29$ ppm, $\delta(^{13}\text{C}) = 1.4$ ppm and $\delta(^{29}\text{Si}) = -21.8$ ppm) derived from *B. Braun AG Sterican®* cannulas, which is marked with § in the corresponding spectra. Quantitative elemental analyses (EA) were carried out using a *HEKAtech* EURO EA instrument equipped with a CHNS combustion analyzer. LIFDI-MS (Liquid Injection Field Desorption Ionization Mass Spectrometry) spectra were recorded on a *Waters* Micromass LCT TOF mass spectrometer equipped with a LIFDI-ion

source (LIFDI 700) from *Linden CMS GmbH*. UV-Vis spectra were recorded on a *Varian, Inc.* Cary 50 spectrophotometer with a Schlenk quartz cuvette. EPR spectra were recorded on a *Jeol* JES-Fa200 ESR spectrometer with a spectrometer frequency of 9.267 GHz (X-band). Generally, samples were prepared in a glovebox and spectra were visualized using OriginPro 2018. Melting Points (M.P.) were determined in sealed glass capillaries under inert gas by a *Büchi* M-565 melting point apparatus. Unless otherwise stated, all commercially available chemicals were purchased from *abcr* or *Sigma-Aldrich* and used without further purification. The compounds [Tipp-Si(IME₄)₂]Cl (**1a**)¹, [Mes-Si(IME₄)₂]Cl (**1b**)², [^tBu₃Si-Si(IME₄)₂]Cl (**5a**)², [^tBu₂MeSi-Si(IME₄)₂]Cl (**5b**)², [^tBu₂MeSi-Si(IEt₂Me₂)₂]Cl (**5c**)², [RuCl₂(*p*-cymene)]₂³, [RhCl₂(C₅Me₅)]₂⁴ and KC₈⁵ were prepared as described in the literature. The compound [^tBu₃Si-Si(IME₄)₂]OTf (**5a-OTf**) was synthesized similarly to the previously published procedure for the anion exchange of NHC-stabilized silyliumylidene ions.⁶

1.2 Synthesis of [^tBu₃Si–Si(IME₄)₂]OTf (**5a-OTf**)

[^tBu₃Si–Si(IME₄)₂]Cl (**5a**) (300.0 mg, 586.7 μmol, 1.0 eq) and KOTf (110.4 mg, 586.7 μmol, 1.0 eq) was suspended in 7 mL THF and stirred at room temperature until the starting material dissolved (5-10 minutes). The cloudy, bright orange suspension was concentrated under reduced pressure to 4-5 mL, filtered and the clear solution was further concentrated under reduced pressure to about 2-3 mL where precipitation began. *n*-Hexane (12 mL) was added to precipitate an orange solid which was collected by filtration, washed with *n*-hexane (3 mL) and after drying under vacuum the product **5a-OTf** (352.3 mg, 563.7 μmol, 96%) was obtained as an orange air- and moisture-sensitive solid.

¹H NMR (500 MHz, CD₃CN, 300 K): δ [ppm] = 3.68 (s, 12H, N_{NHC}CH₃), 2.15 (s, 12H, C_{NHC}CH₃), 1.22 (s, 27H, C(CH₃)₃).

¹H NMR (500 MHz, THF-*d*₈, 300 K): δ [ppm] = 3.85 (s, 12H, N_{NHC}CH₃), 2.21 (s, 12H, C_{NHC}CH₃), 1.25 (s, 27H, C(CH₃)₃).

¹³C{¹H} NMR (126 MHz, CD₃CN, 300 K): δ [ppm] = 164.1 (N_{C_{NHC}N}), 128.7 (C_{NHC}CH₃), 122.0 (q, ¹J_{C–F} = 320.8 Hz, SO₃CF₃), 36.6 (N_{NHC}CH₃), 33.1 (C(CH₃)₃), 26.3 (C(CH₃)₃), 9.2 (C_{NHC}CH₃).

Note: The resonance for the SO₃CF₃ group (quartet) partially overlaps with the resonance for CD₃CN.

¹³C{¹H} NMR (126 MHz, THF-*d*₈, 300 K): δ [ppm] = 162.8 (N_{C_{NHC}N}), 129.0 (C_{NHC}CH₃), 122.4 (q, ¹J_{C–F} = 322.8 Hz, SO₃CF₃), 36.6 (N_{NHC}CH₃), 33.2 (C(CH₃)₃), 26.1 (C(CH₃)₃), 9.4 (C_{NHC}CH₃).

²⁹Si{¹H} NMR (99 MHz, CD₃CN, 300 K): δ [ppm] = 21.7 (SiSi[†]Bu₃), –82.1 (SiSi[†]Bu₃).

²⁹Si{¹H} NMR (99 MHz, THF-*d*₈, 300 K): δ [ppm] = 20.2 (SiSi[†]Bu₃), –84.4 (SiSi[†]Bu₃).

¹⁹F{¹H} NMR (471 MHz, CD₃CN, 300 K): δ [ppm] = –79.3 (SO₃CF₃).

EA: C₂₇H₅₁N₄Si₂SO₃F₃ calculated [%]: C (51.89), H (8.23), N (8.97), S (5.13).

measured [%]: C (52.17), H (8.46), N (9.24), S (4.96).

M.P.: 157-158 °C (decomposition, color change to black).

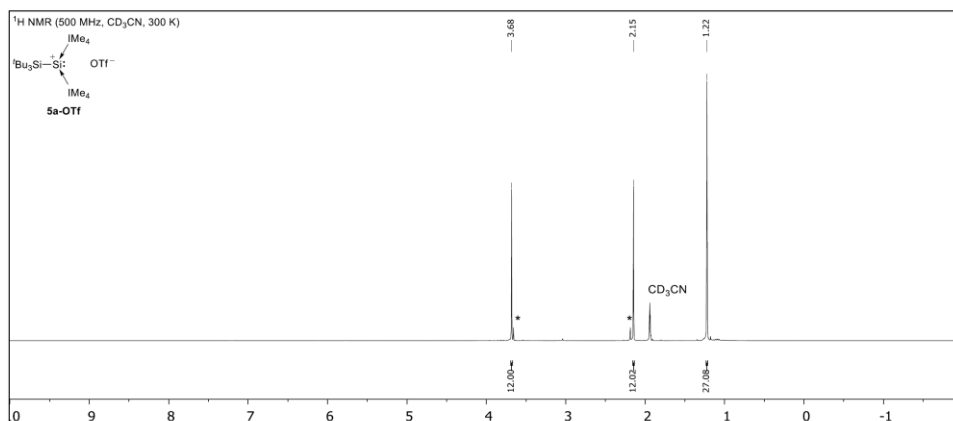


Figure S1 ¹H NMR spectrum of [**Bu**₃Si-Si(Ime₄)₂]OTf (**5a-OTf**) in CD₃CN at 300 K. Residual imidazolium triflate [Ime₄·HOTf] from the precursor synthesis is marked with *.

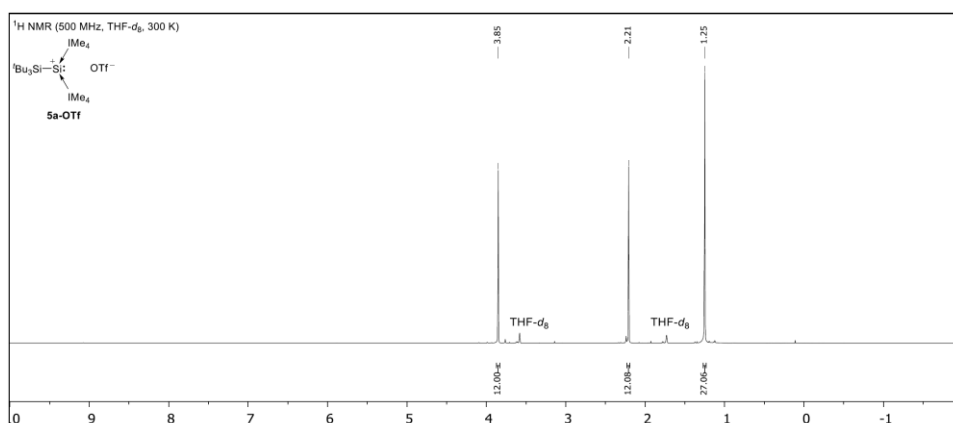


Figure S2 ¹H NMR spectrum of [**Bu**₃Si-Si(Ime₄)₂]OTf (**5a-OTf**) in THF-*d*₈ at 300 K.

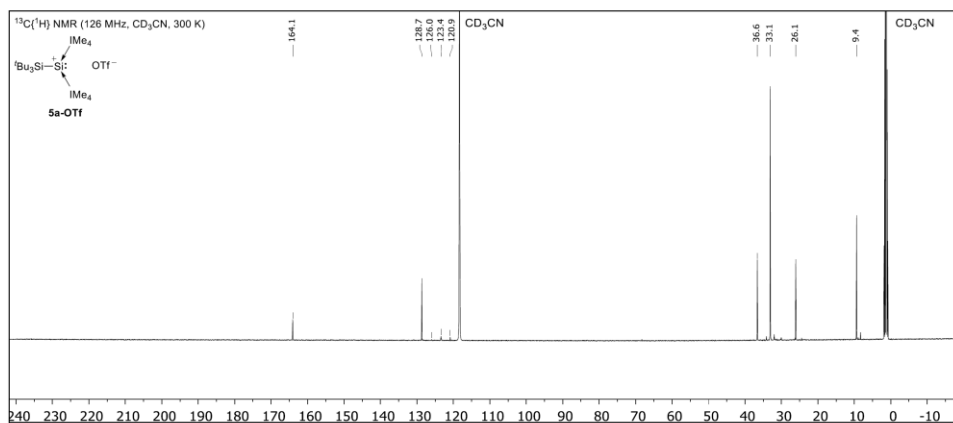


Figure S3 $^{13}\text{C}\{^1\text{H}\}$ NMR spectrum of $[\text{Bu}_3\text{Si}-\text{Si}(\text{Me}_4)_2]\text{OTf}$ (**5a-OTf**) in CD_3CN at 300 K.

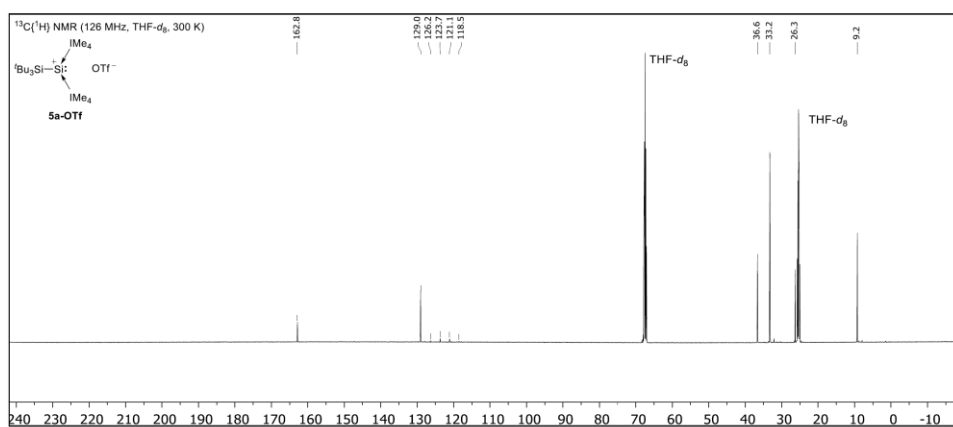


Figure S4 $^{13}\text{C}\{^1\text{H}\}$ NMR spectrum of $[\text{Bu}_3\text{Si}-\text{Si}(\text{Me}_4)_2]\text{OTf}$ (**5a-OTf**) in $\text{THF}-d_8$ at 300 K.

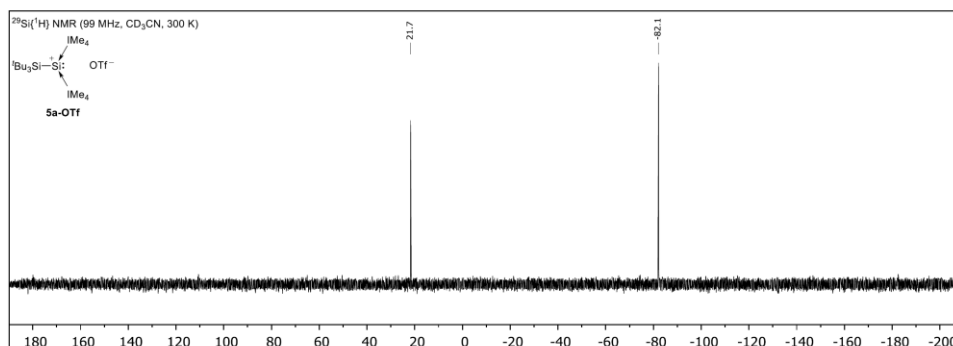


Figure S5 ²⁹Si{¹H} NMR spectrum of [^tBu₃Si-Si(Ime₄)₂]OTf (**5a-OTf**) in CD₃CN at 300 K.

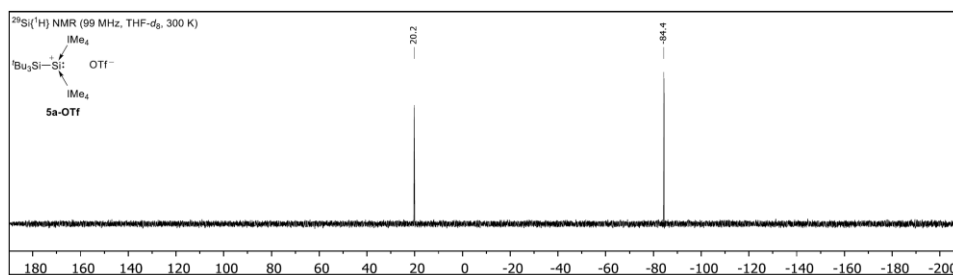


Figure S6 ²⁹Si{¹H} NMR spectrum of [^tBu₃Si-Si(Ime₄)₂]OTf (**5a-OTf**) in THF-*d*₈ at 300 K.

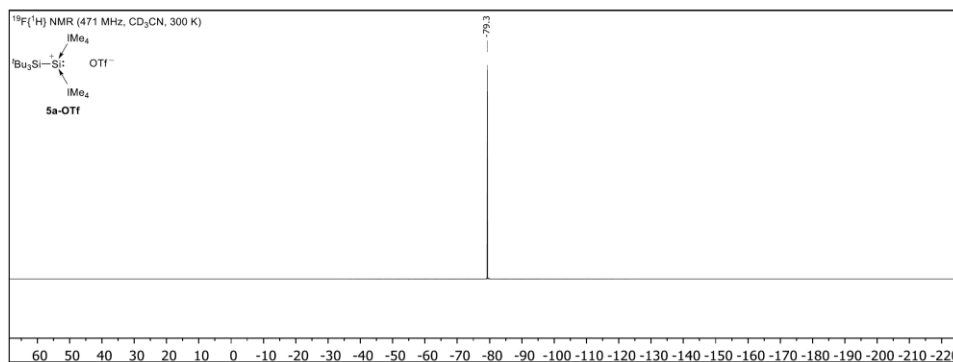
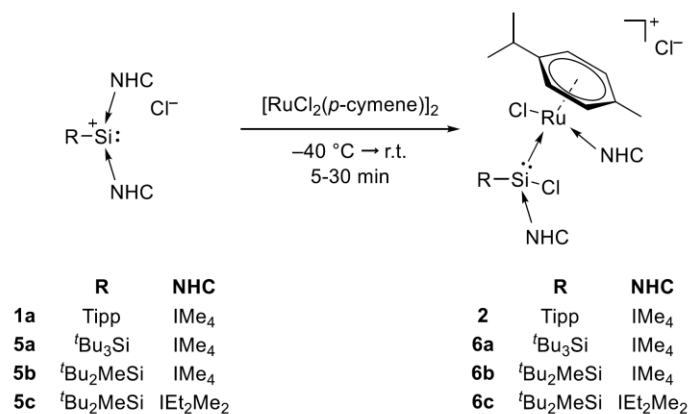
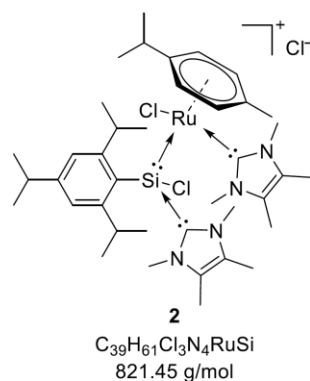


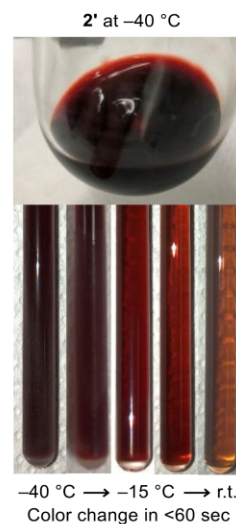
Figure S7 ¹⁹F{¹H} NMR spectrum of [^tBu₃Si-Si(Ime₄)₂]OTf (**5a-OTf**) in CD₃CN at 300 K.

1.3 General Synthetic Procedure for $[R-Si(NHC)Cl \rightarrow RuCl(NHC)(p-cym)]Cl$ 

Silyliumylidene chloride $[R-Si(NHC)_2]Cl$ (**1a** or **5a-c**) (1.0 eq) and $[RuCl_2(p-cymene)]_2$ (0.5 eq) were mixed, cooled to $-40\text{ }^\circ\text{C}$ and pre-cooled ($-40\text{ }^\circ\text{C}$) MeCN (3-10 mL) was added. The reaction mixtures were stirred at $-40\text{ }^\circ\text{C}$ until all starting material had dissolved (5-30 minutes) and then warmed to room temperature. The solutions were quickly concentrated under reduced pressure to about 1-3 mL. A mixture of toluene and Et₂O (1:1, 5-15 mL) was added and the orange-red solutions were stored at $-35\text{ }^\circ\text{C}$ for 3-10 days. The formed (microcrystalline) precipitate was collected by filtration, washed with benzene or toluene (2 mL) and Et₂O (2×2 mL) and after drying under vacuum the complexes $[R-Si(NHC)Cl \rightarrow RuCl(NHC)(p-cymene)]Cl$ (**2** and **6a-c**) were isolated as orange air- and moisture-sensitive solids.

1.3.1 [Tipp-Si(IME₄)Cl → RuCl(IME₄)(*p*-cymene)]Cl (**2**)

Note: (a) Upon addition of cold MeCN to the starting materials the solution turns deep red. Warming of this solution leads to an almost instantaneous color change to orange at temperatures higher than -20 to -15 °C. We presume that the deep red species (**2'**) is in fact the silyliumylidene transition metal complex before insertion into the M–Cl bond and migration of one coordinated NHC moiety, whereas the orange species is complex **2**. Low-temperature ²⁹Si NMR at -35 °C of **2'** revealed a resonance at -21.1 ppm (cf. Figure S16), which is in line with the -20.5 ppm observed for the silyliumylidene ruthenium complex **3** and corresponds well with the calculated NMR shift for **2'** (-23.4 ppm). Isolation of the silyliumylidene complex in a clean fashion was not possible. The insertion reaction occurs too fast, preventing any kind of work up. Utilization of solvents with a significantly lower melting point did not give the desired product (for example, carrying out the reaction in THF led to complete polymerization of the solvent); (b) Full decomposition of **2** occurs in solution within roughly 4 hours (cf. Figure S15) at room temperature. No silicon containing species could be identified. **2** is stable for at least 3 days at -35 °C in MeCN solution.



Batch size: **1a:** 100.0 mg, 194.1 μ mol, 1.0 eq.

[RuCl₂(*p*-cymene)]₂: 59.4 mg, 97.0 μ mol, 0.5 eq.

Yield: 56.6 mg (68.9 μ mol, 36%) as an orange solid.

SC-XRD: Suitable crystals were obtained by cooling a concentrated solution of **2** in MeCN to -35 °C.

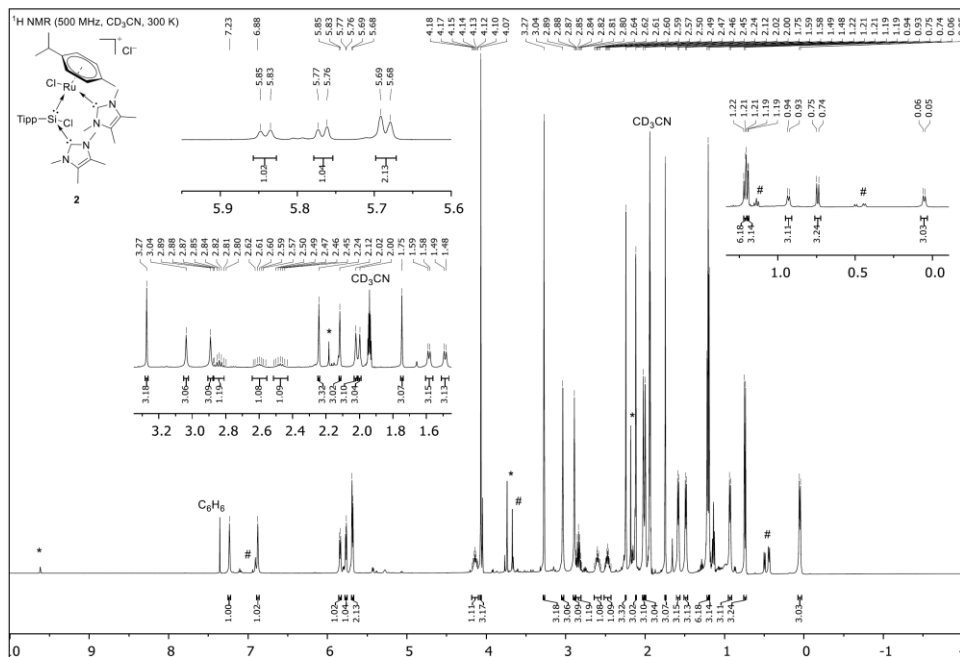


Figure S8 ¹H NMR spectrum of [Tipp-Si(IME₄)Cl-RuCl(IME₄)(*p*-cymene)]Cl (**2**) in CD₃CN at 300 K. Residual imidazolium chloride [IME₄⁺ HCl] from the synthesis of **1a** and from the decomposition of **2** is marked with *. Beginning decomposition is marked with #.

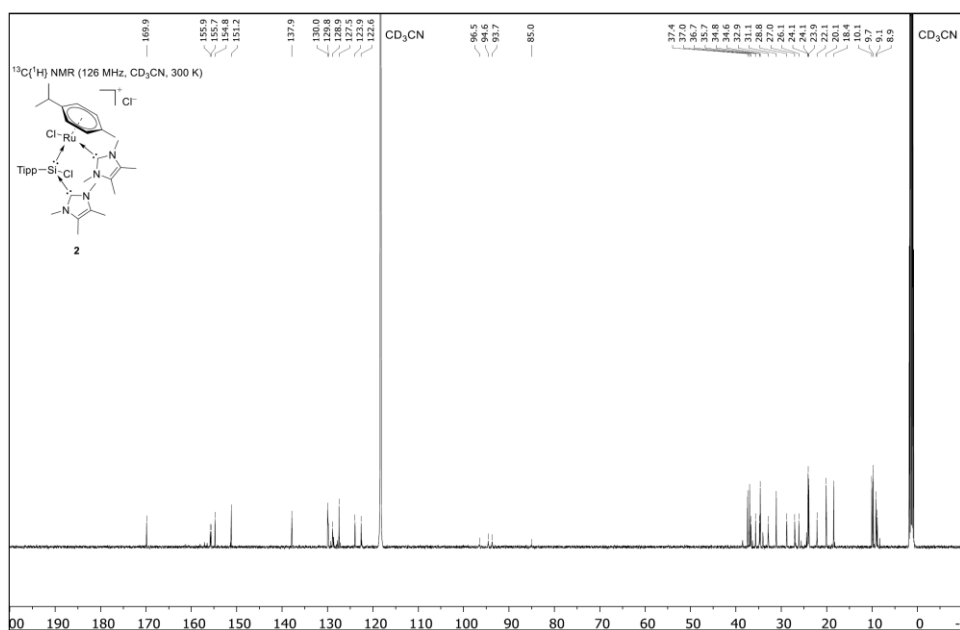


Figure S9 ¹³C{¹H} NMR spectrum of [Tipp-Si(IME₄)Cl-RuCl(IME₄)(*p*-cymene)]Cl (**2**) in CD₃CN at 300 K.

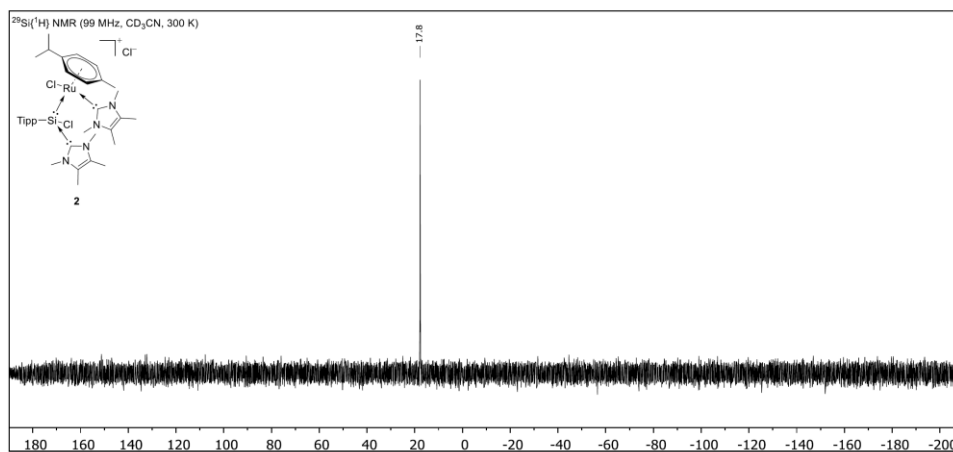


Figure S10 ²⁹Si{¹H} NMR spectrum of [Tipp-Si(IME₄)Cl→RuCl(IME₄)(*p*-cymene)]Cl (**2**) in CD₃CN at 300 K.

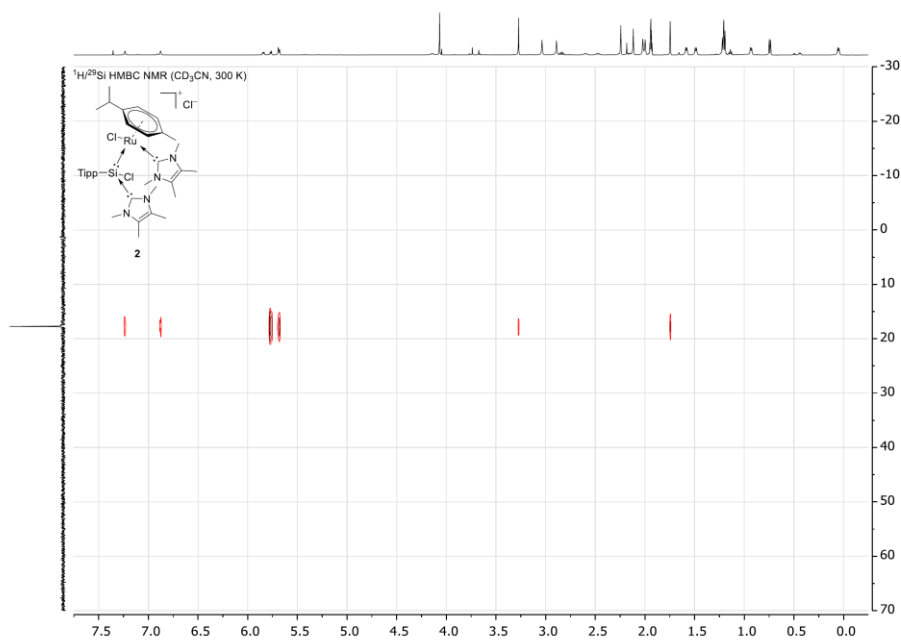


Figure S11 ¹H/²⁹Si HMBC NMR spectrum of [Tipp-Si(IME₄)Cl→RuCl(IME₄)(*p*-cymene)]Cl (**2**) in CD₃CN at 300 K.

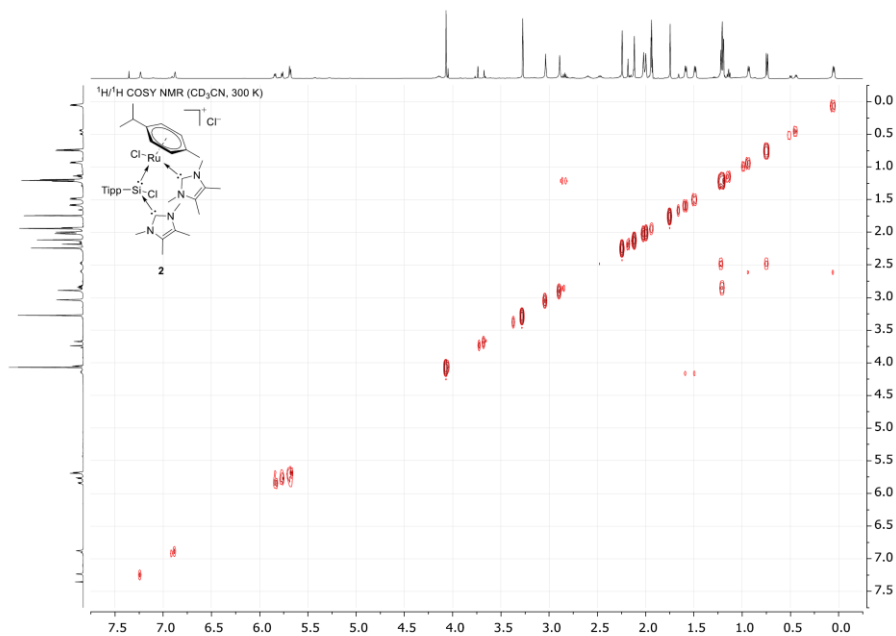


Figure S12 $^1\text{H}/^1\text{H}$ COSY NMR spectrum of $[\text{Tipp-Si}(\text{IME}_4)\text{Cl}\rightarrow\text{RuCl}(\text{IME}_4)(p\text{-cymene})]\text{Cl}$ (**2**) in CD_3CN at 300 K.

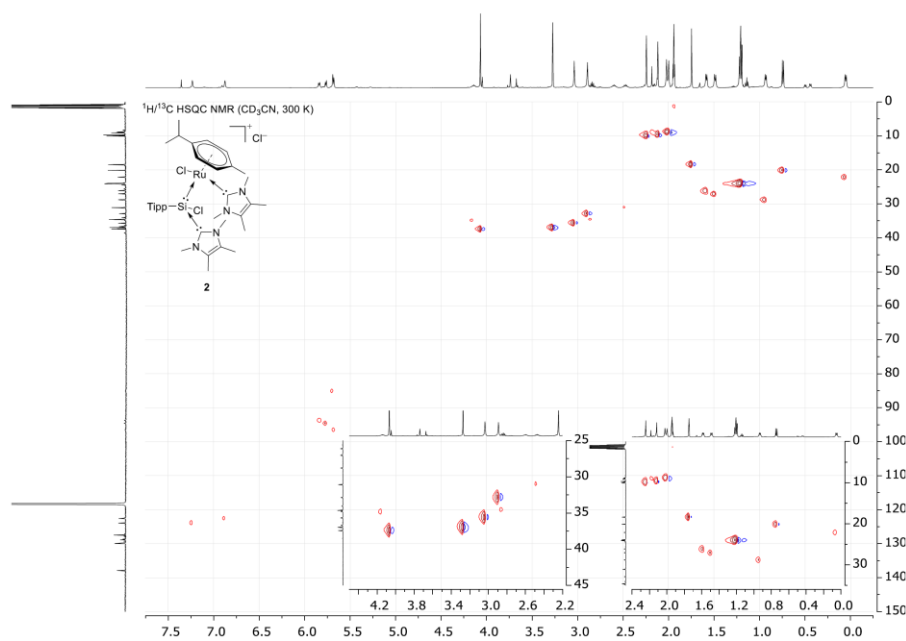


Figure S13 $^1\text{H}/^{13}\text{C}$ HSQC NMR spectrum of $[\text{Tipp-Si}(\text{IME}_4)\text{Cl}\rightarrow\text{RuCl}(\text{IME}_4)(p\text{-cymene})]\text{Cl}$ (**2**) in CD_3CN at 300 K.

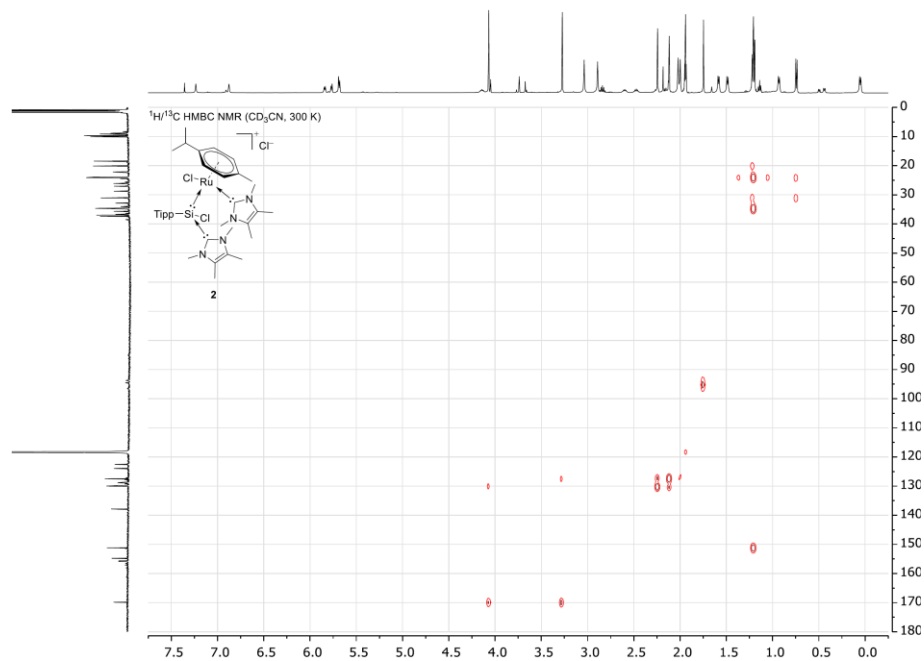


Figure S14 $^1\text{H}/^{13}\text{C}$ HMBC NMR spectrum of $[\text{Tipp-Si}(\text{IME}_4)\text{Cl} \rightarrow \text{RuCl}(\text{IME}_4)(p\text{-cymene})]\text{Cl}$ (**2**) in CD_3CN at 300 K.

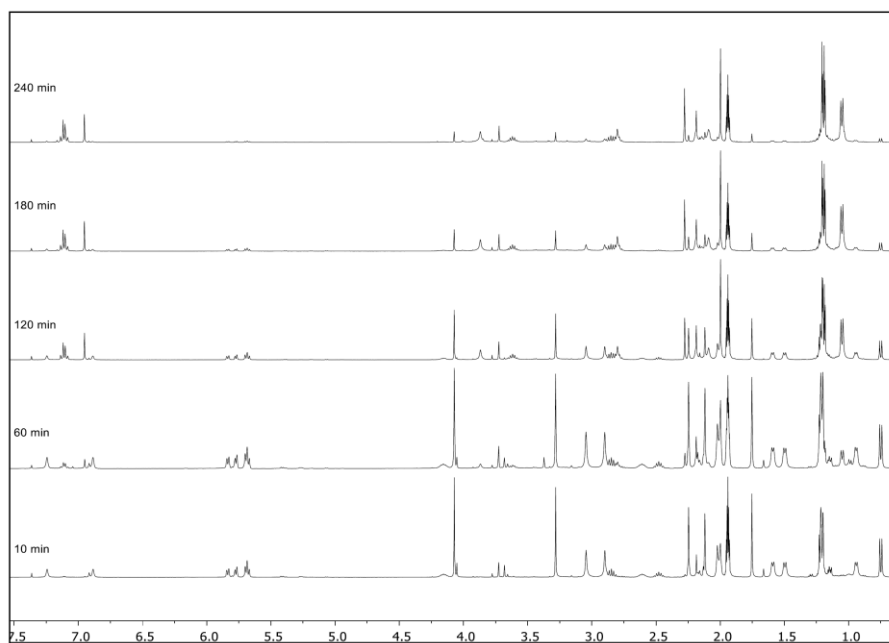


Figure S15 Time resolved ^1H NMR spectra of $[\text{Tipp-Si}(\text{IME}_4)\text{Cl} \rightarrow \text{RuCl}(\text{IME}_4)(p\text{-cymene})]\text{Cl}$ (**2**) in CD_3CN showing the decomposition in solution at room temperature.

S15

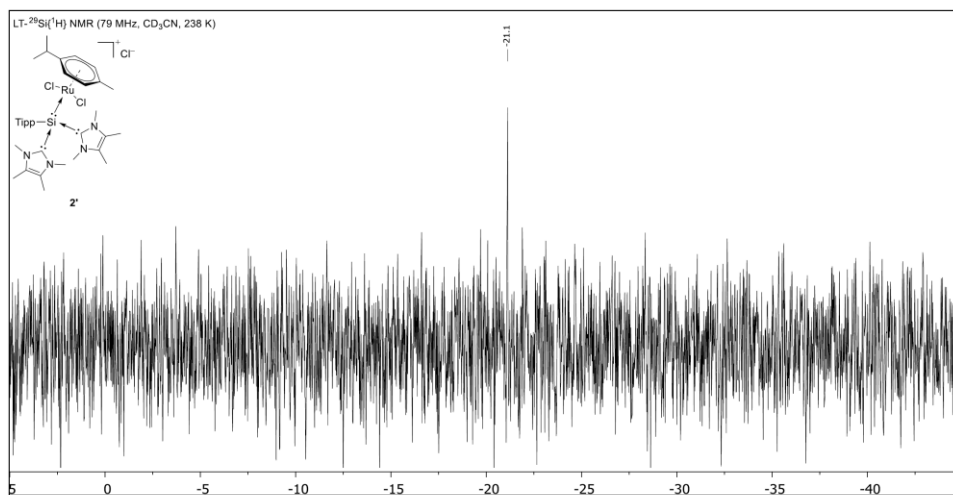
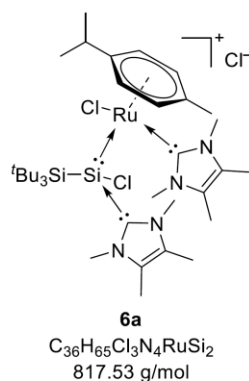


Figure S16 Low temperature $^{29}\text{Si}\{^1\text{H}\}$ NMR of the deep red species observed during the synthesis of **2** at -35°C / 238 K in CD_3CN , indicating the presence of the complex $[\text{Tipp-Si}(\text{Me})_2 \rightarrow \text{RuCl}_2(\textit{p}\text{-cymene})]\text{Cl}$ (**2'**).

1.3.2 [^tBu₃Si-Si(IMEt)₃Cl→RuCl(IMEt)₄(*p*-cymene)]Cl (6a)

Note: The complex decomposes in solution at room temperature to an unidentified mixture of products.

Batch size: 5a: 100.0 mg, 195.6 μmol, 1.0 eq.

[RuCl₂(*p*-cymene)]₂: 59.9 mg, 97.8 μmol, 0.5 eq.

Yield: 102.6 mg (125.5 μmol, 64%) as an orange solid.

SC-XRD: Suitable crystals were obtained by slow diffusion of Et₂O into a concentrated solution of 6a in MeCN at -35 °C.

¹H NMR (500 MHz, CD₃CN, 300 K): δ [ppm] = 5.91 (dd, ³J_{H-H} = 6.2, ⁴J_{H-H} = 0.9 Hz, 1H, C_{*p*-cym}Har), 5.56 (dd, ³J_{H-H} = 5.9, ⁴J_{H-H} = 1.2 Hz, 1H, C_{*p*-cym}Har), 5.42 (dd, ³J_{H-H} = 6.2, ⁴J_{H-H} = 1.2 Hz, 1H, C_{*p*-cym}Har), 5.18 (dd, ³J_{H-H} = 5.9, ⁴J_{H-H} = 0.9 Hz, 1H, C_{*p*-cym}Har), 4.15 (s, 3H, NNHC→SiCH₃), 3.86 (s, 3H, NNHC→RuCH₃), 2.99 (s, 3H, NNHC→RuCH₃), 2.90 (s, 3H, NNHC→SiCH₃), 2.61 (sept, ³J_{H-H} = 6.9 Hz, 1H, CH(CH₃)₂), 2.20 (s, 3H, CNHC→SiCH₃), 2.15 (s, 3H, CNHC→RuCH₃), 1.99 (s, 3H, C_{*p*-cym}CH₃), 1.86 (s, 3H, CNHC→RuCH₃), 1.83 (s, 3H, CNHC→SiCH₃), 1.25 (s, 27H, Si((C(CH₃)₃)₃)), 1.22 (d, ³J_{H-H} = 6.9 Hz, 3H, CH(CH₃)₂), 1.17 (d, ³J_{H-H} = 6.9 Hz, 3H, CH(CH₃)₂).

¹³C{¹H} NMR (126 MHz, CD₃CN, 300 K): δ [ppm] = 172.1 (NC_{NNHC→Ru}N), 155.2 (NC_{NNHC→Si}N), 131.2 (CNHC→SiCH₃), 128.9 (CNHC→RuCH₃), 128.7 (CNHC→SiCH₃), 127.1 (CNHC→RuCH₃), 124.6 (C_{*p*-cym}-ⁱPr), 101.4 (C_{*p*-cym}Har), 94.2 (C_{*p*-cym}CH₃), 91.1 (C_{*p*-cym}Har), 85.0 (C_{*p*-cym}Har), 83.9 (C_{*p*-cym}Har), 37.7 (NNHC→RuCH₃), 37.6 (NNHC→RuCH₃), 36.8 (NNHC→SiCH₃), 36.4 (NNHC→SiCH₃), 33.1 (Si((C(CH₃)₃)₃)), 31.5 (CH(CH₃)₂), 26.4 (Si((C(CH₃)₃)₃)), 22.4 (CH(CH₃)₂), 21.8 (CH(CH₃)₂), 17.7 (C_{*p*-cym}CH₃), 9.8 (CNHC→RuCH₃), 9.8 (CNHC→RuCH₃), 9.7 (CNHC→SiCH₃), 8.5 (CNHC→SiCH₃).

$^{29}\text{Si}\{^1\text{H}\}$ NMR (99 MHz, CD_3CN , 300 K): δ [ppm] = 29.4 (Si/Ru), 23.3 (SiⁱBu₃).

EA: $\text{C}_{36}\text{H}_{65}\text{Cl}_3\text{N}_4\text{RuSi}_2$ calculated [%]: C (52.89), H (8.01), N (6.85).

measured [%]: C (53.12), H (8.23), N (7.11).

M.P.: 122-123 °C (decomposition, color change to black).

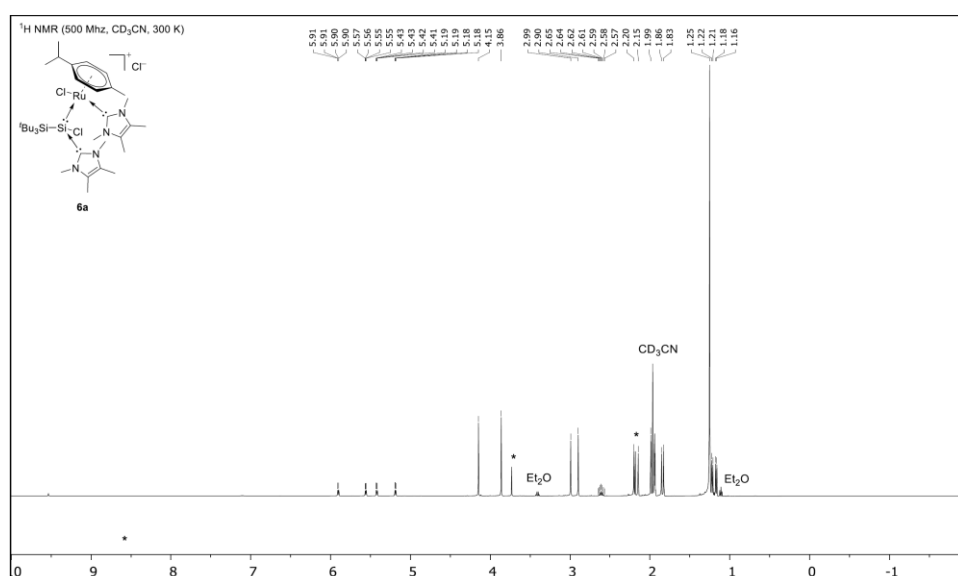


Figure S17 ^1H NMR spectrum of $[\text{Bu}_3\text{Si}-\text{Si}(\text{Ime}_4)\text{Cl} \rightarrow \text{RuCl}(\text{Ime}_4)(p\text{-cymene})]\text{Cl}$ (**6a**) in CD_3CN at 300 K. Residual imidazolium chloride $[\text{Ime}_4\text{HCl}]$ from the synthesis of **5a** and from the decomposition of **6a** is marked with *.

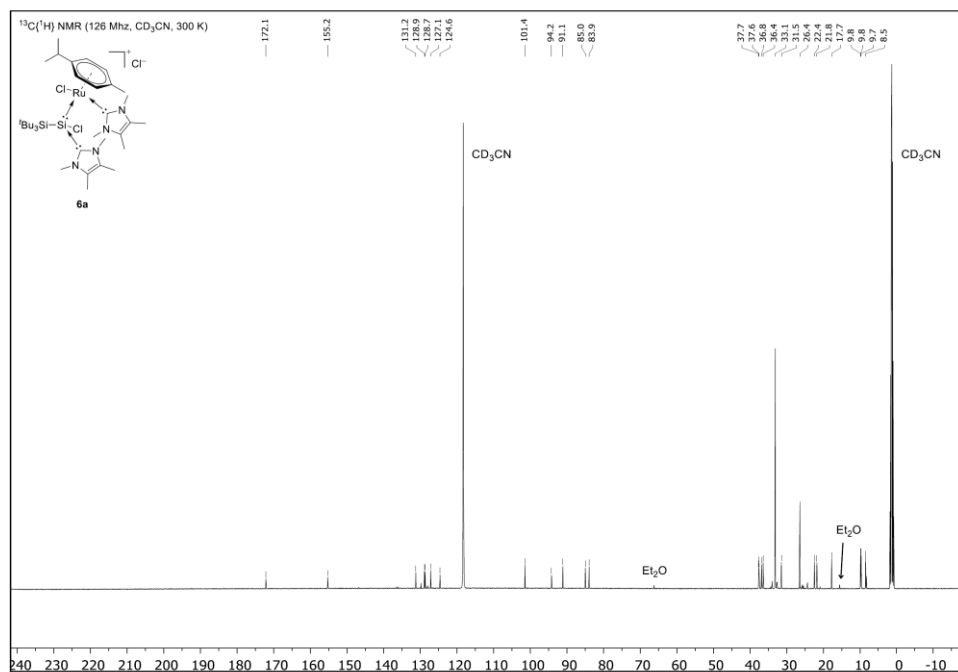


Figure S18 ¹³C{¹H} NMR spectrum of [^tBu₃Si-Si(Ime₄)Cl→RuCl(Ime₄)(*p*-cymene)]Cl (**6a**) in CD₃CN at 300 K.

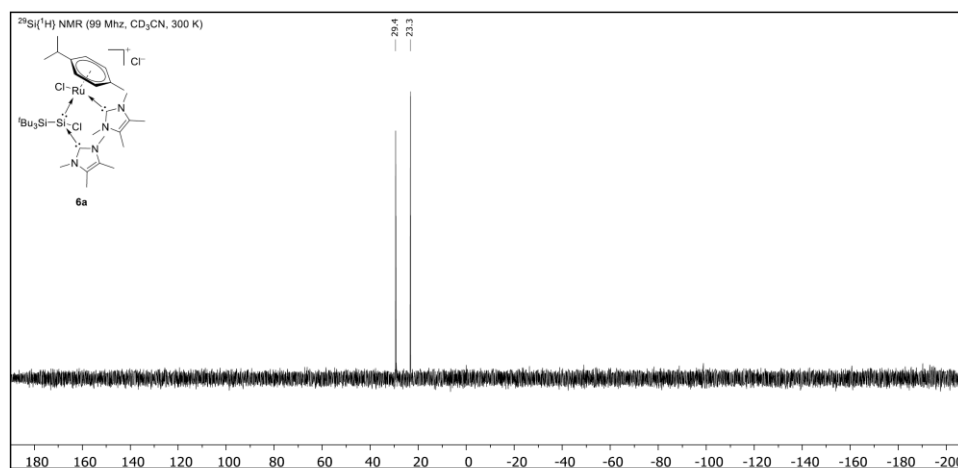


Figure S19 ²⁹Si{¹H} NMR spectrum of [^tBu₃Si-Si(Ime₄)Cl→RuCl(Ime₄)(*p*-cymene)]Cl (**6a**) in CD₃CN at 300 K.

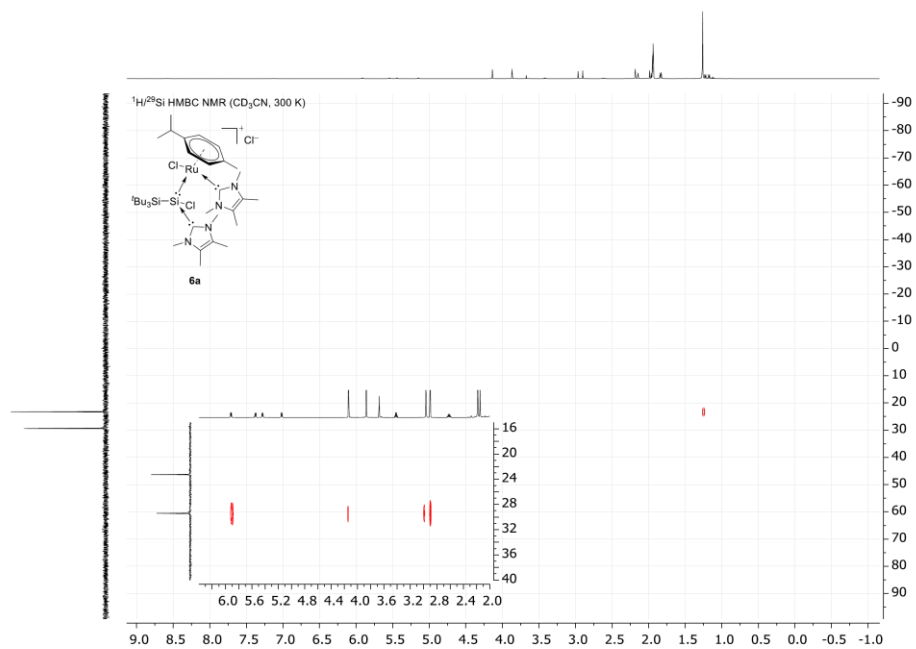


Figure S20 $^1\text{H}/^{29}\text{Si}$ HMBC NMR spectrum of $[\text{Bu}_3\text{Si}-\text{Si}(\text{IME}_4)\text{Cl} \rightarrow \text{RuCl}(\text{IME}_4)(p\text{-cymene})]\text{Cl}$ (**6a**) in CD_3CN at 300 K.

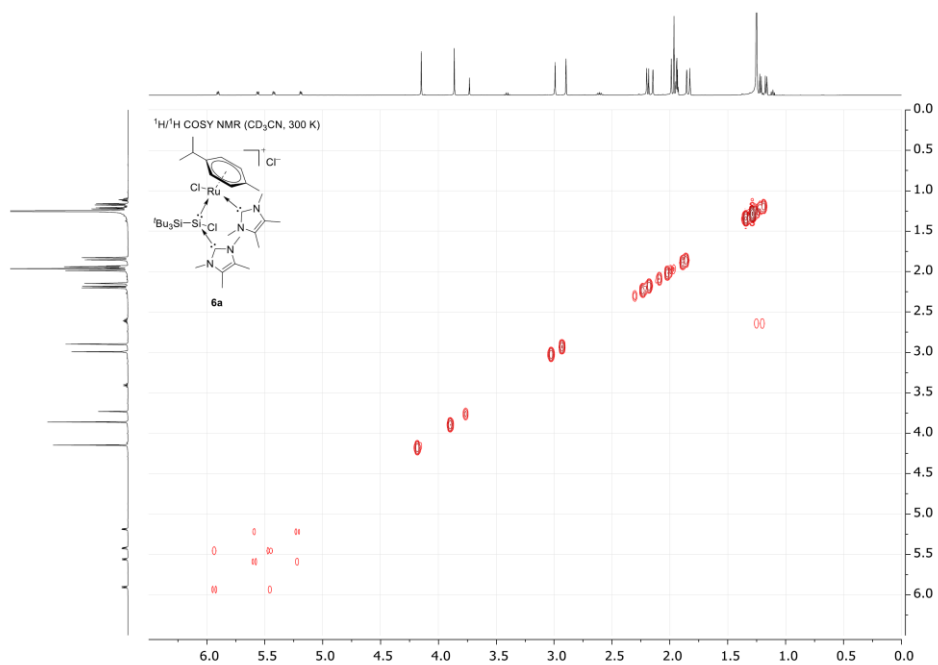


Figure S21 $^1\text{H}/^1\text{H}$ COSY NMR spectrum of $[\text{Bu}_3\text{Si}-\text{Si}(\text{IME}_4)\text{Cl} \rightarrow \text{RuCl}(\text{IME}_4)(p\text{-cymene})]\text{Cl}$ (**6a**) in CD_3CN at 300 K.

S20

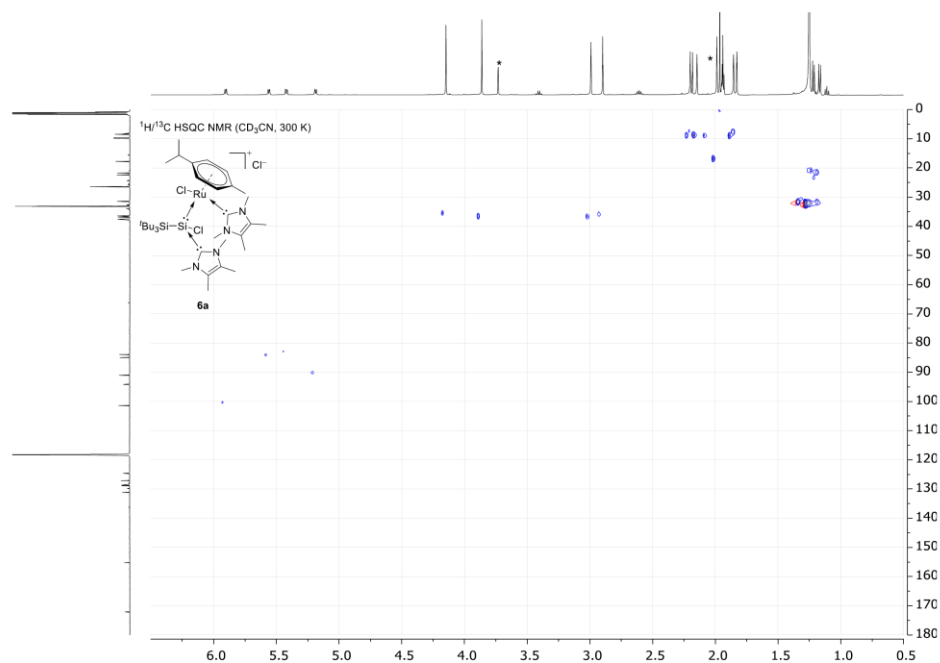


Figure S22 $^1\text{H}/^{13}\text{C}$ HSQC NMR spectrum of $[\text{tBu}_3\text{Si-Si}(\text{IME}_4)\text{Cl} \rightarrow \text{RuCl}(\text{IME}_4)(p\text{-cymene})]\text{Cl}$ (**6a**) in CD_3CN at 300 K.

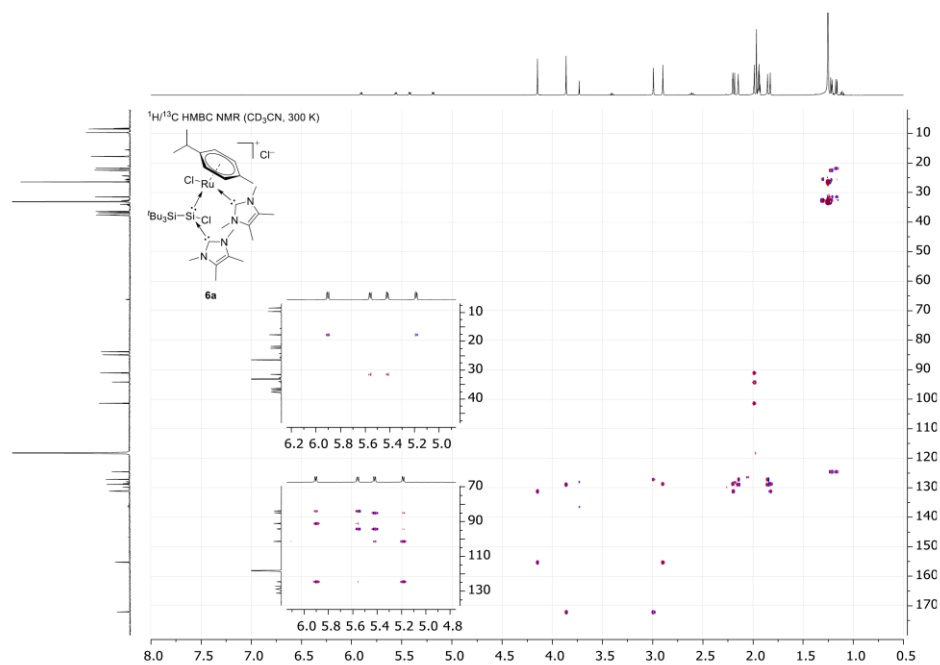
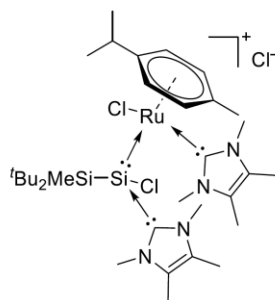


Figure S23 $^1\text{H}/^{13}\text{C}$ HMBC NMR spectrum of $[\text{tBu}_3\text{Si-Si}(\text{IME}_4)\text{Cl} \rightarrow \text{RuCl}(\text{IME}_4)(p\text{-cymene})]\text{Cl}$ (**6a**) in CD_3CN at 300 K.

1.3.3 [^tBu₂MeSi–Si(Ime₄)Cl→RuCl(Ime₄)(*p*-cymene)]Cl (6b)

6b

C₃₃H₅₉Cl₃N₄RuSi₂
775.45 g/mol

Note: The complex decomposes in solution at room temperature to an unidentified mixture of products.

Batch size: 5b: 50.0 mg, 106.6 μmol, 1.0 eq.

[RuCl₂(*p*-cymene)]₂: 32.6 mg, 53.3 μmol, 0.5 eq.

Yield: 46.4 mg (59.8 μmol, 58%) as an orange solid.

¹H NMR (500 MHz, CD₃CN, 300 K): δ [ppm] = 5.94 (dd, ³J_{H-H} = 6.0 Hz, ⁴J_{H-H} = 1.2 Hz, 1H, C_{*p*-cym}Har), 5.65 (dd, ³J_{H-H} = 6.1 Hz, ⁴J_{H-H} = 1.1 Hz, 1H, C_{*p*-cym}Har), 5.16 (dd, ³J_{H-H} = 6.0 Hz, ⁴J_{H-H} = 1.1 Hz, 1H, C_{*p*-cym}Har), 4.87 (dd, ³J_{H-H} = 6.1 Hz, ⁴J_{H-H} = 1.2 Hz, 1H, C_{*p*-cym}Har), 4.09 (s, 3H, NNHC→SiCH₃), 3.84 (s, 3H, NNHC→RuCH₃), 2.96 (s, 3H, NNHC→RuCH₃), 2.89 (s, 3H, NNHC→SiCH₃), 2.66 (sept, ³J_{H-H} = 7.0 Hz, 1H, CH(CH₃)₂), 2.21 (s, 3H, CNHC→SiCH₃), 2.14 (s, 3H, CNHC→RuCH₃), 2.11 (s, 3H, C_{*p*-cym}CH₃), 1.85 (s, 3H, CNHC→RuCH₃), 1.83 (s, 3H, CNHC→SiCH₃), 1.26 (s, 9H, Si(C(CH₃)₃)₂CH₃), 1.24 (d, ³J_{H-H} = 7.0 Hz, 3H, CH(CH₃)₂), 1.19 (d, ³J_{H-H} = 7.0 Hz, 3H, CH(CH₃)₂), 0.72 (s, 9H, Si(C(CH₃)₃)₂CH₃), 0.35 (s, 3H, Si(C(CH₃)₃)₂CH₃).

¹³C{¹H} NMR (101 MHz, CD₃CN, 300 K): δ [ppm] = 172.7 (NC_{NHC→Ru}N), 155.3 (NC_{NHC→Si}N), 130.6 (CNHC→SiCH₃), 128.8 (CNHC→RuCH₃), 128.8 (CNHC→SiCH₃), 127.1 (CNHC→RuCH₃), 124.7 (C_{*p*-cym}-*i*Pr), 99.8 (C_{*p*-cym}Har), 94.4 (C_{*p*-cym}CH₃), 87.7 (C_{*p*-cym}Har), 87.5 (C_{*p*-cym}Har), 87.2 (C_{*p*-cym}Har), 38.0 (NNHC→RuCH₃), 37.4 (NNHC→RuCH₃), 35.9 (NNHC→SiCH₃), 35.8 (NNHC→SiCH₃), 31.2 (Si(C(CH₃)₃)₂CH₃), 30.9 (CH(CH₃)₂), 29.8 (Si(C(CH₃)₃)₂CH₃), 24.4 (Si(C(CH₃)₃)₂CH₃), 23.9 (Si(C(CH₃)₃)₂CH₃), 23.2 (CH(CH₃)₂), 20.9 (CH(CH₃)₂), 17.6 (C_{*p*-cym}CH₃), 9.9 (CNHC→RuCH₃), 9.6 (CNHC→RuCH₃), 9.5 (CNHC→SiCH₃), 8.3 (CNHC→SiCH₃), 0.8 (Si(C(CH₃)₃)₂CH₃).

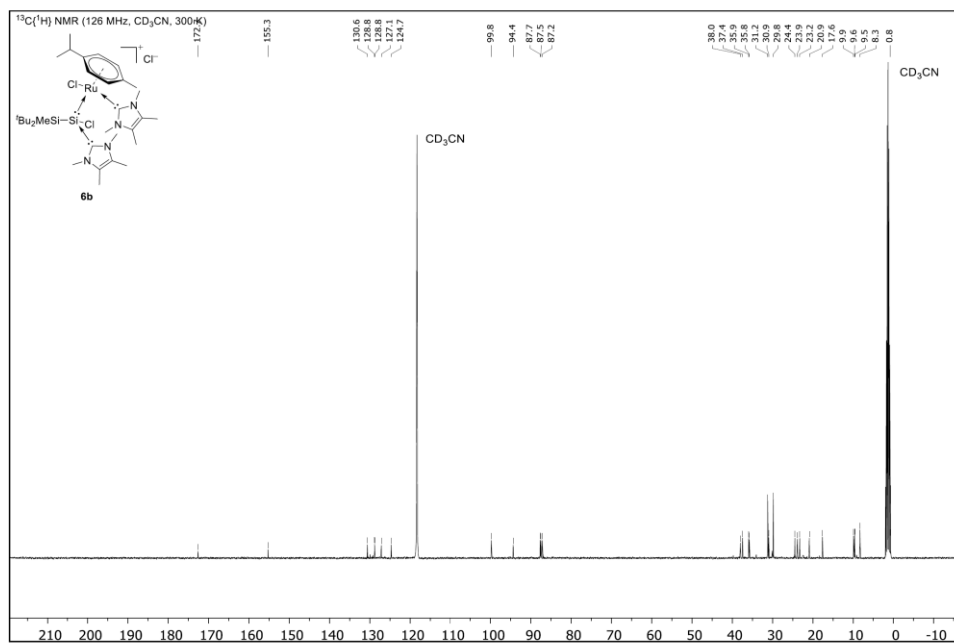


Figure S25 ¹³C{¹H} NMR spectrum of [^tBu₂MeSi-Si(Ime₄)Cl→RuCl(Ime₄)(*p*-cymene)]Cl (**6b**) in CD₃CN at 300 K.

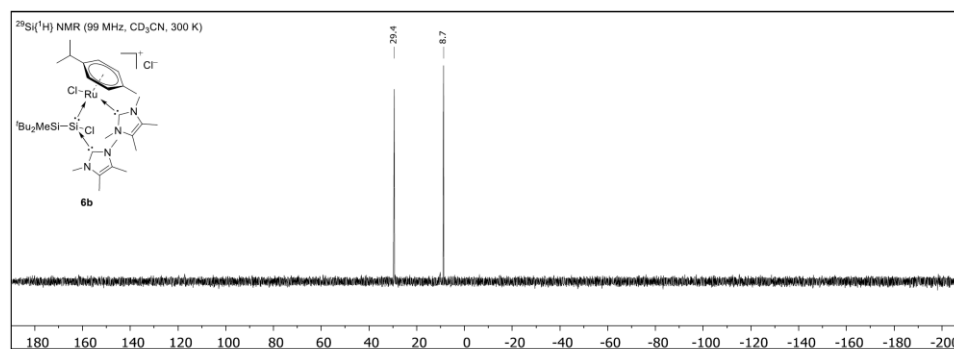


Figure S26 ²⁹Si{¹H} NMR spectrum of [^tBu₂MeSi-Si(Ime₄)Cl→RuCl(Ime₄)(*p*-cymene)]Cl (**6b**) in CD₃CN at 300 K.

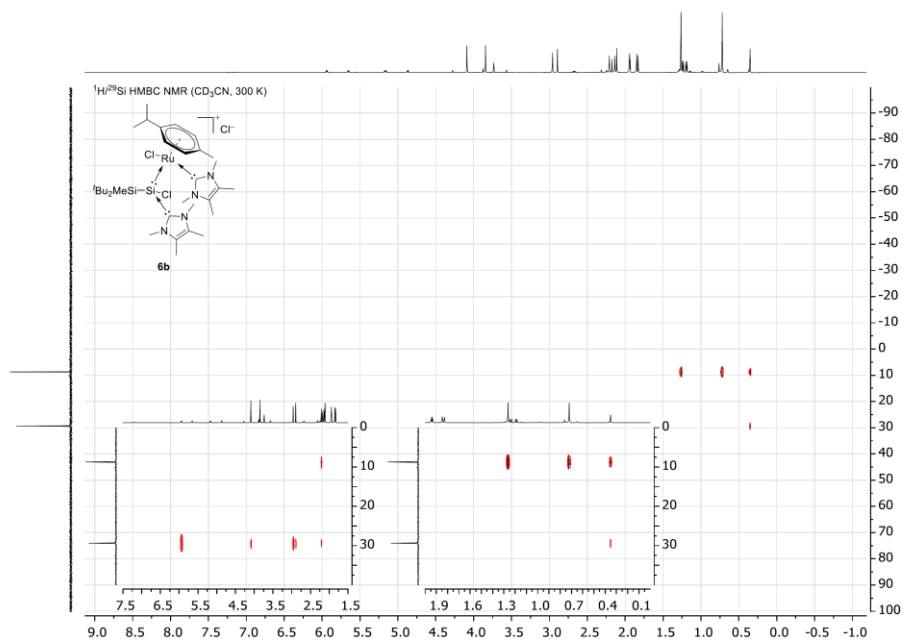


Figure S27 ¹H/²⁹Si HMBC NMR spectrum of [^tBu₂MeSi-Si(IME₄)Cl→RuCl(IME₄)(*p*-cymene)]Cl (**6b**) in CD₃CN at 300 K.

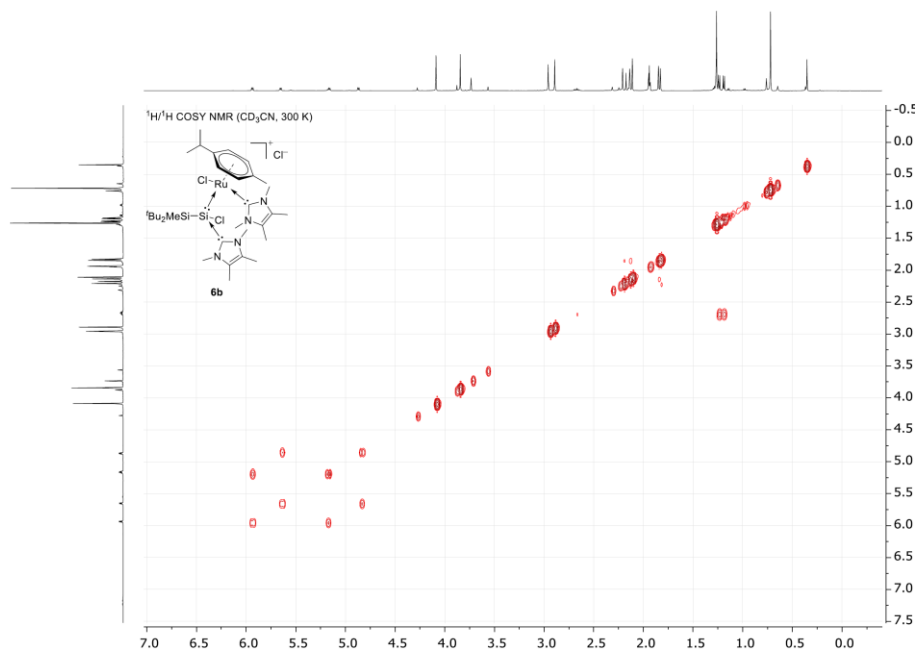


Figure S28 ¹H/¹H COSY NMR spectrum of [^tBu₂MeSi-Si(IME₄)Cl→RuCl(IME₄)(*p*-cymene)]Cl (**6b**) in CD₃CN at 300 K.

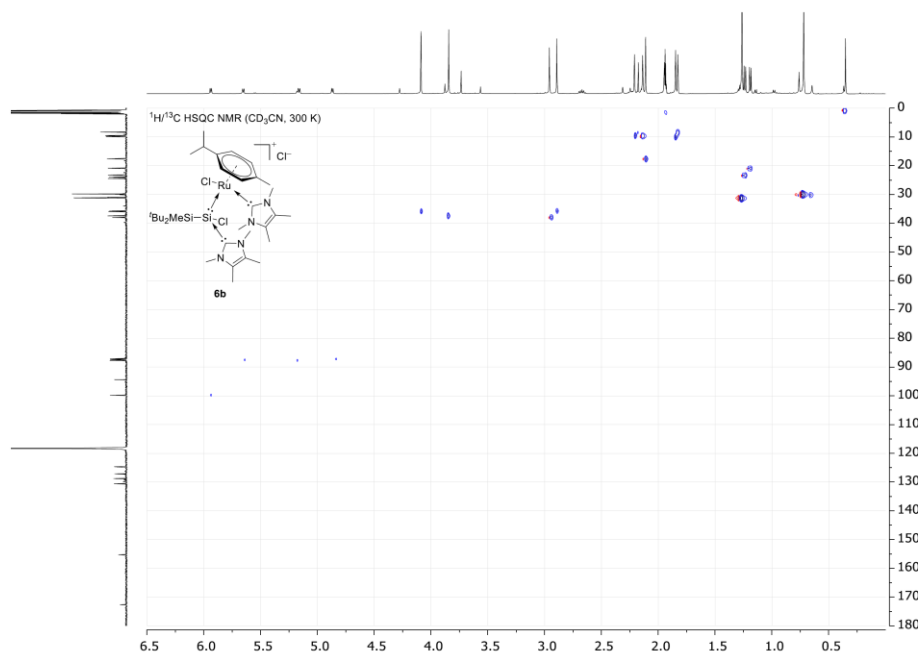


Figure S29 $^1\text{H}/^{13}\text{C}$ HSQC NMR spectrum of $[\text{Bu}_2\text{MeSi-Si}(\text{IMe}_4)\text{Cl} \rightarrow \text{RuCl}(\text{IMe}_4)(p\text{-cymene})]\text{Cl}$ (**6b**) in CD_3CN at 300 K.

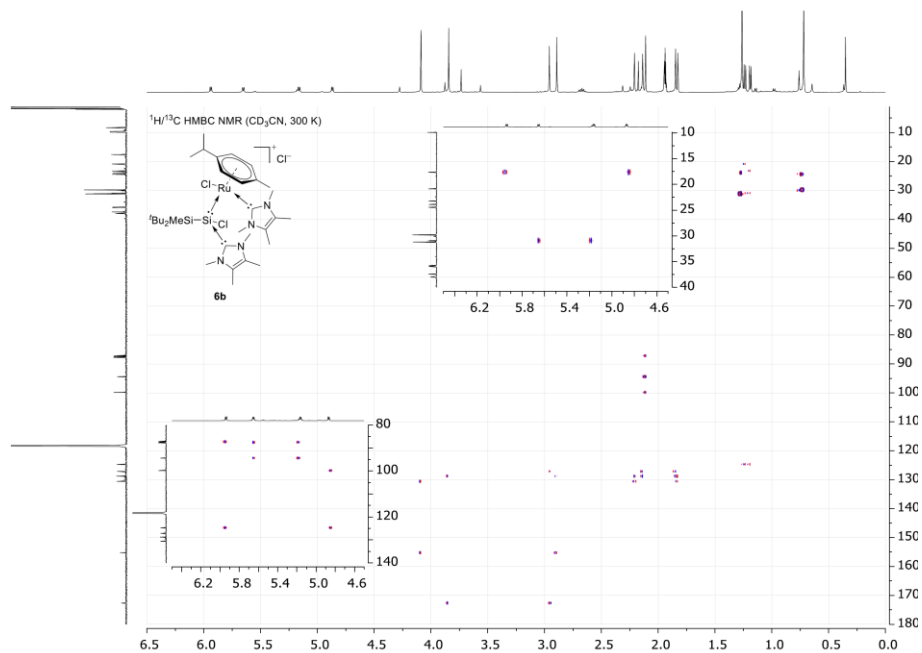
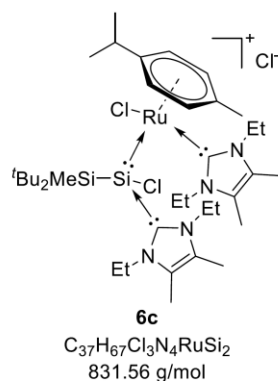


Figure S30 $^1\text{H}/^{13}\text{C}$ HMBC NMR spectrum of $[\text{Bu}_2\text{MeSi-Si}(\text{IMe}_4)\text{Cl} \rightarrow \text{RuCl}(\text{IMe}_4)(p\text{-cymene})]\text{Cl}$ (**6b**) in CD_3CN at 300 K.

1.3.4 [^tBu₂MeSi–Si(IEt₂Me₂)Cl]→RuCl(IEt₂Me₂)(*p*-cymene)]Cl (6c)

Note: (a) The complex decomposes in solution at room temperature to an unidentified mixture of products; (b) The reaction takes longer to complete than the reactions with the *IMe*₄-stabilized silyliumylidene ions (~30 minutes vs. 1-3 minutes) due to the increased steric hindrance of the NHCs. Attempts to isolate the silyliumylidene complex (analogous to **2'**) failed. The rate determining step appears to be the coordination of the silyliumylidene **5c** to the transition metal precursor with the insertion reaction occurring significantly faster. At low temperature (to slow down the insertion step) no coordinating reaction was observed.

Batch size: **5c:** 50.0 mg, 95.2 μmol, 1.0 eq.

[RuCl₂(*p*-cymene)]₂: 29.1 mg, 47.6 μmol, 0.5 eq.

Yield: 35.3 mg (42.5 μmol, 45%) as an orange solid.

¹H NMR (500 MHz, CD₃CN, 300 K): δ [ppm] = 6.13 (dd, ³J_{H-H} = 6.4 Hz, ⁴J_{H-H} = 1.4 Hz, 1H, C_{*p*-cym}Har), 5.73 (dd, ³J_{H-H} = 5.9 Hz, ⁴J_{H-H} = 1.6 Hz, 1H, C_{*p*-cym}Har), 5.38 (dd, ³J_{H-H} = 6.4 Hz, ⁴J_{H-H} = 1.4 Hz, 1H, C_{*p*-cym}Har), 5.00 (dd, ³J_{H-H} = 5.9 Hz, ⁴J_{H-H} = 1.6 Hz, 1H, C_{*p*-cym}Har), 4.89 (dq, ²J_{H-H} = 14.3 Hz, ³J_{H-H} = 7.1 Hz, 1H, NNHC→SiCH₂CH₃), 4.56 – 4.46 (m, 2H, NNHC→SiCH₂CH₃, NNHC→RuCH₂CH₃), 4.35 (dq, ²J_{H-H} = 14.2 Hz, ³J_{H-H} = 7.1 Hz, 1H, NNHC→RuCH₂CH₃), 3.88 (dq, ²J_{H-H} = 14.2 Hz, ³J_{H-H} = 7.1 Hz, 1H, NNHC→SiCH₂CH₃), 3.75 (dq, ²J_{H-H} = 14.3 Hz, ³J_{H-H} = 7.1 Hz, 1H, NNHC→RuCH₂CH₃), 2.68 (sept, ³J_{H-H} = 6.9 Hz, 1H, CH(CH₃)₂), 2.51 (dq, J = 13.9, 7.0 Hz, 1H, NNHC→RuCH₂CH₃), 2.37 – 2.31 (m, 1H, NNHC→SiCH₂CH₃), 2.26 (s, 3H, CNHC→SiCH₃), 2.20 (s, 3H, CNHC→RuCH₃), 2.12 (s, 3H, C_{*p*-cym}CH₃), 1.99 (s, 3H, CNHC→SiCH₃), 1.96 (s, 3H, CNHC→RuCH₃), 1.43 (t, ³J_{H-H} = 7.1 Hz, 3H, NNHC→SiCH₂CH₃), 1.31 (d, ³J_{H-H} = 6.9 Hz, 3H, CH(CH₃)₂), 1.30 – 1.26 (m, 12H, Si(C(CH₃)₃)₂CH₃, NNHC→RuCH₂CH₃), 1.25 (d, ³J_{H-H} = 6.9 Hz, 3H, CH(CH₃)₂), 1.11 (t, ³J_{H-H} = 7.1 Hz, 3H, NNHC→RuCH₂CH₃), 0.86 – 0.81 (m, 12H, Si(C(CH₃)₃)₂CH₃, NNHC→SiCH₂CH₃), 0.37 (s, 3H, Si(C(CH₃)₃)₂CH₃).

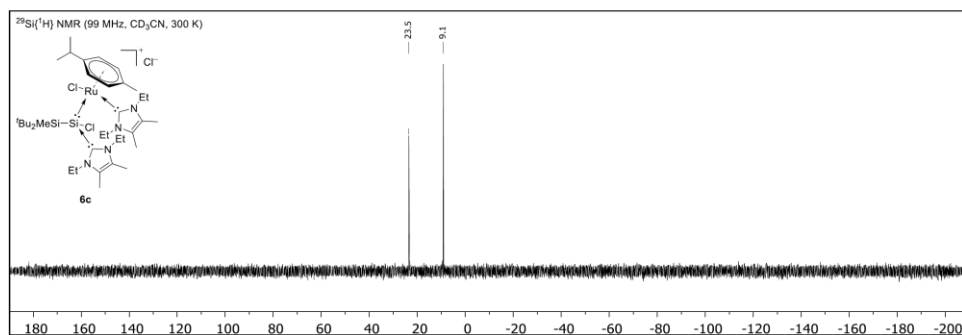


Figure S33 $^{29}\text{Si}\{^1\text{H}\}$ NMR spectrum of $[\text{Bu}_2\text{MeSi}-\text{Si}(\text{IEt}_2\text{Me}_2)\text{Cl} \rightarrow \text{Ru}(p\text{-cymene})\text{Cl}(\text{IEt}_2\text{Me}_2)]\text{Cl}$ (**6c**) in CD_3CN at 300 K.

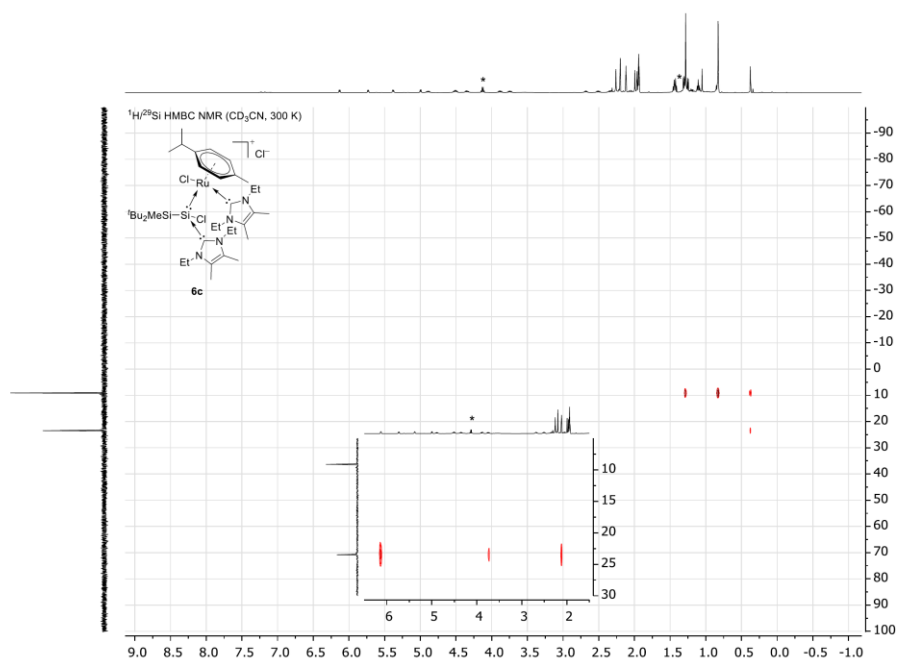


Figure S34 $^1\text{H}/^{29}\text{Si}$ HMBC NMR spectrum of $[\text{Bu}_2\text{MeSi}-\text{Si}(\text{IEt}_2\text{Me}_2)\text{Cl} \rightarrow \text{Ru}(p\text{-cymene})\text{Cl}(\text{IEt}_2\text{Me}_2)]\text{Cl}$ (**6c**) in CD_3CN at 300 K. Imidazolium chloride $[\text{IEt}_2\text{Me}_2 \cdot \text{HCl}]$ from the silyliumylidene precursor is marked with *.

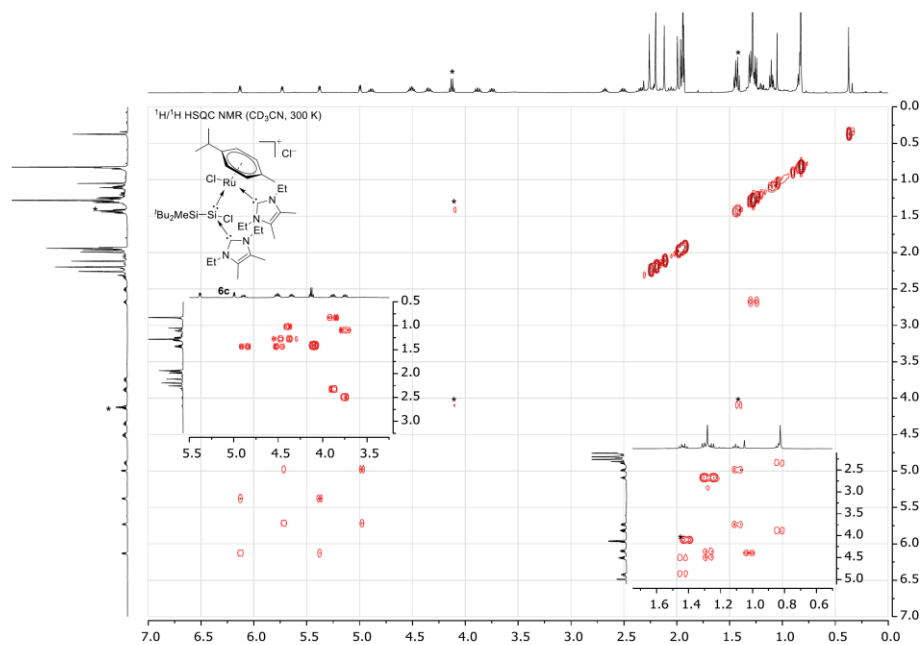


Figure S35 $^1\text{H}/^1\text{H}$ HSQC NMR spectrum of $[\text{tBu}_2\text{MeSi}(\text{I}(\text{Et}_2\text{Me}_2)\text{Cl})\text{Ru}(p\text{-cymene})\text{Cl}(\text{I}(\text{Et}_2\text{Me}_2))\text{Cl}]$ (**6c**) in CD_3CN at 300 K. Imidazolium chloride $[\text{I}(\text{Et}_2\text{Me}_2)\text{HCl}]$ from the silyliumylidene precursor is marked with *.

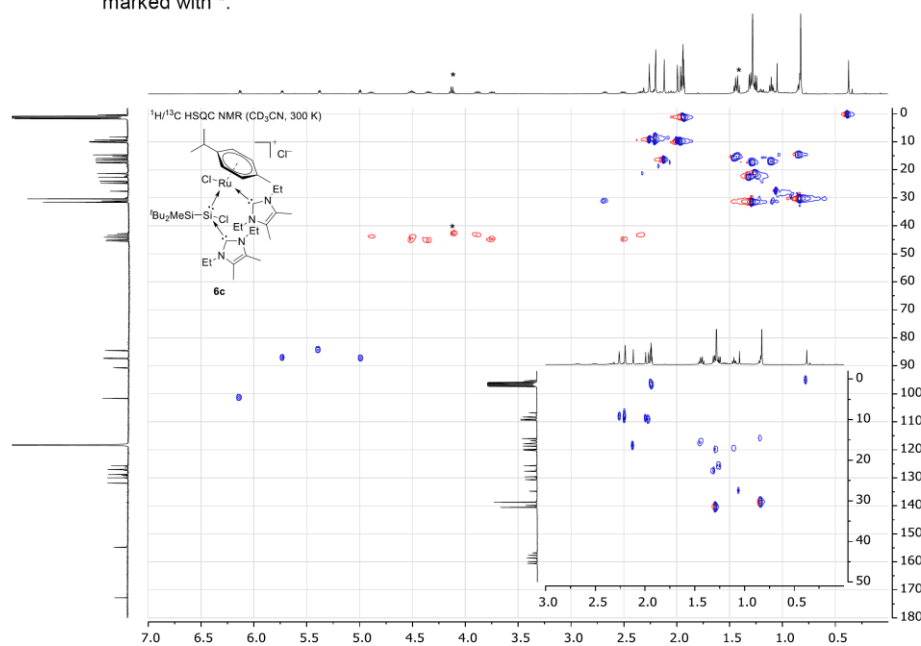


Figure S36 $^1\text{H}/^{13}\text{C}$ HSQC NMR spectrum of $[\text{tBu}_2\text{MeSi}(\text{I}(\text{Et}_2\text{Me}_2)\text{Cl})\text{Ru}(p\text{-cymene})\text{Cl}(\text{I}(\text{Et}_2\text{Me}_2))\text{Cl}]$ (**6c**) in CD_3CN at 300 K. Imidazolium chloride $[\text{I}(\text{Et}_2\text{Me}_2)\text{HCl}]$ from the silyliumylidene precursor is marked with *.

S31

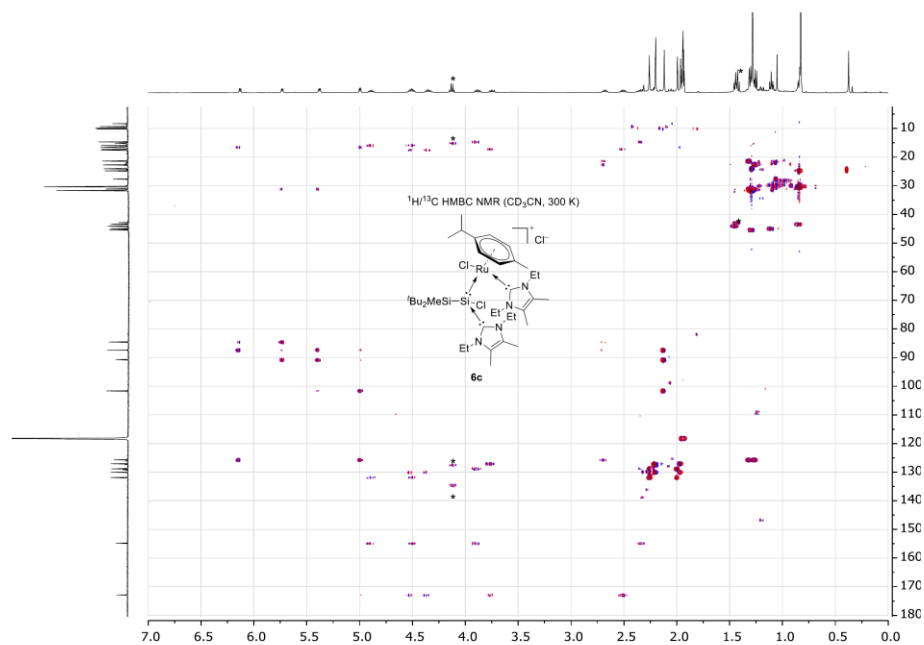
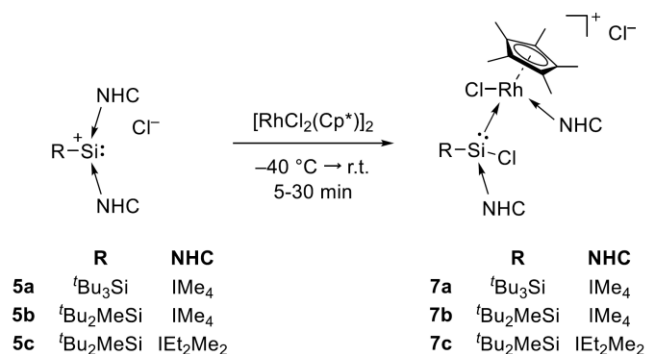


Figure S37 $^1\text{H}/^{13}\text{C}$ HMBC NMR spectrum of $[\text{Bu}_2\text{MeSi}-\text{Si}(\text{IEt}_2\text{Me}_2)\text{Cl} \rightarrow \text{Ru}(\text{p}\text{-cymene})\text{Cl}(\text{IEt}_2\text{Me}_2)]\text{Cl}$ (**6c**) in CD_3CN at 300 K. Imidazolium chloride $[\text{IEt}_2\text{Me}_2\text{HCl}]$ from the silyliumylidene precursor is marked with *.

1.4 General Synthetic Procedure for $[R-Si(NHC)Cl \rightarrow RhCl(NHC)(Cp^*)]Cl$ 

Silyliumylidene chloride $[R_3Si-Si(NHC)_2]Cl$ (**5a-c**) (1.0 eq) and $[RhCl_2(Cp^*)]_2$ (0.5 eq) were mixed, cooled to $-40\text{ }^\circ\text{C}$ and pre-cooled ($-40\text{ }^\circ\text{C}$) MeCN (3-10 mL) was added. The reaction mixtures were stirred at $-40\text{ }^\circ\text{C}$ until all starting material had dissolved (5-30 minutes) and then warmed to room temperature. The solutions were quickly concentrated under reduced pressure to about 1-3 mL. A mixture of toluene and Et₂O (1:1, 5-15 mL) was added and the orange-red solutions were stored at $-35\text{ }^\circ\text{C}$ for 3-10 days. The formed crystals/precipitate was collected by filtration, washed with benzene or toluene (2 mL) and Et₂O (2×2 mL) and after drying under vacuum the complexes **7a-b** were isolated as orange to orange-red air- and moisture-sensitive solids/crystals. In the case of **7c** (R = Si^tBu₂Me, NHC = IEt₂Me₂) the product could only be detected and assigned *via* ²⁹Si NMR spectroscopy (*cf.* Figure S56) due to competing side reactions.

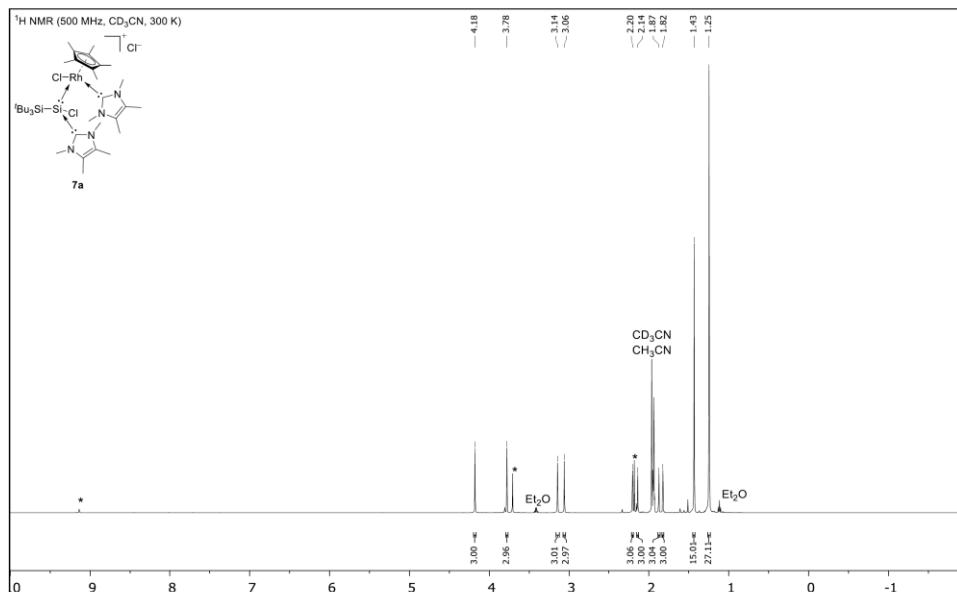


Figure S38 ¹H NMR spectrum of [^tBu₃Si-Si(IME₄)Cl→RhCl(IME₄)(Cp^{*})]Cl (**7a**) in CD₃CN at 300 K. Small amounts of residual imidazolium chloride from the precursor [IME₄·HCl] are marked with *.

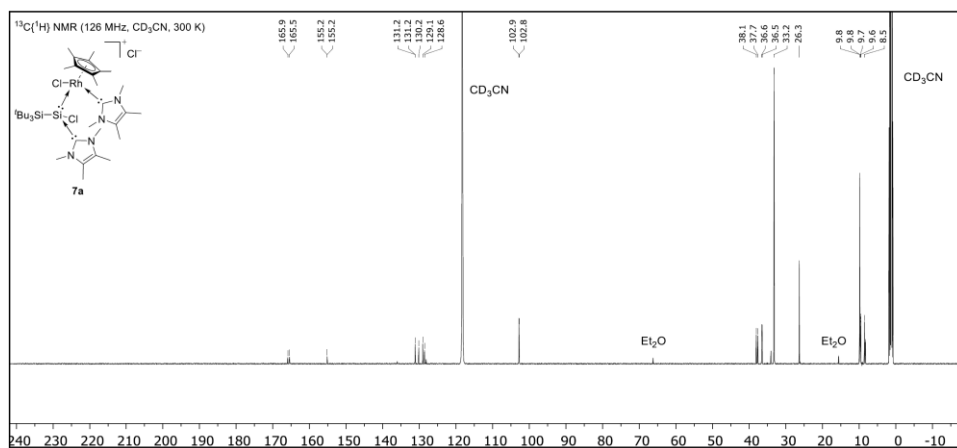


Figure S39 ¹³C{¹H} NMR spectrum of [^tBu₃Si-Si(IME₄)Cl→RhCl(IME₄)(Cp^{*})]Cl (**7a**) in CD₃CN at 300 K.

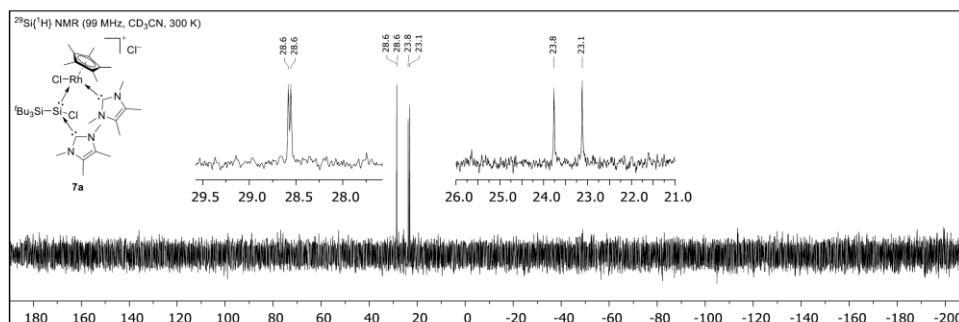


Figure S40 ²⁹Si{¹H} NMR spectrum of [**7a**] in CD₃CN at 300 K.

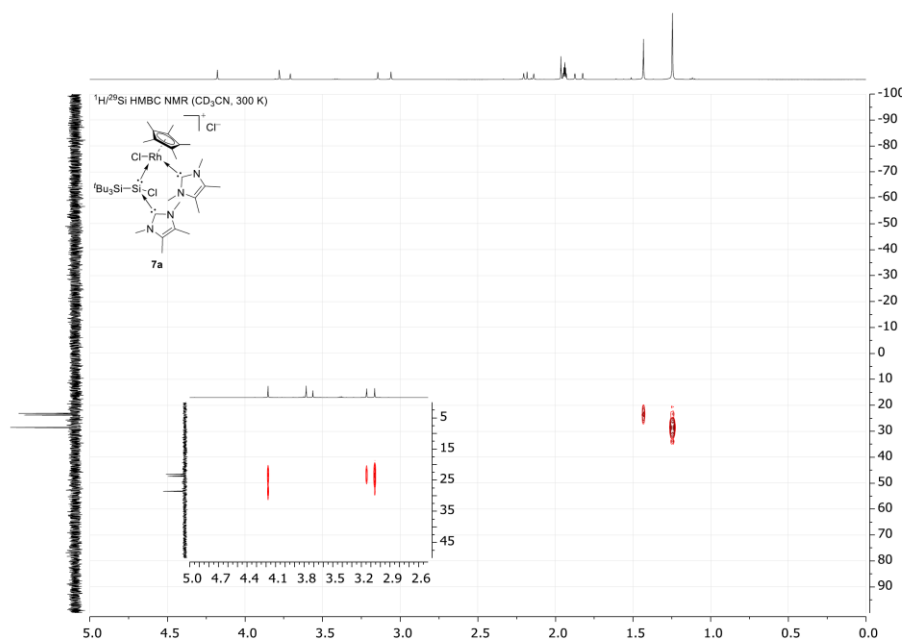


Figure S41 ¹H/²⁹Si HMBC NMR spectrum of [**7a**] in CD₃CN at 300 K.

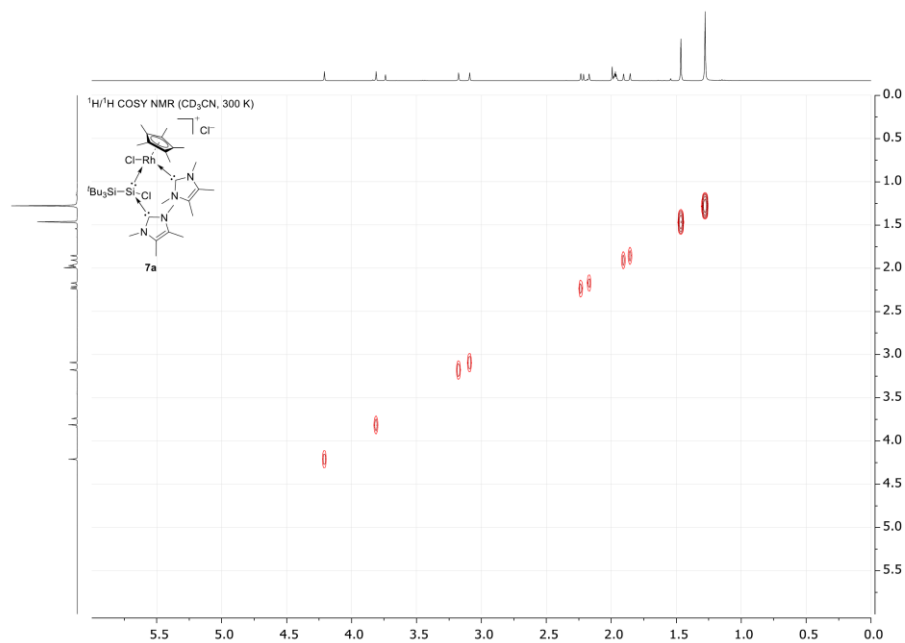


Figure S42 ¹H/¹H COSY NMR spectrum of $[\text{Bu}_3\text{Si}-\text{Si}(\text{IME}_4)\text{Cl} \rightarrow \text{RhCl}(\text{IME}_4)(\text{Cp}^*)]\text{Cl}$ (**7a**) in CD₃CN at 300 K.

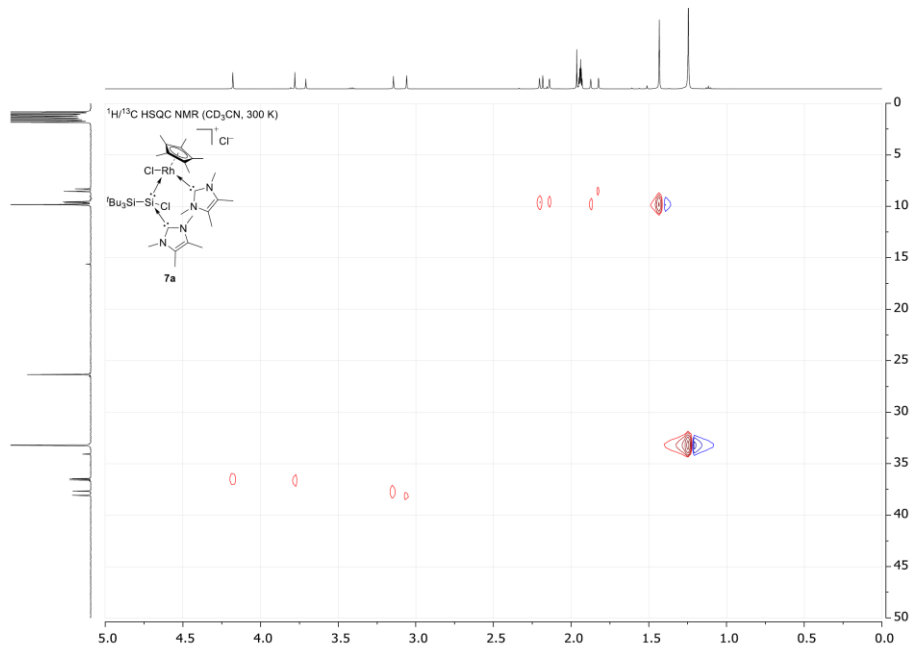


Figure S43 ¹H/¹³C HSQC NMR spectrum of $[\text{Bu}_3\text{Si}-\text{Si}(\text{IME}_4)\text{Cl} \rightarrow \text{RhCl}(\text{IME}_4)(\text{Cp}^*)]\text{Cl}$ (**7a**) in CD₃CN at 300 K.

S37

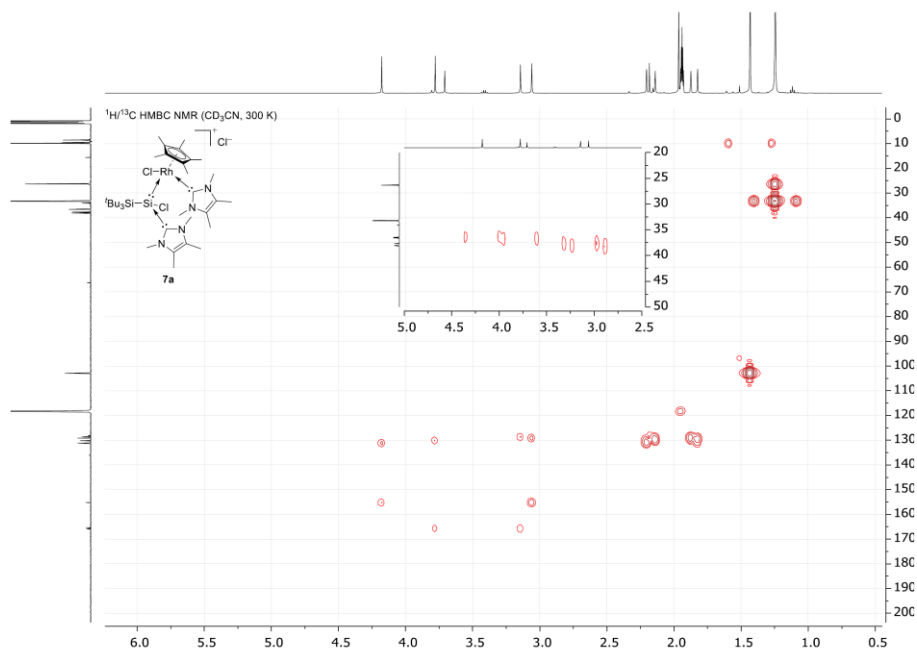


Figure S44 $^1\text{H}/^{13}\text{C}$ HMBC NMR spectrum of $[\text{tBu}_3\text{Si-Si}(\text{IMe}_4)\text{Cl} \rightarrow \text{RhCl}(\text{IMe}_4)(\text{Cp}^*)]\text{Cl}$ (**7a**) in CD_3CN at 300 K.

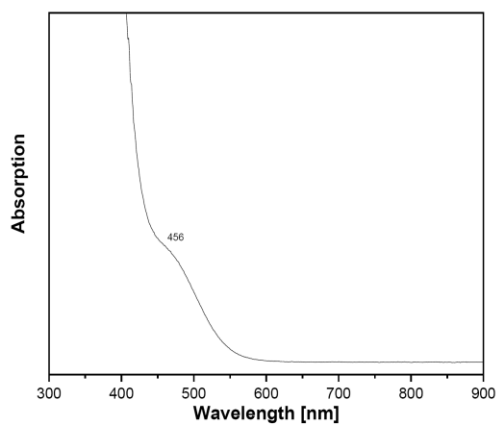
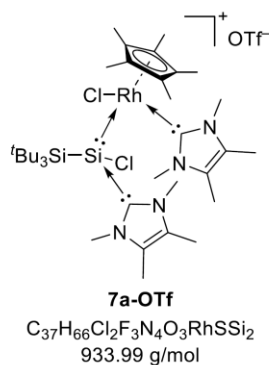


Figure S45 UV-Vis spectrum (300-900 nm) of $[\text{tBu}_3\text{Si-Si}(\text{IMe}_4)\text{Cl} \rightarrow \text{RhCl}(\text{IMe}_4)(\text{Cp}^*)]\text{Cl}$ (**7a**) in toluene at room temperature ($c = 5.0 \times 10^{-4}$ mol/L). $\lambda_{\text{max}} = 456$ nm.

(b) [^tBu₃Si–Si(Ime₄)Cl→RhCl(Ime₄)(Cp^{*})]OTf (**7a-OTf**)

To determine whether insertion into the Rh–Cl bond takes place or if the reaction occurs from an NHC-stabilized chlorosilylene, we synthesized **5a-OTf** (*vide supra*) and utilized it in a reaction similar to that described in section 1.4 for the synthesis of **7a**.

[^tBu₃Si–Si(Ime₄)₂]OTf (**5a-OTf**) (30.0 mg, 48.0 μmol, 1.0 eq) was mixed with [RhCl₂(Cp^{*})]₂ (14.8 mg, 24.0 μmol, 0.5 eq) and cooled to –35 °C. Pre-cooled (–35 °C) CD₃CN (0.5 mL) was added and the suspension was stirred for 5 minutes and then transferred to a *J*-Young NMR tube.

¹H NMR (500 MHz, CD₃CN, 300 K): δ [ppm] = 4.17 (s, 3H, N_{NHC→Si}CH₃), 3.78 (s, 3H, N_{NHC→Rh}CH₃), 3.13 (s, 3H, N_{NHC→Rh}CH₃), 3.06 (s, 3H, N_{NHC→Si}CH₃), 2.19 (s, 3H, C_{NHC→Si}CH₃), 2.14 (s, 3H, C_{NHC→Rh}CH₃), 1.87 (s, 3H, C_{NHC→Rh}CH₃), 1.82 (s, 3H, C_{NHC→Si}CH₃), 1.44 (s, 15H, C₅(CH₃)₅), 1.25 (s, 27H, Si(C(CH₃)₃)₃).

Note: ¹H NMR data are the same as **7a**.

¹³C{¹H} NMR (126 MHz, CD₃CN, 300 K): δ [ppm] = 165.8 (d, ¹J_{Rh–C} = 60.0 Hz, NC_{NHC→Rh}N), 155.2 (d, ²J_{Rh–C} = 2.7 Hz, NC_{NHC→Si}N), 131.1 (C_{NHC→Si}CH₃), 130.2 (C_{NHC→Rh}CH₃), 129.1 (C_{NHC→Si}CH₃), 128.6 (C_{NHC→Rh}CH₃), 122.1 (q, ¹J_{C–F} = 320.9 Hz, SO₃CF₃), 102.8 (d, ¹J_{Rh–C} = 4.8 Hz, C₅(CH₃)₅), 38.0 (N_{NHC→Si}CH₃), 37.6 (N_{NHC→Rh}CH₃), 36.6 (N_{NHC→Rh}CH₃), 36.4 (N_{NHC→Si}CH₃), 33.2 (Si(C(CH₃)₃)₃), 26.3 (Si(C(CH₃)₃)₃), 9.8 (C₅(CH₃)₅), 9.8 (C_{NHC→Rh}CH₃), 9.6 (C_{NHC→Si}CH₃), 9.5 (C_{NHC→Rh}CH₃), 8.5 (C_{NHC→Si}CH₃).

Note: (a) ¹³C NMR data (for comparison, cf. Figure S47) are the same as **7a** except for the additional resonance corresponding to the triflate anion (122.1 ppm (q, ¹J_{C–F} = 320.9 Hz). (b) The resonance for the SO₃CF₃ group (quartet) partially overlaps with the resonance for CD₃CN.

$^{29}\text{Si}\{^1\text{H}\}$ NMR (99 MHz, CD_3CN , 300 K): δ [ppm] = 28.7 (d, $^2J_{\text{Si-Rh}} = 2.8$ Hz, Si^iBu_3), 23.4 (d, $^1J_{\text{Si-Rh}} = 63.8$ Hz, Si^oRh).

Note: ^{29}Si NMR (for comparison, cf. Figure S48) data are the same as **7a**.

$^{19}\text{F}\{^1\text{H}\}$ NMR (471 MHz, CD_3CN , 300 K): δ [ppm] = -79.3 (SO_3CF_3).

Note: Only the resonance corresponding to a free triflate anion could be observed.

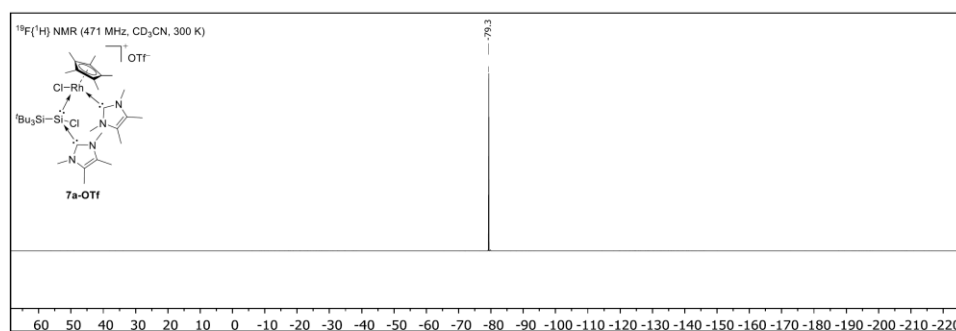


Figure S46 $^{19}\text{F}\{^1\text{H}\}$ NMR spectrum of $[\text{tBu}_3\text{Si-Si}(\text{Ime}_4)\text{Cl}\rightarrow\text{RhCl}(\text{Ime}_4)(\text{Cp}^*)]\text{OTf}$ (**7a-OTf**) in CD_3CN at 300 K.

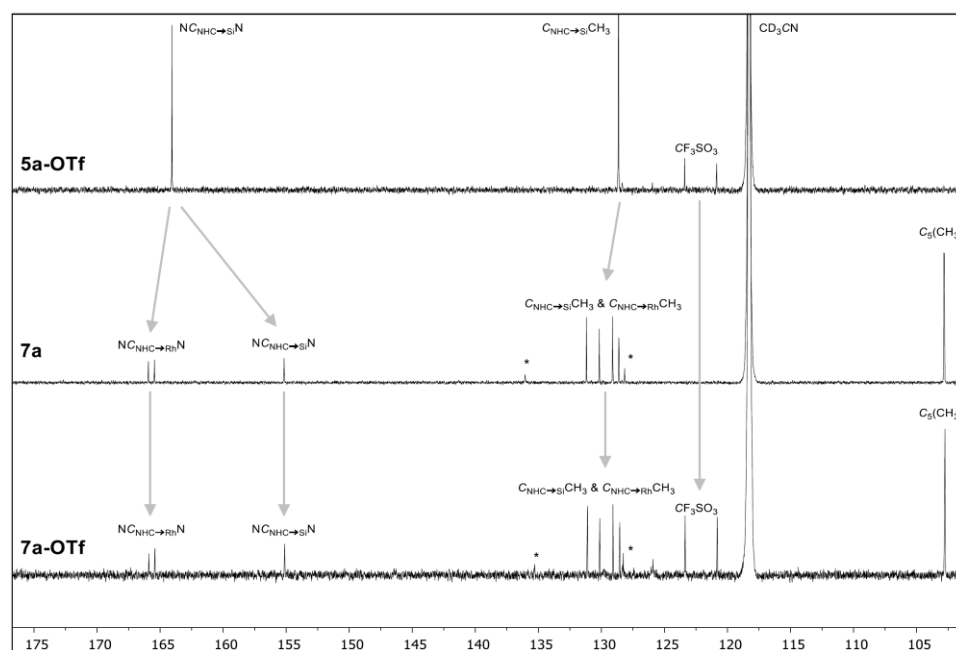


Figure S47 Section (180-100 ppm) of the $^{13}\text{C}\{^1\text{H}\}$ NMR spectra of **5a-OTf** (top), **7a** (middle) and **7a-OTf** (bottom) in CD_3CN at 300 K. Small amounts of residual imidazolium chloride $[\text{Ime}_4^+\text{Cl}^-]$ from the synthesis of **5a/5a-OTf** are marked with *.

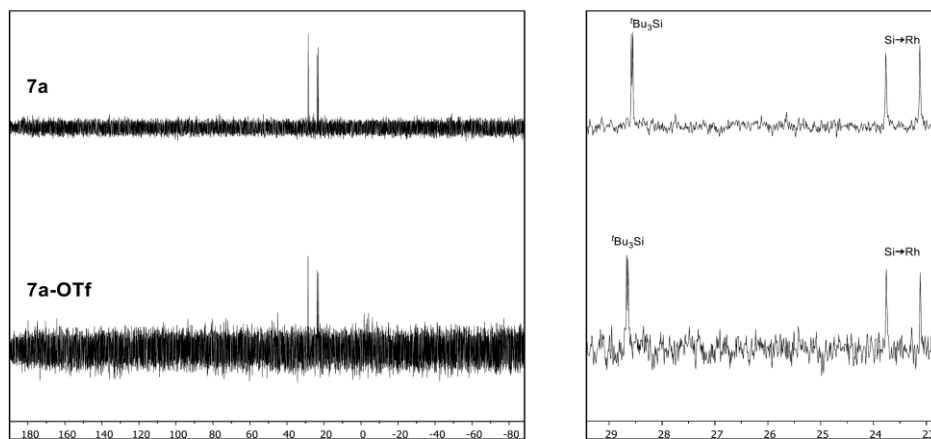
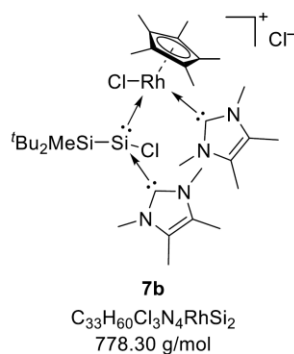


Figure S48 $^{29}\text{Si}\{^1\text{H}\}$ NMR spectrum of **7a** (top) and **7a-OTf** (bottom) in CD_3CN at 300 K.

1.4.2 [^tBu₂MeSi–Si(IME₄)Cl→RhCl(IME₄)(Cp^{*})]Cl (**7b**)

Batch size: **5b:** 50.0 mg, 106.6 μmol, 1.0 eq.

[RhCl₂(Cp^{*})]₂: 32.9 mg, 53.3 μmol, 0.5 eq.

Yield: 51.5 mg (66.2 μmol, 62%) as an orange-red solid.

SC-XRD: Suitable single crystals were obtained by slow diffusion of Et₂O into a concentrated solution of **7b** in MeCN at –35 °C.

¹H NMR (500 MHz, CD₃CN, 300 K): δ [ppm] = 4.15 (s, 3H, N_{NHC}→SiCH₃), 3.79 (s, 3H, N_{NHC}→RhCH₃), 3.15 (s, 3H, N_{NHC}→RhCH₃), 3.11 (s, 3H, N_{NHC}→SiCH₃), 2.22 (s, 3H, C_{NHC}→SiCH₃), 2.13 (s, 3H, C_{NHC}→RhCH₃), 1.86 (s, 3H, C_{NHC}→RhCH₃), 1.84 (s, 3H, C_{NHC}→SiCH₃), 1.47 (s, 15H, C₅(CH₃)₅), 1.21 (s, 9H, Si(C(CH₃)₃)₂CH₃), 0.74 (s, 9H, Si(C(CH₃)₃)₂CH₃), 0.41 (s, 3H, Si(C(CH₃)₃)₂CH₃).

¹³C{¹H} NMR (126 MHz, CD₃CN, 300 K): δ [ppm] = 165.9 (d, ¹J_{Rh–C} = 59.2 Hz, NC_{NHC}→RhN) 154.9 (d, ²J_{Rh–C} = 2.5 Hz, NC_{NHC}→SiN), 130.8 (C_{NHC}→SiCH₃), 130.0 (C_{NHC}→RhCH₃), 129.2 (C_{NHC}→SiCH₃), 128.4 (C_{NHC}→RhCH₃), 102.3 (d, ¹J_{Rh–C} = 4.8 Hz, C₅(CH₃)₅), 38.4 (N_{NHC}→RhCH₃), 36.6 (N_{NHC}→SiCH₃), 36.6 (N_{NHC}→RhCH₃), 35.8 (N_{NHC}→SiCH₃), 31.3 (Si(C(CH₃)₃)₂CH₃), 29.9 (Si(C(CH₃)₃)₂CH₃), 24.7 (Si(C(CH₃)₃)₂CH₃), 24.1 (Si(C(CH₃)₃)₂CH₃), 9.9 (C_{NHC}→RhCH₃), 9.7 (C₅(CH₃)₅), 9.6 (C_{NHC}→RhCH₃), 9.5 (C_{NHC}→SiCH₃), 8.3 (C_{NHC}→SiCH₃), –0.8 (Si(C(CH₃)₃)₂CH₃).

²⁹Si{¹H} NMR (99 MHz, CD₃CN, 300 K): δ [ppm] = 23.9 (d, ¹J_{Si–Rh} = 62.1 Hz, Si/Rh), 11.9 (d, ²J_{Si–Rh} = 1.3 Hz, Si^tBu₂Me).

EA: C₃₃H₆₀Cl₃N₄RhSi₂ calculated [%]: C (50.93), H (7.77), N (7.20).
measured [%]: C (51.19), H (7.92), N (7.56).

M.P.: 138–139 °C (decomposition, change to red-brown oil).

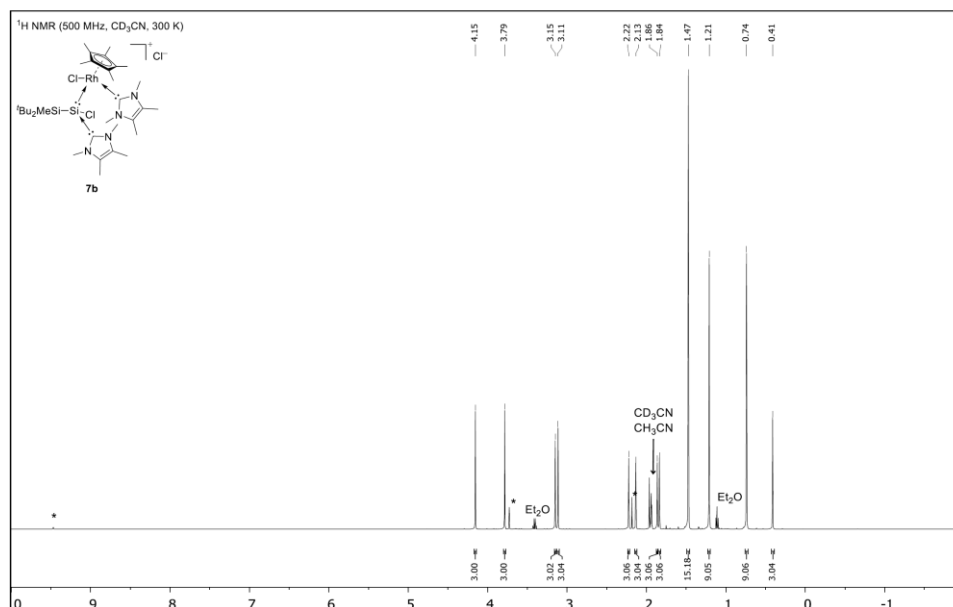


Figure S49 ¹H NMR spectrum of $[\text{Bu}_2\text{MeSi}-\text{Si}(\text{IME}_4)\text{Cl} \rightarrow \text{RhCl}(\text{IME}_4)(\text{Cp}^*)]\text{Cl}$ (**7b**) in CD₃CN at 300 K. Small amounts of residual imidazolium chloride from the precursor $[\text{IME}_4\cdot\text{HCl}]$ are marked with *.

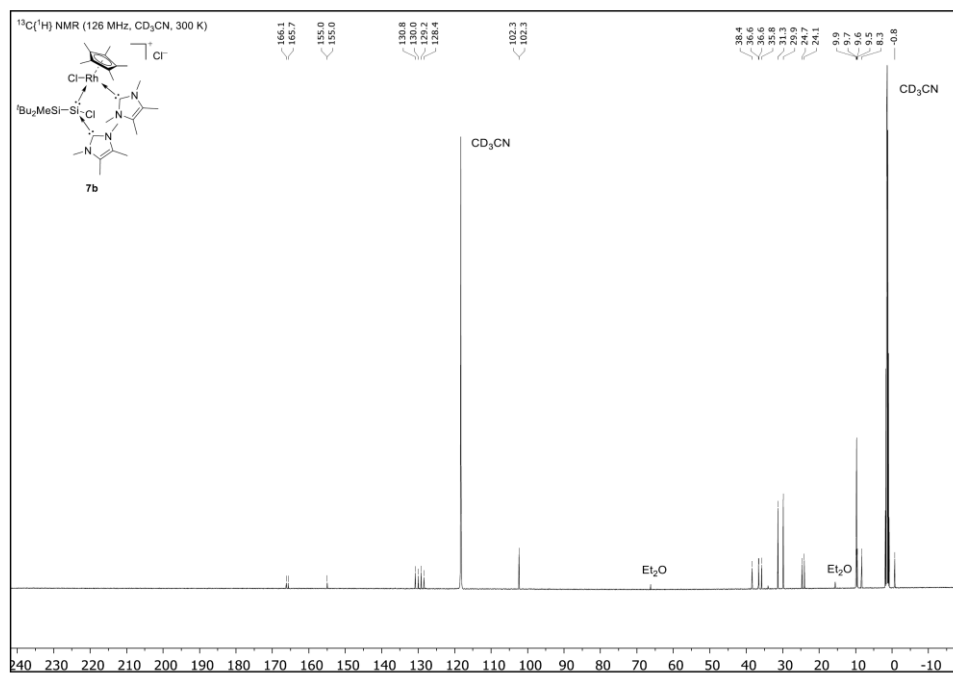


Figure S50 ¹³C{¹H} NMR spectrum of $[\text{Bu}_2\text{MeSi}-\text{Si}(\text{IME}_4)\text{Cl} \rightarrow \text{RhCl}(\text{IME}_4)(\text{Cp}^*)]\text{Cl}$ (**7b**) in CD₃CN at 300 K.

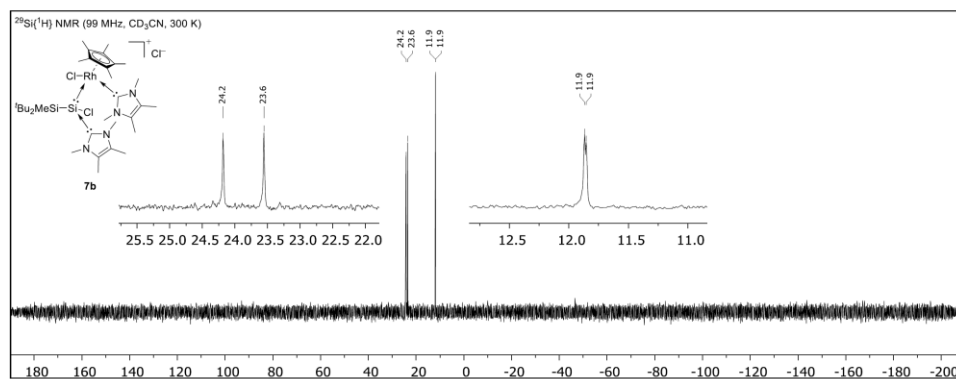


Figure S51 ²⁹Si{¹H} NMR spectrum of [**7b**] in CD₃CN at 300 K.

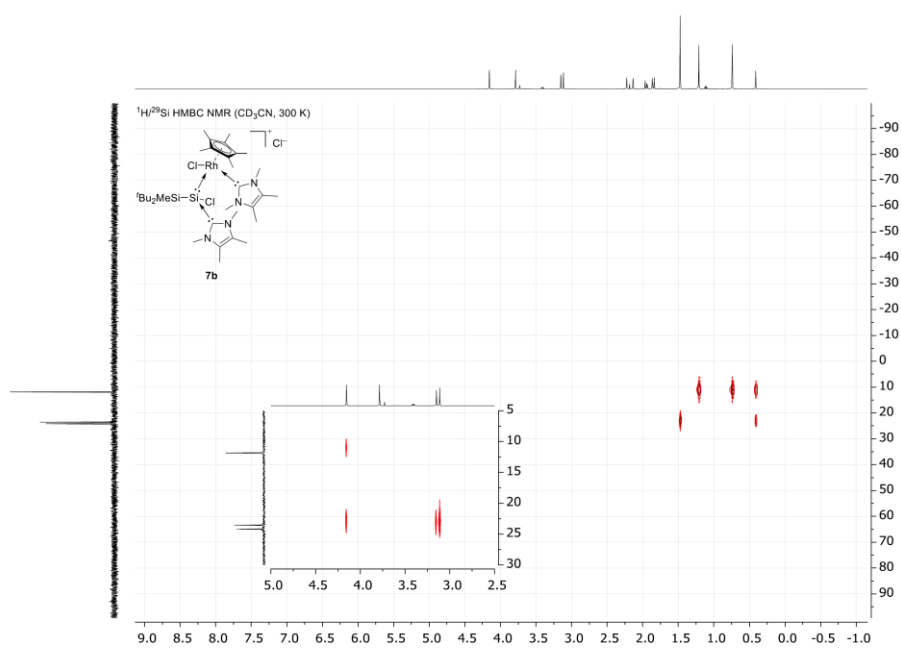


Figure S52 ¹H/²⁹Si HMBC NMR spectrum of [**7b**] in CD₃CN at 300 K.

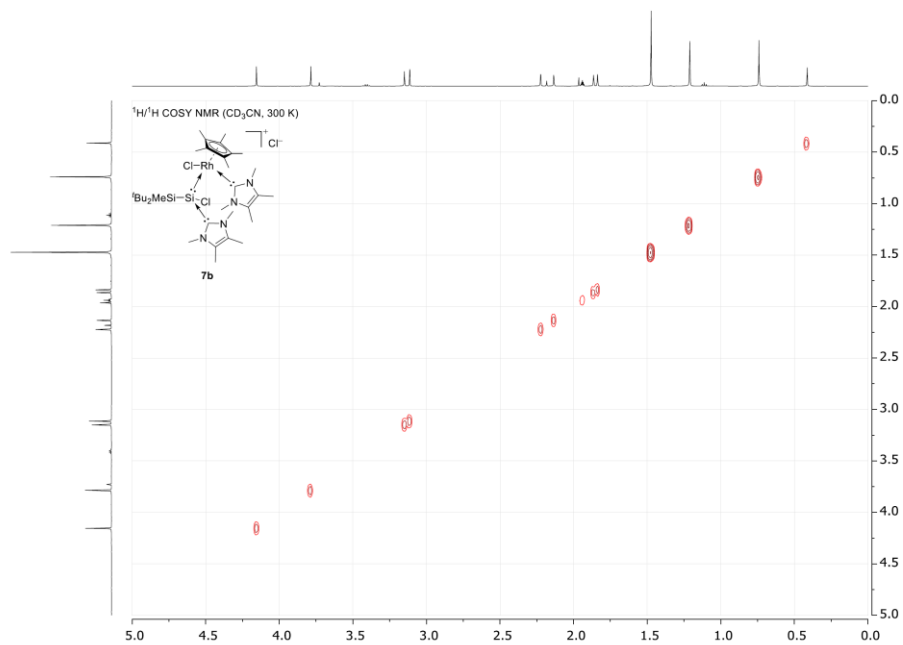


Figure S53 ¹H/¹H COSY NMR spectrum of $[\text{Bu}_2\text{MeSi}-\text{Si}(\text{IME}_4)\text{Cl} \rightarrow \text{RhCl}(\text{IME}_4)(\text{Cp}^*)]\text{Cl}$ (**7b**) in CD₃CN at 300 K.

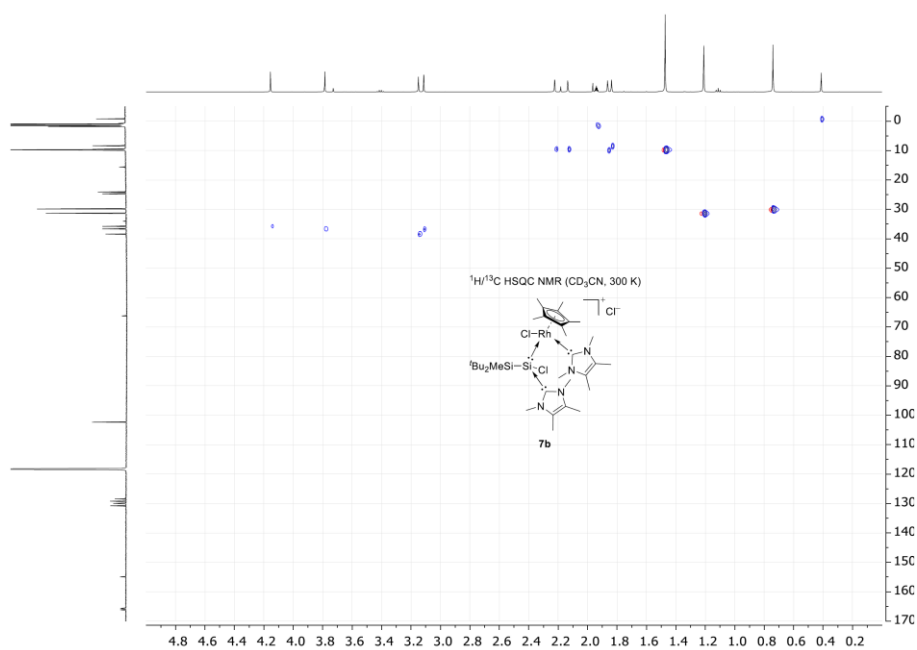


Figure S54 ¹H/¹³C HSQC NMR spectrum of $[\text{Bu}_2\text{MeSi}-\text{Si}(\text{IME}_4)\text{Cl} \rightarrow \text{RhCl}(\text{IME}_4)(\text{Cp}^*)]\text{Cl}$ (**7b**) in CD₃CN at 300 K.

S45

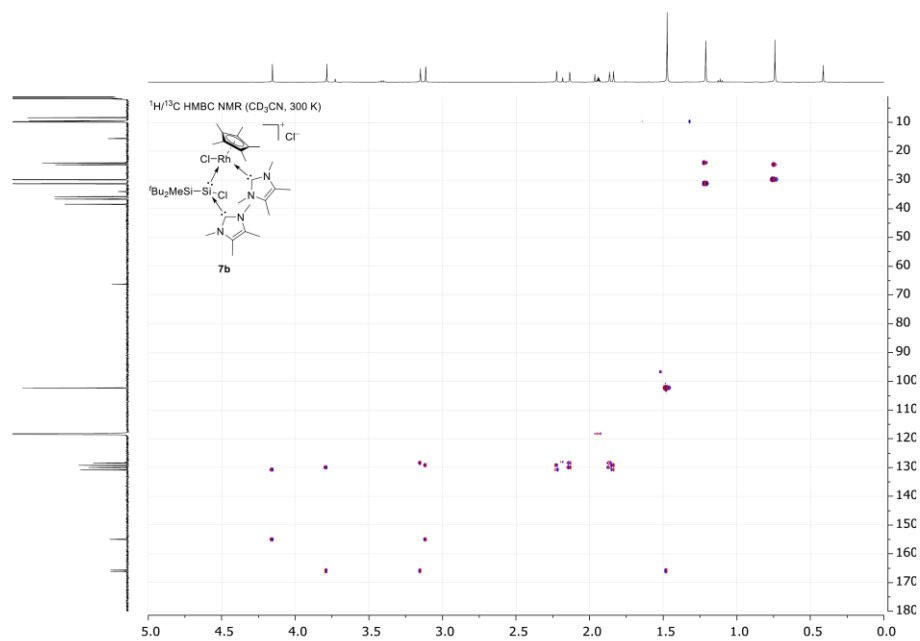
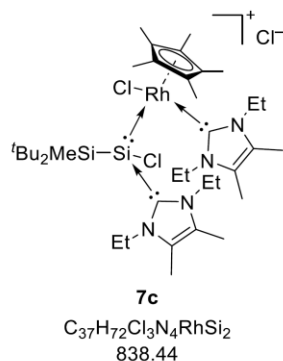


Figure S55 $^1\text{H}/^{13}\text{C}$ HMBC NMR spectrum of $[\text{Bu}_2\text{MeSi}-\text{Si}(\text{IME}_4)\text{Cl} \rightarrow \text{RhCl}(\text{IME}_4)(\text{Cp}^*)]\text{Cl}$ (**7b**) in CD_3CN at 300 K.

1.4.3 [^tBu₂MeSi–Si(IEt₂Me₂)Cl→RhCl(IEt₂Me₂)(Cp⁺)]Cl (**7c**)

Synthesis of complex **7c** was attempted in the same fashion as the other complexes. However, multiple reaction products were observed upon NMR analysis. The desired complex is only present with 35-40% in the reaction mixture and purification attempts were unsuccessful. Temperature and solvent variation during the synthesis did not change the obtained results significantly except for more decomposition products at higher temperatures.

Interestingly, only the signals at 18.6 and 12.8 ppm (assigned to **7c**) in the ²⁹Si NMR exhibit coupling to a rhodium atom ($s = \frac{1}{2}$). The other signals do not exhibit any coupling and hence formation of other coordination complexes with rhodium can be excluded. Chemical shifts and coupling constants are in line with the other complexes.

²⁹Si{¹H} NMR (99 MHz, CD₃CN, 300 K): δ [ppm] = 18.6 (d, ¹J_{Si–Rh} = 65.8 Hz), 12.8 (d, ²J_{Si–Rh} = 1.9 Hz).

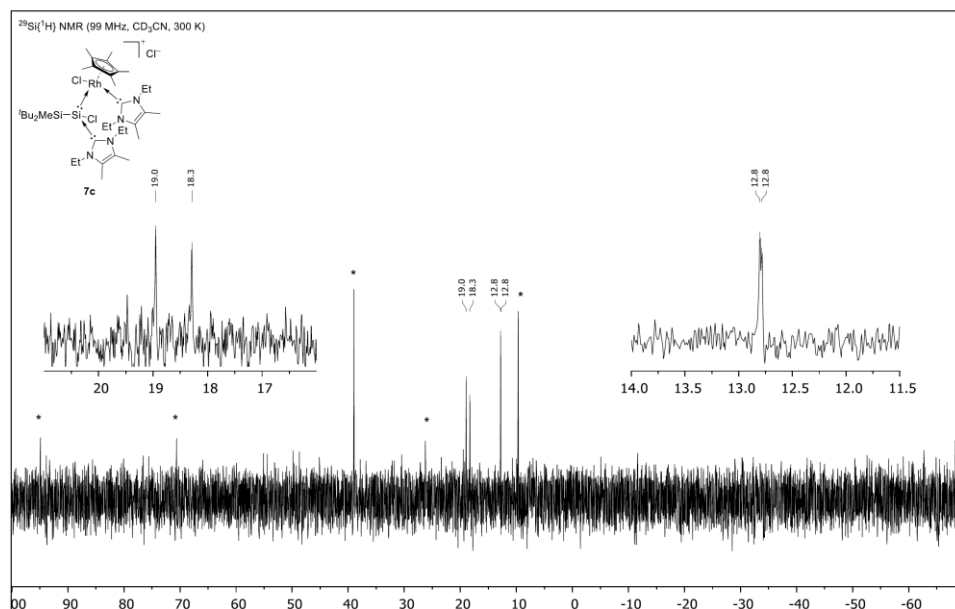
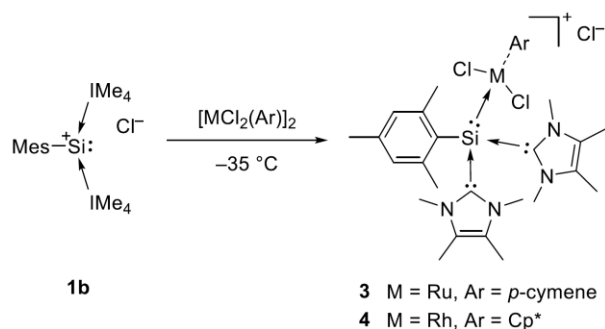
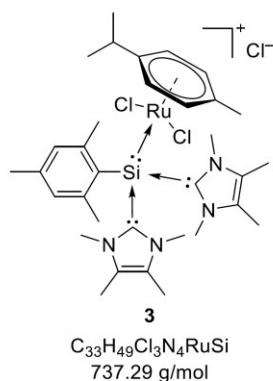


Figure S56 $^{29}\text{Si}\{^1\text{H}\}$ NMR spectrum of $[\text{tBu}_2\text{MeSi-Si}(\text{IEt}_2\text{Me}_2)\text{Cl} \rightarrow \text{RhCl}(\text{IEt}_2\text{Me}_2)(\text{Cp}^*)]\text{Cl}$ (**7c**) in CD_3CN at 300 K. Unknown side products are marked with *.

1.5 General Synthetic Procedure for $[R-Si(NHC)_2 \rightarrow MCl_2(Ar)]Cl$ 

Note: Since $[Mes-Si(IME_4)_2]Cl$ is not stable for a prolonged time in MeCN solution², care must be taken that these reactions are carried out quickly once the starting material is dissolved; **(b)** Due to the very fast decomposition of complexes **3** and **4** in solution, we were not able to isolate the complexes in a clean fashion. Decomposition even occurs slowly at $-35\text{ }^\circ\text{C}$. Hence, NMR measurements were carried out immediately after mixing the starting materials.

$[Mes-Si(IME_4)_2]Cl$ (**1b**) (1.0 eq) and $[MCl_2(Ar)]_2$ (0.5 eq) were mixed, cooled to $-35\text{ }^\circ\text{C}$ and pre-cooled ($-35\text{ }^\circ\text{C}$) CD_3CN (0.5 mL) was added. The deep red reaction mixtures were transferred to a J-Young NMR tube and immediately frozen in liquid nitrogen to stop decomposition. After allowing the NMR samples to thaw the measurements were carried out immediately.

1.5.1 [Mes-Si(IMe₄)₂→RuCl₂(*p*-cymene)]Cl (**3**)

Note: Complex **3** decomposes rapidly in solution at room temperature to an unidentified mixture of products in less than 2 hours. Decomposition is faster than in the case of **2** (~4 hours). During decomposition, large amounts of precipitate are formed that are no longer soluble in organic solvents (presumably the Si-containing part polymerizes and precipitates, as no silicon species can be observed in the NMR after complete decomposition). The major discernable products after decomposition are imidazolium chloride [IMe₄·HCl] and free *p*-cymene. The complex was characterized based on the similarity of the ²⁹Si NMR resonance to the crystallographically characterized complex **4**.

Batch size: **1b:** 30.0 mg, 69.6 μmol, 1.0 eq.

[RuCl₂(*p*-cym)]₂: 21.3 mg, 34.8 μmol, 0.5 eq.

²⁹Si{¹H} NMR (99 MHz, CD₃CN, 300 K): δ [ppm] = -20.5 (MesSi).

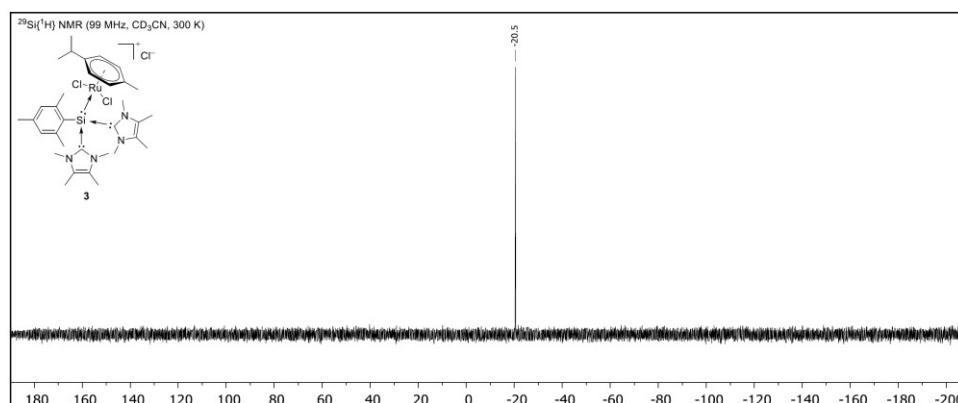
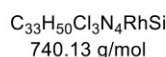
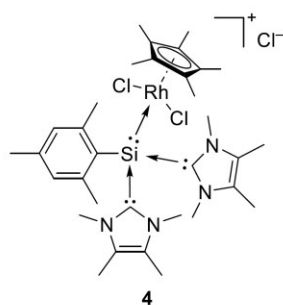


Figure S57 ²⁹Si{¹H} NMR spectrum of [Mes-Si(IMe₄)₂→RuCl₂(*p*-cymene)]Cl (**3**) in CD₃CN at 300 K.

1.5.2 [Mes-Si(IME₄)₂→RhCl₂(Cp*)]X (4, X = Cl, [RhCl₃Cp*])(a) [Mes-Si(IME₄)₂→RhCl₂(Cp*)]Cl (4)

Note: (a) Complex 4 decomposes rapidly in solution at room temperature to an unidentified mixture of products in less than 3 hours. Decomposition is somewhat slower than for complex 3, presumably due to the increased stability of the Cp* ligand in acetonitrile solution; (b) During decomposition, large amounts of precipitate are formed that are no longer soluble in organic solvents (most likely the Si-containing part polymerizes and precipitates, as no silicon species can be observed in the NMR after complete decomposition); (c) Furthermore, during decomposition, the formation of a new anion [RhCl₃Cp*]⁻ can be observed (Figure S58 and Figure S61) and the amount of imidazolium chloride [IME₄-HCl] increases progressively during measurement. After full decomposition, the major discernable products are imidazolium chloride and several Cp* containing species; (d) Due to the decomposition of 4 occurring even at low temperatures, it was not possible to obtain single crystals of 4. However, single crystals of 4-RhCl₃Cp* could be obtained from the same reaction mixture. 4-RhCl₃Cp* can also be selectively synthesized by using one equivalent of [RhCl₂(Cp*)]₂ instead of 0.5 eq (vide supra). 4-RhCl₃Cp* does not appear to be more stable than 4.

Batch size: 1b: 50.0 mg, 116.0 μmol, 1.0 eq.

[RhCl₂(Cp*)]₂: 35.8 mg, 58 μmol, 0.5 eq.

¹H NMR (500 MHz, CD₃CN, 300 K): δ [ppm] = 6.99 (s, 1H, C_{mes}H), 6.94 (s, 1H, C_{mes}H), 4.23 (s, 3H, N_{NHC}→SiCH₃), 3.50 (s, 3H, N_{NHC}→RhCH₃), 3.35 (s, 3H, N_{NHC}→RhCH₃), 2.80 (s, 3H, N_{NHC}→SiCH₃), 2.47 (s, 3H, C_{NHC}→SiCH₃), 2.29 (s, 3H, C_{mes,para}CH₃), 2.21 (s, 3H, C_{NHC}→RhCH₃), 2.15 (bs, 6H, C_{mes,ortho}CH₃), 2.10 (s, 3H, C_{NHC}→RhCH₃), 1.69 (s, 3H, C_{NHC}→SiCH₃), 1.18 (s, 15H, C₅(CH₃)₅).

Note: The resonance of the ortho methyl (2.15 ppm) groups of the silyliumylidene ion ligand overlap with a resonance for imidazolium chloride (2.17 ppm)

²⁹Si{¹H} NMR (99 MHz, CD₃CN, 300 K): δ [ppm] = -24.2 (d, ¹J_{Si-Rh} = 66.9 Hz, MesSi).

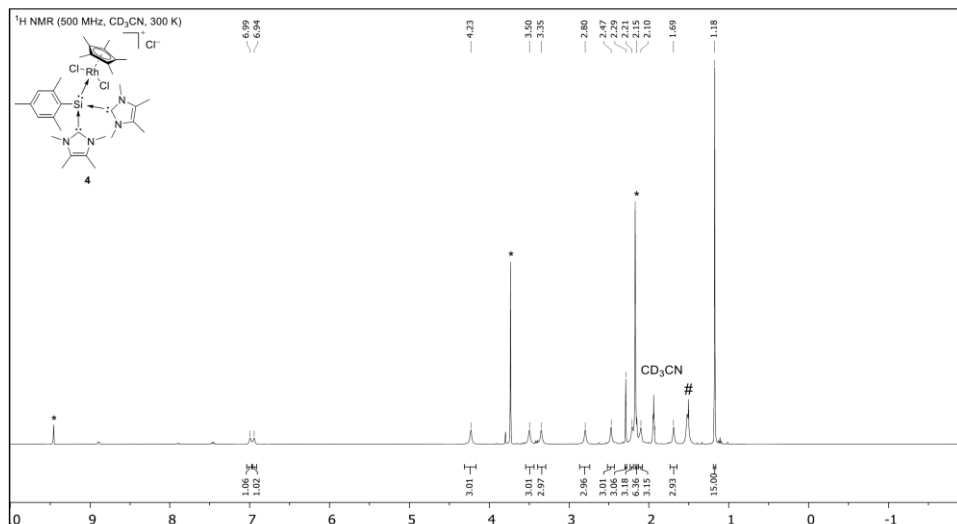


Figure S58 ^1H NMR spectrum of $[\text{Mes-Si}(\text{IMe}_4)_2\text{-RhCl}_2(\text{Cp}^*)]\text{Cl}$ (**4**) in CD_3CN at 300 K. The resonances for imidazolium chloride $[\text{IMe}_4\text{-HCl}]$ (marked with *) increase significantly during decomposition and therefore also increase during measurement. The resonance corresponding to the $[\text{RhCl}_3\text{Cp}^*]^-$ anion also increases during measurement (marked with #).

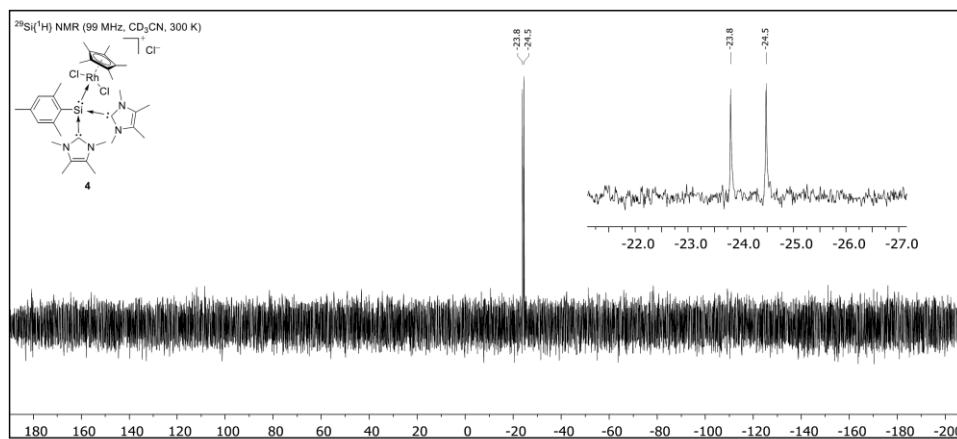


Figure S59 $^{29}\text{Si}\{^1\text{H}\}$ NMR spectrum of $[\text{Mes-Si}(\text{IMe}_4)_2\text{-RhCl}_2(\text{Cp}^*)]\text{Cl}$ (**4**) in CD_3CN at 300 K. No silicon-containing decomposition products can be observed, even after full decomposition.

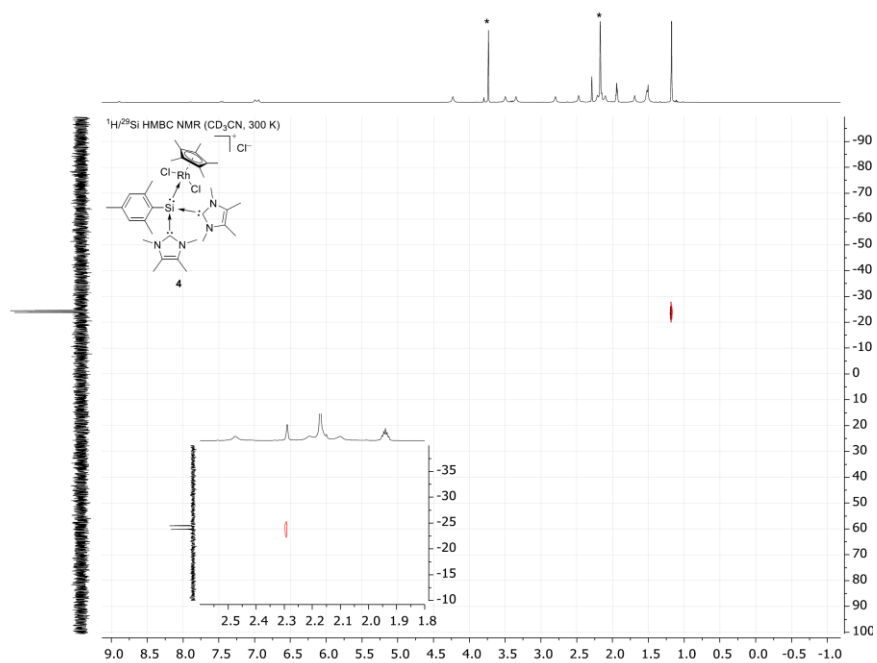


Figure S60 $^1\text{H}/^{29}\text{Si}$ HMBC NMR spectrum of $[\text{Mes-Si}(\text{Me}_4)_2\text{-RhCl}_2(\text{Cp}^*)]\text{Cl}$ (**4**) in CD_3CN at 300 K. Imidazolium chloride $[\text{Ime}_4\text{HCl}]$ is marked with *.

(b) [Mes-Si(IME₄)₂→RhCl₂(Cp*)][RhCl₃(Cp*)] (4-RhCl₃Cp*)

Note: (a) **4-RhCl₃Cp*** was analyzed with the same procedure as described for **4** (cf. section 1.5) except 1.0 eq of [RhCl₂(Cp*)]₂ were used instead of 0.5 eq.; (b) The cationic part of the complex remains the same regardless of the stoichiometry of the reaction; only the anionic part changes from Cl⁻ to [RhCl₃Cp*]⁻ if an equimolar (or excess) amount of transition metal precursor is utilized. The new anion is also formed during decomposition of **4**, albeit not quantitatively; (c) ²⁹Si NMR data of **4** (Figure S59) and **4-RhCl₃Cp*** (Figure S62) is identical. ¹H NMR data (Figure S58 & Figure S61) for the cationic parts are the same. The ¹H NMR spectrum of **4-RhCl₃Cp*** shows an additional resonance for the second Cp* ring (1.56 ppm (C₅(CH₃)₅)).

¹H NMR (500 MHz, CD₃CN, 300 K): δ [ppm] = 7.00 (s, 1H, C_{mes}H), 6.94 (s, 1H, C_{mes}H), 4.23 (s, 3H, N_{NHC}→SiCH₃), 3.50 (s, 3H, N_{NHC}→RhCH₃), 3.34 (s, 3H, N_{NHC}→RhCH₃), 2.78 (s, 3H, N_{NHC}→SiCH₃), 2.48 (s, 3H, C_{NHC}→SiCH₃), 2.29 (s, 3H, C_{mes,para}CH₃), 2.21 (s, 3H, C_{NHC}→RhCH₃), 2.16 (bs, 6H, C_{mes,ortho}CH₃), 2.10 (s, 3H, C_{NHC}→RhCH₃), 1.69 (s, 3H, C_{NHC}→SiCH₃), 1.56 (s, 15H, [RhCl₃(C₅(CH₃)₅)]), 1.18 (s, 15H, C₅(CH₃)₅).

²⁹Si{¹H} NMR (99 MHz, CD₃CN, 300 K): δ [ppm] = -24.1 (d, ¹J_{Si-Rh} = 67.0 Hz, MesSi).

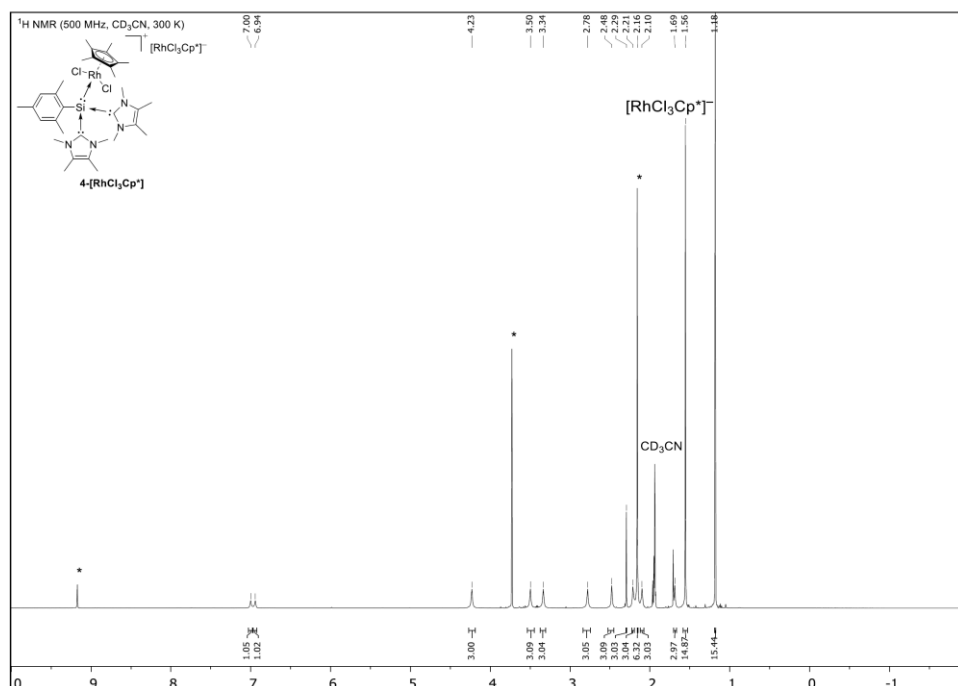


Figure S61 ¹H NMR spectrum of [Mes-Si(IME₄)₂→RhCl₂(Cp*)][RhCl₃(Cp*)] (**4-RhCl₃Cp***) in CD₃CN at 300 K. The resonances for imidazolium chloride [IME₄·HCl] (marked with *) increase significantly during decomposition and therefore also increase during measurement. No increase of the signal assigned to [RhCl₃Cp*]⁻ can be observed.

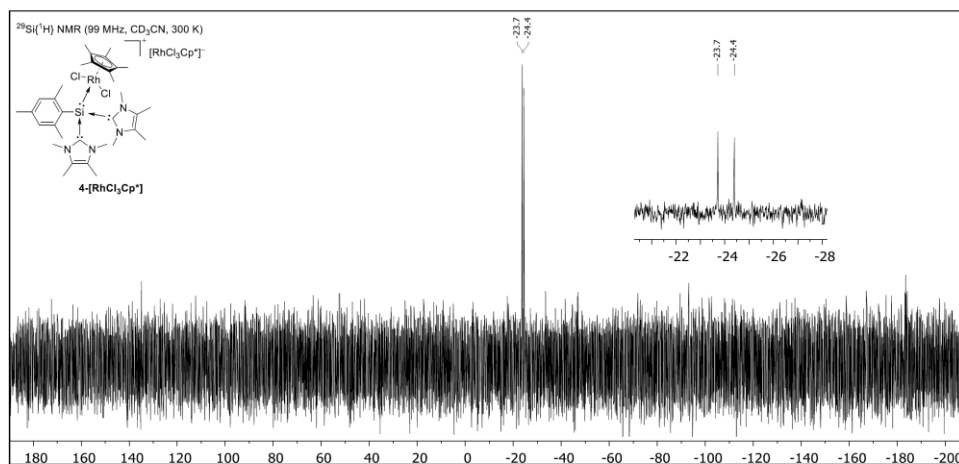


Figure S62 ²⁹Si{¹H} NMR spectrum of [Mes-Si(Me₄)₂-RhCl₂(Cp*)][RhCl₃(Cp*)] (**4-RhCl₃Cp***) in CD₃CN at 300 K.

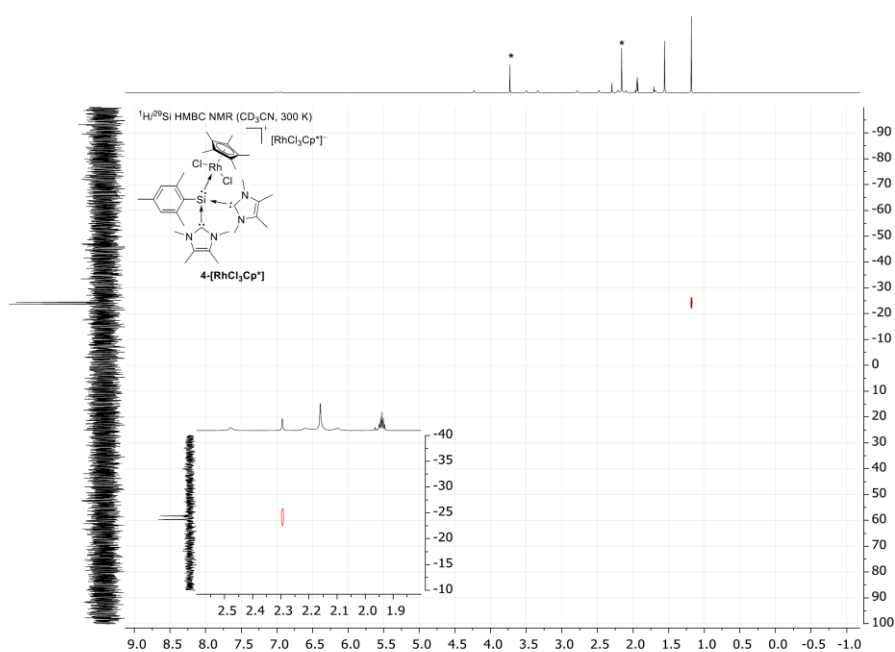
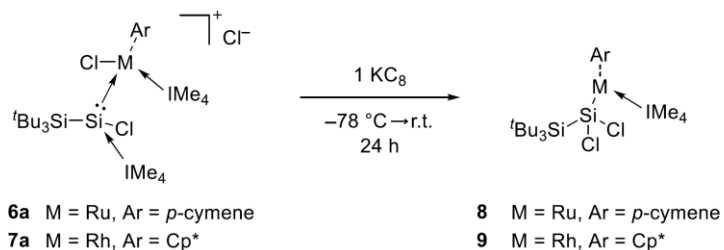
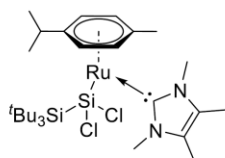


Figure S63 ¹H/²⁹Si HMBC NMR spectrum of [Mes-Si(Me₄)₂-RhCl₂(Cp*)][RhCl₃(Cp*)] (**4-RhCl₃Cp***) in CD₃CN at 300 K.

1.6 General Synthetic Procedure for [^tBu₃Si–SiCl₂–M(IMe₄)(Ar)]

[^tBu₃Si–Si(IMe₄)Cl→MCl(IMe₄)(Ar)]Cl (**6a** (M = Ru, Ar = *p*-cymene), **7a** (M = Rh, Ar = Cp*)) (1.0 eq) and K₂C₈ (1.0 eq) were mixed, cooled to –78 °C and pre-cooled (–78 °C) THF (20 mL) was added rapidly while stirring. The mixtures were stirred at –78 °C for 4 hours, then slowly warmed to room temperature overnight (~16 hours) and then stirred at room temperature for an additional 4 hours. The solvent was removed under reduced pressure and the residue was extracted with toluene (3×7 mL). The solvent was removed under reduced pressure and the residue was dried for 5 hours (60 °C, ~5×10^{–3} mbar) to remove free IMe₄ via sublimation. The residues were dissolved in a minimal amount of toluene and after crystallization at –35 °C, filtration and drying under vacuum, complexes **8** and **9** were obtained as air- and moisture sensitive solids.

Note: Complexes **8** and **9** are stable in solution at room temperature for at least four weeks.

1.6.1 [^tBu₃Si–SiCl₂–Ru(IMe₄)(*p*-cymene)] (**8**)**8**

C₂₉H₅₃Cl₂N₂RuSi₂
657.90 g/mol

Batch size: **6a:** 100.0 mg, 122.3 μmol, 1.0 eq.

KC₈: 16.5 mg, 122.3 μmol, 1.0 eq.

Yield: 45.5 mg (69.2 μmol, 57%) as a bright green solid.

SC-XRD: Suitable single crystals were obtained by storing a concentrated solution of **8** in toluene at –35 °C.

Note: No NMR data could be recorded due to **8** being paramagnetic.

EPR (toluene, c = 5 × 10⁻⁵ mol/L, 286 K): *g* = 2.1062.

LIFDI-MS: calculated: 657.2168 (C₂₉H₅₃Cl₂N₂RuSi₂).
measured: 657.1815 (**8**).

EA: C₂₉H₅₃Cl₂N₂RuSi₂ calculated [%]: C (52.94), H (8.12), N (4.26).
measured [%]: C (52.45), H (8.12), N (4.05).

M.P.: 169–170 °C (decomposition, color change to black).



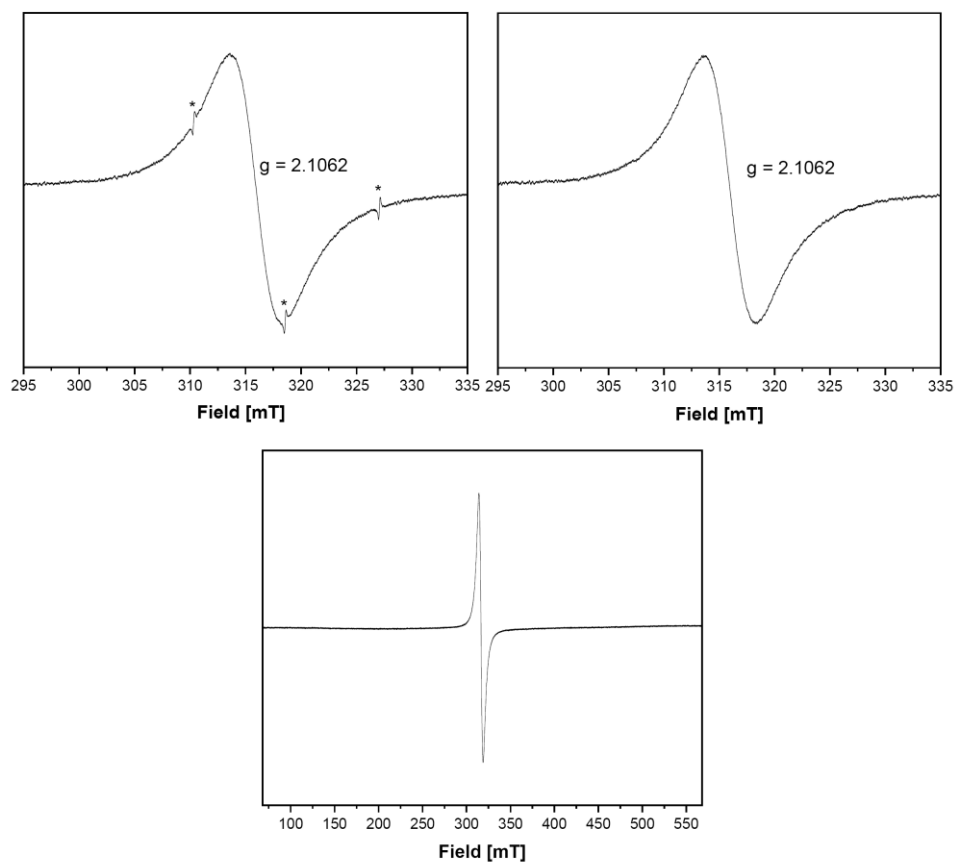


Figure S64 X-band EPR-spectra of [$t\text{Bu}_3\text{Si-SiCl}_2\text{-Ru(IME}_4\text{)(}p\text{-cymene)}$] (**8**) in toluene ($c = 5.0 \times 10^{-5}$ mol/L, 286 K) (top left: including standard (marked with *), top right: excluding standard, bottom: from 70 to 570 mT).

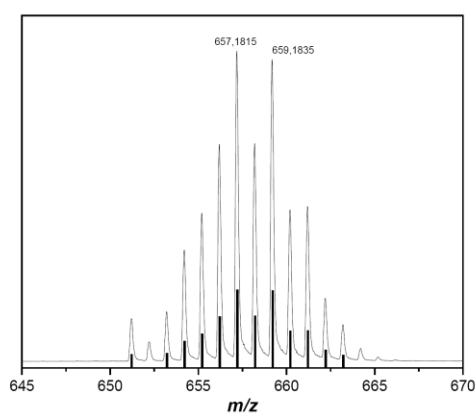


Figure S65 LIFDI-MS spectrum (detailed view) of [$t\text{Bu}_3\text{Si-SiCl}_2\text{-Ru(IME}_4\text{)(}p\text{-cymene)}$] (**8**) in toluene (line: measured spectrum; bars: simulated spectrum).

S58

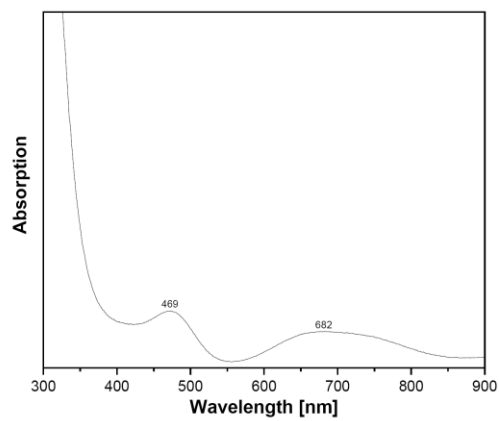
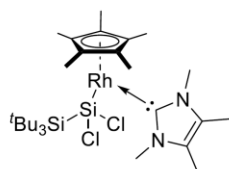


Figure S66 UV-Vis spectrum (300-900 nm) of $[\text{Bu}_3\text{Si}-\text{SiCl}_2-\text{Ru}(\text{IME}_4)(p\text{-cymene})]$ (**8**) in toluene at room temperature ($c = 5.0 \times 10^{-4} \text{ mol/L}$). $\lambda_{\text{max}} = 469 \text{ nm}$ & 682 nm .

1.6.2 [^tBu₃Si–SiCl₂–Rh(IMe₄)(Cp^{*})] (**9**)**9**

C₂₉H₅₄Cl₂N₂RhSi₂
660.74 g/mol

Batch size: **7a:** 100.0 mg, 121.9 μmol, 1.0 eq.

KC₈: 16.5 mg, 121.9 μmol, 1.0 eq.

Yield: 52.3 mg (79.2 μmol, 65%) as a dark grey-black solid.

SC-XRD: Suitable single crystals were obtained by storing a concentrated solution of **9** in toluene at –35 °C.

Note: No NMR data could be recorded due to **9** being paramagnetic.

EPR (toluene, c = 5 × 10⁻⁵ mol/L, 286 K): g = 2.1003.

LIFDI-MS: calculated: 659.2258 (C₂₉H₅₄Cl₂N₂RhSi₂).
measured: 659.1942 (**9**).

EA: C₂₉H₅₄Cl₂N₂RhSi₂·0.5(C₇H₈) calculated [%]: C (55.23), H (8.27), N (3.96).
measured [%]: C (55.29), H (8.39), N (3.75).

M.P.: 191-192 °C (decomposition, change to black oil).

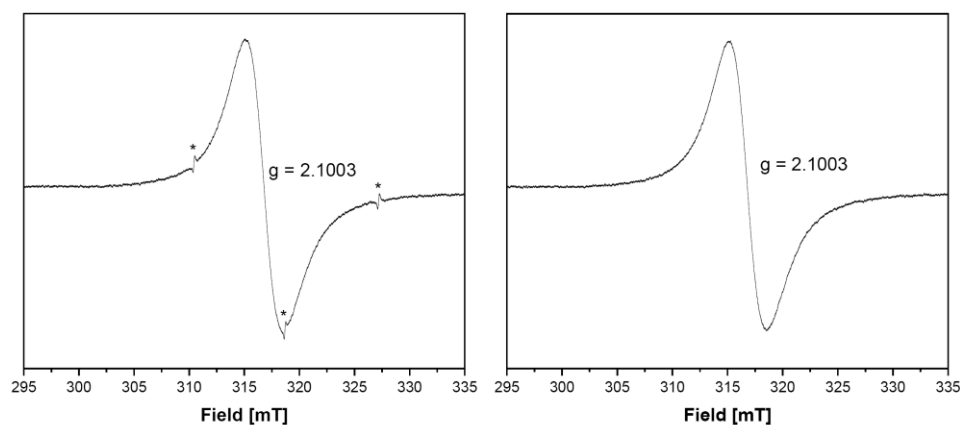


Figure S67 X-band EPR-spectra of [^tBu₃Si–SiCl₂–Rh(Cp^{*})(IMe₄)] (**9**) in toluene (c = 5.0 × 10⁻⁵ mol/L, 286 K) (left: including standard (marked with *), right: excluding standard).

S60

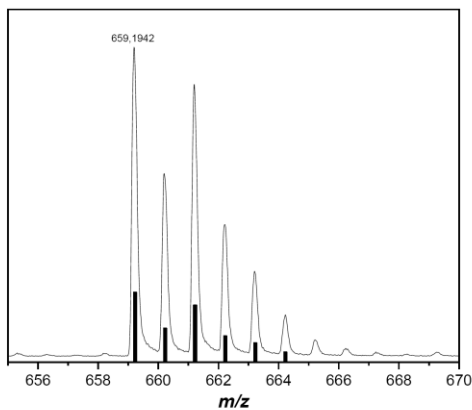


Figure S68 LIFDI-MS spectrum (detailed view) of $[\text{Bu}_3\text{Si-SiCl}_2\text{-Rh}(\text{Cp}^*)(\text{IMe}_4)]$ (**9**) in toluene; (line: measured spectrum; bars: simulated spectrum).

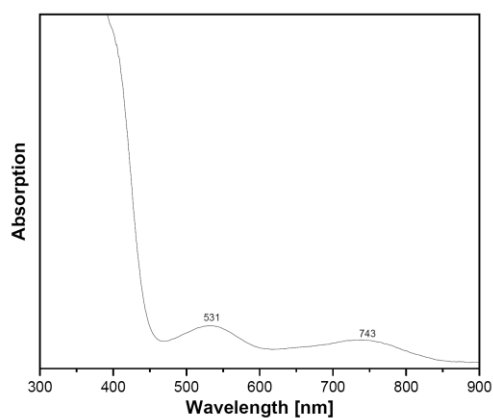
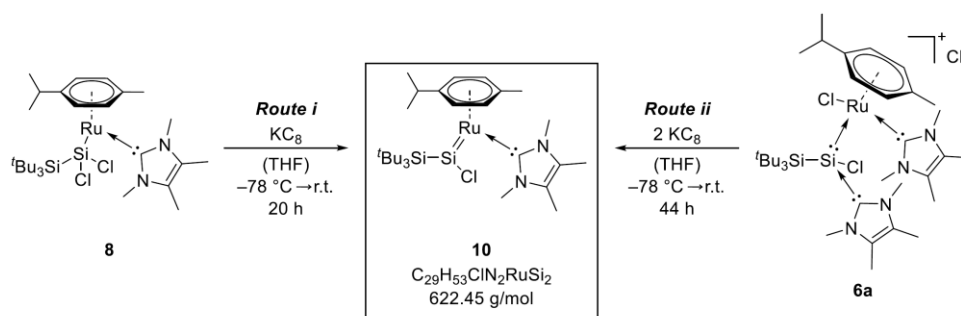


Figure S69 UV-Vis spectrum (300-900 nm) of $[\text{Bu}_3\text{Si-SiCl}_2\text{-Rh}(\text{Cp}^*)(\text{IMe}_4)]$ (**9**) in toluene at room temperature ($c = 1.5 \times 10^{-3} \text{ mol/L}$). $\lambda_{\text{max}} = 531 \text{ nm}$ & 743 nm .

1.7 Synthesis of [^tBu₃Si–Si(Cl)=Ru(IMe₄)(*p*-cymene)] (10)

Complex **10** can be synthesized either from **8** through one electron reduction and abstraction of one chloride (**Route i**) or through two-electron reduction and abstraction of two chlorides directly from **6a** (**Route ii**). Isolation of **8** prior to further reduction gives a cleaner reaction and higher yields.

Route i: [^tBu₃Si–SiCl₂–Ru(IMe₄)(*p*-cymene)] (**8**) (50.0 mg, 76.0 μmol , 1.0 eq) and KC_8 (10.3 mg, 76.0 μmol , 1.0 eq) were mixed, cooled to $-78\text{ }^\circ\text{C}$ and pre-cooled ($-78\text{ }^\circ\text{C}$) THF (10 mL) was added rapidly while stirring. The mixture was slowly warmed to room temperature over a period of 4 hours (color change from green→brown→red) and then stirred overnight at room temperature (~16 hours). The solvent was removed under reduced pressure and the residue was extracted with hexane (3×5 mL). The solution was concentrated under reduced pressure and then stored at $-35\text{ }^\circ\text{C}$ for 1 week. The microcrystalline precipitate was collected by filtration, washed with cold hexane ($-35\text{ }^\circ\text{C}$, 1×0.5 mL) and after drying under vacuum **10** (29.9 mg, 48.0 μmol , 63%) was obtained as a dark red air- and moisture sensitive solid.

Route ii: [^tBu₃Si–Si(IMe₄)Cl→RuCl(IMe₄)(*p*-cymene)]Cl (**6a**) (100.0 mg, 122.3 μmol , 1.0 eq) and KC_8 (33.1 mg, 244.6 μmol , 2.0 eq) were mixed, cooled to $-78\text{ }^\circ\text{C}$ and pre-cooled ($-78\text{ }^\circ\text{C}$) THF (20 mL) was added rapidly while stirring. The mixture was stirred at $-78\text{ }^\circ\text{C}$ for 4 hours, then slowly warmed to room temperature overnight (~16 hours) and then stirred at room temperature for an additional 24 hours. The solvent was removed under reduced pressure and the residue was extracted with hexane (3×8 mL). The solution was concentrated under reduced pressure and then stored at $-35\text{ }^\circ\text{C}$ for 10 days. The microcrystalline precipitate was collected by filtration, washed with cold hexane ($-35\text{ }^\circ\text{C}$, 1×0.5 mL) and after drying under vacuum **10** (31.4 mg, 50.5 μmol , 41%) was obtained as a dark red air- and moisture sensitive solid.

SC-XRD: Suitable single crystals were obtained by storing a concentrated solution of **10** in *n*-hexane at $-35\text{ }^{\circ}\text{C}$.

^1H NMR (500 MHz, C_6D_6 , 300 K): δ [ppm] = 4.78 (m, 4H, $\text{C}_{p\text{-cym}}\text{Har}$), 3.42 (s, 6H, $\text{N}_{\text{NHC}}\text{CH}_3$), 2.44 (sept, $^3J_{\text{H-H}} = 6.9\text{ Hz}$, 1H, $\text{CH}(\text{CH}_3)_2$), 2.26 (s, 3H, $\text{C}_{p\text{-cym}}\text{CH}_3$), 1.67 (s, 6H, $\text{C}_{\text{NHC}}\text{CH}_3$), 1.56 (s, 27H, $\text{Si}((\text{C}(\text{CH}_3)_3)_3)$), 1.39 (d, $^3J_{\text{H-H}} = 6.9\text{ Hz}$, 6H, $\text{CH}(\text{CH}_3)_2$).

$^{13}\text{C}\{^1\text{H}\}$ NMR (126 MHz, C_6D_6 , 300 K): δ [ppm] = 188.5 ($\text{N}_{\text{C}_{\text{NHC}}\text{N}}$), 123.8 ($\text{C}_{\text{NHC}}\text{CH}_3$), 108.5 ($\text{C}_{p\text{-cym}}\text{-iPr}$), 94.0 ($\text{C}_{p\text{-cym}}\text{CH}_3$), 81.7 ($\text{C}_{p\text{-cym}}\text{Har}$), 78.7 ($\text{C}_{p\text{-cym}}\text{Har}$), 36.6 ($\text{N}_{\text{NHC}}\text{CH}_3$), 32.8 ($\text{CH}(\text{CH}_3)_2$), 32.6 ($\text{Si}((\text{C}(\text{CH}_3)_3)_3)$), 25.5 ($\text{CH}(\text{CH}_3)_2$), 24.9 ($\text{Si}((\text{C}(\text{CH}_3)_3)_3)$), 21.8 ($\text{C}_{p\text{-cym}}\text{CH}_3$), 9.4 ($\text{C}_{\text{NHC}}\text{CH}_3$).

$^{29}\text{Si}\{^1\text{H}\}$ NMR (99 MHz, C_6D_6 , 300 K): δ [ppm] = 240.6 ($\text{Si}=\text{Ru}$), 4.7 (Si^iBu_3).

LIFDI-MS: calculated: 622.2479 ($\text{C}_{29}\text{H}_{53}\text{ClN}_2\text{RuSi}_2$).
measured: 622.2941 (**10**).

EA: $\text{C}_{29}\text{H}_{53}\text{ClN}_2\text{RuSi}_2$ calculated [%]: C (55.96), H (8.58), N (4.50).
measured [%]: C (56.23), H (8.84), N (4.59).

M.P.: 149-150 $^{\circ}\text{C}$ (decomposition, color change to black).

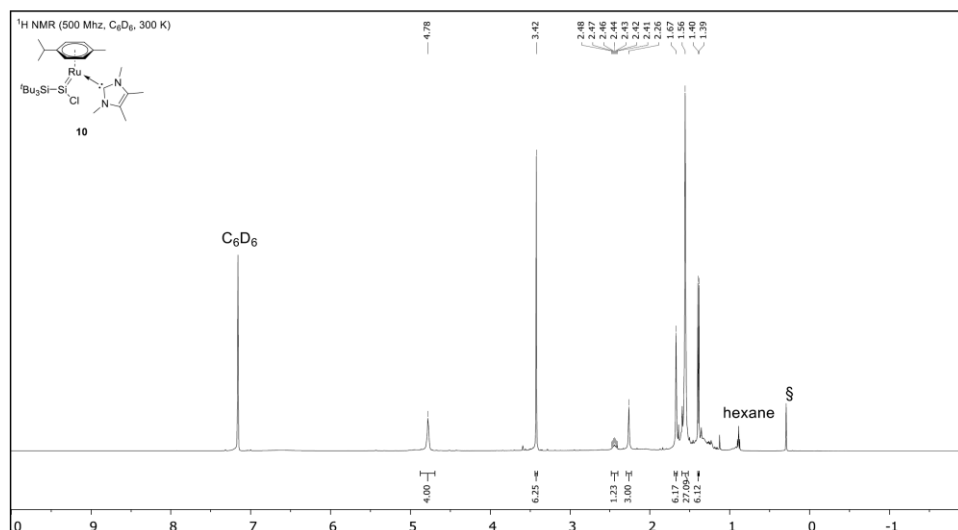


Figure S70 ^1H NMR spectrum of $[\text{Bu}_3\text{Si-Si}(\text{Cl})=\text{Ru}(\text{IME}_4)(\text{p-cymene})]$ (**10**) in C_6D_6 at 300 K. Silicone grease is marked with S.

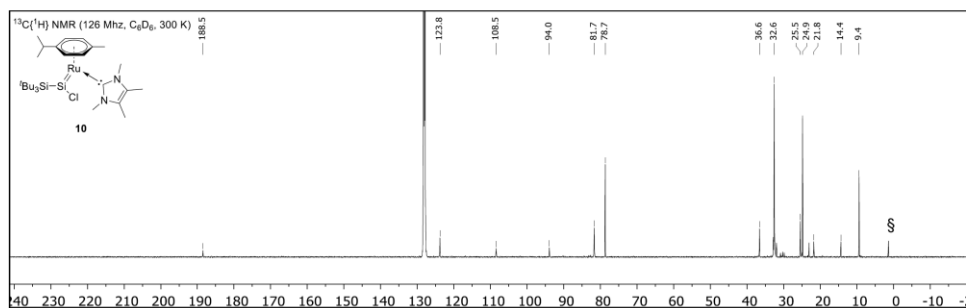


Figure S71 ¹³C{¹H} NMR spectrum of [¹Bu₃Si–Si(Cl)=Ru(Ime₄)(*p*-cymene)] (**10**) in C₆D₆ at 300 K. Silicone grease is marked with §.

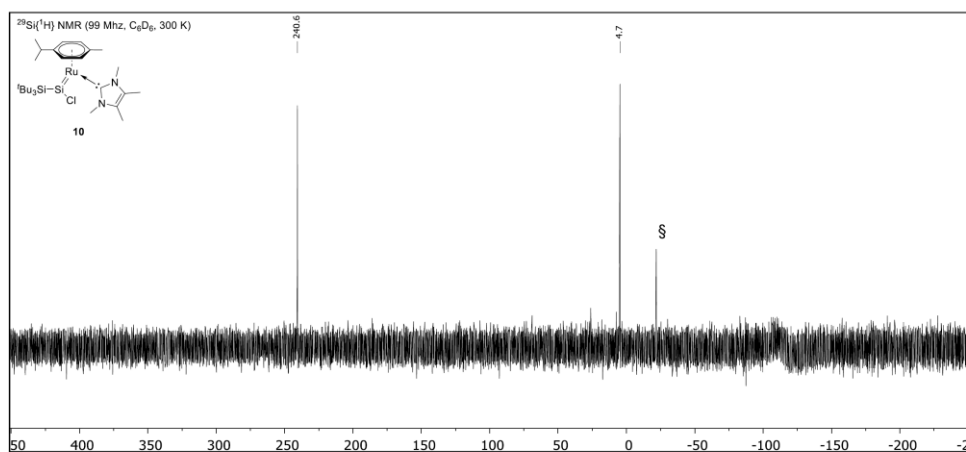


Figure S72 ²⁹Si{¹H} NMR spectrum of [¹Bu₃Si–Si(Cl)=Ru(Ime₄)(*p*-cymene)] (**10**) in C₆D₆ at 300 K. Silicone grease is marked with §.

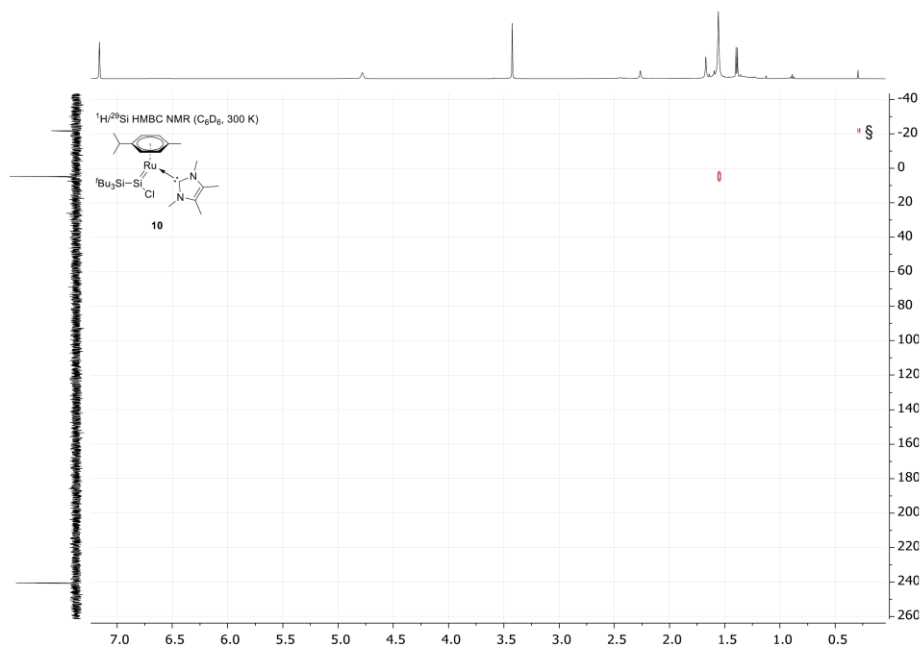


Figure S73 ¹H/²⁹Si HMBC NMR spectrum of [¹Bu₃Si–Si(Cl)=Ru(Ime₄)(*p*-cymene)] (**10**) in C₆D₆ at 300 K. Silicone grease is marked with §.

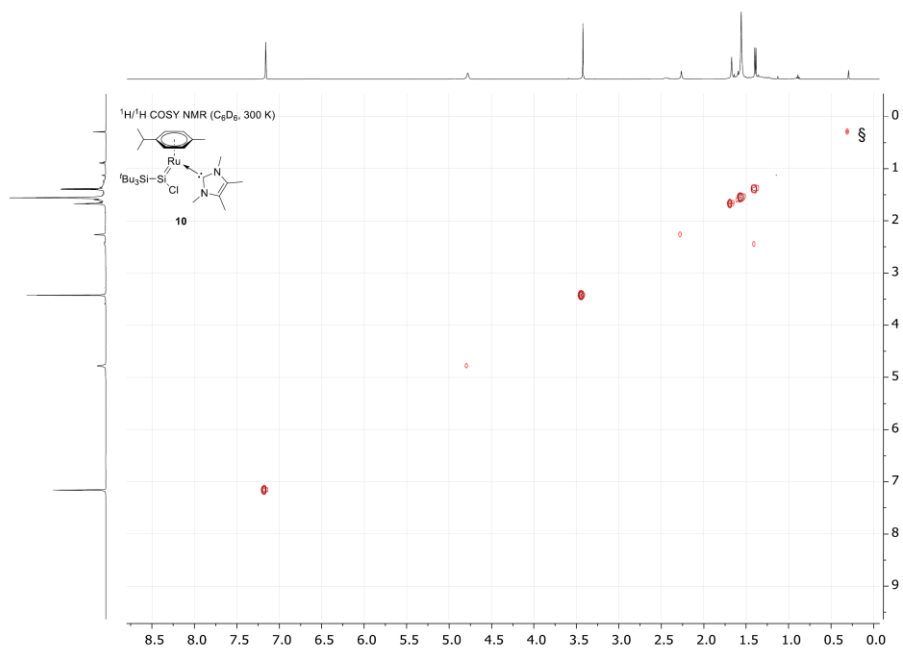


Figure S74 ¹H/¹H COSY NMR spectrum of [¹Bu₃Si–Si(Cl)=Ru(Ime₄)(*p*-cymene)] (**10**) in C₆D₆ at 300 K. Silicone grease is marked with §.

S65

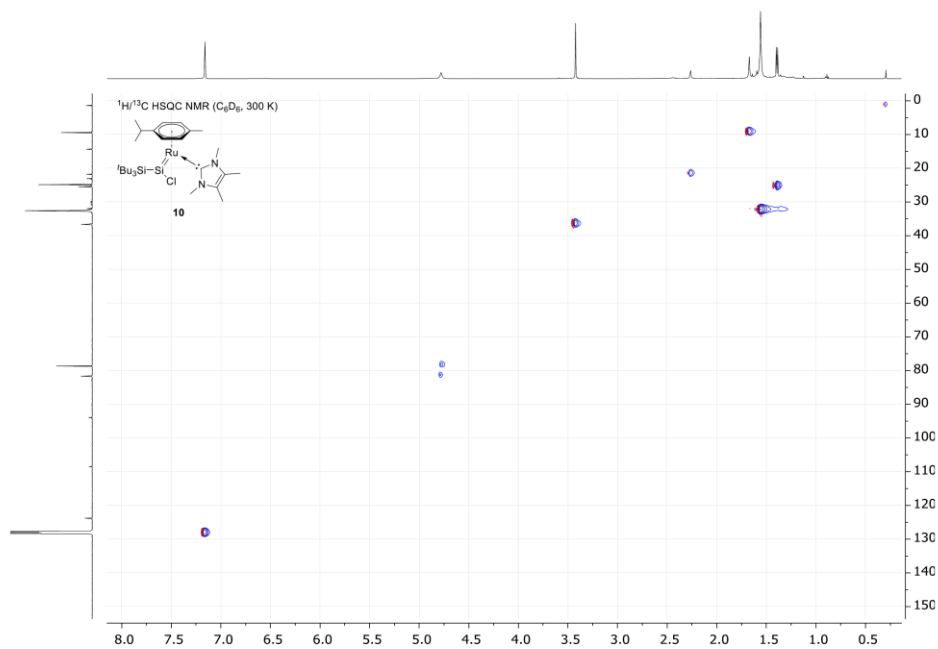


Figure S75 ¹H/¹³C HSQC NMR spectrum of [^tBu₃Si–Si(Cl)=Ru(Ime₄)(*p*-cymene)] (**10**) in C₆D₆ at 300 K.

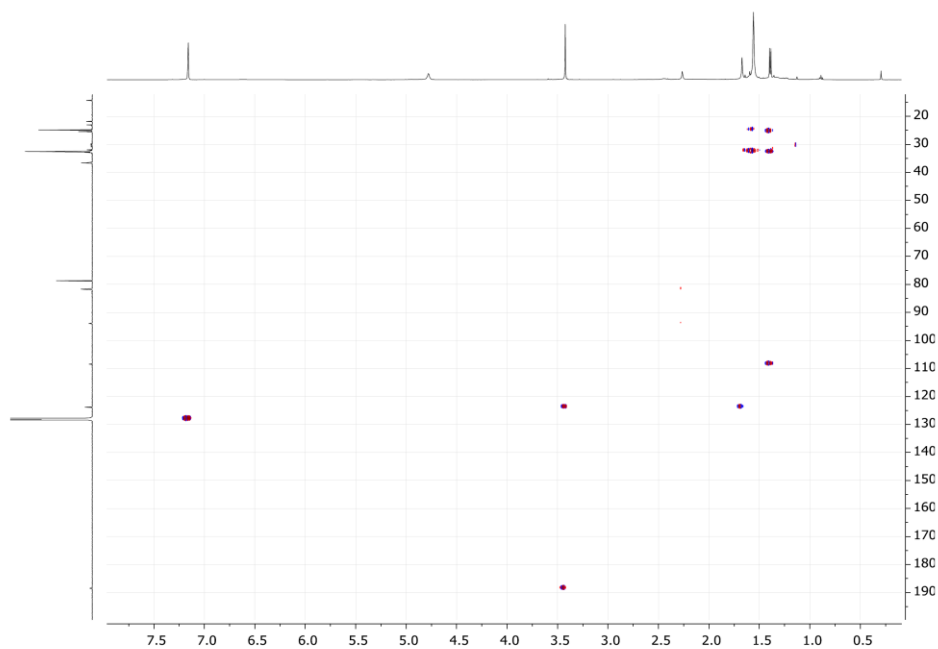


Figure S76 ¹H/¹³C HMBC NMR spectrum of [^tBu₃Si–Si(Cl)=Ru(Ime₄)(*p*-cymene)] (**10**) in C₆D₆ at 300 K.

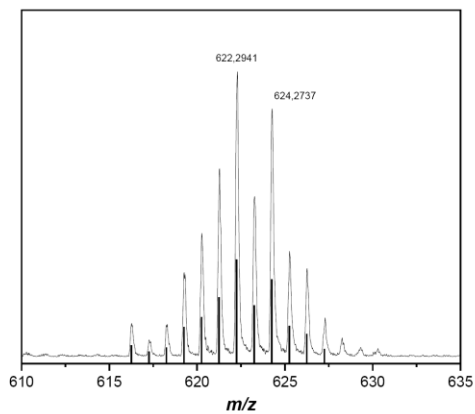


Figure S77 LIFDI-MS spectrum (detailed view) of [$\text{Bu}_3\text{Si-Si}(\text{Cl})=\text{Ru}(\text{IME}_4)(p\text{-cymene})$] (**10**) in toluene; (line: measured spectrum; bars: simulated spectrum).

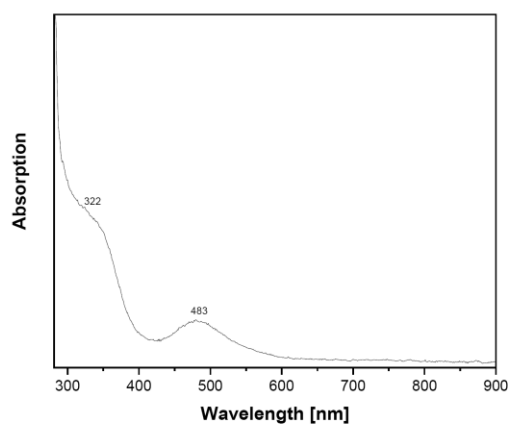
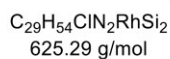
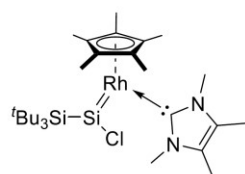


Figure S78 UV-Vis spectrum (280-900 nm) of [$\text{Bu}_3\text{Si-Si}(\text{Cl})=\text{Ru}(\text{IME}_4)(p\text{-cymene})$] (**10**) in toluene at room temperature ($c = 5.0 \times 10^{-5} \text{ mol/L}$). $\lambda_{\text{max}} = 322 \text{ nm}$ & 483 nm .

Note: We also attempted reduction of Rh complex **7a** with two eq. of KC_8 as well as reduction of **9** with one equivalent of KC_8 . In both cases a deep purple compound can be obtained. Based on the ^{29}Si NMR shifts ($\delta(^{29}Si)$ [ppm] = 260.7 (d, $^1J_{Si-Rh}$ = 130.3 Hz, SiRh), 1.6 (d, $^2J_{Si-Rh}$ = 7.1 Hz, tBu_3Si) and the LIFDI-MS data (Figure S79), we presume this purple complex is the to **10** analogous Rh=Si complex $tBu_3Si-Si(Cl)=Rh(IMe_4)(Cp^*)$. However, we have so far been unable to obtain satisfactory analytical data and therefore this is only included as additional information for the sake of completeness.



LIFDI-MS: calculated: 624.2569 ($C_{29}H_{54}ClN_2RhSi_2$).
measured: 624.3738 ($tBu_3Si-Si(Cl)=Rh(IMe_4)(Cp^*)$).

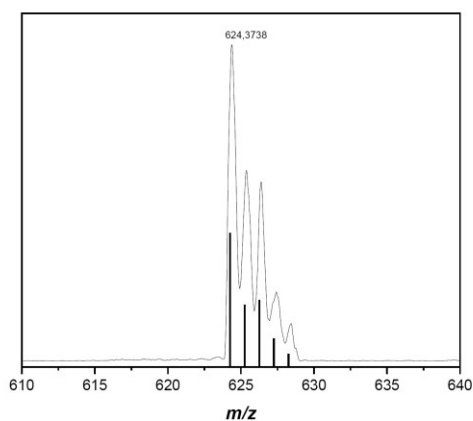


Figure S79 LIFDI-MS spectrum (detailed view) of $[tBu_3Si-Si(Cl)=Rh(IMe_4)(Cp^*)]$ in toluene; (line: measured spectrum; bars: simulated spectrum).

2. X-ray Crystallographic Data

2.1 General Information

The X-ray intensity data of **2**, **4-RhCl₃Cp***, **6a**, **7a**, **7b**, and **8** were collected on an X-ray single crystal diffractometer equipped with a CMOS detector (Bruker Photon-100), an IMS microsource with MoK α radiation ($\lambda = 0.71073 \text{ \AA}$) and a Helios mirror optic by using the APEX III software package.⁷ The X-ray intensity data of **9** and **10** were collected on an X-ray single crystal diffractometer equipped with a CMOS detector (Bruker Photon-100), a rotating anode (Bruker TXS) with MoK α radiation ($\lambda = 0.71073 \text{ \AA}$) and a Helios mirror optic by using the APEX III software package.⁷ The measurements were performed on single crystals coated with the perfluorinated ether Fomblin® Y. The crystals were fixed on the top of a micro sampler, transferred to the diffractometer and frozen under a stream of cold nitrogen. A matrix scan was used to determine the initial lattice parameters. Reflections were merged and corrected for Lorentz and polarization effects, scan speed, and background using SAINT.⁸ Absorption corrections, including odd and even ordered spherical harmonics were performed using SADABS.⁸ Space group assignments were based upon systematic absences, E statistics, and successful refinement of the structures. Structures were solved by direct methods with the aid of successive difference Fourier maps, and were refined against all data using the APEX III software in conjunction with SHELXL-2014⁹ and SHELXLE.¹⁰ All H atoms were placed in calculated positions and refined using a riding model, with methylene and aromatic C–H distances of 0.99 and 0.95 Å, respectively, and $U_{\text{iso}}(\text{H}) = 1.2 \cdot U_{\text{eq}}(\text{C})$. Full-matrix least-squares refinements were carried out by minimizing $\Delta w(F_o^2 - F_c^2)^2$ with SHELXL-97 weighting scheme.¹¹ Neutral atom scattering factors for all atoms and anomalous dispersion corrections for the non-hydrogen atoms were taken from International Tables for Crystallography.¹² The images of the crystal structures were generated by Mercury.¹³ Standard uncertainties of bond distances and (dihedral) angles that include the centroids of aryl ligands were calculated using Diamond 4.6.2.¹⁴ The CCDC numbers CCDC-1976774 (**2**), CCDC-1976772 (**4-RhCl₃Cp***), CCDC-1976773 (**6a**), CCDC-1976776 (**7a**), CCDC-1976775 (**7b**), CCDC-1976777 (**8**), CCDC-1976778 (**9**) and CCDC-1976779 (**10**) contain the supplementary crystallographic data for the structures. These data can be obtained free of charge from the Cambridge Crystallographic Data Centre *via* <https://www.ccdc.cam.ac.uk/structures/>.

2.2 SC-XRD structure of 2 (CCDC-1976774)

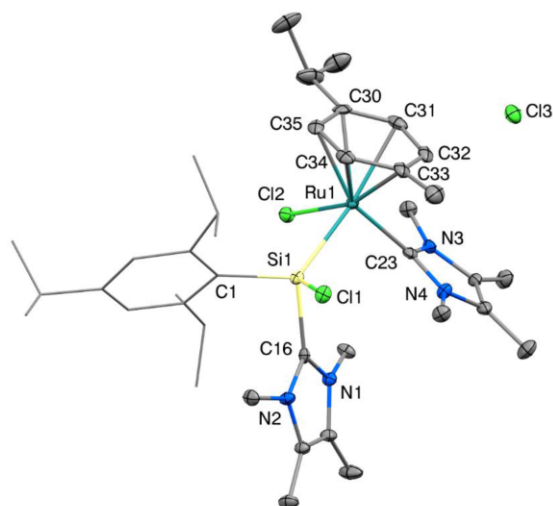


Figure S80 Ellipsoid plot (50% probability level) of the molecular structure of complex **2**. Hydrogen atoms and solvent molecules are omitted and the Tipp substituent is simplified as a wireframe for clarity. Selected bond lengths [Å] and angles [°]: Si1–Ru1 2.409(1), Si1–Cl1 2.167(1), Si1–C1 1.941(4), Si1–C16 1.970(4), Ru1–Cl2 2.404(1), Ru1–C23 2.077(4), Ru1–*p*-cym_⊥ 1.770(1), C1–Si1–Ru1 123.3(1), Si1–Ru1–*p*-cym_⊥ 131.1(1), Cl1–Si1–Ru1–Cl2 –173.1(1), C16–Si1–Ru1–C23 –11.1(2).

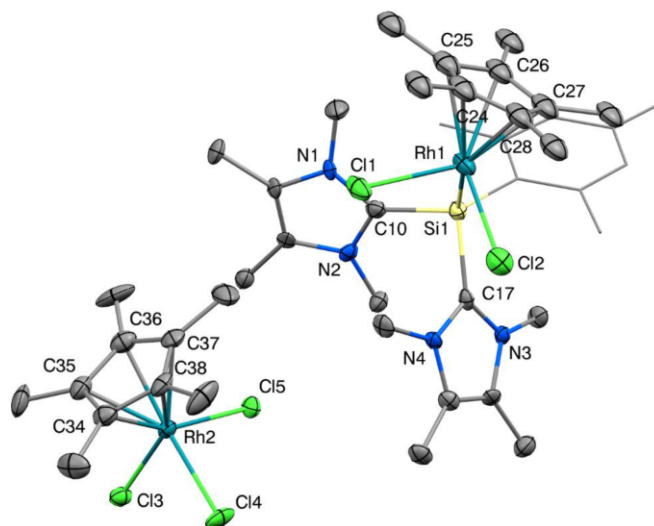
2.3 SC-XRD structure of 4-RhCl₃Cp* (CCDC-1976772)

Figure S81 Ellipsoid plot (50% probability level) of the molecular structure of complex **4-RhCl₃Cp***. Hydrogen atoms and solvent molecules are omitted and the mesityl substituent is simplified as a wireframe for clarity. Selected bond lengths [Å] and angles [°]: Si1–Rh1 2.426(2), Si1–C1 1.899(7), Si1–C10 1.958(7), Si1–C17 1.944(7), Rh1–Cl1 2.420(2), Rh1–Cl2 2.404(2), Rh1–Cp*_⊥ 1.857(1), Si1–Rh1–Cp*_⊥ 132.3(1), Si1–Rh1–Cl1 94.6(1), Si1–Rh1–Cl2 88.9(1), C10–Si1–C17 93.9(3), C1–Si1–C10 110.3(3), C1–Si1–C17 104.4(3), C1–Si1–Rh1 112.7(2), C10–Si1–Rh1 115.3(2), C17–Si1–Rh1 118.5(2), Cl1–Rh1–Cl2 91.6(1), C1–Si1–Rh1–Cp*_⊥ 24.2(2), C1–Si1–Rh1–Cl1 157.0(2), C1–Si1–Rh1–Cl2 –111.5(2), C10–Si1–Rh1–Cl1 29.1(2), C10–Si1–Rh1–Cl2 120.6(2), C17–Si1–Rh1–Cl1 –80.8(2), C17–Si1–Rh1–Cl2 10.7(2).

2.4 SC-XRD structure of 6a (CCDC-1976773)

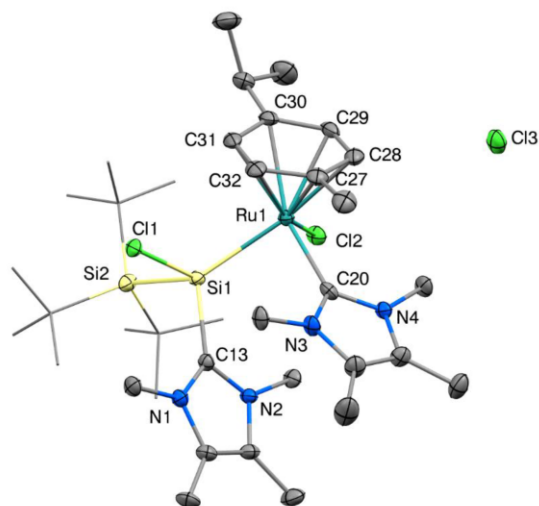


Figure S82 Ellipsoid plot (50% probability level) of the molecular structure of complex **6a**. Hydrogen atoms and solvent molecules are omitted and the $t\text{-Bu}_3\text{Si}$ substituent is simplified as a wireframe for clarity. Selected bond lengths [Å] and angles [°]: Si1–Ru1 2.499(1), Si1–Cl1 2.166(2), Si1–Si2 2.551(2), Si1–C13 2.002(4), Ru1–Cl2 2.427(1), Ru1–C20 2.084(3), Ru1–*p*-cym \perp 1.767(1), Si2–Si1–Ru1 132.6(1), Si1–Ru1–*p*-cym \perp 130.4(1), Cl1–Si1–Ru1–Cl2 $-156.1(1)$, C13–Si1–Ru1–C20 $-0.2(2)$.

2.6 SC-XRD structure of 7b (CCDC-1976775)

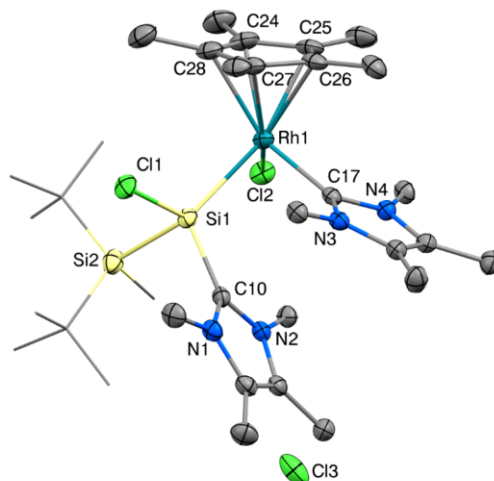


Figure S84 Ellipsoid plot (50% probability level) of the molecular structure of complex **7b**. Hydrogen atoms are omitted and the $t\text{Bu}_2\text{MeSi}$ substituent is simplified as a wireframe for clarity. Selected bond lengths [Å] and angles [°]: Si1–Rh1 2.384(1), Si1–Cl1 2.144(1), Rh1–Cl2 2.415(1), Si1–Si2 2.438(1), Si1–C10 1.978(2), Rh1–C17 2.037(2), Rh1–Cp* $_{\perp}$ 1.890(1), Si2–Si1–Rh1 128.2(1), Si1–Rh1–Cp* $_{\perp}$ 133.6(1), Cl1–Si1–Rh1–Cl2 $-146.8(1)$, Cl1–Si1–Rh1–Cp* $_{\perp}$ $-20.5(1)$, Cl1–Si1–Rh1–C17 114.3(1), C10–Si1–Rh1–C17 $-1.0(1)$.

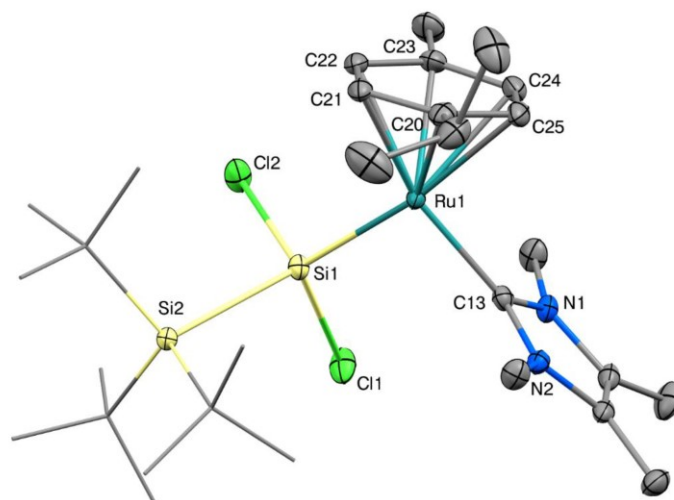
2.7 SC-XRD structure of **8** (CCDC-1976777)

Figure S85 Ellipsoid plot (50% probability level) of the molecular structure of complex **8**. Hydrogen atoms are omitted and the $t\text{Bu}_3\text{Si}$ substituent is simplified as a wireframe for clarity. Selected bond lengths [Å] and angles [°]: Si1–Ru1 2.374(1), Si1–Cl1 2.161(1), Si1–Cl2 2.160(1), Si1–Si2 2.424(1), Ru1–C13 2.064(2), Ru1–*p*-cym \perp 1.756(1), Si2–Si1–Ru1 128.0(1), Si1–Ru1–*p*-cym \perp 134.0(1), Cl1–Si1–Ru1–*p*-cym \perp 139.1(1), Cl1–Si1–Ru1–C13 $-16.9(1)$, Cl2–Si1–Ru1–*p*-cym \perp 29.1(1), Cl2–Si1–Ru1–C13 $-126.9(1)$.

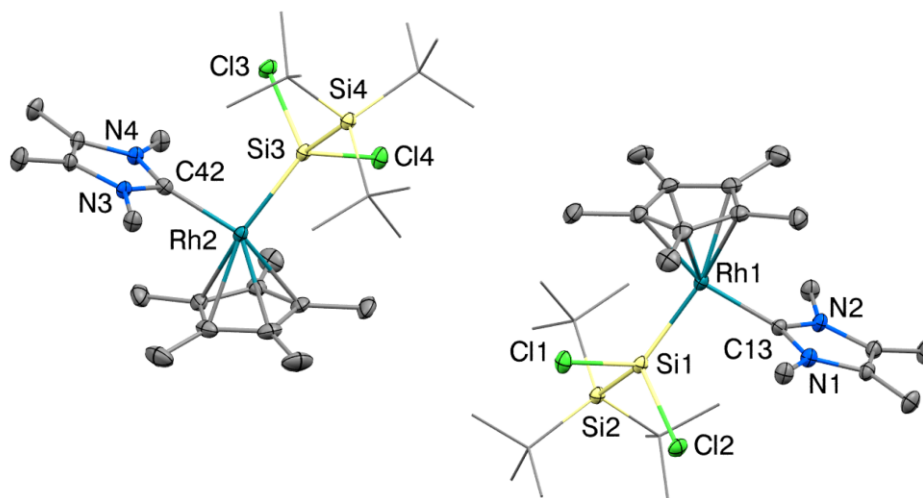
2.8 SC-XRD structure of **9** (CCDC-1976778)

Figure S86 Ellipsoid plot (50% probability level) of the molecular structure of complex **9**. Hydrogen atoms and solvent molecules are omitted and the 'Bu₃Si substituents are simplified as a wireframe for clarity. Selected bond lengths [Å] and angles [°]: Si1–Rh1 2.328(1), Si1–Cl1 2.145(1), Si1–Cl2 2.170(1), Si1–Si2 2.430(1), Rh1–C13 2.033(3), Rh1–Cp*_⊥ 1.911(1), Si2–Si1–Rh1 126.6(1), Si1–Rh1–Cp*_⊥ 135.7(1), Cl1–Si1–Rh1–Cp*_⊥ –16.1(1), Cl1–Si1–Rh1–C13 141.0(1), Cl2–Si1–Rh1–Cp*_⊥ –124.8(1), Cl2–Si1–Rh1–C13 32.3(1), Si3–Rh2 2.331(1), Si3–Cl3 2.146(1), Si3–Cl4 2.171(1), Si3–Si4 2.429(1), Rh2–C42 2.018(3), Rh2–Cp*_⊥ 1.909(1), Si4–Si3–Rh2 126.0(4), Si3–Rh2–Cp*_⊥ 136.1(1), Cl3–Si3–Rh2–Cp*_⊥ 16.1(1), Cl3–Si3–Rh2–C42 –140.8(1), Cl4–Si3–Rh2–Cp*_⊥ 125.4(1), Cl4–Si3–Rh2–C42 –31.6(1).

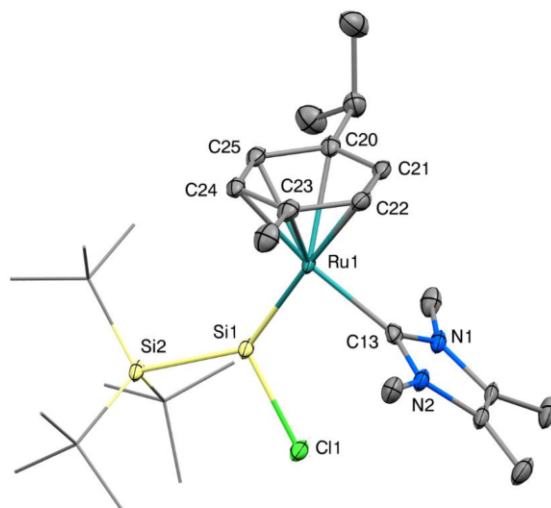
2.9 SC-XRD structure of **10** (CCDC-1976779)

Figure S87 Ellipsoid plot (50% probability level) of the molecular structure of complex **10**. Hydrogen atoms are omitted and the 'Bu₃Si' substituent is simplified as a wireframe for clarity. Selected bond lengths [Å] and angles [°]: Si1–Ru1 2.236(1), Si1–Cl1 2.169(1), Si1–Si2 2.416(1), Ru1–C13 2.055(4), Ru1–*p*-cym_⊥ 1.751(1), Si2–Si1–Ru1 143.8(1), Si1–Ru1–*p*-cym_⊥ 147.7(1), Cl1–Si1–Ru1–*p*-cym_⊥ –175.0(1), Cl1–Si1–Ru1–C13 6.8(1).

2.10 Crystal data and structural refinement parameters

Table S1 Crystal data and structural refinement parameters for compounds 2, 6a, 7a and 7b.

Compound #	2	6a	7a	7b
CCDC #	1976774	1976773	1976776	1976775
Chemical formula	C ₃₃ H ₇₀ Cl ₃ N ₂ RuSi	C ₃₃ H ₆₈ Cl ₃ N ₂ RuSi ₂	C ₃₃ H ₆₈ Cl ₃ N ₂ RuSi ₂	C ₃₃ H ₆₈ Cl ₃ N ₂ RuSi ₂
Formula weight	944.59	858.57	861.40	778.29
Temperature	100(2) K	100(2) K	100(2) K	100(2) K
Wavelength	0.71073 Å	0.71073 Å	0.71073 Å	0.71073 Å
Crystal size	0.316 × 0.334 × 0.494 mm	0.154 × 0.176 × 0.255 mm	0.101 × 0.116 × 0.168 mm	0.212 × 0.298 × 0.324 mm
Crystal habit	clear intense orange fragment	clear intense orange fragment	clear intense red fragment	clear orange-red fragment
Crystal system	orthorhombic	triclinic	tetragonal	monoclinic
Space group	P 2 ₁ 2 ₁ 2 ₁	P -1	I -4	P 2 ₁ /c
Unit cell dimensions	a = 12.1974(10) Å, α = 90° b = 12.7513(11) Å, α = 90° c = 31.0568(3) Å, α = 90° 4830.5(7) Å ³	a = 8.5873(19) Å, α = 100.272(6)° b = 10.536(3) Å, β = 94.576(6)° c = 25.732(6) Å, γ = 103.458(7)° 2209.9(10) Å ³	a = 30.924(7) Å, α = 90° b = 30.924(7) Å, β = 90° c = 9.760(4) Å, γ = 90° 9333(6) Å ³	a = 12.2917(6) Å, α = 90° b = 11.7135(6) Å, β = 95.774(2)° c = 26.4973(18) Å, α = 90° 3795.7(4) Å ³
Volume	1299 g/cm ³	1290 g/cm ³	1226 g/cm ³	1362 g/cm ³
Density (calculated)	0.553 mm ⁻¹	0.622 mm ⁻¹	0.619 mm ⁻¹	0.752 mm ⁻¹
Absorption coefficient	1992	908	3648	1640
F(000)				
Diffractometer	Bruker D8 Venture Duo IMS	Bruker D8 Venture Duo IMS	Bruker D8 Venture Duo IMS	Bruker D8 Venture Duo IMS
Radiation source	IMS microsource, Mo	IMS microsource, Mo	IMS microsource, Mo	IMS microsource, Mo
Theta range for data collection	2.31 to 25.03°	2.03 to 25.35°	2.08 to 31.60°	2.48 to 25.35°
Index ranges	-14<h<14, -15<k<15, -36<l<36	-10<h<10, -12<k<12, -30<l<30	-44<h<45, -45<k<45, -13<l<14	-14<h<14, -14<k<14, -31<l<31
Reflections collected	175495	102323	246899	99017
Independent reflections	8526 [R(int) = 0.0955]	8106 [R(int) = 0.0556]	14537 [R(int) = 0.0769]	6937 [R(int) = 0.0365]
Coverage of independent reflections	99.9%	99.9%	95.7%	99.9%
Absorption correction	Multi-Scan	Multi-Scan	Multi-Scan	Multi-Scan
Refinement method	Full-matrix least-squares on F ²	Full-matrix least-squares on F ²	Full-matrix least-squares on F ²	Full-matrix least-squares on F ²
Refinement program	SHELXL-2016 (Sheldrick, 2016)	SHELXL-2016 (Sheldrick, 2016)	SHELXL-2017 (Sheldrick, 2017)	SHELXL-2016 (Sheldrick, 2016)
Function minimized	Σ w(F _o ² - F _c ²) ²	Σ w(F _o ² - F _c ²) ²	Σ w(F _o ² - F _c ²) ²	Σ w(F _o ² - F _c ²) ²
Data / restraints / parameters	8526 / 66 / 593	8108 / 0 / 463	14537 / 0 / 468	6937 / 0 / 408
Goodness-of-fit on F ²	1.046	1.167	1.117	1.062
Final R indices	7841 data; >2σ(I); R1 = 0.0292, wR2 = 0.0487	7467 data; >2σ(I); R1 = 0.0469, wR2 = 0.1131	10905 data; >2σ(I); R1 = 0.0467, wR2 = 0.0978	6315 data; >2σ(I); R1 = 0.0294, wR2 = 0.0713
Weighting scheme	all data: R1 = 0.0386, wR2 = 0.0517 w = 1/[σ ² (F _o ²) + (0.0159P) ² + 3.1813P] where P = (F _o ² + 2F _c ²)/3	all data: R1 = 0.0517, wR2 = 0.1165 w = 1/[σ ² (F _o ²) + (0.0202P) ² + 11.3934P] where P = (F _o ² + 2F _c ²)/3	all data: R1 = 0.1096, wR2 = 0.1492 w = 1/[σ ² (F _o ²) + (0.0218P) ² + 94.0608P] where P = (F _o ² + 2F _c ²)/3	all data: R1 = 0.0342, wR2 = 0.0760 w = 1/[σ ² (F _o ²) + (0.0305P) ² + 6.5835P] where P = (F _o ² + 2F _c ²)/3
Largest diff. peak and hole	0.335 and -0.344 eÅ ⁻³	2.224 and -1.744 eÅ ⁻³	0.1785 and -1.871 eÅ ⁻³	1.777 and -0.701 eÅ ⁻³
R.I.M.S. deviation from mean	0.057 eÅ ⁻³	0.104 eÅ ⁻³	0.169 eÅ ⁻³	0.066 eÅ ⁻³

S78

Table S2 Crystal data and structural refinement parameters for compounds 4-RhCl₃Cp*, 8, 9, 10.

Compound #	4-RhCl ₃ Cp*	8	9	10
CCDC #	1976772	1976777	1976778	1976779
Chemical formula	C ₂₆ H ₁₆ Cl ₃ NiRh ₂ Si	C ₂₆ H ₁₆ Cl ₃ NiRh ₂ Si ₂	C ₂₆ H ₁₆ Cl ₃ NiRh ₂ Si ₄	C ₂₆ H ₁₆ Cl ₃ NiRh ₂ Si ₂
Formula weight	1090.20	657.88	1413.60	622.43
Temperature	100(2) K	100(2) K	100(2) K	103(2) K
Wavelength	0.71073 Å	0.71073 Å	0.71073 Å	0.71073 Å
Crystal size	0.098 × 0.160 × 0.258 mm	0.100 × 0.204 × 0.258 mm	0.039 × 0.072 × 0.189 mm	0.083 × 0.139 × 0.239 mm
Crystal habit	clear intense red fragment	clear intense green fragment	grey-black fragment	clear intense red plate
Crystal system	orthorhombic	triclinic	triclinic	monoclinic
Space group	P 2 ₁ 2 ₁ 2 ₁	P -1	P -1	P 2 ₁ /n
Unit cell dimensions	a = 9.0670(11) Å, α = 90° b = 17.650(3) Å, α = 90° c = 32.302(5) Å, α = 90°	a = 8.7307(6) Å, α = 104.544(4)° b = 11.6729(10) Å, β = 80.082(3)° c = 18.1360(15) Å, γ = 111.578(2)°	a = 8.4991(6) Å, α = 85.097(3)° b = 19.5364(19) Å, β = 80.082(3)° c = 23.877(2) Å, γ = 79.898(3)°	a = 13.072(3) Å, α = 90° b = 14.981(3) Å, β = 107.024(11)° c = 17.516(4) Å, γ = 90°
Volume	5169.4(13) Å ³	1637.0(2) Å ³	3636.5(6) Å ³	3279.9(13) Å ³
Z	4	2	2	4
Density (calculated)	1.401 g/cm ³	1.335 g/cm ³	1.223 g/cm ³	1.260 g/cm ³
Absorption coefficient	0.955 mm ⁻¹	0.736 mm ⁻¹	0.669 mm ⁻¹	0.652 mm ⁻¹
F(000)	2248	694	1496	1320
Diffractometer	Bruker D8 Venture Duo IMS	Bruker D8 Venture Duo IMS	Bruker D8 Venture	Bruker D8 Venture
Radiation source	IMS microsource, Mo	IMS microsource, Mo	TXS rotating anode, Mo	TXS rotating anode, Mo
Absorption correction	2.22 to 25.35°	2.52 to 25.35°	1.96 to 25.68°	2.20 to 25.35°
Theta range for data collection	-10<math>\leq h \leq 10, -21<math>\leq k \leq 21, -38<math>\leq l \leq 38 <td>-10<math>\leq h \leq 10, -14<math>\leq k \leq 14, -21<math>\leq l \leq 21 <td>-10<math>\leq h \leq 10, -23<math>\leq k \leq 23, -29<math>\leq l \leq 29 <td>-15<math>\leq h \leq 15, -18<math>\leq k \leq 18, -21<math>\leq l \leq 21 </td></td></td>	-10<math>\leq h \leq 10, -14<math>\leq k \leq 14, -21<math>\leq l \leq 21 <td>-10<math>\leq h \leq 10, -23<math>\leq k \leq 23, -29<math>\leq l \leq 29 <td>-15<math>\leq h \leq 15, -18<math>\leq k \leq 18, -21<math>\leq l \leq 21 </td></td>	-10<math>\leq h \leq 10, -23<math>\leq k \leq 23, -29<math>\leq l \leq 29 <td>-15<math>\leq h \leq 15, -18<math>\leq k \leq 18, -21<math>\leq l \leq 21 </td>	-15<math>\leq h \leq 15, -18<math>\leq k \leq 18, -21<math>\leq l \leq 21
Index ranges				
Reflections collected	140074	43724	138631	99553
Independent reflections	9464 [R(int) = 0.0865]	5975 [R(int) = 0.0236]	14584 [R(int) = 0.0496]	6001 [R(int) = 0.0885]
Coverage of independent reflections	99.9%	99.6%	100.0%	100.0%
Absorption correction	Multi-Scan	Multi-Scan	Multi-Scan	Multi-Scan
Refinement method	Full-matrix least-squares on F ²	Full-matrix least-squares on F ²	Full-matrix least-squares on F ²	Full-matrix least-squares on F ²
Refinement program	SHELXL-2017/1 (Sheldrick, 2017)	SHELXL-2016/6 (Sheldrick, 2016)	SHELXL-2017/1 (Sheldrick, 2017)	SHELXL-2017/1 (Sheldrick, 2017)
Function minimized	$\sum w(F_o^2 - F_c^2)^2$	$\sum w(F_o^2 - F_c^2)^2$	$\sum w(F_o^2 - F_c^2)^2$	$\sum w(F_o^2 - F_c^2)^2$
Data / restraints / parameters	9464 / 390 / 738	5975 / 0 / 341	14584 / 0 / 749	6001 / 0 / 332
Goodness-of-fit on F ²	1.079	1.040	1.035	1.136
Final R indices	R = 0.0413, wR2 = 0.1016	R = 0.0169, wR2 = 0.0415	R = 0.0355, wR2 = 0.0854	R = 0.0407, wR2 = 0.1039
all data: R1 = 0.0464, wR2 = 0.1059	all data: R1 = 0.0179, wR2 = 0.0423	all data: R1 = 0.0470, wR2 = 0.0915	all data: R1 = 0.0511, wR2 = 0.1093	
Weighting scheme	w = 1/(σ ² (F _o ²) + 0.0486P) + 14.8769P	w = 1/(σ ² (F _o ²) + 0.0164P) + 1.1024P	w = 1/(σ ² (F _o ²) + 0.0412P) + 6.7178P	w = 1/(σ ² (F _o ²) + 0.0473P) + 6.3380P
Largest diff. peak and hole	where P = (F _o ² + 2F _c ²)/3	where P = (F _o ² + 2F _c ²)/3	where P = (F _o ² + 2F _c ²)/3	where P = (F _o ² + 2F _c ²)/3
R.M.S. deviation from mean	1.005 and -0.939 eÅ ⁻³	0.312 and -0.371 eÅ ⁻³	3.115 and -0.694 eÅ ⁻³	2.371 and -1.082 eÅ ⁻³
	0.107 eÅ ⁻³	0.042 eÅ ⁻³	0.081 eÅ ⁻³	0.110 eÅ ⁻³

3. DFT Calculations

DFT calculations were carried out at the B97-D/def2-SVP level of theory using Gaussian 09.¹⁵⁻¹⁸ Stationary points on the potential energy surface were characterized by harmonic vibrational frequency calculations. NMR shifts were obtained at the HCTH407/def2-SVP//B97-D/def2-SVP level of theory.¹⁹ Table S3 to Table S9 contain the respective relevant data for the NBO analysis of the cationic parts of complexes **2**, **4**, **6a**, **7a**, **8**, **9** and **10**. Table S10 contains the calculated Si–M and Si–C_{NHC} bond lengths, WBIs/MBOs and NPA charges. Figure S88 to Figure S94 contain the respective HOMOs and LUMOs for complexes **2**, **4**, **6a**, **7a**, **8**, **9** and **10** and the detailed calculated mechanism for the formation of complex **2** *via* **2'** is depicted in Figure S95. Table S11 contains the Cartesian coordinates for the calculated structures.

3.1 NBO Analysis of Complexes **2**, **4**, **6a**, **7a**, **8**, **9** and **10**

Table S3 NBO-Analysis of the central Si–Ru moiety in **2**.

3	Occupation	Atom	Polarization	s-character	p-character	d-character
Bond	1.91	Si	43.71%	45.86%	54.04%	0.10%
		Ru	56.29%	14.46%	6.82%	78.71%
Lone pair	1.51	C _{NHC}	×	36.96%	63.04%	0.00%
Empty orbital	0.53	Si	×	14.79%	84.90%	0.31%

Table S4 NBO-Analysis of the central Si–Rh moiety in **4**.

7	Occupation	Atom	Polarization	s-character	p-character	d-character
Bond	1.81	Si	52.57%	32.80%	67.08%	0.12%
		Rh	47.43%	39.03%	6.92%	54.04%
Bond	1.94	C _{NHC}	75.79%	44.15%	55.85%	0.01%
		Si	24.21%	19.79%	79.39%	0.81%
Bond	1.94	C _{NHC}	27.36%	27.70%	71.63%	0.68%
		Si	72.64%	30.69%	69.29%	0.02%

11. Appendix

Table S5 NBO-Analysis of the central Si–Ru moiety in **6a**.

4a	Occupation	Atom	Polarization	s-character	p-character	d-character
Bond	1.81	Si	52.26%	37.80%	62.11%	0.08%
		Ru	47.74%	36.27%	10.96%	52.76%
Bond	1.95	C _{NHC}	78.01%	24.20%	75.53%	0.27%
		Si	21.99%	13.01%	85.98%	1.01%

Table S6 NBO-Analysis of the central Si–Rh moiety in **7a**.

5a	Occupation	Atom	Polarization	s-character	p-character	d-character
Bond	1.79	Si	52.23%	35.60%	64.27%	0.13%
		Rh	47.77%	38.03%	8.80%	53.15%
Bond	1.95	C _{NHC}	76.10%	43.65%	56.35%	0.00%
		Si	23.90%	18.71%	80.44%	0.84%

Table S7 NBO-Analysis of the central Si–Ru moiety in **8**.

8	Occupation	Atom	Polarization	s-character	p-character	d-character
Bond (alpha)	0.96	Si	46.97%	39.33%	60.61%	0.06%
		Ru	53.03%	14.86%	5.83%	79.31%
Bond (beta)	0.92	Si	54.41%	39.26%	60.64%	0.10%
		Ru	45.59%	37.53%	8.72%	53.72%

Table S8 NBO-Analysis of the central Si–Rh moiety in **9**.

9	Occupation	Atom	Polarization	s-character	p-character	d-character
Bond (alpha)	0.97	Si	45.52%	37.69%	62.23%	0.08%
		Rh	54.48%	14.87%	3.69%	81.43%
Bond (beta)	0.93	Si	52.15%	37.30%	62.59%	0.11%
		Rh	47.85%	30.21%	5.17%	64.61%

11. Appendix

Table S9 NBO-Analysis of the central Si–Ru moiety in **10**.

10	Occupation	Atom	Polarization	s-character	p-character	d-character
Bond	1.82	Si	57.16%	53.72%	46.18%	0.10%
		Ru	42.84%	44.44%	15.88%	39.66%
Bond	1.91	Si	29.43%	5.19%	94.58%	0.23%
		Ru	70.57%	3.93%	4.82%	91.25%

Table S10 Calculated Si–M and Si–C_{NHC} bond lengths [Å], NPA charges of Si and Metal atoms, Wiberg Bond Index (WBI) and Mayer Bond Order (MBO) in studied transition metal complexes.

#	Bond length [Å]			NPA charge		WBI/MBO		
	Si–M	Si–C _{NHC}	Si–C _{NHC}	Si	Metal	Si–M	Si–C _{NHC}	Si–C _{NHC}
2	2.392	1.997	x	+1.31	–0.56	0.73/0.83	0.66/0.81	x
4	2.365	1.988	1.986	+1.23	–0.25	0.64/0.81	0.69/0.80	0.69/0.80
6a	2.481	2.030	x	+0.81	–0.53	0.73/0.72	0.69/0.82	x
7a	2.428	2.029	x	+0.74	–0.21	0.64/0.70	0.69/0.81	x
8	2.371	x	x	+0.74	–0.46	0.60/0.86	x	x
9	2.324	x	x	+0.68	–0.21	0.68/0.91	x	x
10	2.225	x	x	+0.62	–0.73	1.35/1.52	x	x

3.2 HOMOs and LUMOs of Complexes 2, 4, 6a, 7a, 8, 9 and 10

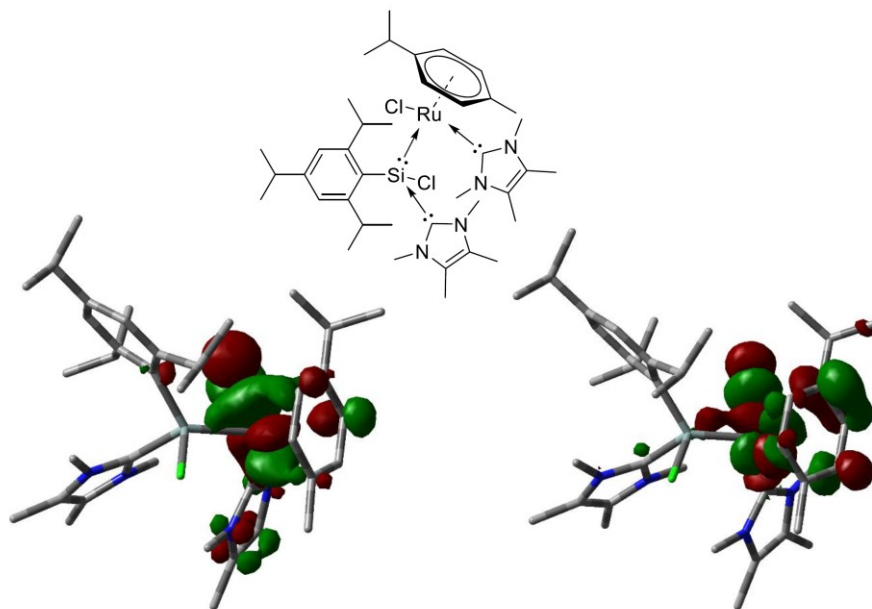


Figure S88 HOMO (left, -7.06 eV) and LUMO (right, -4.46 eV) of 2.

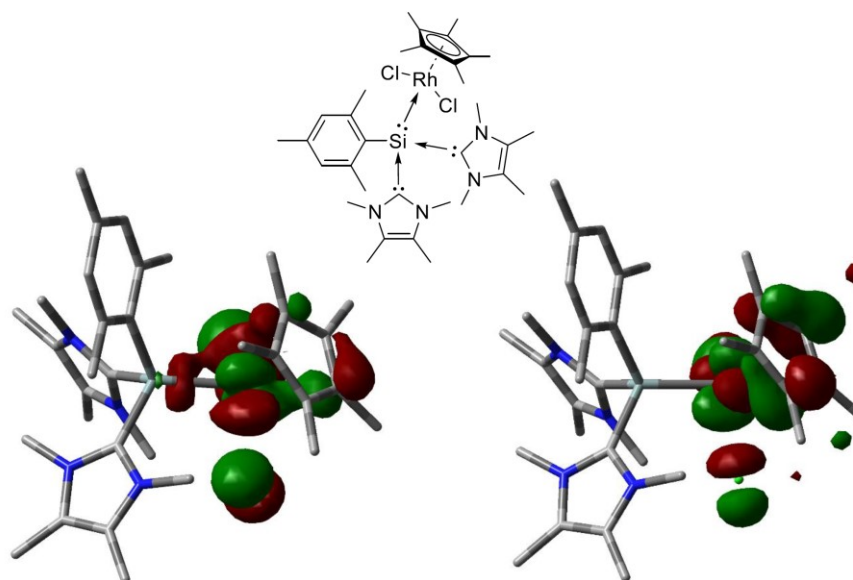


Figure S89 HOMO (left, -6.55 eV) and LUMO (right, -4.71 eV) of 4.

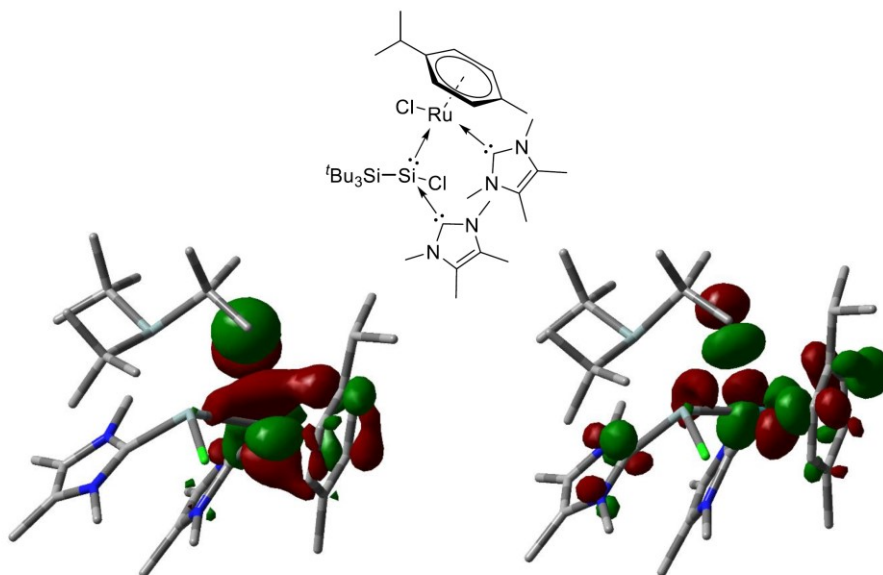


Figure S90 HOMO (left, -6.97 eV) and LUMO (right, -4.62 eV) of 6a.

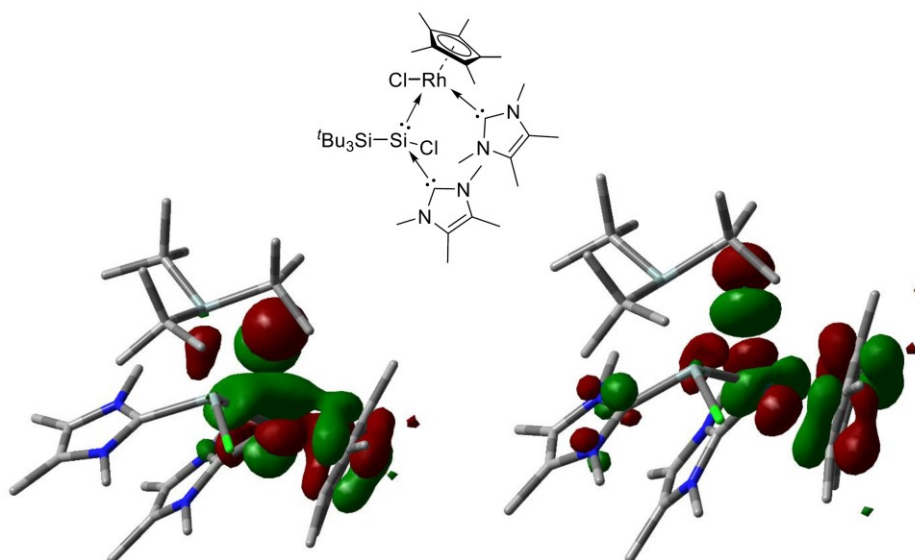


Figure S91 HOMO (left, -7.01 eV) and LUMO (right, -4.82 eV) of 7a.

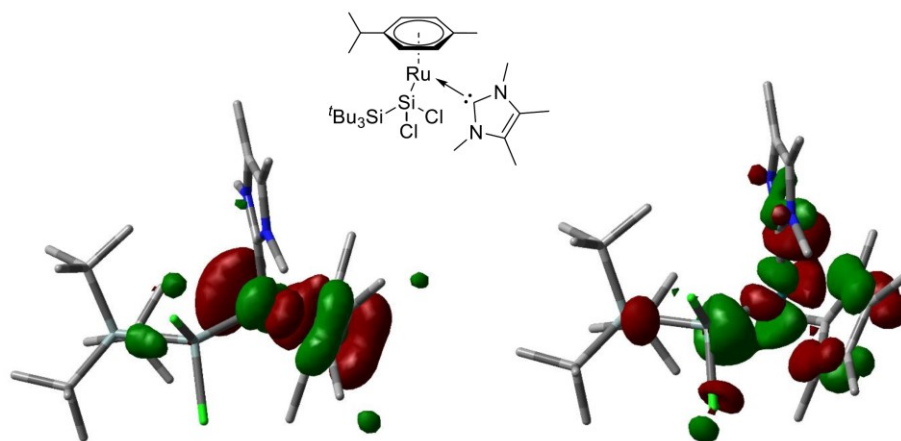


Figure S92 HOMO (left, -3.55 eV) and LUMO (right, -2.58 eV) of **8**.

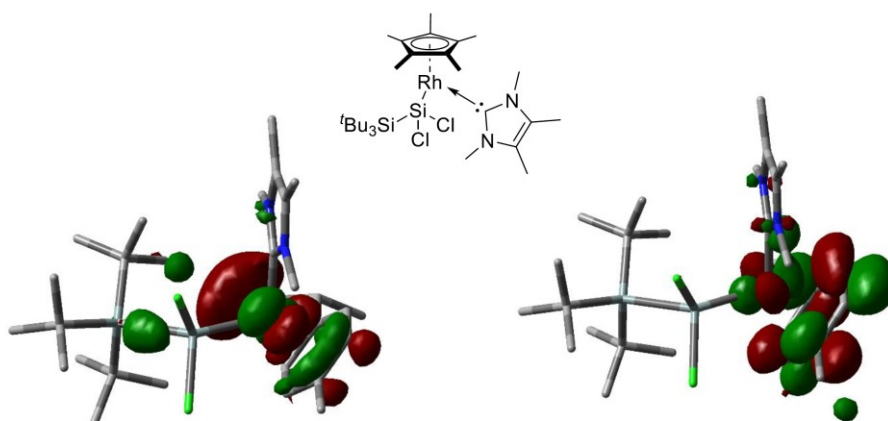


Figure S93 HOMO (left, -3.50 eV) and LUMO (right, -2.80 eV) of **9**.

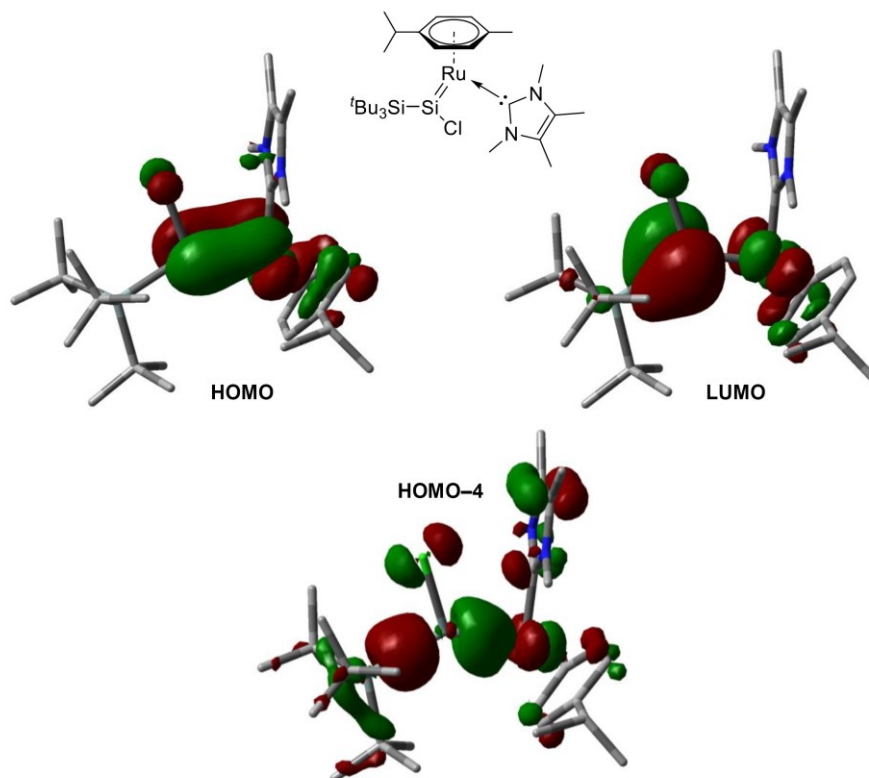
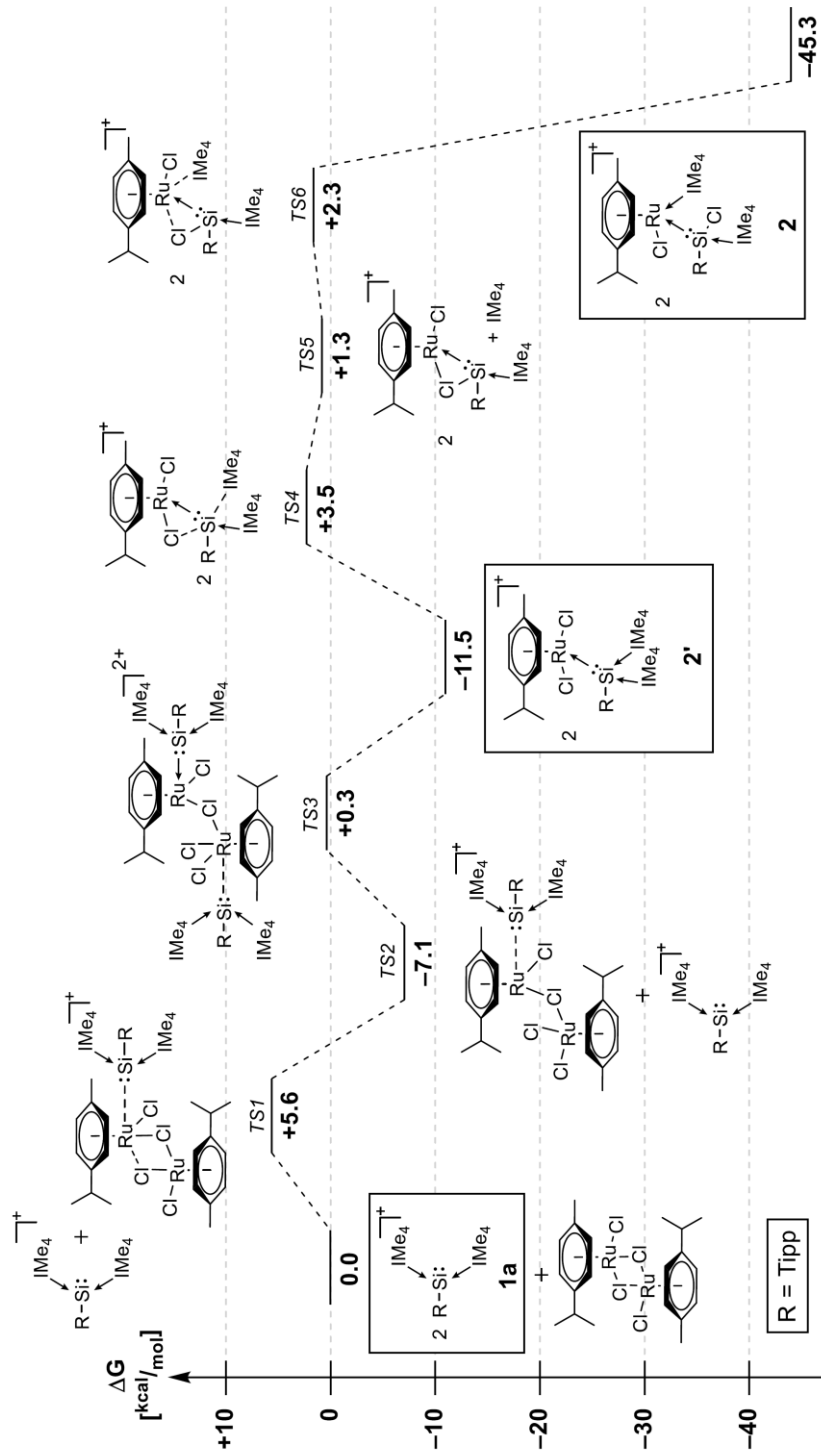


Figure S94 HOMO (top left, -3.52 eV; bonding orbital of Si-Ru π -bond), LUMO (top right, -1.43 eV; anti-bonding orbital of the Si-Ru π -bond) and HOMO-4 (bottom middle, -4.91 eV; σ -orbital of the Si-Ru bond) of **10**.

3.3 Calculated Mechanism for the Formation of **2** via **2'**Figure S95 DFT-derived mechanism for the formation of **2** via **2'**.

S87

3.4 Cartesian Coordinates of the Calculated Structures

Table S11 Cartesian coordinates of the calculated structures

2				4			
Atomtype	X [Å]	Y [Å]	Z [Å]	Atomtype	X [Å]	Y [Å]	Z [Å]
N	0.931894	3.113872	0.88157	N	2.13126	-0.750307	2.118786
C	0.192414	2.161587	0.239417	C	1.922932	0.188473	1.157718
N	-0.722956	2.856971	-0.492854	N	2.866992	1.1557	1.401378
C	-0.595044	4.225749	-0.280497	C	3.605819	0.846444	2.542351
C	0.453037	4.389669	0.597078	C	3.135439	-0.366335	2.99457
Si	0.358907	0.194594	0.5423	Si	0.454904	0.116457	-0.18101
Ru	-1.437389	-1.327611	0.120783	Rh	-1.723396	-0.372155	0.599311
C	-2.914523	0.088865	-0.039598	Cl	-1.356097	-2.809482	0.694572
N	-3.912177	0.077466	-0.989672	C	3.261156	2.276622	0.544019
C	-4.850985	1.08949	-0.768386	C	4.673815	1.734336	3.092873
C	-4.447173	1.753989	0.361814	C	3.518596	-1.180085	4.185892
N	-3.277862	1.120335	0.793347	C	1.47819	-2.052694	2.228706
C	-4.101644	-0.907481	-2.050823	C	1.296678	-1.314517	-1.271745
C	-6.039309	1.30312	-1.648692	N	2.604238	-1.730167	-1.28564
C	-5.047816	2.920869	1.076536	C	2.738071	-2.933188	-1.979453
C	-2.57939	1.545326	1.993836	C	1.479471	-3.258568	-2.433923
C	-1.575872	2.336035	-1.560373	N	0.631698	-2.250436	-2.000164
C	-1.456523	5.23115	-0.970168	C	3.761462	-0.984915	-0.791541
C	1.060691	5.633646	1.156887	C	-0.760757	-2.185642	-2.417635
C	2.158598	2.909168	1.662411	C	0.99686	-4.429222	-3.224374
C	2.195702	-0.024532	-0.054127	C	4.035408	-3.656176	-2.144619
C	3.163598	-0.751129	0.71455	C	0.611758	1.804732	-1.078887
C	4.536003	-0.584105	0.452852	C	0.883619	1.968711	-2.472251
C	5.01399	0.246296	-0.572027	C	0.947513	3.260996	-3.031715
C	4.059497	0.864081	-1.39116	C	0.749424	4.421853	-2.265165
C	2.674127	0.730895	-1.176785	C	0.459341	4.252646	-0.900359
C	2.810821	-1.793883	1.778002	C	0.382319	2.984125	-0.294845
C	3.417401	-1.481442	3.161131	C	1.08711	0.800322	-3.41978
C	1.77408	1.346179	-2.252011	C	0.852242	5.799084	-2.878817
C	1.984035	0.613459	-3.59631	C	0.067925	2.943732	1.188073
C	6.504802	0.413538	-0.825601	Cl	-0.965306	-0.056003	2.889804
C	7.135194	-0.912452	-1.304541	C	-3.704144	0.619132	1.210325
Cl	0.559315	0.42575	2.744446	C	-3.989849	-0.685953	0.722486
C	1.978456	2.864037	-2.431864	C	-3.534048	-0.748552	-0.662583
C	7.23626	0.954603	0.420272	C	-2.96263	0.525929	-1.013307
C	3.257001	-3.197166	1.306066	C	-3.047687	1.377594	0.155579
Cl	-0.793497	-0.994438	-2.218461	C	-4.030593	1.157104	2.56482
C	-1.128996	-3.603258	-0.26982	C	-4.645962	-1.815077	1.451029
C	-2.547197	-3.343418	-0.208796	C	-3.830545	-1.902225	-1.567998
C	-3.107957	-2.668347	0.894031	C	-2.576491	0.998294	-2.382199
C	-2.296399	-2.208051	1.993144	C	-2.889692	2.864361	0.146981

11. Appendix

C	-0.898268	-2.491196	1.922819	H	1.149523	3.361934	-4.106767
C	-0.323143	-3.220745	0.830045	H	0.272294	5.140584	-0.280653
C	-0.572546	-4.297322	-1.497617	H	1.155844	1.152461	-4.464471
C	0.940866	-4.117803	-1.679428	H	0.24824	0.085202	-3.363363
C	-2.908894	-1.543366	3.196938	H	2.014009	0.237285	-3.198459
C	-0.962726	-5.793574	-1.454242	H	1.861853	6.227495	-2.710927
H	4.409519	1.456562	-2.246494	H	0.123827	6.49696	-2.42515
H	5.25748	-1.137215	1.066076	H	0.68228	5.769981	-3.970639
H	0.724869	1.161351	-1.985008	H	0.954834	2.721007	1.808284
H	1.26319	3.261154	-3.178685	H	-0.66586	2.160294	1.438543
H	2.99669	3.084084	-2.80423	H	-0.327592	3.917686	1.524222
H	1.84168	3.421058	-1.488404	H	-0.802743	-1.974387	-3.502821
H	1.274119	0.998212	-4.353808	H	-1.257112	-1.393509	-1.846048
H	1.809701	-0.470076	-3.47771	H	-1.25711	-3.139058	-2.189562
H	3.012442	0.769576	-3.973705	H	1.839897	-5.093552	-3.476722
H	6.619197	1.156556	-1.64007	H	0.514191	-4.109588	-4.168188
H	8.31024	1.108893	0.202044	H	0.252322	-5.013789	-2.649493
H	7.161469	0.237862	1.261041	H	4.768302	-3.065043	-2.729452
H	6.80505	1.918307	0.752517	H	3.864988	-4.60438	-2.681054
H	8.20828	-0.76976	-1.535641	H	4.498378	-3.894273	-1.167247
H	6.627535	-1.290943	-2.211675	H	4.636537	-1.245878	-1.408249
H	7.056268	-1.688787	-0.518715	H	3.980386	-1.225323	0.263747
H	1.716956	-1.82026	1.890752	H	3.569357	0.090867	-0.893085
H	2.898305	-3.972914	2.01046	H	4.363171	2.314149	0.506756
H	4.360021	-3.264811	1.262345	H	2.879396	3.232682	0.940274
H	2.869717	-3.424046	0.296688	H	2.858661	2.136873	-0.46647
H	3.090229	-2.236351	3.902081	H	5.522373	1.850669	2.389531
H	3.108313	-0.484398	3.5202	H	5.067083	1.307528	4.030449
H	4.522879	-1.511591	3.119573	H	4.283424	2.746931	3.312213
H	-2.633433	2.56875	-1.350208	H	3.848572	-2.196518	3.896952
H	-1.433256	1.252082	-1.661389	H	2.658796	-1.295162	4.874004
H	-1.27659	2.821902	-2.505838	H	4.341253	-0.691099	4.733576
H	-1.214344	6.246301	-0.614038	H	2.24397	-2.840985	2.100752
H	-2.531392	5.042676	-0.781712	H	0.686335	-2.159504	1.472869
H	-1.304775	5.206493	-2.067393	H	0.999014	-2.14056	3.216102
H	0.465382	6.511966	0.856182	H	-4.048721	-2.738185	1.333337
H	2.095112	5.780353	0.787673	H	-5.661299	-2.004077	1.046393
H	1.103888	5.603133	2.262394	H	-4.736583	-1.59454	2.52794
H	2.882821	3.686394	1.36583	H	-3.456105	-1.733203	-2.591492
H	2.580782	1.92136	1.434116	H	-4.927973	-2.04289	-1.626502
H	1.945775	2.982477	2.742363	H	-3.393976	-2.832492	-1.161111
H	-4.323067	-0.388327	-2.999244	H	-1.709937	1.679224	-2.336741
H	-4.954087	-1.568113	-1.800921	H	-3.42014	1.556266	-2.837228
H	-3.179551	-1.488474	-2.173001	H	-2.334802	0.157651	-3.054413
H	-6.641392	2.147845	-1.273178	H	-2.088522	3.188939	-0.535373
H	-6.689508	0.406847	-1.680486	H	-2.685332	3.258465	1.155286
H	-5.742241	1.528625	-2.692024	H	-3.837839	3.322023	-0.20615

11. Appendix

H	-5.949507	3.267658	0.543852	H	-4.124373	0.345334	3.304513
H	-4.338459	3.769855	1.145238	H	-4.989407	1.713896	2.522976
H	-5.343239	2.660099	2.112314	H	-3.24148	1.843878	2.91398
H	-3.298702	1.644118	2.825351				
H	-2.082792	2.520257	1.835041				
H	-1.828267	0.792992	2.252685				
H	-3.176099	-3.629583	-1.056672				
H	-4.176107	-2.420744	0.890785				
H	-0.255529	-2.142021	2.735686				
H	0.749458	-3.409775	0.81177				
H	-3.248631	-2.309624	3.922467				
H	-3.787517	-0.938175	2.911496				
H	-2.173101	-0.89619	3.704137				
H	-1.075942	-3.828117	-2.364784				
H	1.248224	-4.521532	-2.660988				
H	1.50272	-4.669304	-0.901686				
H	1.218751	-3.049681	-1.634595				
H	-0.619059	-6.298607	-2.376176				
H	-2.057507	-5.930241	-1.371189				
H	-0.486769	-6.293295	-0.58844				

6a				7a			
Atomtype	X [Å]	Y [Å]	Z [Å]	Atomtype	X [Å]	Y [Å]	Z [Å]
C	-0.972557	2.466978	-2.256578	C	0.860033	-3.734224	-0.144799
C	-2.224359	2.776713	-1.651467	C	2.221478	-3.404685	0.285234
C	-2.229147	3.572969	-0.448578	C	2.832253	-2.645104	-0.750177
C	-1.016534	3.993521	0.125875	C	1.84953	-2.461782	-1.817158
C	0.257876	3.72707	-0.497064	C	0.668817	-3.226508	-1.459412
C	0.250412	2.957402	-1.686989	Rh	1.102159	-1.420057	0.014365
Ru	-0.910991	1.710692	-0.160636	C	2.409885	0.108108	0.257411
C	-2.533299	0.547724	0.260593	N	3.212554	0.362624	1.341875
N	-3.134851	-0.413663	-0.52201	C	4.028148	1.479957	1.131383
C	-4.257901	-0.964872	0.099601	C	3.766106	1.917786	-0.141811
C	-4.402867	-0.302107	1.292084	N	2.797217	1.05604	-0.659201
N	-3.362843	0.632414	1.355466	C	3.31144	-0.430939	2.561721
C	-2.807442	-0.721782	-1.904133	C	2.406813	1.089985	-2.057338
C	-3.269444	1.602897	2.442732	C	4.972903	2.001724	2.164812
C	-5.060017	-2.065678	-0.514293	C	4.330142	3.062632	-0.917625
C	-5.419246	-0.466249	2.375431	C	2.83448	-3.879594	1.564469
C	-3.537197	2.390014	-2.281024	C	4.254206	-2.167116	-0.79032
C	1.568339	4.253193	0.074435	C	2.143008	-1.988801	-3.208712
C	2.241023	5.202721	-0.9426	C	-0.409241	-3.618027	-2.421573
Cl	-0.083411	1.606716	2.135277	C	-0.084954	-4.585174	0.642185
Si	0.539585	-0.263441	-0.551209	Cl	0.284008	-1.562558	2.321941
C	-0.482614	-2.013116	-0.427018	Si	-0.741976	0.07929	-0.479708

S90

11. Appendix

N	-0.737731	-3.039798	-1.30301	C	-0.113527	2.006227	-0.390527
C	-1.49119	-4.044466	-0.696997	N	0.431059	2.532414	0.75101
C	-1.728288	-3.632808	0.591451	C	0.877205	3.832833	0.55722
N	-1.112472	-2.395263	0.725908	C	0.606525	4.144018	-0.752095
C	-0.456907	-3.1366	-2.73669	N	0.003992	3.017556	-1.313107
C	-1.20552	-1.658023	1.981153	C	0.559404	1.890502	2.054667
C	-1.907076	-5.291511	-1.4063	C	-0.367975	3.04876	-2.729442
C	-2.485887	-4.284721	1.699779	C	1.533905	4.636059	1.630271
Cl	0.956067	-0.162123	-2.718417	C	0.858935	5.402305	-1.516574
Si	2.861506	-0.906348	0.307194	Cl	-1.01579	-0.172797	-2.6493
C	2.796507	-1.737253	2.108517	Si	-3.144875	0.1171	0.337236
C	4.217952	-1.874917	2.7194	C	-3.33771	0.989457	2.101334
C	3.642682	-2.212122	-0.981138	C	-4.766911	0.77665	2.668892
C	2.580466	-3.244262	-1.417081	C	-3.733924	-1.749219	0.403925
C	3.954073	0.724662	0.322297	C	-5.27856	-1.875334	0.364781
C	3.609084	1.610413	1.54165	C	-4.190334	1.125515	-1.023554
C	4.833896	-2.984175	-0.358936	C	-3.417877	2.387491	-1.467348
C	4.179094	-1.555815	-2.279506	C	-3.250335	-2.467169	1.685162
C	5.471037	0.41484	0.392609	C	-3.125987	-2.504046	-0.797825
C	3.684594	1.536595	-0.965664	C	-4.474857	0.302418	-2.306666
C	2.157273	-3.147124	2.026871	C	-5.565955	1.577246	-0.471781
C	1.996066	-0.916717	3.14619	C	-2.383713	0.427988	3.179577
C	1.431529	4.928818	1.44664	C	-3.069749	2.510614	1.975564
H	4.526961	-3.650312	0.463952	H	-2.162015	-2.373626	1.83537
H	5.627389	-2.312829	0.012397	H	-3.498009	-3.54649	1.601887
H	5.280891	-3.62607	-1.146614	H	-3.764621	-2.087705	2.585637
H	3.412241	-0.966301	-2.804315	H	-2.024238	-2.500666	-0.730981
H	4.515125	-2.362186	-2.964639	H	-3.414295	-2.079254	-1.774077
H	5.051045	-0.907651	-2.095191	H	-3.4592	-3.563502	-0.776368
H	2.05466	-3.719607	-0.571392	H	-5.757204	-1.375402	1.225014
H	3.065468	-4.046699	-2.012524	H	-5.545346	-2.951593	0.415789
H	1.84341	-2.756619	-2.067152	H	-5.726901	-1.470373	-0.556588
H	5.741344	-0.143535	1.304374	H	-5.125836	-0.566612	-2.118578
H	6.025197	1.376467	0.413272	H	-3.554745	-0.055101	-2.791907
H	5.8357	-0.155151	-0.477198	H	-5.006272	0.955688	-3.029948
H	2.614122	1.77941	-1.062771	H	-6.165002	0.733545	-0.087417
H	3.991215	1.001338	-1.878436	H	-6.138359	2.045625	-1.299363
H	4.245499	2.493717	-0.924279	H	-5.473827	2.332836	0.326299
H	2.526725	1.800031	1.638783	H	-4.049016	2.983027	-2.160576
H	4.126991	2.587043	1.438319	H	-2.514614	2.093895	-2.016499
H	3.964652	1.155599	2.483011	H	-3.126638	3.042681	-0.627946
H	2.052127	-3.560693	3.052014	H	-2.493576	1.039434	4.100257
H	2.771906	-3.858085	1.449224	H	-1.332594	0.441959	2.878693
H	1.153006	-3.126386	1.566371	H	-2.617336	-0.613756	3.444489
H	0.967259	-0.70778	2.839001	H	-3.835405	3.025396	1.369946
H	2.462619	0.056887	3.359791	H	-2.084115	2.72454	1.519901
H	1.965472	-1.488261	4.098225	H	-3.084802	2.972011	2.985452

S91

11. Appendix

H	4.128888	-2.409027	3.688463	H	-4.841588	1.311887	3.638427
H	4.652259	-0.883726	2.937501	H	-4.954241	-0.292242	2.87143
H	4.929535	-2.435292	2.096146	H	-5.571105	1.151044	2.01929
H	-1.412937	-3.265058	-3.276017	H	1.56627	2.097473	2.448284
H	0.184249	-4.01282	-2.928897	H	0.44066	0.801848	1.966075
H	0.041872	-2.22553	-3.083948	H	-0.199316	2.294904	2.74567
H	-2.455724	-5.951644	-0.713951	H	0.881853	4.74109	2.518414
H	-1.031366	-5.84841	-1.791945	H	1.771073	5.645351	1.254936
H	-2.565181	-5.075912	-2.271118	H	2.477286	4.158832	1.961827
H	-3.34152	-3.658781	2.021088	H	1.331143	6.15089	-0.858867
H	-1.844869	-4.449819	2.587139	H	-0.080888	5.834871	-1.910974
H	-2.876577	-5.261203	1.368553	H	1.529767	5.233157	-2.381978
H	-2.265478	-1.616238	2.279279	H	-1.191506	3.768122	-2.877142
H	-0.834605	-0.630695	1.860618	H	-0.68017	2.053556	-3.061534
H	-0.62155	-2.176838	2.759554	H	0.506474	3.376719	-3.31862
H	-2.736471	-1.810612	-2.040954	H	2.875312	0.112663	3.41954
H	-1.856693	-0.235738	-2.162671	H	4.376972	-0.635814	2.768552
H	-3.605544	-0.344245	-2.567274	H	2.756977	-1.365875	2.42697
H	-5.874163	-2.367555	0.166341	H	4.453507	2.239351	3.114057
H	-4.43029	-2.9553	-0.716946	H	5.463691	2.919908	1.799415
H	-5.517153	-1.758085	-1.475612	H	5.765615	1.265767	2.405178
H	-6.040639	0.442924	2.498714	H	3.536542	3.777475	-1.213414
H	-4.943969	-0.671324	3.354899	H	4.834903	2.724481	-1.843852
H	-6.093562	-1.305966	2.135288	H	5.070829	3.605885	-0.306624
H	-4.279479	1.996857	2.653514	H	2.166492	2.121914	-2.355337
H	-2.599757	2.415143	2.13392	H	1.538165	0.436636	-2.199967
H	-2.85667	1.139296	3.356065	H	3.238669	0.727731	-2.688708
H	-3.179702	3.793896	0.048239	H	2.168767	-3.653495	2.418226
H	-1.037154	4.507426	1.089929	H	3.818516	-3.412973	1.743035
H	1.192943	2.708985	-2.181012	H	2.97856	-4.97851	1.536019
H	-0.94004	1.865315	-3.169039	H	4.647753	-1.986844	0.224733
H	-4.201698	1.890215	-1.553102	H	4.343161	-1.22976	-1.365569
H	-3.391608	1.733499	-3.15372	H	4.900234	-2.92482	-1.277354
H	-4.053063	3.306188	-2.62898	H	1.310037	-1.390253	-3.615937
H	2.225373	3.37992	0.202516	H	2.27667	-2.865549	-3.87583
H	0.823197	5.852505	1.381124	H	3.070994	-1.395279	-3.253742
H	2.433027	5.214359	1.816544	H	-1.207764	-4.193076	-1.927724
H	0.971149	4.246829	2.182707	H	0.042094	-4.26343	-3.203393
H	2.419815	4.70303	-1.912646	H	-0.859527	-2.751876	-2.930878
H	3.21616	5.545882	-0.549083	H	-0.121809	-4.246317	1.692804
H	1.609924	6.094615	-1.123863	H	0.25207	-5.641828	0.633567
				H	-1.105565	-4.53977	0.228551

11. Appendix

8				9			
Atomtype	X [Å]	Y [Å]	Z [Å]	Atomtype	X [Å]	Y [Å]	Z [Å]
Ru	-1.378445	-0.617534	-0.422016	C	-1.346717	-3.077038	0.127556
Cl	0.708306	2.478791	-1.400219	C	-2.242386	-2.589419	-0.898104
Cl	1.379434	-0.393733	-2.999151	C	-3.251911	-1.787968	-0.252676
Si	0.718565	0.312408	-1.022475	C	-2.984403	-1.779699	1.167312
Si	2.719084	0.071859	0.311719	C	-1.822275	-2.592682	1.400758
N	-2.465042	2.256172	-0.548842	Rh	-1.237722	-0.762141	0.059496
N	-2.246904	1.618166	1.503279	C	-1.921501	1.121932	0.022463
C	2.091463	0.451139	2.139304	N	-2.125272	1.962017	1.090815
C	1.150348	-0.685003	2.591447	C	-2.733288	3.158235	0.700198
C	1.259394	1.757622	2.163163	C	-2.944812	3.057722	-0.653043
C	3.239907	0.587318	3.165845	N	-2.454012	1.807563	-1.038465
C	4.171343	1.303317	-0.194625	C	-1.81081	1.635535	2.470718
C	5.521346	0.866208	0.427866	C	-2.581132	1.27832	-2.388154
C	4.318513	1.356179	-1.735732	C	-3.021187	4.266372	1.659522
C	3.905579	2.75104	0.287006	C	-3.544026	4.022015	-1.623805
C	3.316039	-1.807463	0.143746	C	-2.173832	-2.956027	-2.348933
C	4.179329	-2.255594	1.347448	C	-4.436983	-1.137388	-0.903424
C	4.140612	-2.026928	-1.149948	C	-3.844126	-1.116775	2.205038
C	2.098513	-2.756033	0.03539	C	-1.216678	-2.904419	2.736443
C	-2.035952	1.199646	0.211299	C	-0.296228	-4.129595	-0.083034
C	-2.894135	3.32379	0.243273	Si	0.742172	-0.241378	-1.039941
C	-2.757627	2.919526	1.548595	Si	2.728065	0.335607	0.216239
C	-2.498988	2.260924	-2.002265	C	2.597095	2.247962	0.701729
C	-3.358882	4.619276	-0.336468	C	3.065497	3.18844	-0.435134
C	-3.033734	3.63338	2.831248	Cl	0.670313	1.39462	-2.500308
C	-2.045067	0.783186	2.674056	Cl	1.374577	-1.856127	-2.378734
C	-2.377601	-2.552105	0.401584	C	4.390399	-0.015991	-0.778177
C	-1.273162	-2.889196	-0.452668	C	5.607882	0.659726	-0.097688
C	-1.195246	-2.391237	-1.784334	C	2.611737	-0.802047	1.820564
C	-2.210183	-1.527514	-2.325764	C	2.270548	-2.248312	1.389363
C	-3.294446	-1.179772	-1.462025	C	4.268872	0.520193	-2.226736
C	-3.387423	-1.699954	-0.131274	C	4.697729	-1.530443	-0.867839
C	-2.553779	-3.135272	1.795128	C	3.916243	-0.825315	2.649668
C	-1.238897	-3.530435	2.484407	C	1.450356	-0.347698	2.73405
C	-3.517026	-4.3434	1.725902	C	3.445004	2.570441	1.956508
C	-2.153441	-1.055483	-3.755163	C	1.122703	2.605442	1.000253
H	1.681296	-1.642324	2.7306	H	3.454119	0.019412	-2.778239
H	0.342089	-0.842093	1.846029	H	5.220765	0.320488	-2.764811
H	0.677569	-0.424298	3.562853	H	4.084691	1.606857	-2.259032
H	0.378215	1.696143	1.501166	H	3.864918	-2.095637	-1.319782
H	1.843035	2.640616	1.859116	H	4.923673	-1.964939	0.12246
H	0.895122	1.933137	3.19961	H	5.595727	-1.676155	-1.505644
H	2.812422	0.750849	4.179369	H	5.753425	0.308029	0.939777
H	3.891295	1.450343	2.939309	H	5.52667	1.760235	-0.076589

S93

11. Appendix

H	3.873627	-0.315712	3.2103	H	6.526713	0.40766	-0.669876
H	5.47784	0.834261	1.531888	H	3.770485	-1.46414	3.547696
H	6.303413	1.60342	0.144966	H	4.211054	0.181394	2.994389
H	5.859239	-0.121997	0.072678	H	4.758568	-1.249951	2.075216
H	4.541764	0.370152	-2.175929	H	0.497163	-0.329998	2.166462
H	5.154435	2.041857	-1.994261	H	1.617296	0.648958	3.178605
H	3.400181	1.741029	-2.212581	H	1.331791	-1.071162	3.568696
H	2.945628	3.143346	-0.087479	H	2.201344	-2.894134	2.291939
H	4.716965	3.405891	-0.097053	H	3.018871	-2.692321	0.714191
H	3.916232	2.832186	1.388991	H	1.290704	-2.279279	0.882374
H	3.610468	-2.249809	2.294696	H	3.088509	2.035928	2.854745
H	5.071815	-1.618704	1.480428	H	3.37971	3.659242	2.170851
H	4.529277	-3.29703	1.1785	H	4.511141	2.320372	1.811501
H	4.390426	-3.106637	-1.235071	H	0.493742	2.509081	0.098788
H	5.092508	-1.469427	-1.152213	H	1.058825	3.660327	1.347752
H	3.567079	-1.738256	-2.047865	H	0.697079	1.963194	1.784234
H	2.458858	-3.804872	-0.04312	H	2.512726	3.008004	-1.372544
H	1.508571	-2.536513	-0.871212	H	4.145123	3.094422	-0.642857
H	1.422811	-2.695495	0.903313	H	2.881652	4.239858	-0.12451
H	-1.970815	1.358786	-2.348754	H	-2.73447	1.614086	3.078104
H	-1.984439	3.154861	-2.393009	H	-1.113106	2.37771	2.897718
H	-3.547215	2.247007	-2.361462	H	-1.343052	0.638899	2.480956
H	-4.222628	4.47905	-1.017188	H	-3.503012	5.108446	1.133019
H	-2.554986	5.109114	-0.922134	H	-2.092186	4.644238	2.132665
H	-3.665973	5.309265	0.468785	H	-3.696452	3.940309	2.476307
H	-3.780957	3.097285	3.451135	H	-4.426247	3.591034	-2.138634
H	-3.424736	4.644921	2.624974	H	-2.815915	4.310638	-2.408062
H	-2.11525	3.739686	3.443608	H	-3.866613	4.938765	-1.100017
H	-3.00106	0.644321	3.215205	H	-2.070853	0.302808	-2.411198
H	-1.302394	1.234533	3.355101	H	-2.103334	1.957415	-3.113754
H	-1.670595	-0.193675	2.327041	H	-3.65059	1.152646	-2.64068
H	-0.462945	-3.514942	-0.073297	H	-2.567524	-3.981266	-2.518534
H	-0.31518	-2.614042	-2.395093	H	-1.1297	-2.93055	-2.706782
H	-4.059896	-0.483419	-1.823236	H	-2.770002	-2.262169	-2.969147
H	-4.212773	-1.38142	0.516459	H	-5.362967	-1.718648	-0.709839
H	-3.042174	-2.350531	2.408579	H	-4.307163	-1.068266	-1.996689
H	-1.438824	-3.860747	3.521056	H	-4.599884	-0.117135	-0.508863
H	-0.528838	-2.687561	2.512641	H	-4.223662	-0.141955	1.846029
H	-0.75081	-4.371959	1.956646	H	-3.281852	-0.942834	3.139788
H	-3.076924	-5.146491	1.102864	H	-4.727476	-1.7402	2.460251
H	-4.487066	-4.057191	1.277749	H	-1.625299	-3.850313	3.151777
H	-3.702737	-4.753163	2.738126	H	-1.42501	-2.102681	3.468661
H	-1.114789	-0.819659	-4.045281	H	-0.122037	-3.016448	2.656908
H	-2.780556	-0.156992	-3.900946	H	-0.776338	-5.107171	-0.29985
H	-2.531851	-1.844689	-4.437688	H	0.331478	-4.257124	0.815016
				H	0.362209	-3.879392	-0.931543

11. Appendix

10				1a			
Atomtype	X [Å]	Y [Å]	Z [Å]	Atomtype	X [Å]	Y [Å]	Z [Å]
Ru	-1.350501	0.747659	-0.509013	C	-1.504431	-0.031915	-0.900279
Cl	0.232663	-2.572259	0.49512	C	-1.057569	-0.485136	0.386825
Si	0.485551	-0.475973	-0.19417	C	-2.022913	-1.081223	1.259295
Si	2.893305	-0.327636	-0.041655	C	-3.374515	-1.155715	0.864219
N	-2.762042	-1.34174	1.239892	C	-3.824327	-0.662792	-0.368293
N	-2.847796	-1.91213	-0.841912	C	-2.865597	-0.114244	-1.23905
C	3.417684	-0.805977	1.806197	Si	0.710473	-0.160711	1.115197
C	2.344743	-0.290774	2.799684	C	1.003475	1.669928	0.54725
C	3.518859	-2.337029	2.012328	N	1.866602	2.321489	-0.295085
C	4.788339	-0.196546	2.187933	C	1.687802	3.705921	-0.218473
C	3.77611	-1.498679	-1.355579	C	0.681179	3.924472	0.693424
C	3.160665	-2.919042	-1.352406	N	0.286871	2.669219	1.153902
C	5.293179	-1.622499	-1.072977	C	2.719323	1.716344	-1.310691
C	3.599755	-0.937245	-2.78577	C	2.477974	4.666864	-1.044613
C	3.303627	1.567377	-0.411462	C	0.061212	5.202903	1.155372
C	4.805083	1.854497	-0.640333	C	-0.794403	2.431444	2.108784
C	2.526232	2.037353	-1.666278	C	-1.662607	-1.695999	2.614332
C	2.80436	2.43986	0.76467	C	-1.855783	-3.226879	2.590138
C	-2.354738	-0.940617	-0.008047	C	-5.291537	-0.737588	-0.765476
C	-3.462398	-2.548874	1.191232	C	-5.879707	0.669769	-1.001052
C	-3.518328	-2.911124	-0.132155	C	-0.555877	0.510421	-1.971321
C	-2.37665	-0.676932	2.471709	C	-0.77176	2.018805	-2.214316
C	-3.986466	-3.228217	2.413632	C	2.047305	-1.184476	0.178399
C	-4.124769	-4.104194	-0.795438	C	-2.444511	-1.05169	3.776493
C	-2.592799	-1.962897	-2.270581	C	-5.491193	-1.63519	-2.005468
C	-1.873012	2.65983	0.551917	C	-0.670929	-0.263234	-3.303394
C	-3.091923	2.116985	0.041907	H	2.423814	2.092174	-2.3065
C	-3.244041	1.777903	-1.341384	H	2.595519	0.625791	-1.288085
C	-2.186605	1.973594	-2.27396	H	3.779121	1.976175	-1.135336
C	-0.976447	2.571972	-1.773492	H	2.197867	5.70291	-0.791433
C	-0.822201	2.920538	-0.401327	H	2.294849	4.519535	-2.127621
C	-1.776999	3.06866	2.011321	H	3.566596	4.554595	-0.873396
C	-0.391383	2.816122	2.624693	H	0.196296	5.355609	2.244322
C	-2.193899	4.5479	2.173193	H	-1.025807	5.224646	0.944649
C	-2.346327	1.64785	-3.737735	H	0.526856	6.055331	0.633244
H	2.659196	-0.530072	3.838683	H	-0.471168	1.65558	2.829576
H	1.371599	-0.786228	2.620338	H	-1.695534	2.06574	1.584059
H	2.192396	0.800165	2.737089	H	-1.019933	3.365846	2.64542
H	3.738995	-2.538152	3.083155	H	-4.10429	-1.616485	1.542878
H	4.335175	-2.789099	1.421643	H	-3.191667	0.247316	-2.22218
H	2.576386	-2.848213	1.754214	H	0.472409	0.35959	-1.605962
H	4.779368	0.907217	2.185036	H	-0.034095	2.411079	-2.942156
H	5.593185	-0.533442	1.509098	H	-1.780639	2.198315	-2.632007
H	5.058119	-0.521763	3.216069	H	-0.687216	2.601987	-1.281023

S95

11. Appendix

H	3.228587	-3.411606	-0.368748	H	0.095999	0.090747	-4.019774
H	3.706746	-3.546656	-2.089908	H	-0.533768	-1.349647	-3.153328
H	2.094286	-2.902178	-1.640887	H	-1.660666	-0.111949	-3.773309
H	5.805339	-0.644335	-1.094186	H	-0.587145	-1.50223	2.800668
H	5.759879	-2.26428	-1.851329	H	-1.545047	-3.672146	3.554958
H	5.495907	-2.090463	-0.094049	H	-2.916835	-3.491536	2.417275
H	2.534711	-0.749633	-3.02554	H	-1.256153	-3.690653	1.782826
H	3.988821	-1.675261	-3.519669	H	-2.121988	-1.482277	4.743697
H	4.162769	0.001353	-2.934263	H	-2.278841	0.042265	3.811385
H	4.953071	2.946889	-0.784289	H	-3.532852	-1.226466	3.675162
H	5.180876	1.350577	-1.549405	H	-5.838721	-1.198859	0.080376
H	5.432166	1.539074	0.212107	H	-6.566536	-1.718495	-2.25359
H	2.61945	3.140813	-1.766489	H	-4.971938	-1.208745	-2.885909
H	1.4552	1.79005	-1.58453	H	-5.092244	-2.652446	-1.831501
H	2.906469	1.587899	-2.597742	H	-6.958186	0.603189	-1.240305
H	3.376398	2.272809	1.693773	H	-5.75812	1.309181	-0.106141
H	1.739428	2.251308	0.983725	H	-5.37421	1.168488	-1.851108
H	2.913287	3.513864	0.498667	N	3.388323	-1.08919	0.47957
H	-1.720431	0.165588	2.194411	C	4.103344	-2.15262	-0.073801
H	-1.819181	-1.377728	3.1209	C	3.183036	-2.946018	-0.721132
H	-3.266369	-0.306547	3.017224	N	1.938125	-2.334193	-0.560455
H	-3.165823	-3.513927	3.102688	C	0.701835	-2.924428	-1.067534
H	-4.530385	-4.147522	2.134422	C	3.360969	-4.221306	-1.478725
H	-4.681159	-2.57714	2.98218	C	5.581876	-2.311997	0.072243
H	-4.620345	-4.745815	-0.045931	C	3.951099	-0.068194	1.354299
H	-3.357791	-4.714617	-1.313865	H	0.831013	-3.194457	-2.129851
H	-4.88114	-3.815384	-1.553482	H	0.455862	-3.836668	-0.492414
H	-3.5437	-1.983285	-2.837359	H	-0.117763	-2.20164	-0.961037
H	-2.003442	-2.866032	-2.519176	H	4.906155	-0.427494	1.768974
H	-2.006918	-1.063781	-2.530506	H	4.125567	0.879586	0.814636
H	-3.896834	1.876213	0.746007	H	3.232555	0.119351	2.178989
H	-4.160817	1.275185	-1.671316	H	5.921869	-3.193468	-0.496658
H	-0.147641	2.73949	-2.468438	H	6.128285	-1.426595	-0.308267
H	0.131945	3.332881	-0.061955	H	5.877074	-2.458486	1.13037
H	-2.51287	2.44656	2.559494	H	3.034103	-4.119862	-2.532538
H	0.361759	3.503686	2.196549	H	4.423127	-4.517863	-1.477067
H	-0.058582	1.78256	2.419527	H	2.773737	-5.045233	-1.027981
H	-0.414645	2.987286	3.717822				
H	-2.178422	4.847242	3.239614				
H	-3.210715	4.722599	1.773224				
H	-1.492748	5.204209	1.620934				
H	-2.740608	2.520106	-4.301394				
H	-3.052392	0.809106	-3.8824				
H	-1.374784	1.368665	-4.185481				

11. Appendix

[RuCl₂(<i>p</i>-cym)]₂				TS1 (+5.6 kcal/mol)			
Atomtype	X [Å]	Y [Å]	Z [Å]	Atomtype	X [Å]	Y [Å]	Z [Å]
C	-3.95386	1.008606	0.437922	C	3.489871	-1.455813	2.114251
C	-3.757442	-0.396076	0.283618	C	4.71448	-0.745743	1.812731
C	-2.978141	-0.918723	-0.816773	C	5.489175	-1.210014	0.712307
C	-2.404344	0.007029	-1.738366	C	5.060524	-2.341439	-0.067362
C	-2.576191	1.415732	-1.545043	C	3.82341	-3.006228	0.209665
C	-3.365397	1.95655	-0.473496	C	3.047605	-2.553044	1.336204
Ru	-1.847073	0.623022	0.309309	Ru	3.484053	-0.866153	-0.01259
Cl	0.372139	1.596753	-0.32971	Cl	1.699628	-1.200206	-1.605786
C	-2.698745	-2.401162	-1.002163	C	5.075602	0.495143	2.585916
C	-3.064496	-3.271126	0.208802	C	3.299712	-4.124182	-0.673537
C	-3.459396	3.43708	-0.217207	C	3.819699	-4.075092	-2.116765
Cl	-0.398155	-1.19326	1.231234	Cl	2.103025	1.13577	0.693435
C	-3.433683	-2.892894	-2.271027	Ru	0.288226	2.21721	-0.678002
H	-1.688835	-0.356569	-2.482162	Cl	-0.403179	3.373411	1.410794
H	-1.991761	2.107644	-2.162801	Si	-1.547972	0.231401	0.227908
H	-4.437131	1.381681	1.347651	C	-2.973711	1.390005	1.030131
H	-4.121329	-1.070537	1.062953	N	-3.815771	2.008024	0.152475
H	-4.43911	3.834174	-0.552224	C	-4.713322	2.845404	0.81125
H	-2.659186	3.974641	-0.756542	C	-4.423261	2.738636	2.149126
H	-3.342485	3.633215	0.864049	N	-3.37101	1.830852	2.255444
H	-1.610269	-2.480963	-1.182089	C	-3.836631	1.779207	-1.285497
H	-2.755133	-4.315931	0.01976	C	-5.750871	3.656738	0.10672
H	-4.158572	-3.272701	0.386495	C	-5.039712	3.416301	3.3282
H	-2.55487	-2.920772	1.123363	C	-2.777464	1.50116	3.540297
H	-3.199094	-3.959274	-2.45161	C	-0.718858	-0.975212	1.614408
H	-3.128536	-2.315831	-3.16363	N	-0.223449	-0.728119	2.868069
H	-4.531488	-2.796359	-2.153726	C	0.06837	-1.914175	3.533983
Cl	-1.599976	1.728721	2.41804	C	-0.213708	-2.934159	2.65936
Ru	1.699591	-0.464101	0.107117	N	-0.652879	-2.338732	1.48069
Cl	0.835508	-1.37033	-1.955798	C	0.187091	0.551581	3.44348
C	3.566428	0.60508	-0.144773	C	-0.865143	-3.151008	0.275462
C	3.104516	0.773959	1.217796	C	-0.123942	-4.414123	2.846397
C	2.755228	-0.337825	2.025197	C	0.602066	-1.950897	4.927957
C	2.850407	-1.682701	1.500931	C	-2.879467	-1.156176	-0.412361
C	3.345892	-1.861642	0.171608	C	-2.934204	-1.649488	-1.75496
C	3.700434	-0.727498	-0.640813	C	-3.662815	-2.814928	-2.063349
H	2.875315	1.784527	1.573876	C	-4.449916	-3.485993	-1.120715
H	2.264444	-0.171211	2.989921	C	-4.491588	-2.938944	0.167534
C	2.366554	-2.854274	2.31267	C	-3.718878	-1.822555	0.548855
H	3.326221	-2.859908	-0.278227	C	-2.274304	-0.96336	-2.940486
H	3.92748	-0.889492	-1.698067	C	-3.361424	-0.545068	-3.96418
C	3.805145	1.828691	-1.011399	C	-5.227386	-4.742086	-1.483842
H	2.059525	-3.686013	1.654601	C	-6.230091	-4.480566	-2.627358
H	3.180423	-3.209978	2.976764	C	-3.879244	-1.414801	2.015602

S97

11. Appendix

H	1.505002	-2.563425	2.938569	C	-3.713479	-2.57694	3.018026
C	3.480101	1.591937	-2.495026	C	0.445322	4.319509	-1.326219
H	3.114004	2.607209	-0.635543	C	1.772739	3.813937	-1.306057
C	5.253336	2.325371	-0.807581	C	1.993709	2.568109	-1.988988
H	3.518771	2.551732	-3.043023	C	0.994713	1.956869	-2.798905
H	4.217401	0.911344	-2.963938	C	-0.285839	2.568925	-2.928771
H	2.473962	1.149304	-2.606718	C	-0.588771	3.685096	-2.089319
H	5.423933	3.25439	-1.384394	C	2.913637	4.414793	-0.502335
H	5.463881	2.534652	0.258846	C	2.494515	5.601841	0.375911
H	5.97683	1.563222	-1.158203	C	-1.217363	2.166777	-4.032284
				Cl	4.577117	0.294664	-1.849724
				C	4.074486	4.789518	-1.451961
				C	3.603076	-5.481067	0.001933
				C	-5.236745	-0.712222	2.232015
				C	-4.266376	-5.895763	-1.844
				C	-1.152621	-1.779683	-3.652543
				H	2.067498	-2.99401	1.506216
				H	2.820346	-1.049852	2.879546
				H	6.351136	-0.614365	0.396235
				H	5.622598	-2.579561	-0.973808
				H	5.533168	0.227724	3.55988
				H	4.173286	1.104751	2.775529
				H	5.795876	1.111257	2.01934
				H	2.201599	-3.983018	-0.710055
				H	3.299288	-4.83778	-2.725155
				H	4.903415	-4.298001	-2.159959
				H	3.637785	-3.079122	-2.556902
				H	3.160545	-6.307092	-0.5869
				H	3.193931	-5.528038	1.03061
				H	4.695708	-5.649611	0.062318
				H	2.950302	2.045807	-1.873481
				H	1.22904	1.017245	-3.306424
				H	-1.599128	4.107834	-2.092995
				H	0.177835	5.162737	-0.6854
				H	-2.279548	2.178503	-3.745827
				H	-1.091933	2.914636	-4.841693
				H	-0.958916	1.184479	-4.447622
				H	3.273265	3.601722	0.158148
				H	3.362373	5.957754	0.961346
				H	2.139563	6.449688	-0.243486
				H	1.690469	5.314947	1.077589
				H	4.926107	5.18353	-0.865746
				H	4.428419	3.910059	-2.021159
				H	3.759053	5.572023	-2.169856
				H	-5.133519	-3.423449	0.913975
				H	-3.633776	-3.191664	-3.092717
				H	1.285252	0.548223	3.544296

11. Appendix

H	-0.088137	1.382159	2.776596
H	-0.271914	0.673333	4.439159
H	-0.11122	-3.95458	0.280376
H	-1.87993	-3.581047	0.259418
H	-0.68365	-2.534338	-0.60995
H	0.171008	-4.641074	3.884368
H	-1.096534	-4.90238	2.644984
H	0.622244	-4.878083	2.171911
H	-0.088811	-1.462419	5.642414
H	0.748602	-2.995694	5.248504
H	1.575286	-1.428254	5.004339
H	-3.567722	1.482176	4.308194
H	-2.321235	0.50597	3.489795
H	-2.010561	2.250355	3.798893
H	-4.283399	2.651807	-1.786953
H	-2.802698	1.652214	-1.638991
H	-4.413798	0.868285	-1.518366
H	-6.3494	4.218078	0.843445
H	-5.294593	4.389718	-0.587851
H	-6.440894	3.019703	-0.480331
H	-4.2888	3.995402	3.899931
H	-5.825067	4.113395	2.991527
H	-5.506527	2.689523	4.022482
H	-3.089409	-0.699774	2.257164
H	-5.320754	-0.32782	3.267502
H	-5.372542	0.13179	1.532557
H	-6.065567	-1.426537	2.067264
H	-3.696628	-2.18122	4.0523
H	-4.551238	-3.296003	2.956602
H	-2.774803	-3.12949	2.845041
H	-1.772129	-0.058853	-2.554615
H	-0.65646	-1.028731	-4.312364
H	-0.47024	-2.073777	-2.84046
H	-1.542739	-2.644096	-4.220318
H	-2.913146	-0.081256	-4.862053
H	-3.917955	-1.437563	-4.307733
H	-4.102561	0.158889	-3.540435
H	-5.803977	-5.045685	-0.587103
H	-6.816998	-5.393626	-2.84297
H	-6.932292	-3.666807	-2.364919
H	-5.700914	-4.190953	-3.555939
H	-4.833552	-6.8198	-2.066581
H	-3.667226	-5.639366	-2.739421
H	-3.566024	-6.107361	-1.013035

11. Appendix

TS2 (-7.1 kcal/mol)				TS3 (+0.3 kcal/mol)			
Atomtype	X [Å]	Y [Å]	Z [Å]	Atomtype	X [Å]	Y [Å]	Z [Å]
N	-0.039434	-0.482025	2.823525	N	3.345115	-1.496851	2.630194
C	-0.514768	-0.77057	1.570901	C	3.851393	-1.437617	1.359554
N	-0.444191	-2.137465	1.482564	N	4.390075	-2.708266	1.186634
C	0.001075	-2.693033	2.678622	C	4.221574	-3.50042	2.309401
C	0.258135	-1.645413	3.527441	C	3.559785	-2.736	3.235905
Si	-1.32831	0.398319	0.139058	Si	4.153762	0.200035	0.199852
Ru	0.279008	2.192422	-0.689377	C	4.846442	-0.775372	-1.4324
Cl	2.083694	1.143568	0.708046	N	6.097164	-0.786749	-2.002109
Ru	3.470787	-0.844833	-0.006428	C	6.088218	-1.502818	-3.193342
Cl	4.515872	0.412916	-1.786581	C	4.810974	-1.992893	-3.356153
C	-2.650486	-0.999608	-0.474943	N	4.074947	-1.530178	-2.269056
C	-2.713039	-1.523516	-1.80388	C	2.680293	-1.874182	-2.005343
C	-3.511381	-2.646985	-2.098589	C	2.692712	-0.37834	3.329173
C	-4.331726	-3.268006	-1.151854	Ru	1.846154	1.937127	-0.323905
C	-4.334492	-2.711614	0.131672	Cl	2.894407	2.36407	1.903641
C	-3.514874	-1.624292	0.496281	C	0.583265	2.317888	-2.102957
C	-2.789178	1.556624	0.878711	C	1.843918	1.869218	-2.568287
N	-3.627881	2.125894	-0.03451	C	3.000998	2.580884	-2.104134
C	-4.545868	2.976794	0.579791	C	2.860959	3.683294	-1.218245
C	-4.272465	2.92801	1.923685	C	1.581215	4.104235	-0.706947
N	-3.207611	2.040268	2.080044	C	0.444907	3.369045	-1.153285
Cl	1.62406	-1.29863	-1.512869	C	1.921892	0.840052	-3.658512
C	0.375764	4.286377	-1.372816	C	1.477684	5.281842	0.248593
C	1.722505	3.833012	-1.318545	C	0.023523	5.515019	0.718791
C	2.001621	2.592211	-1.976867	Cl	0.019749	1.303427	1.272927
C	1.045754	1.926478	-2.795564	C	2.033021	6.578828	-0.368245
C	-0.251608	2.488434	-2.968891	C	5.957654	0.978388	0.805721
C	-0.61747	3.602459	-2.148705	C	7.063988	0.214108	1.379238
C	2.822677	4.489365	-0.500953	C	8.339162	0.77257	1.624308
C	4.004597	4.863529	-1.424625	C	8.643962	2.08742	1.290638
C	-1.131095	2.032721	-4.090355	C	7.62862	2.859613	0.745538
C	4.563358	-0.744092	1.910843	C	6.331019	2.349421	0.547192
C	5.459452	-1.106567	0.866871	Cl	-0.410056	-0.854158	-1.121601
C	5.157561	-2.191063	-0.031608	Ru	-2.02125	-2.317063	0.186688
C	3.959297	-2.955439	0.107861	C	-2.691752	-3.933505	1.58747
C	3.070714	-2.619659	1.196746	C	-1.837343	-4.490104	0.584187
C	3.354943	-1.52903	2.056509	C	-0.504592	-4.030299	0.407145
C	4.806189	0.457295	2.783626	C	-0.14107	-2.8397	1.121762
C	3.567669	-4.057131	-0.857461	C	-0.953759	-2.299615	2.163816
C	3.948402	-5.421871	-0.241052	C	-2.193452	-2.932849	2.477504
C	4.154232	-3.877877	-2.265318	C	0.507019	-4.685182	-0.505553
C	2.348026	5.69571	0.32089	C	1.540281	-5.430667	0.364851
Cl	-0.428481	3.388396	1.372257	C	-2.863148	-2.6789	3.794467
H	2.103509	-3.121722	1.258976	Cl	-2.933989	-3.233026	-1.921287

S100

11. Appendix

H	2.604608	-1.207284	2.782041	Si	-3.676505	-0.425894	-0.148873
H	6.317245	-0.46215	0.64966	C	-4.881246	0.804838	0.869655
H	5.793431	-2.335705	-0.908209	C	-4.739381	1.124809	2.255853
H	5.245568	0.144499	3.752619	C	-5.43783	2.210911	2.817172
H	3.85917	0.991063	2.980993	C	-6.37338	2.961288	2.098005
H	5.502343	1.161382	2.295677	C	-6.590707	2.58219	0.768162
H	2.466279	-3.998467	-0.946646	C	-5.854938	1.563443	0.130287
H	3.715839	-4.627229	-2.949747	C	-3.857215	0.350298	3.233315
H	5.250835	-4.029578	-2.265903	C	-2.703342	1.201633	3.798769
H	3.929118	-2.867573	-2.650209	C	-7.112258	4.129854	2.730849
H	3.625889	-6.244541	-0.906879	C	-6.130873	5.265527	3.093677
H	3.476322	-5.569604	0.750132	C	-6.24241	1.335183	-1.335301
H	5.045302	-5.49702	-0.109881	C	-7.589838	0.586066	-1.41819
H	2.972494	2.104356	-1.835667	C	-5.203263	-1.53415	-0.821646
H	1.323756	0.986026	-3.280104	N	-5.902625	-2.255082	0.10354
H	-1.639651	3.994052	-2.180154	C	-6.871226	-3.050279	-0.505025
H	0.06583	5.131561	-0.753968	C	-6.768178	-2.813397	-1.854969
H	-2.204125	2.046767	-3.848765	N	-5.748468	-1.876882	-2.018704
H	-0.975947	2.748204	-4.923853	C	-5.735893	-2.161752	1.548559
H	-0.839299	1.036605	-4.451232	C	-7.792646	-3.950235	0.251565
H	3.180869	3.707341	0.197319	C	-7.548046	-3.378993	-2.995629
H	3.188837	6.095687	0.917203	C	-5.340779	-1.410306	-3.334796
H	1.989494	6.509653	-0.340312	C	-3.100071	0.96535	-1.478191
H	1.531834	5.413191	1.009364	N	-2.721771	0.851995	-2.788915
H	4.824992	5.301336	-0.825143	C	-2.628534	2.096427	-3.404422
H	4.400824	3.975451	-1.950771	C	-2.909955	3.034843	-2.441746
H	3.69203	5.612067	-2.178978	N	-3.147019	2.333804	-1.266232
C	-2.631728	1.768649	3.386199	C	-2.232846	-0.34021	-3.475785
C	-4.920946	3.630604	3.069867	C	-2.208872	2.265783	-4.826322
C	-5.593217	3.733871	-0.168988	C	-2.975174	4.523592	-2.546748
C	-3.629866	1.849984	-1.465852	C	-3.289367	3.066871	0.000903
C	0.355919	0.815527	3.371536	C	-4.725461	-0.184936	4.400926
C	0.781949	-1.636078	4.925618	C	-7.926587	3.686888	3.964534
C	0.11029	-4.164541	2.911841	C	-6.313655	2.624484	-2.184396
C	-0.675032	-2.999817	0.315287	C	-0.110514	-5.616879	-1.560847
C	-3.665156	-1.205901	1.962966	H	-0.537015	3.566463	-0.730156
H	-4.994226	-3.159177	0.885613	H	-0.302085	1.735899	-2.36007
C	-5.169995	-4.48845	-1.500809	H	3.993225	2.248591	-2.419818
H	-3.498793	-3.044488	-3.119426	H	3.784638	4.211628	-0.889029
C	-1.974571	-0.936285	-3.005275	H	1.681344	1.333529	-4.621977
H	1.454003	0.826769	3.473708	H	1.197174	0.027572	-3.48912
H	0.069935	1.629467	2.689377	H	2.938995	0.423518	-3.747714
H	-0.105425	0.950683	4.364481	H	2.087939	5.013644	1.1327
H	0.088996	-3.793675	0.330602	H	1.978652	7.391654	0.378409
H	-1.686124	-3.439928	0.348888	H	1.431324	6.885625	-1.246214
H	-0.531326	-2.420949	-0.600686	H	3.085794	6.470059	-0.684418
H	0.415395	-4.355519	3.954091	H	-0.0059	6.340001	1.453584

S101

11. Appendix

H	-0.857415	-4.67138	2.733118	H	-0.399369	4.613285	1.199532
H	0.857669	-4.638549	2.246324	H	-0.620424	5.800011	-0.136002
H	0.070919	-1.155863	5.625894	H	0.794	-2.334621	0.861486
H	0.960053	-2.66884	5.268492	H	-0.625586	-1.420354	2.726377
H	1.737304	-1.080568	4.997205	H	-3.693803	-4.34697	1.739055
H	-3.439505	1.727126	4.135159	H	-2.236755	-5.263175	-0.076239
H	-2.126024	0.797812	3.369662	H	-3.960183	-2.621763	3.737468
H	-1.910043	2.561139	3.647344	H	-2.621017	-3.545382	4.443171
H	-4.043428	2.719506	-2.000906	H	-2.472022	-1.773858	4.279748
H	-2.595444	1.685447	-1.802865	H	1.024794	-3.867519	-1.033374
H	-4.228922	0.948933	-1.680716	H	0.67958	-6.018073	-2.223195
H	-6.197812	4.328979	0.535853	H	-0.608981	-6.481958	-1.082835
H	-5.146993	4.431744	-0.904936	H	-0.857421	-5.077127	-2.170236
H	-6.274795	3.055287	-0.718426	H	2.340415	-5.864248	-0.266852
H	-4.202371	4.28038	3.606309	H	1.995118	-4.753067	1.108022
H	-5.749694	4.260737	2.705804	H	1.054626	-6.259809	0.914424
H	-5.338837	2.913051	3.803686	H	-7.352151	3.126592	0.197287
H	-2.864193	-0.503119	2.204072	H	-5.250651	2.473287	3.864362
C	-5.017072	-0.493052	2.184892	H	-1.147833	-0.224263	-3.634178
C	-3.51147	-2.36698	2.970441	H	-2.385654	-1.23523	-2.856308
H	-5.083313	-0.086372	3.213016	H	-2.741142	-0.440185	-4.449426
H	-5.167327	0.333973	1.469507	H	-2.629808	3.947241	-0.043892
H	-5.848977	-1.209988	2.049919	H	-4.331426	3.390524	0.152826
H	-3.477529	-1.965939	4.002232	H	-2.948539	2.437775	0.828402
H	-4.361785	-3.07191	2.920561	H	-2.854967	4.828313	-3.59953
H	-2.584507	-2.937321	2.792199	H	-3.948156	4.906606	-2.184673
H	-1.379663	-0.075226	-2.653655	H	-2.184177	5.022883	-1.956314
C	-1.00345	-1.944702	-3.657986	H	-2.893196	1.743774	-5.522925
C	-3.004664	-0.483053	-4.072224	H	-2.197279	3.335807	-5.091624
H	-0.383656	-1.439045	-4.422589	H	-1.192371	1.858196	-4.992953
H	-0.321403	-2.39878	-2.920976	H	-6.229123	-1.341338	-3.982985
H	-1.564429	-2.753064	-4.164425	H	-4.897254	-0.411016	-3.251245
H	-2.505071	-0.125174	-4.989207	H	-4.606414	-2.110087	-3.766587
H	-3.644502	-1.333857	-4.367682	H	-6.076845	-3.100123	2.013135
H	-3.671106	0.317768	-3.704401	H	-4.670827	-2.015227	1.773736
C	-4.265634	-5.703781	-1.803025	H	-6.310706	-1.309448	1.949915
H	-5.784278	-4.733319	-0.611236	H	-8.486234	-4.446202	-0.447481
C	-6.127678	-4.207991	-2.67785	H	-7.238866	-4.740766	0.795973
H	-6.768916	-5.088421	-2.873657	H	-8.397066	-3.390764	0.991792
H	-6.780045	-3.339858	-2.465566	H	-6.888139	-3.880397	-3.729702
H	-5.560258	-3.992178	-3.603885	H	-8.272994	-4.121801	-2.623594
H	-4.878074	-6.600923	-2.015539	H	-8.114799	-2.591952	-3.531653
H	-3.63159	-5.505443	-2.689262	H	-5.46845	0.723378	-1.807962
H	-3.599358	-5.929208	-0.948295	H	-7.832866	0.326096	-2.466859
				H	-7.589234	-0.338264	-0.816642
				H	-8.400315	1.23379	-1.034031
				H	-6.432849	2.360586	-3.252985

S102

11. Appendix

H	-7.177046	3.256588	-1.907864
H	-5.397766	3.23035	-2.077453
H	-3.412575	-0.495892	2.682122
H	-2.049141	0.579919	4.441163
H	-2.074045	1.636825	3.005119
H	-3.097214	2.023143	4.427205
H	-4.104592	-0.664594	5.177869
H	-5.271254	0.638684	4.892936
H	-5.478171	-0.917497	4.055347
H	-7.822123	4.520908	1.974923
H	-8.493933	4.541778	4.378306
H	-8.642752	2.884563	3.705194
H	-7.257969	3.307569	4.76164
H	-6.678683	6.132441	3.509219
H	-5.403662	4.925354	3.856612
H	-5.563842	5.6049	2.205461
C	7.009616	-1.208998	1.842274
H	9.116807	0.15809	2.090018
H	9.640254	2.502688	1.487519
H	7.827889	3.906422	0.493651
C	5.354433	3.363326	0.081669
C	4.250139	-2.83067	-4.44151
C	7.274735	-1.653682	-4.06179
C	7.255375	-0.037107	-1.527979
C	3.147561	-3.115249	4.607282
C	4.692895	-4.897509	2.417021
C	5.006755	-3.248037	-0.012302
H	2.080756	-0.789144	4.144863
H	3.454392	0.310275	3.730218
H	2.045438	0.173846	2.630235
H	2.107865	-1.840947	-2.94092
H	2.595539	-2.890102	-1.585357
H	2.252398	-1.161228	-1.282377
H	5.363201	-4.263261	0.187353
H	4.272941	-3.297425	-0.819802
H	5.850311	-2.628496	-0.31725
H	4.438805	-5.299648	3.40574
H	4.219884	-5.529322	1.652066
H	5.784174	-4.95103	2.288282
H	2.638504	-2.292066	5.118641
H	2.462942	-3.97553	4.575688
H	4.027472	-3.395333	5.204324
H	8.134018	-0.32242	-2.118393
H	7.077378	1.035894	-1.656338
H	7.425585	-0.203415	-0.439116
H	7.021809	-2.263864	-4.938232
H	7.629802	-0.672026	-4.408867

S103

11. Appendix

H	8.09593	-2.143457	-3.517696
H	3.191781	-3.052412	-4.259774
H	4.333114	-2.313852	-5.408854
H	4.794591	-3.78339	-4.514465
H	6.048762	-1.609844	1.574921
C	8.095745	-2.08045	1.252022
C	7.093447	-1.274308	3.34754
H	7.036078	-2.318797	3.689068
H	8.042278	-0.850803	3.705433
H	6.270897	-0.707322	3.807379
H	7.993716	-3.113097	1.615594
H	8.057893	-2.101705	0.154628
H	9.092208	-1.72311	1.543297
H	4.397506	2.858046	0.031649
C	5.292118	4.516285	1.054434
C	5.72779	3.902975	-1.276346
H	4.549513	5.259258	0.736256
H	5.022228	4.16775	2.057262
H	6.262808	5.027099	1.107753
H	5.035615	4.631068	-1.705829
H	6.681095	4.444659	-1.187605
H	5.879777	3.098464	-2.009504

2'			
Atomtype	X [Å]	Y [Å]	Z [Å]
N	-0.03355	2.594325	1.672632
C	0.287966	1.265762	1.592799
N	0.704179	0.941677	2.851803
C	0.640927	2.039803	3.71062
C	0.181636	3.091794	2.953906
Si	0.033909	0.212031	-0.122141
C	1.402989	-1.1937	-0.227442
C	1.573395	-2.223206	0.757319
C	2.822196	-2.84494	0.93041
C	3.917317	-2.556955	0.094942
C	3.656301	-1.768609	-1.033685
C	2.409615	-1.14401	-1.248725
C	0.353478	-2.832818	1.441966
C	0.614188	-3.579506	2.763268
C	5.290198	-3.157794	0.351952
C	5.253915	-4.700673	0.339265
C	2.119009	-0.672703	-2.673557
C	1.940705	-1.928371	-3.562242
C	1.196628	-0.355492	3.295241
C	0.998491	1.972741	5.159943

TS4 (+3.5 kcal/mol)			
Atomtype	X [Å]	Y [Å]	Z [Å]
N	0.721755	2.297087	-2.349828
C	0.995752	1.561861	-1.236333
N	2.147504	2.107171	-0.731572
C	2.570142	3.186974	-1.502681
C	1.660686	3.307011	-2.527117
Si	-0.042581	0.13298	-0.262938
Ru	-2.42122	-0.016372	-0.312446
Cl	-1.091615	-1.003957	-2.153135
C	2.947379	1.603612	0.384962
C	3.81099	3.96434	-1.209992
C	1.624839	4.245188	-3.686974
C	-0.236754	1.989488	-3.416166
C	0.358772	1.387679	1.68632
N	0.1344	2.731715	1.755696
C	0.400094	3.224039	3.033102
C	0.805987	2.148951	3.789948
N	0.776006	1.044857	2.935944
C	-0.341125	3.58379	0.664996
C	1.15941	-0.293739	3.365546
C	1.193319	2.06547	5.230822

S104

11. Appendix

C	-0.103824	4.505078	3.343186	C	0.224515	4.657606	3.415314
C	-0.548074	3.438481	0.594222	C	1.355734	-1.259564	-0.325378
Ru	-2.330362	-0.016738	-0.306563	C	1.448852	-2.3161	0.644138
Cl	-2.617527	2.039652	-1.630843	C	2.669762	-2.969052	0.889681
C	-2.970491	-1.777088	0.869712	C	3.832623	-2.677027	0.154355
C	-4.024891	-1.589779	-0.092886	C	3.685501	-1.819846	-0.943038
C	-4.619187	-0.306871	-0.188171	C	2.469429	-1.17041	-1.241083
C	-4.170849	0.761045	0.650654	C	0.198647	-2.898593	1.290765
C	-3.202015	0.579087	1.681455	C	-0.365143	-3.947942	0.301939
C	-2.576067	-0.709601	1.740199	C	5.16774	-3.319843	0.496397
C	-4.487961	-2.682338	-1.042614	C	5.661941	-2.847816	1.881103
C	-3.597528	-3.93081	-1.062772	C	2.352994	-0.656813	-2.675772
C	-2.889466	1.680381	2.657199	C	3.515904	0.243045	-3.127453
Cl	-1.555182	-1.198122	-2.297311	C	0.398699	-3.547658	2.672048
C	-5.951711	-3.057607	-0.706734	C	5.098445	-4.860396	0.431683
C	1.077827	1.6197	-1.109481	C	2.201736	-1.882216	-3.611767
N	2.179749	2.23774	-0.578202	Cl	-2.655491	2.123778	-1.500911
C	2.573023	3.317711	-1.365145	C	-3.088417	-1.807323	0.795986
C	1.714995	3.340466	-2.441362	C	-4.167957	-1.528015	-0.116135
N	0.826712	2.28486	-2.269098	C	-4.718202	-0.223389	-0.110455
C	2.962655	1.797565	0.577372	C	-4.185874	0.782334	0.757532
C	3.747057	4.182166	-1.041905	C	-3.180098	0.509819	1.731999
C	1.68759	4.228847	-3.640083	C	-2.612179	-0.806389	1.702926
C	-0.043877	1.85776	-3.37031	C	-4.704483	-2.548172	-1.107098
C	-0.267352	-3.808664	0.411727	C	-6.118473	-2.993982	-0.663848
C	5.877479	-2.630665	1.679305	C	-2.76897	1.5513	2.736482
C	3.171934	0.275312	-3.2732	C	-3.791023	-3.760632	-1.327207
H	4.435027	-1.679498	-1.802145	H	4.536297	-1.694286	-1.625817
H	2.940566	-3.599474	1.715561	H	2.713202	-3.754979	1.652299
H	1.13316	-0.193777	-2.688979	H	1.405288	-0.120953	-2.784646
H	2.840908	0.638384	-4.265001	H	3.277715	0.718426	-4.098223
H	4.13529	-0.24666	-3.4261	H	4.440165	-0.347469	-3.274131
H	3.361542	1.150384	-2.627761	H	3.735156	1.039451	-2.394356
H	1.660662	-1.623178	-4.589142	H	2.035722	-1.541542	-4.652466
H	1.136668	-2.570597	-3.161194	H	1.336971	-2.497168	-3.305986
H	2.876973	-2.516112	-3.614789	H	3.11211	-2.51119	-3.591401
H	5.95457	-2.826591	-0.470861	H	5.90142	-2.980691	-0.261753
H	6.897147	-3.030057	1.839766	H	6.653349	-3.283409	2.110094
H	5.249453	-2.947185	2.535254	H	4.957644	-3.167343	2.674207
H	5.931016	-1.524694	1.682533	H	5.747295	-1.744602	1.921402
H	6.272	-5.111118	0.479459	H	6.093133	-5.300183	0.63615
H	4.849415	-5.082697	-0.616701	H	4.760473	-5.203329	-0.564149
H	4.618422	-5.086698	1.159774	H	4.39304	-5.255462	1.188263
H	-0.378922	-2.027902	1.61772	H	-0.536236	-2.083467	1.380005
H	-1.128834	-4.350076	0.847985	H	-1.232199	-4.477799	0.741094
H	0.486481	-4.561591	0.113994	H	0.411556	-4.703232	0.07764
H	-0.597312	-3.263362	-0.489121	H	-0.673008	-3.467378	-0.641485

S105

11. Appendix

H	-0.347799	-3.839606	3.243458	H	-0.583453	-3.781437	3.124572
H	1.218174	-2.996537	3.482047	H	0.960764	-2.90241	3.371473
H	1.150841	-4.528651	2.577597	H	0.952525	-4.501434	2.585342
H	-0.729492	2.674687	-3.640132	H	-0.864313	2.871495	-3.613897
H	-0.633792	0.981994	-3.069771	H	-0.879698	1.154431	-3.115356
H	0.607693	1.603084	-4.226384	H	0.342184	1.719063	-4.318597
H	2.438834	5.029633	-3.537318	H	2.43153	4.99167	-3.596831
H	0.692796	4.694143	-3.775428	H	0.657095	4.778611	-3.745659
H	1.913867	3.659871	-4.563064	H	1.761291	3.703501	-4.643487
H	3.808411	5.015024	-1.762137	H	3.892064	4.816721	-1.905032
H	4.698138	3.615519	-1.098347	H	4.719901	3.341389	-1.331056
H	3.674227	4.610409	-0.023493	H	3.814058	4.35991	-0.175836
H	4.032512	1.914973	0.336983	H	4.009561	1.628533	0.086676
H	2.766814	0.73243	0.763376	H	2.674184	0.561663	0.595087
H	2.72464	2.400888	1.47213	H	2.805396	2.233033	1.282443
H	-5.337895	-0.098478	-0.985934	H	-5.462435	0.050452	-0.864162
H	-4.562621	1.767645	0.472084	H	-4.538517	1.812879	0.64857
H	-1.79296	-0.880134	2.487756	H	-1.806832	-1.048465	2.40549
H	-2.463796	-2.737271	0.931989	H	-2.617969	-2.788159	0.79084
H	-3.705156	1.769333	3.402609	H	-3.543012	1.643411	3.524736
H	-2.803957	2.651573	2.138707	H	-2.66211	2.539452	2.255284
H	-1.953934	1.481649	3.205973	H	-1.818973	1.286316	3.228224
H	-4.464108	-2.22923	-2.052956	H	-4.792245	-2.01151	-2.072078
H	-3.983829	-4.648008	-1.809654	H	-4.222963	-4.413368	-2.107456
H	-3.599513	-4.439035	-0.078498	H	-3.696144	-4.36292	-0.402709
H	-2.561792	-3.670034	-1.332535	H	-2.787555	-3.440935	-1.652079
H	-6.32106	-3.807675	-1.430701	H	-6.542821	-3.694267	-1.407365
H	-6.621953	-2.179025	-0.744086	H	-6.806673	-2.134498	-0.562026
H	-6.016003	-3.497947	0.307526	H	-6.071168	-3.515344	0.312206
H	1.955708	-0.206513	4.079618	H	1.96633	-0.222742	4.112551
H	0.373983	-0.96552	3.705357	H	0.300913	-0.822708	3.815142
H	1.65721	-0.882874	2.449087	H	1.525344	-0.861073	2.497725
H	0.829201	2.954323	5.633098	H	1.101777	3.058214	5.702286
H	0.383234	1.223584	5.695327	H	0.543248	1.361499	5.786184
H	2.061609	1.700338	5.312601	H	2.239541	1.72366	5.358974
H	0.443054	5.223899	2.703424	H	0.813235	5.329705	2.761876
H	-1.183438	4.73857	3.255447	H	-0.835943	4.970515	3.341906
H	0.19806	4.675275	4.389938	H	0.554264	4.813023	4.456069
H	-1.248823	4.171318	1.024131	H	-0.991321	4.368531	1.082968
H	0.28007	3.979653	0.101549	H	0.513541	4.059104	0.149465
H	-1.103083	2.832019	-0.14227	H	-0.937875	2.991449	-0.050635

11. Appendix

TS5 (+1.3 kcal/mol)				TS6 (+2.3 kcal/mol)			
Atomtype	X [Å]	Y [Å]	Z [Å]	Atomtype	X [Å]	Y [Å]	Z [Å]
N	0.658725	3.256249	-0.652026	C	-0.91829	3.061898	0.828649
C	0.639529	2.111902	0.0797	C	-0.433755	3.680058	-0.37443
N	1.362463	2.37528	1.201769	C	0.931646	4.158947	-0.391796
C	1.849741	3.678698	1.180224	C	1.811523	3.818695	0.649885
C	1.403344	4.236645	0.000616	C	1.35692	3.082399	1.81617
Si	-0.107779	0.326141	-0.183549	C	-0.035377	2.801884	1.926176
Ru	-2.41879	0.07461	0.114803	Ru	0.726374	1.911454	0.052464
Cl	-1.087494	0.338035	-2.180257	Cl	0.8474	1.381646	-2.287088
C	1.598553	1.415085	2.280281	C	-1.34264	3.918807	-1.56519
C	2.683494	4.262086	2.273817	C	-1.90718	5.355222	-1.481245
C	1.62997	5.606146	-0.551501	C	2.331781	2.680136	2.889866
C	-0.030769	3.468174	-1.927428	Si	-0.306234	-0.18233	0.582495
C	1.501648	-0.707018	-0.209368	Cl	-0.056946	-0.457603	2.758787
C	1.725657	-1.760021	0.734058	C	0.439065	-1.994071	0.222032
C	2.986964	-2.374291	0.811239	N	-0.003337	-3.131882	0.835955
C	4.057182	-1.997574	-0.016067	C	0.7936	-4.220147	0.494547
C	3.824056	-0.978644	-0.952358	C	1.748615	-3.745678	-0.376741
C	2.582174	-0.327387	-1.07067	N	1.505224	-2.38485	-0.526734
C	0.644114	-2.28073	1.676841	C	-1.200072	-3.297866	1.666196
C	0.30246	-3.751724	1.353847	C	2.202329	-1.591581	-1.533633
C	5.407186	-2.691937	0.080376	C	2.842461	-4.454613	-1.104968
C	6.000536	-2.590914	1.501351	C	0.544739	-5.601195	1.004493
C	2.480681	0.751993	-2.149462	C	-2.15281	-0.506126	0.120163
C	3.444778	1.925157	-1.876114	C	-3.263958	-0.179664	0.958359
C	1.02196	-2.135619	3.165949	C	-4.551479	-0.648615	0.627492
C	5.296817	-4.165063	-0.370715	C	-4.806541	-1.399728	-0.528378
C	2.693445	0.160699	-3.559258	C	-3.723921	-1.636507	-1.391177
Cl	-2.49784	2.47304	0.334892	C	-2.42049	-1.193278	-1.110965
C	-2.642607	-2.065975	0.583358	C	-3.167946	0.682241	2.219486
C	-3.437629	-1.759165	-0.561027	C	-4.123195	1.896057	2.155891
C	-4.479235	-0.754256	-0.437453	C	-6.201077	-1.873947	-0.919603
C	-4.622508	-0.009989	0.741111	C	-7.170415	-2.031083	0.263909
C	-3.695482	-0.187829	1.843105	C	-1.374355	-1.429252	-2.206041
C	-2.746842	-1.264442	1.764475	C	-1.135487	-2.927621	-2.486271
C	-3.283248	-2.498781	-1.878906	C	3.617645	0.437587	0.322398
C	-4.460403	-3.490471	-2.037151	N	4.488758	0.643408	-0.701854
C	-3.767097	0.703648	3.052616	C	5.484978	-0.339281	-0.751667
C	-1.934249	-3.21655	-2.040464	C	5.224937	-1.193559	0.297787
H	4.643434	-0.683826	-1.620472	N	4.080939	-0.689117	0.930417
H	3.138727	-3.178493	1.540817	C	4.375085	1.73772	-1.66047
H	1.460866	1.161916	-2.149099	C	6.57947	-0.345947	-1.769653
H	3.288129	2.733179	-2.616897	C	5.953787	-2.408371	0.774846
H	4.498539	1.598139	-1.955229	C	3.469044	-1.308711	2.098573
H	3.294868	2.344633	-0.864031	C	-3.438212	-0.139595	3.497674

S107

11. Appendix

H	2.570287	0.948146	-4.327564	C	-1.760636	-0.693436	-3.507439
H	1.962393	-0.643891	-3.760861	C	-6.791395	-0.922242	-1.987881
H	3.710135	-0.262054	-3.664817	C	-2.462398	2.873901	-1.689563
H	6.095856	-2.173398	-0.61564	H	-3.910171	-2.173883	-2.330245
H	7.003317	-3.057127	1.532	H	-5.381782	-0.40668	1.298965
H	5.361026	-3.11964	2.234806	H	-0.418253	-0.973865	-1.899608
H	6.095487	-1.536528	1.823992	H	-0.311911	-3.057855	-3.215281
H	6.289968	-4.652292	-0.340525	H	-2.039872	-3.391056	-2.924067
H	4.900061	-4.239781	-1.400568	H	-0.883527	-3.490917	-1.570058
H	4.619591	-4.729037	0.3	H	-0.96766	-0.829757	-4.26683
H	-0.257966	-1.674395	1.501935	H	-1.874157	0.388597	-3.324938
H	-0.540256	-4.103991	1.979569	H	-2.708678	-1.086694	-3.921138
H	1.169259	-4.407829	1.558042	H	-6.076656	-2.869244	-1.394012
H	0.032979	-3.876341	0.288628	H	-8.111305	-2.501587	-0.076666
H	0.192082	-2.486234	3.809793	H	-7.433003	-1.047344	0.699061
H	1.248162	-1.087724	3.434768	H	-6.735685	-2.657262	1.066108
H	1.912415	-2.74467	3.410721	H	-7.777841	-1.287247	-2.333215
H	0.006132	4.539406	-2.17348	H	-6.121502	-0.838595	-2.864105
H	-1.079995	3.151705	-1.82132	H	-6.924829	0.09107	-1.561349
H	0.461536	2.8928	-2.730521	H	-2.144838	1.080696	2.293325
H	2.263641	6.186862	0.138987	H	-3.932759	2.576293	3.007966
H	0.677642	6.155795	-0.683391	H	-5.180242	1.576706	2.210851
H	2.139554	5.568175	-1.53384	H	-4.002745	2.465424	1.214396
H	2.957739	5.299792	2.022083	H	-3.291438	0.485687	4.399375
H	3.618271	3.688199	2.426112	H	-2.758241	-1.00693	3.567499
H	2.136289	4.282249	3.237041	H	-4.481559	-0.509873	3.504182
H	1.860417	1.96195	3.199281	H	3.288757	-1.747482	-1.43483
H	2.40924	0.71703	2.006911	H	1.95978	-0.530863	-1.403861
H	0.674496	0.840243	2.466198	H	1.868121	-1.915974	-2.535554
H	-5.086745	-0.50827	-1.31541	H	2.886504	-5.509893	-0.787675
H	-5.321193	0.832457	0.771699	H	3.827467	-3.989659	-0.907713
H	-2.061334	-1.426284	2.60295	H	2.679005	-4.430518	-2.200244
H	-1.872763	-2.833165	0.515075	H	1.310133	-6.291573	0.612494
H	-4.617038	0.399362	3.696069	H	-0.448564	-5.975025	0.687289
H	-3.912173	1.753497	2.744237	H	0.574863	-5.639943	2.110662
H	-2.837251	0.634885	3.644572	H	-1.800497	-4.123416	1.246447
H	-3.368131	-1.733215	-2.674945	H	-1.800106	-2.380465	1.653103
H	-1.847367	-3.619196	-3.065624	H	-0.908225	-3.53858	2.703012
H	-1.852754	-4.070994	-1.341328	H	4.166132	1.343807	-2.671767
H	-1.085741	-2.532122	-1.863404	H	5.312582	2.323328	-1.684922
H	-4.400542	-3.994238	-3.019756	H	3.529729	2.373555	-1.356227
H	-5.438958	-2.979608	-1.969106	H	7.192088	-1.258407	-1.666733
H	-4.419634	-4.264974	-1.247268	H	7.250774	0.528526	-1.652931
				H	6.176851	-0.31456	-2.801085
				H	6.773238	-2.65915	0.079135
				H	5.282337	-3.286935	0.848413
				H	6.396634	-2.253929	1.779395

S108

11. Appendix

H	4.195106	-1.359536	2.931223
H	3.132382	-2.335211	1.857816
H	2.598108	-0.709718	2.39965
H	1.317713	4.617281	-1.308512
H	2.881533	4.033942	0.550892
H	-0.397361	2.255542	2.801024
H	-1.954396	2.726287	0.877598
H	2.494536	3.522713	3.592434
H	3.298893	2.398973	2.438703
H	1.940995	1.818623	3.458152
H	-0.701546	3.840191	-2.462755
H	-2.977436	2.992169	-2.65983
H	-3.223275	2.995946	-0.894691
H	-2.052845	1.851743	-1.625144
H	-2.533327	5.567027	-2.368159
H	-1.098679	6.109428	-1.438539
H	-2.537278	5.473488	-0.578104

S109

4. References

- [1] S. U. Ahmad, T. Szilvási and S. Inoue, A facile access to a novel NHC-stabilized silyliumylidene ion and C–H activation of phenylacetylene, *Chem. Commun.* **2014**, *50*, 12619-12622.
- [2] P. Frisch and S. Inoue, NHC-stabilized silyl-substituted silyliumylidene ions, *Dalton Trans.* **2019**, *48*, 10403-10406.
- [3] S. B. Jensen, S. J. Rodger and M. D. Spicer, Facile preparation of η^6 -*p*-cymene ruthenium diphosphine complexes. Crystal structure of $[(\eta^6$ -*p*-cymene)Ru(dppf)Cl]PF₆, *J. Organomet. Chem.* **1998**, *556*, 151-158.
- [4] C. White, A. Yates and P. M. Maitlis, (η^5 -Pentamethylcyclopentadienyl)Rhodium and -Iridium Compounds in *Inorg. Synth.*, **1992**.
- [5] D. Journal of Chemical Physics Reiter, R. Holzner, A. Porzelt, P. J. Altmann, P. Frisch and S. Inoue, Disilene–Silylene Interconversion: A Synthetically Accessible Acyclic Bis(silyl)silylene, *J. Am. Chem. Soc.* **2019**, *141*, 13536-13546.
- [6] P. Frisch, T. Szilvási, A. Porzelt and S. Inoue, Transition Metal Carbonyl Complexes of an *N*-Heterocyclic Carbene Stabilized Silyliumylidene Ion, *Inorg. Chem.* **2019**, *58*, 14931-14937.
- [7] APEX suite of crystallographic software, APEX 3 version 2015.5-2; Bruker AXS Inc.: Madison, Wisconsin, USA, **2015**.
- [8] SAINT, Version 7.56a and SADABS Version 2008/1; Bruker AXS Inc.: Madison, Wisconsin, USA, **2008**.
- [9] G. M. Sheldrick, SHELXL-2014, University of Göttingen, Göttingen, Germany, **2014**.
- [10] C. B. Hübschle, G. M. Sheldrick and B. Dittrich, ShelXle: a Qt graphical user interface for SHELXL, *J. Appl. Cryst.* **2011**, *44*, 1281-1284.
- [11] G. M. Sheldrick, SHELXL-97, University of Göttingen, Göttingen, Germany, **1998**.
- [12] A. J. C. Wilson, International Tables for Crystallography, Vol. C, Tables 6.1.1.4 (pp. 500-502), 4.2.6.8 (pp. 219-222), and 4.2.4.2 (pp. 193-199); Kluwer Academic Publishers: Dordrecht, The Netherlands, **1992**.
- [13] C. F. Macrae, I. J. Bruno, J. A. Chisholm, P. R. Edgington, P. McCabe, E. Pidcock, L. Rodriguez-Monge, R. Taylor, J. van de Streek and P. A. Wood, Mercury CSD 2.0 - new features for the visualization and investigation of crystal structures, *J. Appl. Cryst.* **2008**, *41*, 466-470.
- [14] Diamond – Crystal and Molecular Structure Visualization, Crystal Impact – Dr. H. Putz & Dr. K. Brandenburg GbR, Kreuzherrenstr. 102, 53227 Bonn, Germany, www.crystalimpact.com/diamond.

- [15] A. D. Becke, Density-functional thermochemistry. V. Systematic optimization of exchange-correlation functionals, *J. Chem. Phys.* **1997**, *107*, 8554-8560.
- [16] S. Grimme, Semiempirical GGA-type density functional constructed with a long-range dispersion correction, *J. Comput. Chem.* **2006**, *27*, 1787-1799.
- [17] F. Weigend and R. Ahlrichs, Balanced basis sets of split valence, triple zeta valence and quadruple zeta valence quality for H to Rn: Design and assessment of accuracy, *Physical Chemistry Chemical Physics* **2005**, *7*, 3297-3305.
- [18] M. J. Frisch, G. W. Trucks, H. B. Schlegel, G. E. Scuseria, M. A. Robb, J. R. Cheeseman, G. Scalmani, V. Barone, B. Mennucci, G. A. Petersson, H. Nakatsuji, M. Caricato, X. Li, H. P. Hratchian, A. F. Izmaylov, J. Bloino, G. Zheng, J. L. Sonnenberg, M. Hada, M. Ehara, K. Toyota, R. Fukuda, J. Hasegawa, M. Ishida, T. Nakajima, Y. Honda, O. Kitao, H. Nakai, T. Vreven, J. A. Montgomery, Jr., J. E. Peralta, F. Ogliaro, M. Bearpark, J. J. Heyd, E. Brothers, K. N. Kudin, V. N. Staroverov, R. Kobayashi, J. Normand, K. Raghavachari, A. Rendell, J. C. Burant, S. S. Iyengar, J. Tomasi, M. Cossi, N. Rega, J. M. Millam, M. Klene, J. E. Knox, J. B. Cross, V. Bakken, C. Adamo, J. Jaramillo, R. Gomperts, R. E. Stratmann, O. Yazyev, A. J. Austin, R. Cammi, C. Pomelli, J. W. Ochterski, R. L. Martin, K. Morokuma, V. G. Zakrzewski, G. A. Voth, P. Salvador, J. J. Dannenberg, S. Dapprich, A. D. Daniels, Ö. Farkas, J. B. Foresman, J. V. Ortiz, J. Cioslowski and D. J. Fox, Gaussian 09, Revision E.01, Gaussian, Inc., Wallingford CT, **2009**.
- [19] A. D. Boese and N. C. Handy, A new parametrization of exchange–correlation generalized gradient approximation functionals, *J. Chem. Phys.* **2001**, *114*, 5497-5503.

11.5 Licenses for Copyrighted Content

11.5.1 License for Chapter 4 and 5

Dear Philipp

The Royal Society of Chemistry (RSC) hereby grants permission for the use of your paper(s) specified below in the printed and microfilm version of your thesis. You may also make available the PDF version of your paper(s) that the RSC sent to the corresponding author(s) of your paper(s) upon publication of the paper(s) in the following ways: in your thesis via any website that your university may have for the deposition of theses, via your university's Intranet or via your own personal website. We are however unable to grant you permission to include the PDF version of the paper(s) on its own in your institutional repository. The Royal Society of Chemistry is a signatory to the STM Guidelines on Permissions (available on request).

Please note that if the material specified below or any part of it appears with credit or acknowledgement to a third party then you must also secure permission from that third party before reproducing that material.

Please ensure that the thesis states the following:
Reproduced by permission of The Royal Society of Chemistry
and include a link to the paper on the Royal Society of Chemistry's website.

Please ensure that your co-authors are aware that you are including the paper in your thesis.

Regards
Gill Cockhead
Contracts & Copyright Executive

Gill Cockhead
Contracts & Copyright Executive
Royal Society of Chemistry,
Thomas Graham House,
Science Park, Milton Road,
Cambridge, CB4 0WF, UK
Tel +44 (0) 1223 432134

Journal Title:	Dalton Transactions
Author(s):	P. Frisch, S. Inoue
Volume Number:	48
Year of Publication:	2019
Description of Material:	NHC-stabilized Silyl-substituted Silyliumylidene Ions
Page(s):	10403-10406

Journal Title:	Chemical Communications
Author(s):	P. Frisch, S. Inoue
Volume Number:	54
Year of Publication:	2018
Description of Material:	Coinage Metal Complexes of NHC-stabilized Silyliumylidene Ions
Page(s):	13648-13661

11.5.2 License for Chapter 6



RightsLink®



Home



Help



Email Support



Sign in



Create Account

Transition Metal Carbonyl Complexes of an N-Heterocyclic Carbene Stabilized Silyliumylidene Ion



Author: Philipp Frisch, Tibor Szilvási, Amelie Porzelt, et al

Publication: Inorganic Chemistry

Publisher: American Chemical Society

Date: Nov 1, 2019

Copyright © 2019, American Chemical Society

PERMISSION/LICENSE IS GRANTED FOR YOUR ORDER AT NO CHARGE

This type of permission/license, instead of the standard Terms & Conditions, is sent to you because no fee is being charged for your order. Please note the following:

- Permission is granted for your request in both print and electronic formats, and translations.
- If figures and/or tables were requested, they may be adapted or used in part.
- Please print this page for your records and send a copy of it to your publisher/graduate school.
- Appropriate credit for the requested material should be given as follows: "Reprinted (adapted) with permission from (COMPLETE REFERENCE CITATION). Copyright (YEAR) American Chemical Society." Insert appropriate information in place of the capitalized words.
- One-time permission is granted only for the use specified in your request. No additional uses are granted (such as derivative works or other editions). For any other uses, please submit a new request.

[BACK](#)

[CLOSE WINDOW](#)

11.5.3 License for Chapter 7

Dear Philipp Frisch,

We hereby grant permission for the requested use expected that due credit is given to the original source.

If material appears within our work with credit to another source, authorisation from that source must be obtained.

Credit must include the following components:

- Journals: Author(s) Name(s): Title of the Article. Name of the Journal. Publication year. Volume. Page(s)/(accepted not yet published) Copyright Wiley-VCH Verlag GmbH & Co. KGaA. Reproduced with permission.

If you also wish to publish your thesis in electronic format, you may use the article according to the Copyright transfer agreement:

3. Final Published Version.

Wiley-VCH hereby licenses back to the Contributor the following rights with respect to the final published version of the Contribution:

a. [...]

b. Re-use in other publications. The right to re-use the final Contribution or parts thereof for any publication authored or edited by the Contributor (excluding journal articles) where such re-used material constitutes less than half of the total material in such publication. In such case, any modifications should be accurately noted.

Kind regards

Heike Weller
Rights Manager
Rights & Licenses

Wiley-VCH Verlag GmbH & Co. KGaA
Boschstraße 12
69469 Weinheim
Germany
www.wiley-vch.de

T + (49) 6201 606-585
F + (49) 6201 606-332
rightsDE@wiley.com

WILEY

Journal Title:	Chemistry – A European Journal
Author(s):	Philipp Frisch, Tibor Szilvási and Shigeyoshi Inoue
Volume Number:	n/a
Year of Publication:	2020
Description of Material:	Facile Access to Dative, Single and Double Silicon–Metal Bonds Through M–Cl Insertion Reactions of Base-stabilized Si(II) cations
Page(s):	n/a
DOI:	10.1002/chem.202000866